

Novel Real-time Data Management Modules for General Community-level Grid Based on Centralized V2G System

PhD Thesis

Student: Jie Ru (20388048)

Supervisors: Prof. Mark Gillott

Dr. Rob Shipman

University of Nottingham

Faculty of Engineering

Department of Architecture and Built Environment

August 2025

ABSTRACT

Vehicle-to-Grid (V2G), as an emerging form of temporary energy storage, has been widely studied for its potential applications in grid management, aiming to support peak shaving and power balancing while mitigating the impact of the variable and intermittent output of renewable energy on irregular grid load distributions. Previous research on V2G management and scheduling has seen extensive development at the microgrid level. However, the complexity of electric vehicle (EV) usage behaviours poses significant challenges, limiting the direct applicability of these microgrid-based V2G strategies to community- and region-level centralized frameworks.

To bridge this gap, a centralized V2G scheduling framework was developed and implemented in Python as a simulation-based platform. The framework was designed with the overarching objective of achieving extreme load balancing within community-scale zero-carbon grids. To ensure realism and applicability, the underlying grid model was constructed using operational data from the Nottingham Trent Basin community energy project, a flagship zero-carbon initiative in the UK, in combination with empirical driving and charging behaviour statistics drawn from the MyElectricAvenue project, a national study of electric vehicle users. Three distinct scheduling strategies were evaluated to investigate the operational potential of centralized V2G systems under varying assumptions of vehicle availability and user behaviour. The first strategy prioritized the utilization of active EVs—defined as vehicles that exhibit either driving or charging behaviour within a given day—for meeting load balancing requirements, with idle EVs serving as supplementary resources when the active fleet alone was insufficient. The second strategy preserved the charging behaviour of active EVs entirely and relied exclusively on idle vehicles for V2G operations, a configuration that to some extent reflects the technical feasibility of simplified battery-swapping station paradigms. The third

strategy treated all EVs as fully dispatchable resources, effectively emulating the behaviour of a large-scale stationary storage system and representing an extreme boundary condition for centralized scheduling. This latter scenario further allowed for an exploration of the substitutability of EV-based flexibility against dedicated battery storage facilities.

Results indicate that under current community grid conditions and typical EV usage parameters—including 3.3 kW bidirectional power transfer, 24 kWh battery capacity, full EV ownership, and a 54.87% idle rate—the proposed framework effectively achieves community-level load balancing. Economically and environmentally, Scenarios I and II demonstrate a 49.78% reduction in annual electricity costs and a net negative carbon footprint, confirming the robustness of the control logic. Further sensitivity analysis identified parameter configurations that enhance the efficiency of V2G scheduling. Specifically, when higher charging and discharging power levels are combined with larger EV battery capacities, the number of vehicles required to achieve extreme load balancing within the grid can be significantly reduced, thereby improving the effectiveness of each EV in the scheduling process. However, these gains in operational efficiency are accompanied by higher economic costs and a modest decline in carbon performance, highlighting the trade-offs inherent in configuring system parameters for community-scale V2G applications. Collectively, these findings demonstrate that systematically integrating idle EVs into centralized V2G frameworks provides a scalable, practical approach for balancing community-level power loads, minimizing costs, and advancing carbon neutrality, offering a robust, data-driven foundation for future regional-scale V2G deployment and smart grid development.

ACKNOWLEDGEMENTS

Looking back over the years of my doctoral study, I realise that this journey has been a mixture of excitement, frustration, and long days of work that were often torn down and rebuilt. It has been stressful at times, and I could not have reached this stage without the support I received in many different ways.

First and foremost, I thank my parents for being my strongest support. The path of a PhD is never straightforward, and you have been with me through all its twists and turns. Despite the distance and time difference, you were always the first to give me help when I faced setbacks. I especially remember my mother once saying to me: even if my research is just a small corner of academia, I will always be her pride. Those words stayed with me and kept me going.

My supervisors, Professor Mark Gillott and Dr. Rob Shipman, also deserve my deepest gratitude. They provided me with guidance, yet also allowed me the space to develop my own direction. Our conversations—sometimes very technical, sometimes focused on the bigger picture—helped me to see what I had overlooked. From both of you I learned not only about research, but also how to think critically and to keep moving forward when things did not go as planned.

I would also like to thank my friends and colleagues. Their support, whether through conversations about my research or about everyday life in the UK, made these four years much more manageable. Even when we could not meet often in person, their simple encouragements gave me the strength to continue.

Finally, I want to acknowledge myself. There were times when I doubted whether I would ever finish, but I persevered. This thesis is not only the result of academic work, but also of persistence and determination.

DECLARATION OF GENERATIVE AI AND AI-ASSISTED TECHNOLOGIES IN THE WRITING PROCESS.

During the preparation of this manuscript, the author utilized ChatGPT (developed by OpenAI) to enhance the clarity and readability of the text. The author subsequently reviewed and edited the content as necessary and assumes full responsibility for the final version of the published article.

TABLE OF CONTENTS

Abstract ..... **i**

Acknowledgements ..... **iii**

Declaration of Generative AI and AI-assisted Technologies in the Writing Process. ..... **iv**

List of Tables ..... **ix**

List of Figures ..... **xi**

Chapter 1. Introduction **1**

1.1. Background 1

1.2. What's the gap in knowledge? 5

1.2.1. Grid Side： Technical Challenges and Development Trends in Regional Grid Management 6

1.2.2. EV-Side: Potential of Idle Resources and Behavioural Uncertainty 8

1.2.3. The Need for Standardized Benefit Evaluation Models 9

1.2.4. Key Research Gaps 10

1.3. Current Practice and Research Landscape 11

1.3.1. Core Architecture of V2G Networks 11

1.3.2. Parking-Lot Based Centralized V2G Integration System 15

1.3.3. Control Design for Power Transfer Chain and Data Interaction Chain in V2G Systems 18

1.3.4. V2G Bidirectional Power Rating Design 23

1.3.5. V2G Management Strategy and Control Logic 29

1.4. Deliverable 33

Phase 1: Systematic Literature Review 33

Phase 2: Multi-source Data Modelling and Analysis 33

Phase 3: Optimization Scheme Design 34

Phase 4: Multi-dimensional Benefit Assessment 34

1.5. Objective & Research Methods 35

1.6. Scope of Research, Limitation and Boundaries 38

1.7. Thesis Structure 40

Chapter 2. Literature Review **41**

2.1. Introduction 41

2.2. Literature Analysis methodology 45

2.3. Research Landscape Overview 49
2.3.1. Chronological Development and Paradigm Shifts 49
2.3.2. Geographic Variation and Standardization Barriers 52
2.3.3. Implications for This Study 55
2.4. Community Grid Systems and Real-World Deployments 56
2.4.1. Community-Level Grid Case Studies and Performance 57
2.4.2. Grid-Side V2G Challenges at the Community Level 59
2.5. Bidirectional Charging Interaction in V2G system 65
2.5.1. Foundational Studies in Bidirectional Charging Technologies 65
2.5.2. Data and Coordination Challenges 68
2.6. EV-Side Issues: EV Usage Patterns 71
2.7. V2G Management Strategy 76
2.8. Economic and Policy Considerations 79
2.9. Conclusion 84
Chapter 3. Data Resources and Analysis 88
3.1. Introduction 88
3.2. Data Features 89
3.2.1. Residential Power Load Characteristics 89
3.2.2. Collective Electric Vehicle Usage Characteristics 96
3.2.3. Collective Charging Behaviour Characteristics of Electric Vehicles 98
3.3. Simulation of Collective EV Usage Indicators 102
3.3.1. EV Ownership Rate 102
3.3.2. EV Idling Rate 104
3.3.3. Charging intensity 108
3.3.4. Charging Power Variations 110
3.4. Conclusion 114
Chapter 4. Methodology 116
4.1. Introduction 116
4.2. Research Framework Design 117
4.2.1. Proposed Solution 117
4.2.2. Three-Stage Research Methodology for Centralized V2G System Optimization 121
4.2.3. Who Is It Designed For? 123
4.3. Evaluation Modelling of Components 124
4.3.1. Estimating State-of-Charge Dynamics 126

4.3.2. Modelling Collective EV Behaviour in the Community 128
4.3.3. Simulation-Based Evaluation of Grid Load Dynamics and V2G Optimization Feasibility 130
4.4. Algorithm Design 135
4.4.1. EV Research Database for Usage Patterns on Targeted research day 138
4.4.2. V2G Optimization Management Strategies for Three Designed Scenarios 140
4.4.3. Basic Charging and Discharging Requirements and Logic 147
4.5. Evaluation Principles and Metrics 152
4.6. Simulation Framework of the Main Control Code 155
4.7. Simulation Steps Using the Established Optimization Platform 157
4.8. Conclusion 165
Chapter 5. Simulation Results 166
5.1. Introduction 166
5.2. Result Analysis 167
5.2.1. Scenario I 169
5.2.2. Scenario II 221
5.2.3. Scenario III 229
5.3. Conclusion 236
Chapter 6. Economic and Environmental Evaluation 240
6.1. Introduction 240
6.2.1 Electricity Bill Data Analysis 241
6.2.2. Simulation of Community Grid Electricity Costs under Different V2G Optimization Scenarios 246
6.3. Impacts on Energy Efficiency & Carbon Reduction 266
6.3.1 Carbon Intensity Data Analysis 266
6.3.2. Carbon Intensity Simulation Results for Different V2G Optimization Scenarios 269
6.4. Conclusion 278
Chapter 7. Discussion and Conclusions 281
7.1. Introduction 281
7.2. Summary of Findings 282
7.3. Contributions of Research 285
7.3.1. Development of a Representative Community-Scale Grid Model 286
7.3.2. Identification and Quantification of Collective EV Behavioural Variables 287
7.3.3. Design and Evaluation of a Centralized V2G Management Strategy 288
7.3.4. Policy Implications and Practical Significance 289

7.4. Research Limitation 290
7.5. Potential Work Directions 293
7.6. Conclusion 296
Reference 299
Appendix I: Data Processing 318
Appendix II: Main Logic 329
Appendix III: Data Appendix—2020 Time-of-Use Electricity Tariff Data Provided by LimeJump 344

LIST OF TABLES

Table 1-1. Rated Bidirectional Charging/Discharging Power and Battery Capacities of Mainstream EV Models in the UK Market.....25

Table 1-2. Technical Specifications of CHAdeMO-Compatible V2G Charging Products Available in the UK 27

Table 1-3. Assumption Parameters of Different Battery Situation (Zhao & Baker, 2022). 29

Table 1-4. Structured Framework of the Research Process and Corresponding Outputs. 35

Table 1-5. Mapping of Thesis Units to Objectives, Outputs, and Research Methods 38

Table 2-1. Estimated Revenue Generation Potential for EV Aggregators in STOR, FFR, and EFR Markets (Adapted from Strickland et al., 2019).....50

Table 2-2. Comparative Summary of Key EV Conductive Charging System Standards across Different Regions. 53

Table 2-3. Summary of Global Interface-Level Standards for EV Charging Systems (Part 1): Regional Application, Charging Type, Interface Design, and Communication Protocols.....53

Table 2-4. Summary of Global Interface-Level Standards for EV Charging Systems (Part 2): Electrical Specifications and Technical Features.....54

Table 2-5. Summary of Communication-Layer Standards for EV Charging Systems Worldwide.....55

Table 2-6. Economic Performance Metrics in V2G Studies: Annual Revenue, Battery Degradation Cost, and NPV from 5 Representative Papers.....74

Table 3-1. Peak and valley values of per-unit EV charging load, residential electricity consumption, and PV generation profiles for November. The table highlights the temporal alignment and magnitude of load peaks and valleys, illustrating the combined impact on distribution network demand. 101

Table 3-2. Preliminary estimation of grid stress under varying EV ownership and idling rate combinations, and the corresponding number of idle EVs theoretically required to offset extreme imbalances.....107

Table 3-3. Impact of varying EV charging and discharging power configurations on grid load balancing performance and corresponding V2G participation requirements. The table presents

deviations from ideal load balance and estimates the number of EVs needed to offset power imbalances under different power scenarios, based on November standard day data. 113

Table 4-1. The challenges and the proposed solutions 120

Table 4-2. Simulation Parameters and Variable Configurations in Scenario I–III 164

Table III-1 TIME-OF-USE Electricity Tariff Data (00:00–05:30), 2020, Provided by LimeJump — Part 1 344

Table III-2 TIME-OF-USE Electricity Tariff Data (06:00–11:30), 2020, Provided by LimeJump — Part 2 356

Table III-3 TIME-OF-USE Electricity Tariff Data (12:00–17:30), 2020, Provided by LimeJump — Part 3 369

Table III-4 TIME-OF-USE Electricity Tariff Data (18:00–23:30), 2020, Provided by Limejump — Part 4 381

LIST OF FIGURES

Figure 1-1. Historical and Projected UK Greenhouse Gas Emissions (1990–2100) with Policy-Based Forecast Scenarios. (Source: Huppmann et al., 2018).....1

Figure 1-2. Annual renewable electricity generation in the UK from 2000 to 2020 (Source: IEA (2022), World Energy Statistics and Balances (database), www.iea.org/data-and-statistics). Data expressed in TWh. Light blue: wind power; dark blue: other renewables; green: solar PV. Source: IEA (2022), adapted by author. 3

Figure 1-3. Market Share of EVs in New Car Registrations in the UK, 2018–April 2025 (data compiled from Finder, Zapmap/Uswitch, SMMT via The Guardian and S&P Global, and European Alternative Fuels Observatory; April 2025 data refer to battery electric vehicles [BEVs] only). 3

Figure 1-4. Hierarchical Architecture of Power Grid Management and Data Transmission for Electric Vehicle Charging Services. (Salam et.al., 2024) 7

Figure 1-5. Network Structure of Simple Microgrid (Ouammi, 2021).....12

Figure 1-6. Grid frequency and aggregated power response during a V2G contingency event. (Sturmberg et al., 2024) 17

Figure 1-7. Power Transmission and AC/DC Conversion Structure in a Simplified V2G System (Habib & Kamran, 2014) 21

Figure 1-8. Partial Control Logic for EV Charging and Discharging in V2G Systems (Adapted from Mendes et al., 2016) 30

Figure 2-1. Overview of V2G System Functionality and Key Research Domains. (Ru et.al., 2025) 42

Figure 2-2. Keyword Co-Occurrence Network Derived from V2G Publications (VOSviewer Analysis). (Ru et.al., 2025) 48

Figure 2-3. Schematic Representation of Community-Level V2G Integration and Associated Grid-Side Constraints (Saeed, 2022) 60

Figure 2-4. Typical distributed control architecture of multiple microgrids operating within a shared distribution network. (Saha et.al., 2023) 62

Figure 2-5. Typical power conversion architectures of onboard EV chargers used in V2G systems. (Venkata & Williamson, 2020).....66

Figure 2-6. Centralized V2G Communication Structure Illustrating Interoperability and Data Flow Challenges (Inala, Bose, & Kumar, 2019).....70

Figure 2-7. Battery capacity degradation as a function of depth of discharge (DoD) and state of charge (SoC) cycling profiles in V2G applications. (Kolawole & Al-Anbagi, 2019).....82

Figure 3-1. 500 Households Consumption Powers of 24-hour Time Slot in Specific Duration. 92

Figure 3-2. Average hourly PV generation profiles of the monitored community (29 households) for June and November.....93

Figure 3-3. Daily power profiles of residential electricity demand, PV generation, and resulting net grid load for a 500-household residential community in the United Kingdom. Profiles reflect average values for typical weekdays in summer (June) and winter (November), highlighting diurnal and seasonal variations as well as the impact of PV integration on net load characteristics.....95

Figure 3-4. Typical 24-hour SOC profiles for three representative electric vehicle usage patterns: daytime distributed charging, nighttime concentrated charging, and extended idle periods. Profiles are based on aggregated simulation data reflecting behavioural diversity within the EV fleet. 98

Figure 3-5. Normalized diurnal charging load profile of the electric vehicle fleet. The yellow shaded area denotes the peak PV generation period, highlighting the temporal mismatch between EV charging demand and solar power output.....101

Figure 3-6 (i). Weekday-averaged hourly net grid power profiles for a 500-household UK residential community under varying EV ownership scenarios (25%, 50%, 75%, and 100%) in June. 103

Figure 3-6 (ii). Weekday-averaged hourly net grid power profiles for a 500-household UK residential community under varying EV ownership scenarios (25%, 50%, 75%, and 100%) in November. 104

Figure 3-7. Hourly EV charging power distribution for three representative weeks characterized by high, medium, and low charging frequencies. The curves illustrate how

increased charging intensity shifts the temporal charging pattern and intensifies early-morning demand peaks. 109

Figure 3-8. Hourly net power load profiles under varying EV charging intensities (high, medium, low) for standard weekdays (left column) and weekends (right column) in November. 110

Figure 3-9. Time-of-day distribution of EV charging demand under different charging power levels (3.3 kW, 7 kW, and 10 kW). The figure illustrates increasing temporal concentration of charging activity as power rates rise, with demand clustering around peak residential load periods. 112

Figure 3-10. Time-of-day power load profiles for a community grid under EV charging power levels of 3.3 kW, 7 kW, and 10 kW on standard weekdays in November. The figure highlights the nonlinear increase in peak grid load with higher charging rates and the growing overlap between EV charging demand and residential peak consumption periods. 113

Figure 4-1. Conceptual Framework Illustrating the Influence of Four Key EV Behavioural Parameters on Community-Level Grid Load Dynamics 126

Figure 4-2. Workflow of the proposed centralized V2G optimization scheduling algorithm 137

Figure 5-1. Hourly net-load profiles before and after Scenario I optimization on 21st June with full-standard PV capacity (4 kWp) and default EV parameters. The baseline load profile incorporates both the hourly residential electricity demand and PV generation, while the power-balancing threshold curve represents the calculated extreme-balance parameter. Simulation parameters: bidirectional charging/discharging power = 3.3 kW; EV ownership rate = 1.0; idle rate = 0.5; average hourly charging demand = 0.20455 kWh. 173

Figure 5-2. SOC distribution of dispatched EVs before and after Scenario I optimization under full-standard PV capacity conditions. 174

Figure 5-3. Hourly participation of active and idle EVs in charging and discharging, based on Scenario I optimization. 174

Figure 5-4. Hourly net-load profiles before and after Scenario I optimization on 11th December with full-standard PV capacity (4 kWp) and default EV parameters. Simulation parameters: bidirectional charging/discharging power = 3.3 kW; EV ownership rate = 1.0; idle rate = 0.5; average hourly charging demand = 0.20455 kWh. 175

Figure 5-5. SOC distribution of dispatched EVs before and after Scenario I optimization under full-standard PV capacity conditions on 11th December. 176

Figure 5-6. Hourly participation of active and idle EVs in charging and discharging, based on Scenario I optimization on 11th December. 176

Figure 5-7. Time-of-day power load profiles for the community grid on 21st June under half-capacity PV generation (2 kWp) before and after optimization, showing the baseline load profile (residential demand + PV generation) and the optimized load-balancing reference curve. Simulation parameters: bidirectional charging/discharging power = 3.3 kW; EV ownership rate = 1.0; idle rate = 0.5; average hourly charging demand = 0.20455 kWh..... 178

Figure 5-8. SOC distributions for all EVs participating in V2G scheduling on 21st June under half-capacity PV generation (2 kWp), comparing the start of the day (00:00) and the end of the optimization process (23:00). 179

Figure 5-9. Hourly participation of EVs in V2G scheduling on 21st June under half-capacity PV generation (2 kWp), detailing the number of active EVs charging or discharging and idle EVs charging or discharging at each time step. 179

Figure 5-10. Time-of-day power load profiles for the community grid on 11th December under half-capacity PV generation (2 kWp) before and after optimization, showing the baseline load profile (residential demand + PV generation) and the optimized load-balancing reference curve. Simulation parameters: bidirectional charging/discharging power = 3.3 kW; EV ownership rate = 1.0; idle rate = 0.5; average hourly charging demand = 0.20455 kWh. 180

Figure 5-11. SOC distributions for all EVs participating in V2G scheduling on 11th December under half-capacity PV generation (2 kWp), comparing the start of the day (00:00) and the end of the optimization process (23:00). 181

Figure 5-12. Hourly participation of EVs in V2G scheduling on 11th December under half-capacity PV generation (2 kWp), detailing the number of active EVs charging or discharging and idle EVs charging or discharging at each time step. 181

Figure 5-13. Hourly net-load profiles before and after Scenario I optimization on 21st June without PV generation (0 kWp), along with baseline load (residential demand) and power-balancing threshold curves. Simulation parameters: bidirectional charging/discharging power = 3.3 kW; EV ownership rate = 1.0; idle rate = 0.5; average hourly charging demand = 0.20455 kWh. 182

Figure 5-14. SOC distribution of dispatched EVs before and after Scenario I optimization on 21st June without PV generation (0 kWp). 183

Figure 5-15. Hourly participation of active and idle EVs in charging and discharging, based on Scenario I optimization on 21st June. 183

Figure 5-16. Hourly net-load profiles before and after Scenario I optimization on 11th December without PV generation (0 kWp), along with baseline load (residential demand) and power-balancing threshold curves. Simulation parameters: bidirectional charging/discharging power = 3.3 kW; EV ownership rate = 1.0; idle rate = 0.5; average hourly charging demand = 0.20455 kWh. 185

Figure 5-17. SOC distribution of dispatched EVs before and after Scenario I optimization on 11th December without PV generation (0 kWp). 185

Figure 5-18. Hourly participation of active and idle EVs in charging and discharging, based on Scenario I optimization on 11th December. 185

Figure 5-19. Hourly net-load profiles before and after Scenario I optimization on 21st June with full-standard PV capacity (4 kWp) and default EV parameters. Simulation parameters: bidirectional charging/discharging power = 3.3 kW; EV ownership rate = 0.25; idle rate = 0.5487; average hourly charging demand = 0.20455 kWh. 189

Figure 5-20. SOC distribution of dispatched EVs before and after Scenario I optimization on 21st June with full-standard PV capacity (4 kWp) and default EV parameters (EV ownership rate = 0.25). 189

Figure 5-21. Hourly participation of active and idle EVs in charging and discharging, based on Scenario I optimization on 21st June with full-standard PV capacity (4 kWp) and default EV parameters (EV ownership rate = 0.25). 190

Figure 5-22. Hourly net-load profiles before and after Scenario I optimization on 21st June with full-standard PV capacity (4 kWp) and default EV parameters. Simulation parameters: bidirectional charging/discharging power = 3.3 kW; EV ownership rate = 0.50; idle rate = 0.5487; average hourly charging demand = 0.20455 kWh. 191

Figure 5-23. SOC distribution of dispatched EVs before and after Scenario I optimization on 21st June with full-standard PV capacity (4 kWp) and default EV parameters (EV ownership rate = 0.50). 192

Figure 5-24. Hourly participation of active and idle EVs in charging and discharging, based on Scenario I optimization on 21st June with full-standard PV capacity (4 kWp) and default EV parameters (EV ownership rate = 0.50). 192

Figure 5-25. Hourly net-load profiles before and after Scenario I optimization on 21st June with full-standard PV capacity (4 kWp) and default EV parameters. Simulation parameters: bidirectional charging/discharging power = 3.3 kW; EV ownership rate = 0.75; idle rate = 0.5487; average hourly charging demand = 0.20455 kWh. 194

Figure 5-26. SOC distribution of dispatched EVs before and after Scenario I optimization on 21st June with full-standard PV capacity (4 kWp) and default EV parameters (EV ownership rate = 0.75). 194

Figure 5-27. Hourly participation of active and idle EVs in charging and discharging, based on Scenario I optimization on 21st June with full-standard PV capacity (4 kWp) and default EV parameters (EV ownership rate = 0.75). 195

Figure 5-28. Hourly net-load profiles before and after Scenario I optimization on 21st June with full-standard PV capacity (4 kWp) and default EV parameters. Simulation parameters: bidirectional charging/discharging power = 3.3 kW; EV ownership rate = 1; idle rate = 0; average hourly charging demand = 0.20455 kWh. 198

Figure 5-29. Hourly participation of active and idle EVs in charging and discharging, based on Scenario I optimization on 21st June with full-standard PV capacity (4 kWp) and default EV parameters (EV ownership rate = 1; idle rate = 0)..... 199

Figure 5-30. Hourly net-load profiles before and after Scenario I optimization on 21st June with full-standard PV capacity (4 kWp) and default EV parameters. Simulation parameters: bidirectional charging/discharging power = 3.3 kW; EV ownership rate = 1; idle rate = 0.25; average hourly charging demand = 0.20455 kWh. 200

Figure 5-31. SOC distribution of dispatched EVs before and after Scenario I optimization on 21st June with full-standard PV capacity (4 kWp) and default EV parameters (EV ownership rate = 1; idle rate = 0.25)..... 201

Figure 5-32. Hourly participation of active and idle EVs in charging and discharging, based on Scenario I optimization on 21st June with full-standard PV capacity (4 kWp) and default EV parameters (EV ownership rate = 1; idle rate = 0.25)..... 201

Figure 5-33. Hourly net-load profiles before and after Scenario I optimization on 21st June with full-standard PV capacity (4 kWp) and default EV parameters. Simulation parameters: bidirectional charging/discharging power = 3.3 kW; EV ownership rate = 1; idle rate = 0.75; average hourly charging demand = 0.20455 kWh. 204

Figure 5-34. SOC distribution of dispatched EVs before and after Scenario I optimization on 21st June with full-standard PV capacity (4 kWp) and default EV parameters (EV ownership rate = 1; idle rate = 0.75)..... 204

Figure 5-35. Hourly participation of active and idle EVs in charging and discharging, based on Scenario I optimization on 21st June with full-standard PV capacity (4 kWp) and default EV parameters (EV ownership rate = 1; idle rate = 0.75)..... 205

Figure 5-36. Hourly net-load profiles before and after Scenario I optimization on 21st June with full-standard PV capacity (4 kWp) and default EV parameters. Simulation parameters: bidirectional charging/discharging power = 3.3 kW; EV ownership rate = 0.9; idle rate = 0.6; average hourly charging demand = 0.20455 kWh. 207

Figure 5-37. SOC distribution of dispatched EVs before and after Scenario I optimization on 21st June with full-standard PV capacity (4 kWp) and default EV parameters (EV ownership rate = 0.9; idle rate = 0.6)..... 207

Figure 5-38. Hourly participation of active and idle EVs in charging and discharging, based on Scenario I optimization on 21st June with full-standard PV capacity (4 kWp) and default EV parameters (EV ownership rate = 0.9; idle rate = 0.6)..... 208

Figure 5-39. Hourly net-load profiles before and after Scenario I optimization on 21st June with full-standard PV capacity (4 kWp) and default EV parameters. Simulation parameters: bidirectional charging/discharging power = 3.3 kW; EV ownership rate = 1; idle rate = 0.5487; average hourly charging demand = 0.394958 kWh. 210

Figure 5-40. Hourly net-load profiles before and after Scenario I optimization on 21st June with full-standard PV capacity (4 kWp) and default EV parameters. Simulation parameters: bidirectional charging/discharging power = 3.3 kW; EV ownership rate = 1; idle rate = 0.5487; average hourly charging demand = 0.192591 kWh. 211

Figure 5-41. Hourly net-load profiles before and after Scenario I optimization on 21st June with full-standard PV capacity (4 kWp) and default EV parameters. Simulation parameters: bidirectional charging/discharging power = 3.3 kW; EV ownership rate = 1; idle rate = 0.5487; average hourly charging demand = 0.092093 kWh. 211

Figure 5-42. Hourly net-load profiles before and after Scenario I optimization on 21st June with full-standard PV capacity (4 kWp) and default EV parameters. Simulation parameters: charging power = 10 kW; discharging power = 3.3 kW; EV ownership rate = 1; idle rate = 0.55; average hourly charging demand = 0.20455 kWh. 216

Figure 5-43. Hourly participation of active and idle EVs in charging and discharging, based on Scenario I optimization on 21st June with full-standard PV capacity (4 kWp) and default EV parameters (EV ownership rate = 1; idle rate = 0.55).....216

Figure 5-44. Hourly net-load profiles before and after Scenario I optimization on 21st June with full-standard PV capacity (4 kWp) and default EV parameters. Simulation parameters: charging power = 10 kW; discharging power = 7 kW; EV ownership rate = 1; idle rate = 0.55; average hourly charging demand = 0.20455 kWh. 218

Figure 5-45. Hourly participation of active and idle EVs in charging and discharging, based on Scenario I optimization on 21st June with full-standard PV capacity (4 kWp) and default EV parameters (EV ownership rate = 1; idle rate = 0.55).....218

Figure 5-46. Hourly net-load profiles before and after Scenario I optimization on 21st June with full-standard PV capacity (4 kWp) and default EV parameters. Simulation parameters: battery capacity = 82.5 kWh; charging power = 10 kW; discharging power = 7 kW; EV ownership rate = 1; idle rate = 0.15; average hourly charging demand = 0.20455 kWh.....220

Figure 5-47. Hourly participation of active and idle EVs in charging and discharging, based on Scenario I optimization on 21st June with full-standard PV capacity (4 kWp) and default EV parameters (EV ownership rate = 1; idle rate = 0.15).....221

Figure 5-48. Hourly net-load profiles before and after Scenario II optimization on 21st June with full-standard PV capacity (4 kWp) and default EV parameters. Simulation parameters: battery capacity = 24 kWh; charging power = 3.3 kW; discharging power = 3.3 kW; EV ownership rate = 1; idle rate = 0.55; average hourly charging demand = 0.20455 kWh.....225

Figure 5-49. SOC distribution of dispatched EVs before and after Scenario II optimization on 21st June with full-standard PV capacity (4 kWp) and default EV parameters (EV ownership rate = 1; idle rate = 0.55).....225

Figure 5-50. Hourly participation of active and idle EVs in charging and discharging, based on Scenario II optimization on 21st June with full-standard PV capacity (4 kWp) and default EV parameters (EV ownership rate = 1; idle rate = 0.55).....226

Figure 5-51. Hourly net-load profiles before and after Scenario II optimization on 21st June with full-standard PV capacity (4 kWp) and default EV parameters. Simulation parameters: battery capacity = 82.5 kWh; charging power = 10 kW; discharging power = 7 kW; EV ownership rate = 1; idle rate = 0.15; average hourly charging demand = 0.20455 kWh.....227

Figure 5-52. SOC distribution of dispatched EVs before and after Scenario II optimization on 21st June with full-standard PV capacity (4 kWp) and default EV parameters (EV ownership rate = 1; idle rate = 0.15).....228

Figure 5-53. Hourly participation of active and idle EVs in charging and discharging, based on Scenario II optimization on 21st June with full-standard PV capacity (4 kWp) and default EV parameters (EV ownership rate = 1; idle rate = 0.15).....228

Figure 5-54. Hourly net-load profiles before and after Scenario III optimization on 21st June with full-standard PV capacity (4 kWp) and default EV parameters. Simulation parameters: battery capacity = 24 kWh; charging power = 3.3 kW; discharging power = 3.3 kW; EV ownership rate = 0.35.....231

Figure 5-55. SOC distribution of dispatched EVs before and after Scenario III optimization on 21st June with full-standard PV capacity (4 kWp) and default EV parameters (EV ownership rate = 0.35). 232

Figure 5-56. Hourly participation of active and idle EVs in charging and discharging, based on Scenario III optimization on 21st June with full-standard PV capacity (4 kWp) and default EV parameters (EV ownership rate = 0.35).....232

Figure 5-57. Hourly net-load profiles before and after Scenario III optimization on 21st June with full-standard PV capacity (4 kWp) and default EV parameters. Simulation parameters: battery capacity = 82.5 kWh; charging power = 10 kW; discharging power = 10 kW; EV ownership rate = 0.11.....234

Figure 5-58. SOC distribution of dispatched EVs before and after Scenario III optimization on 21st June with full-standard PV capacity (4 kWp) and default EV parameters (EV ownership rate = 0.11). 235

Figure 5-59. Hourly participation of active and idle EVs in charging and discharging, based on Scenario III optimization on 21st June with full-standard PV capacity (4 kWp) and default EV parameters (EV ownership rate = 0.11).....235

Figure 6-1. Half-Hourly Real-Time Electricity Prices in June 2020 Provided by LimeJump Energy 243

Figure 6-2. The system price of the electricity grid on 21st June, 2020, as provided by LimeJump. 244

Figure 6-3. The system price of the electricity grid on 21st December, 2020, as provided by LimeJump. 245

Figure 6-4. Half-hourly electricity prices under the RTP scheme during the vernal equinox week (17–23 March 2020), based on data from LimeJump. 245

Figure 6-5. Half-hourly RTP electricity prices during the autumnal equinox week (19–25 September 2020), based on data provided by LimeJump. 246

Figure 6-6. Half-hourly distribution of electricity costs on 21st June under Scenario I with full PV installation capacity (4 kWp). All other parameters remain consistent with the baseline configuration (battery capacity = 24 kWh; charging/discharging power = 3.3 kW; EV ownership = 100%; idle rate = 0.5487; average hourly charging demand = 0.20455 kWh). 251

Figure 6-7. Half-hourly electricity cost distribution on 21st June under Scenario I optimization with PV installed capacity of 2 kWp (all other parameters identical to those in Figure 6-6). 251

Figure 6-8. Half-hourly electricity cost distribution on 21st June under Scenario I optimization without PV generation (all other parameters identical to those in Figure 6-6).252

Figure 6-9. Half-hourly electricity cost distribution on 11th December under Scenario I optimization with full PV capacity (all other parameters identical to those in Figure 6-6)...253

Figure 6-10. Half-hourly electricity cost distribution on 11th December under Scenario I optimization with half PV capacity (all other parameters identical to those in Figure 6-6)..253

Figure 6-11. Half-hourly electricity cost distribution on 11th December under Scenario I optimization with no PV capacity (all other parameters identical to those in Figure 6-6). ...254

Figure 6-12. Half-hourly distribution of electricity costs on 21st June under Scenario I with increased EV charging intensity (average hourly charging demand = 0.394958 kWh). All other parameters remain consistent with the baseline configuration. 256

Figure 6-13. Half-hourly distribution of electricity costs on 21st June under Scenario III with increased EV charging intensity (EV ownership = 35%; idle rate = 100%). All other parameters remain consistent with the baseline configuration. 259

Figure 6-14. Half-hourly distribution of electricity costs on 11th December under Scenario III with increased EV charging intensity (EV ownership = 35%; idle rate = 100%). All other parameters remain consistent with the baseline configuration. 259

Figure 6-15. Half-hourly distribution of electricity costs on 21st June under Scenario I with full PV installation capacity (4 kWp). All other parameters remain consistent with the baseline configuration (battery capacity = 82.5 kWh; charging power = 10 kW; discharging power = 7 kW; EV ownership = 100%; idle rate = 15%; average hourly charging demand = 0.20455 kWh). 261

Figure 6-16. Half-hourly distribution of electricity costs on 11th December under Scenario I with full PV installation capacity (4 kWp). All other parameters remain consistent with the baseline configuration. 262

Figure 6-17. Real-time carbon intensity of Great Britain's electricity system on the summer solstice, sourced from the Carbon Intensity API project. 268

Figure 6-18. Real-time carbon intensity of Great Britain's electricity system on the winter solstice, sourced from the Carbon Intensity API project. 268

Figure 6-19. Half-hourly carbon intensity of Great Britain's electricity system during the week of the vernal equinox (17th–23th March 2020), sourced from the Carbon Intensity API project. 268

Figure 6-20. Half-hourly carbon intensity of Great Britain's electricity system during the week of the autumnal equinox (19th–25th September 2020), sourced from the Carbon Intensity API project. 269

Figure 6-21. Half-hourly distribution of carbon emissions on 21st June under Scenario I with no PV installation capacity (0 kWp). All other parameters remain consistent with the baseline configuration (battery capacity = 24 kWh; charging power = 3 kW; discharging power = 3 kW; EV ownership = 100%; idle rate = 55%; average hourly charging demand = 0.20455 kWh). The total daily carbon emissions of the community grid amounted to 1948173.32 kg before optimization, and were reduced to 1923363.92 kg after optimized V2G scheduling.271

Figure 6-22. Half-hourly distribution of carbon emissions on 11th December under Scenario I with no PV installation capacity (0 kWp). The total daily carbon emissions of the community grid were 1716244.18 kg before optimization and decreased to 1657784.68 kg after optimized V2G scheduling. 271

Figure 6-23. Half-hourly distribution of carbon emissions on 21st June under Scenario I & Scenario II with full PV installation capacity (4 kWp). All other parameters remain consistent with the baseline configuration (battery capacity = 24 kWh; charging power = 3 kW; discharging power = 3 kW; EV ownership = 100%; idle rate = 55%; average hourly charging demand = 0.20455 kWh). The total daily carbon emissions of the community grid were 1000715.55 kg before optimization and decreased to –2053303.18 kg after optimized V2G scheduling. 273

Figure 6-24. Half-hourly distribution of carbon emissions on 11th December under Scenario I & Scenario II with full PV installation capacity (4 kWp). The total daily carbon emissions of the community grid were 1331128.40 kg before optimization and decreased to 1259556.52 kg after optimized V2G scheduling. 273

Figure 6-25. Half-hourly distribution of carbon emissions on 21st June under Scenario III with full PV installation capacity (4 kWp; EV ownership = 35%). The total daily carbon emissions of the community grid were 745226.07 kg before optimization and decreased to -2615966.51 kg after optimized V2G scheduling. 275

Figure 6-26. Half-hourly distribution of carbon emissions on 11th December under Scenario III with full PV installation capacity (4 kWp). The total daily carbon emissions of the community grid were 906659.91 kg before optimization and decreased to 779025.97 kg after optimized V2G scheduling. 275

Figure 6-27. Half-hourly distribution of carbon emissions on 21st June under Scenario I & Scenario II with full PV installation capacity (4 kWp). All other parameters remain consistent with the baseline configuration (battery capacity = 82.5 kWh; charging power = 10 kW; discharging power = 7 kW; EV ownership = 100%; idle rate = 15%; average hourly charging demand = 0.20455 kWh). The total daily carbon emissions of the community grid were 1256354.29 kg before optimization and decreased to -1510252.62 kg after optimized V2G scheduling. 277

Figure 6-28. Half-hourly distribution of carbon emissions on 11th December under Scenario I & Scenario II with full PV installation capacity (4 kWp). The total daily carbon emissions of the community grid were 1739441.73 kg before optimization and decreased to 1714790.80 kg after optimized V2G scheduling. 278

CHAPTER 1. INTRODUCTION

1.1. Background

In response to the global climate crisis, countries around the world have committed to reducing carbon emissions, as outlined in international agreements such as the 2015 Paris Agreement (Geske & Schumann, 2018; Noel et al., 2018). In line with this global effort, the UK government has established a legally binding "net-zero" target, aiming to achieve substantial greenhouse gas reductions by 2050 through a combination of technological transition and policy intervention (Geske & Schumann, 2018; Habib et al., 2020). As illustrated in Figure 1-1, which presents historical and projected greenhouse gas emissions in the UK from 1990 to 2100, national emissions are expected to decline sharply after the mid-2020s, reflecting the country's strong policy commitment to decarbonisation.

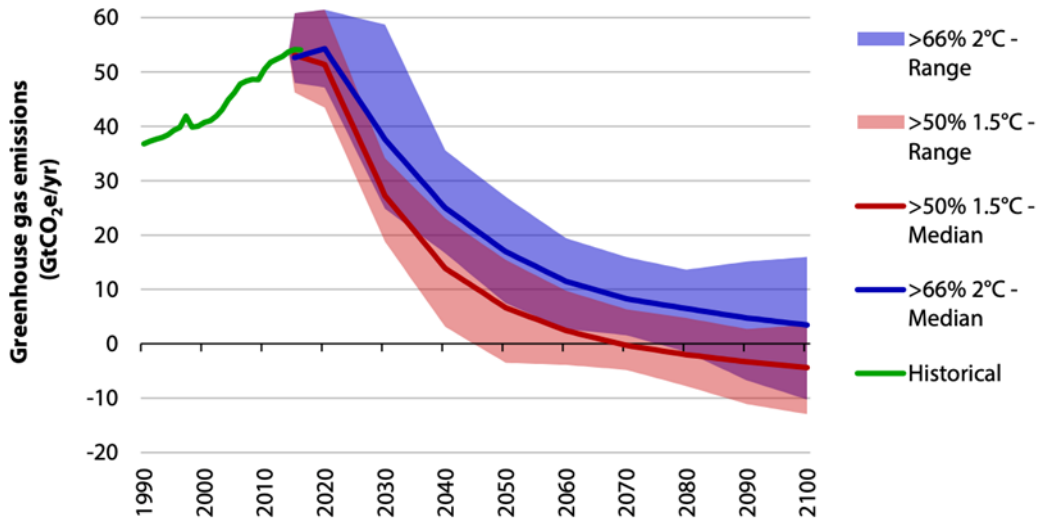


Figure 1-1. Historical and Projected UK Greenhouse Gas Emissions (1990–2100) with Policy-Based Forecast Scenarios. (Source: Huppmann et al., 2018)

Within the broader economy, energy consumption varies significantly across sectors. In the UK, transport, buildings, and industry collectively account for the majority of final energy demand.

Among these sectors, road transport remains one of the largest contributors to national greenhouse gas emissions. According to the UK Department for Transport, transport accounted for approximately 26% of total UK greenhouse gas emissions in 2021, making it the single largest emitting sector of the economy (Department for Transport, 2022). As a result, decarbonising transport has become a central component of the UK's climate strategy.

At the same time, the electricity sector itself has undergone major structural changes as part of the national decarbonisation transition. Coal-fired generation has declined dramatically over the past decade and has now been effectively phased out, while electricity generation from low-carbon sources—particularly wind and solar—has increased substantially. By 2020, low-carbon sources accounted for nearly half of the UK's electricity generation mix (ECUK, 2021). Although this transformation has significantly reduced emissions from electricity production, the growing penetration of intermittent renewable energy introduces new operational challenges for electricity networks. The variability of wind and solar generation often leads to temporal mismatches between electricity supply and demand, placing increasing pressure on grid stability and system dispatch (Bansal et al., 2020; Sharma et al., 2020).

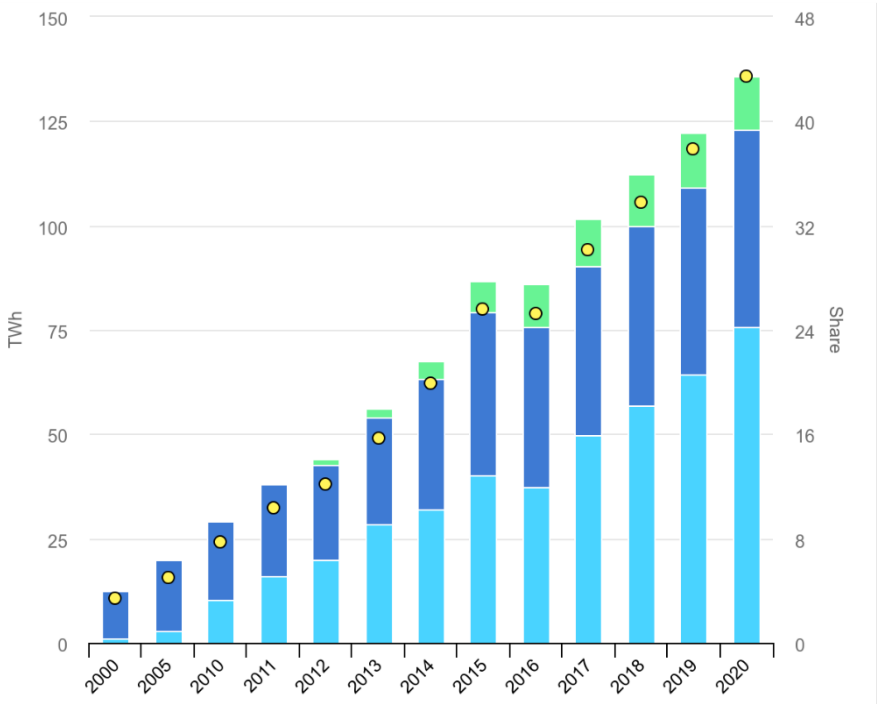


Figure 1-2. Annual renewable electricity generation in the UK from 2000 to 2020 (Source: IEA (2022), World Energy Statistics and Balances (database), www.iea.org/data-and-statistics). Data expressed in TWh. Light blue: wind power; dark blue: other renewables; green: solar PV. Source: IEA (2022), adapted by author.

In parallel with the decarbonisation of electricity supply, the electrification of road transport has emerged as a key policy priority. Electric vehicles (EVs) are widely regarded as one of the most effective pathways for reducing emissions from the transport sector (Noel et al., 2018). Over the past decade, the UK EV market has expanded rapidly. According to official statistics from the UK Department for Transport (2023), the number of battery electric vehicles (BEVs) registered in the UK exceeded 1 million vehicles in 2023, representing a dramatic increase from fewer than 50,000 vehicles in 2015. EV sales have also grown quickly, with battery electric vehicles accounting for approximately 16–17% of all new car registrations in 2023 (Society of Motor Manufacturers and Traders, 2024). This rapid market expansion reflects both technological improvements and strong policy support.

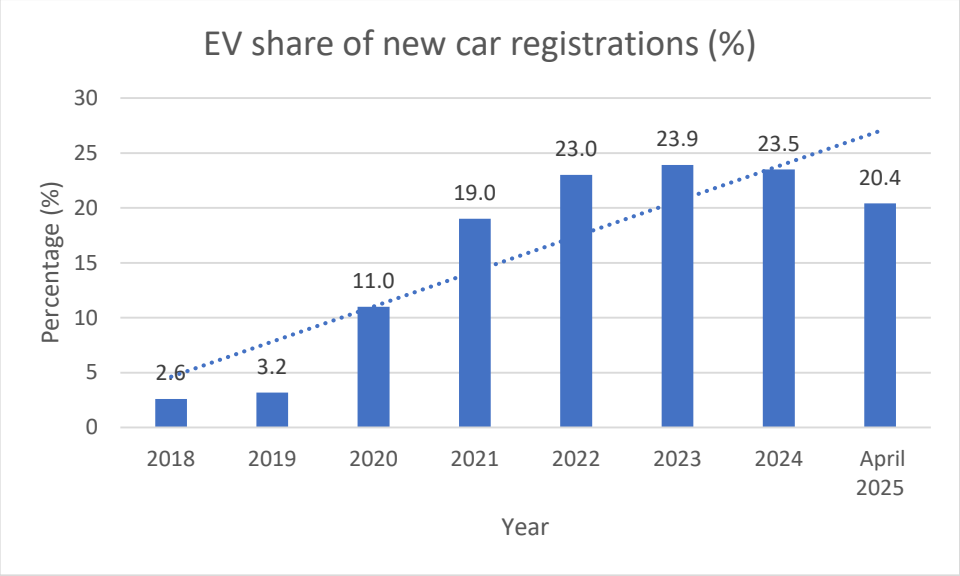


Figure 1-3. Market Share of EVs in New Car Registrations in the UK, 2018–April 2025 (data compiled from Finder, Zapmap/Uswitch, SMMT via The Guardian and S&P Global, and European Alternative Fuels Observatory; April 2025 data refer to battery electric vehicles [BEVs] only).

Several policy instruments have played an important role in accelerating EV adoption in the UK. Government initiatives such as the Plug-in Car Grant, tax incentives for zero-emission vehicles, and large-scale investments in public charging infrastructure have significantly reduced barriers to EV ownership. In addition, the UK government has announced a regulatory phase-out of new petrol and diesel vehicle sales by 2035, which further reinforces the long-term transition toward electric mobility (Department for Transport, 2022). At the same time, improvements in battery technology have contributed to a steady decline in EV costs. The global average cost of lithium-ion battery packs has fallen from more than $1,100 per kWh in 2010 to around $150 per kWh in 2023, substantially narrowing the price gap between electric vehicles and conventional internal combustion vehicles (BloombergNEF, 2023). These technological and policy developments suggest that EV adoption will continue to expand rapidly over the coming decades.

While the primary motivation for EV adoption lies in reducing transport-sector emissions, the large-scale deployment of EV fleets also introduces new opportunities for electricity system management. Unlike conventional energy storage technologies, EV batteries are distributed across large numbers of vehicles and remain parked for a significant proportion of the day. Studies indicate that private vehicles are typically parked for over 90% of their lifetime, implying that a considerable amount of battery capacity remains idle at any given time (Kempton & Tomic, 2005). If appropriately coordinated, this idle storage capacity could be utilised to support electricity grid operations.

This concept underpins the development of vehicle-to-grid (V2G) systems. V2G technology enables bidirectional electricity flows between EV batteries and the power grid through dedicated communication and control infrastructure (Escudero-Garzás et al., 2012; Hoang et al., 2017). Under such arrangements, EVs may charge during periods of low demand or high renewable generation and discharge electricity back to the grid when demand peaks. Although

the primary purpose of EV adoption is to decarbonise road transport, V2G integration represents a potential secondary benefit that could improve the flexibility and stability of future low-carbon electricity systems.

Consequently, the rapid expansion of EV ownership introduces both challenges and opportunities for electricity network management. Uncoordinated charging behaviour could increase peak electricity demand and place additional pressure on local distribution networks. However, with appropriate scheduling and coordination mechanisms, EV fleets may function as distributed energy storage resources capable of supporting load balancing and renewable energy integration. Developing effective strategies to manage these emerging interactions between EV fleets and electricity networks therefore represents an important research challenge in the transition toward integrated low-carbon energy systems.

1.2. What's the gap in knowledge?

As the EV market continues to expand and sustainable energy sources are increasingly integrated into power grids, transmission and distribution systems are facing growing operational pressures. Leveraging V2G frameworks to employ EVs as temporary energy storage assets offers a promising approach to mitigating these pressures, demonstrating clear feasibility from both the grid and EV perspectives. Grid operators can gain additional flexibility in balancing loads, while EV owners have the opportunity to participate in ancillary services without significantly disrupting their mobility requirements. Despite this evident potential, substantial knowledge gaps persist in achieving efficient scheduling of EVs within representative high-level, zero-carbon-oriented grid environments, where the objective is to balance power loads across the network while accounting for the dynamic interactions among supply variability, demand uncertainty, and distributed storage capabilities. Addressing these gaps necessitates a deeper understanding of the technical challenges associated with regional

grid management, the untapped potential of idle EV resources and the behavioural uncertainties of vehicle owners, as well as the development of standardized models for evaluating the economic and operational benefits of V2G integration. The following sections will examine how current research and industry practices fall short in addressing these challenges, highlighting the areas where further investigation is required.

1.2.1. Grid Side: Technical Challenges and Development Trends in Regional Grid Management

On the grid side, the large-scale integration of diversified renewable energy sources and the continuous increase in their output have led to a growing temporal mismatch between renewable energy generation peaks and electricity demand peaks. This asynchrony poses significant challenges to the bidirectional power transmission and dispatch capabilities of high-level grids, particularly at the national and urban backbone levels. To maintain the stability of V2G systems connected to the grid and to reduce the frequency of bidirectional energy interactions and battery cycling, early research predominantly focused on microgrid-based load optimization models. These models reduced overall system response frequency and mutual interference by integrating multiple microgrids in parallel with the main grid.

However, with the emergence of new V2G application scenarios—such as apartment community grids, commercial district grids, and high-speed railway station zones—the traditional microgrid architecture, which assumes fixed usage patterns of individual household electric vehicles, can no longer meet the increasingly complex power load distribution requirements.

More critically, the parallel operation of numerous single-household or small-scale microgrids within the main grid—often functioning independently without unified dispatch coordination—has increased uncertainty in power allocation and system-level optimization. At

the same time, the centralized processing of large volumes of interaction data generated by these distributed microgrids places substantial pressure on data communication, computational resources, and control infrastructure. To address these challenges, many countries and regions have begun implementing hierarchical and multi-layered grid management frameworks that organize grid monitoring and control across multiple administrative and operational levels, such as national, municipal, and community scales (Ma et al., 2019). Figure 1-4 illustrates the hierarchical architecture of the power grid from the perspective of EV charging services, highlighting not only the layered control structure but also the corresponding hierarchical data transmission mechanisms required to support such multi-level coordination. Within this framework, grid management responsibilities and information flows are distributed across different levels to improve scalability and operational efficiency. In particular, urban power systems are increasingly adopting zoned management strategies, in which community- or commercial district-level grids play a more active role in local energy coordination. This approach helps alleviate the growing pressure on city-level grid control centres in terms of both data processing and power distribution.

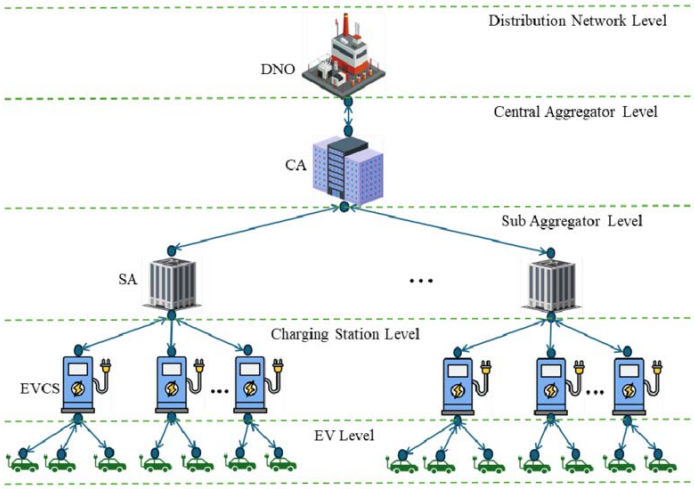


Figure 1-4. Hierarchical Architecture of Power Grid Management and Data Transmission for Electric Vehicle Charging Services. (Salam et.al., 2024)

Consequently, the V2G service model must evolve accordingly. Earlier V2G frameworks primarily focused on isolated or single-user electric vehicle participation within individual microgrids. However, as community-level energy management becomes more prominent, there is a growing need for more centralized and coordinated V2G scheduling mechanisms capable of accommodating the diverse charging and discharging behaviours of large EV populations within community-scale grids.

1.2.2. EV-Side: Potential of Idle Resources and Behavioural Uncertainty

On the EV side, most existing V2G control strategies (Huang & Wu, 2019; Mendes, et.al., 2016) are developed based on simplified assumptions of fixed usage scenarios—typically presuming that the participating EVs operate daily on consistent routes and schedules. However, these assumptions often diverge significantly from real-world usage patterns. In practice, EV usage behaviour is highly variable, and the overall utilization rate of private EVs remains relatively low.

According to statistical research by Habib and Kamran (2014), most EVs are idle for approximately 22 hours per day. Metz and Doetsch (2012) further estimate that, if EVs are enabled with bidirectional grid connectivity at both home and workplace locations, up to 81% of their operational life could be used to support local grid services.

A 2022 survey by the UK Department for Transport on EV user charging behaviour reported that only 41% of battery electric vehicle (BEV) owners and 33% of plug-in hybrid electric vehicle (PHEV) owners drive their vehicles daily. This implies that over 60% of EVs remain unused on a typical day. Combined with continued improvements in battery capacity and vehicle range, this infrequent usage pattern reduces the need for regular charging, thereby limiting both the total connection time and the frequency of EV interaction with the local grid.

The same report also indicates that only 18% of respondents adhere to a consistent daily home charging routine, while nearly 80% charge their vehicles on demand, typically one to three times per week at irregular intervals. This limited grid connection duration, coupled with highly variable user behaviour, significantly reduces the effectiveness of V2G control strategies that rely on deterministic or fixed usage assumptions. Consequently, these uncertainties pose considerable challenges for achieving reliable and scalable grid-level V2G integration in real-world scenarios.

1.2.3. The Need for Standardized Benefit Evaluation Models

In the assessment of both economic and environmental benefits, existing V2G studies have proposed a variety of optimization strategies aimed at improving system cost-effectiveness. However, recent research (Kaur, et.al., 2015; Shams, et.al., 2019; Shi, et.al., 2020) indicates that as the penetration of renewable energy sources within the grid continues to increase, the marginal utility of small-scale systems such as microgrids tends to decline. This trend suggests that traditional microgrid-based V2G implementations are approaching a bottleneck in terms of economic return.

Against the backdrop of an emerging trend toward zonal grid management, it is of practical significance to develop operational simulation and benefit evaluation frameworks specifically tailored to standardized community-level grids in the UK. These grids typically feature diversified energy infrastructures—including generation, storage, and consumption facilities—and are designed with the overarching objective of achieving net-zero emissions.

Developing such standardized models will not only facilitate accurate evaluation of both economic and environmental impacts, but also provide a predictive foundation for the planning and design of future grid systems. Furthermore, a unified modelling and evaluation framework

can help guide the development of regulatory protocols for V2G deployment at the community level, enhancing system interoperability and supporting more effective grid integration.

1.2.4. Key Research Gaps

Building on the challenges and limitations identified across the primary research domains of V2G—including both grid-side and EV-side perspectives—as well as their related fields—particularly as manifested in real-world industry practice, it is evident that several factors continue to hinder the effective development and deployment of V2G systems. Drawing on a comprehensive review of the existing academic literature and current technological advancements in the industry, the following specific research gaps remain under-addressed:

- Centralized Community-Level Management Frameworks: Most current models are built for either household microgrids (Mendes et al., 2016) or distributed P2P configurations (Rahbari-Asr et al., 2016). There is limited research on centralized control of community-level EV clusters, especially under variable and uncertain user participation.
- Behavioural Realism in Availability Modelling: Few studies incorporate real travel data or usage uncertainty into availability forecasting. Models that ignore temporal and spatial heterogeneity in EV behaviour are unlikely to perform reliably in live deployments.
- Integrated Economic and Operational Optimization: Economic evaluations are often detached from operational constraints. For instance, cost-benefit models may overlook grid ramping requirements, transformer constraints, or network topology considerations that directly affect feasibility.
- Scalable Communication Protocols and Interoperability: With growing data volumes and device heterogeneity, scalable, secure, and standardized communication

architectures are needed. While ISO 15118 (International Organization for Standardization, 2019) provides a partial solution, it is still not universally supported, and integration with local DSO (Distribution System Operator) /TSO (Transmission System Operator) platforms remains inconsistent (Hou et al., 2023).

- Lack of Simulation-to-Deployment Pipelines: Many models remain theoretical and have not been validated through field trials or hardware-in-the-loop simulations. Bridging the simulation-reality gap will be critical for real-world impact.

1.3. Current Practice and Research Landscape

Building upon the knowledge gaps identified in Section 1.2 within the current V2G development landscape, this section provides a comprehensive overview of the foundational work established across the industry to support the deployment of V2G systems. It outlines the primary architectural frameworks underpinning V2G networks, details the existing structures and protocols for data transmission and communication, and reviews the V2G market's hardware offerings, including both bidirectional charging and discharging devices and EV models equipped to support V2G functionalities. The common electrical specifications of these devices and vehicles are also discussed, highlighting how they collectively form the technical foundation of the V2G industry.

1.3.1. Core Architecture of V2G Networks

From a system architecture perspective, V2G systems can be conceptualized through two definitional lenses—narrow and broad. In the narrow sense, a V2G system comprises three fundamental components: (1) EVs; (2) grid interface infrastructure, including charging stations, connectors, and communication protocols; and (3) the specific grid nodes to which these EVs are connected. In contrast, the broader definition positions the V2G system as a novel

regulatory unit within the power grid, comprising four interrelated subsystems: source, grid, load, and storage—collectively referred to as the "S-G-L-S" framework (see Figure 1-5).

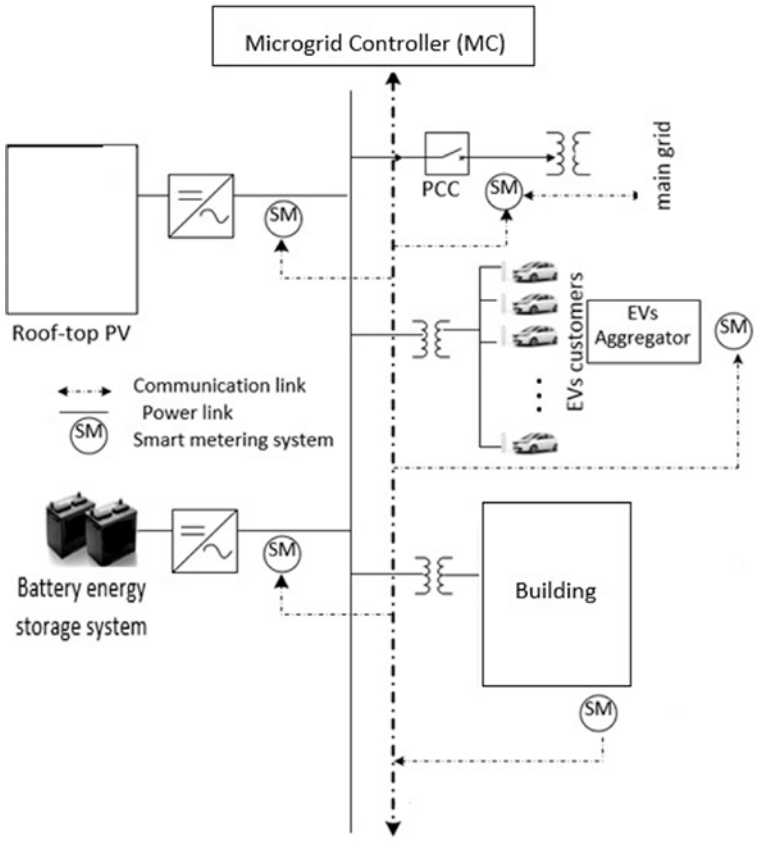


Figure 1-5. Network Structure of Simple Microgrid (Ouammi, 2021).

Note: This schematic illustrates the interconnection and bidirectional coordination between grid, load, generation, and storage subsystems through both power and communication pathways in microgrid.

During the early stages of research (Ahmadian et al., 2017; Chukwu, 2013), EVs were primarily treated as independent, mobile storage units that participated in grid operations via unidirectional power responses, typically for frequency regulation purposes. These early configurations lacked integrated coordination mechanisms with other grid components. However, as the penetration of distributed generation increased, so too did the severity of spatiotemporal mismatches between energy supply and demand, placing growing strain on transmission system stability.

Against this backdrop, system-level V2G integration strategies with coordinated dispatch capabilities have emerged, gradually replacing conventional distributed generation models as the focus of research and development. Among these, the microgrid architecture has gained prominence due to its dual capacity for localized autonomy and system-wide coordination. This makes it the smallest functional unit for optimizing and regulating V2G systems within regional grids. Furthermore, in terms of internal structural design and control logic, the microgrid functions as a modular blueprint for V2G system deployment across larger grid environments, like regional grid and community-level grid, offering a scalable and flexible platform for holistic energy management.

One of the most fundamental microgrid configurations involves the direct integration of EVs with end-user facilities equipped with on-site generation systems. This simple architecture, commonly referred to as Vehicle-to-Building (V2B) or Vehicle-to-Home (V2H), enables bidirectional energy flow between EVs and buildings or households (Karfopoulos & Hatziargyriou, 2015; Ouammi et al., 2019). These systems are typically built upon distributed generation (DG) technologies and are deployed within smart buildings or residential communities as autonomous subsystems aimed at optimizing local power distribution and grid interaction. According to the standard definition adopted by the European Commission's Microgrid Project (ECPM), a microgrid functions as an independent, controllable unit capable of delivering high-quality and reliable power supply to end users.

1. From a technical implementation perspective, microgrid-based V2G systems typically integrate DG units with EV clusters to enable coordinated power management. While implementations may vary, such systems often include the following technical features: The integration of various micro-generation units—including non-dispatchable, semi-dispatchable, and fully dispatchable sources—to efficiently utilize available local

energy. While some microgrids may employ Combined Cooling, Heating, and Power (CCHP) technologies, this is not a defining requirement.

2. They are equipped with power electronic equipment (PEE) that enables dynamic power conversion and distribution between generation sources and end-use loads, effectively resolving electrical coupling conflicts among components.
3. They implement isolation and protection mechanisms designed in accordance with the IEEE 1547.4 standard, utilizing static transfer switches (STS) to facilitate flexible interconnection with the main utility grid (Alsafran, 2023).

This system topology imparts two essential capabilities: first, the ability to achieve internal power self-balancing within the microgrid in response to generation–demand time mismatches; and second, support for seamless transition between grid-connected and islanded operational modes across multiple microgrids. Together, these features significantly reduce operational stress on the main power grid while enhancing the resilience and adaptability of localized energy networks.

Although the microgrid architecture provides a foundational platform for the implementation of V2G systems, it continues to face significant technical challenges in real-world applications. Mouli et al. (2017) highlight that internal components within microgrids—including PEE, control algorithms, and management units—often operate under differing interface protocols and asynchronous response sequences. These inconsistencies lead to structural conflicts during optimization and dispatch processes, which in turn constrain the overall operational efficiency of microgrid systems.

A more critical limitation lies in the current reliance on uniform, centralized control strategies for managing EVs within microgrids (Krueger & Cruden, 2020). Such coarse-grained control models exhibit two major shortcomings: first, they fail to fully harness the distributed energy storage potential of EVs; second, they lack the flexibility to accommodate diverse load

scenarios and user demands. In response to these challenges, researchers (Wei, et.al., 2022) have proposed an innovative architecture known as the centralized Grid-Integrated Vehicle (GIV) system—a large-scale, centralized V2G configuration designed to simultaneously manage multiple EVs within a unified "S-G-L-S" framework. This architecture leverages centralized coordination to facilitate intelligent scheduling, real-time balancing, and integrated energy services across complex power networks.

Compared to decentralized microgrid-based configurations, the centralized GIV model enhances system performance through its centralized coordination of electric vehicle fleets. By integrating a unified management platform, it enables synchronized control across distributed storage units, significantly improving the system's overall flexibility and responsiveness. This centralized approach not only expands the available capacity for peak shaving and energy balancing, but also mitigates operational instabilities that often arise from the parallel interaction of multiple autonomous microgrids. As a result, the centralized GIV architecture is particularly well-suited to complex application scenarios—such as community-level distribution networks—where stability, scalability, and dynamic energy services are essential.

1.3.2. Parking-Lot Based Centralized V2G Integration System

Parking-lot-based V2G networks represent a typical form of centralized integration and have been widely adopted to support large-scale "S-G-L-S" configurations. Unlike microgrid-based V2G systems that typically serve EVs with fixed, predictable usage patterns, the parking-lot-based centralized V2G integration system treats distributed EVs as a unified storage module. Through a centralized V2G control platform, it coordinates power dispatch and transmission across EVs operating under various usage modes, enabling system-wide optimization of regional grids. However, this architecture still relies on traditional centralized control logic that overlooks the heterogeneity of EV behaviours. Consequently, the actual regulatory capacity of

such systems is highly dependent on the real-time number of grid-connected EVs. This stochastic variability undermines predictability and controllability, often leading to secondary regulatory challenges in load balancing and energy absorption within the regional power grid.

To mitigate these limitations, current research increasingly emphasizes enhancing the structural logic of traditional parking-lot-based V2G systems through integrated transmission architectures. Garruto and colleagues (2020) proposed a cross-linked, multi-tiered management model that incorporates centralized, distributed, and microgrid-based interconnection strategies. This system utilizes distributed charging nodes managed via reactive power dispatch methods to regulate EV charging/discharging and associated power parameters. These distributed nodes are topologically interconnected and supervised by a centralized V2G aggregator employing optimized distribution algorithms. The entire system adopts a hierarchical modular design, where local microgrids act as transitional layers between individual EVs and the main grid, thereby improving overall control granularity and operational resilience.

Beyond architectural improvements, researchers have also focused on the internal operational efficiency and scheduling strategies of parking-lot-based V2G systems. Shi (2018) proposed a day-ahead load-transfer scheduling scheme with hourly resolution. Other studies (Sortomme & El-Sharkawi, 2012; Wang et al., 2017) converged on a 30-minute feedback interval, which balances grid peak-shaving profit for aggregators and cost savings for EV users through precise modelling of battery behaviour. Faddel et al. (2018) advanced this further by reducing the interval to 5 minutes, demonstrating improved real-time responsiveness. Experimental evidence from large-scale field trials further illustrates the rapid response capability of V2G systems. As shown in Figure 1-6, a frequency contingency event in the Australian National Electricity Market triggered aggregated discharging from 16 V2G-enabled vehicles, leading to a noticeable reduction in grid import power within approximately one minute. However, large-scale experiments, such as that by He et al. (2012), involving over 400 EVs, revealed that

overly frequent data adjustments could strain automated data processing and compromise system reliability.

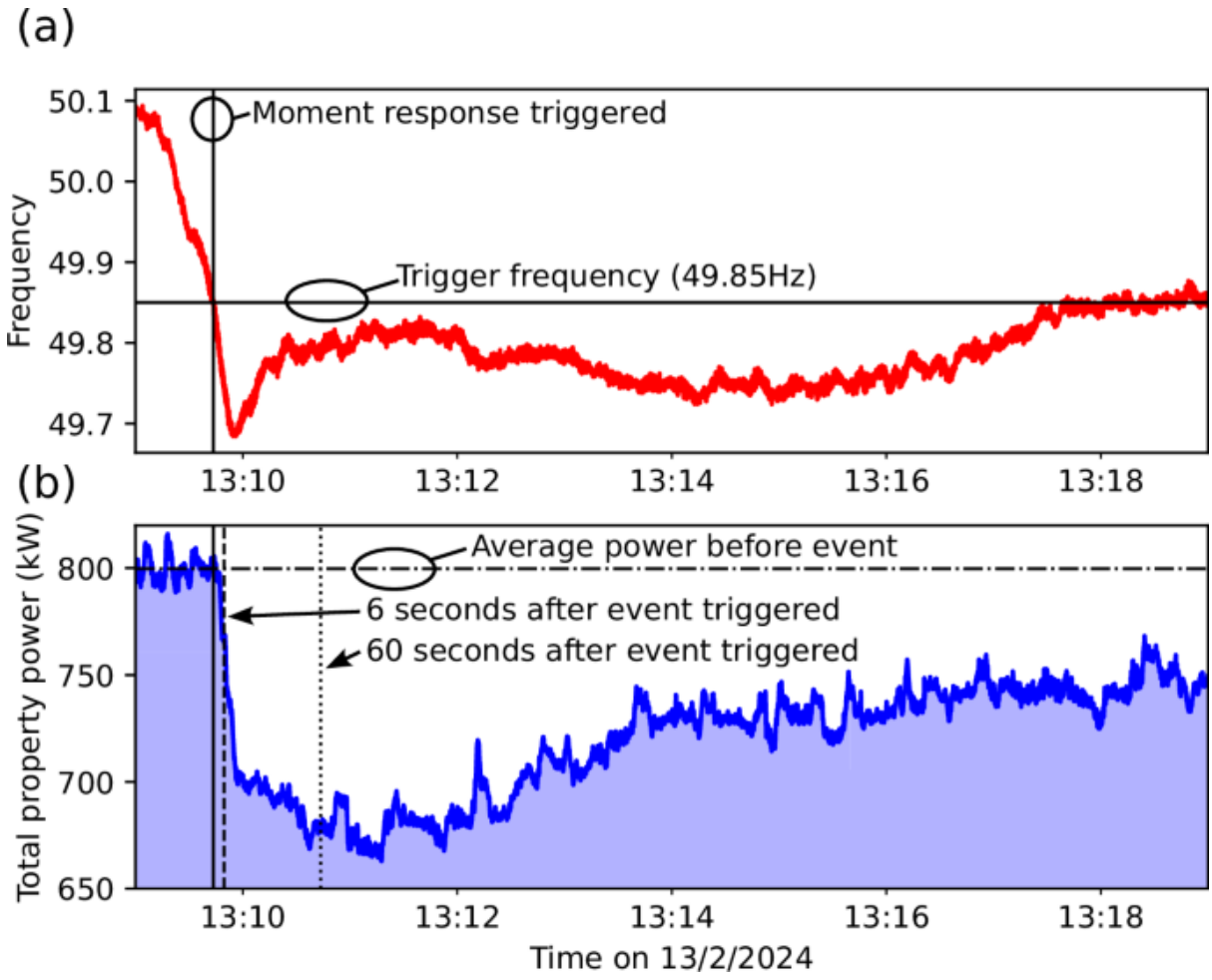


Figure 1-6. Grid frequency and aggregated power response during a V2G contingency event. (Sturmberg et al., 2024)

Note: (a) Frequency of the Australian power system recorded at six residential properties during a contingency event; (b) Total grid import power across the properties, showing a rapid reduction as 16 V2G-enabled electric vehicles respond by discharging power to support the grid.

Recognizing this, Turker and Bacha (2018) suggested a 10-minute interval as the optimal trade-off between response precision and operational cost in small-scale deployments. Building on this insight, Krueger and Cruden (2020) proposed a three-layer hierarchical scheduling model to address calibration delays and data inconsistencies in parking-lot-based V2G systems. In

this model, the first layer handles predictive scheduling based on anticipated EV activity, supported by a modular aggregator strategy using a full-network SQL-based data platform. The second layer provides real-time adjustments to correct for deviations between forecasted and actual power flow. The third layer ensures decentralized fallback operation in the absence of real-time connectivity. Their experimental results confirm that multilayer scheduling significantly enhances the system's regulatory efficiency and temporal responsiveness.

As a technical complement, accurate forecasting of power demand is essential to achieving near-instantaneous V2G responses. Nevertheless, research has shown that mismatches between preset parameters and actual load demand—caused by uncontrollable external variables—can lead to observable delays in the system's dynamic response. The magnitude and duration of such lag effects are directly correlated with the degree of forecast error.

1.3.3. Control Design for Power Transfer Chain and Data Interaction Chain in V2G Systems

The fundamental transmission structure between V2G systems and other grid components consists of two interdependent chains: the power transmission chain and the data response chain, forming a coupled feedback mechanism between high- and low-voltage signal flows. The data response chain is responsible for transmitting information such as EV battery status and regional component load requirements to the V2G centralized management platform. After processing, control instructions are fed back to the power transmission chain, which then regulates power flow in the designated direction and allocates the load accordingly. During this process, the power flow also updates the data chain, enabling dynamic rescheduling. These two chains collectively enable bidirectional signal exchange and multi-modal transformation of information and power between EVs and the regional grid (Liu & Liu, 2021). This dual-chain

architecture serves as the physical foundation for the V2G control and optimization strategies proposed in this study for complex grid environments.

Research on the V2G power transmission chain primarily focuses on the development of V2G aggregators and connectors, aiming to accommodate frequent AC/DC conversions and dynamic changes in electrical parameters (e.g., voltage, current), which are essential to ensuring the stability of V2G circuits (Liu et al., 2013; Zecchino et al., 2019). Figure 1-5 illustrates the overall logic and conversion relationships among participants in a simplified V2G framework, with particular attention to AC/DC transformation processes and internal circuitry within EVs. Due to substantial differences in continuous operating voltages and electrical formats between upstream and downstream nodes, bidirectional aggregators are often integrated with DC chargers, forming terminal hybrid systems that enable continuous energy exchange between high-voltage alternating current (HVAC) and low-voltage direct current (LVDC).

Given current market mechanisms and regulatory constraints, Frequency Containment Reserve (FCR) has been developed as an enabling technology to support rapid, reliable dynamic responses and V2G system integration (Zecchino et al., 2019). Unlike traditional computation models, FCR is evaluated in terms of available instantaneous power (kW) rather than energy throughput. This shift reflects the unique characteristics of EV storage systems, which, although limited in total forward/reverse capacity, are capable of delivering high peak power on demand. As FCR technology becomes increasingly standardized, more EV aggregators are being incorporated into FCR-enabled systems. However, due to its stringent technical requirements, FCR operation critically depends on the real-time reliability of the data response chain, which must provide instantaneous feedback and signal communication to maintain operational integrity.

He and his research team (2021) conducted a theoretical modelling and predictive study on a three-phase, two-stage off-board bidirectional electric vehicle (EV) charger and its associated direct power control scheme. The researchers introduced two novel control strategies—Model Predictive Direct Power Control (MPDPC) and Model Predictive Direct Current Control (MPDCC)—designed to manage the active and reactive power flow within AC/DC aggregator conversion systems. Additionally, the MPDCC approach was employed to regulate constant-current charging in the secondary DC/DC converter stage. This hybrid control architecture addresses the stochastic bidirectional energy transfer requirements inherent in V2G systems and further enables reactive components—such as capacitive and inductive elements in V4G (Vehicle-for-Grid) configurations—to participate in the dynamic regulation of the conversion chain.

Notably, the experimental setup incorporated galvanically isolated DC/DC converters within the power conversion path, enhancing the electrical safety and integrity of the power exchange between the EV and the grid. Compared to the non-isolated composite conversion topologies commonly found in industrial applications, this isolated design significantly improves transmission security and system robustness.

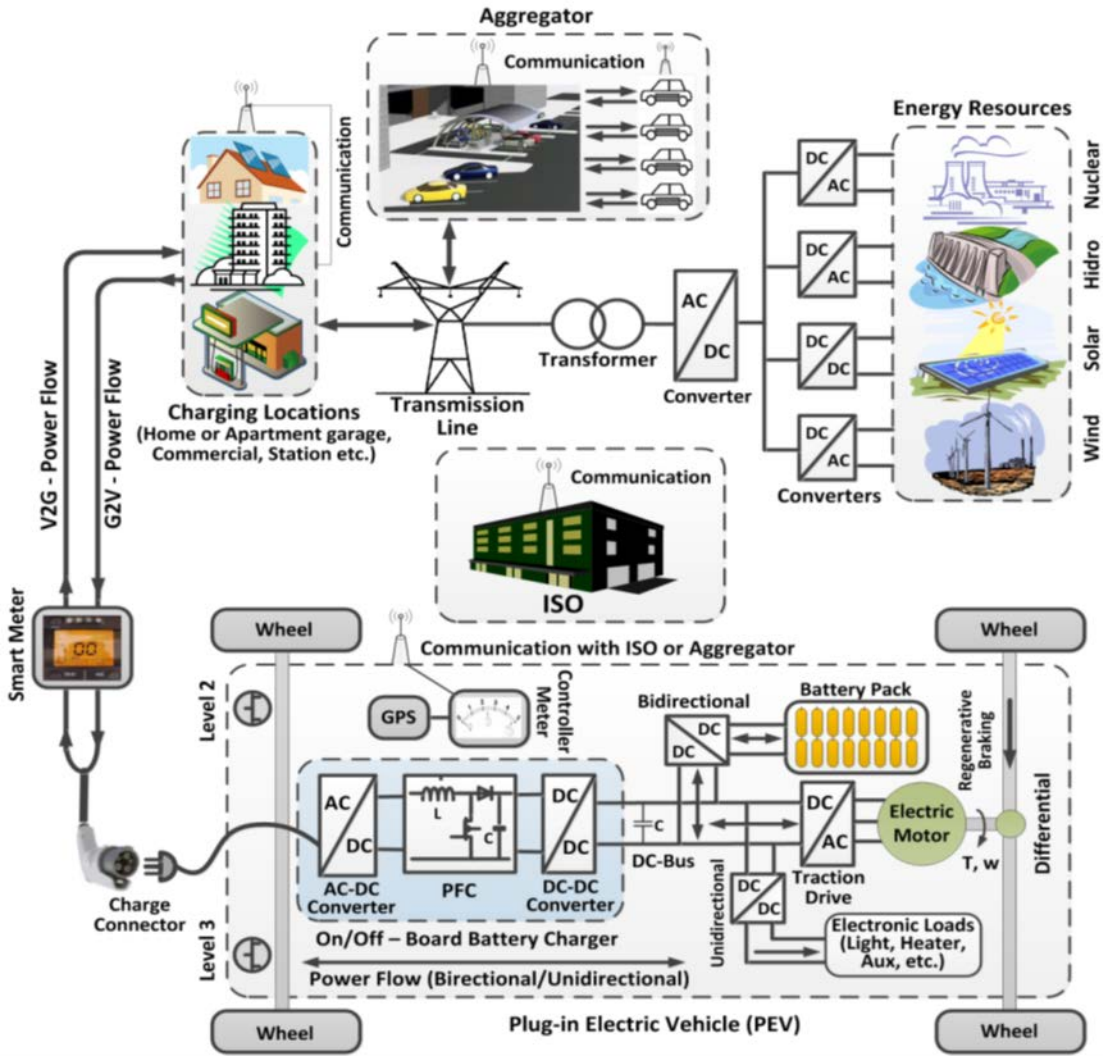


Figure 1-7. Power Transmission and AC/DC Conversion Structure in a Simplified V2G System (Habib & Kamran, 2014)

In the field of V2G data response chain research, beyond widely explored topics such as communication protocols and secure data transmission, recent studies have expanded to include independent V2G terminal logging and scheduling systems for tracking power flow and conversion events (He et al., 2021). These mechanisms are designed to ensure immediate EV-side responsiveness and to address latency mismatches when other grid components operate at different response frequencies. Such structured responses are typically coordinated through embedded serializers and wireless data processing platforms. With further investigation into influencing factors, data response services have increasingly extended to

incorporate real-time electrical performance tracking of EVs and user behaviour monitoring. In addition to battery performance tests conducted in isolation, many current studies (Han & Xiao, 2016; Wang & Zhai, 2016; Zecchino et al., 2019) focus on temporal responses and data stream adjustments during signal conversion processes. These studies evaluate key characteristics of the data response chain, including transmission direction, setpoint linearity, initiation time, maximum activation delay, ramp-up/down time, response precision, and acceptable deviation margins (Han & Xiao, 2016).

Zecchino and colleagues (2019), based on their empirical assessment of V2G CHAdeMO chargers and related data processing systems, proposed several benchmark values for performance parameters within the V2G data response chain. Their modelling results suggest the optimal setpoint linearity should be within 1% of the rated power. In systems without instantaneous response capabilities, at least 50% of rated capacity must be activated within 15 seconds. Fleet-level ramp rate capability should range between 100 kW/s and 300 kW/s. For improved system precision, actual power responses should remain within both 5% of the system setpoint and 0.5% of the rated power (Zecchino et al., 2019).

Moreover, to enhance real-time responsiveness, user behaviour—including access times, dwell durations, and battery state of charge (SoC)—has also been incorporated into response modelling. Some studies (Li et al., 2020; Shi et al., 2020) have explored integrating onboard or mobile GPS terminals into an extended version of the V2G data response chain, aiming to anticipate and adapt to stochastic variations in EV behaviour. However, this expanded scope raises ongoing societal concerns regarding data security and behavioural privacy, which remain unresolved in many implementations (Shi et al., 2020).

1.3.4. V2G Bidirectional Power Rating Design

The bidirectional charging and discharging capability of EVs constitutes a foundational mechanism through which V2G systems respond to dynamic grid load fluctuations. This capability is governed by a combination of factors, including grid capacity constraints, regulatory requirements, and EV-specific conditions such as battery capacity, power tolerance, and the number of EVs actively participating in V2G networks available for grid dispatch.

Higher bidirectional power settings enhance the system's capacity to stabilize sudden load variations, enabling quicker and more effective regulation. Nevertheless, when large EV fleets engage in synchronized high-power charging or discharging, the resulting secondary power peaks can introduce significant transient stress on the grid infrastructure. Furthermore, frequent rapid cycling of power has been associated with accelerated battery degradation, an issue that is discussed in detail in subsequent sections. On the other hand, adopting lower bidirectional power levels can alleviate both battery stress and the risk of secondary peak formation. However, this approach necessitates the involvement of a substantially larger number of EVs to achieve equivalent regulatory output, which becomes particularly challenging during periods of low vehicle availability—such as midday hours when residential EV presence declines, even though excess PV generation demands increased storage capacity.

Supported Bidirectional Charging Standards	EV Models	Battery Capacity (kWh)	Charger Type	Bidirectional Charging Mode	Suggested Bidirectional Power (kW)	Bidirectional Power (kW)	AC Charge Power (kW)	DC Fastcharge Power (kW)
DIN SPEC 70121	MG ZS EV	50.3	Type 2 & CCS	V2L		2.2	11	80
DIN SPEC 70121	MG 4	50.8 /61.7/ 74.2	Type 2 & CCS	V2L		2.2/2.2/2.2	7/7/7	88/140/140
ISO 15118 + Plug & Charge	BYD Atto 3	60.5	Type 2 & CCS	V2L	3.6	2.2	7	80
GB/T (China-market) + ISO 15118 (UK-market) + Plug & Charge	BYD Dolphin Dynamic / Premium	44.9/ 60.5	Type 2 & CCS	V2L	3.6/3.6	3.3/3.3	7/7	60/80
GB/T (China-market) & ISO 15118 (UK-market)	BYD Seal Standard Range /Extend Range/Seal AWD	61.4/ 82.6/ 82.6	Type 2 & CCS	V2L	3.6/3.6/3.6	3.3/3.3/3.3	7/7/7	110/150/150
ISO 15118 + Plug & Charge	Hyundai loniq 5 (MY2025)	74	Type 2 & CCS	V2L		3.6	11	233
ISO 15118 + Plug & Charge	Kia EV6 RWD/AWD/GT	74	Type 2 & CCS	V2L		3.6/3.6/3.6	11/11/11	350/350/350
ISO 15118	Kia EV9 Air RWD/Earth AWD/GT-Line AWD	72.8/ 95/ 95	Type 2 & CCS	V2L		3.6/3.6/3.6	11/11/11	240/240/240
ISO 15118	Kia Niro EV	64.8	Type 2 & CCS	V2L		3.6	11	84
ISO 15118 + Plug & Charge	Genesis GV60/GV70/ G80	74/ 74/ 82.5	Type 2 & CCS	V2L		3.6	11	233

CHAdeMO & ISO15118 (New Vehicle Models)	Nissan Leaf	59	Type 2 & CHAdeMO	V2G/V2L	7(Wallbox Quasar)	3.6	7	100
ISO 15118 + Plug & Charge	Cupra Born	77	Type 2 & CCS	V2G/V2L	Only Adapt Wallbox Quasar 2	TBC	11	170
CHAdeMO & IEC61851	Mitsubishi Outlander, Eclipse Cross	13.8	Type 2 & CHAdeMO	V2G/V2L/V2H		1.5	3.7	60

Table 1-1. Rated Bidirectional Charging/Discharging Power and Battery Capacities of Mainstream EV Models in the UK Market

Note: Data collected from official EV manufacturer websites.

Table 1-1 summarizes the rated bidirectional charging/discharging power and battery capacities of several mainstream EV models currently available in the UK market. The data indicates a strong market inclination toward low-power, symmetrical AC bidirectional transmission. This configuration minimizes the operational stress placed on EV battery management systems while ensuring broad compatibility across various UK regional grid infrastructures. Moreover, such low-power transmission schemes reduce the risk of overloading local distribution networks, aligning well with the technical limitations and regulatory frameworks of the UK grid environment.

It is important to note that while many EVs are also equipped with high-power DC charging capabilities, these functions are primarily reserved for rapid commercial charging at dedicated DC fast-charging stations and are generally not utilized in V2G operations. In contrast to their original design philosophy, even the CHAdeMO protocol—established by the CHAdeMO Association in Japan and originally developed to support high-power, fast DC charging—has adapted its hardware offerings for the UK market to support lower-power, symmetrical AC/DC bidirectional transmission, in line with local V2G deployment needs.

Charging Products	AC/ DC	Max Output Power (kW)	Max Current (A)	Output Voltage Range (V)	Notes
ABB Terra Nova 11 J	DC	±11 kW	36.7	Up to 500V	Accepts all standards
AME	DC	±10 kW	28	50-500	
Delta V2H	DC	5.5 kW	TBC	TBC	
Denso DNEVC-D6075	DC	6.0 kW	TBC	100/200 V (AC)	
Endesa	DC	±10 kW	TBC	TBC	
FERMATA ENERGY FE-15	DC	±15 kW	TBC	TBC	
Honda Power Exporter 9000	AC	9.0 kVA	30	100 V/ 200 V	
Honda Power Manager	DC	5.5 kW	TBC	150-450	

Indra V2G 170911A202	DC	7.4 kW	15	Up to 500V (385-400V normal)	Nissan
Panasonic / LJV1671B	AC	6.0 kW(Charging); 6.7 kW (Discharging)	TBC	202	V2H
Magnum Cap	DC	10 kW	31	Up to 500V (400V normal)	
MiEV power BOX	DC	1.5 kW	15	100	
Nichicon EV Power Station	DC	6 kW	TBC	100/200 V (AC)	
Nichicon Power Mover	DC	4.5 kW	TBC	100 V (AC)	
Princeton Power System	AC	10 kW; 30 kW	40 A; 120 A	500	
Wallbox Quasar	DC	7.2 kW	17.5	150-500	
Takaoka Toko Smaneco	DC	3 kW	TBC	100-200	V2H
TSUBAKIMOTO CHAIN Elink	DC	5 kW	20	150-450	

Table 1-2. Technical Specifications of CHAdeMO-Compatible V2G Charging Products Available in the UK

Note: Data sourced from the official CHAdeMO Association website.

Table 1-2 presents the electrical specifications of CHAdeMO-compatible V2G Charging Products currently deployed in the UK, based on official data provided by the CHAdeMO Association. These figures reflect the broader industry shift toward standardized, grid-friendly lower-power V2G infrastructure that emphasizes stability, interoperability, and long-term battery health. Note that the "Max Output Power (kW)" values represent the maximum power for both charging and discharging operations.

In addition to grid infrastructure influencing EV manufacturers' decisions regarding the rated bidirectional charging/discharging power for V2G applications, another critical factor is the impact of charging intensity and high-rate energy transfer on battery health. In high-sensitivity grid environments characterized by short response times and rapid power fluctuations, V2G

systems frequently trigger real-time charging and discharging cycles of EVs to stabilize power loads. However, such frequent power cycling has raised substantial concerns among researchers regarding its potential to accelerate battery degradation and impair cell balance (Ahmadian et al., 2017; Mouli et al., 2017; Peterson et al., 2010). Peterson and colleagues (2010), for instance, compared the degradation patterns of lithium-ion batteries under conventional daily driving cycles with those subjected to intermittent, high-frequency V2G charge/discharge operations. Their findings indicated that while routine bidirectional charging led to less than 10% capacity loss over thousands of standard use cycles, intermittent, high-rate cycling caused significantly more severe degradation, rapidly eroding battery performance. Other studies (Hu et al., 2015; Shen et al., 2017; Zhao et al., 2022) have similarly confirmed the adverse effects of bidirectional V2G operations on battery longevity. Zhao et al. (2022) conducted fatigue testing on a 40 kWh V2G-enabled NMC battery charged every other day. The results suggested an estimated lifespan of only five years—substantially shorter than those observed under alternative operational modes (see Table 1-3).

Assumption	Unit	EV Battery	V2G	Battery Swap (BS)	Battery Stationary Storage (BSS)
Battery Energy Capacity	kWh	40	40	40	40
Battery Chemistry		Nickel Manganese Cobalt Lithium-Ion Battery (NMC)	NMC	NMC	Lithium Iron Phosphate (LFP)
Degradation model		Wang et.al.			Schimpe et.al.
Charging Frequency		Every 4 Days	Every Other Day	Every Other Day	Every Other Day
Lifetime	Year	8	5	8	36
Capacity (End of 1st Service)	kWh	28			
Capacity (End of Battery Reuse (RU) Service)	kWh	12			

Table 1-3. Assumption Parameters of Different Battery Situation (Zhao & Baker, 2022).

These findings underscore the necessity of optimizing the rated bidirectional power settings not only to enhance grid responsiveness but also to minimize the hidden cost of battery degradation. Aside from advancements in battery chemistry and materials, the strategic configuration of bidirectional charging parameters represents one of the most effective approaches to preserving battery performance and improving the net present value (NPV) of V2G systems.

1.3.5. V2G Management Strategy and Control Logic

As an integral component of integrated energy transition and intelligent grid management, the operational efficiency and system reliability of V2G systems are influenced not only by their internal transmission architecture but also by the broader operating environment and the behaviour of regional grid participants. As highlighted in numerous studies focusing on the optimization of V2G operating environments (Bibak & Tekiner, 2021; Hosseini & Parvania, 2012), the various elements within the power grid—particularly those in the “S-G-L-S” configuration—tend to pursue independent optimization strategies. These strategies often conflict in practical planning constraints, temporal sequencing, flow control, and state transitions, which significantly undermine overall system reliability (Hosseini & Parvania, 2012).

To resolve these conflicts and enable consensus among system components, unified management logic and computational frameworks have been proposed (Geske & Schumann, 2018; Dagdougui et al., 2019). These are typically embedded within centralized management systems or dedicated controllers to regulate and coordinate system operations. However, due to diverging energy objectives and the heterogeneity of system components, no standardized operational protocol for V2G environments has been universally adopted across academic or

industrial domains. In response to these challenges, recent research (Kester et al., 2018; Zahid et al., 2015) has shifted toward developing context-specific optimization and control models that are tailored to particular V2G deployment scenarios. Although the resulting insights—particularly in terms of economic assessment structures—may lack generalizability, the architectural principles and control logics embedded in these models offer valuable reference points for broader applications. Figure 1-8 illustrates a representative example of such control logic, as proposed in the work of Mendes et al. (2016). This schematic outlines a basic structure for managing EV charging and discharging decisions under dynamic grid constraints and optimization targets, providing a practical framework for understanding component interactions in real-world V2G environments.

Algorithm 1 Charging Station Management

Input: T_a, T_p,Ch_T,ϵ,$Time$

Output: Q_x, Q_{N_p},$\overline{u}$

for $i = 1$ to nc **do**
  if $\epsilon(i) = 1$ {Test if there is a parked vehicle} **then**
    if $Ch_T(i) = 1$ {Fast Charge} **then**
      if $Time \geq T_a + T_p - 30minutes$ **then**
        Set $Q_x(i,i)$ to the fast charge value
        Set $Q_{N_p}(i,i)$ to the fast charge value
      else {Use the battery as a grid storage}
        Set $Q_x(i,i)$ to zero
        Set $Q_{N_p}(i,i)$ to zero
      end if
    else {Slow Charge}
      Set $Q_x(i,i)$ to the slow charge value
      Set $Q_{N_p}(i,i)$ to the slow charge value
      Set $\overline{u}(i)$ to the slow charge value
    end if
  end if
end for

Figure 1-8. Partial Control Logic for EV Charging and Discharging in V2G Systems (Adapted from Mendes et al., 2016)

Dagdougui and her research team (2019) developed a demand response framework for V2G systems within standardized microgrids that can be scaled to large-scale “S-G-L-S” grid configurations. In this model, PV systems function as power generation components, while battery energy storage systems (BESS) serve as the storage units. The study focuses on peak load reduction as the sole optimization objective and explores the optimal operational equations of V2G systems under this theoretical constraint.

The researchers formulated a set of management functions and operational strategies for each element within the microgrid system, taking into account their respective dynamic states. By computing PV power output, the SOC of plug-in electric vehicles, and the status of regional storage systems, the study introduced a quadratic dual-cost function. This function defines the range of load regulation during peak events based on a dynamically referenced control load. Within this formulation, M acts as a weighting factor for cost variance, while K introduces the deviation between actual response power and reference power as an additional weighted cost component:

$$J(s,p) = \sum_{t=1}^{T} \Delta t(p_{load}(t) - \bar{p}_{load}(t))^{T} K \Delta t\left(p_{load}(t) - \bar{p}_{load}(t)\right) + (s(t) - \bar{s}(t))^{T} M(s(t) - \bar{s}(t))$$

Peak shaving is achieved by simultaneously adjusting indoor comfort parameters via the Building Management System (BMS) and modifying EV charging patterns. However, the study delivers a cautious conclusion: under interconnected microgrid conditions, the load adjustment capacity—or “adjustment credit”—of a single V2G system is insufficient to meet the peak demand response requirements of the broader external grid. This indicates that microgrids have reached a performance ceiling in this context. Consequently, the findings underscore the necessity of dedicated V2G management schemes designed at the regional grid level,

specifically tailored to large-scale “S-G-L-S” configurations. Such systems are essential for coordinating EV clusters effectively and meeting future demands for scalable, reliable grid interaction and peak load management.

1.4. Deliverable

The primary outcome of this study is the development of an optimized management and dispatch scheme for centralized V2G systems in UK community-level power grids, based on active/idle EV status. The research adopts a systematic four-phase methodology, with each phase yielding independent academic achievements that collectively form a comprehensive V2G optimization solution. Table 1-4 clearly illustrates the main content and corresponding outputs of each research phase.

Phase 1: Systematic Literature Review

Through comprehensive literature analysis, this study first systematically summarizes the overall development trajectory of V2G technology, focusing on: (1) the disciplinary framework and subfield classification of V2G research; (2) evolutionary trends of research hotspots in each subfield; and (3) limitations of existing research. Based on comparative analysis of high-impact literature from the past five years, the study identifies critical gaps in current V2G applications for community-level grids, providing theoretical foundation for subsequent research.

Phase 2: Multi-source Data Modelling and Analysis

This phase integrates three-dimensional measured data from typical UK apartment community grids: (1) consumer-side electricity consumption data; (2) generation data from 4 kWp standard photovoltaic systems; and (3) EV usage behaviour data. Using these real-world datasets, the research constructs a dynamic simulation model to quantitatively analyse time-varying power load distribution characteristics in standard-scale zero-carbon community grids under various EV usage scenarios, establishing a data foundation for subsequent optimization design.

Phase 3: Optimization Scheme Design

Building on Phase 2 simulation results, the study innovatively proposes a V2G optimization management framework with "time-shared power load balancing" as its core objective. The solution particularly focuses on the dispatch potential of idle EV resources, developing a complete management logic containing key components: (1) load balancing algorithms; (2) EV status evaluation system; (3) charging/discharging priority strategies; and (4) real-time control mechanisms. This solution significantly enhances operational stability in community grids.

Phase 4: Multi-dimensional Benefit Assessment

The research conducts comprehensive evaluation of the optimization scheme from both environmental and economic perspectives. For environmental benefits, it quantitatively analyses the scheme's improvement effects on grid carbon emission intensity; for economic benefits, it focuses on assessing the scheme's optimization of total user electricity expenditure. Evaluation results demonstrate that the solution not only effectively balances power load distribution in community grids, but also exhibits significant environmental externalities and economic feasibility.

The entire research process employs a phased progressive design to ensure that outputs from each stage maintain independent academic value while organically integrating into a complete solution, thereby providing theoretical support and technical pathways for the ultimate goal - practical application of community-level V2G systems.

Research Stage	Deliverable	Contents

Stage 1	Literature Review	A systematic bibliometric analysis was conducted, incorporating keyword co-occurrence network mapping and citation tracing techniques to identify and filter high-impact publications in the field of V2G (Vehicle-to-Grid). Building upon this, the current research progress, emerging trends, and existing knowledge gaps were critically examined, culminating in a comprehensive analytical report.	
Stage 2	Data Analysis Report	Using real-world grid data from the Trent Basin zero-carbon residential community in Nottingham, UK—including household electricity consumption, PV generation, and EV usage records from the My Electric Avenue project—a multi-dimensional analysis was conducted. This enabled the development of a time-resolved power distribution model for standardized UK communities, supported by a comprehensive analytical report.	
Stage 3	Optimization Logic	Model Analysis	Based on the temporal power distribution characteristics, potential time slots for EV dispatch were identified to optimize grid flexibility
		Strategy Design	An optimized charging/discharging logic was developed for idle EVs to enhance the overall efficiency of the V2G system, considering grid demand and renewable energy integration
		Algorithm Implementation	The proposed optimization strategy was implemented in Python, where a computational model was constructed to validate the feasibility and effectiveness of the approach.
Stage 4	Economic and Environmental Performance Evaluation	Based on the optimization results, this study evaluates the economic and environmental benefits by comparing the optimized model with the original community grid operation scheme. The assessment employs time-of-use electricity pricing and carbon emission models to systematically quantify performance differences.	

Table 1-4. Structured Framework of the Research Process and Corresponding Outputs.

1.5. Objective & Research Methods

To obtain effective results from the analysis efficiently, essential objectives were required to work out the step-by-step specific research methods shown in Table 1-5. The desired outputs introduce the components and short-term goal to achieve corresponding objectives in more

detail. In addition, some necessary background information is also described as objectives of this research in order to acquire a comprehensive and universal analysis result.

NO	Objectives	Desired Outputs	Research Methods
1	Literature Review and Research Orientation Establishment (Chapter 2)	• Systematically review existing research achievements in V2G field, conducting scientific classification of research domains based on technical characteristics and application scenarios • Conduct in-depth analysis of evolutionary patterns in subfield research directions, examining temporal evolution characteristics and regional differences in research outcomes • Investigate interrelationships between subfields to clarify future research directions and provide theoretical foundation for positioning this study	• Desk-based Study • Literature Review
2	Case Study Grid Power Load Data Integration and Analysis (Chapter 3)	• Build time-series power load databases for community consumption, photovoltaic storage, and EV energy usage based on standardized methods • Calculate baseline distribution of comprehensive grid power load before V2G optimization implementation • Simulate load characteristics under different EV usage scenarios and their impact on overall grid operation • Evaluate technical feasibility of utilizing idle EV resources for grid regulation	• Case Study Project Data Analysis • Python programming for data processing

3	Grid Regulation Evaluation and Core Methodology for V2G Management Solutions (Chapter 4)	• Establish standardized processing methods for community electricity consumption data and photovoltaic power generation data • Propose simulation methods for electric vehicle usage behaviour and charging/discharging characteristics • Construct grid extreme load balancing calculation models • Design comprehensive V2G system management logic framework, including grid status assessment system and EV charging/discharging regulation rules • Develop quantitative evaluation models for assessing economic viability and environmental benefits of V2G systems	• Desk-based Study
4	V2G Optimization Solution Effectiveness Verification and Analysis (Chapter 5)	• Assess implementation effects of optimization solutions under various conditions including EV penetration rates, idle rates, charging/discharging frequencies, and power levels through simulation • Conduct quantitative analysis of optimization efficiency of V2G systems on grid power load distribution	• Desk-based data summary and analysis • Python programming for V2G management optimization framework design • Python programming for grid environment simulation

5	Economic and Environmental Benefit Assessment (Chapter 6)	• Analyse temporal distribution characteristics of dynamic electricity pricing mechanisms • Quantitatively compare changes in community grid electricity costs before and after V2G optimization • Investigate temporal distribution patterns of carbon emissions from regional grid power generation • Evaluate carbon reduction effects achieved through V2G solution implementation	• Python programming for integrated data evaluation

Table 1-5. Mapping of Thesis Units to Objectives, Outputs, and Research Methods

1.6. Scope of Research, Limitation and Boundaries

Building on prior literature that confirms the existence of optimal solutions for community-level grid distribution via topological simulations, this study develops a V2G-based optimized control and management scheme for a standard zero-carbon residential grid in the UK. The system utilizes idle EVs as a virtual energy storage resource, aiming to balance extreme load fluctuations within the local grid.

The selected UK-based community energy model consists of three core components:

1. standard-capacity PV generation facilities (supply side),
2. residential electricity consumers (demand side), and
3. a centralized cluster of idle EVs (storage side).

Regarding bidirectional power control design, this study focuses exclusively on medium- to low-speed V2G power transfer strategies, in alignment with the UK's grid capabilities and load-bearing constraints. High-power V2G transfer scenarios are not considered, as the goal is to enhance grid performance under typical community operating conditions.

From an economic perspective, due to the diverse electricity pricing schemes in practice (e.g., flat rate vs. dynamic pricing) and their varying impacts on the overall cost-effectiveness of grid energy consumption, this study initially constructs an optimization model with grid load balancing as the sole objective. Based on this model, two additional economic optimization strategies are developed under the two pricing schemes, demonstrating that optimal power cost performance can be achieved while maintaining grid stability.

It should be noted that the cost-benefit analysis conducted in this study is limited to system-level power cost optimization. Due to the lack of reliable data on battery degradation, the results do not include calculations of degradation-related costs or the net present value (NPV) of the V2G system—both of which may significantly influence the economic attractiveness of V2G participation for end-users.

Key Contributions of the Study:

1. Literature Review and Research Landscape Mapping

   A systematic review of recent high-impact studies in the V2G domain was conducted, with particular attention to community-level grid optimization and centralized V2G management schemes. Research gaps were identified, and future directions for subdomain development were outlined.
2. Coupled Impact Analysis in Community Energy Systems

   Based on a representative community grid model, the study quantifies the time-based interactions between PV generation, residential demand, and EV storage. The results reveal the contribution strength and temporal distribution patterns of each component to grid load behaviour.
3. V2G-Based Extreme Load Balancing Framework

A complete idle-EV dispatch logic is proposed, including: an algorithm for generating extreme load-balancing curves, a classification scheme for EV availability states, a priority-based charging/discharging strategy, and a control sequence design for system coordination.

4. Multidimensional Validation of the Optimization Scheme

   In addition to quantifying improvements in grid stability (via power balancing) and environmental impact (via carbon emissions reduction), the study also develops an extended version of the V2G scheduling scheme tailored to different electricity pricing models. This confirms the scalability and adaptability of the core optimization framework.

1.7. Thesis Structure

To provide a clear roadmap for the reader, the remainder of this thesis is organised as follows. Chapter 2 presents a comprehensive literature review of V2G integration within community-scale grids, identifying technical, behavioural, and policy gaps that motivate this study. Chapter 3 introduces the multi-source data modelling framework, detailing residential electricity demand, collective EV usage, and charging behaviours that form the basis for simulation. Chapter 4 describes the methodology, including the design of a centralized V2G scheduling algorithm and the evaluation framework for technical feasibility. Chapter 5 presents simulation results under multiple operational scenarios, analysing the performance of the proposed strategy in regulating grid load. Chapter 6 evaluates the economic and environmental impacts of the scheduling approach, including cost reduction and carbon mitigation potential. Finally, Chapter 7 synthesizes the main findings, discusses limitations, and outlines directions for future research.

CHAPTER 2. LITERATURE REVIEW

2.1. Introduction

The global shift toward decarbonized energy systems has entered a decisive stage in the past decade. With the formalization of the 2015 Paris Agreement and subsequent regional net-zero strategies—such as the UK's legally binding target to reach net-zero emissions by 2050—renewable energy integration has accelerated across both national transmission and regional distribution networks (Logan et al., 2020). Yet this transformation has brought with it substantial operational challenges. Renewable energy sources, particularly wind and solar, are inherently intermittent and do not follow the same temporal patterns as conventional demand curves. As a result, a mismatch has emerged between peak electricity generation and peak consumption hours, particularly in urban and suburban areas. This mismatch places considerable stress not only on centralized national transmission grids but more directly on local and community-level distribution infrastructure, where system responsiveness is often limited (Amertet & Gebresenbet, 2024; Kiaee et al., 2015).

Addressing this grid flexibility problem has become one of the central challenges in energy systems research. Among the diverse solutions proposed, the concept of V2G has gained considerable traction (Huda et al., 2020). V2G enables bidirectional energy transfer between EVs and the grid: during periods of low demand or excess generation, EVs absorb energy; during periods of high demand, they discharge it back to the grid. EVs are thus reconceptualized not simply as transport devices but as mobile, distributed energy storage units (Ahmadian et al., 2018; Shang et al., 2023). As EV penetration increases and battery technology improves, the potential aggregate capacity of EV fleets becomes significant. Numerous studies have demonstrated that coordinated V2G participation could reduce peak loads, enhance frequency stability, and even support grid resilience during outage scenarios. The

interconnections between components in a V2G system, depicting both power flow and data exchange pathways, are presented in Figure 2-1.

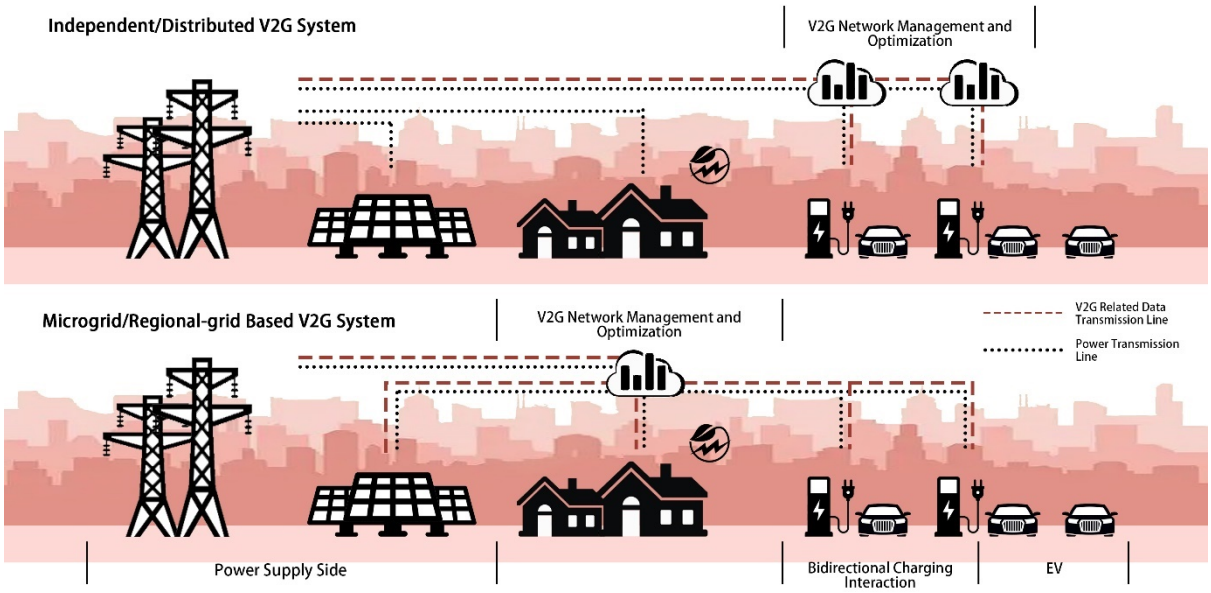


Figure 2-1. Overview of V2G System Functionality and Key Research Domains. (Ru et.al., 2025)

Despite its technical viability, most V2G deployment strategies to date have remained limited in scope and scale. The majority of early implementations have relied on microgrid-based configurations—small-scale systems often centred around individual homes or buildings, with their own renewable generation and storage components. These systems are relatively simple to model and control, often assuming deterministic EV availability based on fixed daily schedules (Hu et al., 2015; Kwon & Choi, 2016). For example, early V2G algorithms often assume that vehicles connect to home chargers overnight and remain stationary during predictable windows. While this assumption simplifies optimization, it is increasingly disconnected from real-world usage data (Huda et al., 2020).

In practice, EV user behaviour is far more varied. A 2022 report by the UK Department for Transport showed that less than half of EV owners charge daily; the majority charge on demand, only once or twice per week, and not necessarily at the same location or time (UK Department

for Transport, 2022). Moreover, most private vehicles are idle for the majority of the day—up to 22 hours in some cases—yet are not reliably connected to the grid during those idle periods (Rachid et al., 2023). This variability significantly reduces the effectiveness of V2G control strategies based on rigid assumptions. Furthermore, existing models rarely account for behavioural heterogeneity across different geographic or demographic segments, such as suburban commuters, commercial fleet operators, or inner-city residents with limited home charging access.

At the same time, there is a broader shift underway in how distribution networks are managed. In response to rising data volumes, voltage control complexity, and localized energy exchange, many urban utilities—particularly in the UK and parts of Europe—are moving toward zonal or community-level grid management structures (Bai & Qiao, 2015; Logan et al., 2020). These structures involve segmenting urban grids into administratively manageable units, such as residential neighbourhoods, business districts, or transit hubs, each with its own dynamic load profile. This evolution away from isolated microgrid systems and toward more coordinated local grid zones introduces new opportunities for centralized V2G coordination. If idle EVs within a defined community zone could be aggregated and managed in real time, they could provide valuable frequency regulation, reactive power support, and even spinning reserve capabilities, particularly during critical peak periods or renewable generation troughs.

However, this potential remains largely underdeveloped in both academic literature and practical deployment. Few existing V2G frameworks are designed specifically to operate at the community level with centralized dispatch logic. Instead, most proposals (e.g. Mendes et al., 2016) focus on peer-to-peer or household-level optimization, where each EV acts autonomously or responds to local price signals. These systems may work in isolated settings but often fail to scale due to data fragmentation, infrastructure limits, and lack of interoperability across devices. More importantly, they are poorly suited to managing the

complex and often unpredictable behaviour of heterogeneous EV users in real-world communities.

Given this context, there is a growing need to reframe the research agenda around V2G. Instead of focusing on isolated technical subsystems—such as converters (e.g. Zahid et al., 2015), protocols (e.g. Sharma & Jain, 2023), or load models in isolation (e.g. Strickland et al., 2019)—future work must emphasize systems-level integration, particularly at the community scale. This includes developing centralized control frameworks capable of aggregating idle EV capacity dynamically, responding to real-time grid needs, and incorporating probabilistic models of user behaviour. In parallel, these systems must align with emerging regional standards for communication, cybersecurity, and economic settlement to ensure both feasibility and scalability.

This literature review aims to reinterpret the V2G research landscape by examining how different thematic domains have evolved, fragmented, and shifted over time. It maps the historical trajectory of the field, identifies the dominant paradigms within each domain, and traces the movement from hardware-focused feasibility studies toward behaviourally aware management strategies. In doing so, it highlights the disconnect between theoretical models and observed EV usage patterns, thereby clarifying where significant research gaps remain for the design of practical, community-level V2G systems.

Ultimately, the purpose of this review is to extract from the literature a set of technological, behavioural, and structural insights that can inform the development of a next-generation V2G management scheme—one that is capable of real-time coordination of idle EVs at the community level, is robust to usage uncertainty, and delivers measurable improvements in grid regulation efficiency. This reframing is essential not only for academic completeness but also for advancing V2G from a promising concept into a deployable system that supports the future

of low-carbon, distributed energy infrastructure. The remainder of this chapter is structured as follows: Section 2.1 introduces the general background of V2G research; Section 2.2 outlines the methodology adopted for this literature review, focusing on the central objective of optimizing centralized V2G efficiency at the community level through the utilization of idle EVs; Section 2.3 provides a comprehensive overview of the existing V2G literature, identifying key research gaps across different subfields; Section 2.4 examines grid-side challenges specific to community-scale V2G deployment; Section 2.5 discusses technological limitations related to bidirectional charging interfaces and communication protocols; Section 2.6 reviews studies on EV user behaviour and its impact on system flexibility; Section 2.7 discusses and synthesizes major prior research findings and practical case studies related to V2G management strategies; Section 2.8 explores V2G management and economic strategies that support practical implementation; and finally, Section 2.9 concludes the chapter with a summary of key findings.

2.2. Literature Analysis methodology

To gain a comprehensive understanding of the long-term research trends and thematic evolution within the field of V2G, this study employs a bibliometric approach to identify and analyse high-impact literature related to "V2G" or "Vehicle to Grid." Using a standardized search query ("V2G" OR "Vehicle to Grid"), a two-dimensional dataset was constructed, capturing both the cumulative citation count and the relative citation rate for each relevant publication from the past decade (2015 to April 2024). These two metrics serve as complementary indicators to assess and rank the influence of each work, resulting in a curated dataset of high-impact publications. To ensure consistency and minimize biases stemming from factors such as the choice of academic database or variations in individual author visibility, all data were collected from NUsearch (University of Nottingham, 2025), an integrated

bibliographic search engine. Incomplete records—such as conference abstracts or publications without accessible full texts—were excluded from the analysis. Subsequently, a qualitative analysis was conducted on the filtered set of research articles to identify secondary research domains within the broader V2G landscape. This analysis examined the distribution of contributions across these subdomains, with particular attention given to works directly relevant to the focus of this study. Notably, a Dynamic Topic Modelling (DTM) framework (Blei & Lafferty, 2006) was applied to trace the evolution of research themes over time and to capture emerging trends within V2G subfields on an annual basis. An analysis of high-impact literature from 2015 to 2024 reveals five dominant subfields within V2G research:

- Power Supply-Side Integration: Research in this domain focuses on coupling V2G systems with intermittent renewable energy sources such as wind and solar. Studies have examined how EV fleets can serve as dynamic buffers to smooth fluctuations in renewable output, reduce reverse power flow during oversupply, and enhance voltage stability in local distribution networks.
- Bidirectional Charging Technology: This subfield includes hardware innovations such as DC-DC and AC-DC converters, inverter designs, resonant networks, and standardization of charging interfaces. Researchers have also developed algorithms for adaptive charging/discharging control under different load conditions, with a growing emphasis on asynchronous and high-disparity bidirectional power flows.
- Data Communication, Protocols, and Cybersecurity: As V2G systems scale, communication protocols have become increasingly critical. This research area includes the development of secure authentication methods, data-sharing standards (e.g., ISO 15118), privacy-preserving computation, and blockchain-based energy trading frameworks.

- EV Battery Systems and Degradation: A significant concern in V2G adoption is battery health. Studies in this field investigate how bidirectional cycling affects degradation rates, battery longevity, and performance under variable load environments. Some findings suggest that, under optimized V2G cycles, battery degradation can be minimized or even slowed, though this remains context-dependent.
- V2G Network Management and Optimization: This category comprises centralized and distributed control architectures, scheduling algorithms, load forecasting tools, and vehicle dispatch models. Earlier works focused on fixed scheduling and static demand-response protocols. More recent contributions incorporate dynamic optimization and real-time grid responsiveness.

A keyword co-occurrence network was constructed using VOSviewer, a widely used bibliometric visualization tool designed to generate scientific knowledge maps from literature datasets (Van Eck & Waltman, 2009). This analysis drew on a curated sample of influential publications in the V2G domain. To enhance thematic clarity, generic and high-frequency technical terms such as "energy" and "engineering" were excluded, and only those keywords appearing five times or more were included in the mapping process.

In the resulting network visualization, node size indicates keyword frequency, while the spatial proximity and linkage density between nodes represent the strength of co-occurrence relationships. The map is organized into colour-coded clusters, each representing a distinct thematic grouping derived from underlying keyword patterns. For example, red-coloured terms are associated primarily with grid-level V2G applications, while yellow clusters reflect a focus on economic analysis. Green groups capture hardware-oriented research, blue nodes emphasize system control and optimization, and purple clusters relate to communication systems and data exchange.

Although the clustering outcome generated by VOSviewer follows a data-driven approach based on statistical proximity rather than manual thematic assignment, several clusters align well with the conceptual framework introduced earlier in the methodology—namely, categories such as bidirectional charging, EV-side behaviour, grid-side integration, and network management. For instance, blue and purple keyword groups correspond closely with themes related to system-level V2G control and communication, while green nodes reflect the hardware and power electronics dimension. This thematic correspondence supports the validity of the subdomain classification proposed in this study, even though the VOSviewer clusters emerge independently from co-occurrence patterns rather than from predefined research categories.

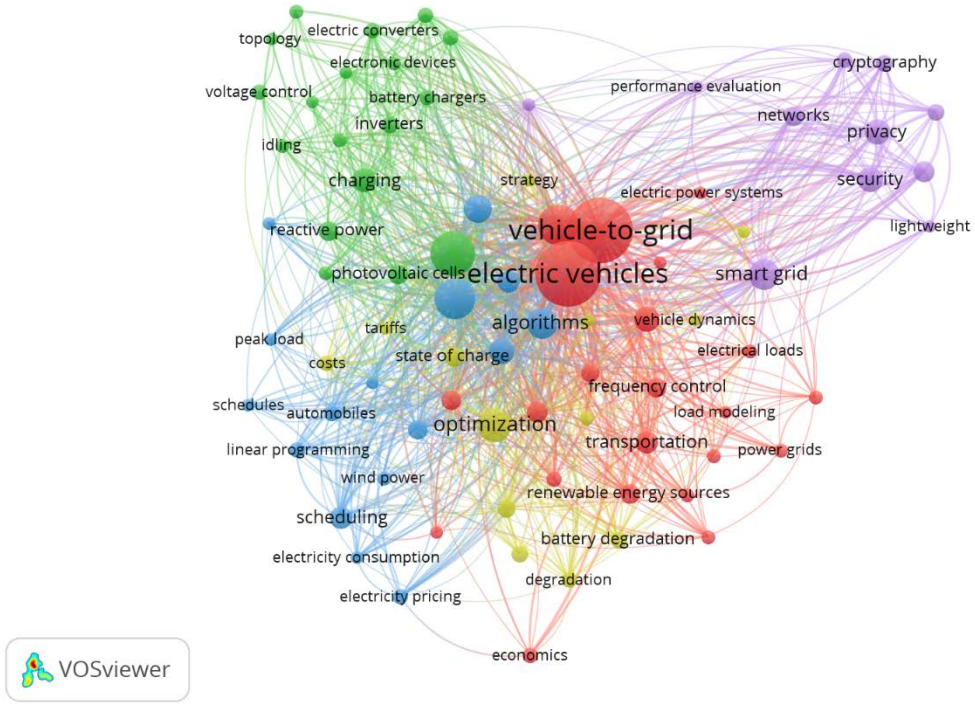


Figure 2-2. Keyword Co-Occurrence Network Derived from V2G Publications (VOSviewer Analysis). (Ru et.al., 2025)

While this classification provides a structured view, the vast majority of studies remain siloed within individual subdomains. Few works attempt to bridge across technical layers (e.g., from hardware to control algorithms), and even fewer integrate user behaviour, economic viability, and grid-level optimization in a unified framework.

2.3. Research Landscape Overview

Over the last decade, V2G research has evolved from theoretical modelling and component-level feasibility studies to a broad, multidisciplinary field encompassing control systems, communication protocols, economic evaluation, behavioural analytics, and energy market integration. However, this expansion has not been uniform; rather, it has resulted in a highly fragmented body of work, with research distributed across loosely connected subdomains and use-case scenarios. This section aims to provide a comprehensive review of the V2G research landscape, both thematically and chronologically, with particular attention to the emergence of centralized management models and community-scale integration—areas most relevant to the research problem of this thesis.

2.3.1. Chronological Development and Paradigm Shifts

Phase 1. Foundations and Hardware Feasibility: In the early stages of V2G research, much attention was directed toward establishing the feasibility of bidirectional energy exchange. Prototypes such as V2H and V2B (Hu et al., 2015; Kwon & Choi, 2016) systems were developed primarily for residential microgrid contexts. Hardware-centric research dominated, focusing on the development of safe, reliable, and cost-effective converters. Researchers introduced resonant converter topologies (e.g., CLLC converters (Zahid et al., 2015)) for bidirectional DC flow and investigated low-loss switching techniques.

These early studies were typically tested under ideal conditions and with fixed usage patterns. EV availability was modelled as constant and predictable, often based on simplistic assumptions such as "connected every night from 6 PM to 7 AM (Shams et al., 2019)". While valuable as proof of concept, these assumptions laid the foundation for what would later emerge as a significant limitation in V2G strategy design.

Phase 2. Diversification and Network Optimization: Around 2019, V2G research began shifting toward grid-level impacts and optimization. Recognizing the limitations of isolated microgrid designs, researchers explored the potential for distributed EV coordination using heuristic scheduling, linear programming, or game-theoretic models. At the same time, researchers started to examine economic performance, such as the net present value (NPV) of V2G participation under different market conditions (e.g. Strickland et al., 2019), especially in frequency regulation services (e.g., FFR and EFR in the UK).

	Short-Term Operating Reserve (STOR)	Firm Frequency Response (FFR)	Enhanced Frequency Response (EFR)
operating regime	06:00-13:00 & 16:30-20:30 weekday	activated by frequency change	adaptive to frequency
standard usage rate	around £100/MWh	—	—
standard availability (utilisation rate listed above)	around £5/MW/hr	around £150/hr (about 20MW)	around £9.50/MW/hr
Estimated revenue from 300 vehicles at 22 kW each	£267,000	£256,000	£323,000
Estimated revenue from 1000 vehicles at 22 kW each	£886,000	£850,000	£1,086,000
Estimated revenue from 3000 vehicles at 22 kW each	£2,670,000	£2,560,000	£3,326,000

Table 2-1. Estimated Revenue Generation Potential for EV Aggregators in STOR, FFR, and EFR Markets (Adapted from Strickland et al., 2019)

A growing number of studies (Bansal et al., 2020) proposed distributed control systems in which each EV or smart charger could independently respond to grid signals. These systems

offered high user autonomy but suffered from data fragmentation, poor scalability, and unpredictable system-level effects. Researchers (e.g. Manzolli et al., 2022) also started to consider stochastic elements in driving behaviour, though most models still assumed semi-regular charging schedules.

Phase 3. Behaviour-Aware, Data-Driven Management Models: The most recent phase of V2G research has seen the emergence of behaviour-aware and community-oriented strategies. Real-world data from smart meters, GPS-enabled EVs, and national travel surveys has enabled more sophisticated modelling of EV availability, charging flexibility, and idle time patterns. Studies have proposed the use of reinforcement learning, model predictive control (MPC), and agent-based simulations to handle real-time decision-making under uncertainty (e.g. Popolizio et al., 2025).

At the same time, the idea of managing V2G participation at the community level began to gain traction. Utilities in the UK, for example, have started to segment distribution zones by postcode or neighbourhood for local energy balancing and congestion management (Santos & Smith, 2023). Some academic proposals suggest that EVs within these zones could be aggregated into virtual energy storage units, with centralized control logic optimizing charge/discharge events based on real-time pricing and demand forecasts.

Yet, even in these forward-looking studies, a gap remains: while technical tools exist for centralized dispatch, there is a lack of system-level models that integrate EV behavioral heterogeneity, localized grid conditions, and standardized communication protocols into a deployable, scalable platform.

2.3.2. Geographic Variation and Standardization Barriers

V2G research also varies significantly by region. In Europe, the emphasis has been on AC-based slow charging systems integrated with home energy management systems (HEMS) (Semsar et al., 2020). Standardization efforts such as ISO 15118 (International Organization for Standardization, 2019) and IEC 61851 (International Electrotechnical Commission, 2017) have progressed steadily, enabling secure plug-and-play V2G communication in pilot projects across Europe and the UK.

In contrast, research in China and Japan has focused more heavily on high-power DC fast-charging systems and battery-swapping stations. The CHAdeMO standard (CHAdeMO Association, 2018), developed in Japan, was one of the first to support V2G functionality. Meanwhile, China's GB/T (Standardization Administration of China [SAC], 2015) and ChaoJi protocols aim to support ultra-high-voltage and high-current scenarios, with more emphasis on infrastructure throughput than on end-user coordination.

These regional disparities reflect divergent national energy priorities: European implementations integrate V2G systems within comprehensive smart grid frameworks with a focus on grid stabilization, while Asian deployments - particularly in China - emphasize large-scale transportation electrification and coordinated energy storage management. The absence of unified international standards continues to impede widespread technology adoption and hinders the development of cross-border interoperability solutions.

Standard Name	Major Applicable Region(s)	Scope	Features
IEC 61851 (International Electrotechnical Commission, 2017)	An international standard consistent with EU 61851 (European standard), extensively referenced or partially adopted by standards in other regions.	· Charging Modes · Control Pilot · Communication Infrastructure	· Defines charging modes (Mode 1–4) · Supports PWM-based low-level communication and ISO 15118 high-level communication

GB/T 18487 (Standardization Administration of China [SAC], 2015c)	China	· Electrical Parameters · Communication Mechanism · Safety Regulations	· Employs CAN bus as the communication protocol · Offers broad compatibility with various DC charging scenarios
CHAdeMO (CHAdeMO Association, 2018)	Japan	· Connector Structure · Charging Procedure · CAN Communication	· Defines rapid-charging DC supports, currently includes Toyota, Mitsubishi, Subaru and Nissan

Table 2-2. Comparative Summary of Key EV Conductive Charging System Standards across Different Regions.

Standard Name	Major Applicable Region(s)	Applicable Charging Type(s)	Connector / Interface Type	Communication Protocol
IEC 62196 (International Electrotechnical Commission, 2022)	International (primarily Europe)	AC + DC	Type 1 Type 2 Combo 1/2	PWM / PLC (ISO 15118)
SAE J1772 (Society of Automotive Engineers, 2017)	North America	Primarily AC-based, with basic DC communication support	Type 1 (5-pin)	PWM + Basic Communication
GB/T 20234 (Standardization Administration of China [SAC], 2015b)	China	AC + DC	Independent AC and DC connectors	CAN (GB/T 27930)
CHAdeMO (CHAdeMO Association, 2018)	Japan	DC	Dedicated DC connector	CAN bus

Table 2-3. Summary of Global Interface-Level Standards for EV Charging Systems (Part 1): Regional Application, Charging Type, Interface Design, and Communication Protocols

Note: This table is Part 1 of a two-part summary. It outlines the geographical coverage, supported charging types, physical connector/interface formats, and associated communication protocols of four major global standards.

Standard Name	Maximum Electrical Parameters	Features

IEC 62196 (International Electrotechnical Commission, 2022)	· AC (Type 2): Maximum 400V / 63A · DC (Combo): Up to 1000V / 500A+	Integrated AC+DC charging Supports PnC feature
SAE J1772 (Society of Automotive Engineers, 2017)	· Level 1: 120V (North American standard) · Level 2: 240V / ≤ 80A	Single-phase AC charging No DC fast charging support (requires pairing with CCS Combo 1)
GB/T 20234 (Standardization Administration of China [SAC], 2015b)	· AC：220V/380V，≤ 32A · DC: Up to 1000V / 600A (continuously expanding)	Separate AC/DC on vehicle side with different connectors Not compatible with Type 2, CCS, or CHAdeMO
CHAdeMO (CHAdeMO Association, 2018)	Up to 1000V / 400A (supports ultra-high speed charging)	Supports bidirectional charging (V2G) Not compatible with CCS connector design

Table 2-4. Summary of Global Interface-Level Standards for EV Charging Systems (Part 2): Electrical Specifications and Technical Features

Note: This table is Part 2 of the two-part summary. It complements Table 2.3. by comparing the maximum supported electrical parameters and highlighting notable technical features of each standard.

Standard Name	Major Applicable Region(s)	Intelligent Functions	Features
ISO 15118 (International Organization for Standardization, 2019)	International (primarily Europe)	· PnC · Supports high-level encrypted communication and authentication (TLS) · V2G	Mandatory support in Europe, but hardware/software implementation is complex, and communication setup time is relatively long
DIN Spec 70121 (CCS) (German Institute for Standardization [DIN], 2014)	International (primarily Europe & North America)	Includes only basic charging communication without encryption	Unidirectional communication standard
SAE J2847 & J2758 (Society of Automotive Engineers [SAE], 2019, Society of Automotive Engineers [SAE], 2018)	North America	Basic communication-oriented	Relatively easy to implement, but limited in high-level functionality

GB/T 27930 (Standardization Administration of China [SAC], 2015a)	China	Defines charger-to-vehicle message formats, handshake procedures, voltage/current parameters, and status codes	Offers stable performance and ease of implementation, supporting high power delivery and a wide voltage range, though the protocol lacks extensibility
CHAdeMO (CHAdeMO Association, 2018)	Japan	First to support bidirectional communication and V2G	Difficult to be compatible with other standards

Table 2-5. Summary of Communication-Layer Standards for EV Charging Systems Worldwide

Note: The information in these tables is compiled from the official documents of the listed standards.

2.3.3. Implications for This Study

The current literature demonstrates that while the technological feasibility of V2G is well established, practical, behaviour-aware, and scalable implementation models—particularly for centralized community-level management of idle EVs—remain scarce. Most research has prioritized either technical hardware (e.g. Zahid et al., 2015) or theoretical optimization (e.g. Ota et al., 2015), without sufficiently addressing how to operationalize these models in environments with irregular user behaviour, infrastructure limitations, and dynamic market conditions.

Existing literature underscores the importance of behavioural flexibility and adaptive dispatch logic in the design of effective V2G systems, yet there remains limited empirical consensus on the structural frameworks through which such systems should be coordinated. Building on this gap, the present study advances the hypothesis that reliable community-level V2G provision may additionally require some form of centralized aggregation framework. Furthermore, for such systems to be viable in practice, they must be aligned with evolving regulatory and standardization environments, particularly in contexts such as the UK where zonal energy planning is becoming increasingly institutionalized.

This thesis builds directly on these insights by proposing and evaluating a centralized V2G control scheme that dynamically utilizes idle EVs to enhance grid regulation efficiency in a community-scale system. The goal is not only to synthesize the technical components of V2G but to assemble them into a functionally cohesive, user-aware, and practically deployable system architecture.

2.4. Community Grid Systems and Real-World Deployments

The integration of large-scale renewable energy sources into the power system has fundamentally transformed the dynamics of load distribution and voltage regulation, especially at the community level (Santos & Smith, 2023). As renewable penetration increases, the challenges faced by regional distribution grids become more complex and less predictable. The traditional grid model—designed for one-way power flow from centralized generators to consumers—has been rendered inadequate by the bidirectional energy exchanges introduced by PV systems, wind farms, and increasingly, EVs with V2G capabilities (Quammi, 2021).

In this new environment, community-level grids—defined as urban or peri-urban network segments serving neighbourhoods, commercial districts, or transport hubs—play a pivotal role. They represent the interface between household and industrial demand, distributed generation assets, and the broader city or national grid (Shams et al., 2019). Yet, despite their importance, current grid-side V2G research and infrastructure planning have not adequately addressed the unique regulatory, technical, and operational challenges inherent to these zones. This section explores those challenges in depth and evaluates the limitations of existing strategies, particularly microgrid-based approaches, in supporting scalable, resilient, and efficient V2G operations within community-level energy systems.

2.4.1. Community-Level Grid Case Studies and Performance

Consistent with the “S-G-L-S” architectural framework introduced earlier for community-level energy systems, most real-world community grid deployments follow a similar structural paradigm. In these systems, distributed energy sources, local grid infrastructure, controllable loads, and energy storage components are integrated within a coordinated operational framework. Empirical studies have demonstrated that such architectures can achieve favourable performance in terms of supply reliability, operational flexibility, and energy sustainability. A representative example is provided by Odetoye et al. (2023), who conducted a multi-year techno-economic and operational assessment of a community-scale microgrid in Nigeria. The studied system integrates solar photovoltaic generation, wind turbines, battery storage, and diesel backup generation, forming a hybrid community energy system capable of supporting local electricity demand. The microgrid supplies a community with an average load of approximately 975 kW and a daily electricity demand of around 23.028 MWh. Their optimisation results indicate that a renewable-dominant configuration combining photovoltaic generation, concentrated solar power, and small hydropower can significantly improve long-term system performance. In particular, the renewable microgrid achieved a levelized cost of electricity (LCOE) of approximately \$0.26 kWh^{-1}, compared with \$1.01 kWh^{-1} for a diesel-based supply system, while the net present cost (NPC) was reduced from \$408 million to \$55.7 million over a 25-year planning horizon. Furthermore, the system was estimated to reduce annual carbon emissions by approximately 7,540 metric tons, demonstrating the potential of coordinated local generation and storage to improve both environmental performance and supply reliability in regions with limited grid infrastructure.

Further insights into the operational characteristics of community grids are provided by Cornélusse et al. (2018), who examined a community microgrid in Belgium. Their work explored the integration of a local energy market within a community grid architecture,

enabling electricity generated within the community to be exchanged through peer-to-peer (P2P) energy trading mechanisms. The proposed framework employs a community microgrid operator that coordinates energy exchanges among participating users while optimizing overall system welfare. Numerical results based on real distribution network data show that coordinated community-level energy trading can substantially improve resource allocation efficiency. In the examined case, the introduction of an internal community market resulted in approximately 54% annual cost savings for the participating users, while also reducing peak demand on the external distribution network. These findings demonstrate that coordinated community energy management can enhance both economic efficiency and grid operational stability by reducing unnecessary energy imports and improving the utilization of locally generated renewable electricity.

Another notable example is the NEOM community energy system case study presented by Alharbi et al. (2025), which investigates the feasibility of a fully renewable community grid. In this study, several hybrid renewable configurations were evaluated using HOMER-based techno-economic modelling for an industrial community in NEOM, Saudi Arabia. The results indicate that a PV-battery configuration achieves a levelized cost of electricity of approximately \$0.112 kWh^{-1} with a net present cost of about \$2.42 million, while a PV–wind–battery hybrid system reduces the LCOE to approximately \$0.0968 kWh^{-1} with an NPC of around \$2.11 million. In addition to economic competitiveness, the study demonstrates that integrating renewable generation with distributed storage resources enables the community grid to achieve zero operational carbon emissions while maintaining stable power supply under varying renewable resource conditions.

These real-world cases illustrate that community-level grid systems built upon coordinated architectures such as the S-G-L-S framework can achieve a balanced performance across reliability, sustainability, and operational efficiency. When compared with conventional power

systems, the advantages of such community-based energy systems become more apparent. Traditional centralized grid systems are typically dominated by large-scale fossil-fuel generation. While this configuration has historically ensured high levels of supply stability and dispatch controllability, it generally exhibits low renewable energy penetration and remains vulnerable to fluctuations in fossil fuel prices and carbon-related regulatory pressures. In contrast, conventional grid systems with substantial renewable integration significantly increase the share of renewable generation but introduce new operational challenges. The intermittent and stochastic nature of renewable resources—such as solar irradiance variability and wind fluctuations—can lead to greater uncertainty in power balancing and grid stability, particularly when renewable penetration becomes high. Moreover, integrating large-scale renewable energy often requires extensive transmission infrastructure upgrades and additional balancing resources, which can increase overall system costs and operational complexity. Community-level grid systems offer an intermediate and potentially more resilient approach. By integrating localized renewable generation, distributed storage, and controllable loads within a coordinated community-scale network, these systems can mitigate renewable intermittency through local balancing mechanisms. Energy storage and demand-side flexibility help stabilize short-term fluctuations, while the localized management of distributed resources reduces transmission losses and enhances system responsiveness. As a result, community grid architectures are increasingly viewed as a promising pathway for achieving high renewable penetration while maintaining grid reliability and operational efficiency.

2.4.2. Grid-Side V2G Challenges at the Community Level

At the core of the grid-side challenge is the growing temporal asynchrony between generation and consumption. Renewable energy output is inherently variable: solar PV generation peaks around midday, while electricity demand typically peaks in the late afternoon or early evening. This mismatch, once mitigated by fossil fuel–based spinning reserves, now requires more

dynamic and localized balancing solutions (Amertet & Gebresenbet, 2024; Huda et al., 2020). Community-level grids are increasingly called upon to absorb generation peaks or meet demand spikes without relying solely on upstream transmission-level intervention.

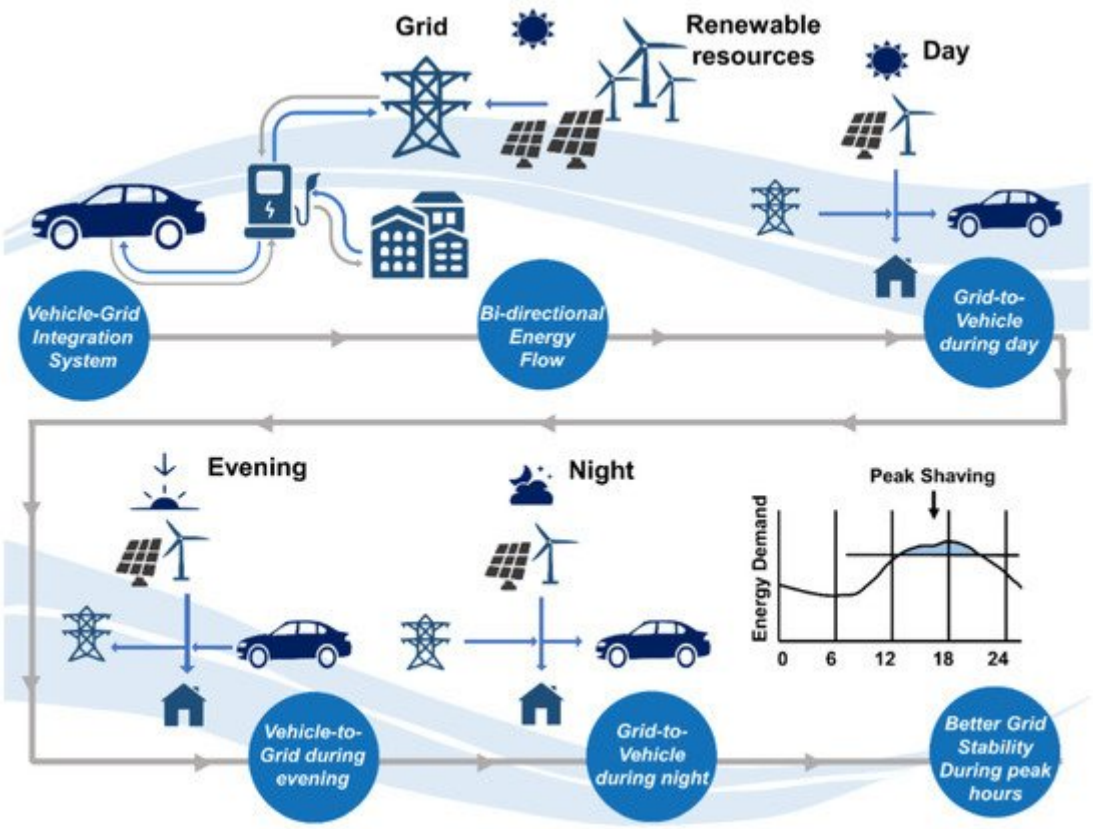


Figure 2-3. Schematic Representation of Community-Level V2G Integration and Associated Grid-Side Constraints (Saeed, 2022)

Note: This diagram outlines a typical setup for V2G systems within a community microgrid, highlighting bidirectional power exchange between electric vehicles and the distribution network. It also reflects key operational challenges such as communication latency, grid congestion, coordination complexity, and system capacity limits.

However, localized balancing is not just a matter of installing batteries. It requires real-time awareness of load dynamics, generation profiles, and flexible storage resources such as idle EVs. The problem is compounded by the non-linear, non-stationary behaviour of modern urban energy consumption (Logan et al., 2020), which includes demand-side phenomena such as heat

pumps, fast chargers, and intelligent appliances—all of which create unpredictable load profiles at the distribution level.

EVs, as mobile and user-controlled devices, offer theoretical flexibility to absorb and dispatch energy as needed (Ahmadian et al., 2018). But leveraging that flexibility in practice is non-trivial. It requires a control system that can dynamically aggregate EVs with highly heterogeneous behaviour—different SOC, arrival/departure times, mobility constraints—and coordinate their participation in a way that aligns with grid needs, not just individual convenience.

Limitations of Microgrid-Based V2G Deployment

A substantial portion of early V2G research has assumed the viability of microgrid-based integration as the primary architecture for implementation. Microgrids—localized energy systems composed of distributed generation, energy storage, and controllable loads—are typically configured to operate autonomously or semi-autonomously, often with fixed EV participation schedules and known load profiles (Quammi, 2021; Shams et al., 2019). This model is useful for small-scale or off-grid scenarios, and it provides a testbed for control algorithms, communication protocols, and battery degradation studies.

However, at the community scale, the microgrid paradigm proves increasingly inadequate for enabling scalable and coordinated V2G deployment. A range of structural limitations hinder its effectiveness in complex urban environments. When multiple microgrids operate in parallel within a shared distribution network, their localized and autonomous control strategies often result in conflicting decisions, redundant regulation actions, and suboptimal allocation of energy resources (Mendes et al., 2016). Figure 2-4 illustrates a typical distributed control architecture adopted in many microgrid systems. Within such architectures, energy management and data exchange are primarily handled at the individual microgrid level, where

local controllers independently manage energy dispatch, charging coordination, and load balancing. As the number of interconnected subsystems grows, the internal control logic and data interactions become increasingly complex, which may lead to overlapping control actions or inconsistent operational decisions across neighbouring microgrids. In the absence of an overarching coordination mechanism, such independently operated systems may achieve local efficiency while undermining broader system-wide objectives.

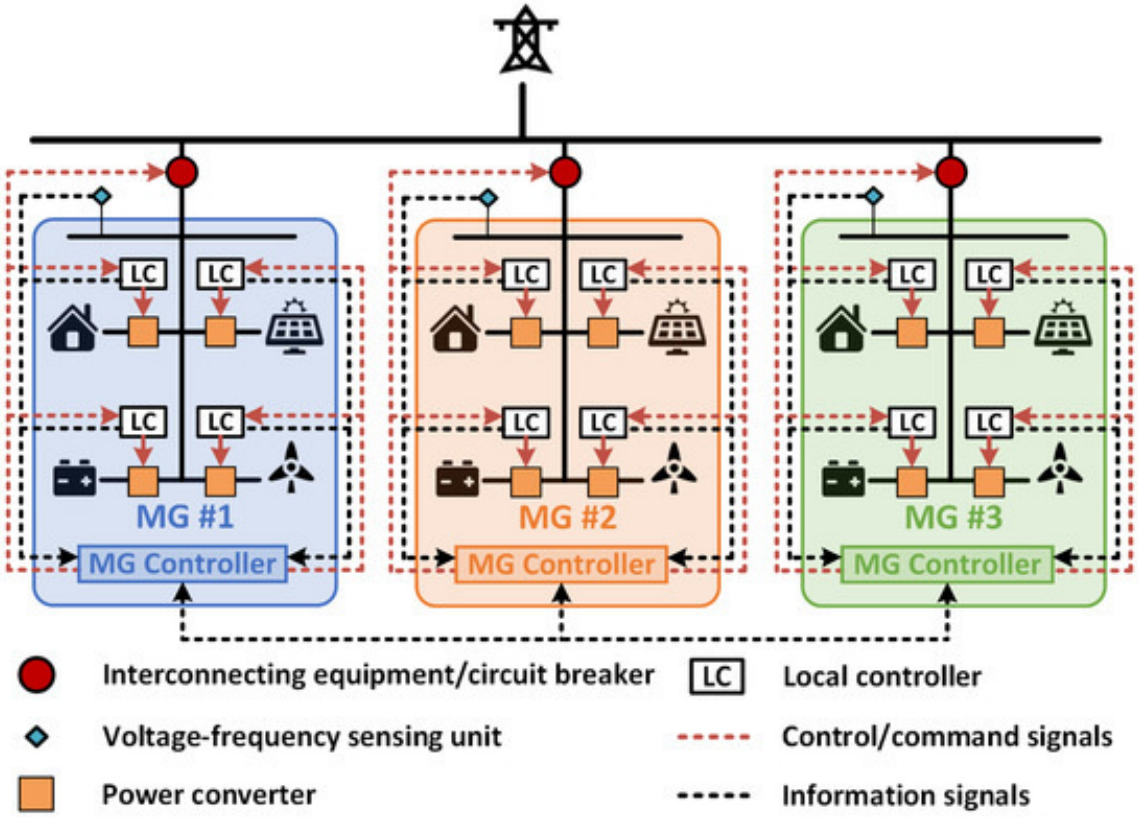


Figure 2-4. Typical distributed control architecture of multiple microgrids operating within a shared distribution network. (Saha et.al., 2023)

Moreover, the scalability of microgrid-based V2G models is constrained by their reliance on high-bandwidth communication and localized computational resources. As the number of participating electric vehicles increases, the communication load and data processing requirements can grow rapidly, particularly in designs that depend on frequent polling or synchronous updates. Another critical issue lies in the fragmentation of operational data.

Typically, SOC values, vehicle availability, and usage profiles are confined within local microgrid controllers, limiting the potential for global optimization or integration with upstream services such as frequency regulation or spinning reserve support. Furthermore, while microgrids are generally capable of buffering small-scale fluctuations, they lack the dynamic flexibility required to manage the broader variability introduced by high-penetration renewables across an entire community. In this context, microgrid-based V2G systems cannot respond effectively to large-scale solar and wind volatility without interconnection and systemic coordination (Alam et al., 2016). Consequently, while microgrids remain relevant for specific or isolated applications, these limitations underscore the necessity of a centralized coordination architecture—one capable of orchestrating the behaviour of distributed EVs, buildings, and energy resources across the entire community—to unlock the full potential of V2G services at scale.

The rapid proliferation of EVs, distributed renewable energy sources, and dynamic demand-side technologies has placed increasing stress on both the physical and digital infrastructures of community-level power grids. Uncoordinated charging and discharging behaviours by EVs can cause significant voltage fluctuations—particularly in low-voltage distribution feeders, where line impedance and transformer capacity tend to be unevenly distributed (Gamit et al., 2019). Furthermore, during periods of high PV output and low local demand, V2G operations without appropriate control mechanisms can exacerbate reverse power flows into upstream networks. This increases the risk of equipment malfunction and may lead to violations of regulatory limits (Ota et al., 2015). Simultaneous discharging by multiple EVs within the same neighbourhood—especially when it overlaps with conventional system peak hours—can also overwhelm substations and feeder lines, pushing them beyond their design capacity. These physical stressors are compounded by a significant lack of grid visibility. Traditional Supervisory Control and Data Acquisition (SCADA) systems were not designed to track the

real-time, granular behaviour of a geographically dispersed and highly mobile fleet of energy storage units (Ebrahimi et al., 2023). In the absence of timely information—such as SOC, spatial distribution, and user intentions—grid operators are effectively unable to leverage the inherent flexibility of EVs for system-level optimization. Taken together, these challenges underscore the inadequacy of current grid management paradigms in addressing the dynamic, high-resolution demands introduced by V2G technologies at the community level. To transform V2G from a source of disruption into a stabilizing force within the grid, the development of new data architectures, control protocols, and operational strategies is urgently needed.

Limitations of Current Literature

While several studies (e.g. Bai & Qiao, 2015) acknowledge the need for centralized control and community-level integration, few provide actionable frameworks or validated architectures. For instance, many proposals (e.g. Quammi, 2021) lack real-world implementation data and instead rely on simplified simulation environments. Others fail to integrate user behaviour in a meaningful way, assuming fixed vehicle availability or uniform participation rates.

Moreover, current economic models (e.g. Li et al., 2020) often ignore grid-side technical constraints such as line capacity, voltage deviation, or transformer aging, leading to overestimation of potential benefits. Similarly, few papers (e.g. Hu et al., 2022) account for the overhead of real-time communication, data processing, or security requirements.

Thus, despite significant progress in individual technical components—such as hardware design, optimization algorithms, or encryption protocols—there remains a critical gap in system-level design that bridges these components into a cohesive, scalable, and deployable community V2G solution.

2.5. Bidirectional Charging Interaction in V2G system

2.5.1. Foundational Studies in Bidirectional Charging Technologies

Bidirectional charging has emerged as a major area of focus in the V2G research landscape, constituting over 40% of publications across multiple years. A substantial portion of this literature centres on the development of advanced power converters and the corresponding communication mechanisms that regulate energy and data exchange between EVs and charging infrastructure. However, disparities in charging standards and device specifications across different regions have resulted in significant limitations to the scalability and transferability of these technological advancements.

From a temporal perspective, research outputs in this domain are heavily influenced by contemporaneous hardware capabilities and tend to be tailored to specific regional contexts. For instance, Zahid et al. (2015) introduced a 3.5-kW DC-DC resonant converter optimized for CLLC topologies—representing a common output benchmark for bidirectional V2G systems at that time. In contrast, Zhu et al. (2023) revisited the same CLLC framework and identified the emergence of substantial double line frequency (DLF) current harmonics when deployed under varying power loads, leading to higher energy losses and operational instability. This illustrates how hardware designs that were once considered state-of-the-art may face critical limitations under evolving grid conditions.

Within the power transmission domain, circuit design and interconnection technologies represent the most intensively studied subcategory—accounting for more than half of the research on bidirectional charging. Typical EV charging systems generally adopt a multi-stage power conversion architecture to interface the grid and the battery system. Figure 2-5 illustrates representative converter layouts used in onboard EV chargers, including the conventional two-stage configuration and alternative single-stage designs. Key contributions in this area include

the development of converters, controllers, inverters, and charging modules. These components facilitate core functions such as dynamic power adjustment (Debbarma & Shrivastwa, 2019), control of asymmetrical bidirectional energy flows (Luo et al., 2022), and support for both AC-DC and DC-DC resonant transformations (Liu et al., 2018; Semsar et al., 2020). Notably, the specific design directions often reflect the interaction between local grid topology and market demands. For example, earlier studies largely relied on two-stage AC-DC and DC-DC converter architectures for V2G-compatible charging systems, whereas more recent research has explored advanced DC-DC and multi-port converter designs capable of supporting high-variance and asymmetrical power exchange scenarios. This transition marks a clear evolution in design philosophy aligned with technological and market developments.

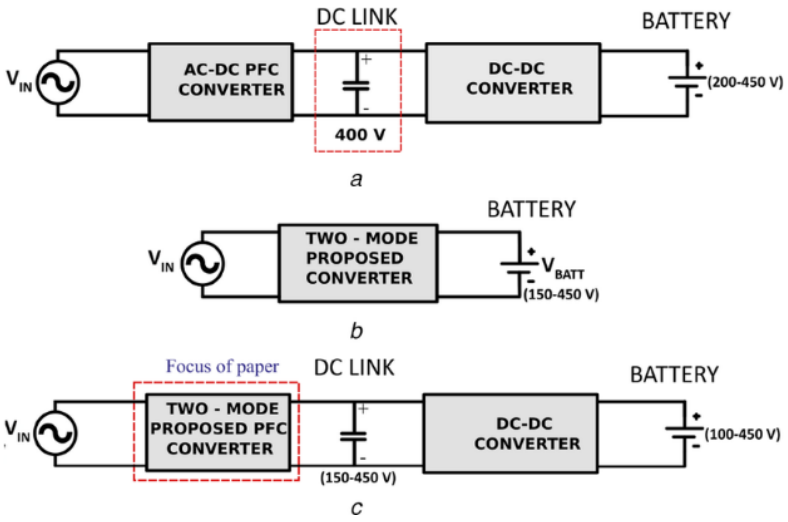


Figure 2-5. Typical power conversion architectures of onboard EV chargers used in V2G systems. (Venkata & Williamson, 2020)

Note: This schematic shows a two-stage bidirectional converter enabling both active charging/discharging and reactive power compensation in V2G operations.

Parallel to hardware advancements, the reliability and security of communication protocols has become the second most frequently addressed issue in bidirectional V2G systems. This research stream—closely linked to progress in hardware interfaces—has concentrated on four

primary areas: optimization of data routing, security enhancement, long-term data management, and compatibility with international standards. Early-stage solutions (e.g., Ming et al., 2017) predominantly relied on cloud-based infrastructures for communication and data storage. However, as bidirectional V2G systems became more complex and exposed to cybersecurity risks, researchers began transitioning toward decentralized models. Recent studies (e.g., Aggarwal et al., 2021; Hassija et al., 2020; Luo et al., 2022) increasingly adopt multi-layer blockchain architectures as alternatives to conventional cloud services. This shift is driven largely by concerns over single points of failure and the growing need for secure, tamper-proof data exchanges in V2G environments.

Over the past decade, approximately 85% of the most cited contributions to V2G communication protocol research have incorporated privacy-preserving technologies. Innovations in this field span a variety of cryptographic techniques, including homomorphic encryption for secure energy transaction processing (Sharma & Jain, 2023), polymorphic signatures for adaptive access control (Bansal et al., 2020), and anonymity-preserving communication frameworks built on Tor protocols (Li et al., 2018).

Despite this technical progress, the formulation of unified international standards has lagged behind, hindered by the fragmented nature of competing solutions and the rapid pace of protocol evolution. ISO 15118 (International Organization for Standardization, 2019), a well-known attempt at standardization, enables secure plug-and-charge interactions through a Public Key Infrastructure (PKI) and digital certificate authentication. However, concerns regarding its reliance on conventional public-key cryptography have intensified, particularly in light of potential threats posed by advances in quantum computing.

Among the reviewed literature, only a limited number of studies (e.g., J. Park et al., 2019; Kester et al., 2019) explicitly address ISO 15118, proposing enhancements to its authentication

mechanisms and context-specific adaptations. To address limitations in traditional cryptographic models, several alternative approaches have recently been proposed. For instance, Chen et al. (2024) developed a cyber-physical co-authentication mechanism for Plug-and-Charge (PnC) environments, utilizing smart contracts to guarantee transaction integrity, user anonymity, and resistance to man-in-the-middle attacks. For resource-constrained EV platforms, Xiao et al. (2025) introduced a lightweight authentication scheme combining Chebyshev chaotic maps with hash-based verification, achieving significant reductions in communication overhead and robust resistance to impersonation. To mitigate risks related to hardware-level attacks, Kaveh et al. (2020) proposed an authentication protocol based on Physically Unclonable Functions (PUFs), which enhances resistance to tampering and reduces resource consumption by over 50% compared to traditional models. Looking toward post-quantum security, Prateek et al. (2024) introduced the QSKA protocol—a superdense coding-based quantum communication framework. Formally verified using the Coq proof assistant, QSKA offers unconditional security and represents a promising candidate for replacing classical cryptographic methods in next-generation V2G systems.

2.5.2. Data and Coordination Challenges

The reviewed research indicates that in centralized V2G applications, beyond the necessity for standardized hardware parameters to ensure compatibility and prevent electrical conflicts within the system, greater challenges arise from data exchange and communication coordination. A key barrier arises from the heterogeneity of EVs and charging infrastructure, which are produced by diverse manufacturers operating with proprietary software ecosystems. In the absence of standardized application programming interfaces (APIs) or universally interoperable communication protocols, achieving seamless, real-time coordination across devices becomes technically infeasible. While emerging standards such as ISO 15118 (International Organization for Standardization, 2019) partially address this issue—enabling

functions like Plug-and-Charge and encrypted communication—support remains inconsistent across vendors and regions (Chen et al., 2024).

Compounding this interoperability gap is the problem of latency in data acquisition and command execution. In order to dispatch thousands of EVs within operational timeframes suitable for ancillary services such as frequency regulation (typically on the order of 5 to 10 minutes (Bansal et al., 2020)), control systems must be resilient to communication delays, asynchronous node behaviour, and intermittent data availability. The failure to address these temporal challenges can significantly degrade system responsiveness and compromise service delivery.

Simultaneously, the integration of vehicle-level data into centralized grid platforms raises pressing concerns around privacy and cybersecurity. Real-time coordination often requires access to sensitive user information—such as vehicle location, trip schedules, and charging habits—which, if not properly protected, can expose users to surveillance risks or data misuse. Without robust privacy-preserving mechanisms, such as federated learning frameworks or secure multiparty computation techniques, user trust in centralized V2G schemes may be severely undermined.

Moreover, centralized control introduces jurisdictional ambiguity, particularly in regulatory environments like the United Kingdom, where community energy zones may span multiple distribution network operator (DNO) territories (Strickland, 2019). In such contexts, questions of data sovereignty, control authority, and legal compliance become nontrivial, posing institutional barriers to cross-zone V2G aggregation and shared dispatch governance (Aggarwal et al., 2021). These interrelated challenges highlight the need for a new generation of communication architectures and policy frameworks that support secure, low-latency, and interoperable V2G coordination at the community scale.

In light of the multifaceted challenges outlined above, transitioning from fragmented, microgrid-based architectures to a centralized, community-oriented V2G management framework emerges not simply as a matter of scale, but as a functional imperative. A robust centralized system would enable the aggregation of idle EVs across spatially defined zones—such as postal districts or DNO service areas—into coherent, dispatchable virtual storage assets (Bai & Qiao, 2015). Such a framework would rely on statistical inference or machine learning models trained on real-world behavioural data to monitor and forecast EV availability, user charging preferences, and anticipated departure times, thereby allowing energy events to be scheduled with both grid requirements and user constraints in mind.

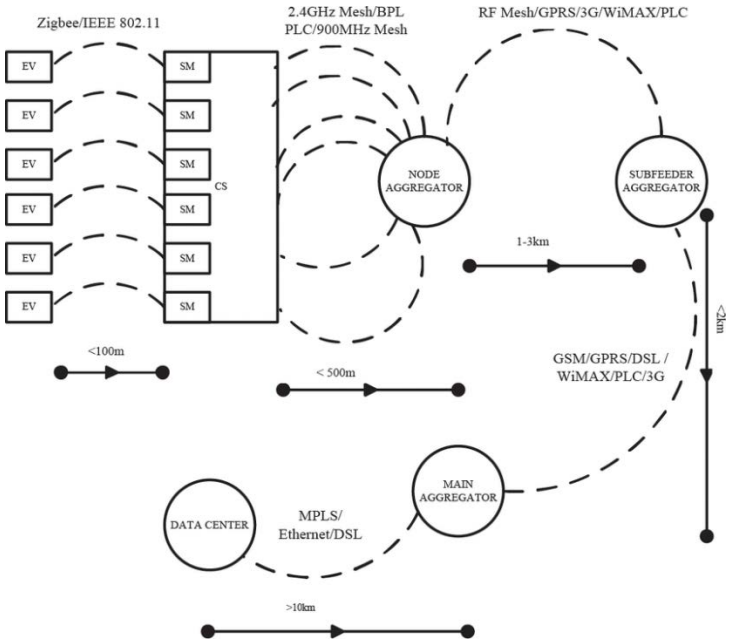


Figure 2-6. Centralized V2G Communication Structure Illustrating Interoperability and Data Flow Challenges (Inala, Bose, & Kumar, 2019)

Note. The illustration shows a central aggregator coordinating charging and discharging across a diverse network of EVs and charging infrastructure. It emphasizes typical technical bottlenecks such as protocol fragmentation, delayed command execution, and potential exposure of user-specific operational data.

Crucially, centralized control would also enable integration with distribution network operators and wholesale electricity markets, facilitating the delivery of ancillary services such as

frequency regulation, voltage support, and peak load management. This interface would allow idle EV capacity to be monetized within market structures, transforming latent flexibility into a tradable grid service (Chandra et al, 2019). To function at scale, the system must also support secure and privacy-compliant communication across a heterogeneous ecosystem of vehicles and chargers, each potentially operating under distinct protocols and ownership regimes (Bansal et al., 2020; Ebrahimi & Rastegar, 2023).

By unifying these capabilities, a centralized V2G platform could relieve stress on local infrastructure while generating new economic value for both users and system operators. Through predictable, contract-based participation schemes, such systems could transition V2G from a largely experimental technology into a standardized and scalable mechanism for grid balancing—anchored in both technical feasibility and economic rationality.

2.6. EV-Side Issues: EV Usage Patterns

The viability of V2G systems, particularly at the community scale, is fundamentally dependent on the availability of EVs for energy dispatch (Ahmadian et al., 2018; Shang et al., 2023). While the technical capacity of modern EV batteries makes them suitable for grid support, the actual extent to which EVs can participate in V2G operations is determined by when, where, and for how long they are idle—and crucially, whether they are connected to a charger during those idle periods (Mokhtar et al., 2022). As such, EV idle time, connectivity, and user charging behaviour form the core parameters of system availability on the vehicle side.

Unfortunately, much of the V2G literature to date has either oversimplified or overlooked the complexity of EV behavioural dynamics. Models (e.g. Mozafar et al., 2018) often treat availability as deterministic or assume fixed participation windows. While these assumptions may hold for tightly controlled experimental settings or corporate fleets, they do not reflect real-world behaviour, particularly among private vehicle owners operating in diverse urban

environments. This section explores the structural and behavioural uncertainties that affect EV availability for V2G, reviews how existing research has attempted to model these factors, and identifies gaps that must be addressed for centralized community-level V2G systems to function effectively.

A frequently cited statistic in the V2G literature is that private vehicles remain idle for over 90% of the day (Rachid et al., 2023). While this figure is broadly accurate in temporal terms, its practical relevance is often overstated or misinterpreted. Crucially, vehicle idleness does not equate to V2G availability: a parked EV is not necessarily connected to a charger, nor is its battery guaranteed to be within a SOC range appropriate for discharging. For grid operators and system designers, the metric of real importance is connectable idle time—the specific intervals during which an EV is not only stationary but also plugged in and technically available for grid dispatch, subject to system and user constraints.

Attempts to quantify this more operationally meaningful metric have drawn on a variety of data sources, including national travel surveys, GPS-tracked mobility logs, and charging infrastructure usage statistics. A notable UK-based study conducted in 2022 using Department for Transport (DfT) household travel survey data found that although vehicles were typically stationary for over 22 hours per day, the average charger connection duration ranged only from 1.5 to 2.3 hours (Electric Vehicle Charging Research Survey with Electric Vehicle Drivers - Research report, April 2022). This large discrepancy highlights a substantial window of “idle-but-unplugged” time, which remains inaccessible to current V2G systems unless user behaviour shifts or enabling technologies—such as robotic or automated charging systems—are adopted to bridge the availability gap.

Furthermore, the temporal distribution of idle and connectable time varies widely across user demographics and driving patterns. For instance, individuals with fixed commuting schedules

tend to exhibit predictable idle windows at residential and workplace locations, which can be effectively integrated into V2G scheduling frameworks (Dagdougui, 2019). In contrast, EVs operating under more dynamic conditions—such as fleet vehicles in commercial districts or large transport vehicles servicing variable routes—tend to follow highly fragmented and non-repetitive patterns of movement (Manzolli et al., 2022; Shirazi et al., 2015). Despite this variability, many existing V2G system designs rely on fleet-level average assumptions, thereby overlooking the behavioural heterogeneity that directly impacts dispatch reliability and system efficiency. Addressing this gap necessitates more granular, user-specific modelling approaches that can accommodate the full spectrum of real-world vehicle usage patterns.

Even among users with relatively stable mobility patterns, charging behavior does not necessarily correlate with idle periods. Statistical results reported by UK Department for Business, Energy & Industrial Strategy (Electric Vehicle Smart Charging Action Plan - Affordable, Sustainable Power for Electric Vehicles, January 2023) has shown that EV owners often charge based on perceived need rather than fixed routine. A significant proportion of users do not plug in every night, and many prefer to charge during daytime hours—particularly in regions with time-of-use tariffs or home PV installations (Alam et al., 2016).

Furthermore, “range anxiety” and concerns about battery degradation influence user decisions around discharging (Strickland et al., 2019). Unless users are confident that participating in V2G events will not compromise their ability to complete the next journey, they may refuse to opt in—even if technically available. This introduces a psychological and informational layer of uncertainty into system-level planning.

From a control systems perspective, this variability presents a fundamental challenge: although battery capacity is physically available, its functional availability is governed by user-perceived utility—an attribute that is neither constant nor entirely rational (Sovacool et al., 2020).

Common deterministic scheduling models (e.g., Modarresi et al., 2019) struggle under these conditions, often resulting in errors in capacity planning and dispatch strategies.

A critical limitation of current V2G management strategies lies in the behavioural modelling of EV users, which often lacks the robustness and adaptability necessary for large-scale deployment. One major concern is the limited generalizability of these models across diverse geographic and socio-economic contexts. Behavioural patterns observed in one region—shaped by local cultural norms, regulatory frameworks, and infrastructure availability—may not be applicable elsewhere. As a result, models trained on region-specific datasets often fail to perform reliably when applied to different settings. For example, all five studies summarized in Table 2.6 optimize V2G management by analysing EV user behaviour, and each demonstrates the economic feasibility and benefits of V2G integration. However, because these studies rely on localized data, their results differ significantly in terms of economic performance. This variability highlights a key issue: the lack of universally applicable evidence to support V2G's economic viability.

No.	Annual Average V2G Revenue	Battery Degradation Cost	Net Present Value (NPV)	Summary
A1(Shirazi et al., 2015)	$14,400	$700 per unit	$24,200 per unit	Limited economic viability of V2G for bus fleets
A2(Gough et al., 2017)	£840	Significant impact on NPV, specific value not provided	£8,400	Economically viable in commercial building scenarios
A3(Koubaa et al., 2021)	€ 29.90	€ 4.46	Not Provided	Significantly reduces operational costs
A4(Steffen et al., 2020)	£1,245.60	£38.62	Not Provided	Considerable economic returns
A5(Popolizio et al., 2025)	€ 3,046.81	Increase 1.96%	Not Provided	High returns achievable through optimized management

Table 2-6. Economic Performance Metrics in V2G Studies: Annual Revenue, Battery Degradation Cost, and NPV from 5 Representative Papers

Furthermore, many existing models (e.g., Ma et al., 2019) operate at relatively low temporal resolution, typically employing hourly or half-hourly time steps. While this level of granularity may suffice for long-term planning or aggregated load forecasting, it is insufficient for real-time grid services that require minute-level responsiveness—particularly in applications such as frequency regulation or contingency support.

To effectively address the limitations outlined above, a centralized V2G coordination system must embed behaviour-aware intelligence capable of capturing user heterogeneity across spatial, temporal, and contextual dimensions. Such a system should not only accommodate variation in individual usage patterns but also evolve dynamically by integrating real-time data streams, refining behavioural profiles, and continuously adapting dispatch strategies in response to both user feedback and grid conditions. As emphasized by Zecchino et al. (2019) in their analysis of V2G and EV responsiveness within complex centralized environments, forecasting modules within this framework must be designed with high temporal resolution and supported by adaptive learning algorithms. This ensures that the system can respond effectively to rapid changes in demand, availability, and grid signals, maintaining stability and maximizing flexibility in real-time operations.

These challenges are further amplified when V2G coordination is scaled to the community level. Unlike fleet-based V2G applications—where vehicles are operated under centralized control and exhibit standardized, predictable usage patterns—community systems must engage with a diverse population of privately owned EVs, each with its own mobility routines, charging preferences, and technological configurations. In such decentralized environments, behavioural uncertainty becomes a dominant constraint on system reliability and responsiveness.

Existing microgrid-oriented models (e.g. Rao et al., 2021), which typically assume homogeneous participation and static charging behaviour within localized zones, are ill-equipped to capture the spatial and temporal variability inherent in real-world community dynamics. As a consequence, they tend to overestimate the aggregate flexibility available from idle EVs while underestimating the operational complexity involved in managing distributed, behaviourally diverse resources. Overcoming these limitations requires a paradigm shift toward system architectures that treat user heterogeneity not as noise to be averaged out, but as a core input to real-time control logic.

2.7. V2G Management Strategy

Distinct from research on the grid-side, which primarily focuses on the design and coordination of various grid devices, studies on V2G management strategies concentrate on integrating EVs into the grid as flexible energy storage resources through dedicated V2G control logic. These strategies simultaneously account for both grid-side and EV-side requirements, enabling coordinated regulation of local loads to achieve specific objectives, such as balancing power distribution across the grid or optimizing overall system-level economic performance.

From the perspective of operational scope, V2G management strategies and their control logic can be classified according to the scale of the serviced grid, the characteristics of the grid load, and the size of the EV fleet being managed. The main categories include centralized V2G management, distributed V2G management, microgrid-based V2G management, and battery-pack-based V2G management, also referred to as battery-swapping station V2G management. These distinct operational modes provide a structured framework for researchers to design refined EV dispatch and control logic, tailored to the capabilities and constraints of each architecture.

Building on these foundational frameworks, researchers have developed various control algorithms adapted to the contemporary hardware capabilities and prevailing operational modes. Early V2G management strategies, exemplified by Sun (2013), employed a simple hierarchical structure from grid operator to V2G aggregator to EV fleet, implementing a real-time Welfare-Maximizing Regulation Allocation (WMRA) algorithm. This framework achieved solutions within O(1/V) of the theoretical optimum while outperforming greedy scheduling approaches. However, such simple architectures lacked consideration for multi-layer grid coordination, relied on centralized communication infrastructure, and raised privacy and data collection concerns. Peng (2017) extended this approach by developing an optimal dispatch strategy for V2G aggregators participating in supplementary frequency regulation. Their work more explicitly incorporated EV-side constraints, such as state-of-charge limits and driving demand, effectively integrating user requirements with grid services and enabling participation in ancillary service markets. Nevertheless, this strategy depended on accurate EV mobility predictions, and computational complexity scaled with fleet size. While Peng (2017) primarily approached the problem from the perspective of EV user requirements, other studies have emphasized market-oriented considerations. For example, Lotfi (2024) proposed a market-based V2G optimization approach, integrating electricity market mechanisms to guide EV dispatch for regulation and spinning reserve services. While effective in economic optimization, this approach was heavily dependent on volatile market prices, which introduced considerable uncertainty.

Beyond these relatively linear hierarchical frameworks, subsequent studies have explored microgrid-integrated V2G management architectures aimed at strengthening interactions between V2G systems and local grid structures. For instance, Iqbal (2020) implemented a hierarchical control scheme within an industrial microgrid, enabling bidirectional energy flows and local control to improve grid stability while reducing disturbances to the main network.

Although this strategy enhances local reliability, its scalability beyond the microgrid boundary remains limited and requires advanced microgrid control infrastructure. Building on this, Zhang (2023) investigated large-scale EV scheduling that incorporates reactive power management to support voltage regulation and broader grid power control. While effective for larger-scale systems, these approaches demand sophisticated communication networks and significant computational resources for real-time operation.

With the advancement of computational power and artificial intelligence, contemporary V2G management strategies increasingly employ deep reinforcement learning (DRL). The enhanced computational capacity available in modern systems enables the implementation of previously proposed complex control logics that were once constrained by computational limitations. In this context, Zhang (2022) and Zhang (2023) developed DRL-based multi-stakeholder hierarchical coordination frameworks that simultaneously consider the grid, aggregators, and EV users. These approaches improve system-level optimization, enable truly flexible integration of EV fleets into grid operations, and allow fast, proactive responses rather than reactive adjustments.

Despite the significant improvements achieved across multiple dimensions—including differing optimization objectives (such as EV user-oriented versus market-oriented strategies), enhanced interaction architectures between V2G systems and power grids, and improved prediction accuracy enabled by large-scale computation and deep learning—three key challenges remain in V2G management research. First, EV availability uncertainty, driven by the mobility of vehicles, complicates scheduling. Second, communication scalability issues arise as large fleets require extensive data exchange. Third, most studies focus on the hierarchical chain from grid operator to aggregator to EV fleet, rather than encompassing community-level grids with distributed generation and local loads, highlighting the research gap addressed in this thesis.

2.8. Economic and Policy Considerations

A substantial body of literature has explored diverse economic strategies aimed at unlocking the financial value of V2G, each varying in their degree of market integration, approaches to risk mitigation, and the design of stakeholder incentives. By systematically comparing these strategies across recent studies, a more nuanced understanding emerges of how V2G systems can be architected to balance economic profitability with technological feasibility and sustained user participation. Particularly within integrated grid systems, where V2G must interact with a complex ecosystem of generation, transmission, and distributed assets, the ability to optimize economic performance holistically becomes critical. In such contexts, well-designed V2G frameworks are not only expected to provide ancillary services or peak shaving benefits, but also to enhance overall grid efficiency and resilience while aligning with broader market structures and regulatory regimes.

A central distinction in economic strategy lies between aggregator-led auction-based models and infrastructure-centric optimization frameworks. Zeng et al. (2020) propose an incentivized group-selling auction mechanism that enables EV users to collectively participate in demand response events, managed through a Vickrey-Clarke-Groves (VCG) auction scheme. This model capitalizes on user participation and game-theoretic pricing to ensure truth-telling and efficient resource allocation, positioning aggregators as market facilitators that reduce transaction costs and optimize price discovery. In contrast, Shirazi et al. (2015) and Noel and McCormack (2014) offer cost-benefit analyses cantered on school bus fleets, examining the NPV of deploying alternatively fuelled buses integrated with V2G capabilities. Their results reveal that large-scale, highly utilized public fleets present the most economically viable environments for V2G, primarily due to the predictable scheduling and high idle periods that allow for optimal grid interaction.

Where Zeng et al. (2020) emphasize auction efficiency and user-driven participation, Shirazi et al. (2015) and Noel and McCormack (2014) focus on infrastructure amortization and the externalities associated with reduced emissions. For example, Noel and McCormack (2014) report significant societal cost savings attributed to decreased particulate matter and greenhouse gas emissions. However, Shirazi et al. (2015) caution against overestimating V2G profitability in regions with harsh climates or underdeveloped frequency regulation markets, illustrating that scale and locational attributes are critical to economic viability. The implication is that while market-based auction models offer flexibility and user engagement, they require sophisticated coordination and depend heavily on market maturity.

Further studies extend the economic discourse by integrating V2G into broader distributed energy storage systems. Research by Geth et al. (2013) and Liu et al. (2021) evaluates the techno-economic impact of V2G in microgrids and distribution networks, comparing unidirectional and bidirectional flow configurations. Geth et al. (2013) demonstrate that V2G-equipped microgrids can significantly reduce peak loads and enhance reliability, especially when combined with renewable energy sources. Liu et al. (2021), employing a heuristic optimization algorithm, assess the optimal sizing of autonomous hybrid PV systems that include V2G parking decks, concluding that co-located renewable-V2G systems offer superior financial performance when appropriately scaled. These findings underscore the relevance of integrated energy system planning, suggesting that V2G must be embedded into a holistic energy architecture to deliver maximum economic benefits.

Another dimension in economic strategy pertains to how tariffs and subsidies shape V2G participation. Keshav et al. (2021) introduce a dynamic tariff-subsidy framework that adapts in real-time to manage congestion and incentivize EV discharge during peak periods. Their approach mitigates the principal-agent problem by aligning grid needs with user incentives, effectively translating demand-side flexibility into measurable financial outcomes. Similar

pricing-driven strategies are evident in works by Chukwu and Mahajan (2018), who analyse profit maximization under multi-objective mixed-variable optimization (MOMVO), and by Vayanos et al. (2020), who apply distributionally robust model predictive control to address uncertainties in user availability and price volatility. These models rely on adaptive pricing and risk-aware scheduling to ensure profitability while maintaining system resilience, reflecting a shift toward sophisticated algorithmic approaches in V2G economics.

A particularly salient issue across the literature is the impact of battery degradation on economic returns. Xu et al. (2022) conduct a cost-benefit analysis that explicitly models degradation costs, finding that while V2G participation can offer positive net revenue, these benefits are sensitive to the depth of discharge cycles and the underlying battery chemistry. Their study supports findings by Wu et al. (2020), who emphasize the need to internalize lifecycle costs within economic modelling. Failure to do so, they argue, can lead to overestimated profitability and diminished user trust. Moreover, Wu et al. (2020) suggest that lifecycle-based incentive schemes, wherein users are compensated proportionally to the incurred battery wear, could align economic incentives with technical realities.

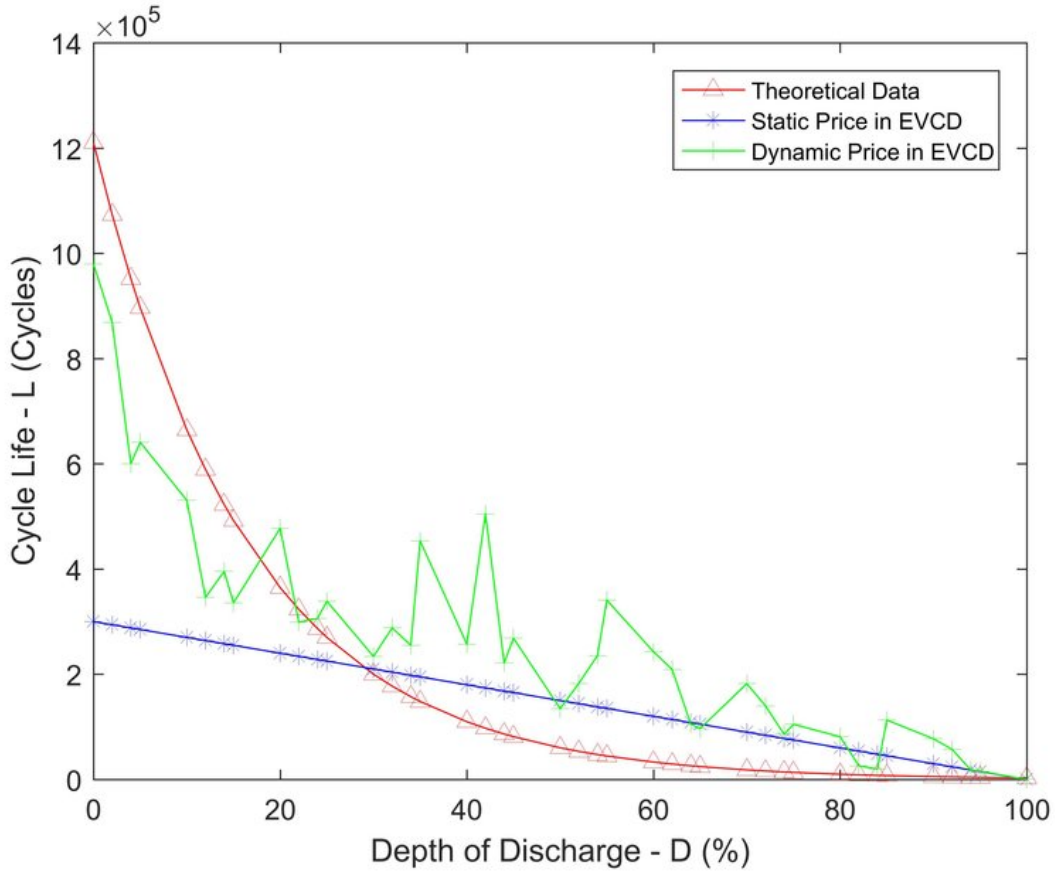


Figure 2-7. Battery capacity degradation as a function of depth of discharge (DoD) and state of charge (SoC) cycling profiles in V2G applications. (Kolawole & Al-Anbagi, 2019)

Note: This figure illustrates the impact of different cycling patterns—specifically varying depths of discharge and charge/discharge frequencies—on the degradation rate of lithium-ion batteries commonly used in electric vehicles with V2G capabilities. The data demonstrate that deeper and more frequent cycling accelerates capacity fade, thereby affecting battery lifespan and economic viability of V2G participation. These insights highlight the importance of incorporating battery degradation models in the optimal scheduling and operation strategies for V2G systems to balance revenue generation and battery health.

Parallel research has examined the spatial and temporal optimization of V2G infrastructure. Sharma et al. (2021) explore the optimal sizing of V2G parking lots within urban microgrids, leveraging energy price forecasting and stochastic modelling to balance investment costs with potential grid service revenues. Their findings align with the broader trend in the literature

emphasizing location-specific planning and demand prediction as fundamental to achieving financial viability. Similarly, Nazari-Heris et al. (2020) propose an integrated planning model that couples V2G-enabled EV fleets with PV charging, highlighting the economic complementarities of aligning solar generation with EV discharge cycles. These studies collectively advocate for the convergence of spatial planning, energy forecasting, and policy design to fully harness V2G's economic potential.

User behaviour and participation willingness also emerge as critical variables in the economic viability of V2G systems. Sierzchula and Nykvist (2017) investigate behavioural determinants of V2G adoption, revealing that economic incentives alone may not suffice; social norms, trust in utilities, and perceived convenience significantly affect user participation. This is echoed in the work of Brouwer et al. (2018), who argue that economic models must account for behavioural heterogeneity and design incentive schemes that accommodate diverse user profiles. Without such considerations, even the most theoretically sound economic strategies may fail to translate into real-world engagement.

Taken together, these studies reveal that V2G economic strategies are inherently multifaceted and highly context-dependent. Auction-based mechanisms, for example, are designed to enhance user engagement and improve market efficiency but typically require mature regulatory frameworks and robust technological infrastructure to function effectively. Cost-benefit analyses focusing on fleet-based deployment underscore the importance of operational scale, usage predictability, and supportive public policy in achieving favourable economic outcomes. Integrated system approaches further demonstrate that the economic value of V2G is maximized when it is strategically aligned with distributed renewable energy sources and governed by intelligent, demand-aware scheduling algorithms. These findings collectively affirm the economic feasibility of establishing large-scale, centralized V2G systems within community-level grids—particularly when system design leverages local renewable

integration and demand-side flexibility. Moreover, studies emphasizing adaptive pricing schemes and degradation-aware dispatch models highlight the critical need to align economic incentives with both technical constraints and evolving user expectations. The growing consensus across the literature is that no single pricing or compensation model can universally optimize V2G profitability. Instead, the effectiveness of any V2G economic strategy must be tailored to the specific characteristics of the local grid infrastructure, regulatory environment, and market conditions. This reinforces the necessity of developing context-sensitive management frameworks and economically optimized participation models. In this regard, hybrid approaches—combining elements of auction-based pricing, dynamic tariffs, infrastructure co-optimization, and user behaviour alignment—have emerged as the most promising path forward for achieving sustainable and scalable V2G integration.

2.9. Conclusion

This chapter has critically examined the evolution, fragmentation, and emerging directions in V2G research, with particular emphasis on the development of centralized, community-scale management systems designed to harness the latent capacity of idle EVs. Through a combined bibliometric and thematic analysis, five major research domains have been identified: integration with renewable power sources, bidirectional charging technologies, communication and cybersecurity frameworks, EV-side behavioural modelling, and economic and policy-oriented strategies. While each of these domains has made substantial technical contributions, collectively they expose enduring limitations that continue to constrain the deployment of scalable, real-world V2G systems.

A central insight arising from this review is the persistent compartmentalization of research within discrete technical silos—such as converter optimization, scheduling logic, or battery lifecycle analysis—with relatively little effort devoted to systems-level integration. Particularly

underrepresented is the question of grid-side coordination at the community level, which is critical for operationalizing V2G systems in dense urban contexts. Early-stage microgrid-oriented models, while valuable for controlled experimentation, are ill-suited to the complexities of managing large, heterogeneous EV populations across interconnected urban zones. They frequently overlook regulatory overlaps, cross-platform interoperability, and the demands of real-time load balancing across dynamic spatial networks.

In addition, the review underscores a pronounced disconnect between theoretical control models and actual patterns of EV usage. Initial V2G frameworks have often relied on fixed assumptions regarding EV availability and user compliance. However, mounting empirical evidence suggests that key behavioural variables—such as charging intensity, plug-in duration, and willingness to participate in grid services—exhibit significant heterogeneity across both time and population segments. These behavioural uncertainties become particularly acute at the community level, where user diversity is amplified, and system performance depends on the probabilistic aggregation of decentralized, user-driven assets. Models that fail to reflect this complexity are unlikely to deliver reliable or efficient performance under operational conditions.

Interoperability and communication latency have also emerged as key bottlenecks in the scaling of V2G architectures. As hardware ecosystems diversify, the absence of universal standards for APIs, communication protocols, and data security mechanisms poses a critical barrier to seamless integration. Although international standards such as ISO 15118 have made progress toward resolving some of these challenges, adoption remains uneven, and few architectures have demonstrated the ability to support secure, low-latency communication across heterogeneous devices and proprietary platforms. In particular, current communication frameworks are often inadequate for time-sensitive ancillary services such as frequency regulation and reactive power support, which require rapid, reliable response times.

From an economic and policy perspective, the literature indicates that the viability of V2G systems depends as much on institutional design as on technological feasibility. Dynamic pricing models, auction-based participation schemes, and degradation-aware compensation mechanisms all show promise in theory but require regulatory maturity, infrastructure readiness, and—crucially—user trust to succeed in practice. Misalignment between technical performance and economic incentives can hinder user engagement and reduce overall system effectiveness. Furthermore, the long-term economic impact of battery degradation, though increasingly well understood, remains a significant constraint on adoption and must be integrated into future cost–benefit analyses.

Taken as a whole, the current body of research suggests that transitioning V2G from conceptual pilot projects to robust, community-scale infrastructure demands a fundamental reorientation in both system architecture and research priorities. Rather than treating behavioural variability, data fragmentation, or regulatory uncertainty as secondary constraints, future models must embed these factors into the core logic of system design. Centralized management frameworks must be equipped with behavioural forecasting capabilities, dynamic scheduling algorithms, and secure communication interfaces that are not only technically effective but also economically viable and socially acceptable.

In doing so, V2G systems can begin to fulfil their promise as a foundational element of next-generation energy infrastructure—capable of enhancing grid stability, supporting renewable integration, and unlocking new forms of distributed energy value. This chapter thus lays the groundwork for the remainder of the thesis. Specifically, it reiterates the central research question: Why do existing V2G scheduling strategies, which are typically based on single-EV usage patterns in microgrid contexts, fail to translate directly to centralized V2G systems serving large-scale grid-level ‘‘S-G-L-S’’ configurations, and how can this limitation be overcome? In response, the overarching research objective of this thesis is to develop an

optimized V2G scheduling strategy that, across diverse EV usage patterns and regional grid scenarios, maximizes the utilization of idle EV storage to achieve spatio-temporal load balancing limits within regional power networks.

CHAPTER 3. DATA RESOURCES AND ANALYSIS

3.1. Introduction

This chapter presents the analysis of the data collected to address the research questions outlined in Chapter 1, with a particular focus on constructing a community-scale power grid model in the standard UK "S-G-L-S" configuration, as well as developing the corresponding EV usage database. The data sources and analytical methods employed will be detailed in Chapter 4 (Methodology).

All data used for constructing the models and databases were sourced from historical records collected through real-world pilot projects. The analysis begins by identifying and summarizing the power distribution patterns of the core components within the standard "S-G-L-S" community configuration: source (S), represented by PV output; grid (G); load (L), corresponding to residential electricity consumption; and potential storage (S), represented by EVs considered as mobile storage units. Within this framework, EVs serve a dual role. On the one hand, they function as temporary storage media that can provide peak shaving for the grid; on the other, as electricity consumers, their diverse technical parameters and usage behaviours introduce additional variability to the community load profile. To capture these dynamics, representative days were selected for detailed analysis, including a summer period (June) and a winter period (November). Data from December were excluded in this stage due to distortions introduced by holiday-related anomalies, which make them less representative of typical seasonal patterns.

Building on the analysis of baseline grid load profiles—derived from the combined effects of household consumption and PV generation—and the corresponding EV charging demand under varying influencing factors, this research develops an integrated community energy

model that incorporates residential demand, PV output, and EV charging behaviour. On the basis of this model, a simplified estimation approach using characteristic values is applied to assess the theoretical feasibility of implementing V2G optimization strategies. Specifically, the analysis examines whether, under current EV usage patterns, idle vehicles within the cluster can be mobilized to provide effective grid regulation and thereby facilitate load balancing.

The remainder of this chapter is structured as follows: Section 3.1 outlines the overall data analysis procedure. Section 3.2 presents the statistical results for the three core components of the community-level grid system—residential electricity consumption, PV generation, and EV usage behaviour. Section 3.3 evaluates the effects of four distinct EV usage indicators on power load distribution within the grid and explores the feasibility of extreme-case optimization using only idle EVs. These extreme scenarios demonstrate the potential of V2G optimization strategies proposed in the methodology and suggest that including active EVs in regulation further enhances feasibility. Finally, Section 3.4 discusses the key findings of the analysis and their broader implications for community-scale grid balancing and V2G implementation.

3.2. Data Features

3.2.1. Residential Power Load Characteristics

The research focuses on a modelled community energy system located in Nottingham, UK, designed with zero-carbon operation as a guiding principle. The case study is based on the Trent Basin development, one of the UK's first operational community energy demonstrator projects integrating distributed generation, shared energy infrastructure and real-time digital monitoring. Phase 1 of this development comprises a total of 76 homes, including 10 apartment units, while the present study specifically considers a subset of 29 homes that are currently being actively monitored. Although this represents a subset of the full development, these dwellings form part of a homogeneous low-carbon residential scheme constructed under the

same design standards and energy strategy, thereby providing a statistically and physically consistent sample for modelling broader community-scale energy interactions.

A real, community-owned PV installation with a peak rated output of 198 kilowatts-peak (kWp), originally designed to supply approximately 50 dwellings, is incorporated into the model. Under optimal solar irradiance conditions, the monitored PV system provides an average generation of approximately 4 kWp per household, which aligns with typical UK residential PV penetration levels and therefore supports the representativeness of the generation profile used in this study. Importantly, the PV system is not hypothetical but physically deployed and grid-connected within the community energy network, enabling the use of measured generation data rather than simulated estimates.

All monitored data employed in this study were obtained from the SCENe project database via the SCENe Things IoT platform (https://data.projectscene.uk/), as described by Shipman & Gillott (2019). The SCENe Things platform was specifically developed to enable high-resolution, IoT-based monitoring of electricity consumption, PV generation and energy flows within the Trent Basin community. The monitoring architecture includes distributed sensors, smart metering infrastructure and cloud-based data aggregation, ensuring temporal continuity, data integrity and traceability. The dataset therefore represents empirically measured, real-world operational behaviour rather than synthetic load or generation profiles.

Trent Basin has been widely referenced in peer-reviewed literature (Rodrigues et al., 2020) and policy-related documentation as a demonstrator for community-scale low-carbon energy systems in the UK (https://www.projectscene.uk/impact/). The integration of residential demand, shared PV generation and community energy governance makes it structurally comparable to emerging UK zero-carbon housing developments. Consequently, the monitored subset of 29 dwellings provides a robust empirical foundation for extrapolating system-level

behaviour in simulations of centralised V2G scheduling within a representative UK community energy context. By grounding the modelling framework in measured operational data from an implemented community energy scheme—rather than in hypothetical or purely synthetic datasets—this study ensures both transparency and external validity in the evaluation of centralised V2G scheduling strategies.

In order to upscale the monitored dataset to a 500-household community—corresponding to the planned full build-out of the Trent Basin development—a per-household normalisation and linear aggregation approach was adopted. Hourly electricity consumption data from the 29 monitored dwellings for the full calendar year of 2019 (Shipman & Gillott, 2019) were first processed to derive a representative per-household demand profile. For each hour *h* of the year (h = 1…8760), the arithmetic mean electricity demand across the 29 dwellings was calculated:

$$\bar{L_h} = \frac{1}{29}\sum_{i=1}^{29} L_{i,h} \tag{3.1}$$

where $L_{i,h}$ represents the measured load of dwelling i at hour h, and $\bar{L_h}$ denotes the mean hourly demand per dwelling.

This procedure results in a standardised 8760-hour per-household load profile reflecting the observed temporal characteristics (daily cycles, seasonal variation, and weather-dependent demand patterns) embedded within the real dataset. The total community demand for 500 dwellings was then estimated through linear scaling:

$$L_{community,h} = 500 \times \bar{L_h} \tag{3.2}$$

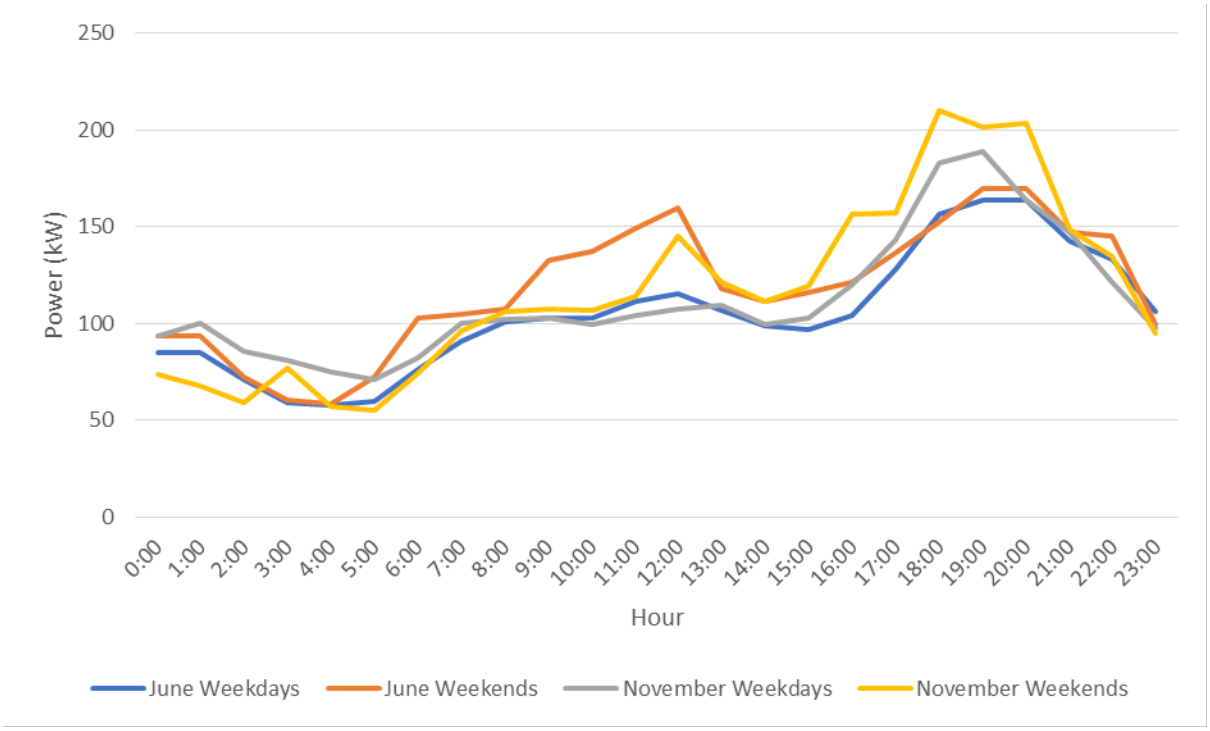


Figure 3-1. 500 Households Consumption Powers of 24-hour Time Slot in Specific Duration.

This approach assumes that the monitored dwellings are representative of the broader development in terms of building typology, occupancy patterns and energy system configuration, which is justified by the homogeneous construction standards and shared energy infrastructure of the Trent Basin scheme (Rodrigues et al., 2020).

For PV generation, a similar normalization strategy was applied. Figure 3-2 illustrates the average hourly PV generation profiles for June and November within the monitored community, representing the mean PV output for each hour from 0:00 to 23:00 (with generation expressed as positive values). These two months were selected to reflect the seasonal variability of solar production. The measured hourly PV generation profile from the community installation was divided by the number of households originally served (29 in the monitored subset) to derive an effective per-household PV generation profile:

$$\bar{G_h} = \frac{G_h}{29} \tag{3.3}$$

where G_h denotes the measured total PV output at hour h.

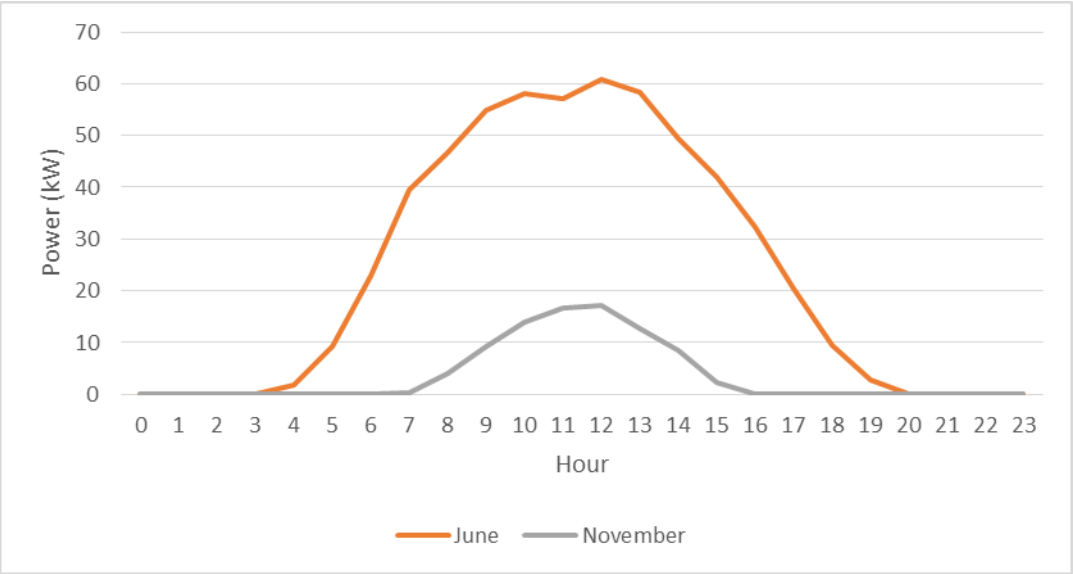


Figure 3-2. Average hourly PV generation profiles of the monitored community (29 households) for June and November

This per-household PV generation profile was then extrapolated to 500 dwellings:

$$G_{community,h} = 500 \times \bar{G_h} \tag{3.4}$$

This scaling effectively represents a full PV adoption scenario across the 500-household community, corresponding to a high-penetration or best-case distributed generation configuration. While this constitutes an upper-bound estimate of total community PV output, it provides a useful benchmark for evaluating V2G scheduling performance under high renewable integration conditions. The linear aggregation method adopted here is consistent with bottom-up residential energy modelling approaches commonly used in community-scale simulations, where representative per-dwelling load profiles are scaled according to projected

dwelling counts. Because the Trent Basin development comprises dwellings constructed under uniform design specifications and similar low-carbon standards, structural load characteristics are expected to scale proportionally with dwelling number. Moreover, averaging across 29 monitored dwellings reduces stochastic individual behaviour effects, thereby producing a smoothed yet empirically grounded demand profile suitable for system-level scheduling analysis.

By extending both consumption and generation datasets through uniform scaling, a baseline energy profile for a 500-household smart grid environment was established. This profile forms the foundation for further simulation of EV integration and V2G interactions under varying behavioural conditions. This section analyses the 24-hour residential electricity load profile of a standard UK apartment community consisting of 500 households. The analysis is based on simulated data derived from real-world observations, focusing on average daily load behaviour during both weekdays and weekends in June (representing summer) and November (representing winter).

The residential load profile typically demonstrates a gradual increase throughout the day, culminating in a distinct evening peak between 18:00 and 21:00. During this period, power demand ranges from approximately 50 kW to 200 kW. The winter load profile, in particular, exhibits a significant peak-to-valley differential, with the maximum intra-day variation reaching 155 kW. The winter evening peak demand is nearly four times higher than the lowest daily load, largely driven by increased heating and lighting needs.

To assess the influence of distributed renewable generation, time-dependent output from 4 kWp PV systems was superimposed on the residential load. The resulting net load profile reveals more pronounced temporal variability and highlights sharper peak-to-valley dynamics, particularly between seasons.

In summer, the net load becomes negative between 06:00 and 18:00, indicating a surplus of PV generation relative to local demand. The maximum net power export during this period reaches approximately 491.67 kW, suggesting that the community has substantial capacity to feed electricity back into the upstream grid. This condition poses considerable challenges for centralized V2G coordination and grid balancing strategies. Conversely, winter PV output is considerably lower, with negative net load values occurring only between 10:00 and 15:00. The peak net export during winter reaches just 62.05 kW, and the corresponding load curve displays relatively moderate fluctuations.

These findings underscore the strong diurnal and seasonal characteristics of residential electricity demand and highlight the variable impact of solar generation. They also point to the operational complexity that distributed generation introduces to grid management and V2G system design.

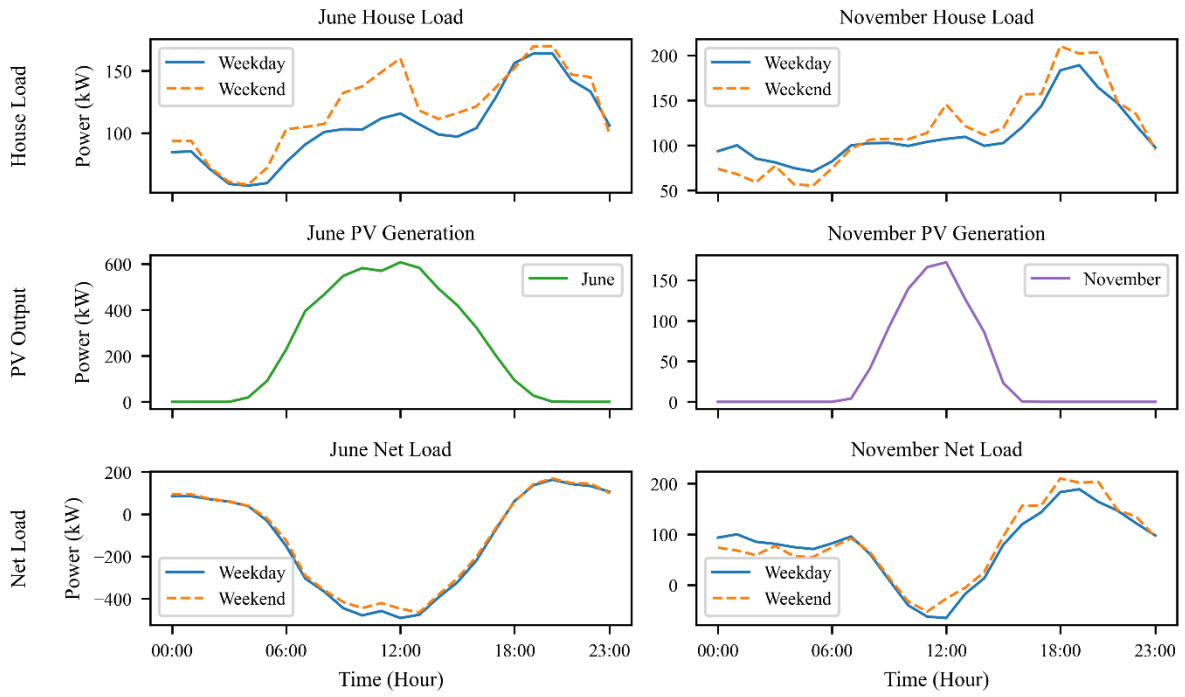


Figure 3-3. Daily power profiles of residential electricity demand, PV generation, and resulting net grid load for a 500-household residential community in the United Kingdom. Profiles reflect

average values for typical weekdays in summer (June) and winter (November), highlighting diurnal and seasonal variations as well as the impact of PV integration on net load characteristics.

3.2.2. Collective Electric Vehicle Usage Characteristics

A key objective of the study was to integrate realistic EV usage patterns into the simulation framework. To this end, empirical data were obtained from the "My Electric Avenue" project, which tracked the driving and charging behaviours of 215 users of the 2011 Nissan LEAF over a period spanning from December 2013 to November 2015 (Quirós-Tortós, Ochoa & Lees, 2015). The LEAF model used in the dataset is characterized by a 24 kWh lithium-ion battery and a standard 3.3 kW charging capability. Notably, the dataset discretizes the state of charge (SOC) into 13 levels, ranging from 0 to 12, corresponding to SOC values from 0% to 100%. This classification facilitates statistical analysis and enhances data processing efficiency. A single, uniform vehicle model was selected to reduce variability introduced by differing technical specifications, such as charging rates, battery capacities, and onboard energy management systems. While this simplification does not capture the full diversity of EV models in the market, the Nissan LEAF represents a typical mid-sized household electric vehicle, and the primary focus of the study is on community-level load profiles and charging patterns. Therefore, this assumption is not expected to significantly impact the overall findings, as the statistical characteristics of the aggregated charging behavior remain representative of a broader EV population.

The dataset includes detailed logs of driving and charging sessions, encompassing key metrics such as start and end times, durations, and battery SOC at each transition point. From these logs, daily behavioural sequences for each vehicle were extracted and classified based on activity patterns. Vehicles were categorized as idle if no driving or charging events occurred during the study day; in this study, the term "idle" exclusively refers to these non-active vehicles, whereas vehicles that experienced driving or charging events on a given day were

categorized as active. For each active vehicle, a daily timeline was constructed by identifying three primary states:

- Departure (Driving) Period: Defined as the continuous interval between the earliest trip initiation and the final trip conclusion on a given day, excluding any embedded charging events.
- Charging Window: Time periods during which the EV was physically connected to the grid and actively drawing power.
- Stationary Phase: Intervals where the vehicle remained stationary and disconnected from the grid, including periods both before and after usage events.

This time-segmented behavioural structure was foundational to the subsequent modelling of battery availability for grid-supportive discharging.

Simulation-based analysis of aggregated EV behaviour within the project reveals substantial variability in usage patterns among the studied vehicle population. By reconstructing representative 24-hour usage profiles, the study identifies significant divergence across several behavioural dimensions: (1) the temporal distribution of charging sessions, (2) frequency of charging events, (3) timing and duration of driving periods, and (4) the proportion of time EVs remain idle throughout the day.

Figure 3-4 presents typical daily SOC trajectories for three distinct usage archetypes, synthesized from aggregated data. These archetypes include: (I) distributed charging during daytime hours, (II) charging concentrated in the evening and nighttime periods, and (III) prolonged vehicle idling with minimal daily activity. Each pattern reflects a different operational context and user behaviour, offering insight into the heterogeneity present within a shared EV fleet.

This behavioural diversity poses a fundamental challenge to the development of effective V2G control strategies. Many existing approaches assume relatively fixed or homogeneous EV behaviour—assumptions that may be suitable in microgrid or residential scenarios, but become inadequate when applied to centralized fleet management. Effective V2G optimization in such environments must therefore account for the dynamic and decentralized nature of real-world EV usage patterns.

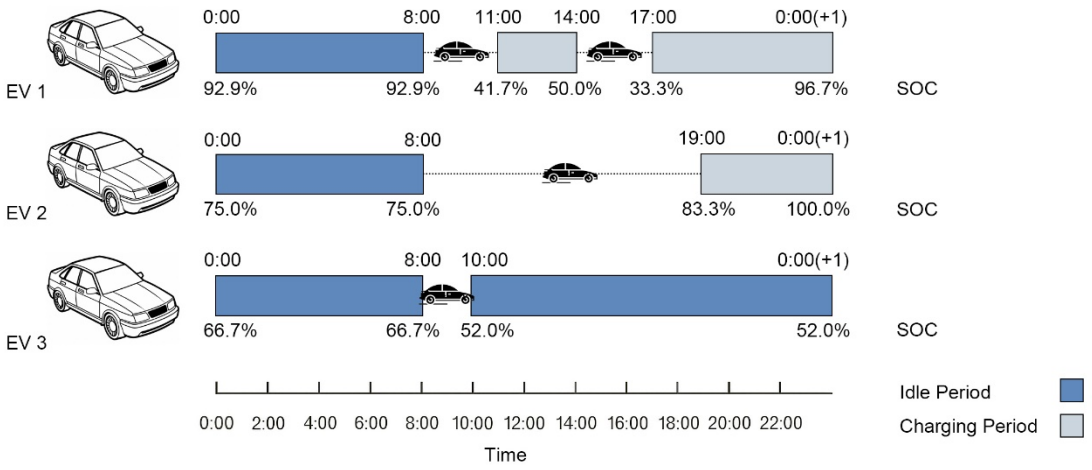


Figure 3-4. Typical 24-hour SOC profiles for three representative electric vehicle usage patterns: daytime distributed charging, nighttime concentrated charging, and extended idle periods. Profiles are based on aggregated simulation data reflecting behavioural diversity within the EV fleet.

3.2.3. Collective Charging Behaviour Characteristics of Electric Vehicles

Longitudinal data obtained from the My Electric Avenue project demonstrate that EVs in real-world community settings exhibit considerable heterogeneity not only in daily operational patterns but also over extended time horizons such as weekly cycles. This heterogeneity is reflected in individual variability regarding charging frequency (e.g., the number of charging events per week) and differences in driving routines between weekdays and weekends. Such multi-scale behavioural variability introduces additional complexity to the optimization of V2G scheduling algorithms.

To systematically characterize representative charging behaviours, a modelling framework has been developed based on aggregated average daily EV usage profiles. Analysis of the project data reveals an average daily utilization rate of approximately 54.87%, indicating that nearly half of the fleet remains inactive on any given day.

Figure 3-5 presents the standardized daily EV charging load profile, which is intended to represent the typical temporal distribution of EV charging demand rather than the detailed variability of individual driving behaviour. The profile was constructed using the charging activity database from the "My Electric Avenue" project introduced earlier in this Chapter. This dataset records the charging behaviour of 215 electric vehicles over a full year, including the exact start and end time of each charging session for every vehicle. In the project, all vehicles are of the same model with identical battery capacity (24 kWh), and residential charging is performed at a fixed power level of 3.3 kW. As a result, the charging energy within any time interval can be directly determined from the duration of the charging session.

To construct the standardized profile, the charging energy associated with each hour was first calculated by identifying the portion of every recorded charging session that falls within hour h. Because the charging power is constant, the charging energy within that hour is obtained by multiplying the charging duration within the hour by the rated charging power. For each hour h, the charging energy values from all vehicles and all observation days across the entire year were then aggregated. The aggregated energy was subsequently normalized by both the total number of observation days D and the fleet size N =215, yielding the average hourly charging energy per vehicle:

$$P_h = \frac{\sum_{d=1}^{D} \sum_{i=1}^{N} E_{i,h,d}}{D \times N} \tag{3.5}$$

where $E_{i,h,d}$ denotes the charging energy of vehicle i in hour h on day d. Through this aggregation and normalization process, the resulting curve represents the average hourly charging demand of a standardized day for the entire EV population in the community, including both active vehicles and idle vehicles. In other words, the profile reflects the expected hourly charging demand averaged across one full year and across all vehicles in the dataset. This approach effectively smooths out day-to-day behavioural fluctuations while preserving the overall temporal characteristics of EV charging demand, thereby providing a representative load profile suitable for system-level simulation and community-level energy management analysis.

Although this averaging procedure inevitably smooths out seasonal differences and weekday–weekend variations, its purpose is to provide a generalized baseline representation of charging demand at the community level. This baseline is used as a behavioural reference distribution for subsequent simulations; the actual modelling of pre- and post-optimization grid net load profiles always relies on the real-time charging and discharging power of individual EVs, rather than this averaged profile.

The aggregated charging load exhibits a pronounced bimodal distribution, characterized by a dominant peak during nighttime hours and a trough throughout the daytime. This standardized load curve serves as a benchmark for assessing the typical influence of individual EV charging behaviour on the broader community grid. It also facilitates further investigations into how variations in EV usage parameters collectively shape the overall power load profile.

As summarized in Table 3-1, EV charging loads display a strong temporal correlation with residential electricity consumption, particularly during peak (18:00–22:00) and off-peak (03:00–07:00) intervals. Notably, the peak magnitudes of EV and residential loads are closely matched (EVs: 0.37 kW per unit; residential: 0.36 kW per household), resulting in a near

doubling of peak load stress on the distribution network—an increase of approximately 103%. Conversely, peak PV generation (10:00–15:00) occurs out of phase with these demand peaks. This temporal mismatch between generation and load exacerbates the spatial-temporal imbalance of power flow, leading to amplified net load fluctuations, with peak-to-valley differences increasing by 139%.

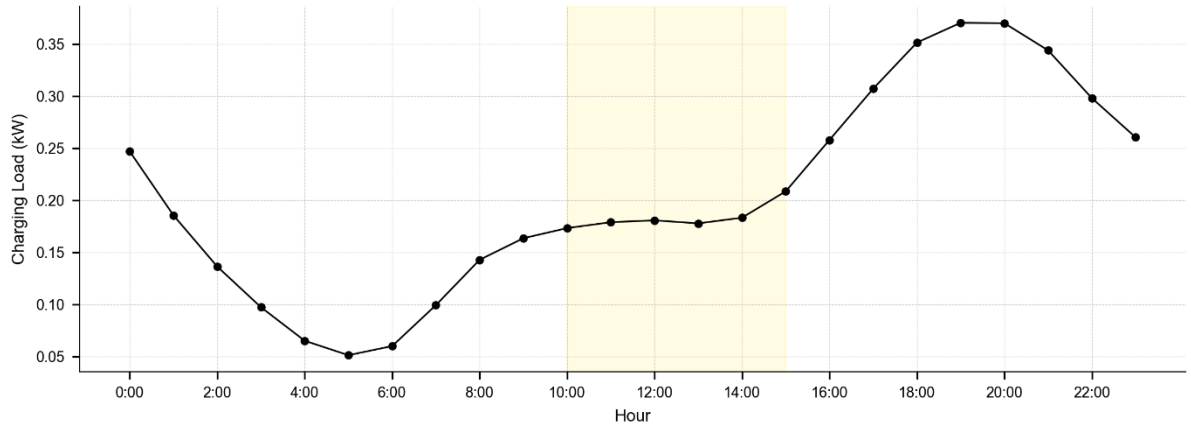


Figure 3-5. Normalized diurnal charging load profile of the electric vehicle fleet. The yellow shaded area denotes the peak PV generation period, highlighting the temporal mismatch between EV charging demand and solar power output.

Elements (per unit)	Peak Loads		Valley Loads	
	Occurrence Time Period	Extreme Value (kW)	Occurrence Time Period	Extreme Value (kW)
House	18:00--22:00	0.363407226	02:00--07:00	0.137720984
PV	06:00--17:00	1.081135257	21:00--03:00 (+1)	0
EV	16:00--00:00 (+1)	0.370264415	03:00--07:00	0.051302963

Table 3-1. Peak and valley values of per-unit EV charging load, residential electricity consumption, and PV generation profiles for November. The table highlights the temporal alignment and magnitude of load peaks and valleys, illustrating the combined impact on distribution network demand.

3.3. Simulation of Collective EV Usage Indicators

3.3.1. EV Ownership Rate

To systematically evaluate the impact of varying EV penetration levels on community grid load distribution, this study establishes four EV ownership scenarios: 25%, 50%, 75%, and 100%. All other usage parameters are held constant across scenarios to isolate the effects of ownership rate. As shown in Figure 3-6, the average per-EV hourly charging load profile for weekdays is superimposed onto the net residential electricity consumption curve of a 500-household community. The comparison is conducted for representative weekdays in June (summer) and November (winter).

The results indicate that increasing the EV ownership rate leads to a substantial amplification in grid load variability, particularly in the peak-to-valley differential. At full EV adoption (100% ownership), the maximum load difference in June exceeds 800 kW—representing a 22.6% increase relative to the baseline fluctuation in the absence of EV charging loads. This trend underscores a critical challenge: under existing usage patterns, large-scale EV integration will significantly intensify temporal imbalances in community power demand. The analysis reveals a strong temporal alignment between EV charging activity and residential energy consumption, especially during the evening peak (18:00–21:00). This coincidence further accentuates the load curve's inherent peakiness, increasing the burden on local distribution infrastructure. Although the November scenario exhibits a smaller absolute increase in peak-to-valley load difference—16.61% lower than in June—this is largely attributable to seasonal reductions in PV generation capacity. Nevertheless, as EV ownership rises, the contribution of EV charging to total real-time peak demand becomes increasingly significant, growing from 23.56% to 55.21%. This confirms the emerging dominance of EV loads in shaping grid demand patterns.

These seasonal variations in peak-shaving requirements—driven by both load seasonality and EV market penetration—highlight the necessity for dynamic, real-time optimization of V2G control strategies. In particular, adaptive regulation algorithms must be developed that adjust threshold parameters in accordance with seasonal load characteristics and fluctuating EV stock levels. Such seasonally responsive V2G frameworks are essential to effectively mitigate varying peak load pressures throughout the year. Furthermore, the findings emphasize the importance of integrating EV charging load profiles into monthly peak load forecasting models. Doing so can significantly improve the accuracy of seasonal V2G strategy planning, while providing a more precise representation of how real-time EV ownership levels influence overall grid load distribution.

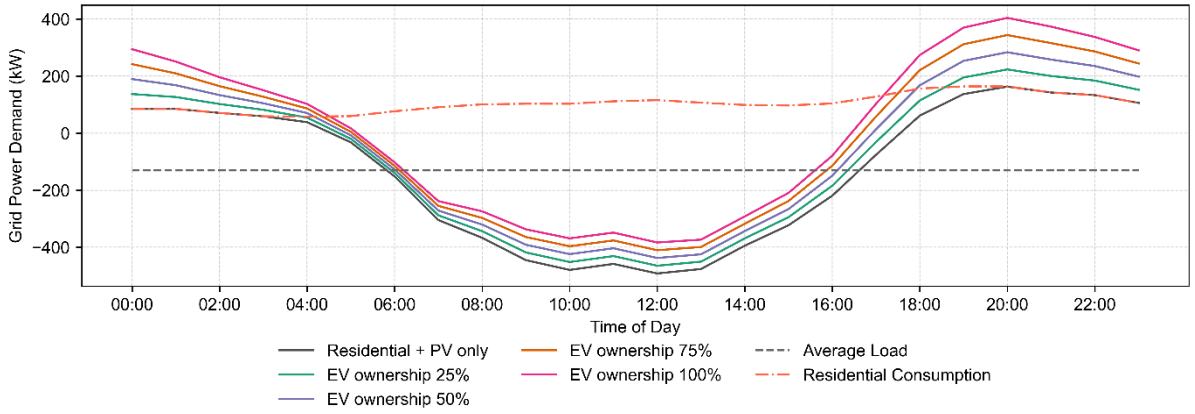


Figure 3-6 (i). Weekday-averaged hourly net grid power profiles for a 500-household UK residential community under varying EV ownership scenarios (25%, 50%, 75%, and 100%) in June.

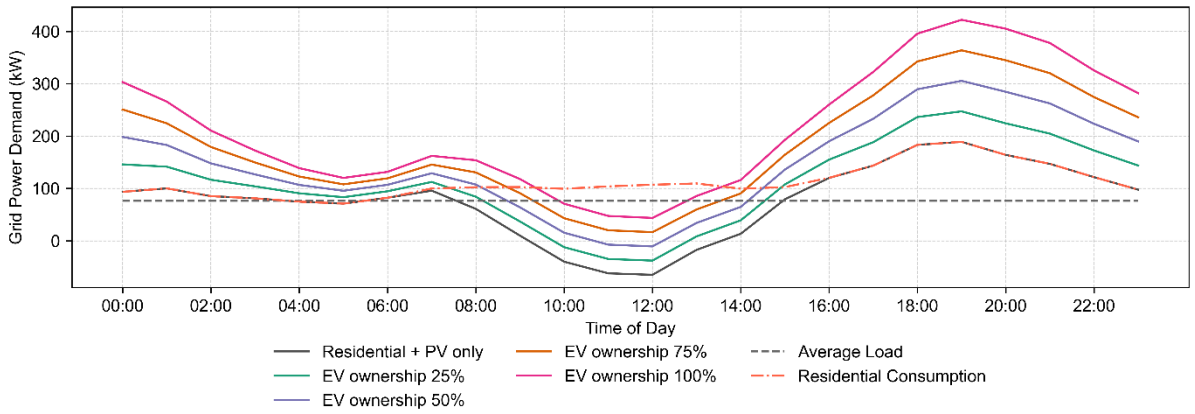


Figure 3-6 (ii). Weekday-averaged hourly net grid power profiles for a 500-household UK residential community under varying EV ownership scenarios (25%, 50%, 75%, and 100%) in November.

Note: The profiles are computed by averaging across all weekdays within the respective month, using the same aggregation method as in Figure 3-3 but applied to a monthly dataset rather than the full year. The net power at each hour h is calculated as:

$$NetP_h = \overline{P_h^{res}} - \overline{P_h^{PV}} + S_h \times N_{EV} \tag{3.6}$$

where $\overline{P_h^{res}}$ and $\overline{P_h^{PV}}$ are the mean residential consumption and mean PV generation at hour h averaged over all weekdays of the month, S_h is the standardized per-vehicle weekday charging profile derived from that month's data (see Figure 3-5), and $N_{EV} = ownership\% \times 500$ is the number of EVs corresponding to the specified ownership level. These curves represent the typical weekday net load for the month and illustrate how increasing EV penetration affects both peak intensity and the overall shape of the diurnal load profile.

3.3.2. EV Idling Rate

Longitudinal data from the My Electric Avenue project reveal substantial variability in the daily utilization of the monitored fleet of 215 EVs. Throughout the observation period, the number of actively used vehicles per day ranged from fewer than 10 to nearly 200, corresponding to an

idling rate spectrum from approximately 4.7% to 93%. This variation indicates that, in practice, a significant portion of EVs may be inactive and potentially available for grid-related functions, particularly V2G applications.

However, the number of EVs available for V2G dispatch is jointly constrained by both the ownership rate and the idling rate. To assess the combined influence of these two factors on grid load dynamics, this study conducts four scenario-based simulations. The purpose of this analysis is not to optimize dispatch itself, but rather to construct and illustrate a set of baseline net-load models that integrate residential electricity demand, PV generation, and EV charging consumption under different ownership–idling configurations. These models serve as the foundational framework upon which the V2G scheduling strategies developed in later chapters are designed and tested. For clarity of exposition, November is selected as the representative winter month, as it avoids the atypical effects of December holidays while still reflecting characteristic seasonal load and generation conditions. The analysis is therefore based on the average standardized net residential load curve for November, with the four representative cases summarized in Table 3-2:

1. High ownership (100%) – Low idling (25%)
2. High ownership (100%) – High idling (75%)
3. Low ownership (25%) – Low idling (25%)
4. Low ownership (25%) – High idling (75%)

To evaluate the effects of these scenarios on grid performance, a limit load balance reference curve was established as a benchmark. This curve reflects ideal load balancing conditions and serves to quantify the deviation introduced by EV integration under various behavioural conditions. The analysis focuses on the added stress these deviations place on V2G load balancing algorithms.

From an energy balance perspective, where PV generation is treated as negative load and electricity consumption as positive, the November data show that when active EVs account for approximately 38% of households, the daily charging demand of the fleet becomes equivalent to the community's average daily residential electricity consumption. At this threshold, EV charging emerges as the dominant load on the distribution system. In contrast, for June—when PV generation significantly exceeds local demand—the community's net electricity usage is −3032.05 kWh/day. Under these conditions, when the number of active EVs reaches 62% of households, the cumulative charging demand is sufficient to absorb the entire PV-induced energy surplus, thereby neutralizing the community's net export to the upstream grid.

With respect to peak load stress, two critical periods are evaluated:

1. the midday PV generation peak in summer, where the challenge lies in absorbing surplus energy;
2. the evening load peak in winter, driven by coincident residential and EV charging demand.

The results indicate that during the summer midday period, even with full EV activation (100% of households), autonomous charging offsets only ~37% of the PV surplus. This highlights the limited capacity of unmanaged charging behaviour to align with peak generation. In contrast, during winter evenings, once 52% of households have actively charging EVs, the EV load alone is already equivalent to the residential load peak—effectively doubling the grid's instantaneous demand during that period.

From a V2G strategy design perspective, the preceding analysis highlights the potential regulatory role of idle EVs in community-level grids. Even without altering their original travel or charging behaviours, a certain proportion of idle vehicles could in principle contribute to balancing power distribution. For example, idle EVs may serve to absorb excess PV generation

during summer surplus periods, or to supply power during winter peak demand. Table 3-2 summarizes the maximum net power imbalances observed across the four scenarios, together with the corresponding number of idle EVs that would theoretically be required to offset these imbalances through bidirectional exchange at a fixed rate of 3.3 kW per vehicle. These simple estimations suggest that only a modest share of idle EVs would be sufficient to achieve near-optimal balancing in periods of peak exchange, thereby indicating that the temporary storage potential of idle EVs could provide a meaningful foundation for the design of V2G optimization strategies explored in subsequent chapters.

Benchmark Scenarios	Peak Loads		Valley Loads	
	Maximum Power Difference (kW)	Required EV Amounts (Charge)	Maximum Power Difference (kW)	Required EV Amounts (Discharge)
High Ownership Rate (100%) – Low Idle Rate (25%)	238.496578	73	-156.12169	48
High Ownership Rate (100%) – High Idle Rate (75%)	156.048708	48	-143.37403	44
Low Ownership Rate (25%) – Low Idle Rate (25%)	145.742725	45	-141.78057	43
Low Ownership Rate (25%) – High Idle Rate (75%)	125.130758	38	-138.59366	42

Table 3-2. Preliminary estimation of grid stress under varying EV ownership and idling rate combinations, and the corresponding number of idle EVs theoretically required to offset extreme imbalances.

Note: The estimation is based on standardized daily net load profiles for a representative November weekday. Values represent deviations from the limit load balance reference curve and provide a simple calculation of the number of idle EVs that would be needed to offset these deviations, assuming a bidirectional transfer capacity of 3.3 kW per vehicle. This calculation is intended solely as a boundary-case estimation to illustrate the theoretical feasibility of leveraging idle EVs as temporary storage for community-level load balancing, thereby motivating the design approach developed in subsequent chapters.

3.3.3. Charging intensity

This study investigates the impact of EV charging intensity on load profiles using empirical data from 215 monitored EVs. To capture distinct charging intensity conditions, three representative weekly periods were selected corresponding to high, medium, and low charging intensity. The selection was made using a standardized metric defined as the ratio of the total cumulative charging duration across the fleet in a given week to the sum of daily active EVs over the same seven-day period. This ratio provides a normalized measure of average charging intensity per active vehicle per week, effectively accounting for fluctuations in both vehicle availability and charging behaviour. Based on this metric, the week with the highest ratio, the median week, and the lowest ratio were identified as representative cases. The corresponding cumulative weekly charging durations were 4,295 hours, 2,383 hours, and 1,008 hours, respectively. These three periods thus reflect systematically defined high-, median-, and low-intensity charging conditions, allowing the analysis to isolate the influence of charging intensity variation on the integrated community net-load model (comprising residential demand, PV generation, and EV charging).

Standardized 24-hour average charging load curves per EV, as illustrated in Figure 3-7, reveal pronounced differences in charging behaviour across the three intensity levels. In the high-intensity charging week, a distinct secondary load peak emerges prior to 05:00, with charging demand reaching approximately 170.5% of that observed in the medium-intensity scenario. A comparison of the per-vehicle hourly charging power distributions across the high-, medium-, and low-intensity conditions further demonstrates that total charging energy consumption is strongly and positively correlated with charging intensity. This finding confirms that higher charging intensity is associated with a substantial increase in both aggregate energy consumption and instantaneous load demand.

Scenario-based simulations for November, assuming a full EV ownership rate of 100% (500 EVs), further highlight the grid-level consequences of varying charging frequencies. As depicted in Figure 3-8, the weekday peak load under the high-frequency charging scenario increases by 394.5 kW—a 240.3% rise relative to the baseline condition—while the trough load increases by only 161.2 kW. This leads to a peak-to-valley load difference that is approximately 1.8 times greater than the original baseline, significantly amplifying load imbalance across the daily cycle.

The observed nonlinear distortion of the load distribution, induced by changes in charging intensity, demonstrates the limitations of using static or average load assumptions in EV integration planning. It also underscores the need for dynamic load scheduling models that incorporate charging probability density functions to accurately represent the stochastic nature of large-scale EV clusters. Conventional fixed-pattern models—commonly used in microgrid-based frameworks—are insufficient in capturing this variability and, if applied to larger networks, may lead to suboptimal or inefficient grid regulation strategies.

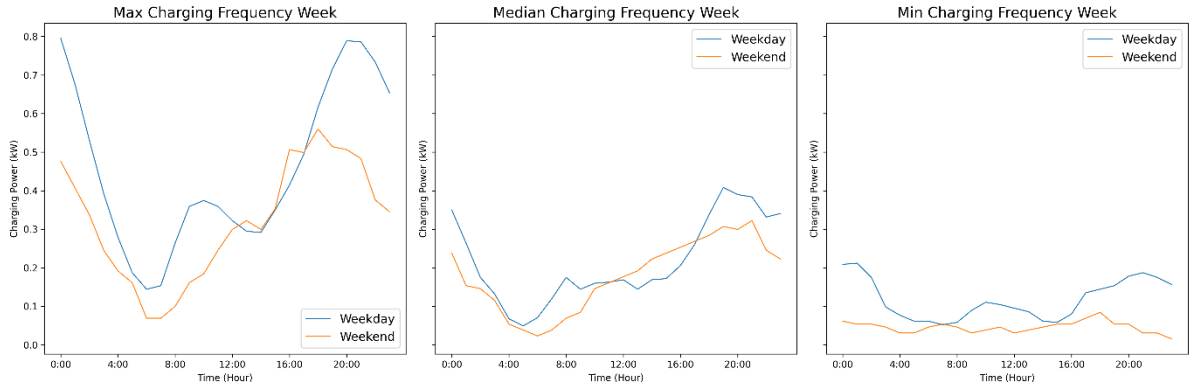


Figure 3-7. Hourly EV charging power distribution for three representative weeks characterized by high, medium, and low charging frequencies. The curves illustrate how increased charging intensity shifts the temporal charging pattern and intensifies early-morning demand peaks.

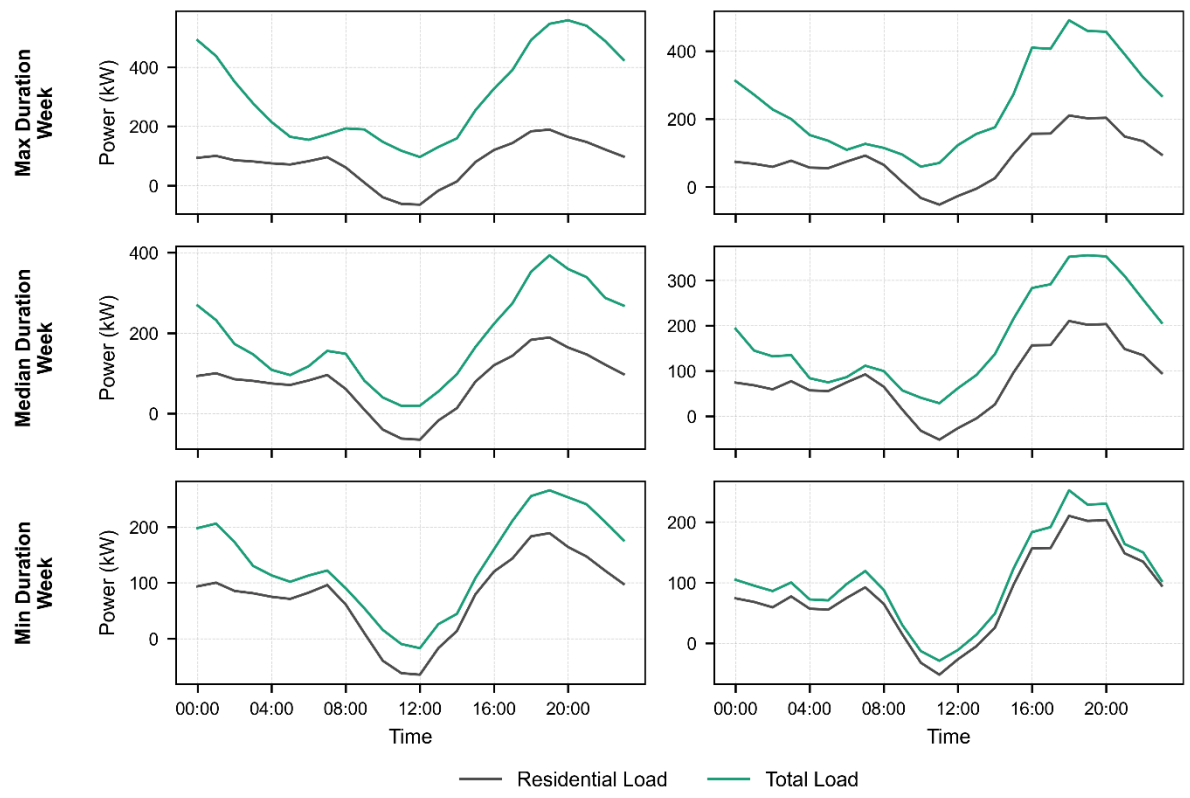


Figure 3-8. Hourly net power load profiles under varying EV charging intensities (high, medium, low) for standard weekdays (left column) and weekends (right column) in November.

Note: The six subplots are arranged in three rows (top to bottom: high, medium, low charging intensity) and two columns (left: weekday, right: weekend). The comparison illustrates that higher charging intensity significantly elevates peak demand and widens peak-to-valley disparities, thereby exacerbating grid imbalance.

3.3.4. Charging Power Variations

This section analyses the impact of increased EV charging power on load distribution characteristics, following the simulation framework established earlier. Using empirical charging behaviour data based on a 3.3 kW charging baseline, simulations were conducted for increased charging powers of 7 kW and 10 kW, while holding all vehicle usage patterns constant.

The results reveal a marked temporal aggregation effect associated with higher charging power. Specifically, the time-based Gini coefficient—a metric used to assess temporal concentration of charging activity—increases from 0.2675 at 3.3 kW to 0.3046 at 7 kW and 0.3169 at 10 kW. This effect indicates a stronger concentration of charging within limited time windows, which notably coincide with peak periods of residential electricity demand (Figure 3-9). Further analysis of grid-level load profiles (Figure 3-10) confirms that, if unmanaged, increasing EV charging power leads to a substantial rise in community-level peak demand. Moreover, the grid peak load exhibits a nonlinear growth trend, suggesting that continued reliance on higher charging rates as a means of achieving faster charging may intensify rather than mitigate grid load imbalance.

To systematically examine the potential of idle EVs as temporary storage for community-level grid balancing, Table 3-3 provides a simplified estimation of the effects of three representative charging/discharging configurations—3.3 kW, 7 kW, and 10 kW—on peak and valley load compensation. These calculations do not involve detailed V2G optimization; rather, they follow the same straightforward estimation method used in earlier sections, quantifying the deviation from an idealized load balance reference curve and approximating the number of EVs that would be needed to offset these imbalances under each configuration. The results suggest that while 10 kW charging can marginally reduce the number of vehicles required for valley load absorption—by about 327% compared with the baseline—it simultaneously exacerbates peak-time imbalance, increasing the required compensation by 106.23 kW. In contrast, an asymmetric configuration featuring 7 kW charging and 10 kW discharging appears most favourable: it stabilizes daily regulation demand (with EV availability variation kept within ±13.4%) and reduces the frequency of dispatch, indicating a potentially more battery-friendly and system-efficient pathway. Importantly, this exercise is not intended as a full optimization, but rather as an indicative assessment that demonstrates the plausibility of developing idle EVs

as a flexible storage resource. The insights gained here frame the rationale for the more detailed V2G scheduling analysis presented in the following chapters.

Overall, these results suggest that charging power optimization must go beyond the goal of faster energy delivery and instead be integrated into broader grid balancing strategies. Configurations that balance charging and discharging asymmetrically can yield improved operational stability while enhancing both grid support and battery longevity.

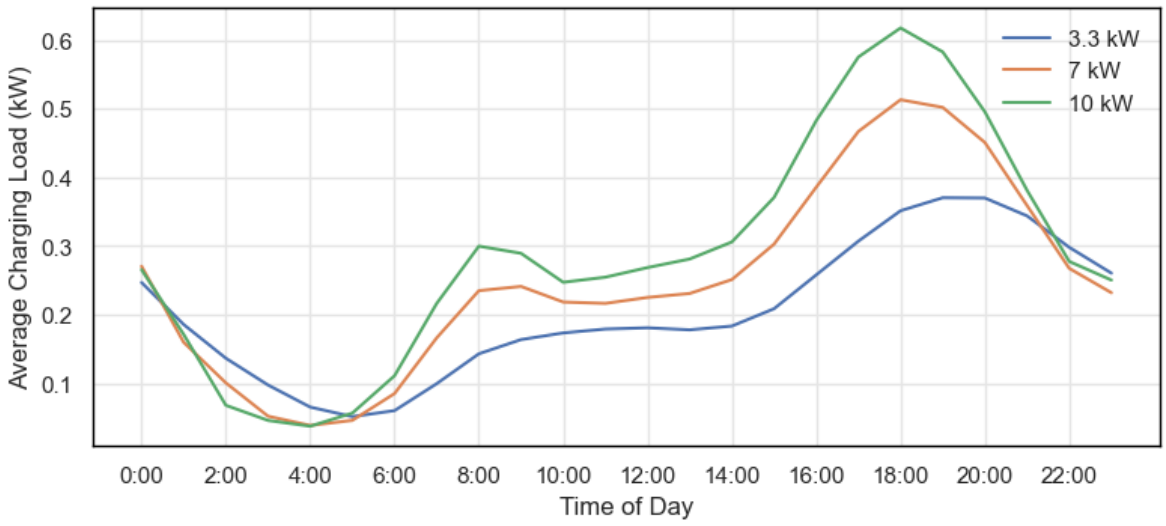


Figure 3-9. Time-of-day distribution of EV charging demand under different charging power levels (3.3 kW, 7 kW, and 10 kW). The figure illustrates increasing temporal concentration of charging activity as power rates rise, with demand clustering around peak residential load periods.

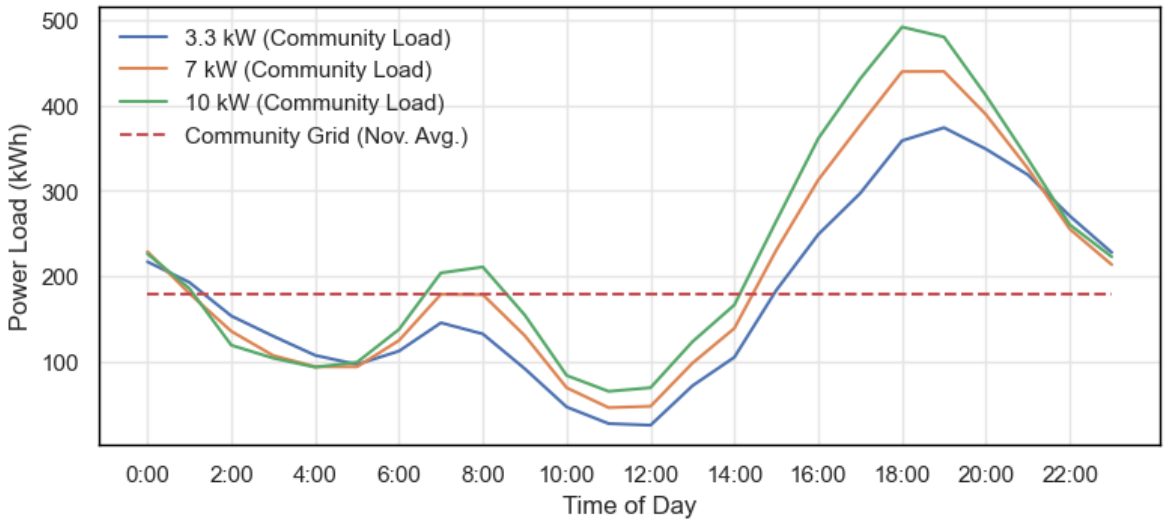


Figure 3-10. Time-of-day power load profiles for a community grid under EV charging power levels of 3.3 kW, 7 kW, and 10 kW on standard weekdays in November. The figure highlights the nonlinear increase in peak grid load with higher charging rates and the growing overlap between EV charging demand and residential peak consumption periods.

Discharging Power	Charging Power	Peak Loads		Valley Loads	
		Maximum Power Difference (kW)	Required EV Amounts (Charge)	Maximum Power Difference (kW)	Required EV Amounts (Discharge)
3.3 kW	3.3 kW	195.559561	60	-153.03878	47
	7 kW	261.392628	80	-130.90498	19
	10 kW	301.794030	92	-109.14008	11
7 kW	3.3 kW	195.559561	28	-153.03878	47
	7 kW	261.392628	38	-130.90498	19
	10 kW	301.794030	44	-109.14008	11
10 kW	3.3 kW	195.559561	20	-153.03878	47
	7 kW	261.392628	27	-130.90498	19
	10 kW	301.794030	31	-109.14008	11

Table 3-3. Impact of varying EV charging and discharging power configurations on grid load balancing performance and corresponding V2G participation requirements. The table presents deviations from ideal load balance and estimates the number of EVs needed to offset power imbalances under different power scenarios, based on November standard day data.

3.4. Conclusion

Large-scale, centrally managed EVs represent not only a vital asset for future community-level V2G regulation systems, but also a key determinant in shaping grid operation dynamics through their aggregated usage behaviour. Using a representative UK-based residential community of 500 households and real-world EV usage data, this chapter presents a comprehensive analysis of the dual role that aggregated EVs play within local grid systems. By examining four pivotal parameters—EV ownership rate, idle time ratio, charging intensity, and charging power—this study quantifies their respective impacts on grid load distribution. The results highlight a strong spatiotemporal correlation between EV charging patterns and residential electricity demand, forming a positive feedback mechanism that amplifies the daily peak-to-valley load difference by 12.25% to 49.03%.

In particular, under a full EV penetration scenario (100% ownership), EV charging contributes up to 55.21% of the total load during peak hours. With high-frequency charging behaviour, the grid's peak load surges by as much as 240.3%. Nevertheless, the current usage behaviour of EVs exhibits limited capacity to mitigate low-load (valley) periods, with even fully active fleets absorbing only 37% of the valley load. The introduction of high-power charging technologies (e.g., 10 kW) further exacerbates temporal load imbalances, as evidenced by an 18.5% increase in the time-based Gini coefficient, indicating greater load concentration.

To enable a quantitative assessment of how large-scale, centralized V2G systems can contribute to balancing power distribution within high-tier community grids, the study in this chapter applies the power distribution model and monthly net load threshold curves (with the calculation method for these reference values detailed in Chapter 4). The analysis indicates that, even under the restrictive condition of engaging only idle EVs, community-level power balancing requirements can still be met. Moreover, an asymmetric power configuration (10 kW

charging / 7 kW discharging) is shown to stabilize dispatch variability within ±13.4%. Importantly, idealized simulations suggest that mobilizing only 3.8–5.4% of idle EVs would suffice to balance power at critical peak points. Together, these findings provide a robust theoretical foundation for the design of intelligent V2G systems capable of accommodating heterogeneous and dynamic EV usage patterns, while also demonstrating the practical feasibility of leveraging idle EVs as a flexible storage resource. This evidence underpins the methodological framework developed in this study and its proposed strategies for enhancing power distribution within community grids.

CHAPTER 4. METHODOLOGY

4.1. Introduction

The ultimate objective of this research is to develop an optimized centralized V2G management model tailored for a standard-scale, community-level power grid environment in the UK, following the "S-G-L-S" configuration. This model is designed to support a zero-carbon energy transition by enhancing the load balancing capabilities of regional power grids. Specifically, it aims to achieve optimal distribution of power demand and supply within localized grid networks by leveraging the latent energy storage capacity of idle EVs, thereby improving the overall efficiency and responsiveness of a centralized V2G system.

To accomplish this, the study adopts a quantitative modelling approach grounded in real-world data from community grid projects and electric vehicle usage patterns. Using Python-based simulation techniques, the research constructs an operational framework for optimizing centralized V2G vehicle coordination, with the goal of aligning power load distribution with system stability constraints. The methodology involves both the design and implementation of computational algorithms for managing EV charging and discharging schedules, as well as the formulation of control logic governing energy exchange within the grid. To assess the feasibility and effectiveness of the proposed V2G optimization strategy, a comparative quantitative evaluation is performed across multiple operational scenarios.

This chapter is structured into four main sections. The first section outlines the overall research framework, detailing the major phases of the study along with the corresponding methodological approaches. The second section introduces the community-scale power grid model and the EV fleet modelling process, explaining the analytical procedures used to capture realistic system dynamics. The third section describes the construction of the V2G optimization

scheme, including the underlying logic for vehicle coordination and the algorithmic strategies for power allocation. The final section presents a summary of the methodological design and lays the groundwork for the subsequent evaluation and analysis presented in later chapters.

4.2. Research Framework Design

The design of this research framework is derived from the problems revealed in Chapter 2 through the literature review. To address these issues, the study proposes a centralized V2G system optimization model for standardized community-scale power grids, providing a clear roadmap from the identification of system requirements to the formulation of optimization logic. Following this logic, the section sets out the proposed solution to the problems identified, outlines the three-stage research methodology developed on this basis, and concludes by clarifying the beneficiaries of the resulting framework.

4.2.1. Proposed Solution

In response to the current state of V2G research and the practical challenges hindering its large-scale deployment, this study focuses on key unresolved issues in the development of optimized control strategies for centralized V2G systems within community-scale power grids. Based on a systematic review of existing literature and simulated data from representative case studies, several critical technical bottlenecks were identified at the community grid level. These include, but are not limited to:

- the need for standardized characterization of low-carbon community grid features,
- accurate modelling of EV usage behaviour under diverse real-world conditions,
- quantitative evaluation of V2G efficiency in power load optimization, and
- the establishment of a comprehensive economic assessment framework at the community scale.

To address these challenges systematically, the study proposes an innovative solution framework. The technical pathway and implementation strategy are detailed in Table 1-5, which presents a side-by-side comparison of the specific challenges identified and the corresponding targeted solutions adopted in this research. This table serves as a structured roadmap guiding the design and execution of the proposed optimization strategy.

Challenges	Solutions	Methodologies
Standardized Modelling of Power Load Distribution in a UK Zero-Carbon Community Grid	• A simulation model of a standard-scale (500-household) zero-carbon community grid was developed based on real operational data from small-scale community grids, using data expansion techniques. • Grid components were categorized into three primary subsystems: energy storage (PV systems), energy consumption (residential loads), and energy regulation (EV clusters). A typical daily time-of-use load distribution model was established accordingly. • Combined simulations using both "extreme characteristic days" and "regular pattern days" were conducted to comprehensively represent the annual load distribution.	• Real-world electricity consumption data and PV generation outputs from apartment communities were scaled equivalently to construct a 500-household benchmark model. • Seasonal daily load curves were modelled with emphasis on solstice days (e.g., summer and winter solstices), which exhibit distinct seasonal features. • To account for differences in weekday and weekend usage patterns, monthly average statistics were applied to enhance model accuracy.
Modelling of EV Usage Scenarios in Centralized Parking Environments	• A classification system for EV usage states was established to simulate state-of-charge (SOC) fluctuation curves under various user behaviour patterns throughout the day. • A multi-scenario database was developed based on key parameters such as EV penetration rate and idle rate.	• Actual driving and charge/discharge data were used to determine EV operating conditions and to calculate SOC time-variant curves for typical days. • A stochastic sequence replication method was applied to expand the scenario database under different usage conditions.

Quantitative Design of V2G Regulation Mechanisms	• A set of quantitative indicators was defined to trigger V2G participation in grid regulation. • A reference curve for power-load balancing and an evaluation standard for adjustment capacity was established. • A hierarchical scheduling and control strategy for EVs was designed.	• Baseline load curves (original scheduling curves) were generated by integrating data from both energy consumption and storage subsystems. • Hourly monthly averages were used to construct benchmark curves for extreme load balancing scenarios. • The deviation between the original and benchmark curves was analysed to determine the required V2G adjustment capacity. • EVs were classified and scheduled based on idle state and SOC thresholds.
Quantitative Evaluation Framework for Optimization Benefits	• A typical time-of-use electricity pricing scheme was used to simulate the economic performance of the community grid. • Carbon emission reductions before and after optimization were calculated using per-kWh carbon intensity factors.	• A comprehensive benefit evaluation framework was developed at the community grid level, avoiding isolated component-level analysis. • The robustness of the optimization strategy was verified under economic volatility conditions using variable electricity pricing scenarios. • Regional real-time carbon intensity data were integrated to quantify emissions reduction resulting from the optimization.

Table 4-1. The challenges and the proposed solutions

4.2.2. Three-Stage Research Methodology for Centralized V2G System Optimization

To address the limitation that existing V2G scheduling strategies—largely developed for microgrid contexts and based on single-EV usage patterns—cannot be directly applied to centralized V2G systems operating within large-scale ‘‘S-G-L-S’’ configurations, this study develops a novel scheduling framework grounded in logical modelling. The central aim of the framework is to increase the utilization of idle EV storage in order to achieve extreme spatio-temporal balancing of power loads within regional grids. Once the framework is established, its performance is systematically evaluated using real-world case data to assess operational effectiveness across technical, economic, and environmental dimensions. To ensure a coherent and progressive research design, the methodology is structured into three interrelated stages, with each stage building upon the findings of the previous one to form an integrated pathway toward the optimization of centralized V2G scheduling strategies.

Stage One: Quantitative Modelling of Community Grid Load and generation Profiles

As the foundation for simulating and testing the proposed optimization logic, this stage focuses on constructing a data-driven, quantitative model of power load distribution within a representative UK community power grid of approximately 500 households, oriented towards a zero-carbon transition. Using Python as the primary analytical tool, real-world operational data from relevant pilot projects is processed to identify the dynamic load behaviours of major system components. These include generation units (e.g., PV systems), household and community-level consumption loads, and EV charging demands. The goal of this stage is to generate a representative model of load distribution patterns across the "S-G-L-S" architecture, forming the foundational structure for later optimization.

Stage Two: Development of the Optimization Control Framework

In this stage, an optimization control framework is developed to enhance the scheduling efficiency of idle EVs within the centralized V2G system. The framework builds upon the load distribution model and the refined simulation of EV usage and charging–discharging behaviours established in Stage One. By integrating these components, the framework enables a more precise representation of both grid demands and user behaviour. Python-based algorithmic tools are employed to design and simulate a coordinated scheduling strategy, which dynamically adjusts EV charging and discharging activities in order to maximize grid–load balance. To further accommodate the heterogeneity of grid environments and EV usage scenarios, three distinct scheduling modes are designed within the framework. This multi-scheme approach ensures that both power load distribution across the grid and the operational efficiency of EV scheduling can be simultaneously optimized.

Stage Three: Evaluation of Economic Efficiency and Environmental Impact

Building upon the scheduling logic developed in Stage Two to achieve extreme spatio-temporal balancing of power loads, the third stage extends the analysis beyond load distribution and EV dispatch efficiency to examine the broader economic and environmental implications of the proposed optimization framework. In this phase, the model is assessed under a range of scenarios with a dual focus: first, on the economic efficiency of grid operation, and second, on the environmental impact as reflected in carbon emissions. To quantify these outcomes, the optimization logic is tested against empirical tariff structures of the UK power grid and contemporaneous data on carbon intensity. This integration enables a comparative evaluation of energy cost savings and carbon reduction potential before and after the application of the optimized scheduling strategy. By doing so, Stage Three not only demonstrates the operational

effectiveness of the proposed V2G management model but also substantiates its practical feasibility and contribution to long-term sustainability goals.

4.2.3. Who Is It Designed For?

The design framework and interim findings of this study offer valuable decision-making support and practical guidance for various stakeholders within the V2G ecosystem.

For national energy policy makers, the dynamic year-round load distribution model—developed based on a standard UK zero-carbon apartment community (500 households)—systematically quantifies the spatiotemporal characteristics and combined effects of residential electricity consumption, PV generation, and EV charging behaviours. This provides not only benchmark data for constructing standardized zero-carbon community grid models, but also supports higher-level power grids in optimizing cross-regional energy dispatch, improving load forecasting accuracy, and formulating targeted V2G incentive mechanisms. Notably, the proposed idle-EV scheduling strategy identifies threshold values for EV storage availability under different load conditions, offering a quantitative basis for designing dynamic subsidy policies tied to grid stress and real-time electricity prices, as well as demand-response reward schemes.

For electricity market operators, the community grid load simulation model developed in this research addresses key challenges in current electricity pricing mechanisms. The model accurately represents a baseline load curve that accounts for the impact of EV adoption and PV integration, while also projecting the synergistic effects of increasing EV penetration and renewable energy capacity. These outcomes will significantly improve the precision of real-time pricing models, enhance supply-demand balancing efficiency, and increase the grid's renewable energy absorption capacity. The dataset and model outputs can be directly applied

to power market decision support systems, offering scientific insights for refining pricing mechanisms in spot and ancillary service markets.

For the EV industry, this study proposes an optimal charging/discharging power allocation strategy tailored to the UK's V2G market. Simulation results confirm the efficiency advantages of asymmetric charge-discharge configurations and identify ideal power ratios for specific application scenarios. These insights provide direct technical reference for the design of EV powertrains, charging infrastructure specifications, and the standardization of V2G communication protocols. The findings are especially relevant for determining critical technical parameters such as interface circuit design and rated power configuration, contributing to the harmonization and advancement of industry standards.

For end-users, the study establishes a benchmark indicator system for residential electricity consumption, enabling users to align with standard values, adjust usage patterns according to real-time pricing, and strategically plan EV charging and discharging. Empirical analysis shows that adopting the proposed consumption strategies significantly increases household V2G revenues while reducing annual electricity expenses at the community level. This win–win outcome—enhancing both user benefits and grid stability—underscores the real-world applicability of the study. The user-oriented behavioural guidance framework presented herein can help maximize economic returns for participants while contributing to overall grid balancing.

4.3. Evaluation Modelling of Components

This section outlines the modelling framework and analytical methods employed to investigate the impact of EV usage patterns on the load balancing capacity of community-level V2G systems. The methodology builds on the data analysis in Chapter 3 and is constructed using two core empirical resources: the Trent Basin zero-carbon community dataset in the UK

(providing residential demand and PV generation profiles) and the EV charging and usage behaviour database developed under the UK My Electric Avenue project. These datasets were integrated to establish a comprehensive community net-load model that captures the joint dynamics of household consumption, renewable generation, and EV-related electricity demand.

Within this framework, two methodological components are emphasized. First, EV charging behaviour is parameterized by fitting empirical charging data to generate time-varying SOC trajectories, from which individual vehicle availability and usage states can be simulated across different time periods. Second, for the net-load model, three key demand curves are defined to support subsequent evaluation: the original net power demand curve, the baseline net power demand curve, and the reference curve representing the theoretical load-balance threshold. Finally, a computational approach is introduced to define and quantify the scheduling requirements necessary to achieve power balance, together with the calculation method for determining the corresponding EV dispatch demand.

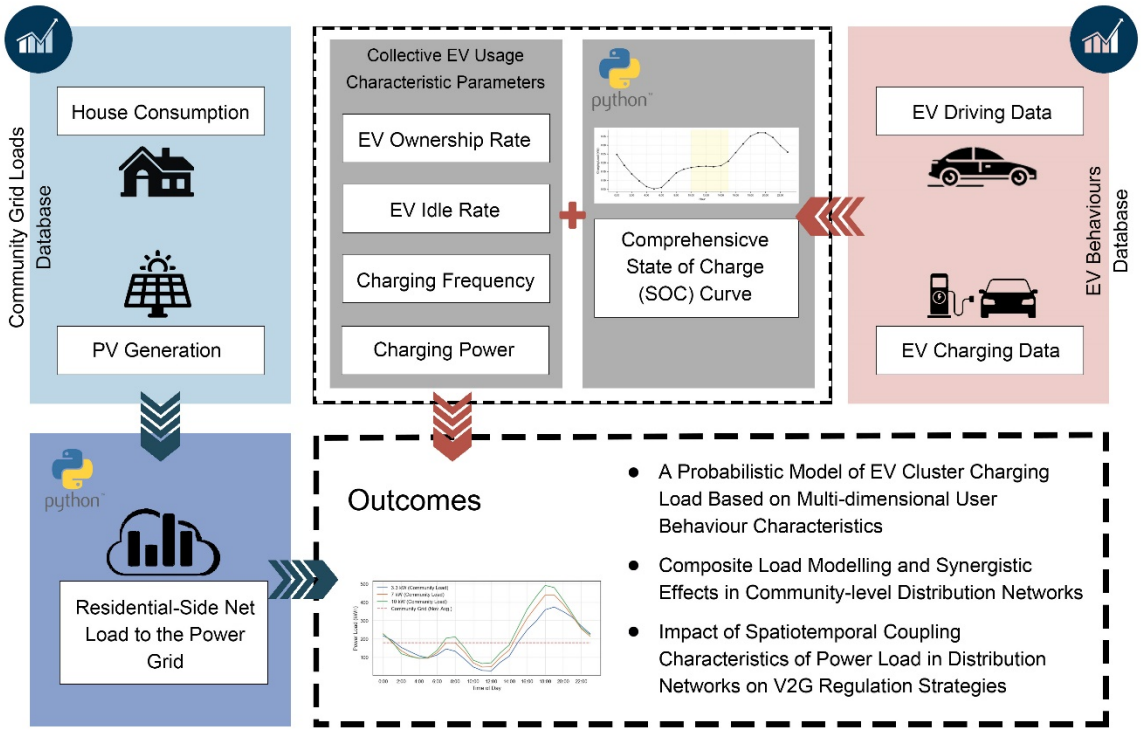


Figure 4-1. Conceptual Framework Illustrating the Influence of Four Key EV Behavioural Parameters on Community-Level Grid Load Dynamics

4.3.1. Estimating State-of-Charge Dynamics

Accurate modelling of the SOC across the different operational phases of active vehicles—namely charging, stationary, and driving—is essential for evaluating V2G readiness and discharge potential. In this study, the term idle refers exclusively to vehicles that exhibit no driving or charging events during the entire day and are therefore excluded from SOC trajectory estimation. For active vehicles, SOC trajectories during charging periods were estimated using a linear growth model derived from recorded session boundaries and known vehicle specifications. Given the start and end times and SOC values for each charging event, the SOC at any intermediate point in time *t* (expressed in hours) was approximated as:

$$SOC(t) = min(SOC_{end}, SOC_{start} + \frac{(t - t_{start}) \times P_{new}}{E_{bat}}) \quad (4.1)$$

Where:

- $SOC(t)$ is the estimated state of charge at time *t* [%],
- SOC_{start} is the recorded state of charge at the beginning of the charging event [%],
- SOC_{end} is the recorded state of charge at the end of the charging event [%],
- t_{start} is the start time of the charging session [h],
- P_{new} is the effective charging power, accounting for on-board charger specifications and connection limits [kW],
- E_{bat} is the nominal battery capacity of the vehicle [kWh].

This formulation assumes constant power input and uniform battery efficiency throughout the charging window. Once the estimated SOC reaches the recorded end value, it is held constant

for the remainder of the session, indicating that the battery has completed charging but remains grid-connected.

During idle periods in the My Electric Avenue dataset—defined as intervals where no driving or charging events were logged, resulting in missing SOC records—SOC values were inferred using heuristic rules grounded in the temporal sequence of observed events. It should be noted that the term *idle* here does not imply that the vehicle remains grid-connected; rather, it refers to periods of non-activity in the dataset during which SOC must be estimated indirectly. The following rules were applied:

- If the idle period follows a completed charging event and precedes driving, SOC is held constant at the end-of-charge level.
- When the idle interval precedes a charging session, SOC is set equal to the upcoming charging session's start value (This rule does not imply that the vehicle is assumed to autonomously reach this level during the idle period; rather, it reflects the fact that the subsequent charging session in the dataset already provides a measured SOC at its onset. The rule therefore uses the observed SOC at the beginning of the next charging event as a boundary condition to backfill the preceding idle interval).
- When a driving period is followed by an idle phase with no subsequent charging, the end-of-use SOC is not recorded. In such cases, the community-average starting SOC at the initiation of charging is used as a proxy, which is reasonable for large EV clusters and has negligible impact on aggregate results.
- For midnight-to-morning idle periods without prior SOC data, the value from the previous evening is carried forward where available. Otherwise, the average SOC at the end of charging is used as a substitute, representing the typical state of vehicles after completing overnight charging and before departure the following morning. Given the

scale of large EV clusters, this approximation is considered reasonable and introduces only negligible error.

For all time intervals outside of the defined Charging Window and Idle Phase—including the Departure (Driving) Period and other periods during which the EV is inferred to be unavailable for V2G participation (e.g., idle periods occurring between two distinct driving intervals)—the SOC values are uniformly set to '-1'. This sentinel value serves as a logical flag, indicating that the corresponding vehicle is not available for scheduling or energy balancing during those times. The use of this placeholder simplifies subsequent logical operations in the V2G optimization process, allowing efficient identification and filtering of vehicles based on their inferred availability status.

These estimation rules enable the construction of time-continuous SOC profiles across both active and inactive periods, ensuring a comprehensive representation of battery status throughout the day.

4.3.2. Modelling Collective EV Behaviour in the Community

The constructed SOC database facilitates simulation of aggregate vehicle behaviour at the community level. The analysis focuses on four primary behavioural metrics that significantly influence grid load modulation:

- EV Ownership Rate: This is defined as the proportion of households in the community with access to an EV. For a 500-household model, ownership levels are varied systematically to assess impacts under different adoption scenarios.
- Idle Rate: Idle rate measures the percentage of EVs that remain unused on a specific study day. Adjusting this parameter enables simulation of diverse engagement levels. To calibrate this, daily usage profiles from historically active vehicles were randomly sampled and reallocated across days to simulate higher or lower idle conditions.

- Charging Intensity: Charging intensity is quantified as the average daily charging duration per active EV. Following the approach described in Section 3.3.3, three representative weeks were selected to capture high, medium, and low charging intensity conditions. Specifically, a standardized metric was used, defined as the total cumulative charging duration of all EVs during a week divided by the sum of daily active EVs over the same seven-day period. This metric directly provides the average daily charging hours per active vehicle, effectively accounting for fluctuations in both vehicle availability and charging behaviour. Based on this metric, the weeks with the maximum, median, and minimum ratios were identified as representative cases. For each of these weeks, distinct EV charging load curves were generated to represent the varying intensity levels. Multiplying these curves by the specified charging power yields the average daily energy consumption per active EV under each charging intensity scenario.
- Charging Power: Three distinct charging power scenarios were considered—3.3 kW (baseline), 7 kW, and 10 kW—to reflect different levels of infrastructure availability. SOC curves for the higher-power cases were recalculated while keeping the behavioural sequences unchanged.

Through this parameterized simulation, a comprehensive database is first generated to capture the SOC trajectories of all EVs on the selected study day under varying conditions defined by different influencing factors. This database, constructed according to the specified parameter settings, serves as the foundational input for the subsequent V2G scheduling framework developed in this research. It enables systematic evaluation of how these factors shape the effectiveness of the proposed V2G optimization strategy in achieving balanced intraday power distribution within the community grid, while also determining their implications for the overall efficiency of EV dispatch.

4.3.3. Simulation-Based Evaluation of Grid Load Dynamics and V2G Optimization Feasibility

To quantitatively evaluate the load adjustment required from a V2G system over a specific period, this study defines three key power demand profiles based on the overall load characteristics of a standard community-level grid: the original net power demand curve, the baseline net power demand curve, and the reference curve. These three curves together provide a structured framework for assessing the extent to which V2G operations are required to reshape the community grid load profile. For clarity, the relationships among these three curves can be illustrated with reference to the simulation results presented in Chapter 5, particularly Figure 5-1, where their interactions are visualized within the optimized dispatch process. The evaluation itself is conducted over a 24-hour time horizon with an hourly time resolution, enabling the analysis to capture the temporal dynamics of community electricity demand and the corresponding adjustments required from coordinated EV charging and discharging.

The baseline net power demand curve is defined as residential consumption minus PV generation, effectively representing the grid profile without any EV-related demand. This curve serves as the foundational load profile for assessing V2G's regulatory capacity.

$$P_{baseline}(t) = P_{residential}(t) - P_{PV}(t) \tag{4.2}$$

Where:

- $P_{residential}(t)$ represents the scaled residential consumption at hour t.
- $P_{PV}(t)$ is the solar generation from the PV system.

Meanwhile, the original net power demand at each time step is calculated by summing the residential electricity consumption and the EV charging demand under uncontrolled charging

scenarios (i.e., without V2G coordination), and then subtracting the power generated from PV systems:

$$P_{original}(t) = P_{residential}(t) + P_{EV}(t) - P_{PV}(t) \quad (4.3)$$

Where:

- $P_{residential}(t)$ represents the scaled residential consumption at hour t.
- $P_{EV}(t)$ represents the total EV charging demand at hour t, calculated as the number of EVs actively charging at that time multiplied by the charging power per vehicle.
- $P_{PV}(t)$ is the solar generation from the PV system.

To determine the magnitude of load adjustment required from V2G, the baseline curve is evaluated against a reference curve. Unlike a time-varying trajectory, the reference curve is constructed as a constant value over all 24 hours of the target day. Its magnitude is calculated as the monthly average residential electricity consumption minus the monthly average PV generation, plus the total charging demand of all active EVs on the target day, evenly distributed across 24 hours. This formulation serves two fundamental objectives: it captures the seasonal characteristics of community-level net load and establishes a long-term equilibrium benchmark that mitigates distortions arising from short-term fluctuations on atypical days, while simultaneously preserving the actual EV charging demand corresponding to the specific study day.

The decision to average the non-EV components of the reference load on a monthly rather than daily basis is methodologically motivated. At the current stage of EV penetration, EV charging represents only a limited proportion of total community electricity demand. Consequently, whether the community functions as a net exporter or net importer to the upstream grid is primarily determined by conventional residential consumption and PV generation rather than

EV charging. Under this condition, the monthly average hourly net demand (residential load minus PV generation) effectively represents a stable “baseline operating point” of the community. This constant value reflects the fundamental supply–demand balance excluding EVs and avoids overemphasising short-term irregularities.

Adopting daily averages would marginally increase temporal precision but introduce unnecessary volatility into the reference signal. Apart from exceptional days (e.g., major holidays), the daily average residential electricity consumption within a given month remains relatively stable, with differences mainly arising between weekdays and weekends. Using daily averages would therefore produce a reference value that fluctuates slightly from day to day. Although such variations may appear minor, they would impose additional data management and coordination burdens both within the community’s centralised control framework and at the upstream grid level, without delivering commensurate analytical benefits. From a computational and operational perspective, the incremental precision does not justify the increased complexity.

From the perspective of seasonal PV generation, monthly resolution is also sufficient. Seasonal changes in solar irradiance and daylight duration manifest predominantly at the monthly scale rather than through systematic daily shifts. Moreover, since the reference curve relies on historical data to approximate current conditions, pursuing daily-level accuracy does not necessarily enhance predictive reliability. On the contrary, it may amplify weather-induced deviations. For example, if the historical data for 6th June corresponded to a rainy day while the current year’s 6th June is exceptionally sunny, a daily-average-based reference would substantially overestimate net demand due to underestimated PV generation, thereby enlarging prediction error. A monthly average smooths such meteorological variability, sacrificing superficial precision in exchange for greater robustness and stability.

Importantly, the monthly averaging procedure applies only to conventional residential demand and PV generation, thereby preserving their seasonal characteristics. EV charging demand, in contrast, is treated with greater flexibility to reflect actual user behaviour. As described in Chapter 3, the total daily EV charging demand in the community is calculated as the product of (i) the average daily charging energy of a single active EV and (ii) the total number of active EVs on the target day. In practical implementation, the number of active EVs is reported by vehicle owners one day in advance.

The average daily charging demand of a single active EV is derived from the "My Electric Avenue" dataset compiled in Chapter 3. In this database, each active EV contributes a 24-hour SOC record for each day of activity. For each defined charging window within a data set, the energy charged is computed as the SOC increment multiplied by the battery capacity. Summing the charging energy across all charging windows yields the total daily charging demand for that EV on that specific day. By aggregating the daily charging demand across all recorded data sets over one year and dividing by the total number of active-day records, the mean daily charging demand of a representative active EV is obtained.

This annual-level averaging enhances statistical robustness by diluting the influence of extreme or atypical behaviours. For instance, charging demand may be unusually low on a day with limited vehicle use or unusually high on a day with intensive travel. Averaging across a full year ensures that the estimated daily charging demand reflects typical usage patterns and covers the majority of realistic scenarios. Consequently, the forecasted EV demand used in the reference curve is more reliable and less sensitive to outliers.

Through this construction, the methodology approximates a flat net-demand target aligned with the monthly equilibrium level, thereby alleviating stress on upstream transmission networks, while preserving the genuine aggregate charging requirements of EV users on the target day.

The hourly deviation between the baseline curve and this constant benchmark quantifies the adjustment required from V2G scheduling. Specifically, this deviation defines the charging and discharging modulation that EVs must undertake to reshape the community load profile in response to grid-level operational objectives.

To verify the feasibility of the study's objective—namely, utilizing idle EVs in a community to supplement V2G functions for local grid support—an estimation-based validation is conducted. Specifically, under the assumption that the usage trajectories of active EVs remain unchanged on the target day, the proposed method calculates the power mismatch between the original net power demand curve and the reference curve. This mismatch represents the most demanding adjustment scenario for the V2G system. If this worst-case scenario can be accommodated solely by mobilizing idle EVs for bidirectional regulation—charging to absorb surplus generation and discharging to alleviate deficits—then incorporating optimization for active EVs as well would further enhance system reliability. Therefore, satisfying this extreme case serves as strong evidence for the overall feasibility of the proposed approach. The deviation between the actual and reference curves, denoted as

$$\Delta P(t) = P_{original}(t) - P_{ref}(t) \tag{4.4}$$

and is interpreted as the additional power required (or surplus to be absorbed) for balancing.

The minimum number of EVs required to compensate for this power gap through discharging is computed using:

$$N_{EV}(t) = \lceil \frac{\Delta P(t)}{P_{discharge}} \rceil \tag{4.5}$$

Where $P_{discharge}$ is the standard discharging power per vehicle. This value represents the dispatch demand necessary to maintain power balance; in other words, at times of peak demand, at least this number of EVs must be available and capable of discharging to the community grid. By analogy, during load valleys the required number of EVs available for charging is obtained using the same formulation, with the denominator replaced by the charging power. The ceiling function ensures that partial vehicle capacities are rounded up to whole units for deployment planning. This formulation enables quantification of resource adequacy for V2G-based grid stabilization under varying behavioural and technical conditions.

4.4. Algorithm Design

In the data processing stage, a comprehensive community-level power distribution model was developed. This model includes demand-side loads, supply-side generation, and community EV clusters characterized by diverse usage patterns. It captures the temporal power distribution across the community grid and provides a reference for the monthly peak power load balance under an uncontrolled scenario, i.e., without any external regulation or intervention. Building upon this foundational model, the study proceeds to its core objective: the design of an optimized V2G management strategy and charging/discharging logic for EV clusters. The proposed framework aims to coordinate the charging behaviour of EVs in a way that does not disrupt their normal usage patterns, while maximizing the overall efficiency of energy exchange between the grid and EVs. This is achieved by leveraging both active and idle EVs—especially by tapping into the latent energy exchange potential of idle EVs—to meet the combined power balancing needs of the grid and the EV fleet.

Section 4.4 elaborates on the core optimization framework in three main parts. Figure 4-2 illustrates the overall control logic of the optimized V2G scheduling algorithm developed in this study. The figure provides a high-level overview of the algorithmic workflow, while the

detailed logic of each component is explained separately in the following subsections. Section 4.4.1 describes the construction of a daily EV database. Unlike Section 4.3, which focuses on empirical data analysis, this subsection represents a key preparatory stage within the centralized V2G optimization framework. In this context, the EV database functions as an input module for the optimization algorithm. Based on user-defined parameter settings, the procedures introduced in this section generate the EV dataset required for subsequent scheduling calculations and simulation outcomes. Section 4.4.2 then introduces three optimization scenarios, each corresponding to a distinct V2G scheduling strategy with its own EV dispatch logic. These scenarios represent alternative operational approaches for coordinating charging and discharging activities within the community grid. Finally, Section 4.4.3 defines the fundamental operational rules governing EV charging and discharging within the proposed framework. This subsection specifies the control constraints and decision logic applied during the scheduling process, which ensure consistent and feasible implementation of the algorithm across the different optimization scenarios.

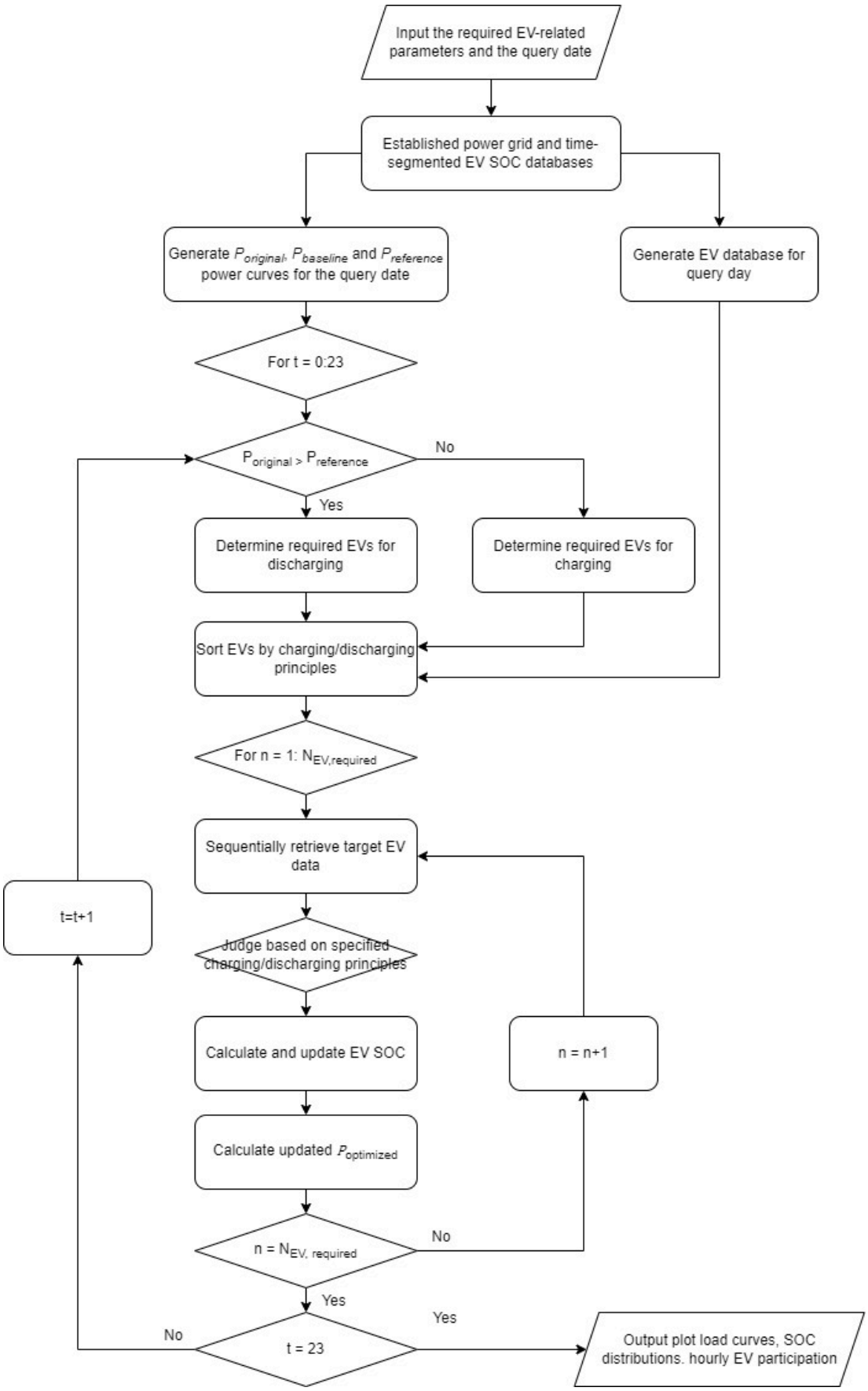


Figure 4-2. Workflow of the proposed centralized V2G optimization scheduling algorithm

4.4.1. EV Research Database for Usage Patterns on Targeted research day

Within the V2G optimization framework, the first step requires users to specify the target simulation day along with the basic composition of the EV fleet, particularly the penetration rate and the idling ratio. These parameters serve as the foundational inputs for constructing a synthetic EV fleet database representative of the community under study. By defining EV ownership and the proportion of vehicles available for idle-based participation, the model establishes the boundary conditions for simulating grid performance under varying usage scenarios and for evaluating the potential of V2G to enhance load balancing. The total number of EVs in the community fleet for a given scenario is then computed as:

$$N_{EV-User} = 500 \times EV_{penetration} \tag{4.6}$$

where $EV_{penetration}$ denotes the proportion of households equipped with electric vehicles.

Based on the assumed idling ratio, the number of idle and active vehicles is then determined by:

$$N_{idle} = N_{EV-User} \times EV_{idle\,ratio} \tag{4.7}$$

$$N_{active} = N_{EV-User} \times (1 - EV_{idle\,ratio}) \tag{4.8}$$

To align the constructed dataset with the user-defined scenario parameters—including EV penetration rate, idling ratio, and the specified target day—the model first computes the exact number of total, active, and idle EVs required for the simulation. These targets are then reconciled with the empirical SOC database built from historical EV records for the corresponding day. Because the empirical dataset rarely matches the required fleet composition exactly, an adjustment procedure is applied to ensure internal consistency:

- If the number of active EVs is insufficient, additional active vehicle profiles are randomly sampled from records of other days. These duplicated entries are assigned new virtual ID labels to distinguish them within the dataset.
- Similarly, if the number of idle EVs is inadequate, additional idle vehicle profiles are also randomly selected and incorporated, each assigned a new virtual ID.
- Conversely, if there is a surplus of either active or idle EVs, excess entries are randomly removed from the dataset to match the desired ratios.

Through this iterative calibration process, a synthetic dataset is constructed for the target day. This database contains the SOC profile for each EV across 24 hours and is used as the foundation for subsequent V2G optimization simulations.

For idle EVs without recorded SOC data on the study day, virtual IDs are first assigned to match the required number of idle vehicles. These EVs are treated as new entries in the dataset. Subsequently, their initial SOC values must be defined. If a given EV (identified by its ID) is classified as idle on the study day but was active on the previous day—meaning its SOC profile is available from the day before—then its SOC at 23:00 on the previous day is used as the initial SOC value for the current day.

However, if the EV was not active on the previous day and thus lacks a recorded SOC profile, an alternative estimation method is applied. This involves introducing an auxiliary statistical parameter: the distribution of SOC values at the start of charging events across all EVs in the dataset. First, the start-of-charge SOC values from all charging records are collected and grouped into 13 SOC levels (from 0 to 12, corresponding to 0% to 100% SOC). A weighted distribution histogram is then constructed to represent the likelihood of each SOC level.

Based on this distribution, the expected number of idle EVs in each SOC category is calculated. From each category, the number of idle EVs that already have initial SOC values from the

previous day is subtracted. The remaining number of EVs in each SOC level is then randomly assigned to the virtual idle EV IDs with no historical SOC data, preserving the overall statistical distribution.

4.4.2. V2G Optimization Management Strategies for Three Designed Scenarios

Scenario I: Prioritizing Active EVs with Idle EVs as Supplemental Resources

This scenario is designed for community environments where EVs exhibit regular and predictable usage patterns, and where the proportion of active vehicles remains relatively high throughout the day, resulting in fewer idle vehicles available for grid regulation. The strategy primarily utilizes the fleet of actively operating EVs to balance power fluctuations in the grid. Idle EVs are engaged only as supplemental resources when the power imbalance exceeds the modulation capacity of active EVs—such as during peak demand hours or under unexpected supply surpluses.

The rationale of this scenario is twofold. First, it focuses on active EVs as the primary regulating resource, with idle EVs engaged only when additional flexibility is required. Second, by requiring active vehicles to connect during their stationary phases—when they are already parked on-site—the strategy enables real-time participation in grid balancing without disrupting habitual driving routines. By respecting habitual vehicle usage in this way, the approach strikes a practical balance between operational feasibility and grid-level optimization, while simultaneously expanding the effective storage potential of the V2G system.

The simulation is conducted over a standard 24-hour period, from 00:00 to 24:00, with a temporal resolution of one hour. Based on the methodology established previously, the active and idle EV populations are first identified for the target day, and a time-resolved SOC database is constructed accordingly.

Beginning at hour 0, an hourly optimization schedule is constructed across the 24-hour simulation window. At each time step, the power gap between the baseline net power demand curve and the reference curve is calculated to determine the appropriate V2G action—either charging or discharging—and the magnitude of energy adjustment required.

Specifically, if $P_{original}(t)$, as defined in Equation (4.3) of Section 4.3.3—namely, the sum of the baseline net power demand ($P_{baseline}(t)$) and the EV charging load at time *t* ($P_{EV}(t)$) — falls below the corresponding reference value, the system initiates a charging response. Conversely, when the combined load $P_{original}(t)$ exceeds the reference curve, the system triggers a discharging response to mitigate the surplus.

Charging Case:

If the baseline net demand plus the time-specific mandatory EV charging demand $P_{EV,potential}(t)$ remains lower than the reference value, the system determines that additional EV charging should be activated to absorb surplus generation. The parameter $P_{EV,potential}(t)$ represents the total charging power required at time *t* for EVs whose SOC falls below the minimum threshold specified in the V2G management scheme. In this study, a minimum SOC level of 20% is imposed to ensure that vehicles maintain a basic level of battery availability. Whenever an EV's SOC drops below this threshold, the control system classifies the vehicle as requiring mandatory charging and initiates charging until the SOC reaches the minimum acceptable level. Consequently, $P_{EV,potential}(t)$ corresponds to the aggregated charging demand of all such vehicles at time *t*, which can be expressed as the product of the fixed charging power and the number of EVs that must be charged to restore the minimum SOC requirement.

After accounting for this mandatory charging demand, if the resulting net demand still remains below the reference level, additional EV charging is scheduled. The available active EVs (i.e., those currently parked within the community and connected to the charging infrastructure) are first sorted in ascending order of SOC, thereby prioritizing vehicles with lower battery levels. The detailed rules governing the charging assignment and prioritization process are provided in Section 4.4.3. Charging is then allocated sequentially at the fixed charging power P_{charge} until the required number of vehicles to be charged, $N_{charge,required}$ is reached. This number is determined according to the following expression:

$$N_{charge,required}(t) = \left\lceil \frac{\left| P_{baseline}(t) + P_{EV,potential}(t) - P_{ref}(t) \right|}{P_{charge}} \right\rceil \quad (4.9)$$

If the pool of active EVs is insufficient to satisfy the required number of charging vehicles, idle EVs are subsequently dispatched. These are also prioritized in ascending order of SOC, following the same selection logic as for active EVs, until the total number of vehicles $N_{charge,required}$, real matches the requirement, or until all available EVs have been utilized. It is important to emphasize that all EVs selected for charging must comply with the eligibility criteria defined in Section 4.4.3, particularly those related to the SOC thresholds established under the EV charging management framework. This ensures that the charging process respects the operational constraints of the battery systems and aligns with the mobility needs of vehicle owners.

The SOC of each participating EV is updated for the next time step, with strict enforcement of the upper limit to ensure that the battery capacity never exceeds 100%:

$$SOC(t+1) = SOC(t) + \frac{P_{charge} \times 1\ hour}{E_{bat}} \times 100\% \quad (4.10)$$

For the subsequent hour, the system reorders the list of available EVs based on their updated SOC values, ensuring that vehicle selection for V2G operations aligns with the latest battery states and availability conditions. The updated grid load at hour t is then given by:

$$P_{optimized}(t) = P_{baseline}(t) + P_{EV,potential}(t) + P_{charge} \times N_{charge,real} \tag{4.11}$$

Discharging Case:

If the baseline net demand exceeds the reference, discharging is required. Available active EVs are sorted in descending order of SOC. Discharging is assigned similarly using a fixed discharging power $P_{discharge}$, with the number of required vehicles given by:

$$N_{discharge,required}(t) = \left\lceil \frac{\left| P_{baseline}(t) + P_{EV,potential}(t) - P_{ref}(t) \right|}{P_{discharge}} \right\rceil \tag{4.12}$$

As before, idle EVs are added if active EVs alone are insufficient, and the final deployed fleet size is denoted $N_{discharge,real}$. With strict enforcement of the lower capacity threshold defined in Section 4.4.3 to ensure that battery levels never fall below the prescribed discharge limit, each participating vehicle's SOC is updated as:

$$SOC(t+1) = SOC(t) - \frac{P_{discharge} \times 1\ hour}{E_{bat}} \times 100\% \tag{4.13}$$

The updated SOC values are assigned to their respective EV IDs and will serve as the basis for reordering the vehicle pool at the next time step, thereby informing subsequent V2G decisions based on real-time battery status. The optimized grid power at hour t becomes:

$$P_{optimized}(t) = P_{baseline}(t) + P_{EV,potential}(t) - P_{discharge} \times N_{charge,real} \tag{4.14}$$

Scenario II: Idle-EV-Only V2G Strategy Without Altering Active EV Charging Behaviour

This scenario is designed under the assumption that it is currently impractical to immediately alter EV users' habitual charging and driving behaviours. It specifically targets community energy environments where EV usage rates are low and the proportion of idle vehicles is relatively high. To preserve the original usage patterns of active EVs, this approach leverages only idle EVs to support grid power balancing.

By exclusively using idle EVs, this strategy avoids interfering with user routines and reduces the frequency of charge/discharge cycles for individual EVs, thereby minimizing battery degradation and preserving battery life and user net present value (NPV). Moreover, the scenario indirectly tests the feasibility of replacing other forms of stationary energy storage with idle EVs as temporary mobile storage assets for local grid stabilization.

Additionally, this approach can be seen as a simplified variant of a battery-package-based V2G management scheme, offering preliminary evidence on whether idle EV clusters—managed independently from users' daily routines—can serve as effective, decentralized grid-balancing units.

Similar to Scenario I, the operational logic follows an hour-by-hour schedule across a standard 24-hour simulation window. However, only idle EVs are eligible for dispatch. First, the power gap to be balanced—defined as the absolute difference between the original net demand curve $P_{original}(t)$ and the reference curve $P_{ref}(t)$—is computed at each time step (shown in Eq.(4.4)). Notably, because active EVs' charging behaviors are no longer optimized under this scheme, their charging demand remains part of the net load and must be accounted for when calculating the required corrective power:

$$N_{charge,required}(t) = \lceil \frac{\left|P_{original}(t) - P_{ref}(t)\right|}{P_{charge}} \rceil = \lceil \frac{\Delta P(t)}{P_{charge}} \rceil \quad (4.15)$$

$$N_{discharge,required}(t) = \lceil \frac{\left|P_{original}(t) - P_{ref}(t)\right|}{P_{discharge}} \rceil = \lceil \frac{\Delta P(t)}{P_{discharge}} \rceil \quad (4.16)$$

Idle EVs are then sorted in ascending order of their SOC values for charging (or descending for discharging). They are sequentially selected for charging or discharging until either the number of required vehicles is met or no additional idle EVs satisfy the operational constraints defined in Section 4.4.3.

Each selected vehicle's state of charge (SOC) is updated according to the following formulations. As in the previous operational steps, both charging and discharging processes strictly follow the operational constraints defined in Section 4.4.3. In particular, during charging the SOC is capped to ensure that the battery level does not exceed its physical upper limit of 100%. Conversely, during discharging the SOC is constrained to remain above the prescribed lower bound of 0, thereby preventing over-discharge and ensuring battery protection. For charging, the SOC update is calculated according to Equation (4.10). For discharging, the SOC update follows Equation (4.13). The updated SOC values are recorded for each EV using its unique vehicle ID and are subsequently used to reorder the available EV fleet at the next time step according to their SOC levels, thereby ensuring that the scheduling decisions in the following interval reflect the latest battery conditions of all vehicles. Consequently, the grid load after V2G adjustment at hour t is calculated as:

For charging:

$$P_{optimized}(t) = P_{original}(t) + P_{charge} \times N_{charge,real} \quad (4.17)$$

For discharging:

$$P_{optimized}(t) = P_{original}(t) - P_{discharge} \times N_{charge,real} \quad (4.18)$$

Scenario III: Unrestricted Charging/Discharging of All EVs

This scenario investigates the modulation capacity of a centralized V2G system under special circumstances in which all EVs are continuously available—such as during pandemic-related lockdowns when most individuals work from home. In such contexts, a large proportion of EVs remain idle and can be freely dispatched by the V2G system at any time. As a result, the entire EV fleet effectively functions as a stationary battery energy storage system with fixed capacity. This approach explores the potential for centralized V2G systems to serve as a temporary substitute for conventional stationary battery storage infrastructure.

Data Preparation: To simulate this environment, all EVs in the research-day dataset are treated as idle, regardless of their original status. A unified replacement process is conducted whereby the state of charge (SOC) of each EV ID is randomly reassigned based on the initial SOC distribution observed for idle EVs, as outlined in earlier sections.

V2G Dispatch Method: Following this, the system calculates the number of EVs required to balance grid load fluctuations at each time step t, using the same approach as in Scenarios I and II. However, since all EVs remain stationary (i.e., no driving activity occurs), there is no vehicle-induced energy consumption. Consequently, the power variations to be compensated stem solely from residential electricity demand and rooftop PV generation. The number of EVs required for charging or discharging is determined as:

$$N_{charge,required}(t) = \lceil \frac{|P_{baseline}(t) - P_{ref}(t)|}{P_{charge}} \rceil \quad (4.19)$$

$$N_{discharge,required}(t) = \lceil \frac{|P_{baseline}(t) - P_{ref}(t)|}{P_{discharge}} \rceil \quad (4.20)$$

Dispatch Logic: The dispatch logic mirrors that of the previous two scenarios. When the baseline net power demand falls below the reference curve, the system enters the charging phase. EVs are sorted in ascending order of SOC and selected sequentially until either the required number of EVs is reached or no further EVs meet the eligibility criteria defined in Section 4.4.3. Conversely, when the baseline exceeds the reference, the system initiates discharging by sorting EVs in descending order of SOC and dispatching them accordingly.

SOC Update and Grid Load Optimization: Each participating EV's SOC is updated using the following formulations. For the charging process, the SOC update is calculated according to Equation (4.10), whereas for the discharging process the SOC update follows Equation (4.13). SOC values are assigned to corresponding EV IDs and used for sorting at the next time step. The optimized net grid load at time t is updated as:

Charging phase:

$$P_{optimized}(t) = P_{baseline}(t) + P_{charge} \times N_{charge,real} \tag{4.21}$$

Discharging phase:

$$P_{optimized}(t) = P_{baseline}(t) - P_{discharge} \times N_{charge,real} \tag{4.22}$$

4.4.3. Basic Charging and Discharging Requirements and Logic

Design of SOC Threshold for Charging/Discharging Decisions: The decision threshold $SOC_{criterion}$ is established based on the mode value of the initial state of charge ($SOC_{start,mode}$) observed at the beginning of recorded charging sessions. This statistical measure reflects the typical remaining battery level when users plug in their vehicles, thereby representing the approximate energy requirement of the most prevalent driving behaviours in the community.

The criterion is thus designed to preserve a sufficient energy reserve for users' routine travel needs and minimize the risk of V2G interventions compromising daily mobility. The threshold is defined as:

$$SOC_{criterion} = 100\% - SOC_{start,mode} \tag{4.23}$$

Charging/Discharging Logic in Scenario I

- Special Charging Requirement: If an active EV's SOC falls below the threshold $SOC_{criterion}$, the vehicle is prioritized for charging regardless of whether the current V2G schedule calls for charging or discharging. Charging continues until the SOC exceeds the threshold.

- Charging Logic and Conditions: For all available EVs with $SOC_{criterion} \leq SOC < 100\%$, and during time steps where the system identifies a need for V2G charging, eligible EVs are sorted in ascending order of SOC and charged sequentially. Once an EV reaches $SOC = 100\%$, it exits the charging pool.

- Discharging Logic and Conditions: For all available EVs with $SOC_{criterion} \leq SOC \leq 100\%$, and during time steps where discharging is required, EVs are sorted in descending order of SOC and discharged until their SOC drops to $SOC \leq SOC_{criterion}$, at which point they exit the discharging pool.

Charging/Discharging Logic in Scenarios II and III

- Charging Logic and Conditions: For available EVs with $0 \leq SOC < 100\%$, and during time steps when V2G charging is needed, EVs are sorted by ascending SOC and charged sequentially. Vehicles exit the charging pool once they reach $SOC = 100\%$.

- Discharging Logic and Conditions: For EVs with $SOC_{criterion} < SOC \leq 100\%$, and during periods requiring V2G discharging, EVs are sorted in descending order of SOC and discharged until they reach $SOC \leq SOC_{criterion}$, at which point they are no longer eligible for discharging.

SOC Update Mechanism for V2G Scheduling

In order to ensure the accuracy and consistency of SOC updates within the V2G scheduling framework, a differentiated update mechanism is designed for two distinct categories of EVs (active EVs and idle EVs). The primary objective of this mechanism is to align the simulated SOC evolution with the real-world constraints imposed by vehicle availability, without altering the original mobility patterns recorded in the dataset.

For active EVs, the SOC update process must account for off-site periods during which the vehicle is unavailable for grid interaction. These periods are denoted in the original SOC data by placeholder values (e.g., -1), indicating the vehicle's absence. The update logic ensures that such entries remain untouched during scheduling, thus preserving the vehicle's original usage trajectory. When the EV is on-site, its SOC is updated based on the charging or discharging actions it undergoes. However, if an EV departs following a scheduling event and later returns, it is necessary to recalculate the SOC at the return time by offsetting the previously updated departure SOC with the energy presumed to be consumed during its absence, as inferred from the original SOC difference over the same period,

$$SOC_{end,opmized} = SOC_{start,optimized} - \frac{(t - t_{start}) \times P_{new}}{E_{bat}} \tag{4.24}$$

Or,

$$SOC_{start,optimized} - SOC_{end,opmized} = SOC_{start,original} - SOC_{end,original} \quad (4.25)$$

This adjustment is crucial for maintaining internal consistency between the optimized dispatch outcomes and the EV's inferred energy usage behaviour during non-participation periods.

In contrast, idle EVs are treated as continuously available resources over the entire scheduling interval. Their SOC evolution is governed by a forward-propagation mechanism, wherein the SOC is initialized to a given starting value and subsequently updated in response to each scheduling action. Once a vehicle has been selected for charging or discharging in a particular time slot, all subsequent SOC values are iteratively updated to reflect this change, thereby ensuring that the simulated energy state remains consistent with the cumulative effect of scheduling decisions over time. Since idle EVs do not experience interruptions in availability, their SOC update process is comparatively straightforward and does not require retrospective adjustments.

This dual-mode SOC update framework is embedded within the overall dispatch algorithm, enabling dynamic and accurate tracking of vehicle energy states while strictly adhering to mobility constraints. It serves as a foundational component for evaluating scheduling strategies under realistic operational conditions, ensuring that both spatial-temporal availability and energy dynamics are coherently integrated within the simulation environment. The pseudocode illustrating this logic is presented as follows:

```
// Initialize updated_SOC_matrix as a deep copy of the original SOC data matrix
updated_SOC_matrix = deep_copy(original_SOC_matrix)
// Loop over each EV in the dataset
for each EV in EV_list:
    if EV is active:  // Active EV with time-varying availability
        departure_SOC = null  // To store SOC at departure before off-site period
        offsite_start_hour = null  // Track when vehicle goes off-site
```

```
    // Iterate through each hour of the day
    for hour from 0 to 23:
        current_original_SOC = original_SOC_matrix[EV][hour]
        if current_original_SOC == -1:
            // Vehicle is off-site at this hour: no scheduling possible
            updated_SOC_matrix[EV][hour] = -1
            // If vehicle just left this hour (previous hour was on-site)
            if hour > 0 and original_SOC_matrix[EV][hour-1] != -1 and departure_SOC == null:
                departure_SOC = updated_SOC_matrix[EV][hour-1]
                offsite_start_hour = hour
            continue  // Skip to next hour
        else:
            // Vehicle is on-site: participate in scheduling
            // Apply scheduling update: calculate new SOC based on dispatch decisions
            updated_SOC = ScheduleUpdate(EV, hour, updated_SOC_matrix[EV][hour])
            updated_SOC_matrix[EV][hour] = updated_SOC
            // Check if vehicle just returned from off-site period
            if departure_SOC != null and hour > 0 and original_SOC_matrix[EV][hour-1] == -1:
                // Calculate SOC difference during off-site time from original data
                original_delta_SOC = original_SOC_matrix[EV][offsite_start_hour - 1] - current_origin
al_SOC
                // Adjust updated SOC at return time by subtracting energy consumed off-site
                corrected_SOC = departure_SOC - original_delta_SOC
                // Update SOC to corrected value to maintain consistency
                updated_SOC_matrix[EV][hour] = corrected_SOC
                // Reset departure tracking variables
                departure_SOC = null
                offsite_start_hour = null

    else:  // Idle EV, available full 24 hours
        // Initialize current SOC with starting SOC
        current_soc = original_SOC_matrix[EV][0]
        // Iterate through each hour, updating SOC based on scheduling
        for hour from 0 to 23:
            if EV is scheduled at hour:
                // Update current SOC based on charging or discharging power
                current_soc = ScheduleUpdate(EV, hour, current_soc)
```

// Assign updated SOC for this hour
updated_SOC_matrix[EV][hour] = current_soc

4.5. Evaluation Principles and Metrics

Beyond assessing the effectiveness of V2G scheduling in flattening grid power fluctuations, this study also quantitatively evaluates the environmental and economic benefits of each optimization scenario. Specifically, it measures improvements in carbon emissions (i.e., environmental friendliness) and total electricity costs (i.e., economic efficiency), thereby providing a holistic assessment of V2G's multi-dimensional value for community-scale grids.

For the evaluation of carbon emissions, this study utilizes data from the '2019 Real-Time Carbon Intensity of the Electricity System in Great Britain', jointly published by the Carbon Intensity API (National Energy System Operator), Environmental Défense Fund Europe, the University of Oxford Department of Computer Science, and WWF (Carbon Intensity API et al., 2019). This dataset provides hourly carbon intensity values (in kg CO_2/kWh), which are used to estimate emissions both before and after V2G optimization.

The carbon emissions at each hour t are calculated by multiplying the grid's hourly net power demand by the corresponding carbon intensity factor. Specifically, before optimization, the original net power demand $P_{original}(t)$ is used, while after optimization, the adjusted value $P_{optimized}(t)$ is employed. If the net demand is negative (i.e., PV generation exceeds local load), the excess generation is assumed not to be absorbed and thus excluded from emission accounting.

The hourly carbon emissions are calculated as:

$$C_t = E_t \times CF_t \tag{4.26}$$

where E_t is the electricity consumption in hour t (in kWh), and CF_t is the corresponding carbon emission factor (in kg CO_2/kWh).

The daily carbon emissions are obtained by summing emissions across all 24 hours:

$$C_{day} = \sum_{t=0}^{23} C_t = \sum_{t=0}^{23} (E_t * CF_t) \tag{4.27}$$

Similarly, the annual carbon emissions are calculated by aggregating daily emissions across all 365 days of the year:

$$C_{year} = \sum_{d=1}^{365} C_{day,d} = \sum_{d=1}^{365} (\sum_{t=0}^{23} (E_{t,d} * CF_{t,d})) \tag{4.28}$$

where $E_{t,d}$ represents electricity consumption during hour t on day d, and $CF_{t,d}$ is the carbon intensity for that hour.

In a similar manner, the economic performance of V2G optimization is evaluated by comparing total electricity costs before and after optimization, using time-of-use electricity pricing. For this purpose, the study adopts the '2020 time-of-use electricity tariff data' provided by LimeJump, a recognized UK-based energy trading platform. This pricing scheme reflects the real-time cost of electricity throughout the day and is used to assess how V2G strategies can reduce electricity expenditures through intelligent load shifting.

The methodology parallels that of the carbon emission analysis: for each hour, the grid's net power demand is multiplied by the corresponding electricity price. Specifically, the pre-optimization demand is denoted by $P_{original}(t)$, while the post-optimization demand is denoted by $P_{optimized}(t)$. When the grid net demand is negative—i.e., when PV generation exceeds the load—it is assumed that this surplus power cannot be absorbed or exported, and is therefore excluded from the billing calculation. This treatment reflects the absence of explicit

export tariffs in the RTP dataset and avoids assigning unrealistically high revenues to the unoptimized system, which would otherwise appear to "sell" electricity back to the grid at the full retail purchase price. In contrast, the optimized case is evaluated under the assumption of community-level coordination and supporting V2G infrastructure (based on the S-G-L-S configuration), which allows surplus power to be exported at the system price provided by LimeJump. Although conservative, this approach ensures that both scenarios are assessed on a consistent basis, without artificially inflating the baseline performance while still capturing the realistic economic potential unlocked by optimization.

The hourly electricity bill is computed as:

$$B_t = E_t \times BF_t \tag{4.29}$$

where E_t is the electricity consumption in hour t (in kWh), and BF_t is the corresponding time-of-use electricity price (in p/kWh).

The daily electricity bill is obtained by summing across 24 hours:

$$B_{day} = \sum_{t=0}^{23} B_t = \sum_{t=0}^{23} (E_t * BF_t) \tag{4.30}$$

The annual electricity bill is then calculated by summing all daily bills over the course of a year:

$$B_{year} = \sum_{d=1}^{365} B_{day,d} = \sum_{d=1}^{365} (\sum_{t=0}^{23} (E_{t,d} * BF_{t,d})) \tag{4.31}$$

where $E_{t,d}$ is the electricity consumption at hour t on day d, and $BF_{t,d}$ is the price of electricity at that specific hour. Negative values of $E_{t,d}$ therefore represent surplus generation, which is treated as net income.

4.6. Simulation Framework of the Main Control Code

Building upon the detailed methodological framework and control algorithms outlined in the preceding sections, and drawing from the historical database constructed through prior data preprocessing, this study developed a centralized V2G scheduling and control algorithm tailored for community-scale electricity networks. To facilitate a clear understanding of its operational logic, a Python-based simulation framework was implemented, encompassing parameter initialization, data integration, EV population synthesis, reference curve computation, dispatch execution, performance evaluation, and result storage:

1. Parameter Initialization
    - Define key parameters: EV ownership rate, idle rate, charging/discharging power, battery capacity, average hourly charging power (with suggested values derived from the My Electric Avenue project database provided at the user input stage), and target simulation date.
    - Select dispatch strategy: Strategy I (Active + Idle EV coordination), Strategy II (Idle EV only, net load tracking), or Strategy III (Idle EV only, baseline tracking).
2. Data Acquisition and Preprocessing
    - Load datasets: residential load profiles, photovoltaic (PV) generation, EV state-of-charge (SOC) records, EV charging logs, half-hourly electricity prices, and carbon intensity.
    - Convert timestamps, align datasets to hourly resolution, and prepare them for analysis.
3. EV Population Generation (Section 4.4.1)

- Active EVs: For the required number of vehicles, extract SOC profiles from the target day or synthetically expand using historical SOC data.
- Idle EVs: Generate SOC profiles based on observed SOC level distributions from charging logs, keeping SOC constant throughout the day.
- Assign unique identifiers to all synthetic EV entries.

4. Reference Curve and Baseline Calculation (Section 4.3.3)
    - Compute the baseline net load: household demand minus PV output.
    - Determine the reference curve: compute the corresponding reference curve based on the user-defined strategy. In Scenarios I and II, the reference curve incorporates both the average hourly values of the monthly $P_{baseline}$ and the EV charging demand of the study day, whereas in Scenario III it includes only the average hourly values of the monthly $P_{baseline}$.
    - For active EVs, incorporate expected charging demand into the baseline.
5. Dispatch Strategies (Section 4.4.2 & Section 4.4.3)
    - Strategy I: Actively schedule both active and idle EVs to minimize deviation from the reference curve, considering SOC thresholds.
    - Strategy II: Adjust idle EV charging/discharging to align the original net load with the reference curve.
    - Strategy III: Adjust idle EV charging/discharging to align the baseline (without active EV charging) with the reference curve.
    - SOCs are updated hourly based on charging/discharging actions, constrained by battery capacity and SOC limits.
6. Performance Evaluation
    - Calculate hourly and total CO_2 emissions before and after dispatch using carbon intensity data.

- Compute electricity costs using half-hourly price signals.
- Compare total cost and emissions pre- and post-optimization.

7. Result Visualization
    - Plot load curves (original, optimized, baseline, and reference).
    - Show SOC distributions before and after dispatch.
    - Visualize hourly participation counts for charging and discharging.
    - Plot half-hourly CO_2 emissions and electricity costs.
8. Output Storage
    - Save updated SOC profiles for active and idle EVs.
    - Export EV participation logs and evaluation metrics.

4.7. Simulation Steps Using the Established Optimization Platform

This section outlines the simulation procedure implemented on the established optimization platform. These steps define how the case-study simulations are conducted, and the resulting outputs are analysed in Chapter 5. The simulation framework was developed with reference to real-world data and operational characteristics of UK residential communities. It combines grid-level load profiles with empirical EV usage data to reproduce realistic community energy consumption patterns and mobility behaviours. The core logic is built upon a multi-layer optimization model that simultaneously considers grid demands, EV availability, user behaviour heterogeneity, and system-level control objectives. To account for the diversity of energy consumption and vehicle mobility patterns, the simulation considers three distinct operational scenarios. To reflect the diversity of EV-grid interaction models under real-world community conditions, the simulation study examines three representative scenarios. The first scenario models a typical high-EV-utilization environment commonly found in urban or suburban residential communities, where a large proportion of vehicles are regularly used, and

their availability for V2G participation fluctuates in line with predictable commuting patterns. This setting is used to evaluate how V2G coordination can be integrated into normal community operations without disrupting everyday mobility needs. The second scenario explores a low-EV-utilization context, where a significant proportion of EVs remain idle for extended periods. This condition could result from low adoption rates or limited daily travel demand. From a systems perspective, this scenario is functionally equivalent to a V2G infrastructure model based on battery-swapping stations, where idle EV batteries can be decoupled from vehicles and repurposed as flexible energy storage units. The control logic in this case assumes high availability of stationary batteries and focuses on optimizing their integration into grid balancing operations. The third scenario simulates an exceptional case in which EV usage is nearly absent—such as during public lockdown periods or widespread remote working arrangements, where most vehicles remain unused for days or weeks. Under these conditions, the role of EVs as mobile storage assets is effectively replaced by a fixed battery energy storage (BES) system embedded within the community grid. This scenario allows for an evaluation of the V2G management logic in a setting structurally similar to current fixed BES deployments and provides a useful reference for comparing the operational efficiency of EV-based storage versus traditional stationary systems.

Within each scenario, a unique V2G scheduling logic is applied to manage bidirectional charging and discharging processes in response to time-varying power demand at the community level. The design of these control strategies emphasizes the dynamic allocation of idle EVs as distributed energy storage, ensuring that energy is discharged during peak demand periods and recharged when excess capacity is available. At the same time, mobility constraints are respected to ensure that EVs remain operational for users' transportation needs. The simulation platform was developed using Python, with key dependencies such as NumPy and

Pandas providing the necessary data manipulation, time-series modelling, and computational efficiency to simulate large-scale multi-agent systems.

The data used in the simulation originates from real community-level grid operations and EV behaviour logs, as introduced in Chapter 3. This includes hourly electricity consumption data, hourly PV generation data, and EV travel and charging logs. These datasets were pre-processed and expanded through statistical equivalence techniques to create a robust simulation environment capable of capturing day-to-day operational dynamics as well as longer-term seasonal fluctuations. Representative days were selected to reflect typical and extreme power demand patterns—for example, peak days during winter with high heating loads, and low-demand days in summer characterized by reduced occupancy or minimal heating/cooling needs. This approach ensures that the model is not only calibrated against average conditions but also stress-tested under the most demanding scenarios a real system might face. Through a series of 24-hour simulation cycles, the model evaluates key performance indicators such as the temporal distribution of power flows within the community grid, the effectiveness of peak shaving and load levelling, and the efficiency of idle EV integration into the energy system. One of the primary goals of the simulation is to determine whether the control logic developed for each scenario can adaptively coordinate large numbers of EVs while responding to rapid fluctuations in demand. This is especially crucial given the inherently stochastic nature of EV usage, user preferences, and weather-influenced electricity consumption.

In the simulation experiments, specific attention is given to the factors most likely to influence the attainment of extreme load-balancing conditions and the efficiency of EV scheduling under the proposed optimization framework, together with the parameter ranges assigned to each factor. On the generation side, PV output is modelled at three representative levels: a standard installed capacity of 4 kWp, a reduced capacity of 2 kWp, and a baseline case without PV generation. The 4 kWp standard capacity per household is based on the typical installed PV

capacity defined for each household in the Trent Basin project, as described in Section 4.3.1 of this chapter. These cases allow for the assessment of how different levels of solar penetration influence the behaviour and outcomes of V2G scheduling strategies.

On the EV side, the simulations examine key parameters including EV ownership rate (25%, 50%, 75%, and 100%), idle rate (25%, 50%, and 75%), and bidirectional charging/discharging power (3.3 kW, 7 kW, and 10 kW, covering the most common medium-to-low charging rates, with corresponding discharging rates considered). In addition, the analysis partially explores how variations in charging intensity—defined here as the charging intensity over a given time interval—can alter the target curve for extreme load balancing, thereby affecting the performance of V2G dispatch strategies aimed at achieving temporal load equilibrium.

A controlled-variable simulation approach is adopted to minimize the influence of extraneous factors. Given space limitations, not all possible parameter combinations and results are presented. For factors other than charging/discharging power, the simulations consistently employ the baseline charging model derived from the empirical EV database, representing a charging rate of 3.3 kW together with the associated real-world driving and charging patterns. This ensures that the modelled conditions remain as close as possible to actual operational behaviour, thereby preserving the validity of results and avoiding distortions that could arise from secondary synthetic modelling. In determining the boundary ownership and idle rates of EVs that allow the community grid to achieve extreme load-balancing conditions under current parameter settings (3.3 kW bidirectional charging/discharging power and 24 kWh battery capacity), further simulations were conducted to explore how different combinations of EV technical specifications might enhance scheduling efficiency while maintaining system balance. These explorations focus on parameter configurations commonly observed in the EV market, such as larger battery capacities and higher charging/discharging power. For cases involving increased charging power, charging behaviour was recalculated using the methodology

presented in Section 4.3.3, with SOC trajectories adjusted to reflect the higher power rates while remaining consistent with the original empirical driving and charging database.

For scenarios with increased battery capacity, the modelling adopted a proportional scaling approach to simplify computational complexity and avoid an unmanageable proliferation of parameter combinations. Specifically, SOC trajectories from the 24 kWh baseline case were linearly scaled to represent larger battery sizes. This inevitably amplifies driving-related energy consumption and introduces some inaccuracy, since real-world behaviour may diverge from such scaled assumptions. In practice, charging and driving behaviours are strongly influenced by the SOC values displayed to users, and thus accurately extrapolating behaviour from lower-capacity EVs to higher-capacity ones is inherently challenging. Survey evidence from the UK Department for Transport (2022) indicates that EV users tend to adjust charging behaviour based on the remaining SOC percentage. With larger battery capacities, range anxiety is alleviated, reducing the likelihood of intermediate charging outside the community grid. Consequently, more charging events occur upon return to the community, effectively shifting additional energy demand to the local grid. In simulations involving both higher battery capacity and higher bidirectional charging power, this behavioural effect is approximated by proportionally scaling driving-related energy consumption. While this approach cannot fully capture the exact behavioural shifts of users, it allows the model to incorporate the potential increase in local energy demand associated with larger battery capacity and altered charging patterns. For combinations of different charging/discharging power levels and battery capacities, the simulation experiments were conducted exhaustively, with all possible configurations enumerated and compared. However, in the analysis presented in Chapter 5, the discussion is limited to two representative cases: the baseline configuration derived from the EV database (3.3 kW bidirectional charging/discharging power and 24 kWh battery capacity),

and a contrasting configuration that reflects a favourable pairing of higher charging power with lower discharging power.

Table 4-2 summarizes the set of factors that may influence the effectiveness of the V2G optimization framework proposed in this chapter, together with the parameter levels assigned to each factor for simulation. The table identifies the variables most likely to affect the attainment of load-balancing objectives in the community grid and specifies the parameter ranges used to quantify their impact. By systematically varying these factors while holding other conditions constant, the study enables a controlled examination of how each variable, at different magnitudes, contributes to the feasibility of achieving power load balancing and to the performance of EV scheduling optimization. The simulation results reported in Chapter 5 are structured around the experimental sequence and parameterization provided in this table, allowing for a detailed assessment of EV dispatch outcomes and the resulting temporal distribution of power flows under different influencing conditions. This approach provides not only a validation of the proposed V2G framework's robustness under diverse operating scenarios but also insights into the most efficient configurations of idle EV utilization required to sustain load-balancing performance.

Variable		Value	Representative Day		Other Parameter Settings			
			Summer Typical Day (21st June)	Winter Typical Day (11th December)	Bidirectional Charging/Discharging Power (Database: 3.3 kW)	EV Ownership rate (Database: 100%)	EV Idle Rate (Database: 54.87%)	Average Hourly Charging Demand (Database: 0.20455 kWh)
PV Capacity		Full Standard Capacity (4 kWh)	✓	✓	3.3 kW	100%	50%	0.20455 kWh
		Half Standard Capacity (2 kWh)	✓	✓	3.3 kW	100%	50%	0.20455 kWh
		No PV Installations (0 kWh)	✓	✓	3.3 kW	100%	50%	0.20455 kWh
EV Participation Level (PV Capacity Setting: 4 kWh)	Ownership Rate	25%	✓		3.3 kW		54.87%	0.20455 kWh
		50%	✓		3.3 kW		54.87%	0.20455 kWh
		75%	✓		3.3 kW		54.87%	0.20455 kWh
		100%	✓		3.3 kW		54.87%	0.20455 kWh
	Idle Rate	0%	✓		3.3 kW	100%		0.20455 kWh
		25%	✓		3.3 kW	100%		0.20455 kWh
		50%	✓		3.3 kW	100%		0.20455 kWh
		75%	✓		3.3 kW	100%		0.20455 kWh
	Charging intensity	High (0.394958 kWh)	✓		3.3 kW	100%	54.87%	
		Medium (0.192591 kWh)	✓		3.3 kW	100%	54.87%	
		Low (0.092091 kWh)	✓		3.3 kW	100%	54.87%	
Charging/Discharging Power		Bidirectional Standard Low Power (3.3 kW)	✓			Optimal Value for Power Load Balancing	Optimal Value for	0.20455 kWh

					Power Load Balancing	
High-Power Charging, Low-Power Discharging	✓			Optimal Value for Power Load Balancing	Optimal Value for Power Load Balancing	0.20455 kWh
High-Power Charging, Medium-Power Discharging	✓			Optimal Value for Power Load Balancing	Optimal Value for Power Load Balancing	0.20455 kWh
Optimal Power–Capacity Combination	✓			Optimal Value for Power Load Balancing	Optimal Value for Power Load Balancing	0.20455 kWh

Table 4-2. Simulation Parameters and Variable Configurations in Scenario I–III

Note: The Average Hourly Charging Demand reported in the table is calculated as the mean hourly charging demand of active EVs in the reference curve described in Section 4.3.3.

4.8. Conclusion

In conclusion, this study proposed a comprehensive methodology for harnessing the flexible energy storage potential of electric vehicles within a community-level, centralized V2G system. Rather than limiting the analysis to idle vehicles, the framework considers different combinations of active and idle EV participation. Specifically, three complementary optimization strategies were designed: Scenario I prioritizes the scheduling of active EVs with idle EVs providing supplementary support; Scenario II relies solely on idle EVs; and Scenario III assumes that all EVs are continuously available, effectively treating them as idle. Collectively, these strategies maximize the temporary storage capacity offered by idle EVs while accounting for realistic patterns of vehicle availability, thereby enabling the community grid to approach extreme power–load balancing across time periods and enhancing overall system stability and efficiency.

The methodology is implemented through a real-time data-driven simulation framework, supported by custom-developed algorithms in Python. All input datasets—ranging from household electricity consumption, PV generation, to detailed EV usage profiles— are drawn from real historical records: the first two from the UK energy system and the latter from the My Electric Avenue project, ensuring that the modelled behaviour closely reflects the operational characteristics of a typical UK residential community with a zero-carbon orientation. For each scenario, the V2G management logic is encoded programmatically to simulate the power modulation process hour by hour, under different assumptions of EV availability and user behaviour. This enables a dynamic evaluation of how centralized V2G systems can balance grid load, while also reducing carbon emissions and lowering electricity costs, offering both environmental and economic benefits. The outcomes and performance validation of this methodology are presented and discussed in detail in the following sections.

CHAPTER 5. SIMULATION RESULTS

5.1. Introduction

This chapter presents the simulation results evaluating the effectiveness of a centralized V2G optimization management strategy tailored for zero-carbon-oriented community energy systems in the UK. Using the methodological framework introduced in Chapter 4, the simulation aims to test the feasibility and performance of a dynamic V2G control system capable of integrating EVs into local grid operations at the community scale. By simulating various usage environments and demand scenarios, this chapter demonstrates how idle EV resources can be coordinated to enhance power distribution, alleviate peak loads, and improve grid flexibility without compromising the mobility needs of EV users.

Building on the simulation procedures outlined in Section 4.7 of the Methodology (Chapter 4), together with the influencing factors and parameter settings defined at varying levels, this chapter examines the performance of different scenarios under alternative parameter environments in achieving temporal power load balancing within the community grid and in determining the corresponding EV dispatch outcomes. The analysis of dispatch efficiency focuses on the extent to which EVs are utilized effectively across different time periods, assessed through comparisons of the number and composition of dispatched vehicles (in terms of the proportions of idle and active EVs) as well as the distribution of SOC before and after optimization. To evaluate the effectiveness of load-balancing at the system level, the optimized scenarios are benchmarked against a baseline case without V2G participation, thereby allowing a clear assessment of performance improvements across the relevant power balance metrics. The concluding section of this chapter synthesizes the findings from these simulations and provides a limited discussion of how the results address the research gaps identified in the Introduction (Chapter 1) and the Literature Review (Chapter 2). It also considers, through the

lens of the simulation outcomes, whether the scheduling optimization framework developed in the Methodology (Chapter 4) demonstrates both scalability and effectiveness for EV coordination in community-level grids aligned with the UK's net-zero transition.

5.2. Result Analysis

Based on the simulation logic established in Chapter 4, a Python-based simulation platform was developed to evaluate the operational performance of a community grid integrated with V2G under different usage scenarios. The platform enables the simulation of community-level power distribution and time-dependent EV scheduling under realistic operating conditions. It incorporates several datasets derived from the earlier Trent Basin project, including a residential electricity consumption database for the community grid and centralized PV generation datasets representing three deployment conditions: no PV installation, partial-capacity PV installation, and full-capacity PV installation. In addition, the platform integrates EV SOC behaviour datasets corresponding to different charging power levels (3.3 kW, 7 kW, and 10 kW), allowing the model to capture variations in charging dynamics across different charging infrastructures.

To perform a simulation, the user inputs several key parameters following the platform prompts. These include the simulation date and the PV deployment condition (no PV, partial-capacity PV, or full-capacity PV). In addition, several EV-related parameters describing the community fleet must be specified, including the EV ownership rate, idle rate, average hourly charging demand, charging power, and discharging power. Finally, the user selects one of the predefined V2G scheduling strategies (Scenario I, Scenario II, or Scenario III). Based on these inputs, the platform generates a set of simulation outputs describing system behaviour under the specified configuration. The primary outputs include (i) the temporal distribution of net grid power before and after optimization, (ii) the number of active and idle EVs participating in charging

or discharging during each time interval, and (iii) the SOC distributions for all participating EVs at the beginning and end of the optimization process. These results allow the effectiveness of the implemented V2G scheduling strategy to be evaluated in terms of both EV dispatch behaviour and its influence on the community grid power profile.

The results presented in this chapter are generated by systematically varying the key input parameters defined in Chapter 4. A stepwise parameter testing approach is adopted, in which individual parameters are adjusted sequentially to identify the critical combinations required for the proposed V2G scheduling strategies to achieve optimal grid power regulation. This approach makes it possible to determine the threshold conditions under which the designed control strategies can effectively balance community grid demand and supply. In addition, the performance of the scheduling framework is examined under extreme operating conditions, such as scenarios where the community grid contains no PV generation capacity, in order to evaluate the robustness of the proposed strategies.

This section applies the simulation framework established in Chapter 4 to evaluate the performance of the three proposed V2G management scenarios under varying community grid characteristics and EV utilization patterns. The objective is to verify the effectiveness of each strategy in achieving extreme load-balancing limits in community-scale power distribution while ensuring rational scheduling of EV resources. The structure of this section follows the three designed V2G scheduling strategies—Scenario I, Scenario II, and Scenario III. For each scenario, modelling results are presented under different parameter configurations and evaluated using three complementary indicators: (i) the temporal distribution of net grid power before and after optimization, (ii) the number of active and idle EVs participating in charging or discharging during each time interval, and (iii) the SOC distributions for all participating EVs at the start and end of the optimization process. Together, these indicators provide a comprehensive assessment of the peak-shaving capability of the community grid and the

rationality of EV utilization under each parameter combination. The economic and environmental implications of the optimized operational results will be further analysed and discussed in Chapter 6.

5.2.1. Scenario I

Scenario I is designed to address centralized V2G scheduling in the context of existing community grid conditions and prevailing EV usage patterns. In this configuration, the scheduling framework prioritizes the coordination of active EVs—vehicles that are connected to the grid during the simulation period—while idle EVs are deployed in a supporting role to complement the operation of active EVs. The overarching objective is to achieve an extreme load-balancing condition within the community grid, thereby minimizing temporal deviations in net power flow.

A key principle in this scenario is the full utilization of the connection periods of active EVs to support the V2G dispatch process, while maintaining complete adherence to the vehicles' original usage schedules. This ensures that V2G participation does not interfere with owners' travel needs or alter their daily mobility patterns. To safeguard this balance, the charging and discharging thresholds are determined with reference to real-world operational data: specifically, it is set as 1 minus the mode of all initial SOC values at the start of charging, which approximates the typical energy consumption required for a single EV trip. Compared with directly calculating energy consumption from the SOC at departure and the SOC at the start of recharging—which can underestimate consumption for vehicles that opportunistically charge during trips—this 1-minus-mode approach provides a buffer to account for such in-trip charging. This threshold setting reflects the typical daily driving energy requirement, ensuring that V2G operations deliver load-balancing benefits without compromising the availability of EVs for routine transportation demands.

5.2.1.1. Impact of PV Capacity on Scenario I Load-Balancing Performance

To quantitatively examine the influence of PV generation—a primary factor directly shaping grid load profiles—on the performance of Scenario I in achieving load-balancing and peak-shaving objectives, the simulation is conducted using the three representative PV parameter settings specified in Section 4.7, following the methodology outlined therein.

For all simulations in this stage, the bidirectional charging/discharging rate was fixed at 3.3 kW, consistent with the original EV dataset, thereby ensuring that results remain representative of observed operational conditions. The charging intensity parameter was set to the algorithm's default value, derived from the annual EV charging database as the average per-active vehicle hourly charging demand of 0.20455 kWh. As detailed in the methodology (Chapter 4), this value is used solely for the calculation of the daily extreme-balance parameter (daily power-balance reference value) and is not applied directly in the pre- or post-optimization modelling of the community net power load, which is computed from the real-time power consumption or discharge of EVs. To ensure comparability across different PV penetration levels, a consistent set of EV fleet configurations was applied, with ownership and idle rates defined in accordance with the simulation design procedure in Section 4.7. Specifically, these values were taken from the EV database reported in Table 4-2, where the baseline ownership rate is 100% and the idle rate is 54.87% (rounded to 50% for subsequent explanation and calculation). By holding these parameters constant, the analysis isolates the impact of varying PV capacity on the ability of the proposed V2G optimization strategy to achieve extreme load-balancing conditions.

Given that PV generation can lead to the community's net load reference values—that is, the daily power-balance reference values calculated according to the methodology outlined in Chapter 4—particularly during periods of high insolation or minimal production, two

characteristic dates were selected to test the scheduling strategy under such boundary conditions: 21 June, representing peak annual PV generation, and 11 December, representing the lowest annual PV output. All parameter variations were simulated for both dates, allowing for a direct comparison of V2G performance in mitigating load extremes across both maximum and minimum renewable generation contexts.

5.2.1.1-(i) Performance Results under Full-Capacity PV Generation (4 kWp)

Figure 5-1 illustrates the diurnal net-load profiles for the community grid on 21 June—representing the seasonal peak of PV generation—under the condition of full-standard PV capacity (4 kWp), bidirectional charging/discharging power of 3.3 kW, EV ownership and idle rates most closely aligned with the empirical database (100% ownership, 50% idle rate), and a charging intensity corresponding to the database-derived mean hourly charging energy of 0.20455 kWh per active EV. The comparison between pre-optimization and Scenario I-optimized load curves clearly shows the algorithm's capability to reduce extreme load deviations despite the substantial midday PV surplus. Correspondingly, Figure 5-2 presents the distribution of EVs across different SOC levels before and after optimized day, while Figure 5-3 depicts the hourly number and composition of EVs engaged in charging or discharging—disaggregated into active EV discharging, active EV charging, idle EV discharging, and idle EV charging.

Simulation results indicate that the high PV output in June drives the calculated extreme-balance parameter (daily power-balance reference value) to − 161.63763018 kW, a negative value reflecting a net generation surplus over community demand. In the absence of auxiliary storage facilities, this inevitably leads to partial PV spillover into the grid. The post-optimization curves reveal that between 16:00 and 17:00, the net-load trajectories before and after optimization almost coincide. SOC distribution analysis confirms that during this interval,

all available EVs have reached their maximum storage capacity, leaving no further margin for PV absorption. This finding validates the appropriateness of the extreme-balance parameter as derived from the underlying system data, under current system conditions.

From the EV dispatch perspective, the substantial PV surplus imposes storage demands predominantly between 06:00 and 18:00, peaking at 12:00 when no active EVs are available for charging and idle EV engagement reaches 174 units (out of 250 idle EVs). Active EV participation is constrained by mobility patterns, resulting in minimal availability during the midday storage-demand peak. Nevertheless, during discharge-heavy periods—particularly from 00:00 to 05:00 and 18:00 to 21:00—active EVs bear the majority of the load-balancing burden. After 21:00, most active EVs have depleted their discharge potential, shifting the responsibility for residual load-levelling almost entirely to idle EVs. This early withdrawal of active EVs from post-21:00 discharge operations is also attributable to the discharge lower-bound threshold adopted in this study, which was set to the statistical mode of daily driving-related SOC consumption in the EV database. While this relatively conservative threshold safeguards against any adverse impact on users' daily mobility requirements, it also leads to an earlier cessation of active EV participation in late-evening discharge, thereby transferring the remaining balancing tasks to idle EVs.

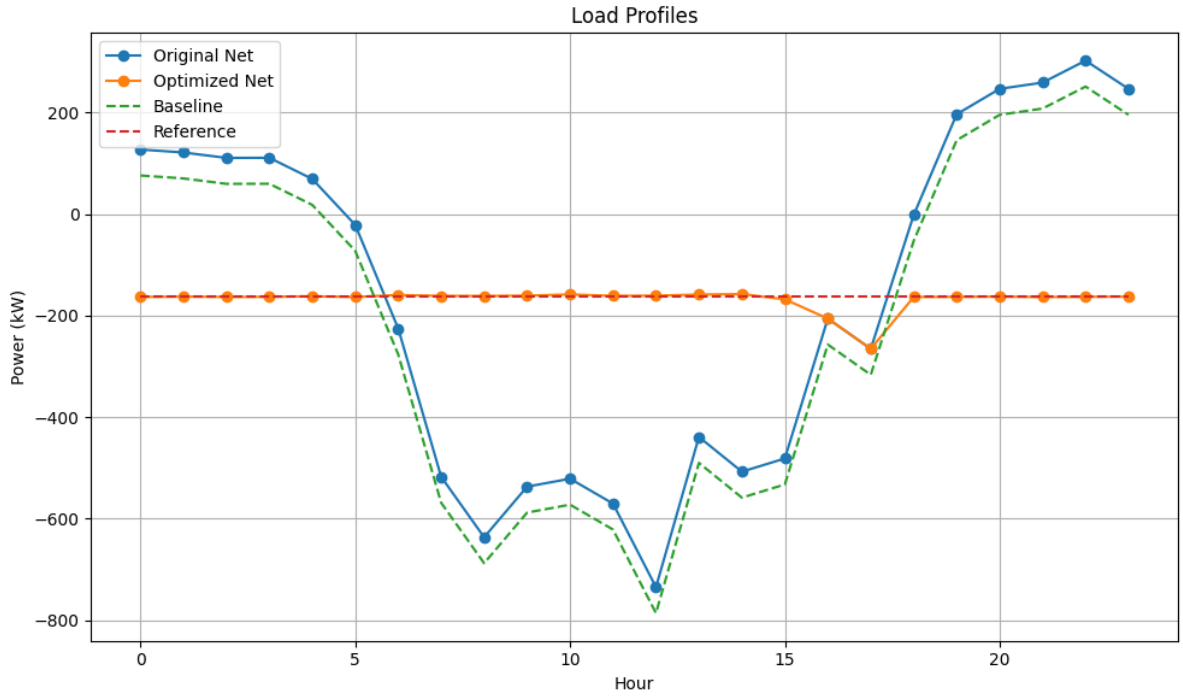


Figure 5-1. Hourly net-load profiles before and after Scenario I optimization on 21st June with full-standard PV capacity (4 kWp) and default EV parameters. The baseline load profile incorporates both the hourly residential electricity demand and PV generation, while the power-balancing threshold curve represents the calculated extreme-balance parameter. Simulation parameters: bidirectional charging/discharging power = 3.3 kW; EV ownership rate = 1.0; idle rate = 0.5; average hourly charging demand = 0.20455 kWh.

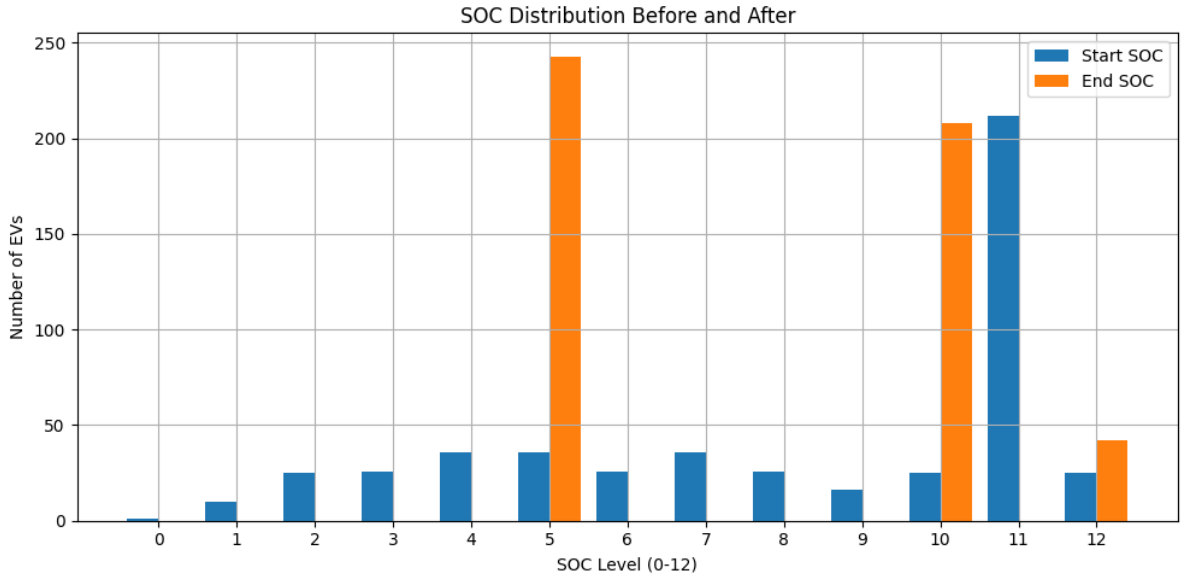


Figure 5-2. SOC distribution of dispatched EVs before and after Scenario I optimization under full-standard PV capacity conditions.

Note: The methodology constrains the discharging threshold at SOC Level 5. As a result, following evening discharging events, a substantial proportion of active EVs converge at this SOC level.

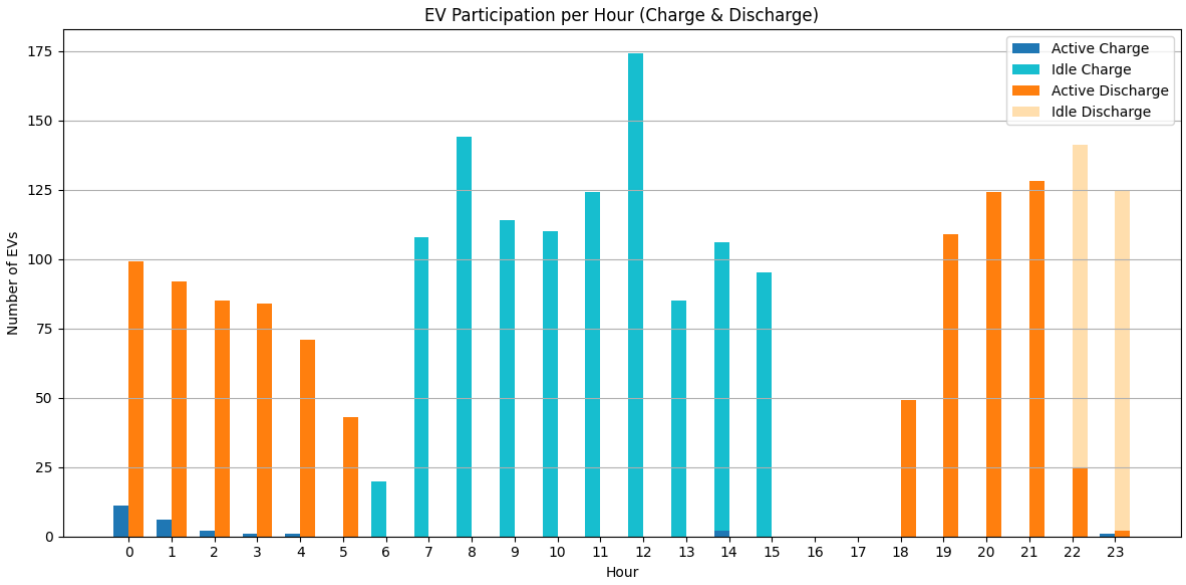


Figure 5-3. Hourly participation of active and idle EVs in charging and discharging, based on Scenario I optimization.

Similarly, the same parameter configuration was applied to simulate the winter characteristic day, when PV generation reaches its seasonal minimum, in order to examine the pre- and post-optimisation power load distribution and EV dispatch patterns. As illustrated in Figure 5-4, the reduced PV generation results in a less pronounced fluctuation in power load compared to the summer case, with the lowest net power value reaching only – 96.29632342 kW at 11:00. Consequently, the demand on EV dispatch is markedly lower than in the high-PV scenario. Although the V2G strategy prioritizes active EVs, at this time most active vehicles are either away on trips or have already reached full charge in earlier periods, leaving only idle EVs available. Therefore, the peak dispatch volume at 11:00—requiring a total of 68 EVs to absorb the modest surplus generation—consists entirely of idle EVs.

Throughout the day, the overall electricity demand consistently exceeds PV supply, yielding a positive extreme balancing threshold of 125.55088861 kW. This is corroborated by the SOC distributions presented in Figure 5-5, which compare the states of charge of all EVs at the start of the day and after optimisation. The SOC profiles appear more evenly distributed than in the summer case, with no instances of surplus PV generation exceeding the aggregate storage capacity of the EV fleet. As a result, the overall dispatch pressure on EVs is substantially reduced relative to the high-PV scenario.

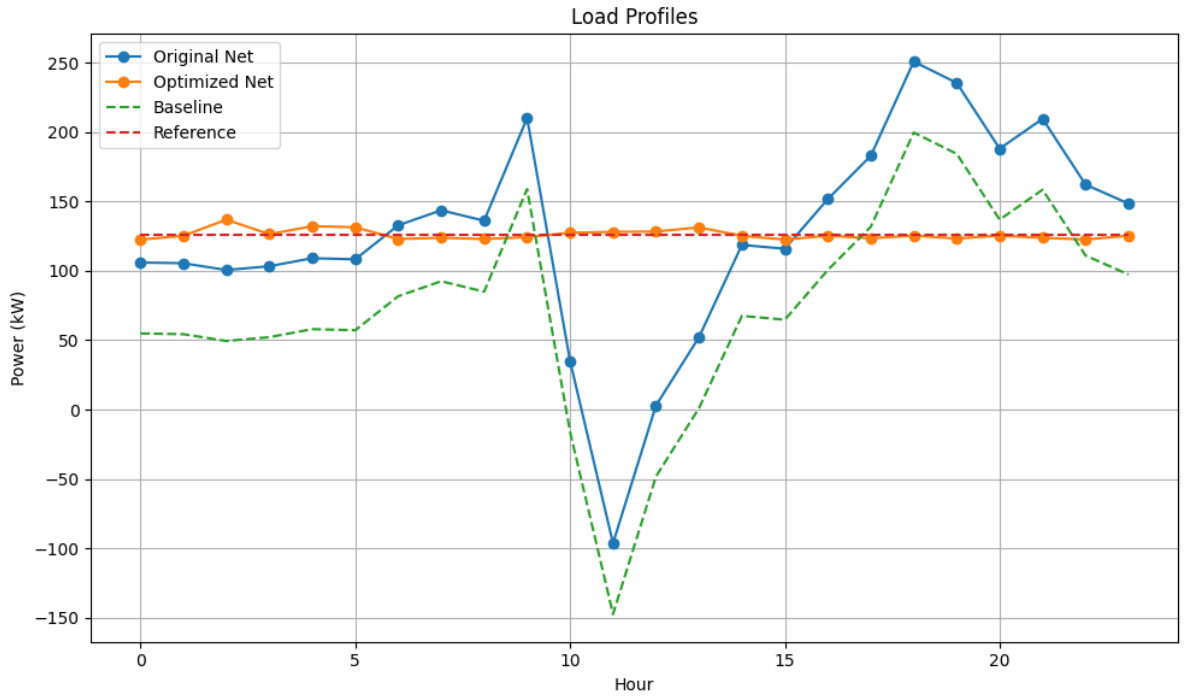


Figure 5-4. Hourly net-load profiles before and after Scenario I optimization on 11th December with full-standard PV capacity (4 kWp) and default EV parameters. Simulation parameters: bidirectional charging/discharging power = 3.3 kW; EV ownership rate = 1.0; idle rate = 0.5; average hourly charging demand = 0.20455 kWh.

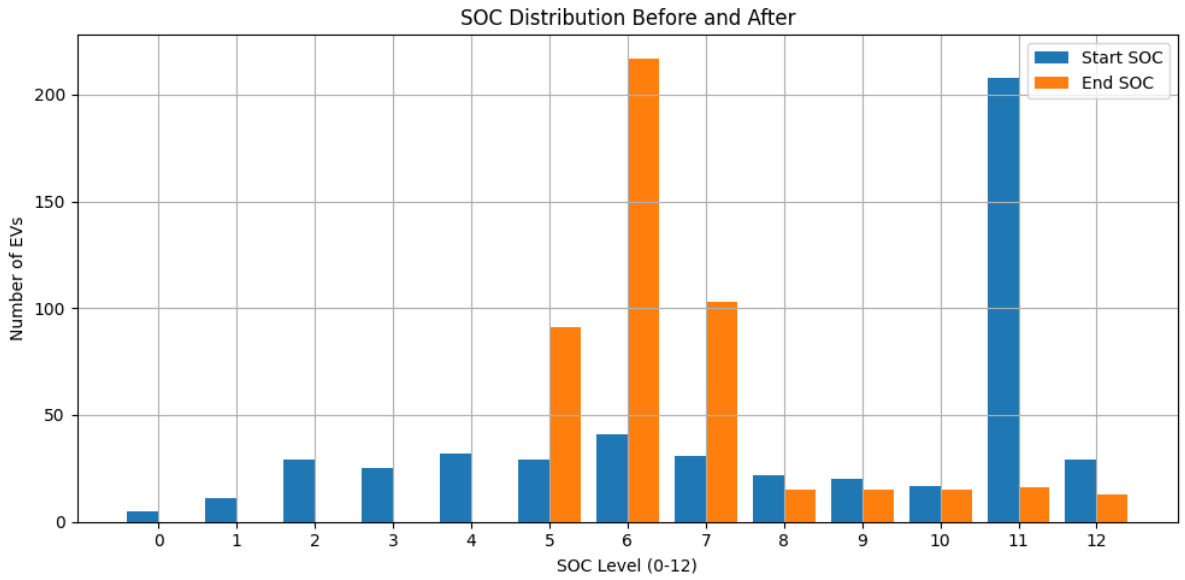


Figure 5-5. SOC distribution of dispatched EVs before and after Scenario I optimization under full-standard PV capacity conditions on 11th December.

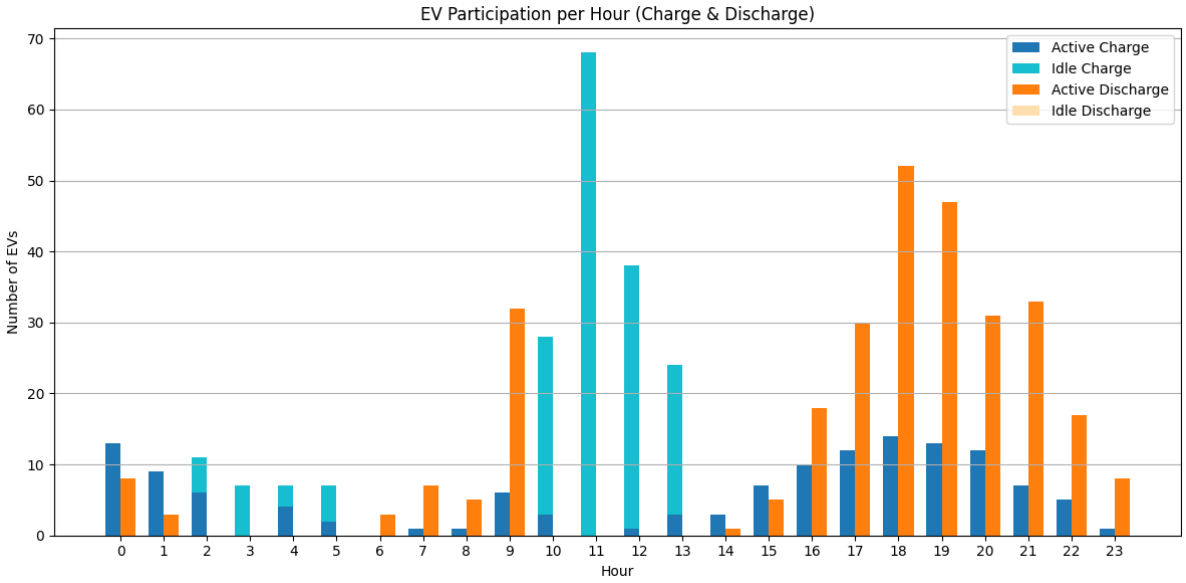


Figure 5-6. Hourly participation of active and idle EVs in charging and discharging, based on Scenario I optimization on 11th December.

5.2.1.1-(ii) Performance Results under Half-Capacity PV Generation (2 kWp)

The half-capacity PV generation scenario is introduced as an intermediate benchmark between the zero-PV and full-capacity PV configurations, allowing for a quantitative assessment of how

PV availability—particularly during production peaks—affects the overall EV scheduling dynamics. All other simulation parameters are kept identical to those used in the full-capacity PV case, ensuring that any observed differences are attributable solely to PV output. As in the previous analysis, results are presented for both the summer and winter characteristic days, including the community grid's time-varying load profiles before and after optimization, the distribution of EV SOC levels at the start of the study day and after optimization, and the detailed temporal pattern of EV dispatch.

For the summer characteristic day (Figure 5-7), the optimized power balance reference under the half-capacity PV model converges almost perfectly to zero (−1.09760499 kW). This near-zero balance indicates that the community grid is capable of achieving complete self-sufficiency, with negligible net power exchange with the upstream grid. From the perspective of EV scheduling (Figures 5-8 and 5-9), the dynamics differ substantially from those in the 4 kWp full-capacity case. Here, the most significant dispatch peak occurs at 23:00, corresponding to the late-night demand surge, where 93 active EVs are mobilized to discharge and balance the load. A second peak appears at 12:00—coinciding with the midday PV production peak—where 91 idle EVs are engaged for charging. This dual-peak pattern contrasts sharply with the full-capacity scenario, where the midday PV surplus created a single dominant dispatch peak across the entire day.

The time-series load distribution confirms that, under half-capacity PV conditions, the total PV output imposes a far lower storage burden on EVs than in the full-capacity case. The community grid achieves self-sufficiency without significant surplus spillover, enabling EVs to fully absorb all PV-generated electricity while still retaining unused storage capacity. In contrast, under the 4 kWp scenario, PV output during the 16:00–17:00 interval exceeded available storage, leaving part of the surplus unutilized. This finding underscores the balancing

effect of reduced PV capacity, which both alleviates midday storage saturation and distributes scheduling requirements more evenly across the day.

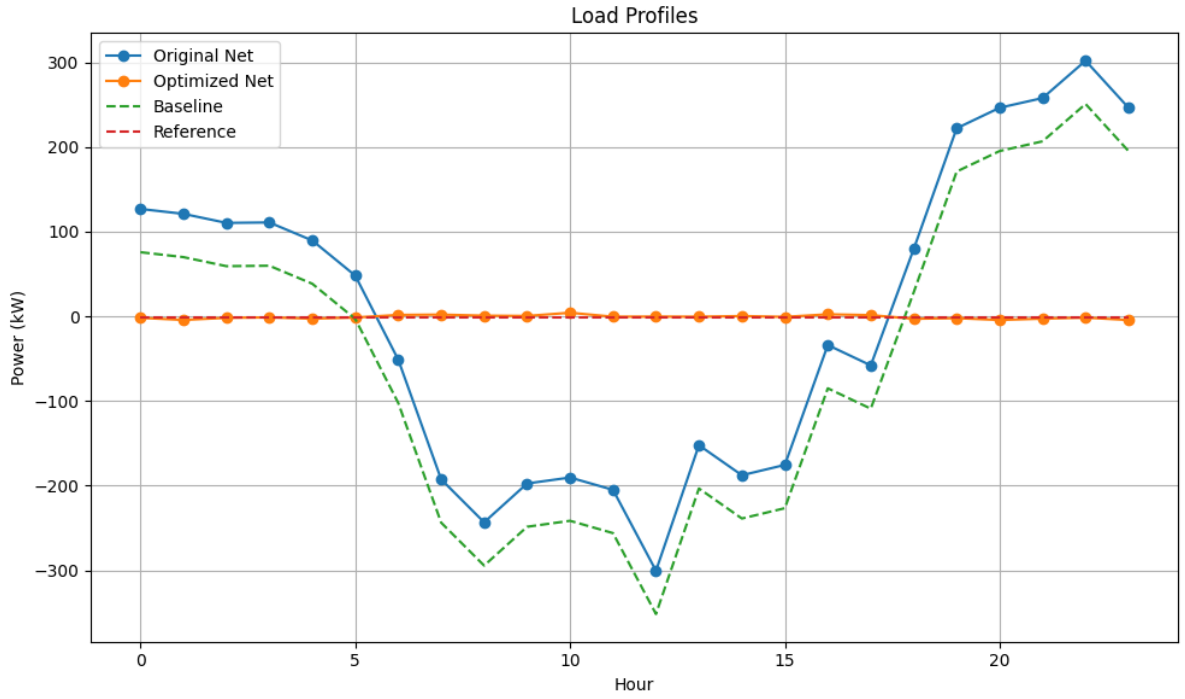


Figure 5-7. Time-of-day power load profiles for the community grid on 21st June under half-capacity PV generation (2 kWp) before and after optimization, showing the baseline load profile (residential demand + PV generation) and the optimized load-balancing reference curve. Simulation parameters: bidirectional charging/discharging power = 3.3 kW; EV ownership rate = 1.0; idle rate = 0.5; average hourly charging demand = 0.20455 kWh.

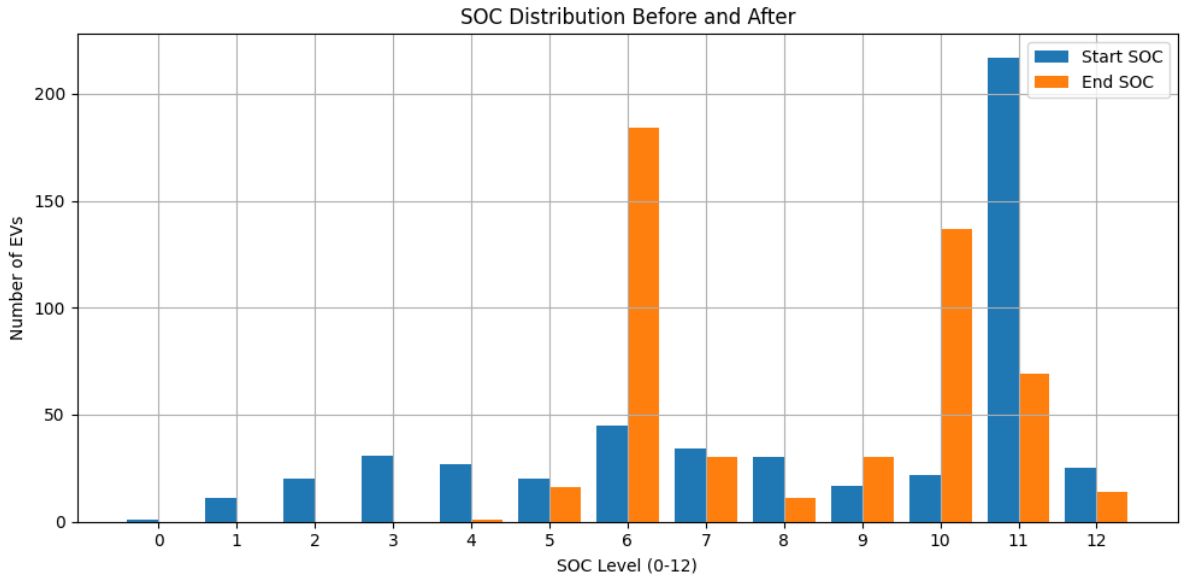


Figure 5-8. SOC distributions for all EVs participating in V2G scheduling on 21st June under half-capacity PV generation (2 kWp), comparing the start of the day (00:00) and the end of the optimization process (23:00).

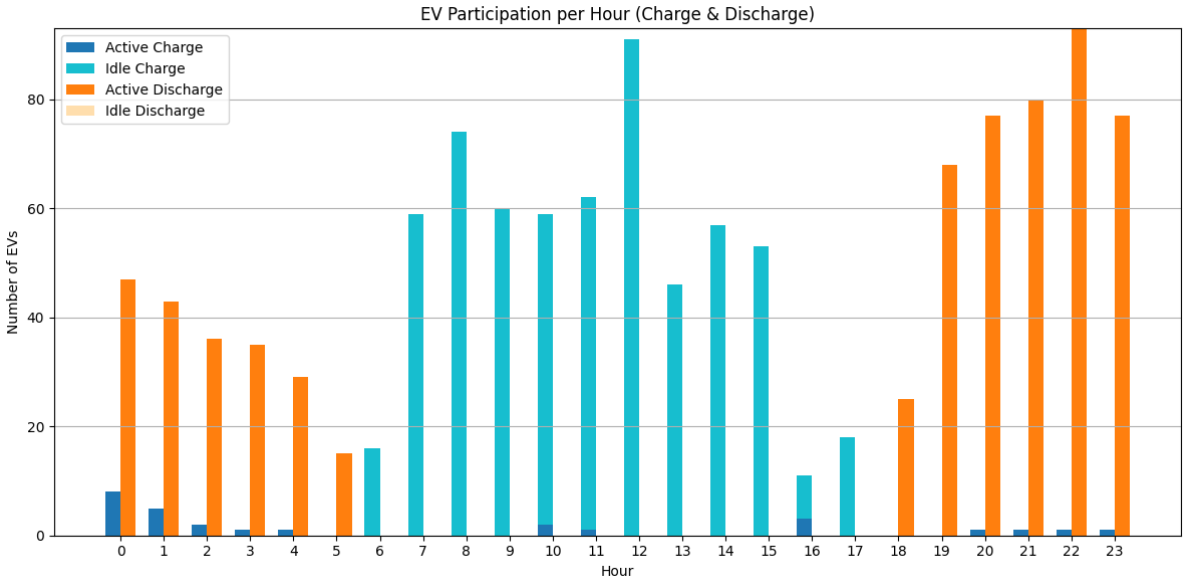


Figure 5-9. Hourly participation of EVs in V2G scheduling on 21st June under half-capacity PV generation (2 kWp), detailing the number of active EVs charging or discharging and idle EVs charging or discharging at each time step.

In contrast, the reduction in both PV generation during winter and the installed PV capacity results in a markedly higher reference value for the extreme power-balancing threshold, reaching 143.3223203 kW—an increase of approximately 16% compared to the full-capacity PV scenario. However, under these conditions, the dispatch burden on EVs is substantially reduced. The peak dispatch demand occurs between 18:00 and 19:00, requiring 47 and 46 active EVs, respectively, to discharge in order to balance the community load—approximately half the peak dispatch volume observed in summer. Correspondingly, the post-optimisation SOC distribution of EVs is no longer concentrated exclusively in the high-SOC range but shifts towards mid-range SOC values. This indicates that, under conditions of limited PV generation, EVs are not required to absorb excessive amounts of surplus energy; instead, charging is primarily directed towards meeting the daily mobility needs of the vehicles.

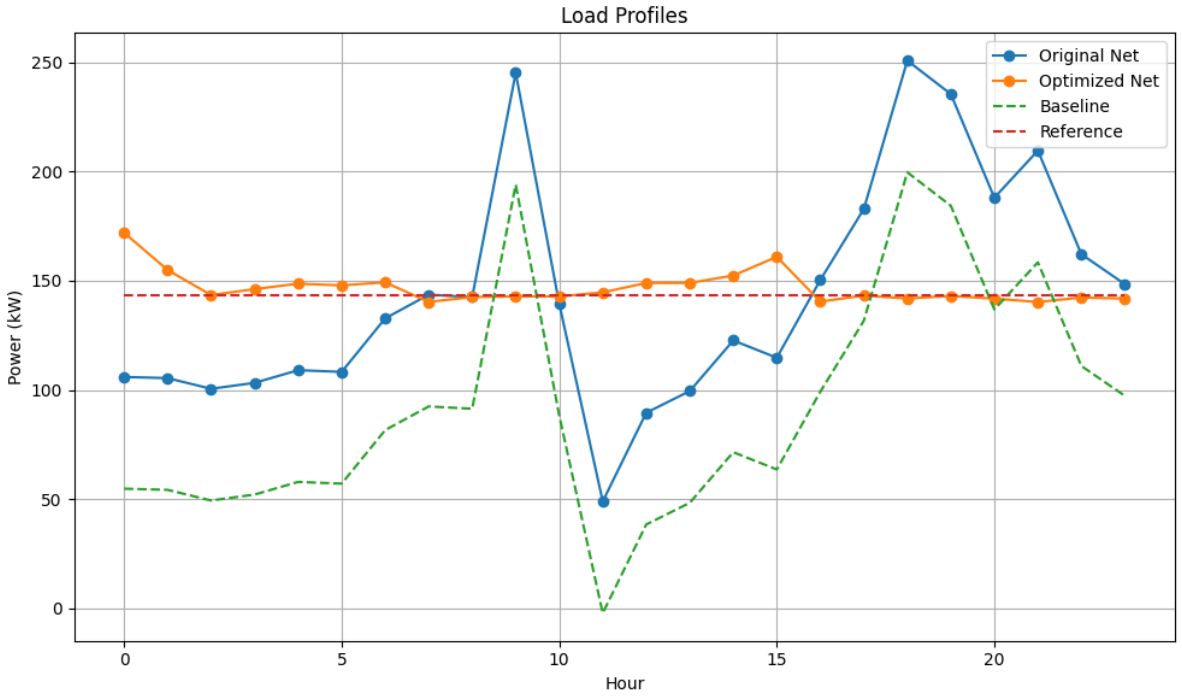


Figure 5-10. Time-of-day power load profiles for the community grid on 11th December under half-capacity PV generation (2 kWp) before and after optimization, showing the baseline load profile (residential demand + PV generation) and the optimized load-balancing reference curve. Simulation parameters: bidirectional charging/discharging power = 3.3 kW; EV ownership rate = 1.0; idle rate = 0.5; average hourly charging demand = 0.20455 kWh.

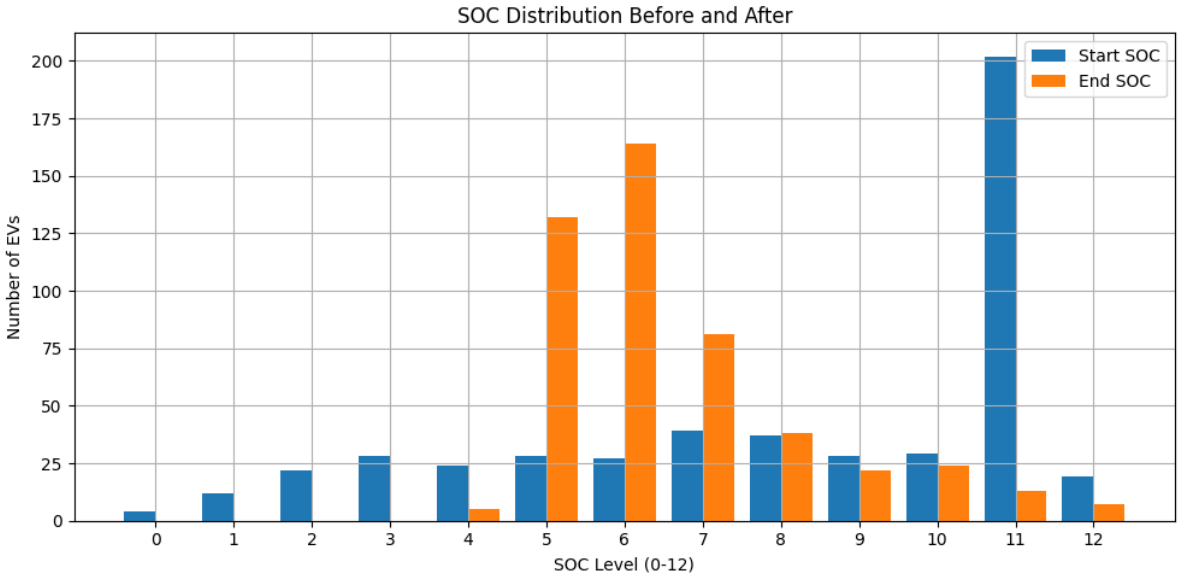


Figure 5-11. SOC distributions for all EVs participating in V2G scheduling on 11th December under half-capacity PV generation (2 kWp), comparing the start of the day (00:00) and the end of the optimization process (23:00).

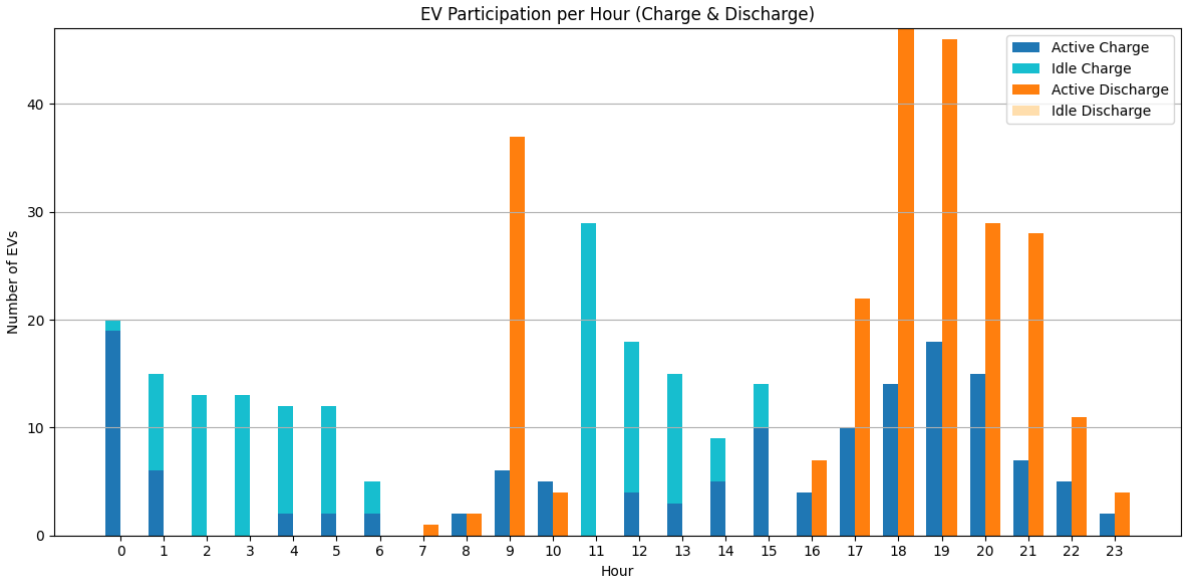


Figure 5-12. Hourly participation of EVs in V2G scheduling on 11th December under half-capacity PV generation (2 kWp), detailing the number of active EVs charging or discharging and idle EVs charging or discharging at each time step.

5.2.1.1-(iii) Performance Results without PV Generation (0 kWp)

The 0 kWp PV generation reference scenario was designed to examine V2G dispatch in a community grid entirely devoid of local generation, i.e., without any photovoltaic contribution. In this configuration, the upstream grid consistently provides unidirectional power supply to the community, and the optimization objective shifts from managing bidirectional power imbalances—with frequent direction reversals and large peak-to-valley fluctuations—to smoothing a unidirectional supply-demand mismatch. The focus is to maintain a constant and stable demand profile toward the upstream grid by balancing the temporal variation in local consumption.

Under such conditions, the pre-optimization hourly net-load profile is determined solely by household consumption patterns and EV charging behaviour. Consequently, the evening peak

after 18:00 emerges as the dominant driver for EV dispatch. As illustrated in Figure 5-13, when operating under identical parameter settings but without PV support, the application of Strategy I in a summer characteristic day results in a dispatch pattern where EVs act purely as temporary energy buffers, transferring stored power to offset short-term demand peaks without the need to absorb surplus renewable generation.

From Figure 5-15, it can be observed that the small number of idle EVs participating in the dispatch serve only a transient storage function, avoiding excessive reliance on idle EV capacity. This stands in sharp contrast to the full-PV scenario, where up to 174 idle EVs were required to absorb the extreme surplus output during the midday PV generation peak, making idle EVs a critical resource for balancing in that case.

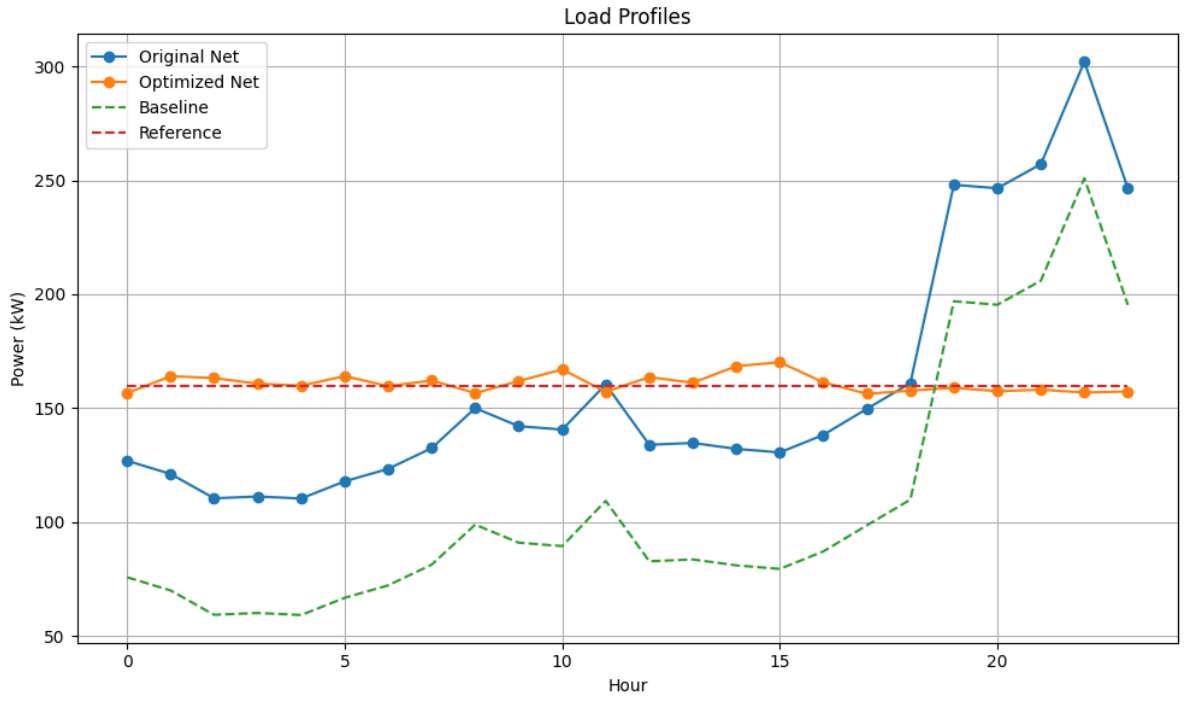


Figure 5-13. Hourly net-load profiles before and after Scenario I optimization on 21st June without PV generation (0 kWp), along with baseline load (residential demand) and power-balancing threshold curves. Simulation parameters: bidirectional charging/discharging power = 3.3 kW; EV ownership rate = 1.0; idle rate = 0.5; average hourly charging demand = 0.20455 kWh.

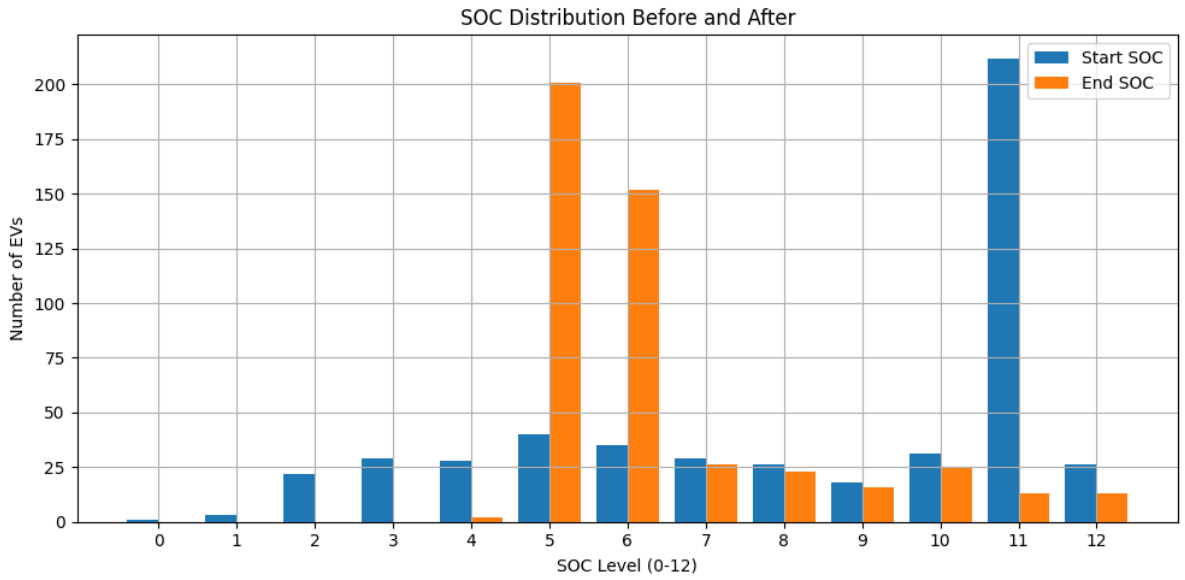


Figure 5-14. SOC distribution of dispatched EVs before and after Scenario I optimization on 21st June without PV generation (0 kWp).

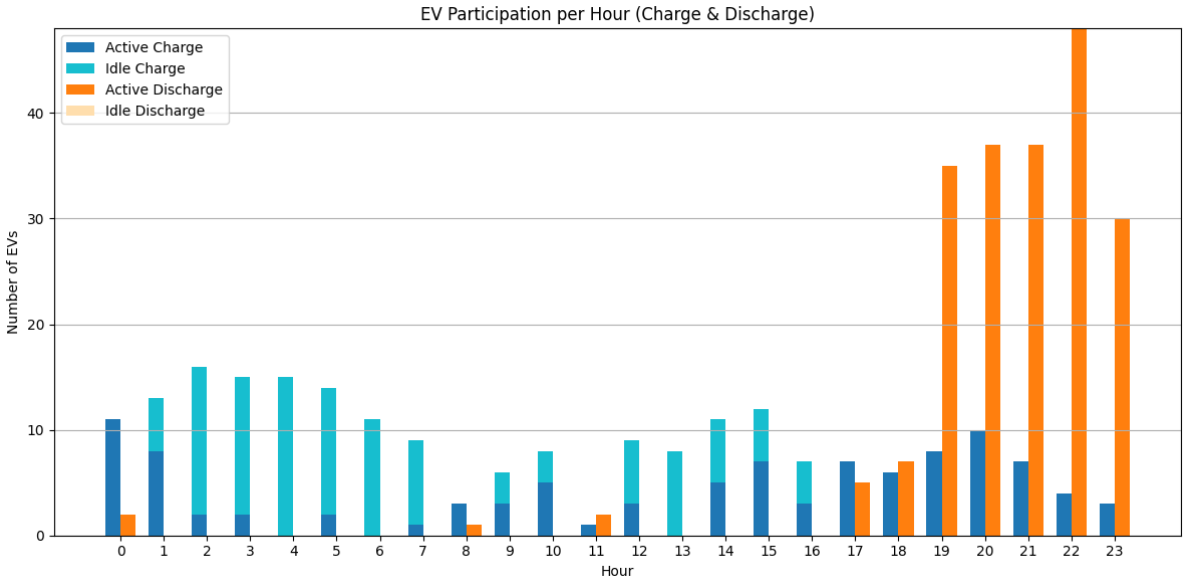


Figure 5-15. Hourly participation of active and idle EVs in charging and discharging, based on Scenario I optimization on 21st June.

Similarly, the underlying logic of power-balancing dispatch in winter under the 0 kWp PV generation scenario remains consistent with the summer case. In the absence of PV generation, the community grid is no longer subject to the pronounced seasonal variability characteristic of solar output. Instead, fluctuations in the net-load profile are driven primarily by the seasonal

patterns of residential electricity consumption. However, compared to the strong volatility of PV output, the seasonal variation in household demand is far less significant. As a result, the reference values for the power-balance limit remain nearly identical across seasons, calculated at 159.4424202 kW for the summer day and 161.09375199 kW for the winter day.

A subtle difference emerges in the dispatch dynamics, however, due to the dual-peak demand profile observed in winter residential consumption. Specifically, two distinct load peaks occur between 09:00–12:00 and 17:00–21:00, both markedly above the daily average. These peaks induce two corresponding dispatch periods during which more than 40 active EVs are required to discharge in order to stabilize the community net-load. Nevertheless, the overall dispatch intensity in this scenario is significantly lower than that observed under the full-PV case for the same season. In fact, the winter dispatch volume under 0 kWp conditions amounts to roughly half of the EV dispatch required when the system operates with full-capacity PV, reflecting the reduced balancing pressure when no surplus PV generation is present.

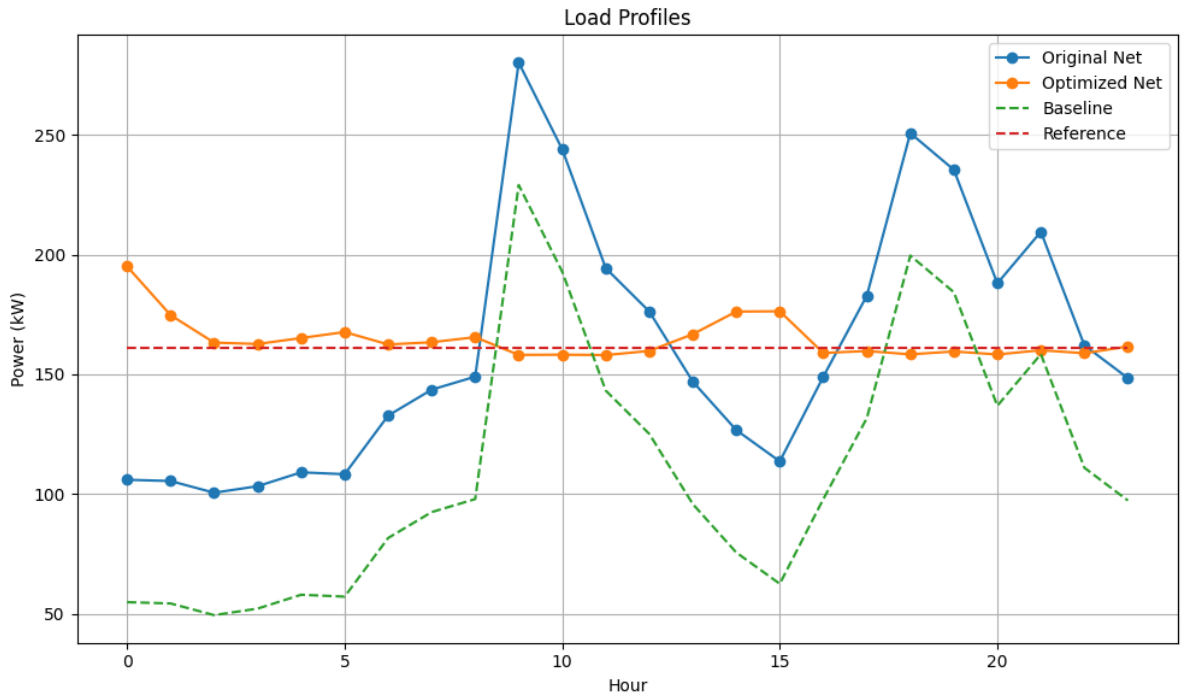


Figure 5-16. Hourly net-load profiles before and after Scenario I optimization on 11th December without PV generation (0 kWp), along with baseline load (residential demand) and power-balancing threshold curves. Simulation parameters: bidirectional charging/discharging power = 3.3 kW; EV ownership rate = 1.0; idle rate = 0.5; average hourly charging demand = 0.20455 kWh.

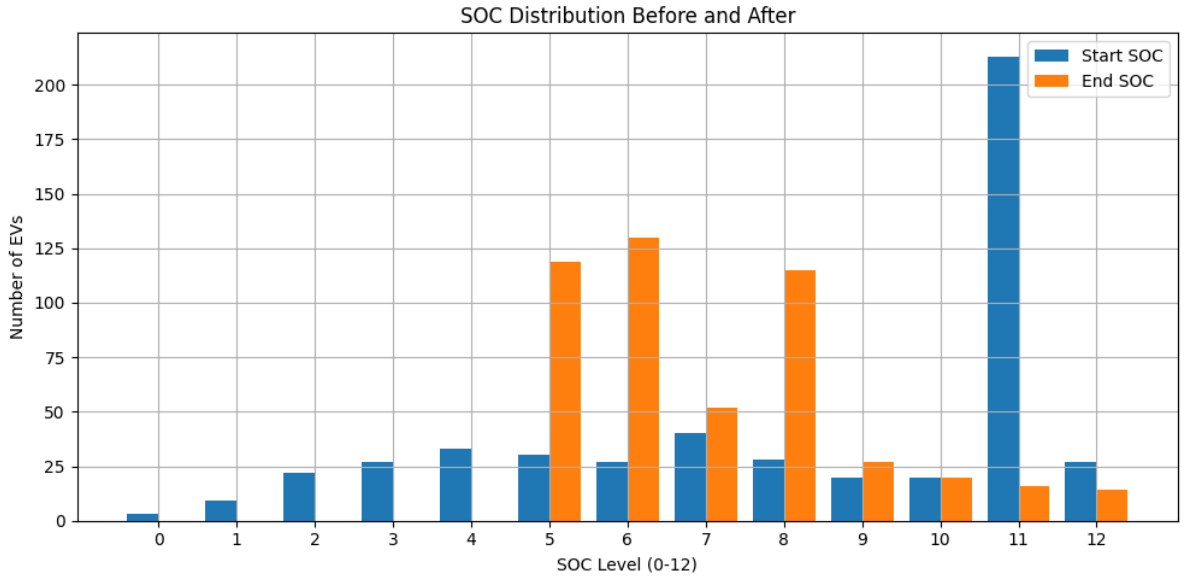


Figure 5-17. SOC distribution of dispatched EVs before and after Scenario I optimization on 11th December without PV generation (0 kWp).

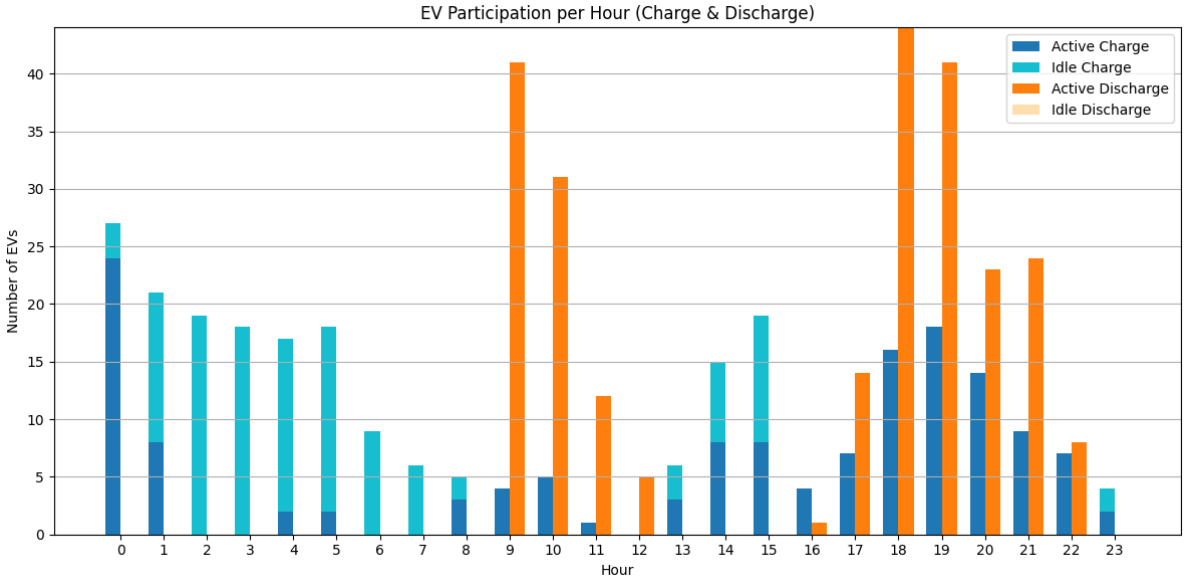


Figure 5-18. Hourly participation of active and idle EVs in charging and discharging, based on Scenario I optimization on 11th December.

5.2.1.2. Impact of EV Participation Level on Load-Balancing Performance in Scenario I

The degree of EV participation directly determines both the availability of vehicles for V2G dispatch during the study horizon and the structural composition of the participating fleet, i.e., the relative proportions of active and idle EVs. As discussed in Chapter 3, the temporal distribution of EV charging demand exhibits a pronounced evening and nighttime peak, largely aligned with residential load patterns but distinctly misaligned with the diurnal profile of PV generation. This temporal mismatch implies that the level of EV participation plays a decisive role in determining whether the system can successfully achieve load balancing at critical extremities of the net-load curve—for instance, during midday hours in summer when PV output surges and surplus generation must be absorbed. Building upon this observation, the subsequent analysis focuses on examining how varying degrees of EV participation influence the system's capacity to perform peak shaving and valley filling at these extreme moments, and the extent to which different participation levels can effectively meet the balancing requirements.

Participation rates are therefore particularly consequential during these extreme periods, as insufficient engagement of EVs may compromise the ability to smooth load fluctuations effectively. Moreover, changes in the fleet composition—specifically, the ratio of active to idle EVs—introduce further complexity. Since active EVs can only participate when connected to the community grid and when their SOC conditions permit, whereas idle EVs can be dispatched at any time within the optimization framework, the balance between these two categories directly influences the feasibility of stabilizing net-load extremes. Beyond their role in peak balancing, active EVs also shape the baseline net-load profile of the community grid due to their inherent charging behaviour, thereby exerting an additional layer of influence on the overall dispatch outcome.

5.2.1.2-(i) EV Ownership Rate

The absolute number of EVs within a community grid fundamentally determines both the maximum power absorption capacity at critical load-extreme periods and the aggregate storage capability over a 24-hour cycle. Based on the mobility dataset employed in this study, the average daily utilization rate of EVs is 45.13%, corresponding to an idle rate of 54.87%. Using this empirical idle rate as a benchmark, a controlled simulation framework was established in which all other parameters were fixed to ensure comparability. Specifically, the bidirectional charging and discharging power of each EV was set at 3.3 kW, the average hourly charging demand at 0.20455 kWh, and the PV generation capacity at its full-installation level of 4 kWp, modelled under summer peak solar conditions to capture the most challenging balancing scenarios. Within this controlled setting, four gradients of EV ownership were examined—25%, 50%, 75%, and 100%—in order to assess the capacity of the system to achieve load balancing at extreme conditions under varying levels of EV penetration. The objective of this analysis is to identify the minimum EV ownership rate that, given the current empirical usage intensity (as reflected by the observed idle rate and average hourly charging demand), can satisfy load-balancing requirements at peak stress points while simultaneously maximizing the efficiency of EV dispatch.

- **Case 1: EV Ownership Rate at 25%**

In Case 1, when the EV ownership rate is limited to 25%, the number of vehicles available for V2G dispatch within the community grid is relatively small. Under this configuration, the total fleet comprises 125 EVs, of which 57 are classified as active and 68 as idle. As shown in Figure 5-19, the contribution of these EVs to the net-load profile is modest, given their relatively low aggregate charging capacity. Consequently, the overall temporal pattern of the load curve remains largely governed by the interplay between residential electricity demand and PV generation. Examination of Figures 5-20 and 5-21, which illustrate the final SOC distribution

of participating EVs and their hourly dispatch behaviour, further clarifies these dynamics. During peak PV generation hours (07:00–17:00), the system's capacity to absorb surplus solar output is constrained simultaneously by the low charging power of individual EVs and the limited number of vehicles available for dispatch. In this period, charging and discharging activities rely predominantly on idle EVs, with their role becoming almost exclusive after 05:00.

Before 15:00, the 3.3 kW charging power per vehicle restricts the rate at which excess PV output can be absorbed, preventing the system from fully utilizing the surplus generation. Between 15:00 and 17:00, this limitation becomes even more apparent: with the storage capacity of the available EV fleet effectively saturated, additional PV output can no longer be absorbed, resulting in an optimized net-load profile that closely overlaps with the baseline curve. A similar limitation arises after 17:00, when the system attempts to dispatch EVs for load reduction. Although discharging occurs at the rated 3.3 kW per vehicle, the small number of available EVs proves insufficient to offset the real-time power imbalance, thereby preventing the net load from being brought back toward the theoretical balancing curve.

The SOC distribution at the end of the day underscores this inadequacy. Between 18:00 and 23:00, extensive discharging depletes much of the energy stored during midday hours, leaving a large portion of EVs in the lower SOC range (Level 2), particularly since idle EVs are not restricted by a lower discharging threshold. This outcome indicates that, under current usage assumptions, a 25% ownership rate allows the EV fleet to provide limited peak-shaving capability but falls short of achieving a fully balanced net-load distribution. The result highlights the inherent vulnerability of low-ownership scenarios, where insufficient fleet size and restricted charging/discharging power jointly undermine the effectiveness of V2G optimization.

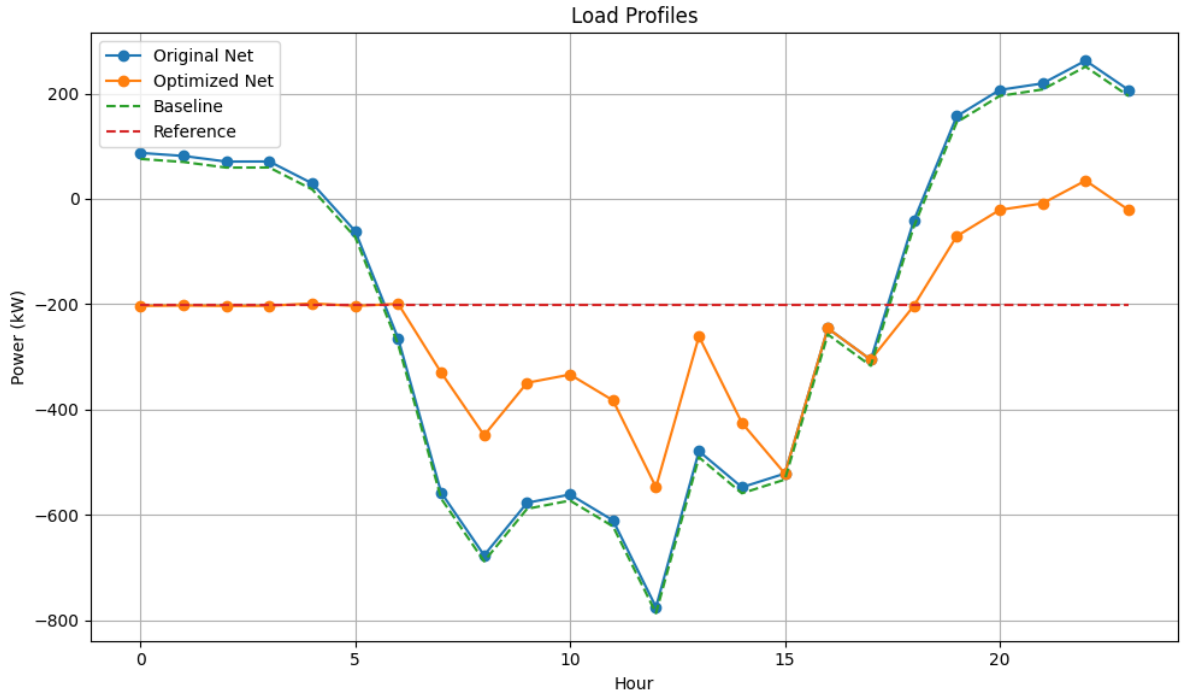


Figure 5-19. Hourly net-load profiles before and after Scenario I optimization on 21st June with full-standard PV capacity (4 kWp) and default EV parameters. Simulation parameters: bidirectional charging/discharging power = 3.3 kW; EV ownership rate = 0.25; idle rate = 0.5487; average hourly charging demand = 0.20455 kWh.

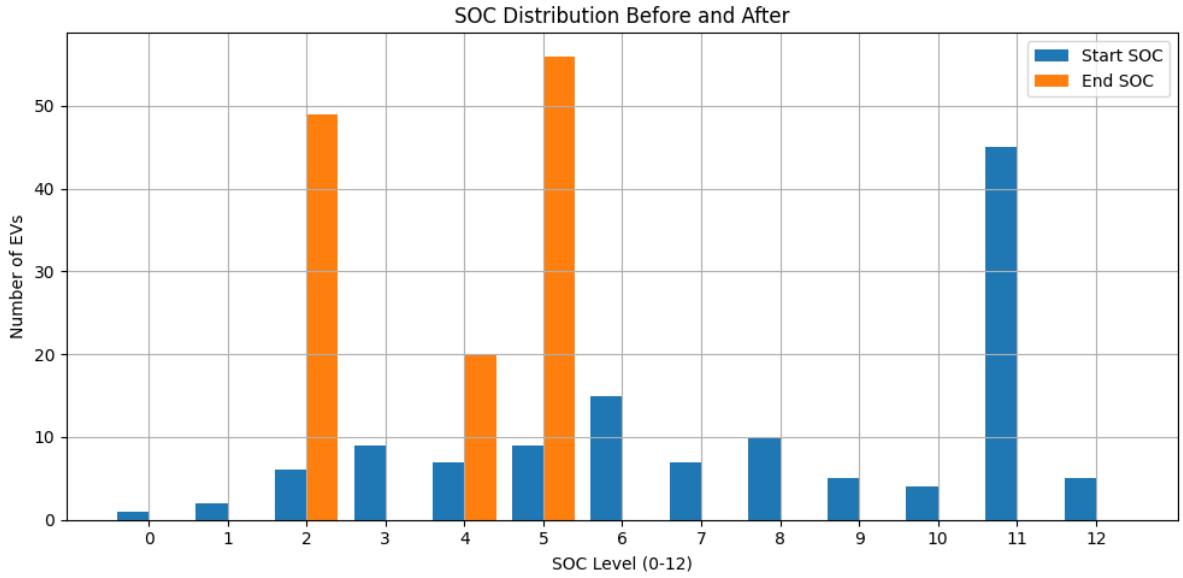


Figure 5-20. SOC distribution of dispatched EVs before and after Scenario I optimization on 21st June with full-standard PV capacity (4 kWp) and default EV parameters (EV ownership rate = 0.25).

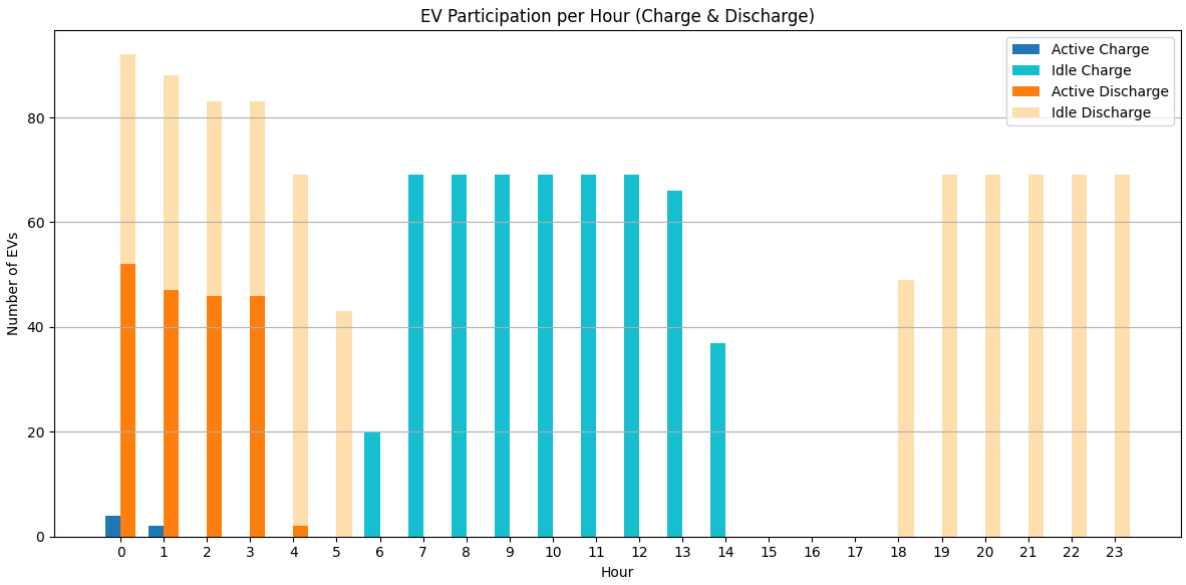


Figure 5-21. Hourly participation of active and idle EVs in charging and discharging, based on Scenario I optimization on 21st June with full-standard PV capacity (4 kWp) and default EV parameters (EV ownership rate = 0.25).

- **Case 2: EV Ownership Rate at 50%**

When the EV ownership rate is set to 50%, the community microgrid includes a total of 250 EVs. Based on the mobility patterns extracted from the empirical EV travel database, this fleet comprises approximately 114 active EVs and 136 idle EVs. Using the same parameter settings as in Scenario I to ensure comparability, the resulting 24-hour net-load distribution is illustrated in Figure 5-22. Compared with the 25% ownership case, the increased availability of EVs substantially enhances the system's ability to absorb surplus PV generation during daytime hours (06:00–17:00). A greater number of hours within this interval now achieve the target load-balancing profile. Furthermore, during the evening residential peak, the system is also able to maintain the net-load curve within the predefined balancing threshold, demonstrating a more robust load-smoothing capability. Importantly, the former limiting factor observed in Case 1—namely, the insufficient aggregate charging/discharging rate per unit time, defined as the product of rated EV power and the number of dispatchable EVs—no longer constrains system performance. Instead, the primary bottleneck shifts toward the total storage capacity of

the EV fleet, which remains inadequate to fully absorb the surplus PV output between 12:00 and 17:00.

From the perspective of vehicle dispatch, the optimized SOC distribution reveals a clear improvement. Unlike in the 25% case, EVs participating in V2G operations do not end the day at critically low SOC levels. This ensures that idle EVs, even if activated as active EVs on the following day, will retain sufficient charge to meet normal mobility requirements without compromising travel behaviour. Thus, at a 50% ownership level, the system demonstrates both enhanced grid balancing capability and improved sustainability of EV participation across consecutive days.

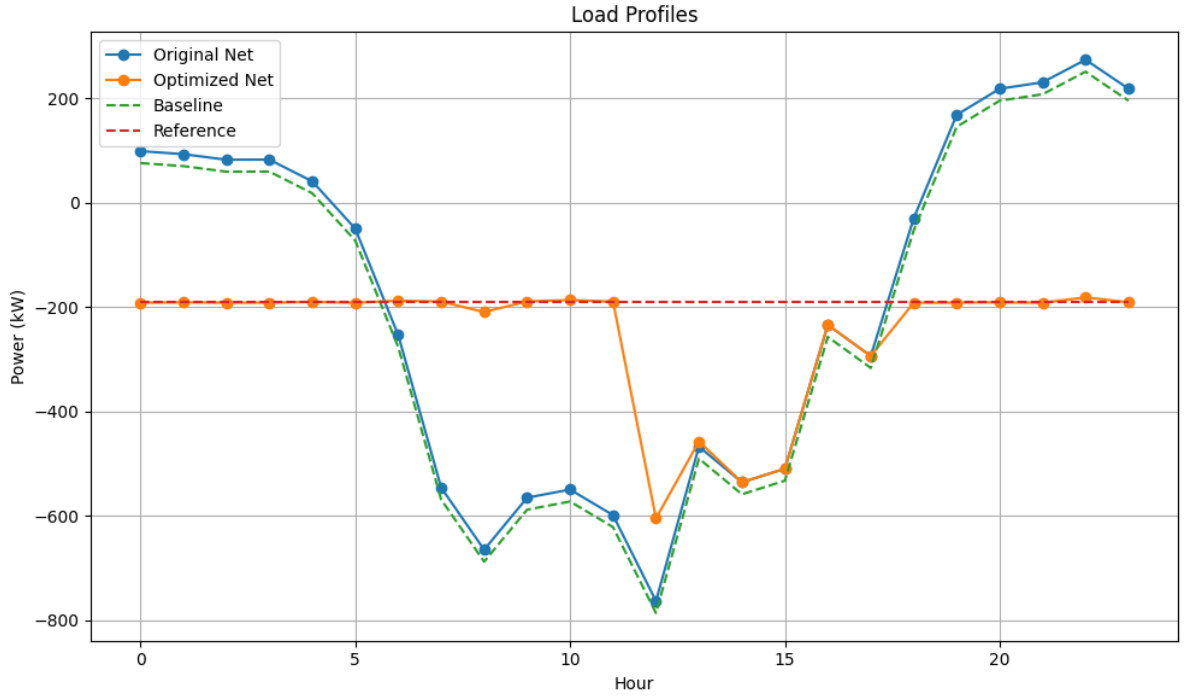


Figure 5-22. Hourly net-load profiles before and after Scenario I optimization on 21st June with full-standard PV capacity (4 kWp) and default EV parameters. Simulation parameters: bidirectional charging/discharging power = 3.3 kW; EV ownership rate = 0.50; idle rate = 0.5487; average hourly charging demand = 0.20455 kWh.

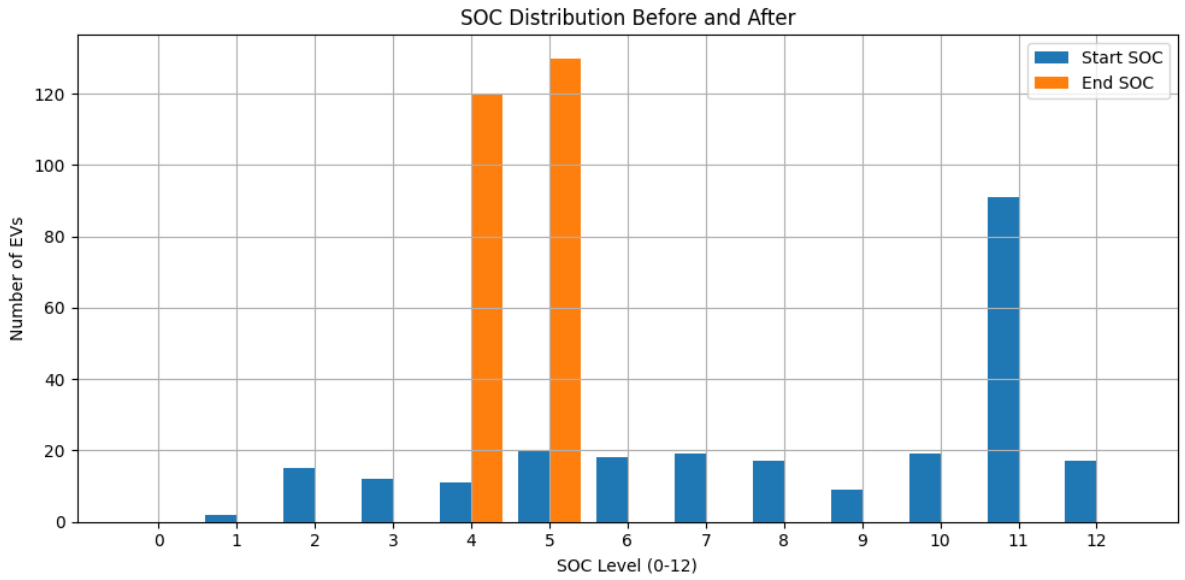


Figure 5-23. SOC distribution of dispatched EVs before and after Scenario I optimization on 21st June with full-standard PV capacity (4 kWp) and default EV parameters (EV ownership rate = 0.50).

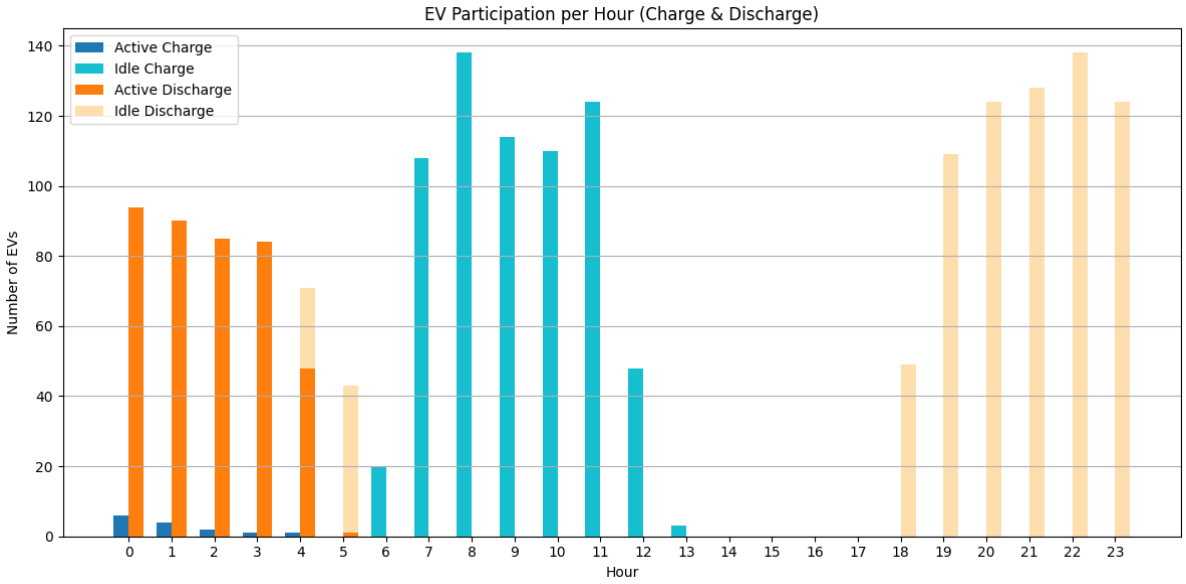


Figure 5-24. Hourly participation of active and idle EVs in charging and discharging, based on Scenario I optimization on 21st June with full-standard PV capacity (4 kWp) and default EV parameters (EV ownership rate = 0.50).

- **Case 3: EV Ownership Rate at 75%**

When the EV ownership rate increases to 75%, the community microgrid contains a total of 375 EVs, of which approximately 169 are active EVs and 206 are idle EVs. Compared with Case 2, the net-load profile under this case shows further improvement, particularly during critical periods where the system load closely converges toward the reference curve of the predefined balancing threshold. The enhanced dispatch capacity of the larger EV fleet enables more effective smoothing of fluctuations, and the overall load profile exhibits a high degree of stability.

From the dispatch perspective, both the number of EVs participating in V2G operations and their final SOC levels after optimization show notable enhancement relative to the 50% case. The increased fleet size strengthens the system's ability to absorb surplus PV output during midday hours, reducing the duration of unbalanced intervals by approximately two hours compared with Case 2. Consequently, a greater volume of excess PV generation is stored during the day, which in turn provides stronger support for peak shaving during evening demand periods. At the same time, the optimized SOC distribution indicates that the majority of dispatched EVs retain sufficiently high energy levels at the end of the day, with SOC values concentrated in levels 7 to 9. This corresponds to an energy reserve consistent with the modal value of typical single-trip energy consumption in the dataset (approximately 42% SOC), thereby ensuring that V2G participation does not compromise EV owners' mobility requirements on the following day.

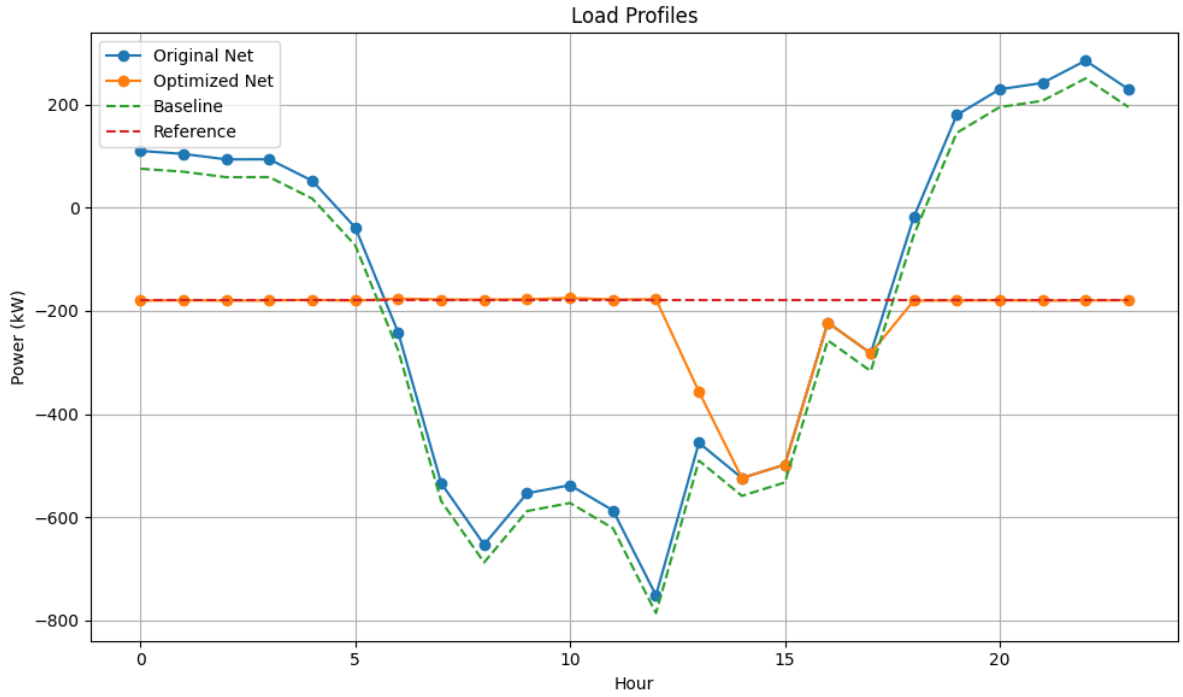


Figure 5-25. Hourly net-load profiles before and after Scenario I optimization on 21st June with full-standard PV capacity (4 kWp) and default EV parameters. Simulation parameters: bidirectional charging/discharging power = 3.3 kW; EV ownership rate = 0.75; idle rate = 0.5487; average hourly charging demand = 0.20455 kWh.

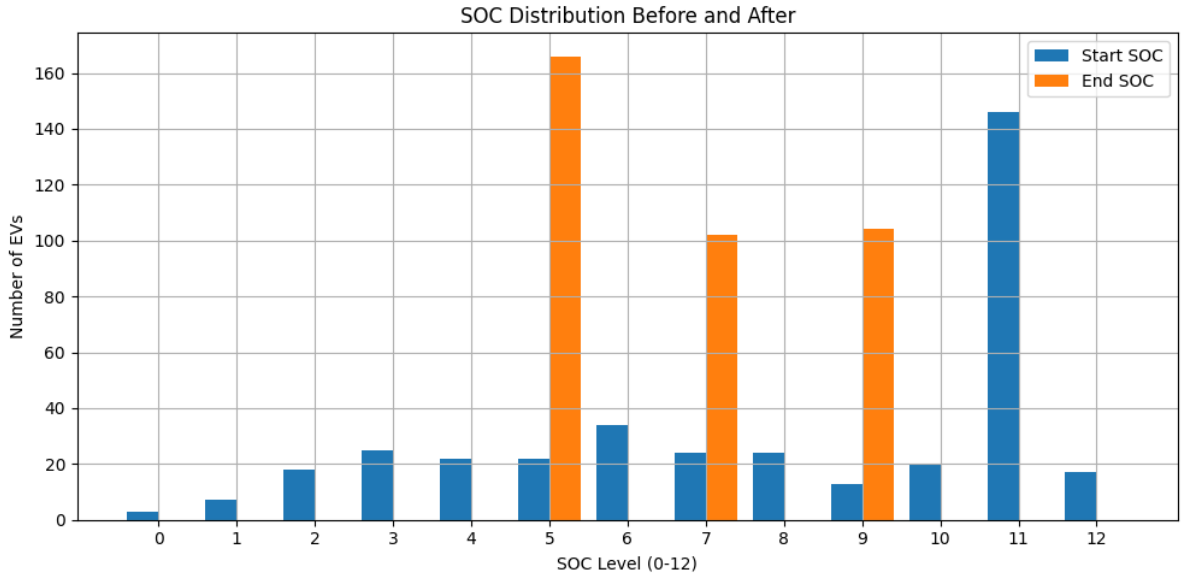


Figure 5-26. SOC distribution of dispatched EVs before and after Scenario I optimization on 21st June with full-standard PV capacity (4 kWp) and default EV parameters (EV ownership rate = 0.75).

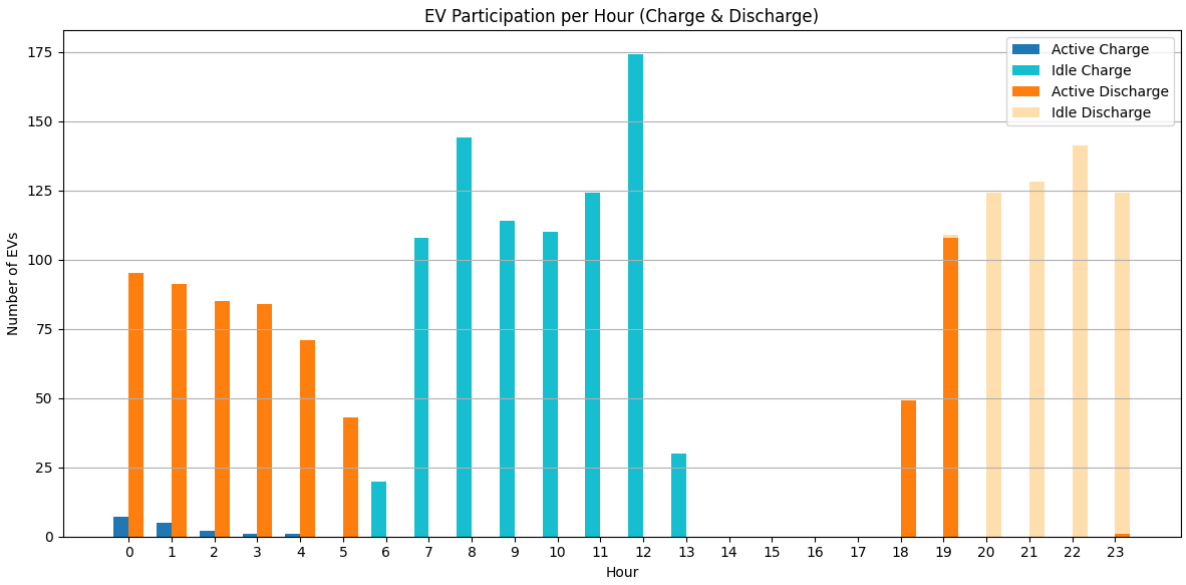


Figure 5-27. Hourly participation of active and idle EVs in charging and discharging, based on Scenario I optimization on 21st June with full-standard PV capacity (4 kWp) and default EV parameters (EV ownership rate = 0.75).

- **Case 4: EV Ownership Rate at 100%**

In Case 4, the EV ownership rate within the community microgrid is set to 100%. Based on the behavioural data of the EV fleet, the composition of active and idle EVs in this setting (ownership at 100%, with an idle rate of 54.87%) is essentially consistent with the proportions used in Figures 5-1 through 5-3, where the idle rate was approximated at 50%. By comparing the results with the previous three cases, a distinct pattern emerges. During periods of extreme system stress—most notably at the midday PV production peak—the abundant availability of EVs ensures that low per-vehicle charging and discharging power is no longer the limiting factor in achieving load balancing. In this case, the collective charging and discharging rates are already sufficient to match the instantaneous fluctuations of the net load.

This outcome highlights a critical threshold condition: under the operational parameters of the current system, once the EV ownership rate surpasses approximately 50%, further increasing the bidirectional charging power capacity of individual EVs has little or no marginal effect on

the V2G optimization outcome. Beyond this point, the only determinant of balancing effectiveness is the aggregate storage capacity of the EV fleet. However, even at full ownership, the available storage capacity remains insufficient to absorb the entirety of midday surplus PV generation. Specifically, between 16:00 and 17:00, all dispatchable EVs reach their maximum SOC, leaving no residual storage capability. As a result, the net-load profile during this interval fails to converge fully with the predefined balancing curve, leaving residual mismatches unaddressed.

To overcome this limitation, one potential pathway would be to increase the per-vehicle battery capacity (currently 24 kWh in this study). This approach is technologically feasible and aligns with the ongoing trend of battery capacity expansion in the EV industry. In addition, increasing the overall EV ownership rate within the community grid also proves to be both effective and feasible, as it directly enlarges the aggregate storage capacity available for V2G dispatch. By contrast, relying on a higher idle rate to secure additional storage availability during PV peak hours is much less realistic, as it contradicts the expected increase in EV utilization in the future. Overall, the results demonstrate that idle EVs play a substantial and valuable role in enabling peak shaving and valley filling, yet the system cannot rely solely on raising the idle EV rate to achieve full load-balancing performance.

5.2.1.2-(ii) EV Idling Rate

In the current community grid configuration, the availability of active EVs during critical load conditions—either at midday valleys requiring charging to absorb surplus PV output or at evening peaks requiring discharging support—remains relatively limited. Many active EVs are not physically connected to the grid during midday hours, while others fail to meet discharging conditions during evening peaks. As a result, the realization of load-balancing objectives in both midday surplus absorption and evening peak shaving relies heavily on the contribution of

idle EVs. Consequently, the idling rate becomes a decisive factor in shaping system-level performance. Its influence manifests primarily in two dimensions: first, the ability to provide instantaneous charging or discharging power at net-load extremities in order to achieve balance at critical points; and second, the aggregate capacity to absorb and store surplus PV generation on days characterized by high solar output.

To better approximate realistic EV usage conditions and to capture the scheduling flexibility of EVs under extreme load conditions, the subsequent simulations focus on scenarios where the EV ownership rate is fixed at 100%, while the idling rate varies across 0%, 25%, 50%, and 75%. All other parameters are kept consistent with the empirical dataset to preserve fidelity of the analysis, including a bidirectional charging/discharging power of 3.3 kW, a uniform EV battery capacity of 24 kWh, and an average hourly charging demand of 0.20455 kWh. The test environment corresponds to a highly challenging case: the summer solstice (21st June), when PV generation reaches its seasonal maximum, thereby amplifying the load-balancing challenge. In addition, a boundary case with an EV ownership rate of 90% and an idling rate of 60% is included to illustrate the threshold condition under which the V2G system, leveraging idle EVs, is still able to achieve load-balancing at critical net-load extremities. This boundary scenario not only provides a quantified reference point for the structural requirements needed to ensure system stability, but also demonstrates that under the current community grid conditions and EV usage patterns, it is possible to fully achieve extreme load balancing through the effective scheduling of idle EVs.

- **Case 1: EV Idling Rate = 0% (Ownership Rate = 100%)**

Case 1 serves as the reference scenario, representing an extreme condition in which the community grid consists entirely of active EVs with no idle EVs available. Under this configuration, the V2G system effectively loses its capacity to absorb surplus PV generation during midday hours—the very period when storage potential is most critical. Instead, the

majority of EVs participating in V2G scheduling remain in a continuous discharging state throughout the day to support load-balancing operations. This reliance on uninterrupted discharge becomes particularly pronounced during the evening demand peak, where more than 140 EVs are simultaneously dispatched for discharging. Such a state, however, is inherently unsustainable, as vehicles rapidly deplete their stored energy reserves without any opportunity to recharge. Consequently, the system is unable to maintain stable operation over extended periods. This case thus highlights a critical structural limitation: in the absence of idle EVs, relying solely on active EVs under current usage conditions is insufficient to achieve load-balancing at net-load extremities.

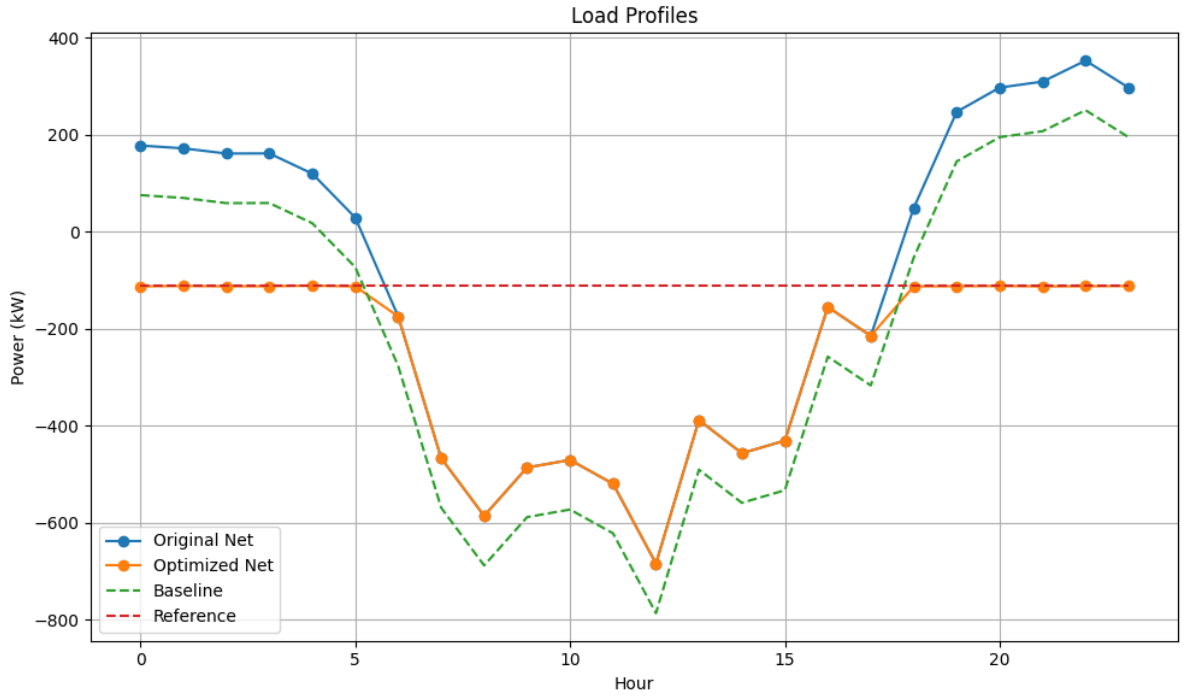


Figure 5-28. Hourly net-load profiles before and after Scenario I optimization on 21st June with full-standard PV capacity (4 kWp) and default EV parameters. Simulation parameters: bidirectional charging/discharging power = 3.3 kW; EV ownership rate = 1; idle rate = 0; average hourly charging demand = 0.20455 kWh.

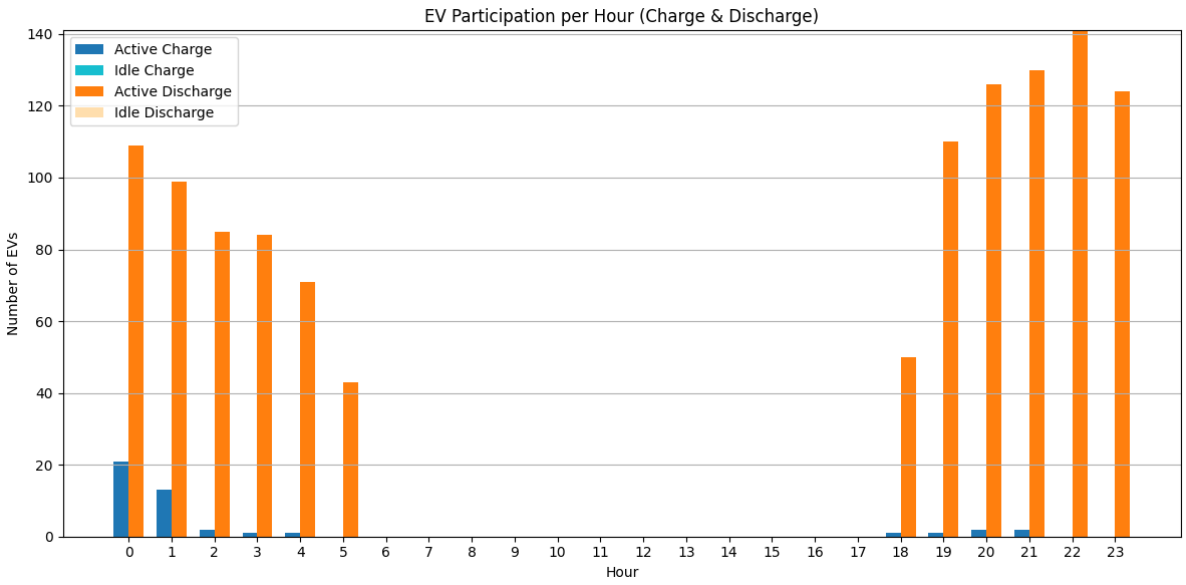


Figure 5-29. Hourly participation of active and idle EVs in charging and discharging, based on Scenario I optimization on 21st June with full-standard PV capacity (4 kWp) and default EV parameters (EV ownership rate = 1; idle rate = 0).

- **Case 2: EV Idling Rate = 25% (Ownership Rate = 100%)**

When the EV idling rate increases to 25%, the community grid consists of 375 active EVs and 125 idle EVs, leading to a marked improvement in the system's ability to absorb surplus PV generation during midday peak hours. Interestingly, the absolute number of idle EVs under this condition is almost identical to that observed in the scenario with a 50% ownership rate and an idling rate of 54.87% (as shown in Figures 5-22 to 5-24). However, despite the numerical similarity in idle EV counts, and after discounting potential biases arising from the stochastic nature of data sampling in the simulation process, a closer analysis reveals substantive structural differences in the final scheduling outcomes. Specifically, in the present case, the relatively large pool of active EVs ensures that during the evening peak demand period—when discharging is required—the system can rely primarily on active EVs to maintain load-balancing performance. In contrast, the scenario depicted in Figure 5-24, characterized by fewer active EVs, relies almost entirely on idle EVs to provide peak-shaving capacity. Nonetheless, in terms of midday absorption of surplus PV generation, both cases demonstrate

comparable performance, indicating that the primary distinction lies in the structural allocation of responsibilities between active and idle EVs across different periods of the day. This further highlights that the contribution of idle EVs is most critical during load extremities rather than in sustaining continuous balancing throughout the day.

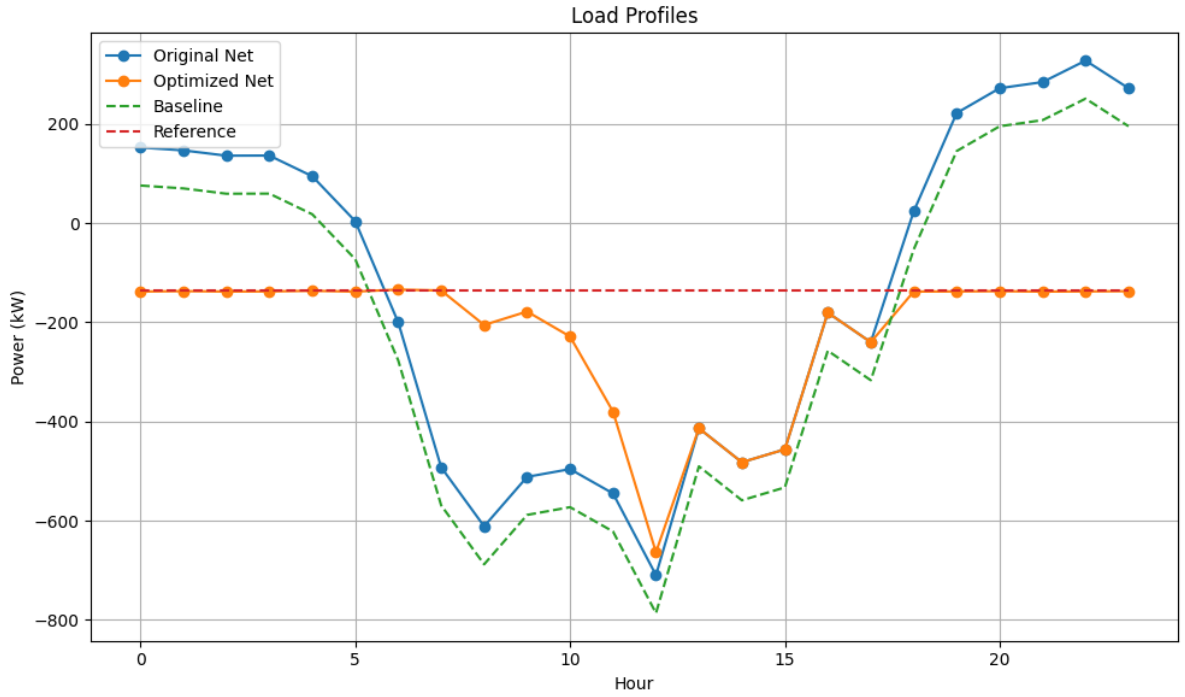


Figure 5-30. Hourly net-load profiles before and after Scenario I optimization on 21st June with full-standard PV capacity (4 kWp) and default EV parameters. Simulation parameters: bidirectional charging/discharging power = 3.3 kW; EV ownership rate = 1; idle rate = 0.25; average hourly charging demand = 0.20455 kWh.

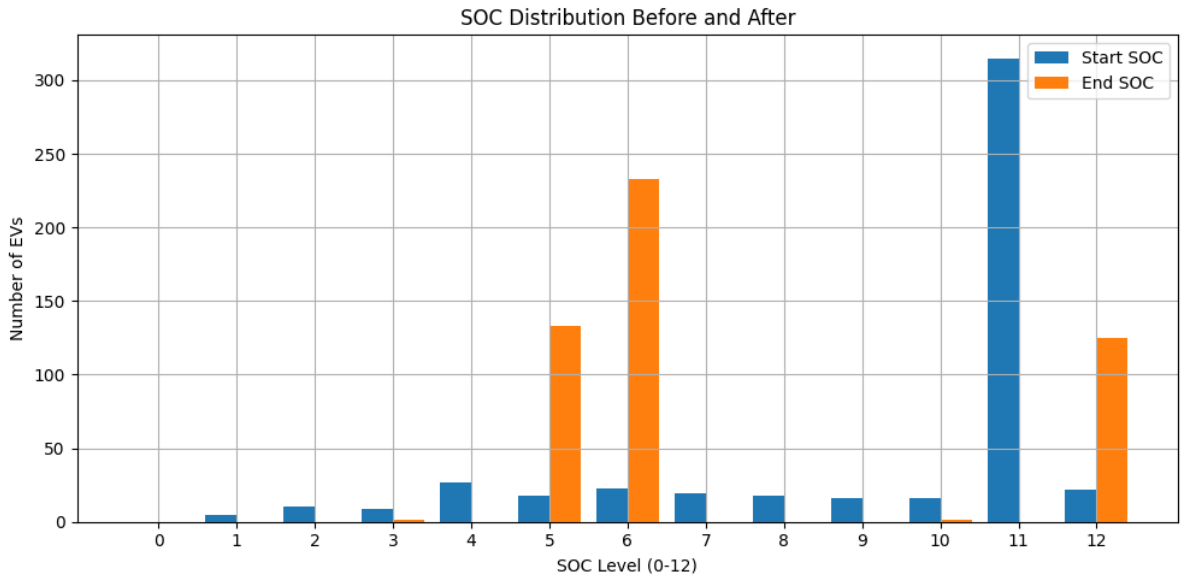


Figure 5-31. SOC distribution of dispatched EVs before and after Scenario I optimization on 21st June with full-standard PV capacity (4 kWp) and default EV parameters (EV ownership rate = 1; idle rate = 0.25).

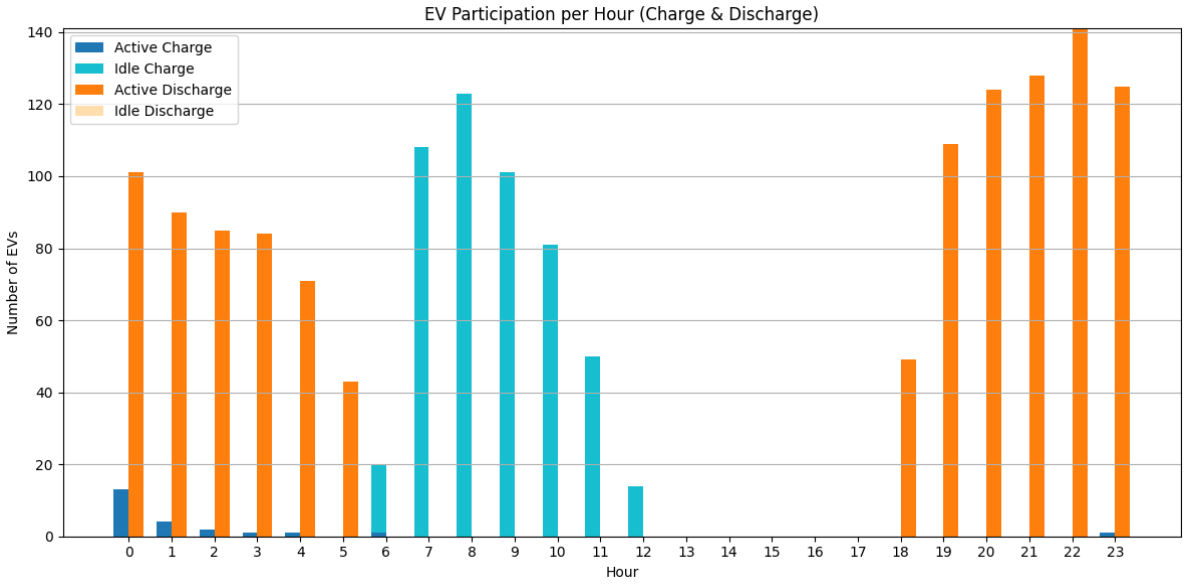


Figure 5-32. Hourly participation of active and idle EVs in charging and discharging, based on Scenario I optimization on 21st June with full-standard PV capacity (4 kWp) and default EV parameters (EV ownership rate = 1; idle rate = 0.25).

- **Case 3: EV Idling Rate = 50% (Ownership Rate = 100%) — Consistent with Current EV Usage Patterns**

In Case 3, the simulation parameters are aligned with those applied in Figures 5-1 through 5-3, representing a condition where the EV idling rate (50%) closely reflects the observed real-world usage pattern. The corresponding results for net-load distribution and EV scheduling are illustrated in Figures 5-1 to 5-3. Compared with the preceding two scenarios, this configuration achieves near-complete alignment with the system's theoretical load-balancing limits, as the optimized net-load curve effectively matches the predefined balance threshold across most time intervals. A notable feature of this case lies in the clear temporal division of labour between active and idle EVs in the scheduling process. Active EVs are primarily dispatched during evening peak demand periods to provide discharging capacity and ensure load balancing, while idle EVs are predominantly scheduled during midday troughs to absorb surplus PV generation. This structural differentiation in scheduling highlights the complementary roles of active and idle EVs, with each type of vehicle contributing to balancing at distinct extremities of the net-load curve.

The SOC distributions of EVs at the end of the simulation day further reinforce this division of function. Idle EVs, having absorbed surplus electricity during trough periods, exhibit a post-optimization SOC distribution clustered at higher levels, particularly around level 10 and level 12, indicating substantial retained energy reserves. In contrast, active EVs, heavily utilized for discharging during the evening peak, converge toward the lower SOC boundary at level 5, which corresponds to the minimum discharge threshold set in the optimization model. Importantly, despite this extensive use, the final SOC levels of active EVs remain sufficient to meet mobility requirements on the following day, thereby ensuring that the optimization process does not compromise transportation functionality.

- **Case 4: EV Idling Rate = 75% (Ownership Rate = 100%)**

Case 4 represents a parameter setting that reflects atypical usage days observed in the empirical EV dataset, where vehicle utilization rates are comparatively low and a larger proportion of

EVs remain idle. Under this condition, the optimized net-load distribution curve almost perfectly aligns with the theoretical balance threshold, suggesting that this scenario approximates a potential boundary state in which the EV fleet is capable of fully absorbing surplus PV generation during midday production peaks.

From the perspective of scheduling dynamics, the maximum number of EVs simultaneously dispatched reaches 175, which does not exhaust the total idle EV reserve, leaving additional flexibility within the system. This indicates that, even under conditions of extreme PV surplus, the system maintains sufficient headroom to accommodate further variability. However, due to the relatively limited number of active EVs in this case, the burden of evening peak demand balancing is almost entirely borne by idle EVs through discharging. As a result, the final SOC distribution of all participating EVs converges toward mid-range levels: active EVs cluster at level 5, which corresponds to the lower discharge limit, while idle EVs predominantly concentrate between levels 7 and 9. This outcome ensures that all vehicles retain sufficient energy reserves to support either charging or discharging operations on the following day, without compromising their driving requirements.

Overall, this scenario represents a relatively favourable and robust operating condition, in which the system not only achieves effective load balancing across both midday and evening extremes but also preserves operational margins for future scheduling flexibility. However, it is important to emphasize that the high idling-rate condition reflected here corresponds to an atypical, low-utilization state of EV fleets, and thus serves more as a theoretical boundary case than as a realistic operating norm.

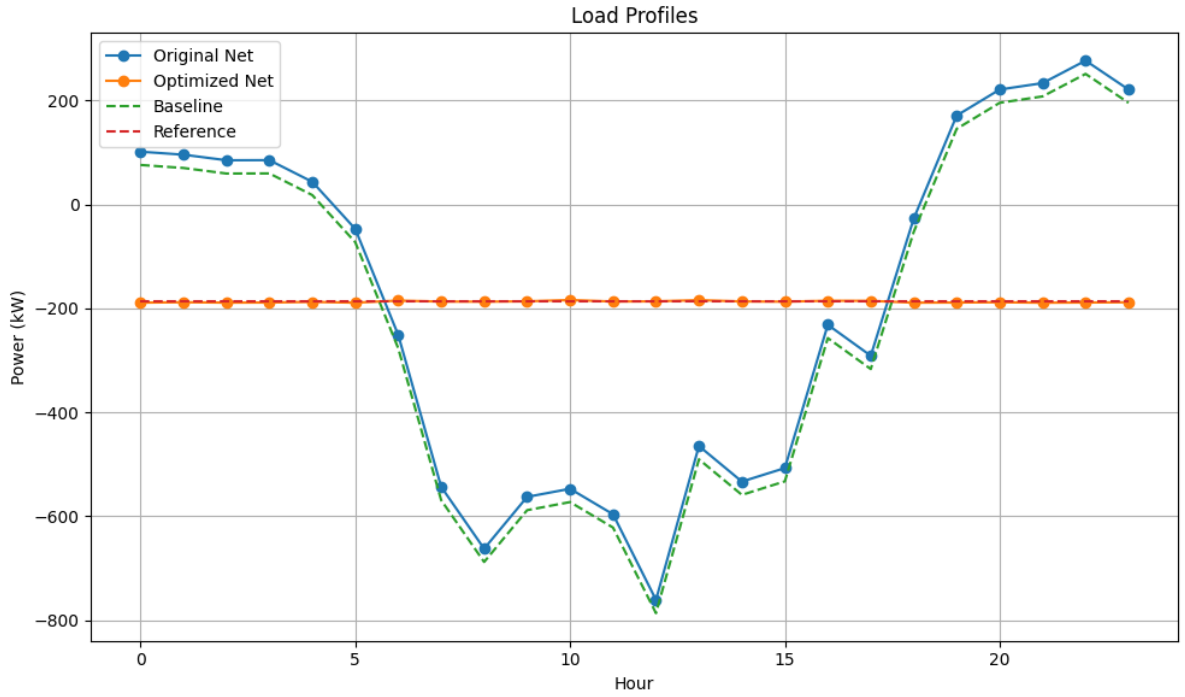


Figure 5-33. Hourly net-load profiles before and after Scenario I optimization on 21st June with full-standard PV capacity (4 kWp) and default EV parameters. Simulation parameters: bidirectional charging/discharging power = 3.3 kW; EV ownership rate = 1; idle rate = 0.75; average hourly charging demand = 0.20455 kWh.

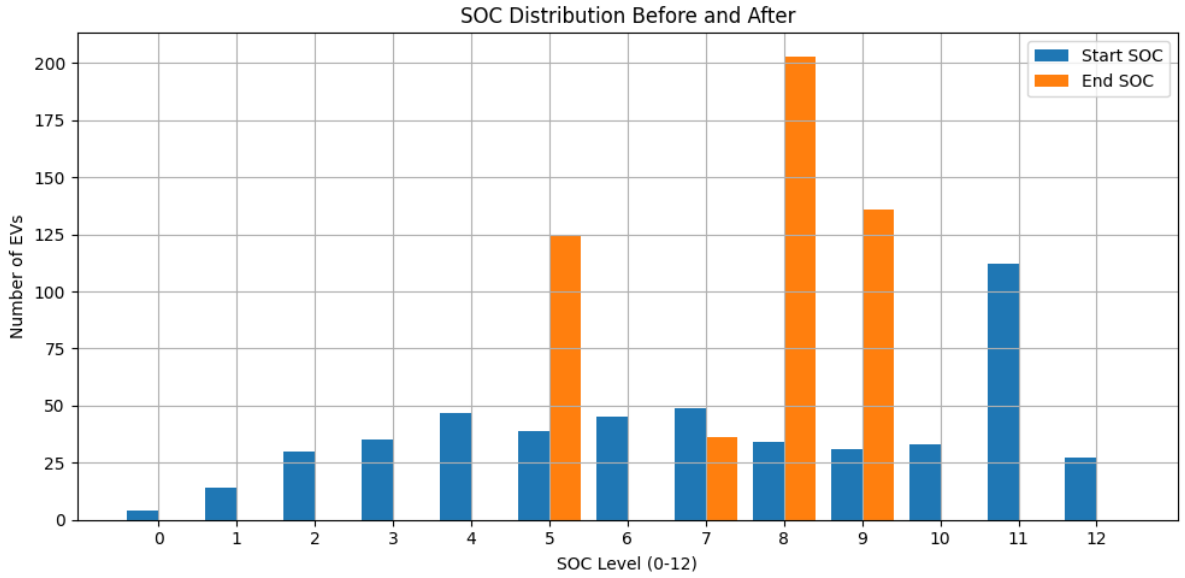


Figure 5-34. SOC distribution of dispatched EVs before and after Scenario I optimization on 21st June with full-standard PV capacity (4 kWp) and default EV parameters (EV ownership rate = 1; idle rate = 0.75).

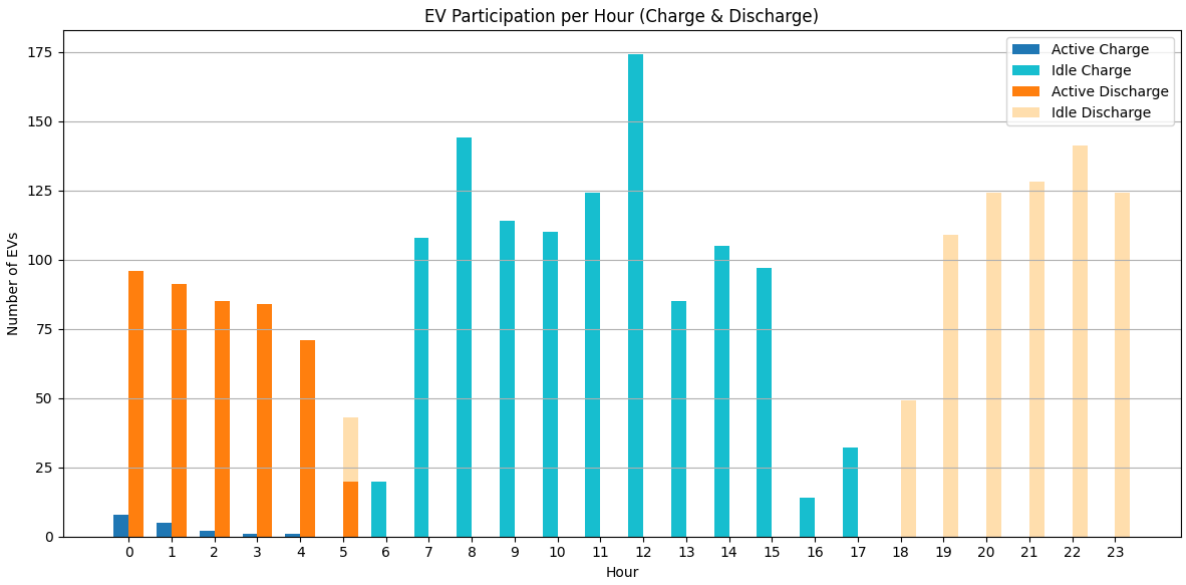


Figure 5-35. Hourly participation of active and idle EVs in charging and discharging, based on Scenario I optimization on 21st June with full-standard PV capacity (4 kWp) and default EV parameters (EV ownership rate = 1; idle rate = 0.75).

The exploration of boundary conditions is essential to identify the thresholds under which the EV fleet can fully satisfy the extreme scheduling requirements of the community grid. Three criteria must be simultaneously met in such boundary cases: first, the instantaneous charging or discharging power must be sufficient to balance grid loads during both peak and valley hours; second, the aggregate storage capacity of the EV fleet must be able to completely absorb surplus PV generation during periods of maximum output; and third, the final SOC distribution at the end of the day should concentrate around mid-range levels. A mid-range SOC distribution not only reflects high scheduling efficiency but also ensures that sufficient reserves are preserved to meet both the following day's V2G requirements and the mobility needs of EV users.

To identify these boundary conditions, a combinatorial enumeration method was employed by testing pairs of EV ownership and idling rate values under the specific operational background of the studied community grid, which comprises 500 residential households and rooftop PV

systems with a maximum installed capacity of 4 kWp. The EV usage model is constrained by current empirical data: vehicles are dispatched based on mobility demand while preserving observed charging frequencies, battery capacity is fixed at the relatively low value of 24 kWh, and the bidirectional charging/discharging power is limited to 3.3 kW.

The results indicate that the optimal configurations capable of achieving perfect load-balancing while maintaining high EV utilization efficiency—and remaining realistic in terms of actual and future EV usage patterns—are either (i) an EV ownership rate of 100% with an idling rate of 55%, or (ii) an EV ownership rate of 90% with an idling rate of 60%. Both parameter combinations satisfy the dual requirements of balancing instantaneous load extremes and absorbing midday PV surpluses, while ensuring that final SOC levels cluster around the mid-range. Notably, the configuration with 100% ownership and 55% idling aligns closely with the observed daily average idling rate in the empirical EV dataset, thereby reinforcing the validity and practical feasibility of leveraging idle EVs for large-scale V2G scheduling.

It is important to emphasize, however, that these optimal combinations are not universally transferable. Rather, they are contingent on the specific grid and EV parameter settings considered here, particularly the relatively low bidirectional power transfer capacity (3.3 kW) and the modest EV battery size (24 kWh). These constraints inherently limit the scalability of the results and suggest that, under future conditions where higher charging/discharging powers and larger battery capacities become standard, the boundary conditions for achieving efficient load-balancing may shift substantially.

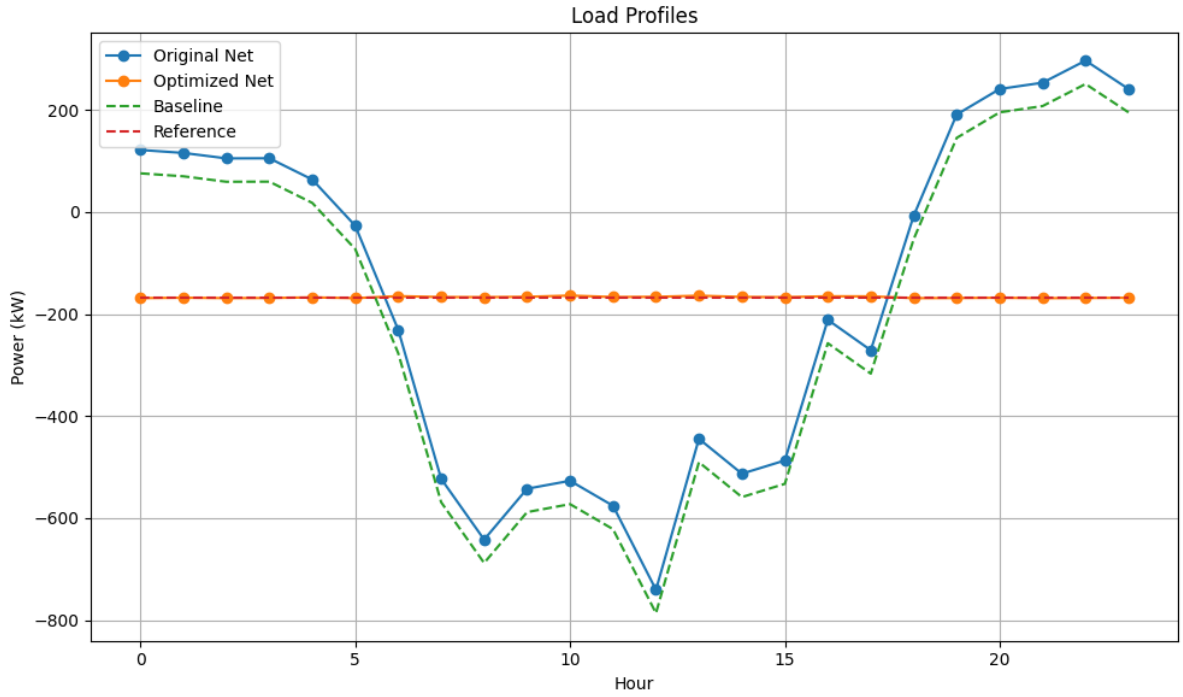


Figure 5-36. Hourly net-load profiles before and after Scenario I optimization on 21st June with full-standard PV capacity (4 kWp) and default EV parameters. Simulation parameters: bidirectional charging/discharging power = 3.3 kW; EV ownership rate = 0.9; idle rate = 0.6; average hourly charging demand = 0.20455 kWh.

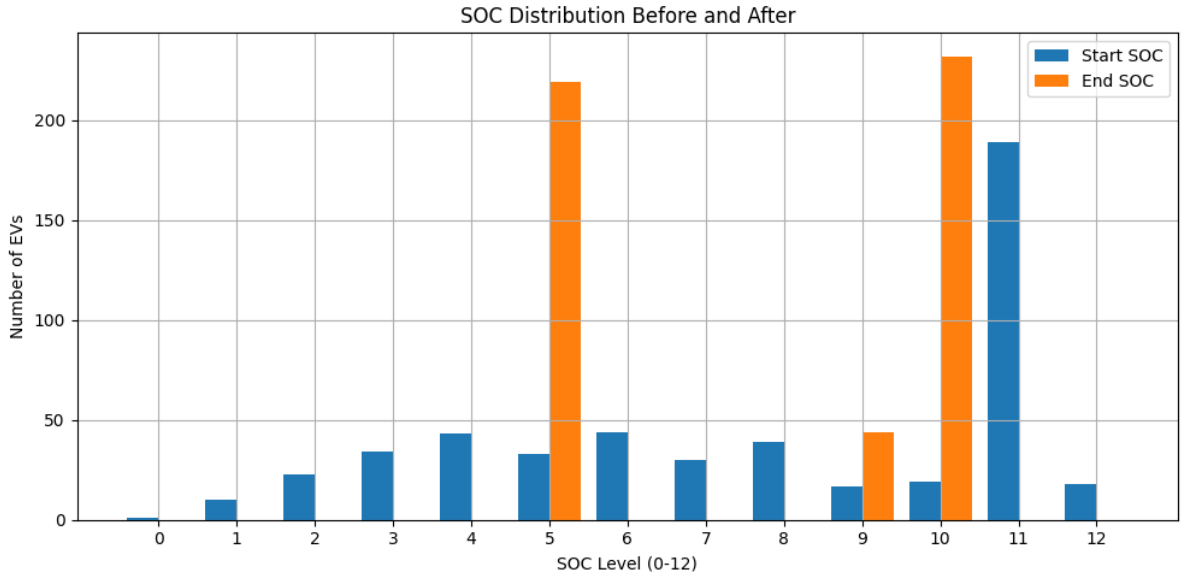


Figure 5-37. SOC distribution of dispatched EVs before and after Scenario I optimization on 21st June with full-standard PV capacity (4 kWp) and default EV parameters (EV ownership rate = 0.9; idle rate = 0.6).

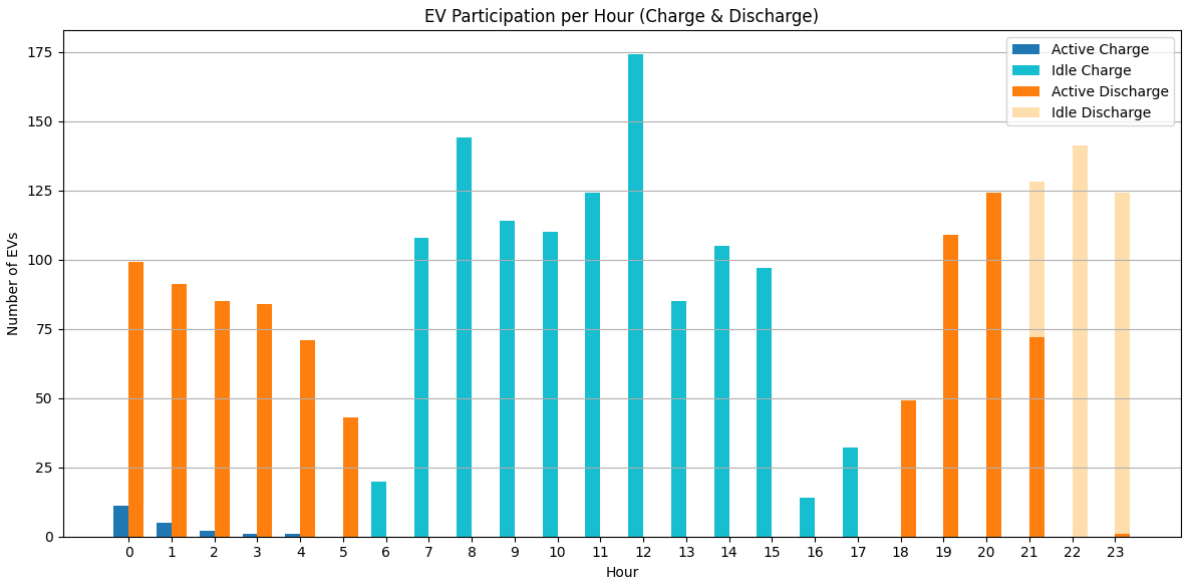


Figure 5-38. Hourly participation of active and idle EVs in charging and discharging, based on Scenario I optimization on 21st June with full-standard PV capacity (4 kWp) and default EV parameters (EV ownership rate = 0.9; idle rate = 0.6).

5.2.1.2-(iii) Charging Intensity

The impact of charging intensity on V2G management primarily manifests in two aspects: the modification of daily EV driving and charging patterns, and the variation in the net-load balancing threshold of the community grid. To evaluate this effect, three representative weeks identified in Chapter 3—corresponding to the highest, median, and lowest charging frequencies—were selected for simulation. From each representative week, the mid-week day was chosen as the benchmark "standard day," and the corresponding EV usage and charging profiles were extracted and combined with the extreme grid environment of June 21st (summer solstice, maximum PV output) to perform V2G optimization modeling. For each case, the average hourly charging demand was also computed: 0.394958 kW for the high-frequency week, 0.192591 kW for the median-frequency week, and 0.092093 kW for the low-frequency week. These values were used to derive the net-load balancing thresholds against which optimization results were evaluated.

To ensure comparability and reduce the influence of confounding variables, all other parameters were kept consistent with those applied in the previous scenarios, including a PV system installed at its maximum rated capacity of 4 kWp, bidirectional charging/discharging power of 3.3 kW, an EV ownership rate of 100%, and an idling rate of 54.87%.

The simulation results reveal that differences in charging intensity significantly alter the pre-optimization net-load profiles, leading to marked variations in the calculated balancing thresholds. Figures 5-39 to 5-41 illustrate the optimized net-load distributions for the high-, median-, and low-frequency standard days, with corresponding balancing thresholds of –123.90990268 kW, –169.44247768 kW, and –192.05452768 kW, respectively. While these variations do not substantially affect the absolute number of EVs scheduled in the V2G optimization process, the magnitude of the balancing threshold directly determines the residual transmission pressure exerted on the upstream grid. In other words, lower charging frequencies reduce both the overall daily electricity demand reflected in the net-load curve and the fleet's capacity to absorb surplus PV generation during midday peaks, even though the scheduling capability of the EV fleet itself remains relatively stable across cases.

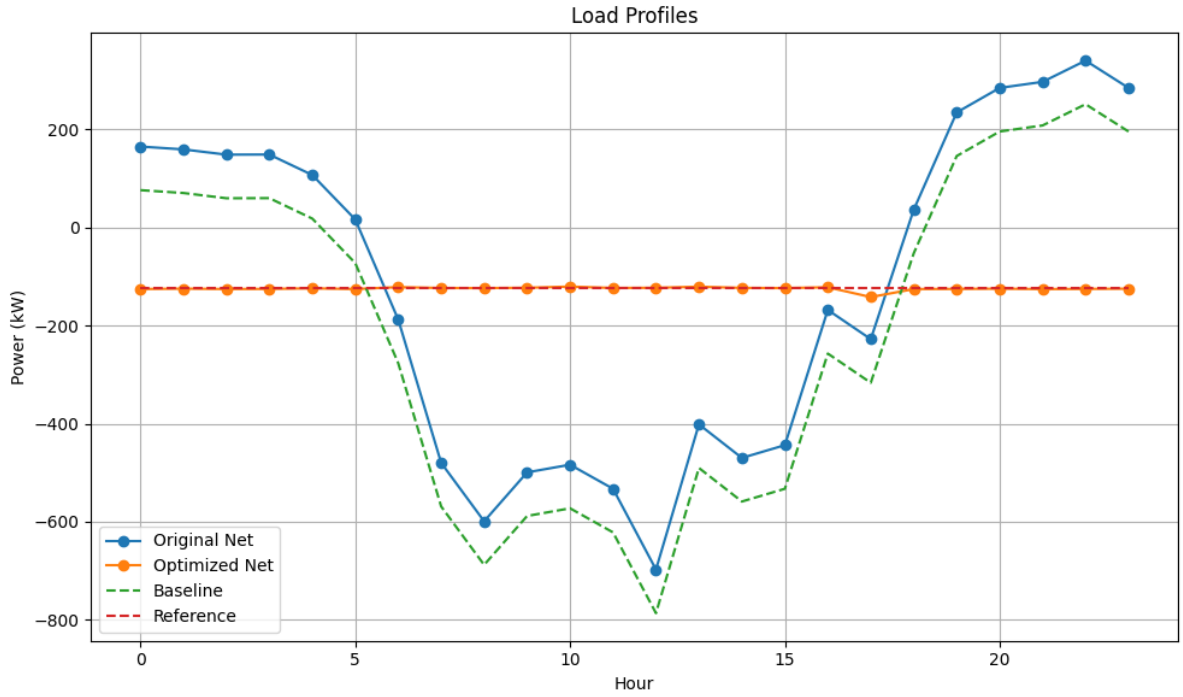


Figure 5-39. Hourly net-load profiles before and after Scenario I optimization on 21st June with full-standard PV capacity (4 kWp) and default EV parameters. Simulation parameters: bidirectional charging/discharging power = 3.3 kW; EV ownership rate = 1; idle rate = 0.5487; average hourly charging demand = 0.394958 kWh.

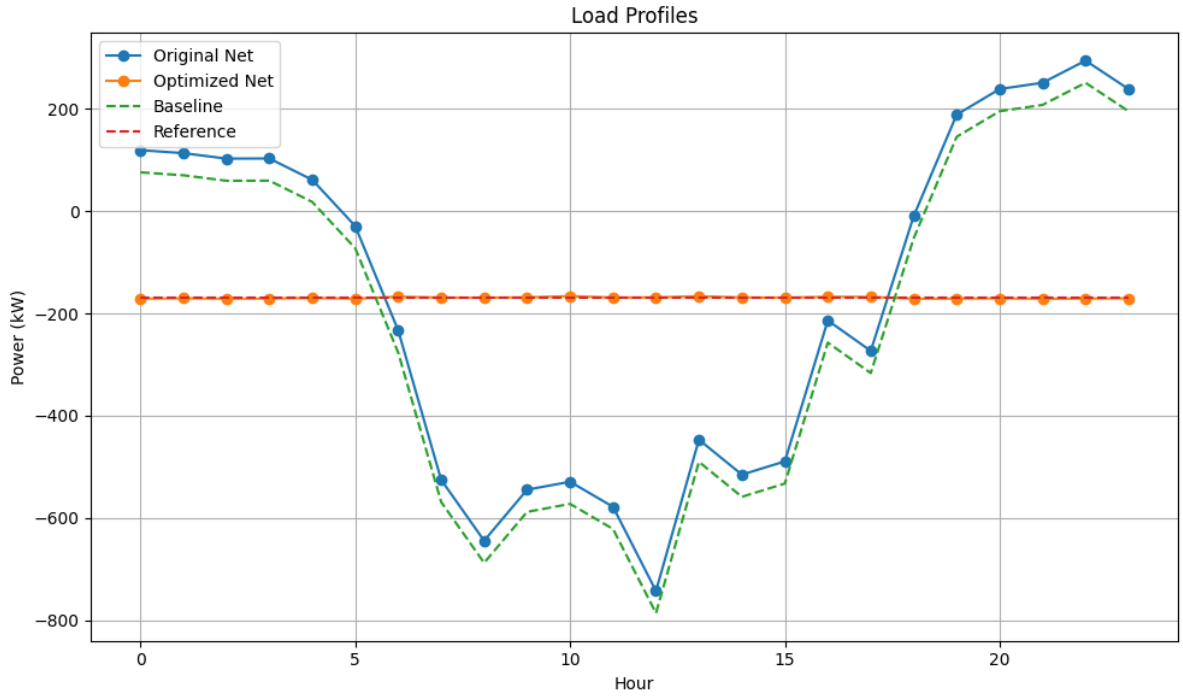


Figure 5-40. Hourly net-load profiles before and after Scenario I optimization on 21st June with full-standard PV capacity (4 kWp) and default EV parameters. Simulation parameters: bidirectional charging/discharging power = 3.3 kW; EV ownership rate = 1; idle rate = 0.5487; average hourly charging demand = 0.192591 kWh.

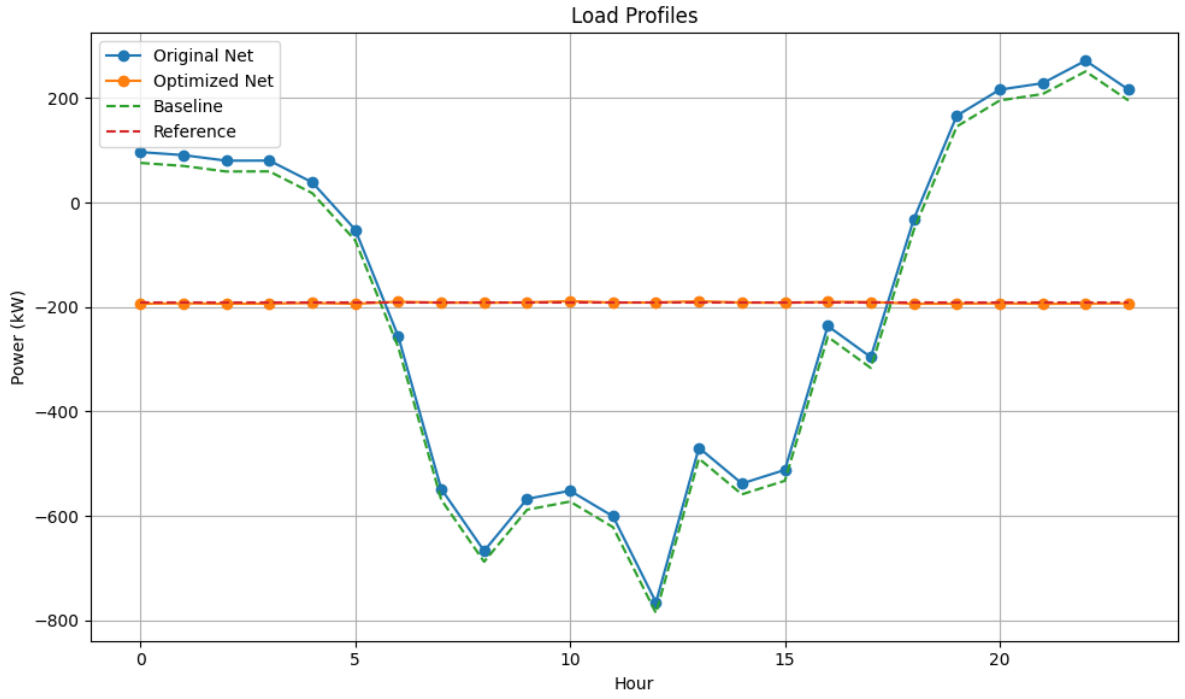


Figure 5-41. Hourly net-load profiles before and after Scenario I optimization on 21st June with full-standard PV capacity (4 kWp) and default EV parameters. Simulation parameters: bidirectional charging/discharging power = 3.3 kW; EV ownership rate = 1; idle rate = 0.5487; average hourly charging demand = 0.092093 kWh.

5.2.1.3. Impact of EV Charging/Discharging Power on Load-Balancing Performance in Scenario I

Charging and discharging power is a critical determinant of the efficiency of V2G scheduling, as it directly influences the distribution of extreme values in the community grid's net-load profile. An increase in charging power introduces a secondary peak during periods of concentrated EV charging—an artificial load peak that does not originate from the intrinsic interaction of residential demand and PV generation. Nevertheless, higher charging power significantly enhances the system's ability to accommodate surplus PV generation, particularly at the midday production peak, by reducing the number of EVs required to absorb the excess

electricity. This improvement in efficiency not only lowers the scheduling burden but also makes dispatching patterns more rational. Similarly, higher discharging power enables the system to achieve peak shaving during evening demand hours with fewer EVs, thereby alleviating the tension between the total number of EVs that must be scheduled throughout the day and the maximum number of available EVs that can be dispatched at load extremes. From the perspective of system design, therefore, identifying the optimal combination of charging and discharging power is essential for maximizing EV dispatch efficiency and for determining the minimal ownership and idling rates required to achieve reliable load balancing.

In the simulation, an enumeration-based approach was employed to systematically explore the effects of different charging and discharging power configurations. Consistent with the empirical EV battery capacity of 24 kWh observed in the dataset, three common levels of charging power (3.3 kW, 7 kW, and 10 kW) and three corresponding levels of discharging power (3.3 kW, 7 kW, and 10 kW) were selected to construct nine distinct power-pairing scenarios. For cases where charging power exceeded the baseline of 3.3 kW, EV charging behaviour was modelled using the behavioural framework developed in Chapter 3, which allowed the higher charging powers to be realistically incorporated into daily mobility-driven charging patterns. Each synthetic charging profile was subsequently superimposed onto the residential plus PV net-load curve of June 21—representing the stress-test condition of the community grid—to generate the raw pre-optimization net-load models.

To assess scheduling efficiency under each power configuration, the enumeration method was further extended by systematically pairing every charging–discharging combination with varying levels of EV ownership and idling rates, incremented in 5% steps. This procedure enabled the identification of boundary ownership–idling rate combinations that yielded the highest dispatch efficiency for each charging/discharging power setting. The evaluation criteria included both the optimization performance of load balancing and the overall efficiency of EV

utilization. Given the large number of possible parameter combinations across the nine charging/discharging power scenarios, the following discussion focuses only on several representative cases, highlighting their associated boundary ownership and idling configurations to illustrate the broader trends.

- **Case 1: Baseline and Boundary Scenario with Standard EV Parameters (Battery Capacity = 24 kWh; Charging/Discharging Power = 3.3 kW; EV Ownership = 100%; Idle Rate = 55%)**

The parameter configuration in Case 1 mirrors the baseline conditions of current EV usage patterns, thereby serving as a representative benchmark. Under this setting, the temporal distribution of community net load and the corresponding EV scheduling behaviour remain broadly consistent with the outcomes previously illustrated in Figures 5-1 to 5-3. The choice of 100% EV ownership combined with an idle rate of 55% also represents one of the feasible boundary conditions for the bidirectional charging/discharging power of 3.3 kW.

Simulation results demonstrate that, under these assumptions, the collective storage capacity of the EV fleet is sufficient to fully absorb the surplus PV generation exceeding the load-balancing threshold across the entire solar production period. Even at the instantaneous PV peak, the available EV capacity ensures complete absorption of the generation surplus, thereby maintaining instantaneous power balance without curtailment. However, a critical limitation of this configuration lies in the relatively low bidirectional transfer power of 3.3 kW. This constraint necessitates the dispatch of a large number of EVs to address instantaneous imbalances during both the midday trough and the evening demand peak. As a result, the overall number of scheduled EVs increases significantly compared to higher transfer power settings. This effect is particularly pronounced in the midday period, where the absorption of excess PV generation becomes heavily dependent on idle EVs. Consequently, the availability

of idle EVs emerges as a strictly binding condition to guarantee real-time power balance at these critical moments.

- **Case 2: Boundary Modelling of Asymmetric High-Charging Power Configuration for Mitigating Midday Net-Load Extremes (Battery Capacity = 24 kWh; Charging = 10 kW; Discharging = 3.3 kW; EV Ownership = 100%; Idle Rate = 55%)**

This case investigates the efficiency of V2G scheduling under an asymmetric bidirectional power transfer configuration, where the charging power is substantially higher than the discharging power. The rationale for this setup lies in the seasonal behaviour of the community grid: during summer, the grid is subjected to its highest fluctuations, with the most pronounced single-direction power extremes occurring around midday, coinciding with the peak of PV generation. At this time, the net-load curve typically reaches its deepest valley, and EVs must be dispatched for charging in order to absorb the excess solar output and restore power balance. Consequently, the midday PV peak generally represents the period of maximum EV dispatch requirements within a day. By adopting a higher charging power, the intention is to reduce the number of EVs required specifically to absorb the instantaneous midday peak, thereby alleviating the need for extensive dispatches that serve only to counteract this extreme condition. As illustrated in Figure 5-43, increasing the charging power significantly reduces the number of EVs needed during the midday PV peak—from 174 vehicles under the 3.3 kW charging condition to only 58 vehicles at 10 kW. However, the highest dispatch demand shifts toward the evening load peak, where up to 141 EVs are required for discharging. Despite this apparent improvement, the constraint imposed by both the battery capacity (fixed at 24 kWh) and the magnitude of midday PV surplus remains critical. To fully absorb the total PV excess, the system still requires approximately 275 idle EVs to be available during the midday peak. Under such circumstances, simply increasing the charging power does not substantially enhance the overall efficiency of EV utilization.

This case thus highlights an important boundary condition: when the number of EVs required to absorb the total PV surplus energy exceeds the number needed to mitigate instantaneous peak imbalances, further increasing charging power yields diminishing returns in terms of reducing total EV dispatch requirements. Accordingly, the analysis focuses on the minimum number and composition of EVs—distinguishing between active and idle participants—that are necessary to maintain load balance, along with the associated net-load profiles and scheduling dynamics.

To isolate the interplay between charging power and the minimum number of EVs required for PV surplus absorption, a simplified comparative approach was adopted. Rather than introducing hypothetical modifications to actual mobility behaviour—which would be unrealistic given that EV usage patterns, charging intensity, and dispatch behaviours are strongly coupled with battery capacity—the simulation instead applied an equivalent expansion of idle EV battery capacity. Specifically, the capacity was scaled from 24 kWh to 60 kWh, which corresponds to models such as the BYD Atto 3, BYD Dolphin Premium, and BYD Seal Standard Range. Under this enlarged capacity assumption, the total midday surplus could theoretically be absorbed with only 110 idle EVs. At this point, the required EV capacity for surplus absorption falls below the number of EVs needed to cover the evening load peak (140 vehicles). Consequently, the binding constraint on dispatch efficiency shifts from charging capacity during midday surplus absorption to discharging capacity during the evening demand peak.

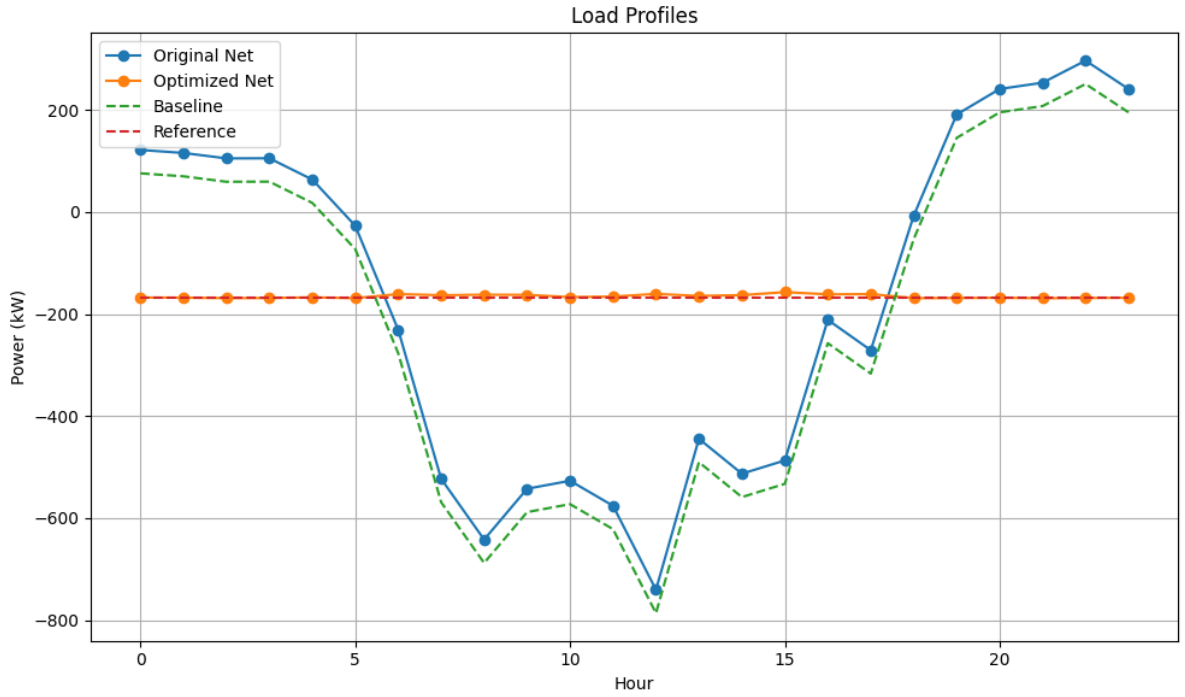


Figure 5-42. Hourly net-load profiles before and after Scenario I optimization on 21st June with full-standard PV capacity (4 kWp) and default EV parameters. Simulation parameters: charging power = 10 kW; discharging power = 3.3 kW; EV ownership rate = 1; idle rate = 0.55; average hourly charging demand = 0.20455 kWh.

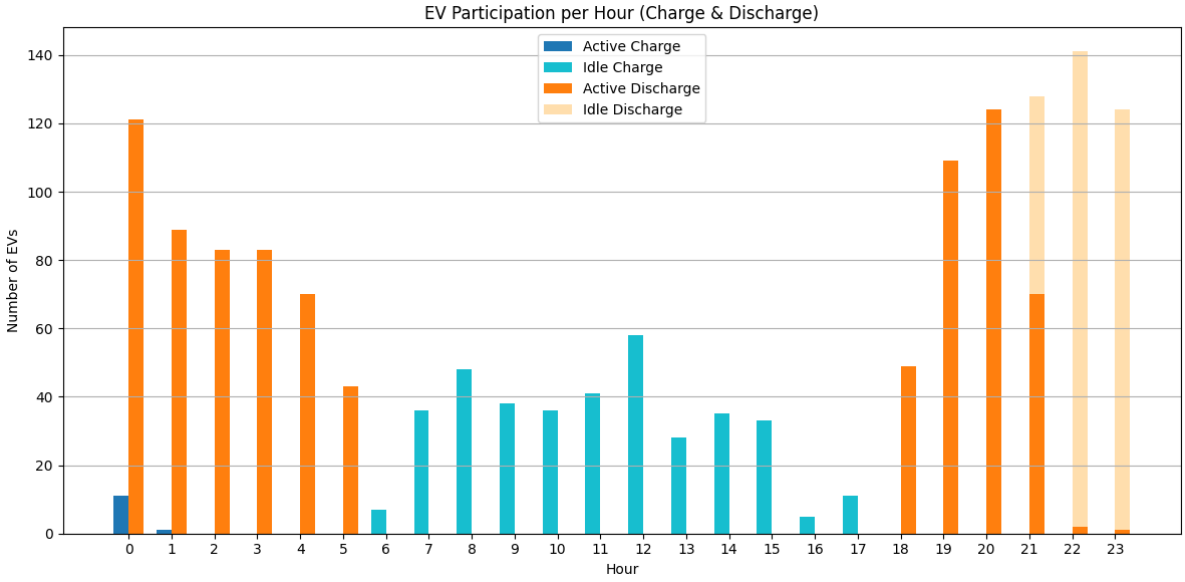


Figure 5-43. Hourly participation of active and idle EVs in charging and discharging, based on Scenario I optimization on 21st June with full-standard PV capacity (4 kWp) and default EV parameters (EV ownership rate = 1; idle rate = 0.55).

- **Case 3. Asymmetric High Charging–Discharging Power Configuration with Balanced Peak–Valley Dispatch Requirements (Battery Capacity = 24 kWh; Charging Power = 10 kW; Discharging Power = 7 kW; EV Ownership = 100%; Idle Rate = 55%)**

This case explores another asymmetric charging–discharging configuration, similar in principle to Case 2, but with an increased discharging power. The purpose of this setup is to investigate whether a more balanced distribution of EV dispatch can be achieved across both midday valley absorption and evening peak supply when battery capacity constraints are temporarily disregarded. Under the baseline condition of a 24 kWh battery capacity, the relationship between the total PV surplus and the available storage capacity imposes an inherent lower bound on the number of idle EVs required to fully absorb excess solar generation—approximately 275 vehicles in this context.

As shown in Figure 5-45, with the combination of a 10 kW charging power and a 7 kW discharging power, the maximum number of EVs required for valley absorption (58 vehicles) becomes nearly equivalent to that required for peak load mitigation (67 vehicles). This relative symmetry indicates that, once the limitation of battery capacity is alleviated (for instance, through future increases in standard EV storage capacity), it is feasible to achieve a more balanced scheduling framework in which EV dispatch requirements at midday and evening extremes converge. Such balance has important implications for enhancing V2G system stability, as it reduces the overall strain on idle EV resources while simultaneously minimizing the disparity in scheduling demand between charging and discharging operations.

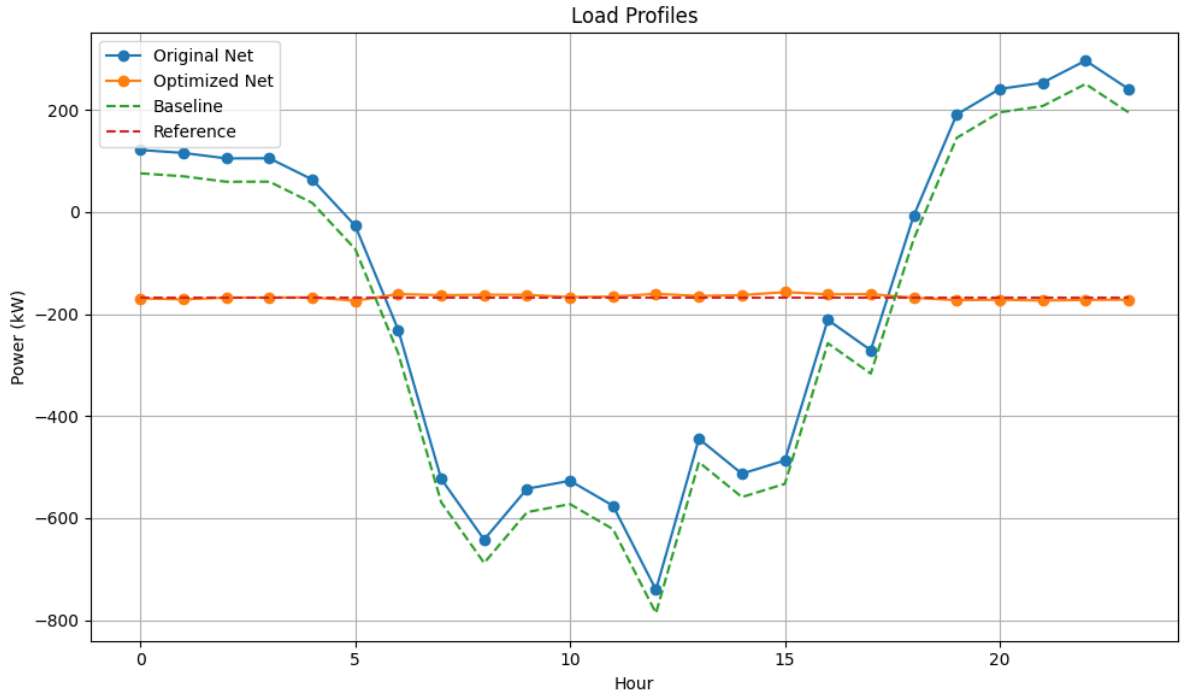


Figure 5-44. Hourly net-load profiles before and after Scenario I optimization on 21st June with full-standard PV capacity (4 kWp) and default EV parameters. Simulation parameters: charging power = 10 kW; discharging power = 7 kW; EV ownership rate = 1; idle rate = 0.55; average hourly charging demand = 0.20455 kWh.

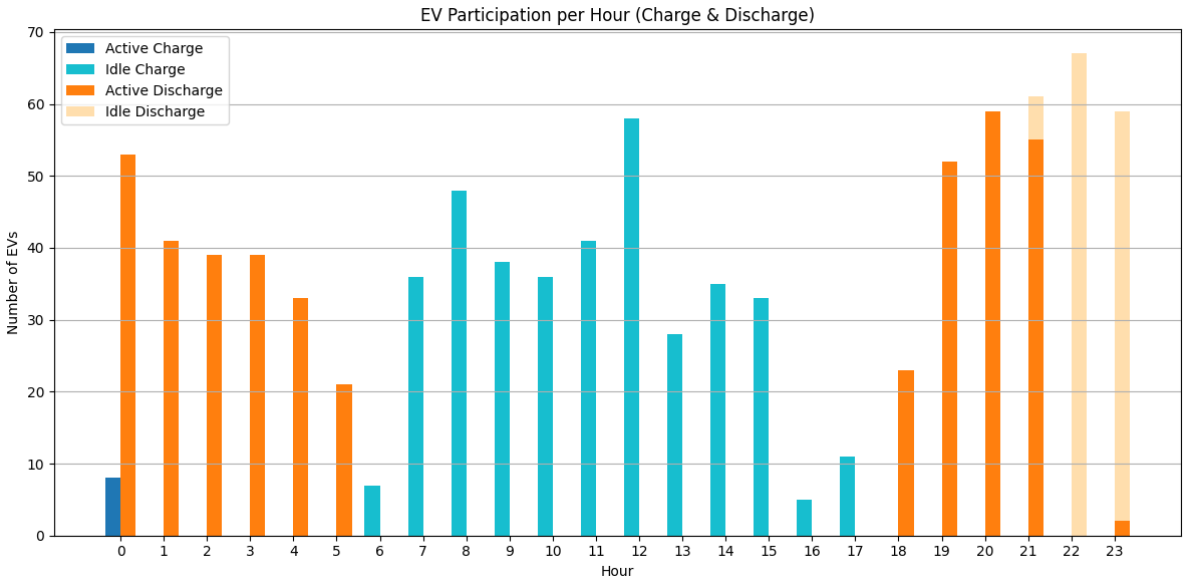


Figure 5-45. Hourly participation of active and idle EVs in charging and discharging, based on Scenario I optimization on 21st June with full-standard PV capacity (4 kWp) and default EV parameters (EV ownership rate = 1; idle rate = 0.55).

- **Case 4. Near-Optimal Configuration under Current Grid Conditions (Battery Capacity = 82.5 kWh; Charging Power = 10 kW; Discharging Power = 7 kW; EV Ownership = 100%; Idle Rate = 15%)**

This case represents a near-optimal configuration derived under the current grid environment and scheduling logic, employing an equivalent scaling approach to approximate the impact of larger EV battery capacities. Although the method is inherently an approximation—since scaling up the battery capacity equivalently increases energy consumption during driving periods, which does not fully reflect real-world behavioural changes in EV usage, charging/discharging profiles, and energy consumption patterns—it is acceptable within the context of this predictive model. This is because, as demonstrated in Chapter 3 and earlier analyses of load distribution, the dominant contributors to community power fluctuations are household demand and PV generation, while autonomous EV charging behaviour plays only a secondary role in shaping aggregate grid profiles. Hence, the simplification introduces tolerable error margins while still offering meaningful insight into system-level dynamics.

The parameter values selected here are consistent with widely adopted specifications in current EV markets and thus representative rather than arbitrary. Charging and discharging powers of 7 kW and 10 kW, respectively, align with common bi-directional residential EVSE configurations. A battery capacity of 82.5 kWh corresponds to contemporary high-capacity passenger EVs such as the BYD Seal AWD or Genesis G80, while an idle rate of 15% reflects typical values observed in empirical EV usage databases during high-frequency operational conditions. Under this configuration, the dispatch requirements become both balanced and minimized: approximately 59 EVs are sufficient to absorb the midday valley extreme, while 69 EVs are required to mitigate the evening peak demand. To fully absorb the total PV surplus at its relative maximum, only 75 EVs are required. This distribution demonstrates a high degree of balance, ensuring that no single factor disproportionately increases the overall EV demand.

Moreover, the system avoids secondary load peaks that may arise from excessive charging power, while the available battery capacity during midday ensures complete absorption of PV surplus generation. Importantly, the number of EVs required to balance instantaneous grid extremes at both midday and evening peaks remains below the total required for surplus absorption, thereby further enhancing dispatch efficiency.

Overall, this case achieves the most favourable balance among all tested configurations, minimizing the total EV demand while simultaneously smoothing load fluctuations and maintaining realistic operational parameters. Within the present technical and behavioural landscape, this parameter set can be regarded as a near-optimal solution for maximizing V2G scheduling efficiency and ensuring grid stability in high-PV-penetration communities.

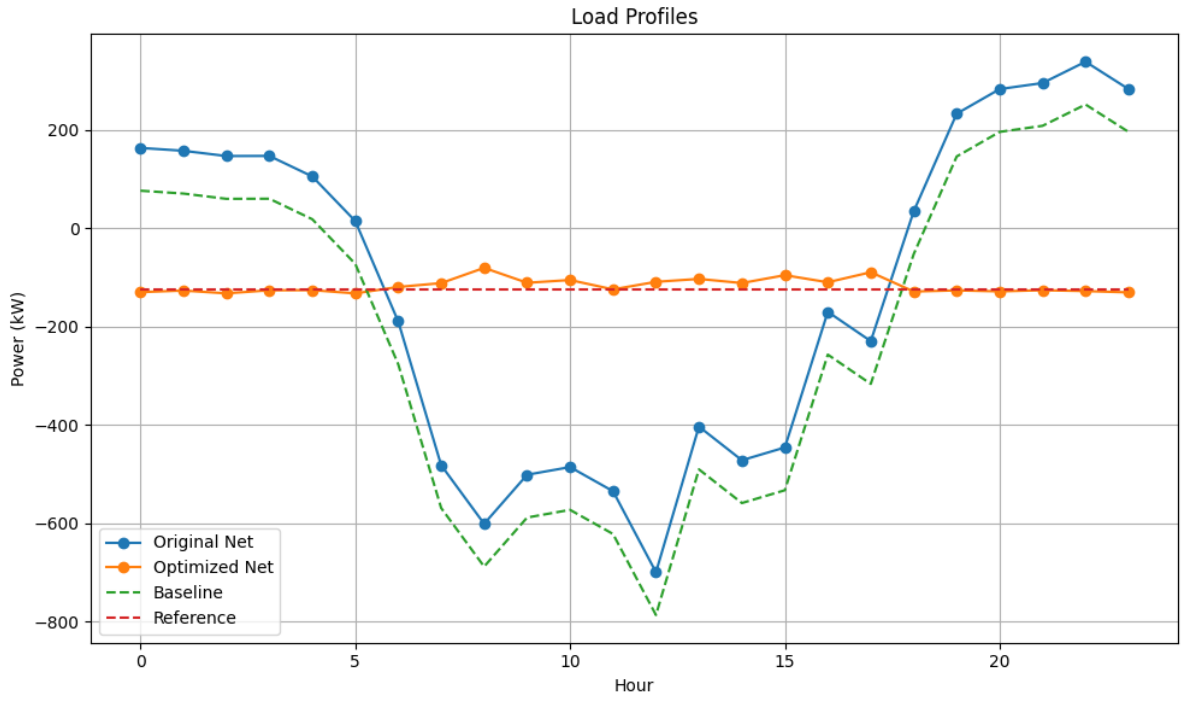


Figure 5-46. Hourly net-load profiles before and after Scenario I optimization on 21st June with full-standard PV capacity (4 kWp) and default EV parameters. Simulation parameters: battery capacity = 82.5 kWh; charging power = 10 kW; discharging power = 7 kW; EV ownership rate = 1; idle rate = 0.15; average hourly charging demand = 0.20455 kWh.

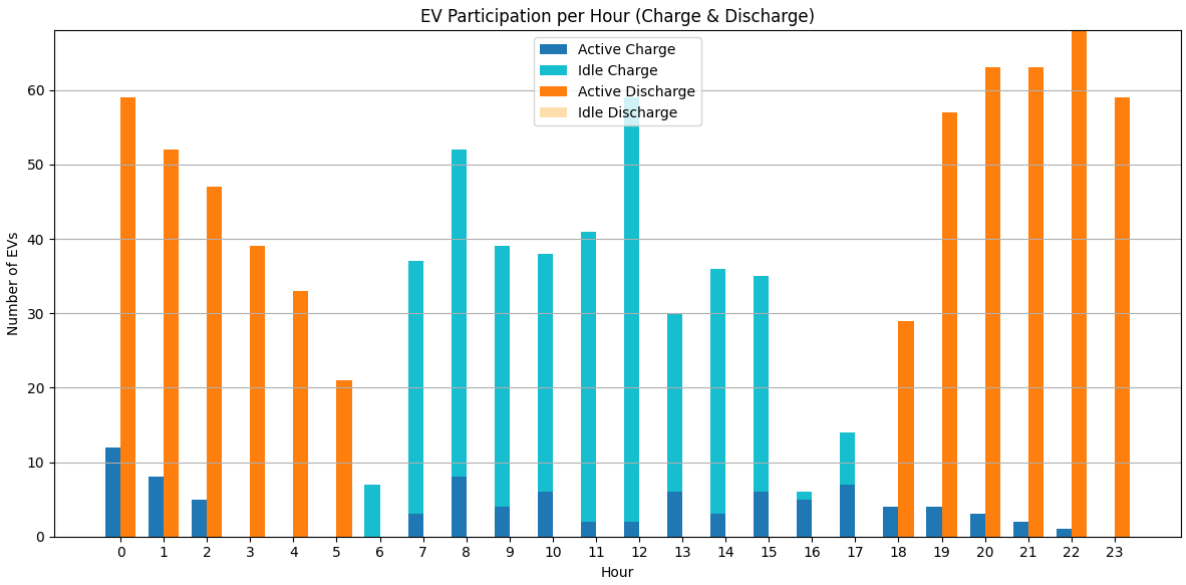


Figure 5-47. Hourly participation of active and idle EVs in charging and discharging, based on Scenario I optimization on 21st June with full-standard PV capacity (4 kWp) and default EV parameters (EV ownership rate = 1; idle rate = 0.15).

5.2.2. Scenario II

Scenario II introduces a scheduling methodology distinct from that of Scenario I, in which no forced V2G charging management is imposed on active EVs. Instead, the system relies exclusively on idle EVs for V2G participation, thereby enabling a systematic exploration of boundary parameter configurations—including EV charging/discharging power, EV ownership rate, and EV idle rate—under this alternative scheduling paradigm. This framework is conceptually aligned with a battery swap–based V2G management model, where the management of energy exchange is effectively shifted from vehicles in active operation to a pool of idle battery packs stored in centralized swap stations.

In this context, the parameter of battery ownership corresponds to the ratio between the total number of available battery packs in the swap station and the number of EVs within the community grid. Importantly, this ratio is determined by market demand for swapping frequency and may exceed 100%, since the number of battery packs stored in the station can

be greater than the number of EVs physically present in the system. For consistency with the preceding analysis, the EV ownership rate is still defined as the ratio of EVs within the community grid to the number of households, while in this scenario the idle rate reflects the proportion of idle battery packs relative to the number of EVs in the community grid. Scenario II, therefore, provides a technical and managerial perspective for defining the boundary conditions required to achieve load-balancing performance under a battery-swap-based V2G system.

One of the primary advantages of this scheduling method lies in its preservation of EV user autonomy, since individual driving and charging behaviours remain unaffected. At the same time, the management logic becomes substantially simpler compared with Scenario I, as the scheduling only involves idle EVs (or idle battery packs in the case of battery swap stations), without requiring explicit modelling of the uncertainties associated with active EV usage patterns.

For the subsequent analysis, the same enumeration-based approach employed in Scenario I is adopted, generating a variety of parameter combinations (shown in Table 4-2) by varying charging power, discharging power, EV ownership rate, and idle rate. Each configuration is then evaluated based on its impact on the temporal distribution of community net-load and the corresponding EV scheduling requirements, allowing for the identification of parameter sets that represent near-optimal trade-offs between load-balancing performance and scheduling efficiency. In this context, scheduling efficiency refers not only to the overall effectiveness of dispatch but also to the avoidance of inefficient outcomes in which a large number of EVs must be mobilized to address imbalances at a single time interval, yet provide little or no contribution at other times. By focusing on parameter settings that minimize such redundant dispatch, the analysis ensures that V2G operations achieve extreme load-balancing conditions for the community grid while making the most effective use of available EV resources.

Given that all dispatch operations in Scenario II rely solely on idle EVs, the determination of boundary parameter configurations is reduced to assessing the quantitative relationships among five key requirements: the total number of idle EVs needed for morning peak shaving, the number required for midday charging, the maximum idle EV demand at the midday net-load minimum caused by peak PV generation, the number required for evening peak shaving, and the maximum idle EV demand at the evening load peak. These interdependencies define the feasible boundary conditions for V2G scheduling under the Battery Swap–based paradigm. The following case studies illustrate representative boundary configurations under different charging and discharging power scenarios.

- **Case 1. Boundary Definition under Standard Symmetrical Low Charging and Discharging Power (Charging Power = 3.3 kW; Discharging Power = 3.3 kW; Battery Capacity = 24 kWh; EV Ownership = 100%; EV Idle Rate = 55%)**

The analysis of Case 1 indicates that, under the given configuration, the dominant factor determining the number of EVs required to achieve power balance in the community grid is the absorption of excess PV generation during midday. Specifically, the total surplus electricity produced by PV exceeds the grid's reference equilibrium level by a significant margin, while the relatively small 24 kWh battery capacity of individual EVs constrains the amount of surplus that each vehicle can store. As a result, a large number of idle EVs must be mobilised during this period, substantially exceeding the numbers required for load balancing at the morning and evening peaks.

As illustrated in Figure 5-49, however, the SOC distribution of EVs after the optimisation process demonstrates that the evening discharging operations, which are scheduled to alleviate peak loads, do not deplete the energy stored during midday charging. In other words, while the midday surplus necessitates a broad mobilisation of idle EVs to absorb generation, the aggregate stored energy proves more than sufficient to cover evening peak demand, leaving

SOC levels within a mid-range band. This outcome indicates that the EV fleet retains unused storage capacity even after evening discharge, thereby preserving flexibility for subsequent charging and discharging cycles on the following day and ensuring the continuity and sustainability of V2G scheduling.

From the perspective of a battery swap station, the analysis suggests that the ratio of reserve battery packs to active ones is approximately 11:9, which means that users have constant and reliable access to fully charged replacement batteries. This ensures that EV mobility needs are never compromised, as every battery swap provides sufficient residual energy to support the average driving demand. While this guarantees user convenience, it also implies a significantly higher infrastructure cost for the swap station. For instance, in a community of 500 households with both EV ownership and utilization rates reaching 100%, the corresponding swap station would need to be equipped with at least 612 battery packs to satisfy operational requirements. This highlights the inherent trade-off between ensuring user reliability and controlling the economic costs of large-scale battery deployment.

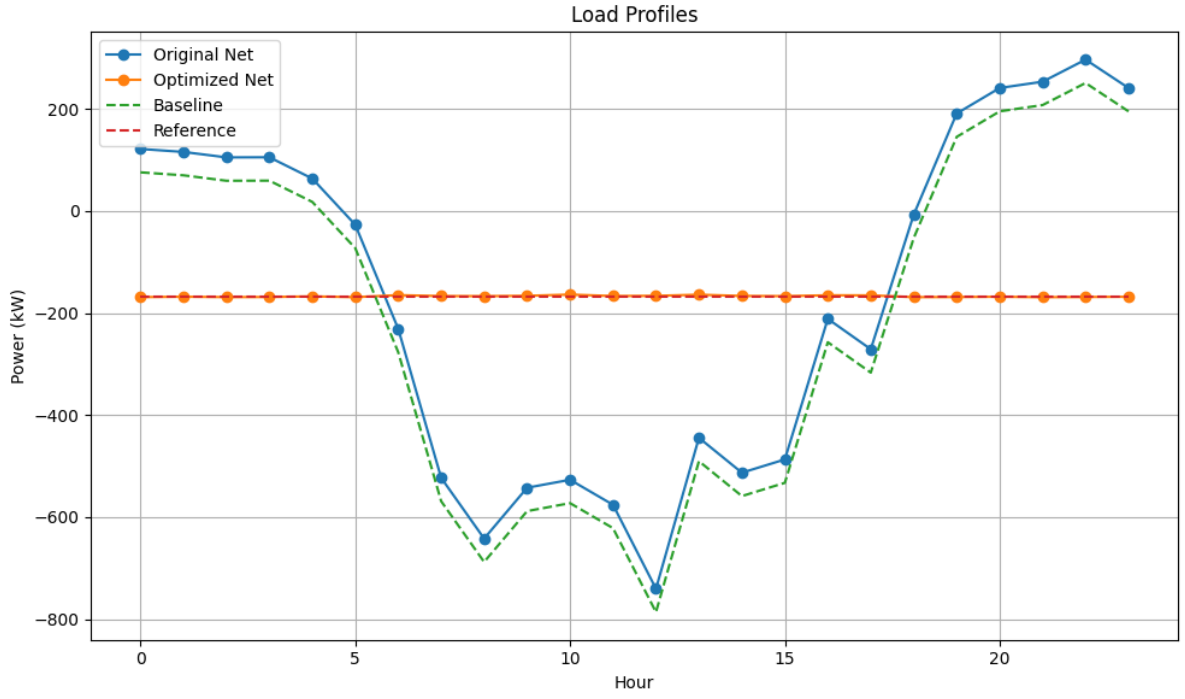


Figure 5-48. Hourly net-load profiles before and after Scenario II optimization on 21st June with full-standard PV capacity (4 kWp) and default EV parameters. Simulation parameters: battery capacity = 24 kWh; charging power = 3.3 kW; discharging power = 3.3 kW; EV ownership rate = 1; idle rate = 0.55; average hourly charging demand = 0.20455 kWh.

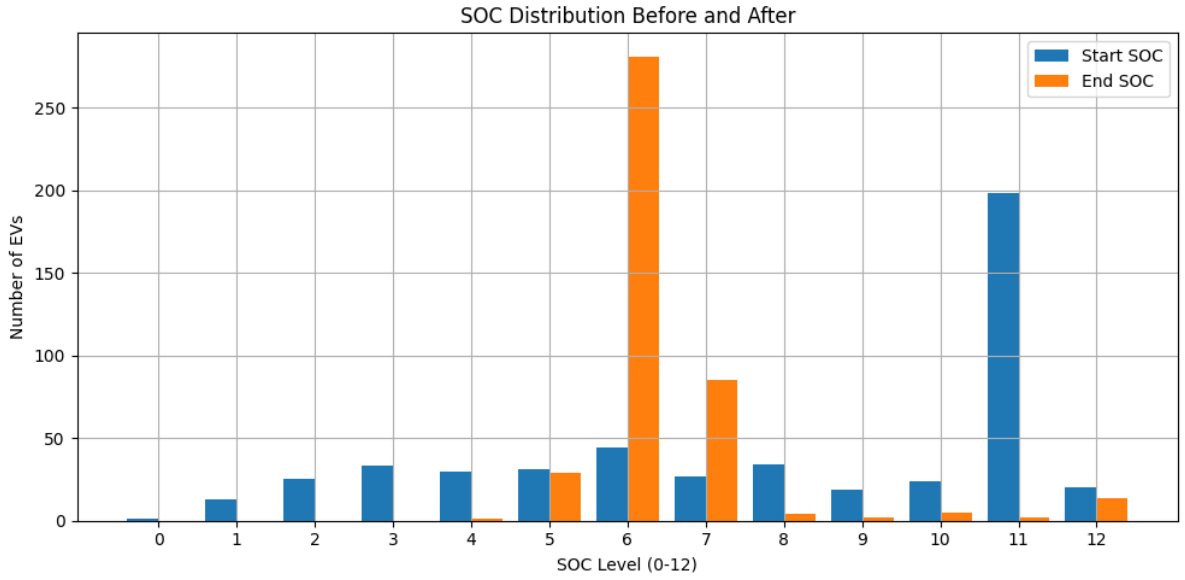


Figure 5-49. SOC distribution of dispatched EVs before and after Scenario II optimization on 21st June with full-standard PV capacity (4 kWp) and default EV parameters (EV ownership rate = 1; idle rate = 0.55).

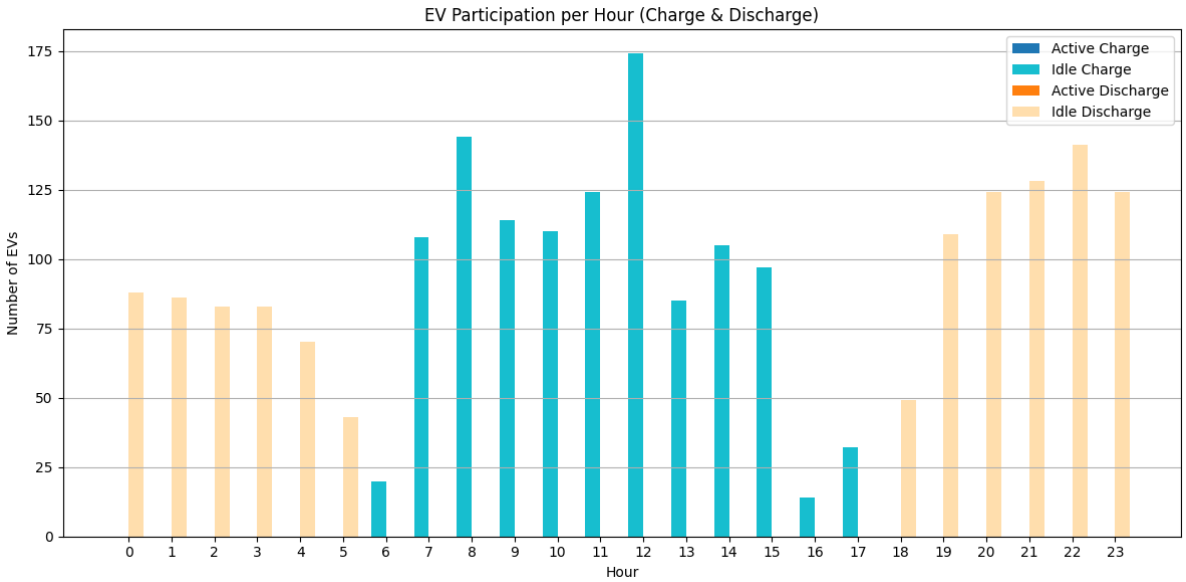


Figure 5-50. Hourly participation of active and idle EVs in charging and discharging, based on Scenario II optimization on 21st June with full-standard PV capacity (4 kWp) and default EV parameters (EV ownership rate = 1; idle rate = 0.55).

- **Case 2. Boundary Definition under High Charging and Discharging Power with Enlarged Battery Capacity (Charging Power = 10 kW; Discharging Power = 7 kW; Battery Capacity = 82.5 kWh; EV Ownership = 100%; EV Idle Rate = 15%)**

In Case 2, an equivalent scaling method, consistent with the approach adopted in Scenario I, is employed to identify an optimal parameter configuration under the management framework of Scenario II. The selected parameters reflect realistic values currently observed in the EV market, thereby representing a plausible configuration for future deployment. Under this setting, all grid balancing operations are achieved through the contribution of only 75 idle EVs, highlighting the efficiency of the model. The post-optimization distribution of SOC further demonstrates that most vehicles stabilize around level 6, a threshold defined as 1 minus the mode of the initial charging SOC values in the database used in the methodology, which approximates the typical energy consumption required for a single EV trip. This suggests that, under prevailing community grid conditions, the strategy can generally maintain sufficient residual capacity for routine mobility needs on the following day, thereby achieving overall power balance with the involvement of only a relatively small share of idle EVs.

From the perspective of battery swap station design, this configuration also implies an economically efficient ratio of reserve to active battery packs. Specifically, when viewed solely from the standpoint of grid optimization, the required reserve-to-active battery ratio is as low as 3:17, which is sufficient to guarantee effective scheduling for community-level load balancing. In practice, swap stations are likely to maintain a higher number of spare batteries to safeguard user convenience and ensure uninterrupted availability. Nevertheless, the identified ratio can be regarded as a theoretical lower bound, below which reliable scheduling

could not be achieved. Any additional reserve capacity beyond this threshold would simply improve operational flexibility without being strictly necessary for grid optimization. This finding carries important implications, as it demonstrates the technical feasibility of deploying battery swap stations within community-scale distribution networks in the United Kingdom. By providing a cost-effective reserve capacity ratio while maintaining reliability, Scenario II illustrates that battery swap–based V2G systems can reconcile the dual objectives of minimizing infrastructure cost and delivering stable load-balancing performance.

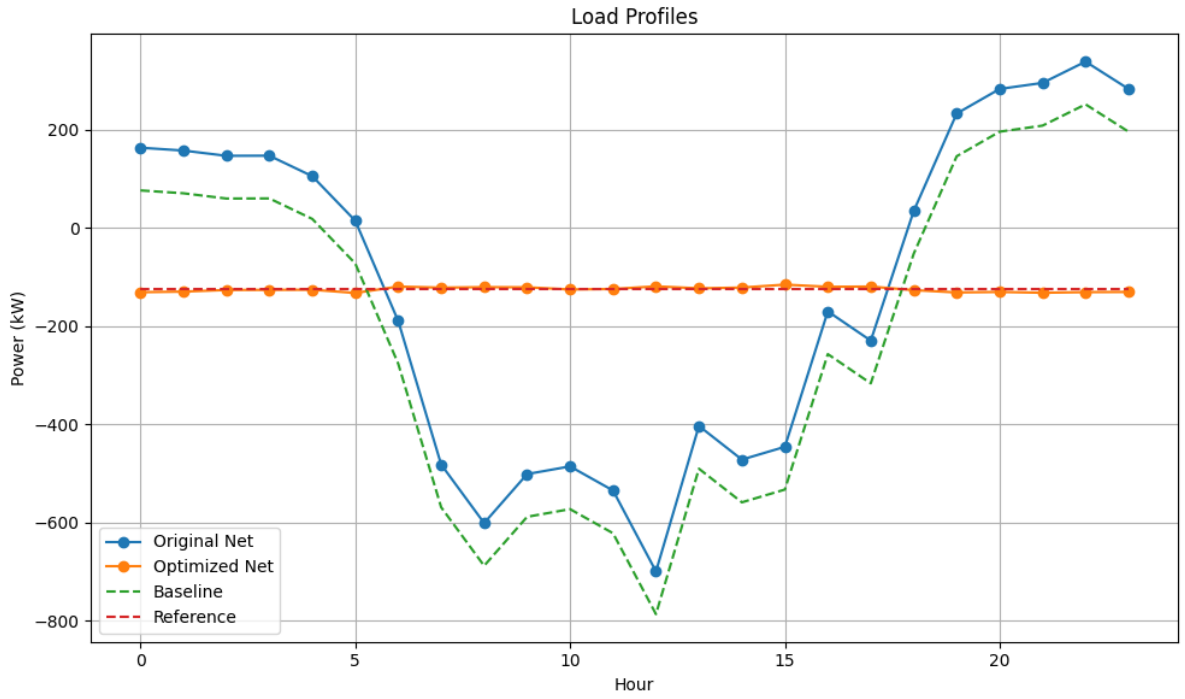


Figure 5-51. Hourly net-load profiles before and after Scenario II optimization on 21st June with full-standard PV capacity (4 kWp) and default EV parameters. Simulation parameters: battery capacity = 82.5 kWh; charging power = 10 kW; discharging power = 7 kW; EV ownership rate = 1; idle rate = 0.15; average hourly charging demand = 0.20455 kWh.

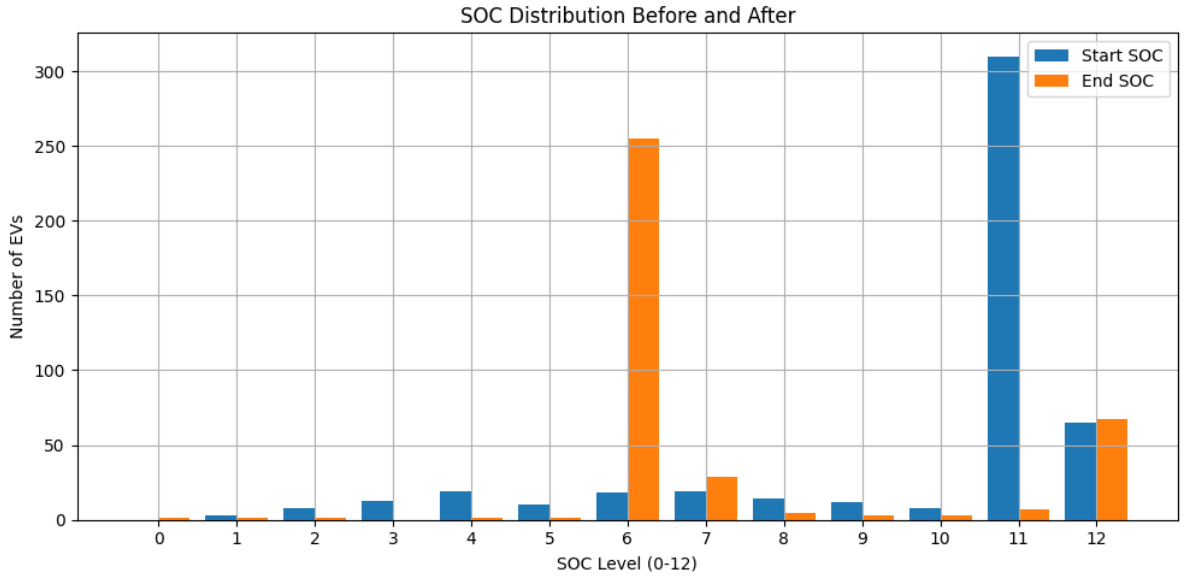


Figure 5-52. SOC distribution of dispatched EVs before and after Scenario II optimization on 21st June with full-standard PV capacity (4 kWp) and default EV parameters (EV ownership rate = 1; idle rate = 0.15).

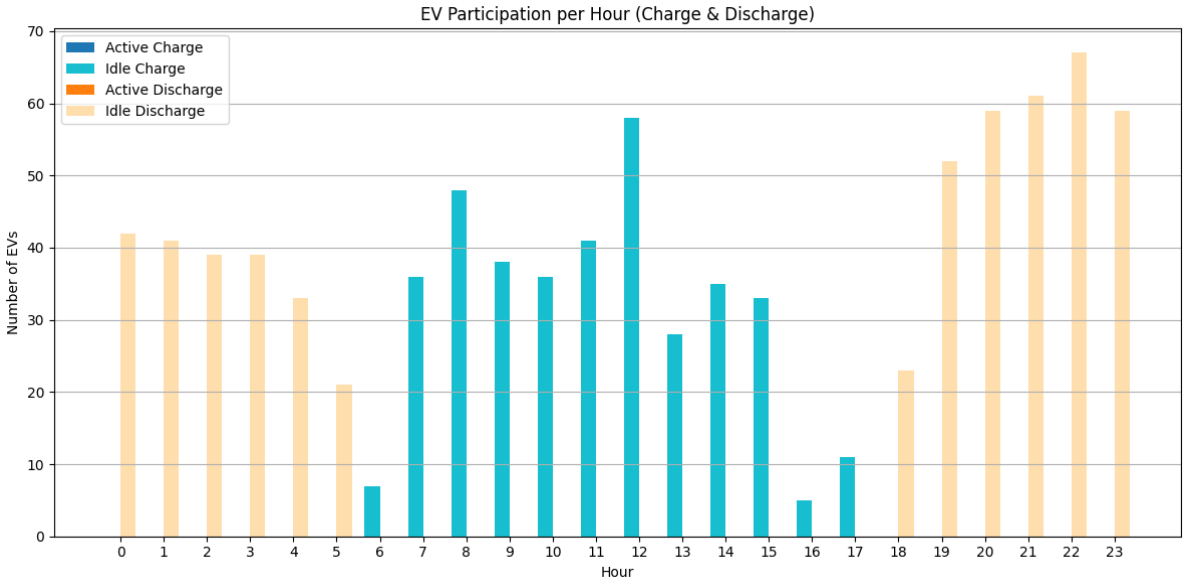


Figure 5-53. Hourly participation of active and idle EVs in charging and discharging, based on Scenario II optimization on 21st June with full-standard PV capacity (4 kWp) and default EV parameters (EV ownership rate = 1; idle rate = 0.15).

5.2.3. Scenario III

Scenario III investigates an extreme boundary condition in which all EVs are assumed to be continuously available for grid scheduling, corresponding to an idle rate fixed at 100%. In this case, the analysis focuses solely on EV ownership as the determining factor for system capacity. This setting is of particular interest because it conceptually demonstrates the potential substitutability of fixed battery energy storage stations by V2G systems. When all EVs are fully dispatchable, V2G can theoretically replace stationary battery storage in balancing power fluctuations within a community grid.

However, unlike Scenario I and Scenario II, this extreme case eliminates the impact of EV driving-related charging consumption on the grid power profile, thereby amplifying the imbalance observed in periods of high PV generation. During summer, when PV generation significantly exceeds local demand, the surplus can become increasingly large. If V2G scheduling were to indiscriminately absorb all excess PV output, the aggregated EV fleet would inevitably reach a fully charged state after several consecutive days, leaving no further storage capacity available and rendering the system ineffective.

To address this issue, the management logic introduced in Chapter 4 defines the extreme power balancing reference value as the average of hourly net power over a one-month period, rather than simply the daily maximum or minimum imbalance. This design ensures that even on days when PV generation surpasses consumption, the V2G system maintains the capability to sell electricity back to the grid on an hourly basis, thereby sustaining power balance at the community level. Crucially, this approach prevents excessive accumulation of stored energy within EV batteries and ensures the continuity of dispatchability, a feature that preserves the long-term sustainability of Scenario III. The validation of this scheduling method also confirms

the feasibility of adopting the reference value definition proposed in Chapter 4, since it effectively guarantees both real-time power equilibrium and system sustainability.

In this section, the analysis will therefore examine the load distribution of the community grid after optimization under Scenario III, along with the corresponding scheduling performance of the EV fleet. By evaluating these outcomes under the assumption of full EV availability, the study aims to identify the optimal configuration parameters that can support system operation under such extreme conditions and clarify the practical implications of V2G as a substitute for fixed energy storage solutions.

- **Case 1: Critical Values under a Low Bidirectional Charging–Discharging Power Model (Charging Power = 3.3 kW; Discharging Power = 3.3 kW; Battery Capacity = 24 kWh; EV Ownership = 35%)**

In Case 1, the absence of EV driving-related charging consumption fundamentally alters the definition of the extreme power balancing reference value, which is recalculated as –214.60039915 kW. Under this condition, the total surplus PV generation above the reference value is reduced compared to Scenarios I and II. Consequently, the total number of EVs required to absorb the full surplus generation decreases, with fewer than 160 EVs (corresponding to an ownership rate of approximately 32%) being sufficient to maintain balance. However, the most critical scheduling challenge arises at the time of maximum PV output, which coincides with the grid's minimum load valley. At this point, 174 EVs (an ownership rate of 35%) must be dispatched simultaneously to accommodate the surplus. This shift indicates that, in Scenario III, the limiting factor for scheduling efficiency is no longer the tension between relatively low battery capacity and high cumulative PV surplus, but rather the insufficient charging power available to manage the deepest valley of the load profile.

Even under these restrictive conditions, the total EV fleet required to achieve extreme load balancing remains substantially lower than the minimum idle EV availability observed under identical charging–discharging parameters in Scenarios I and II. This outcome highlights the efficiency advantages of the extreme scheduling framework when charging consumption is excluded from the system's load dynamics. Moreover, the SOC distribution after optimization, as shown in Figure 5-55, further validates the sustainability of this approach. The SOC levels of the scheduled EVs cluster around the mid-range level 5, ensuring adequate reserve capacity to support discharge operations during the early morning peak of the following day, while simultaneously preventing excessive accumulation of stored energy. This balance between maintaining discharge capability and avoiding overcharging underscores the long-term operational viability of the proposed scheduling strategy under low bidirectional power conditions.

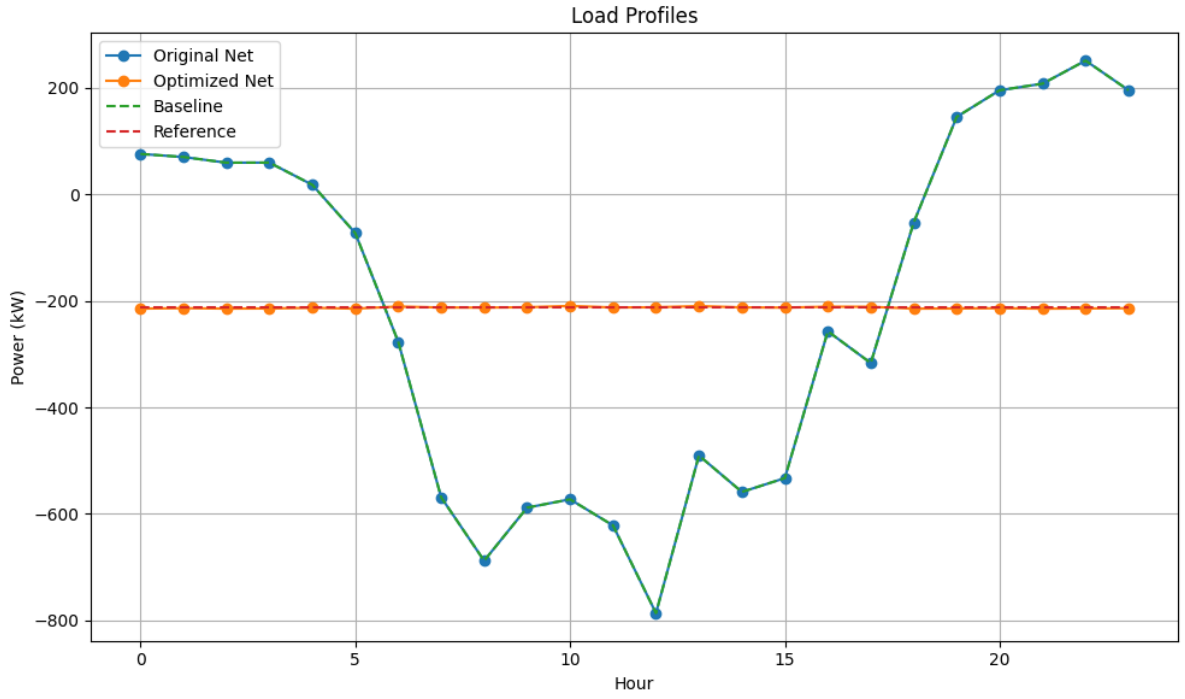


Figure 5-54. Hourly net-load profiles before and after Scenario III optimization on 21st June with full-standard PV capacity (4 kWp) and default EV parameters. Simulation parameters: battery

capacity = 24 kWh; charging power = 3.3 kW; discharging power = 3.3 kW; EV ownership rate = 0.35.

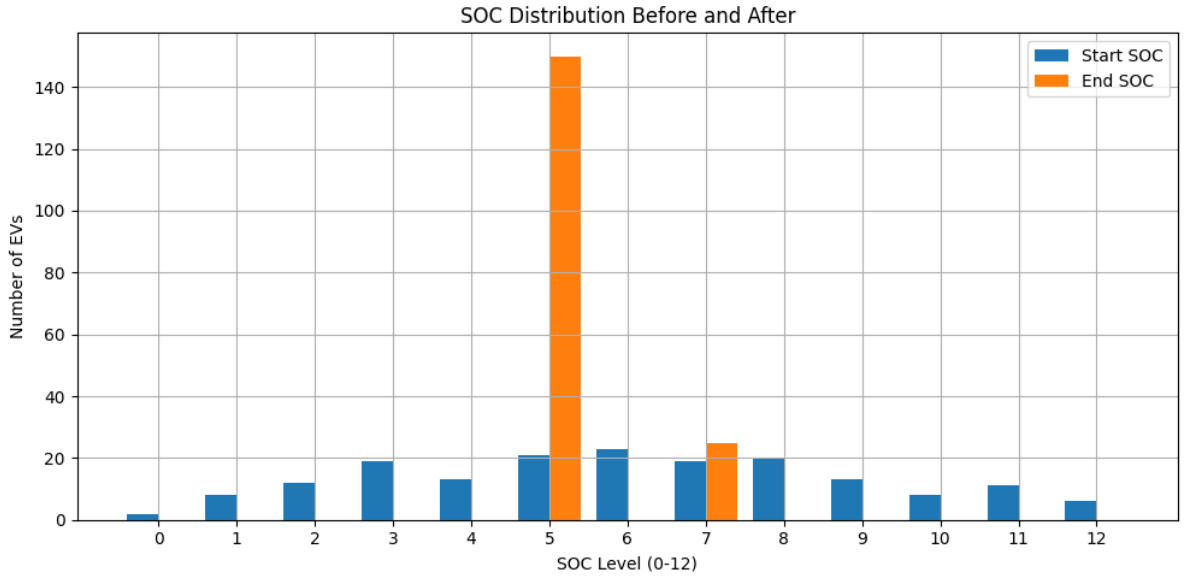


Figure 5-55. SOC distribution of dispatched EVs before and after Scenario III optimization on 21st June with full-standard PV capacity (4 kWp) and default EV parameters (EV ownership rate = 0.35).

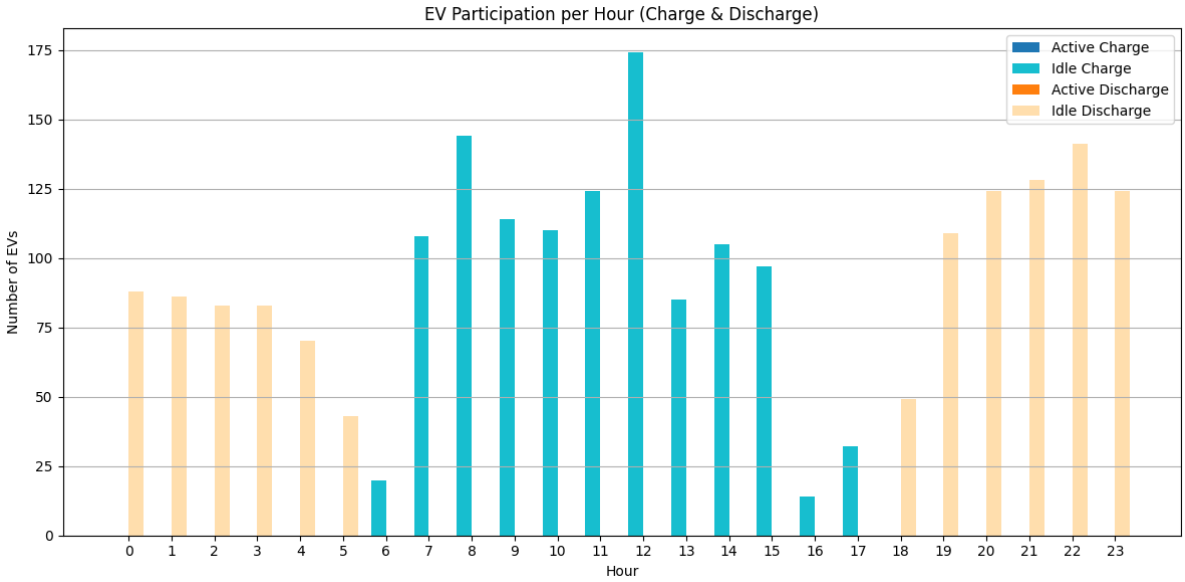


Figure 5-56. Hourly participation of active and idle EVs in charging and discharging, based on Scenario III optimization on 21st June with full-standard PV capacity (4 kWp) and default EV parameters (EV ownership rate = 0.35).

- **Case 2: Optimized Boundary Parameter Combination Based on Market-Oriented EV Characteristics (Charging Power = 10 kW; Discharging Power = 10 kW; Battery Capacity = 82.5 kWh; EV Ownership = 11%)**

Building upon the findings of Case 1, Case 2 explores an optimized configuration of EV parameters designed to further reduce the total number of vehicles required for dispatch while enhancing overall scheduling efficiency. In this case, both charging and discharging power are increased to 10 kW, and battery capacity is expanded to 82.5 kWh. Under these enhanced parameters, the minimum number of EVs required at the critical scheduling points is significantly reduced. Specifically, only 55 EVs are needed to manage the load at the valley extreme, 47 EVs to mitigate the evening peak, and 55 EVs to absorb the total PV surplus relative to the extreme balancing reference value. These nearly aligned requirements across different critical conditions demonstrate that the system achieves a balanced scheduling configuration, thereby maximizing EV dispatch efficiency under the scenario's extreme assumptions.

The remarkably low dispatch requirement under this configuration highlights a key insight: even in the absence of stationary battery storage facilities, a relatively small number of EVs with enhanced technical parameters can sustain the community grid's load balancing needs. From a system design perspective, this finding is significant not merely because larger batteries increase individual storage capacity, but because it demonstrates the potential for a limited EV fleet—when equipped with sufficiently high charging/discharging power and storage capacity—to substitute for dedicated battery storage stations in community-level grids. This substitution is not a trivial observation; it reflects the feasibility of leveraging mobile, user-owned storage assets as a reliable system resource under realistic availability rates. Furthermore, when considering Scenarios I and II, where EV daily driving consumption is explicitly included, a similar parameter configuration (10 kW charging power, 7 kW

discharging power and 82.5 kWh capacity) requires only approximately 15% of the total community households to provide idle EVs for scheduling. Such an idle availability rate is both realistic and achievable across the majority of days throughout the year, thereby reinforcing the practical viability of this approach.

These findings reinforce the broader conclusion that the establishment of dedicated stationary battery storage stations may not be necessary for community grids with sufficient EV penetration and appropriately designed parameter configurations. Instead, the V2G system, when optimized, provides a technically feasible and economically efficient alternative that aligns with real-world market conditions and user behaviour, while maintaining long-term operational sustainability.

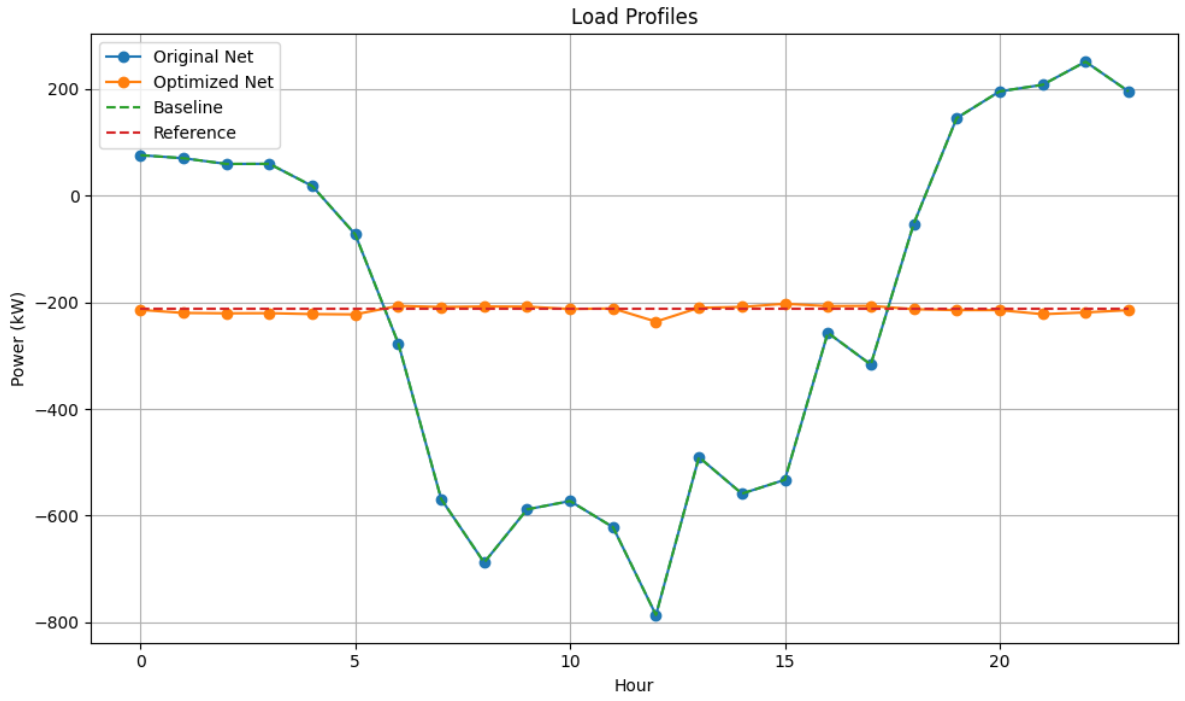


Figure 5-57. Hourly net-load profiles before and after Scenario III optimization on 21st June with full-standard PV capacity (4 kWp) and default EV parameters. Simulation parameters: battery capacity = 82.5 kWh; charging power = 10 kW; discharging power = 10 kW; EV ownership rate = 0.11.

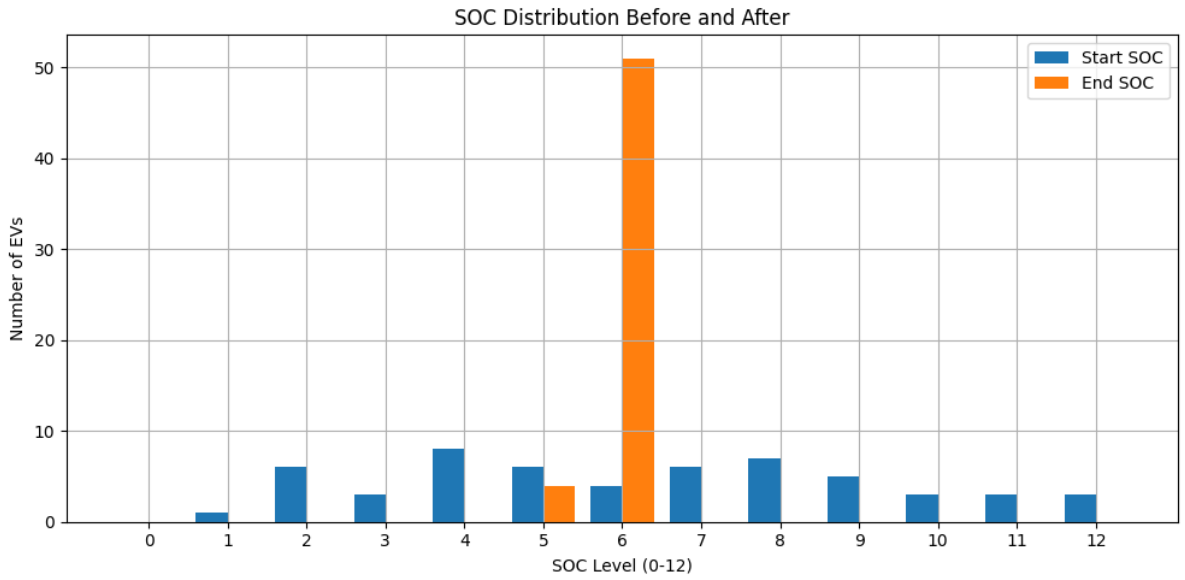


Figure 5-58. SOC distribution of dispatched EVs before and after Scenario III optimization on 21st June with full-standard PV capacity (4 kWp) and default EV parameters (EV ownership rate = 0.11).

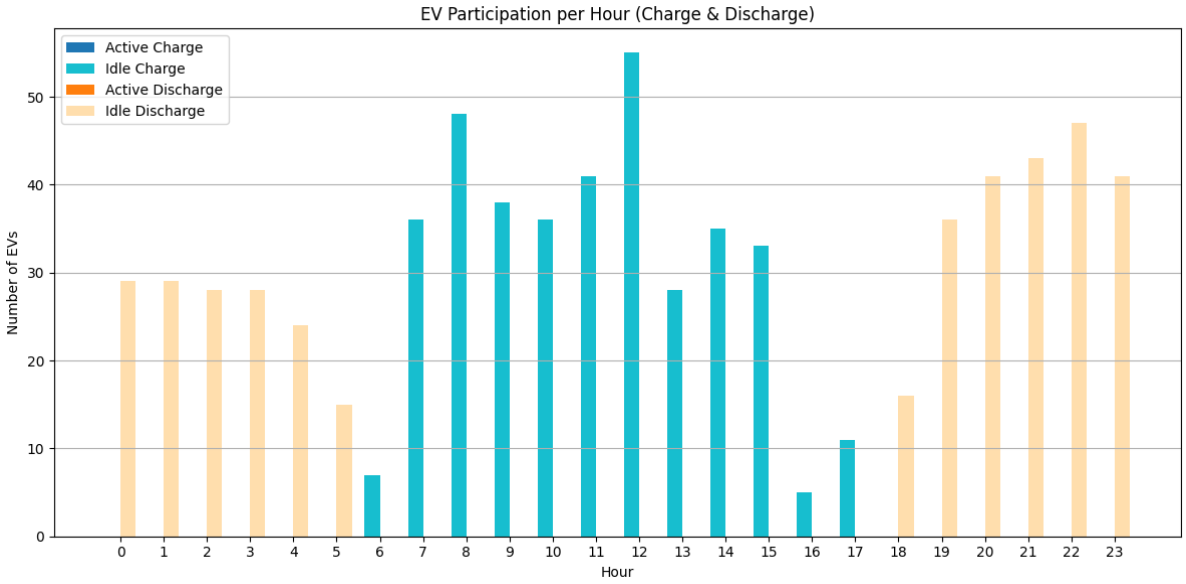


Figure 5-59. Hourly participation of active and idle EVs in charging and discharging, based on Scenario III optimization on 21st June with full-standard PV capacity (4 kWp) and default EV parameters (EV ownership rate = 0.11).

5.3. Conclusion

In conclusion, the simulation results presented in Chapter 5 provide compelling evidence that improving the scheduling efficiency of idle EVs within a centralized V2G framework can enable community-level distribution networks in the UK to achieve extreme load balancing across different time periods. By employing real-world UK distribution grid data together with empirically derived EV behaviour models, this chapter validated the methodological framework proposed in Chapter 4 through the evaluation of three distinct scenarios, each tested under their respective boundary conditions.

The analyses systematically investigated the impact of several key factors on V2G performance, including varying PV installation capacities, seasonal variations, EV fleet composition (ownership and idle rate), charging intensity, and bidirectional charging and discharging power levels. To ensure robustness, simulations were conducted on representative days characterized by extreme load conditions, thereby enabling the identification of both feasible scheduling strategies and optimal parameter combinations. The results clearly demonstrate that under the current baseline configuration of community grids and EV parameters (battery capacity = 24 kWh; charging power = 3.3 kW; discharging power = 3.3 kW), Scenario I—where active EVs participate in scheduling with idle EVs providing supplementary capacity—can achieve extreme load balancing when ownership reaches 100% and the idle rate is at least 55%. Similarly, Scenario II—where the charging behaviour of active EVs is preserved and only idle EVs are dispatched—was shown to produce comparable balancing outcomes with improved scheduling efficiency under equivalent conditions. In the extreme case represented by Scenario III, where all EVs are treated as idle and freely dispatchable, the minimum boundary requirement was further reduced to 35%, confirming the potential of V2G to achieve balancing with even fewer vehicles under highly favourable conditions.

To address the inherent limitations posed by low charging/discharging power and small battery capacities—particularly in absorbing midday PV surplus or mitigating demand extremes—this chapter further introduced an equivalent scaling approach based on typical EV market parameters. Through this optimization, the highest scheduling efficiency was achieved under the following configurations: for Scenarios I and II, battery capacity = 82.5 kWh, charging power = 7 kW, discharging power = 10 kW, EV ownership = 100%, and idle rate = 15%; for Scenario III, battery capacity = 82.5 kWh, charging power = 10 kW, discharging power = 10 kW, and EV ownership = 11%. These configurations not only enhanced the efficiency of EV scheduling but also ensured a balanced load distribution within the community grid.

Moreover, the results derived from Scenario II highlighted the potential of the battery swapping station model, demonstrating its feasibility in UK community grids by improving both EV utilization efficiency and grid-level balancing. Finally, the findings of Scenario III illustrated that under conditions of complete scheduling flexibility, a relatively small subset of EVs is sufficient to maintain extreme load balancing. This provides strong theoretical support for the proposition that, with carefully designed parameter configurations and realistic idle availability, V2G systems can substitute for stationary battery storage facilities in community-level grids. Collectively, these conclusions reinforce the central claim of this research: that through optimized scheduling and parameter design, V2G technology can serve as a technically viable and economically efficient strategy for achieving sustainable load balancing in community-level power systems.

In addition to quantitatively identifying optimal scheduling strategies and parameter settings for EVs under diverse grid and usage environments—such as varying ownership rates and idle availability—the simulations presented in this chapter also provide validation for several of the key assumptions established earlier in the dissertation. In particular, the results corroborate the prediction made in Chapter 3 that grid stabilization can be achieved without altering existing

EV usage habits or travel frequencies, simply by retaining and intelligently scheduling a sufficient pool of idle EVs, all while maintaining user satisfaction. The findings further confirm that, under the proposed centralized control logic, EVs with highly heterogeneous usage patterns—from daily commuters to occasional users—can be effectively coordinated as a unified virtual energy storage system. This directly addresses one of the central challenges identified in the literature review in Chapter 2, namely, the difficulty of applying generalized V2G strategies across settings characterized by diverse user behaviours and operational environments.

Moreover, the detailed analysis of scheduling distributions under different parameter conditions—particularly those required to achieve temporal load balancing at the community scale—highlights important limitations in many existing V2G modelling approaches. Earlier studies, often based on simplified microgrid configurations with only a small number of EVs operating under fixed or predetermined schedules, have been valuable for illustrating the fundamental principles of V2G. However, such models have limited applicability when extended to real-world community energy systems, where user behaviour, charging availability, and grid conditions introduce significant variability and uncertainty. In contrast, the centralized strategy investigated in this study is explicitly designed with scalability and operational flexibility in mind. The optimization framework developed in Chapter 4 enables coordinated control across large EV fleets connected to a shared distribution network, allowing the system to respond dynamically to variations in grid demand, user charging requirements, and temporal operational constraints. The simulation results therefore demonstrate that the proposed framework can support coordinated V2G scheduling within complex ‘S-G-L-S’ architectures, which are increasingly characteristic of next-generation smart community energy systems. In doing so, the simulations address another gap frequently observed in the literature: the disconnect between V2G algorithms developed for isolated experimental microgrids and the

operational realities of community-scale energy networks. The results presented in this chapter indicate that the proposed centralized V2G control logic provides a practical pathway for bridging this gap. By enabling coordinated dispatch of distributed EV storage resources, the framework extends the potential benefits of V2G from small-scale experimental demonstrations to broader system-level applications. This capability is particularly relevant for future integration with upstream grid operators seeking to utilize distributed storage assets as part of wider energy-balancing and demand-management strategies. The economic and carbon implications associated with such integration, particularly from the perspective of community grid operations, will be examined in detail in Chapter 6. While the simulation results presented in this chapter demonstrate clear operational advantages of the proposed approach, several methodological limitations should also be acknowledged. These will be discussed more comprehensively in Section 7.4 (Research Limitations) of Chapter 7. In particular, that section will examine the constraints associated with the datasets used in this study, including the community electricity demand model derived by scaling standard UK residential consumption profiles to represent a 500-household community grid, as well as the EV behavioural dataset based on a single vehicle model and usage pattern. These data assumptions may introduce a degree of numerical uncertainty into the optimized simulation results presented here, and their potential influence on the findings will be analysed in the concluding discussion of the thesis.

CHAPTER 6. ECONOMIC AND ENVIRONMENTAL EVALUATION

6.1. Introduction

Chapter 5 examined three centralized V2G scheduling strategies designed for community electricity networks in the United Kingdom, evaluating their performance under varying grid characteristics and patterns of EV utilization. The analysis compared the temporal distribution of net power in the grid before and after optimization, as well as the operational behaviour of EVs under each scheduling strategy. The results demonstrated that, given current EV usage conditions—including ownership rates, idle rates, and utilization frequency—the proposed strategies can effectively coordinate both active and idle EVs to maximize the mitigation of peak–valley imbalances within the community grid. This is particularly evident in extreme operational periods, such as summer midday intervals when substantial PV generation produces one-directional power surpluses. By strategically absorbing or supplying power during these intervals, the strategies achieve near-optimal load balancing across the community network. The quantitative findings from Chapter 5 thus confirmed the effectiveness of the proposed approaches in enhancing power equilibrium.

Building on this foundation, the present chapter shifts focus from power balancing to broader performance dimensions, namely economic viability and environmental sustainability, as evaluated using the methodology established in Chapter 4. Historical datasets are employed to conduct a quantitative assessment at the community grid level, examining the economic performance and energy efficiency of the strategies under different grid conditions. This dual-perspective evaluation is intended to demonstrate that the benefits of the proposed approaches

extend beyond load balancing, delivering measurable gains in both cost savings and carbon emission reduction.

In particular, the economic assessment incorporates findings from the real-time tariff analysis, which, as a by-product of the research, informed the development of an additional V2G optimization method oriented toward real-time economic maximization. This supplementary method—formulated for the two prevailing tariff structures—leverages real-time operational data to incentivize user participation in V2G dispatch by enabling direct financial benefits. Such an approach lays the groundwork for future user-driven V2G electricity trading markets, providing an operational logic framework capable of integrating economic motivation with grid stability objectives.

The remainder of this chapter is organized as follows. Section 6.2 presents the time-of-use distribution patterns for the two existing tariff structures and evaluates the economic effectiveness of the grid balancing parameters embedded within the proposed strategies. The section then reports the economic performance of the scheduling approaches under different grid scenarios, concluding with the formulation of a real-time data-driven, economically optimized V2G scheduling strategy. Section 6.3 follows a parallel structure for environmental assessment, beginning with an analysis of the temporal distribution of carbon intensity in the UK electricity grid and proceeding to quantify the net carbon impact of the proposed strategies at the community grid level. Finally, Section 6.4 summarizes the key findings and implications of the chapter.

6.2.1 Electricity Bill Data Analysis

Within the context of the UK electricity market, two primary tariff structures enable flexible pricing based on real-time grid conditions, including electricity demand and renewable generation supply. The first is the Time-of-Use (ToU) tariff, which implements fixed time

blocks with predefined electricity rates that correspond to typical demand patterns throughout the day (Ofgem, 2025). ToU tariffs are typically published in advance and exhibit high predictability, resulting in low risk for consumers. This tariff model is particularly favourable for fundamental energy storage technologies and unidirectional smart charging (V1G) systems, which have relatively limited flexibility in their operation.

Common ToU tariffs in the UK include Economy 7 (E7), which provides seven off-peak hours (generally from midnight to 7 am, although this varies by supplier) and seventeen standard-rate hours, and Economy 10 (E10), which offers twelve off-peak hours split into multiple blocks (e.g., 9 pm to 9 am, with further subdivisions such as midnight to 5 am, 1 pm to 4 pm, and 8 pm to 10 pm) and twelve standard-rate hours (Ofgem, 2025).

The second tariff type is Real-Time Pricing (RTP), where electricity prices are highly dynamic and updated frequently—typically every half hour or hour—based on market conditions such as wholesale prices and supply-demand balances. RTP tariffs are linked to mechanisms such as the National Grid's Balancing Mechanism and the day-ahead/intraday electricity markets. While this pricing scheme introduces higher risk due to potential volatility, it allows users with flexible demand, such as those participating in V2G systems, to capitalize on low prices during periods of renewable energy surplus or high supply, while avoiding periods of peak pricing.

Given these characteristics, this study adopts RTP data provided by LimeJump Energy for June 2020 as the economic benchmark to evaluate the feasibility and robustness of the proposed centralized V2G management strategy, which leverages the storage potential of idle EVs (such prices are typically published one day in advance rather than intraday in practical V2G applications). The dataset consists of half-hourly electricity prices across the entire month, enabling an assessment of the economic benefits and challenges under real-world dynamic price conditions.

Figure 6-1 presents a dot plot of the half-hourly electricity prices for June 2020, as recorded by LimeJump. The distribution of points illustrates the lack of a clear daily pricing pattern under the RTP scheme, highlighting the unpredictability and volatility of electricity prices throughout the 24-hour cycle. Notably, the data also include instances of negative electricity prices, indicating time periods when consumers would be effectively paid to consume electricity, creating profitable opportunities for V2G-enabled EV charging.

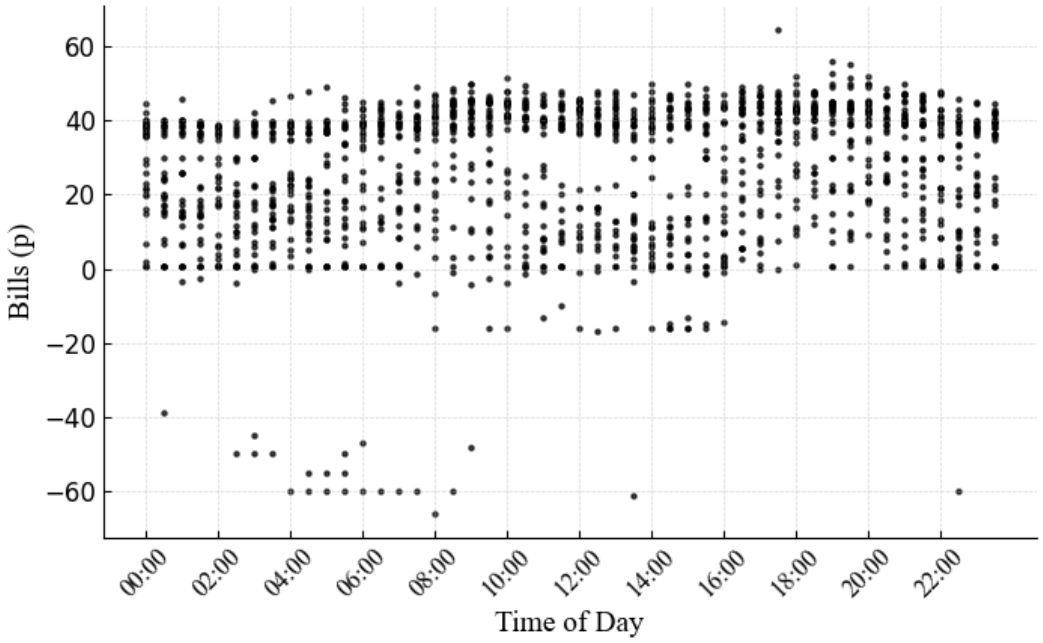


Figure 6-1. Half-Hourly Real-Time Electricity Prices in June 2020 Provided by LimeJump Energy

Note: The plot displays electricity price variation (pence per kWh) over 24 hours for each day of June 2020. The vertical axis shows the electricity price, while the horizontal axis represents the time of day in hours.

To further substantiate the claim that electricity prices under the RTP scheme exhibit no discernible or consistent fluctuation patterns over a 24-hour cycle, several representative time windows were selected for closer examination. Specifically, daily electricity prices were

extracted for both the summer solstice (see Figure 6-2) and the winter solstice (see Figure 6-3), which respectively represent extreme conditions in terms of PV generation potential and residential electricity demand. Additionally, weekly price distributions were analysed for the weeks surrounding the vernal equinox (see Figure 6-4) and the autumnal equinox (see Figure 6-5), which represent more balanced seasonal conditions.

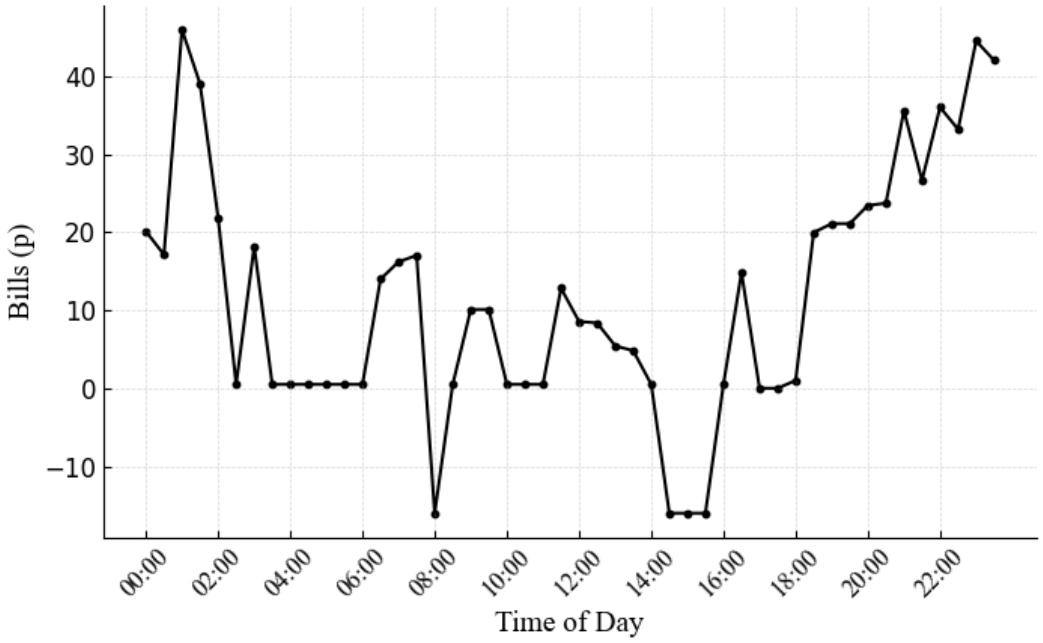


Figure 6-2. The system price of the electricity grid on 21st June, 2020, as provided by LimeJump.

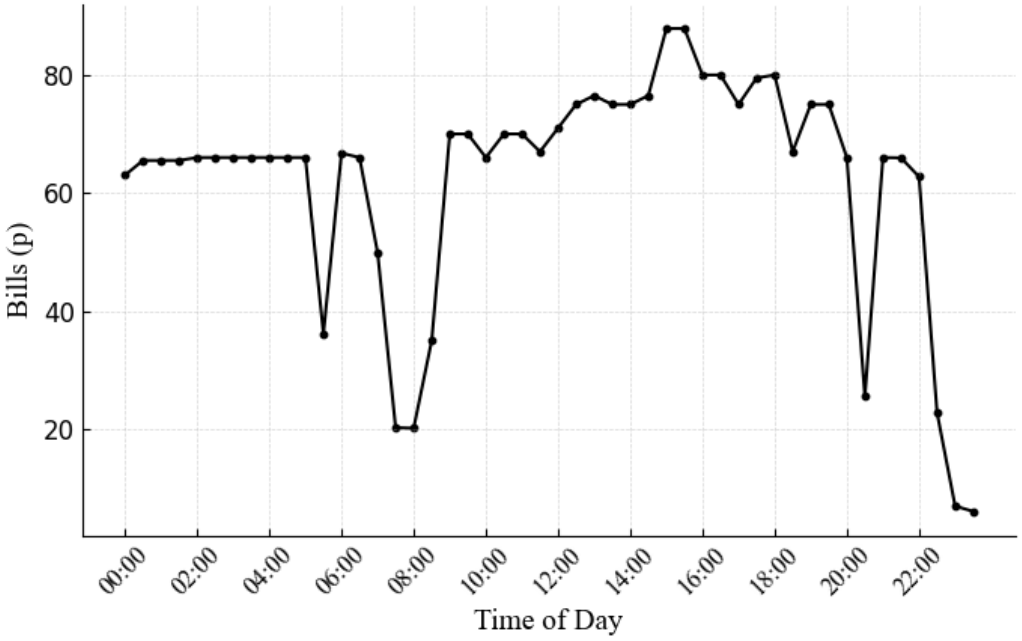


Figure 6-3. The system price of the electricity grid on 21st December, 2020, as provided by LimeJump.

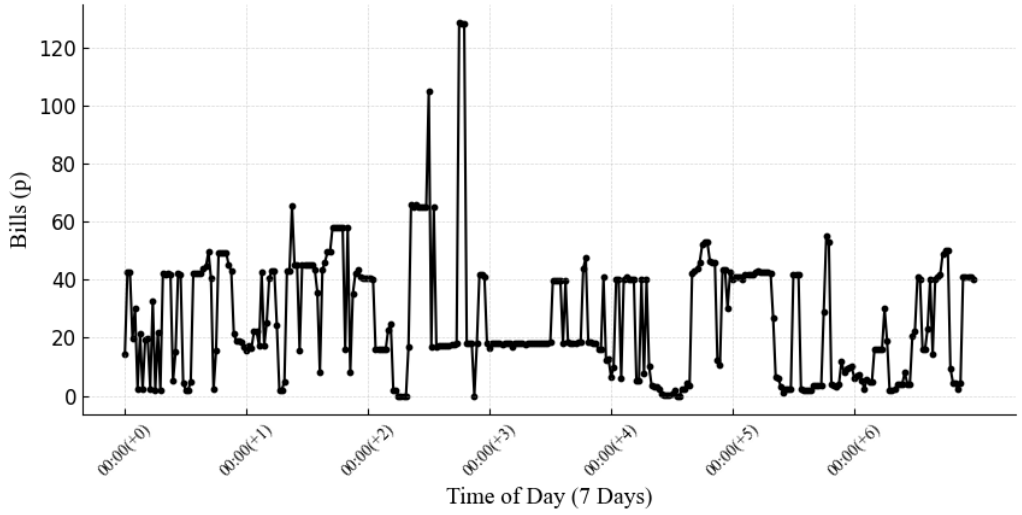


Figure 6-4. Half-hourly electricity prices under the RTP scheme during the vernal equinox week (17–23 March 2020), based on data from LimeJump.

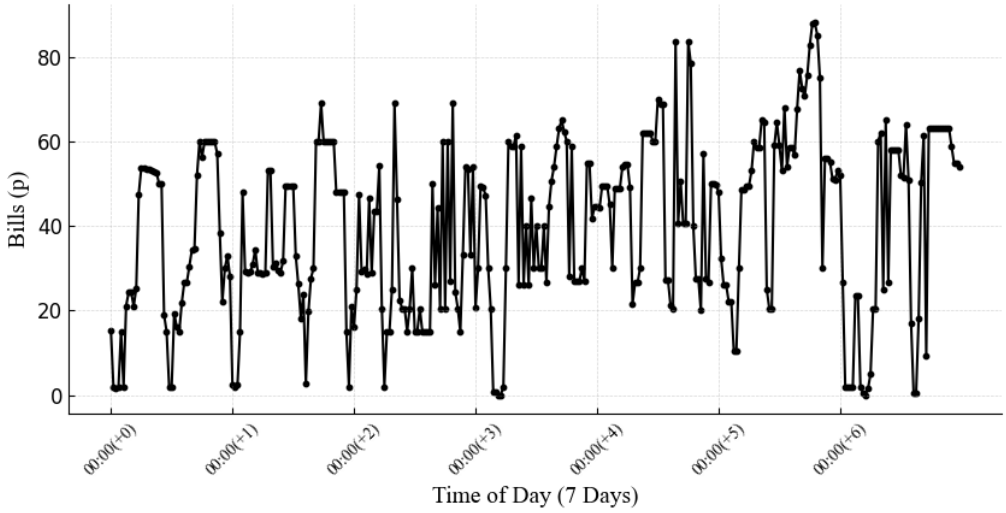


Figure 6-5. Half-hourly RTP electricity prices during the autumnal equinox week (19–25 September 2020), based on data provided by LimeJump.

6.2.2. Simulation of Community Grid Electricity Costs under Different V2G Optimization Scenarios

The optimization framework developed in this research was designed from the outset with the explicit objective of achieving an extreme balance in the temporal distribution of community grid power loads. Consequently, for all parameter configurations that successfully meet the design goal, the resulting load distribution over the 24-hour study period converges toward a straight line that closely approximates the reference value of extreme load balancing. The only variations arise from the calculation of the reference value itself, which explicitly incorporates household electricity demand, PV generation, and baseline EV charging consumption prior to optimization. As a result, changes in PV installation capacity or in the composition of the EV fleet (e.g., ownership rate, idle rate, and charging intensity) inevitably lead to shifts in the daily reference value of extreme load balancing, thereby altering the total volume of unidirectional power exchanged with the upstream grid on a given day.

In the subsequent economic evaluation, the tariff model adopted was a Real-Time Pricing (RTP) scheme characterized by irregular fluctuations in electricity prices. Within this context, the optimization task can be interpreted as assigning dynamic weightings—determined by the hourly RTP price levels—to a uniform hourly power distribution defined by the balancing reference curve, thereby yielding the total daily cost outcome. It is important to note that under an RTP framework, where both the magnitude and the temporal pattern of price fluctuations are uncertain, it is neither practical nor conceptually valid to construct a scheduling scheme that deliberately operates against the price distribution. Such an approach would not only be unfeasible under real-world operational constraints but would also violate the fundamental principle underpinning this study, namely the balancing of power exchanges between the community grid and the upstream grid.

Nevertheless, despite the volatility of RTP tariffs, there remains a degree of structural consistency between the temporal distribution of prices and demand patterns. By overlaying the hourly residential net electricity consumption from the Trent Basin project with the RTP data, it can be observed that, although some discrepancies exist, the general pattern holds: electricity prices tend to be higher during peak demand hours and lower during off-peak periods. Against this backdrop, the balancing reference curve adopted in this research—defined as a flat hourly load profile over the 24-hour horizon—demonstrates superior economic performance. Instead of producing an hourly cost trajectory that is uniformly lower than the pre-optimization profile, the optimized balancing curve achieves cost reduction through a reallocation of load relative to the RTP price structure. In the unoptimized case, higher consumption tends to coincide with higher price periods while lower consumption occurs during lower price periods, leading to a cost amplification effect. By contrast, the optimized profile redistributes part of the demand toward low-price hours, while simultaneously reducing consumption during high-price hours. Although this does not guarantee that the cost in every individual hour is lower,

the aggregate outcome after price-weighted integration is a significant reduction in total daily electricity expenditure. This outcome confirms that a balanced power distribution not only satisfies the technical requirement of achieving extreme load balancing but also provides clear economic advantages under realistic tariff conditions.

In this section, detailed analyses are presented on the hourly electricity cost curves corresponding to different parameter configurations and influencing factors. These simulations illustrate how the proposed V2G optimization framework interacts with varying PV capacities, EV fleet characteristics, and operational assumptions, thereby providing insights into the cost-effectiveness of the scheduling strategies across multiple scenarios.

6.2.2.1. Impact of PV Installation Capacity on Optimized Time-of-Use Electricity Cost Profiles

The impact of PV installation capacity on the electricity cost curve is illustrated in Figures 6-6 through 6-11. It should be noted that the underlying V2G schedule was optimized to achieve extreme power-load balancing rather than cost minimization; the resulting time-of-use electricity cost curve is obtained by superimposing the real-time RTP prices onto the optimized load profile. These figures present the distribution of electricity costs before and after optimization, together with the corresponding daily cost totals, for three representative PV configurations: full installation capacity (4 kWp), half installation capacity (2 kWp), and no PV. The analysis is conducted under a fixed set of baseline parameters (battery capacity = 24 kWh; charging power = 3.3 kW; discharging power = 3.3 kW; EV ownership rate = 1; idle rate = 0.5487; average hourly charging demand = 0.20455 kWh), with V2G scheduling performed according to the Scenario I management logic on both a representative summer day and a representative winter day. For cost calculation, the pre-optimization community grid is assumed to lack centralized coordination equipment and therefore has no ability to intelligently export electricity to the upstream grid. In such a case, whenever net power within the

community grid becomes negative (i.e., PV generation exceeds internal demand), the electricity cost is set to zero rather than reflecting potential revenues from export. This approach was adopted because the RTP dataset does not include explicit electricity export prices, and in practice, the Smart Export Guarantee (SEG) prices are typically much lower than the grid purchase price. If the pre-optimization load profile were instead evaluated using the same system price for both buying and selling electricity, periods with excess PV generation would unrealistically imply that the community is selling electricity at the purchase price, artificially inflating the apparent economic performance of the unoptimized system. By contrast, the optimized load profiles, determined using the extreme power-load balancing reference values, generally maintain net positive community power for most hours of the day, with negative net power occurring only under specific conditions, such as peak PV generation days. This ensures that the cost evaluation of the optimized system does not suffer from the same distortions, providing a more realistic comparison of economic performance. By contrast, the optimized system is assumed to be equipped with centralized control infrastructure and a community-scale V2G system based on the 'S-G-L-S' configuration, thereby enabling the community to sell surplus electricity to the upstream grid at the system price provided by LimeJump.

A particular phenomenon emerges in the summer representative day (21st June), where instances of electricity oversupply in the upstream grid drive market prices down to zero or even into negative territory. According to the optimization logic, however, the community grid is required to maintain a stable and balanced unidirectional power exchange with the upstream network across all time intervals. As a result, during these negative pricing periods the optimized community grid continues to export electricity, leading to intervals of zero or even negative revenue. It should be noted that, although stopping electricity exports during negative pricing periods could improve short-term economic performance, this approach would introduce two critical challenges. First, it would require a substantial additional storage

capacity in idle EV batteries to absorb the surplus electricity, which is not available under typical community conditions. Second, during peak PV generation periods, a large number of EVs would need to be simultaneously engaged in charging to absorb the excess power and prevent reverse flow to the upstream grid. Such a scenario is highly impractical in daytime EV scheduling and would impose significant operational pressure on the fleet, substantially reducing the overall efficiency of EV coordination. Therefore, the optimization logic maintains unidirectional exports even during negative price intervals, prioritizing stable load balancing and practical feasibility over marginal short-term economic gains. Nevertheless, a comparison of Figures 6-6 to 6-8 shows that when PV installation capacity decreases from 4 kWp to 0 kWp, the corresponding increase in daily electricity cost for the optimized community grid averages only £68.56. This is significantly lower than the cost increase observed in the unoptimized grid under the same PV variations, which averages £894.98. Such a discrepancy highlights the effectiveness of the optimization framework in absorbing and utilizing PV generation, thereby improving the economic performance of the community grid. More importantly, it demonstrates that the optimized system is capable of maintaining profitability across all time periods during summer conditions when PV output is at its seasonal peak.

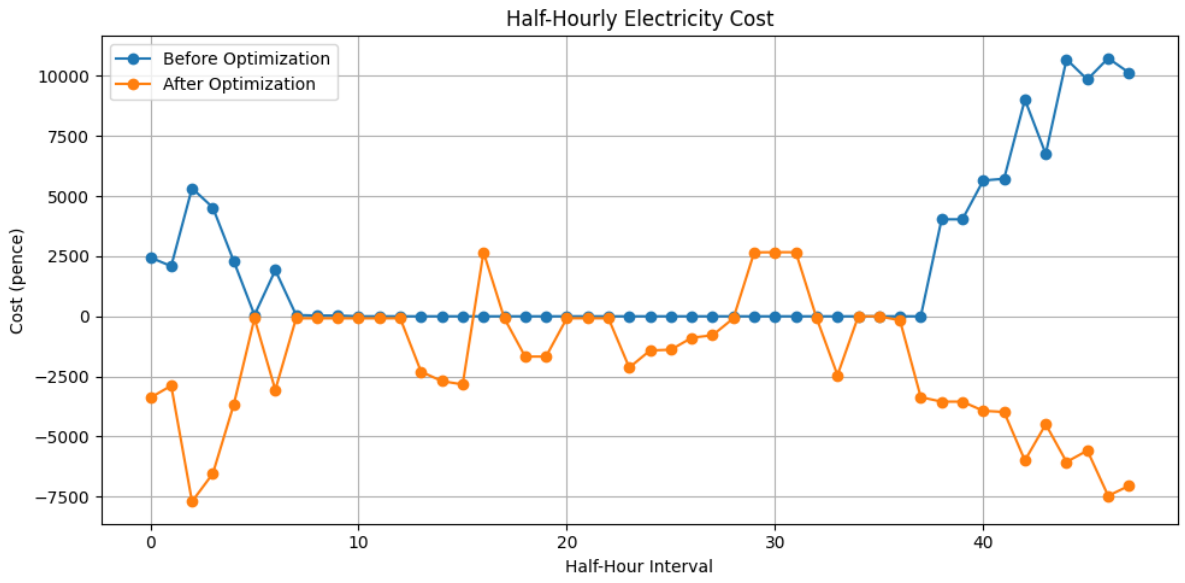


Figure 6-6. Half-hourly distribution of electricity costs on 21st June under Scenario I with full PV installation capacity (4 kWp). All other parameters remain consistent with the baseline configuration (battery capacity = 24 kWh; charging/discharging power = 3.3 kW; EV ownership = 100%; idle rate = 0.5487; average hourly charging demand = 0.20455 kWh).

Note: During the period from 08:30 to 18:30, the optimized system consistently exported electricity to the upstream grid, resulting in zero or even negative revenues due to instances of over-supply and depressed market prices. Nevertheless, the system maintained a clear net economic advantage over the entire day. The total daily electricity cost for the unoptimized community grid amounted to £954.24, whereas under the optimized Scenario I configuration, the daily electricity cost was reduced to –£931.49, demonstrating a net profit.

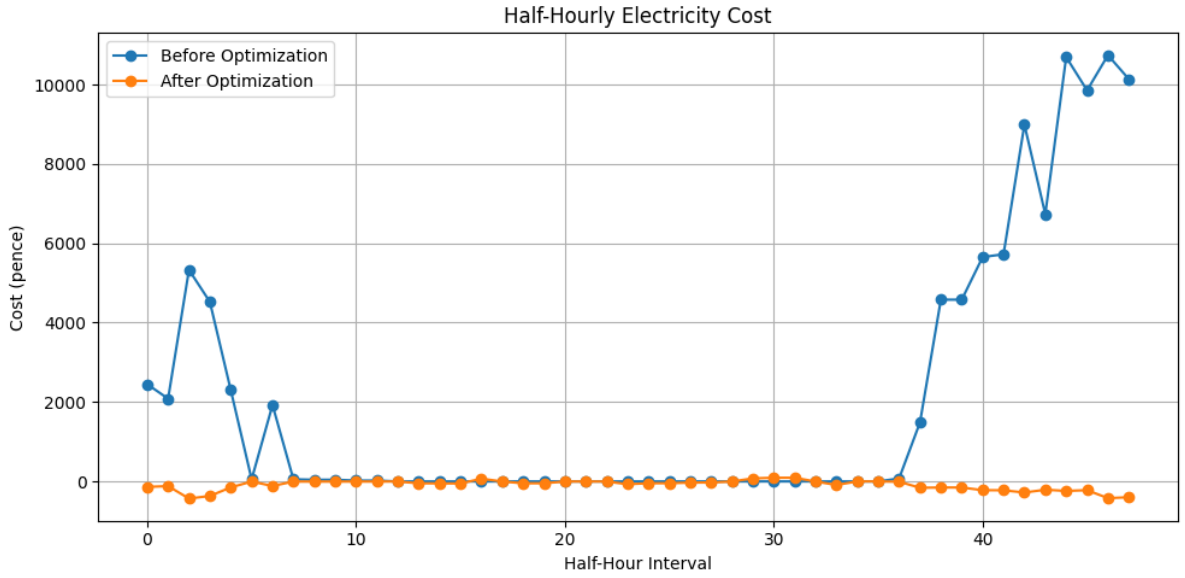


Figure 6-7. Half-hourly electricity cost distribution on 21st June under Scenario I optimization with PV installed capacity of 2 kWp (all other parameters identical to those in Figure 6-6).

Note: With a reduced PV installed capacity of 2 kWp, the reference value for load balancing was set at –6.211 kW, resulting in the optimized load profile oscillating around this threshold. Under this configuration, the total daily electricity cost for the unoptimized community grid was £980.79, whereas the optimized grid achieved a significantly lower total of –£42.72.

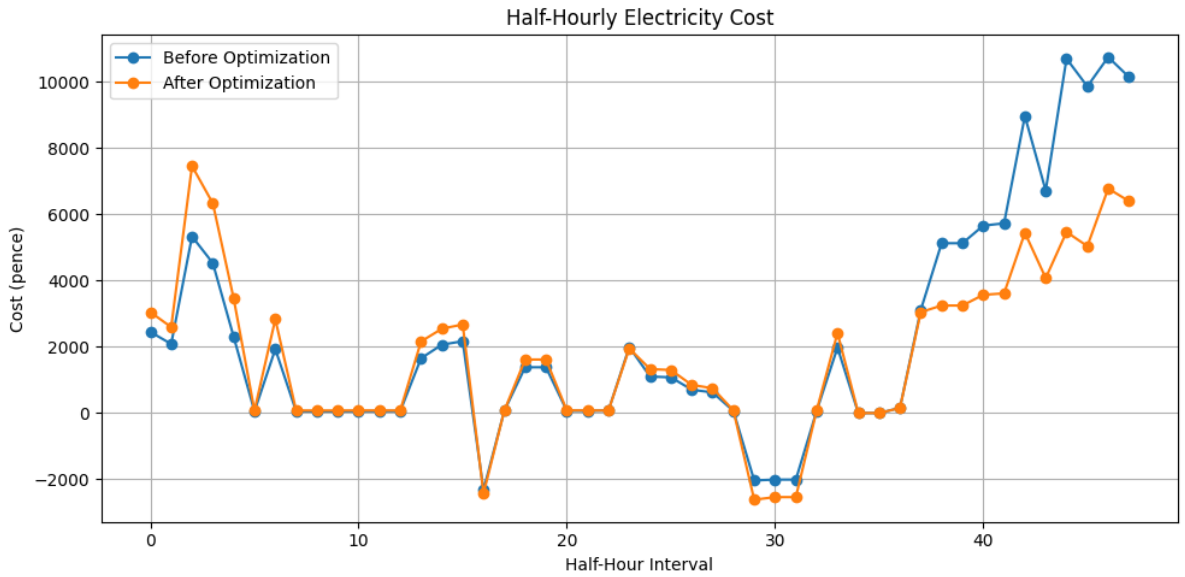


Figure 6-8. Half-hourly electricity cost distribution on 21st June under Scenario I optimization without PV generation (all other parameters identical to those in Figure 6-6).

Note: In the absence of PV contribution, the community grid exhibited a substantially higher dependence on upstream power supply. Under this condition, the total daily electricity cost of the unoptimized grid amounted to £1091.36, whereas the optimized grid reduced the cost to £858.46, highlighting the effectiveness of the proposed balancing strategy even without local renewable generation.

In winter (Figures 6-9 to 6-11), the situation differs substantially as PV output is markedly lower and the community grid functions primarily as a net electricity consumer reliant on the upstream grid. Under these conditions, the optimization logic redistributes power demand by shifting a portion of consumption toward midday hours when electricity prices are relatively low, thereby alleviating demand during evening peak hours when prices are highest. Although the reduction in total electricity costs is more constrained than in summer due to limited PV availability, the optimized scheduling still yields meaningful savings by mitigating reliance on high-cost electricity periods. This outcome underscores the robustness of the proposed optimization strategy across different seasonal contexts, ensuring both technical feasibility in load balancing and enhanced cost efficiency.

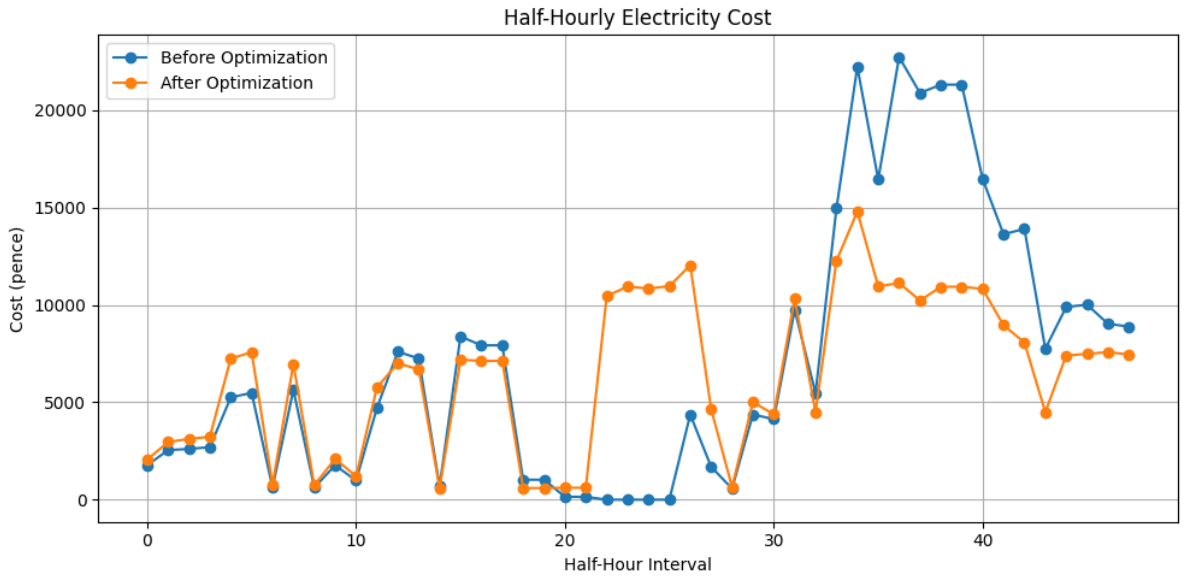


Figure 6-9. Half-hourly electricity cost distribution on 11th December under Scenario I optimization with full PV capacity (all other parameters identical to those in Figure 6-6).

Note: On this winter characteristic day, the total daily electricity cost of the unoptimized community grid was £3366.35, while the optimized grid reduced the cost to £3101.69. This demonstrates that the V2G-based balancing strategy effectively lowers electricity expenditure even during periods of limited PV generation.

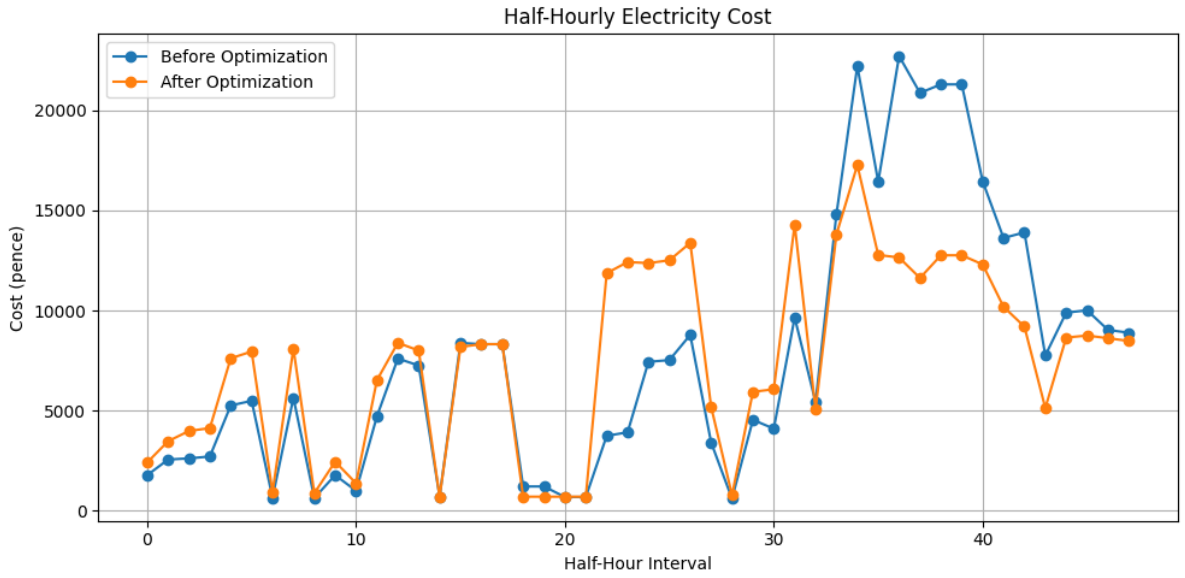


Figure 6-10. Half-hourly electricity cost distribution on 11th December under Scenario I optimization with half PV capacity (all other parameters identical to those in Figure 6-6).

Note: On this day with half PV capacity, the total daily electricity cost of the unoptimized community grid was £3673.19, while the optimized grid reduced the cost to £3591.21. The results indicate that the V2G-based optimization strategy continues to improve economic performance even under reduced PV generation conditions.

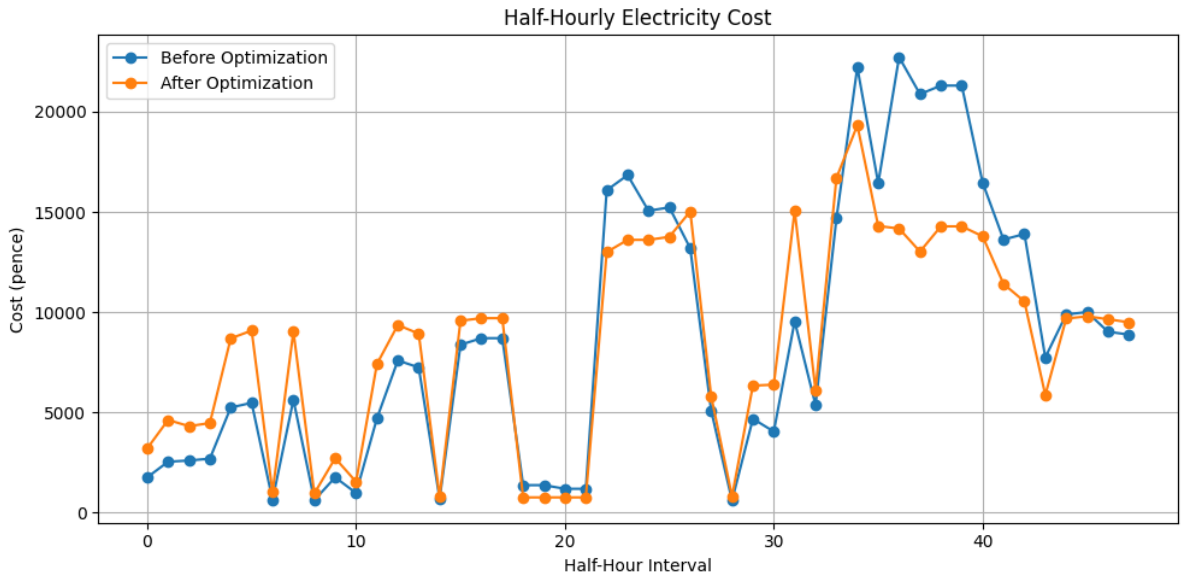


Figure 6-11. Half-hourly electricity cost distribution on 11th December under Scenario I optimization with no PV capacity (all other parameters identical to those in Figure 6-6).

Note: On this day with no PV generation, the total daily electricity cost of the unoptimized community grid was £4160.32, whereas the optimized grid reduced the cost to £4041.52. The results demonstrate that the V2G-based optimization continues to provide economic benefits even in the absence of PV generation.

6.2.2.2. Impact of EV Fleet Composition Parameters on the Post-Optimization ToU Electricity Cost Curve

The composition parameters of the EV fleet—namely ownership rate, idle rate, and charging intensity—play a critical role in shaping the optimized time-of-use electricity cost curve. Their influence manifests primarily through changes in the absolute number of active EVs and the resulting average charging demand per unit time, both of which directly affect the net load

distribution of the community grid and the corresponding load-balancing reference value. Specifically, a higher number of active EVs under a given ownership–idle rate configuration leads to simultaneous increases in the baseline net load curve of the community grid and in the daily reference value for power balancing. However, due to the inherent randomness of charging increments across hours and the unpredictability of real-time electricity prices, the relative economic change between the original load curve and the balanced reference curve cannot be straightforwardly quantified.

This phenomenon becomes more evident when comparing optimization outcomes under different scenarios. For example, in the boundary configuration where bidirectional charging and discharging capacities remain identical (battery capacity = 24 kWh; charging/discharging power = 3.3 kW; average hourly charging demand = 0.20455 kWh; EV ownership = 100%; idle rate = 55%), Scenarios I and II share the same parameter settings for the active EV population (summer load distribution shown in Figure 5-48, corresponding cost distribution in Figure 6-6). By contrast, Scenario III differs only in the absence of active EVs, with 35% of households instead holding exclusively idle EVs (summer distribution on 21st June shown in Figure 5-54, with cost distribution in Figure 6-14). Under Scenarios I and II, the original daily electricity costs of the community grid were £954.24, reduced after optimization to a profit of £931.49. In Scenario III, however, the original daily cost was markedly lower at £737.29, and optimization further improved the outcome to a profit of £1186.95. Notably, in Scenario III the higher load-balancing reference value resulted in additional electricity export to the upper grid during midday hours with zero or even negative prices, leading to higher costs in those specific intervals. Nevertheless, the aggregate outcome demonstrated superior profitability compared to cases with larger active EV populations.

A second boundary case is illustrated in Figure 6-12, where charging intensity is maximized (average hourly charging demand = 0.394958 kWh) while all other parameters remain identical

to those of Scenario I with full PV installation (battery capacity = 24 kWh; charging/discharging power = 3.3 kW; EV ownership = 100%; idle rate = 55%). The corresponding power distribution is shown in Figure 5-39. In this case, the increase in charging intensity raised both the net community load curve and the daily load-balancing reference value (from −161.64 kW in Figure 6-6 to −124.30 kW). As a result, the original daily cost increased from £954.24 to £1161.93, while the post-optimization profit decreased from £931.49 to £695.38.

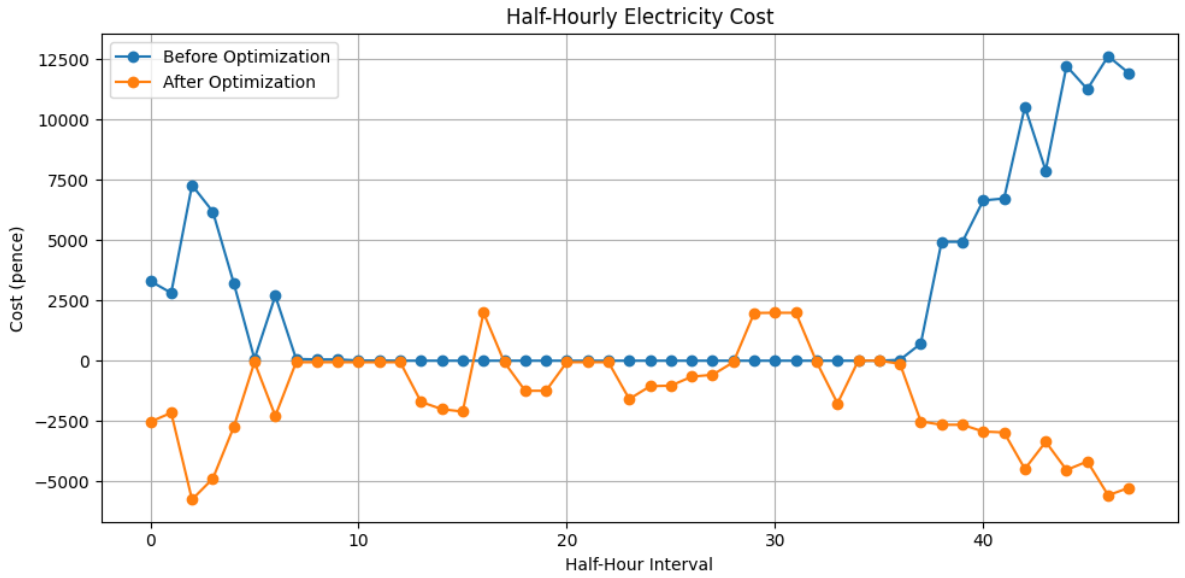


Figure 6-12. Half-hourly distribution of electricity costs on 21st June under Scenario I with increased EV charging intensity (average hourly charging demand = 0.394958 kWh). All other parameters remain consistent with the baseline configuration.

This finding confirms that variations in the absolute number of active EVs and the average charging demand per unit time—that is, the charging intensity—have a pronounced impact on electricity costs. More importantly, it highlights the trade-off between maximizing the flexibility offered by larger active EV populations and charging demands, and maintaining economic efficiency under fluctuating tariff conditions. Nevertheless, even when all parameter configurations are designed as boundary conditions that satisfy the primary objective of load-

balancing equilibrium—namely, equalized bidirectional power transfer between the community grid and the upper-level grid—the intrinsic influence of EV fleet composition on total electricity consumption remains unavoidable. In other words, while optimization ensures the technical requirement of balancing load stress, the absolute number of active EVs and their charging intensity fundamentally reshape the baseline consumption profile, thereby determining the magnitude of the total electricity cost even under identical balancing constraints. From a broader perspective, this indicates that achieving technical equilibrium in power exchange does not necessarily guarantee economic optimality. Instead, the inherent coupling between physical balancing constraints and the stochastic nature of EV demand underscores the role of fleet composition parameters as structural drivers of system-level economic performance. This insight reinforces the importance of incorporating behavioural and demographic dimensions of EV adoption into the design of V2G optimization strategies, particularly in community-level grid planning, where both physical stability and economic viability must be simultaneously ensured.

6.2.2.3. Electricity Cost Profiles under Boundary Parameter Configurations with Low Bidirectional Charging Power and Limited Battery Capacity

Under boundary configurations that reflect low bidirectional charging/discharging power and limited battery capacity—consistent with current EV usage—Scenarios I and II were evaluated to quantify their impact on community-level electricity costs after optimization. In both schemes, the system is parameterized with a battery capacity of 24 kWh, charging and discharging power of 3.3 kW, and an average hourly charging demand of 0.20455 kWh. Under these conditions, full EV ownership with an idle rate of 55% constitutes the critical threshold at which the load-balancing reference can be met. The half-hourly cost distributions and daily totals on 21st June and 11th December are shown in Figures 6-6 and 6-9, respectively.

Annualizing across the full year, total community electricity expenditure decreases from £788507.67 before optimization to £396061.51 after optimization—nearly a 50% reduction.

By contrast, Scenario III assumes an extreme but informative setting in which all EVs are treated as idle (i.e., fully dispatchable), thereby removing the impact of active-use charging from the net-load trajectory. With the same technical parameters but reduced EV ownership, a threshold of 35% ownership suffices to achieve the load-balancing reference. The corresponding half-hourly cost distributions for 21st June and 11th December are presented in Figures 6-13 and 6-14. On an annual basis, electricity costs fall from £563401.23 pre-optimization to £130903.61 post-optimization, approximately one quarter of the baseline. The larger saving relative to Scenarios I and II arises because the absence of charging-related consumption amplifies the economic value of PV energy that is stored and subsequently utilized.

These findings demonstrate that the pronounced differences in outcomes across Scenarios I, II, and III are not simply a matter of technical feasibility but rather stem from their distinct economic implications. Specifically, when EV charging demand is absent—as in Scenario III—the stored PV generation achieves a disproportionately greater economic effect, since no portion of the renewable energy is offset by concurrent EV consumption. In contrast, Scenarios I and II, which involve active or partial EV charging, inherently reduce the net economic value of PV by coupling renewable availability with additional demand. Thus, the superior cost reduction observed under Scenario III reflects the amplification of PV's contribution in the absence of EV-related load, underscoring how the interaction between EV usage patterns and local renewable generation fundamentally shapes the economic performance of V2G optimization.

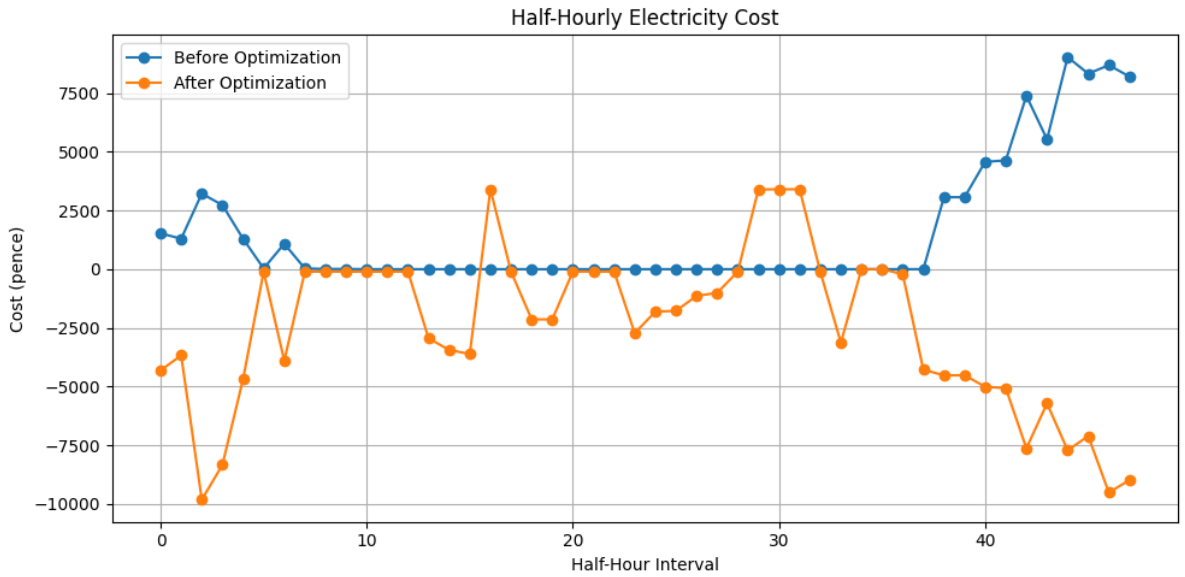


Figure 6-13. Half-hourly distribution of electricity costs on 21st June under Scenario III with increased EV charging intensity (EV ownership = 35%; idle rate = 100%). All other parameters remain consistent with the baseline configuration.

Note: The total daily electricity cost of the community grid was £737.29 before optimization, whereas after implementing the optimized V2G scheduling, the cost was reduced to -£1186.95.

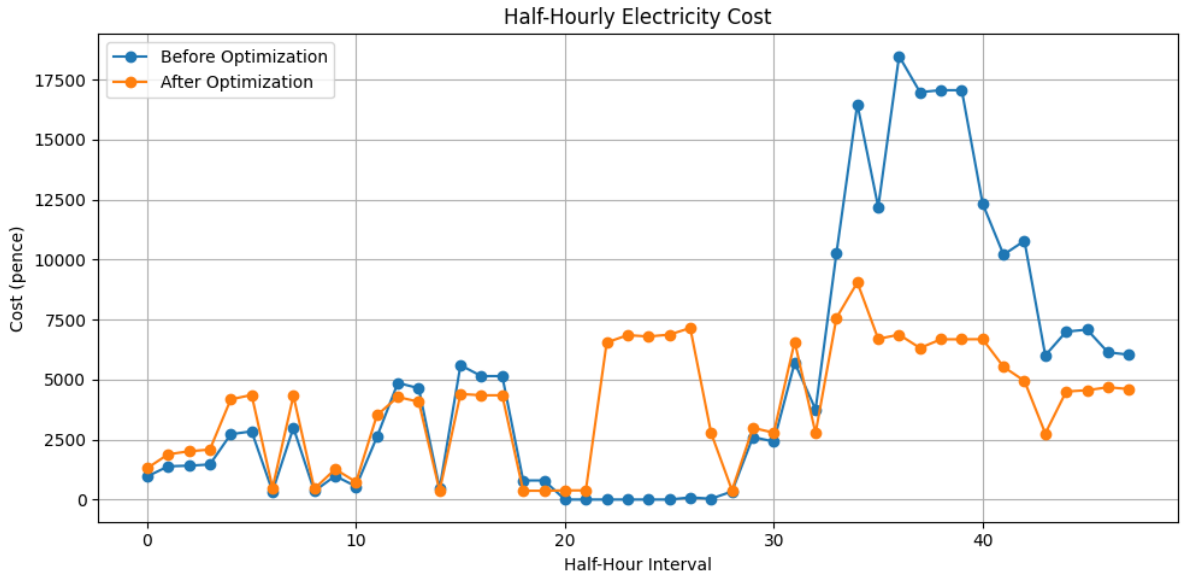


Figure 6-14. Half-hourly distribution of electricity costs on 11th December under Scenario III with increased EV charging intensity (EV ownership = 35%; idle rate = 100%). All other parameters remain consistent with the baseline configuration.

Note: The total daily electricity cost of the community grid was £2349.84 before optimization, whereas after implementing the optimized V2G scheduling, the cost was reduced to £1904.23.

6.2.2.4. Electricity Cost Profiles under Market-Feasible EV Parameter Configurations and Current Grid Conditions

For Scenario I and Scenario II, the optimal EV boundary parameter configurations under current market-acceptable power levels and community grid conditions were determined based on the simulations presented in Chapter 5. Using calibrated EV behaviour parameters—battery capacity = 82.5 kWh; charging power = 10 kW; discharging power = 7 kW; average hourly charging demand = 0.20455 kWh—and controlling for EV ownership = 100% and idle rate = 15%, the boundary conditions necessary to achieve extreme load balancing within the community grid were established. Under these settings, the half-hourly electricity cost distributions for the summer reference day (21st June) before and after optimization are shown in Figure 6-15, while the corresponding distributions for the winter reference day (11th December) are presented in Figure 6-16.

Annual simulations under these conditions estimate that the total daily electricity cost of the community grid was £1002700.62 prior to optimization and reduced to £636182.23 after optimization. Notably, the use of equivalently scaled EV battery capacities in the simulations increased the total charging demand, while the reduced idle rate led to a higher absolute number of active EVs. This amplified the overall EV charging energy consumption, resulting in a 27.17% increase in the pre-optimization annual cost compared to the "Boundary Parameter Configurations with Low Bidirectional Charging Power and Limited Battery Capacity" scenario, and a 60.63% increase in the post-optimization annual cost. These results demonstrate that, within a fully implemented S-G-L-S grid including EV power consumption, enhancing bidirectional charging power and EV battery capacity to maximize EV dispatch efficiency may inadvertently reduce economic performance. It should be noted that, under unchanged

household demand and driving requirements, simply increasing EV battery capacity or bidirectional charging power would not inherently alter the total energy consumption of the fleet. However, user charging behaviour is influenced by the SOC displayed on the vehicle battery. According to the 2022 survey by the UK Department of Transport, EV users tend to adjust their charging decisions based on the remaining battery percentage. When battery capacity is increased, users experience less SOC-related anxiety, which reduces the likelihood of charging at locations outside the community grid. Consequently, more charging occurs upon return to the home community grid, effectively shifting additional energy consumption into the local grid. In the simulations with higher battery capacities and bidirectional charging power, this behavioural effect was approximated by proportionally scaling the driving-related energy consumption. Although this approach cannot quantitatively capture the precise impact of altered user behaviour, it ensures that the simulation accounts for the potential increase in local energy demand resulting from changes in charging patterns.

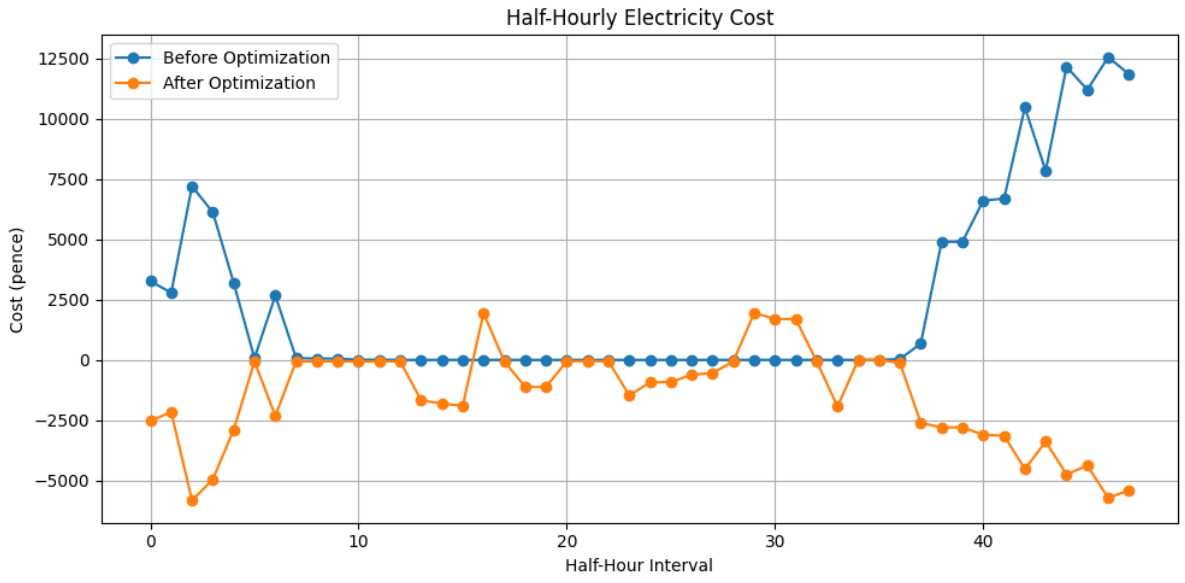


Figure 6-15. Half-hourly distribution of electricity costs on 21st June under Scenario I with full PV installation capacity (4 kWp). All other parameters remain consistent with the baseline configuration (battery capacity = 82.5 kWh; charging power = 10 kW; discharging power = 7 kW; EV ownership = 100%; idle rate = 15%; average hourly charging demand = 0.20455 kWh).

Note: The total daily electricity cost of the community grid was £ 1154.35 before optimization, whereas after implementing the optimized V2G scheduling, the cost was reduced to -£710.96.

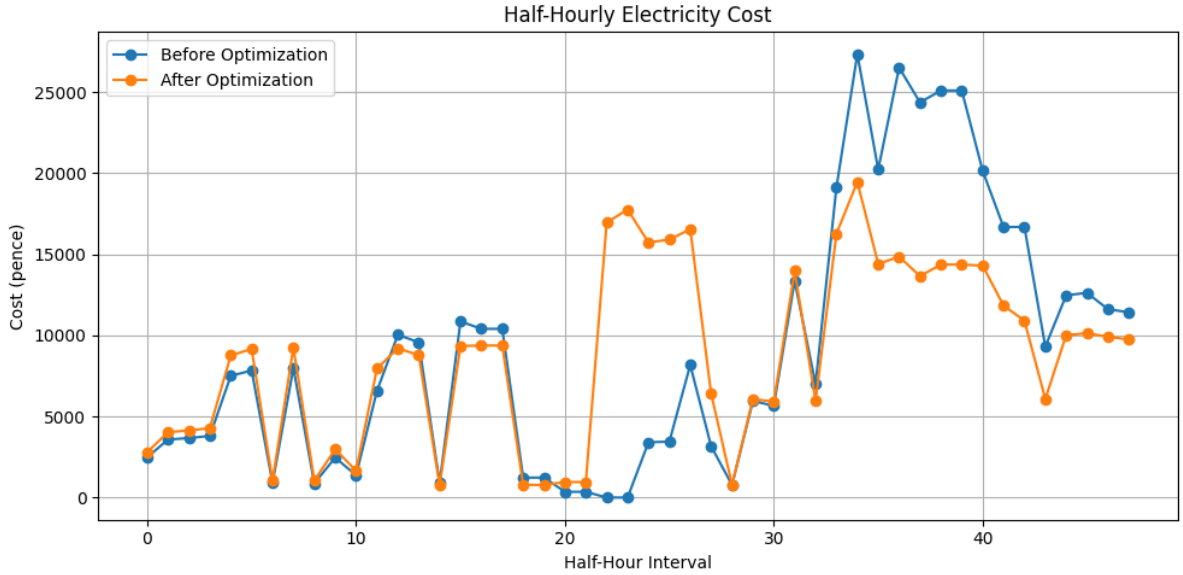


Figure 6-16. Half-hourly distribution of electricity costs on 11th December under Scenario I with full PV installation capacity (4 kWp). All other parameters remain consistent with the baseline configuration.

Note: The total daily electricity cost of the community grid was £ 4339.90 before optimization, whereas after implementing the optimized V2G scheduling, the cost was reduced to £ 4196.89.

For Scenario III, under the current market-acceptable EV power levels and optimal EV boundary parameter configurations, the simulations presented in Chapter 5 indicate that, with battery capacity = 82.5 kWh, charging power = 10 kW, discharging power = 10 kW, and average hourly charging demand = 0.20455 kWh, controlling EV ownership at 11% constitutes the boundary condition necessary to achieve extreme load balancing in the community grid. Since EVs in this scenario do not contribute to either grid power consumption or generation, modifications to their parameters do not fundamentally alter the grid environment. Consequently, the electricity cost simulations under these settings are identical to those obtained for the “Boundary Parameter Configurations with Low Bidirectional Charging Power

and Limited Battery Capacity" scenario. This outcome further confirms that, under the extreme conditions represented by Scenario III, adjustments to EV parameters have no discernible impact on the overall economic performance of the community grid.

To clarify how electricity cost savings are allocated among residents, two alternative benefit-sharing mechanisms are proposed, reflecting different levels of social cohesion and organisational structure within the community.

For communities characterised by a high degree of mutual trust and collective orientation, a contribution-weighted daily settlement scheme can be adopted. Under this approach, the total daily net profit or net expenditure of the community microgrid is allocated in proportion to each household's net energy contribution. The net contribution of household i on day d is defined as

$$C_{i,d} = \overline{PV}_{i,d} + E_{i,d}^{V2G,dis} - E_{i,d}^{self} \tag{6.1}$$

where $\overline{PV}_{i,d}$ represents the per-household share of community PV generation (given the centralised PV installation), $E_{i,d}^{V2G,dis}$ denotes the V2G discharge energy, and

$$E_{i,d}^{self} = E_{i,d}^{res} + E_{i,d}^{V2G,ch} \tag{6.2}$$

corresponds to total self-consumption, consisting of residential load and EV charging demand on that day.

Let Π_d denote the total net economic outcome of the community microgrid on day d. The allocated benefit to household i is then given by

$$B_{i,d} = \Pi_d \times \frac{C_{i,d}}{\sum_{j=1}^{N} C_{j,d}} \tag{6.3}$$

where N is the total number of households.

This mechanism is straightforward and particularly suitable for communities with long-term shared interests. It explicitly recognises the positive contribution of V2G participants to the overall economic performance of the microgrid and ensures that bidirectional power exchange is reflected in proportional benefit allocation. However, because settlement is based solely on the aggregate daily net balance, temporal variations in electricity prices are not explicitly captured. In practice, identical power exchanges at different hours may yield substantially different economic values under time-of-use or real-time pricing. By relying on daily net results, this approach smooths temporal price signals and consequently attenuates the economic premium associated with strategically timed V2G charging and discharging.

In contrast, for communities in which households operate more independently and require greater economic transparency, a more granular internal pricing mechanism can be introduced. In this framework, internal electricity prices are jointly determined by community members. The internal PV selling price and V2G discharge price at hour t are defined as proportional to the upstream grid's real-time retail tariff $p_t^{grid,sell}$, namely

$$p_t^{PV,int} = \alpha_{PV} p_t^{grid,sell} \tag{6.4}$$

$$p_t^{V2G,int} = \alpha_{V2G} p_t^{grid,sell} \tag{6.5}$$

where $\alpha_{V2G} > \alpha_{PV}$. The higher coefficient applied to V2G discharge results in a slightly higher internal selling price for V2G electricity, and the price differential serves as compensation for battery degradation and related operational costs.

Settlement is conducted on an hourly basis. For household i at hour t, self-consumption is defined as

$$E_{i,t}^{self} = E_{i,t}^{res} + E_{i,t}^{V2G,ch} \tag{6.6}$$

, which is similar to Equation (6.2).

When the community microgrid operates in a net import state, i.e., total demand exceeds local generation and electricity must be purchased from the upstream grid, the weighted unit supply cost is calculated as

$$\bar{p}_t^{import} = \frac{E_t^{grid,imp} p_t^{grid,sell} + E_t^{V2G,tot} p_t^{V2G,int}}{E_t^{grid,imp} + E_t^{V2G,tot}} \tag{6.7}$$

Accordingly, the hourly benefit of household iii is expressed as

$$B_{i,t} = \overline{PV}_{i,t} p_t^{PV,int} + E_{i,t}^{V2G,dis} p_t^{V2G,int} - E_{i,t}^{self} \bar{p}_t^{import} \tag{6.8}$$

Conversely, when the community operates in a net export state, meaning that local generation exceeds demand and surplus electricity is exported to the upstream grid, the valuation of PV generation and V2G discharge reflects a weighted combination of internal consumption and grid export. Specifically,

$$\bar{p}_t^{PV,export} = \frac{E_t^{load,tot} p_t^{PV,int} + E_t^{grid,exp} p_t^{grid,buy}}{E_t^{load,tot} + E_t^{grid,exp}} \tag{6.9}$$

$$\bar{p}_t^{V2G,export} = \frac{E_t^{load,tot} p_t^{V2G,int} + E_t^{grid,exp} p_t^{grid,buy}}{E_t^{load,tot} + E_t^{grid,exp}} \tag{6.10}$$

Meanwhile, the cost assigned to self-consumption is derived from internal generation sources:

$$\bar{p}_t^{self} = \frac{E_t^{PV,tot} p_t^{PV,int} + E_t^{V2G,tot} p_t^{V2G,int}}{E_t^{PV,tot} + E_t^{V2G,tot}} \quad (6.11)$$

The corresponding hourly benefit of household i is therefore calculated according to Equation (6.8). Through this proportional and temporally resolved allocation framework, both internal transactions and external exchanges are consistently reflected in household-level settlements. Although this hourly internal pricing mechanism improves economic fairness and fully preserves the temporal value of flexibility provided by V2G, it entails higher administrative and computational complexity. Accurate metering, real-time data aggregation, and a sufficiently capable local or cloud-based management platform are required to perform hourly clearing. Consequently, while economically rigorous and more reflective of marginal value signals, this mechanism is most appropriate for communities equipped with advanced digital infrastructure and formalised governance structures.

6.3. Impacts on Energy Efficiency & Carbon Reduction

6.3.1 Carbon Intensity Data Analysis

To evaluate the impact of the proposed optimization strategy on energy efficiency, a methodology analogous to that used for economic assessment was adopted. From a macro-level grid perspective, the analysis estimates the reduction in carbon emissions by comparing the net power-related carbon content of the community electricity network before and after the implementation of the optimized scheduling scheme. Data for the carbon intensity of electricity generation were sourced from the 2019 Real-Time Carbon Intensity of the Electricity System in Great Britain, provided through the Carbon Intensity API, a collaboration between the National Energy System Operator, the Environmental Defence Fund Europe, the University of Oxford Department of Computer Science, and WWF. Similar to the economic evaluation

process, representative single-day profiles and continuous week-long periods were first selected to characterize the temporal distribution of carbon intensity. Figures 6-17 to 6-20 present the hourly carbon intensity patterns for the Great Britain electricity system during the weeks containing the summer solstice, winter solstice, spring equinox, and autumn equinox, respectively. Unlike household electricity demand or PV generation, which often display pronounced diurnal cycles with distinct peak and off-peak periods, the daily carbon intensity profile exhibits no such strong regularity. However, a recurring feature is the appearance of a daily peak—or near-peak—in carbon intensity between approximately 16:00 and 20:00, coinciding closely with the residential demand peak. From the perspective of V2G power management aimed at minimizing total carbon emissions, shaping the community's net power profile to more closely align with a theoretical power balance curve—whereby demand during high-carbon-intensity hours is reduced and redistributed to periods of lower carbon intensity—can effectively decrease the total net carbon emissions of the community grid over a 24-hour cycle.

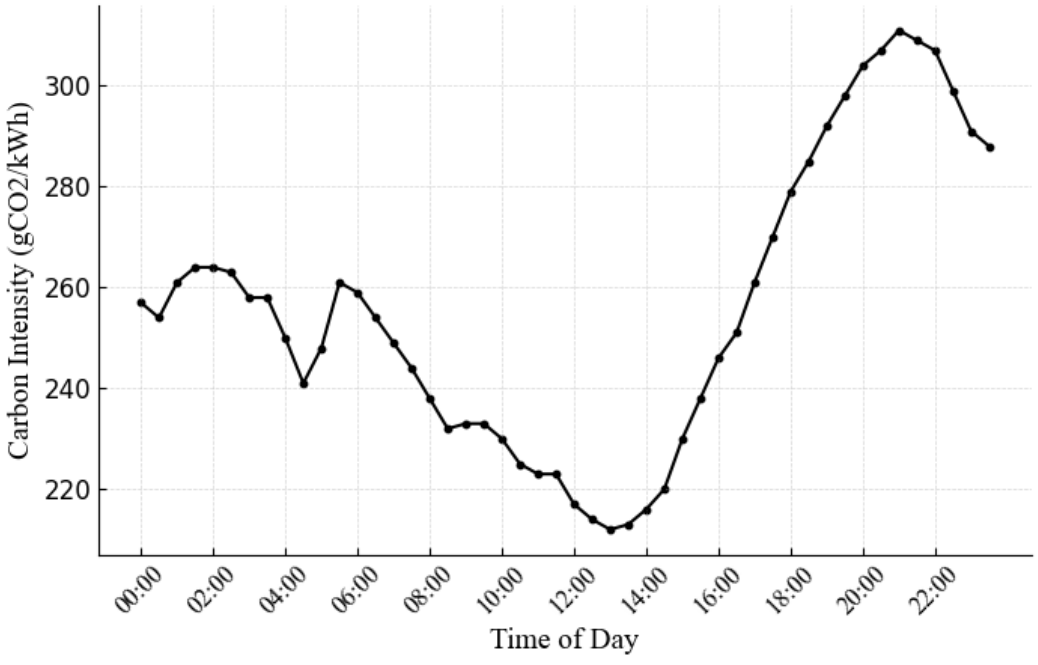


Figure 6-17. Real-time carbon intensity of Great Britain's electricity system on the summer solstice, sourced from the Carbon Intensity API project.

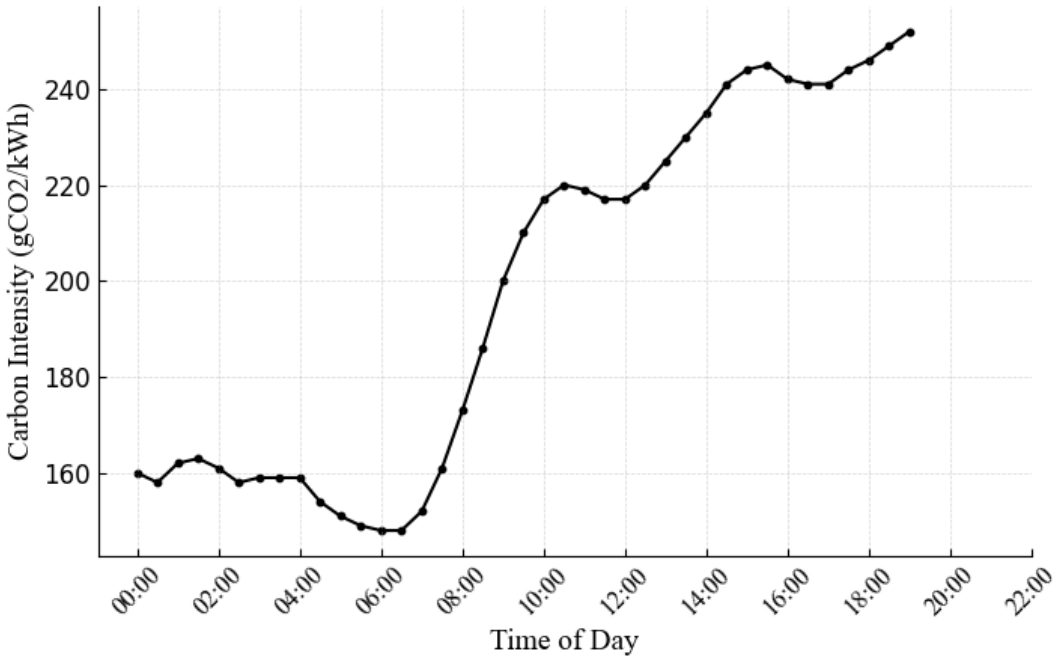


Figure 6-18. Real-time carbon intensity of Great Britain's electricity system on the winter solstice, sourced from the Carbon Intensity API project.

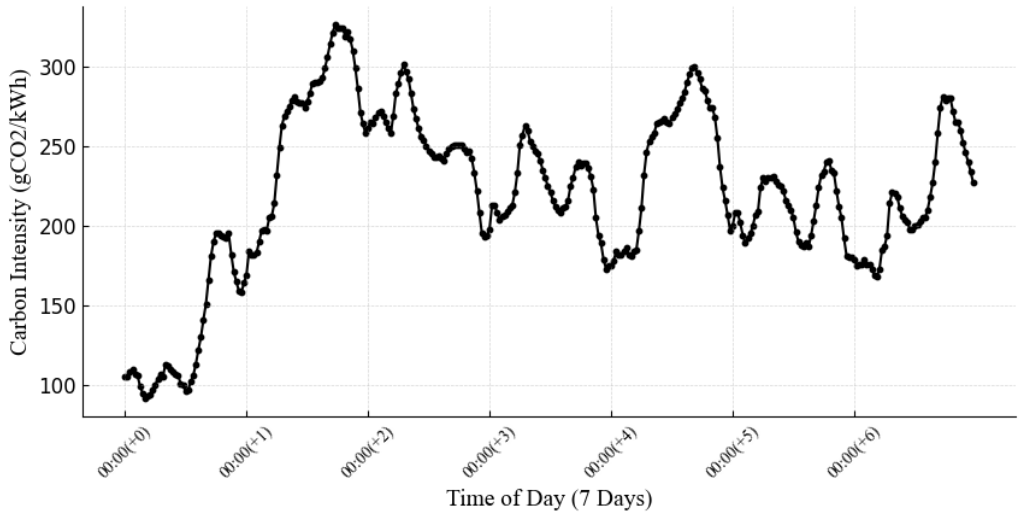


Figure 6-19. Half-hourly carbon intensity of Great Britain's electricity system during the week of the vernal equinox (17th–23th March 2020), sourced from the Carbon Intensity API project.

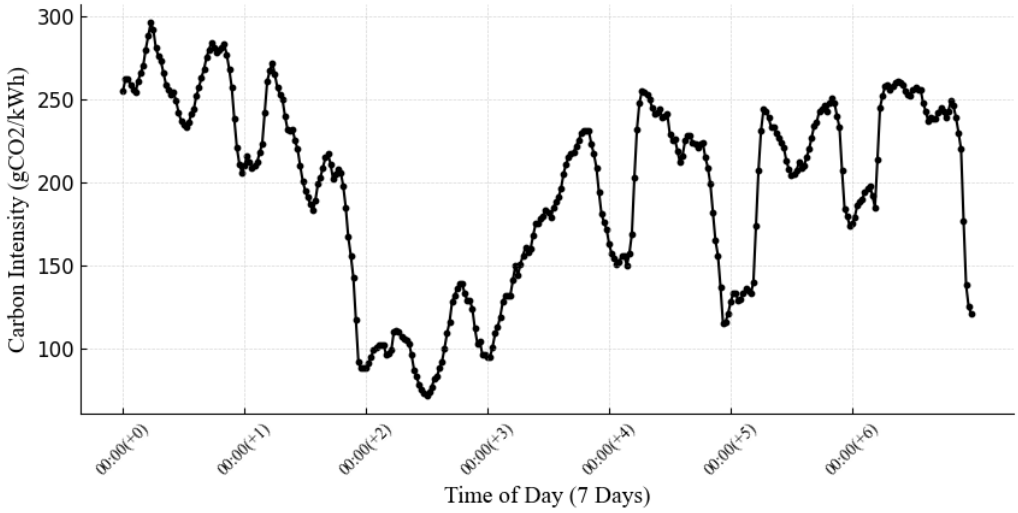


Figure 6-20. Half-hourly carbon intensity of Great Britain's electricity system during the week of the autumnal equinox (19th–25th September 2020), sourced from the Carbon Intensity API project.

6.3.2. Carbon Intensity Simulation Results for Different V2G Optimization Scenarios

6.3.2.1. Factors Influencing the Post-Optimization Carbon Intensity Profile

Similar to the preceding discussion on economic performance, any parameter that directly affects the net power load of the community grid—such as PV installation capacity or the structural characteristics of the EV population described in Section 6.2—also exerts a significant influence on the carbon intensity of the grid after the implementation of V2G optimization. In essence, the environmental friendliness of the optimized system is inherently tied to the same determinants that govern cost performance.

A key challenge arises from the inherently unpredictable temporal dynamics of carbon intensity in the upstream grid. In some cases, carbon intensity follows a linear increase over time; in others, it decreases, or it may even exhibit bimodal patterns. Under such conditions, the potential for further carbon intensity reduction through purely mathematical redistribution of power flows—i.e., altering weight factors in the optimization framework to shift load

temporally—is limited. Figures 6-21 and 6-22, which depict the time-varying distribution of carbon emissions for summer and winter representative days in the absence of PV generation, illustrate this constraint.

Nonetheless, the optimization strategies significantly enhance the efficiency with which locally generated PV electricity is utilized. By reducing dependence on the upstream grid and, in some cases, enabling reverse power flows back to the higher-level grid, the overall carbon intensity of the community system can be lowered. This effect is particularly pronounced when PV output is abundant. For example, as shown in Figures 6-23 and 6-24, with identical EV scheduling parameters, optimization during the summer representative day enabled reverse transmission to the upstream grid, reducing total carbon emissions to –2053303.18 kg. Even during the winter representative day, when PV availability was lower, optimization still yielded a 5.38% reduction in carbon emissions compared to the pre-optimization case.

In parallel, the composition of the EV population—defined by factors such as idle rate, ownership level, and charging intensity—directly determines the aggregate daily charging demand of EVs. This, in turn, influences the community grid's reliance on external electricity and thereby alters total carbon emissions. The mechanisms mirror those observed in the economic evaluation, and thus need not be reiterated here in detail. What can be emphasized, however, is that attempts to optimize carbon emissions solely by adjusting EV dispatch according to temporal variations in carbon intensity are both technically challenging and conceptually misaligned with the foundational goal of V2G management in this study, which is to maintain grid load balance as the primary objective.

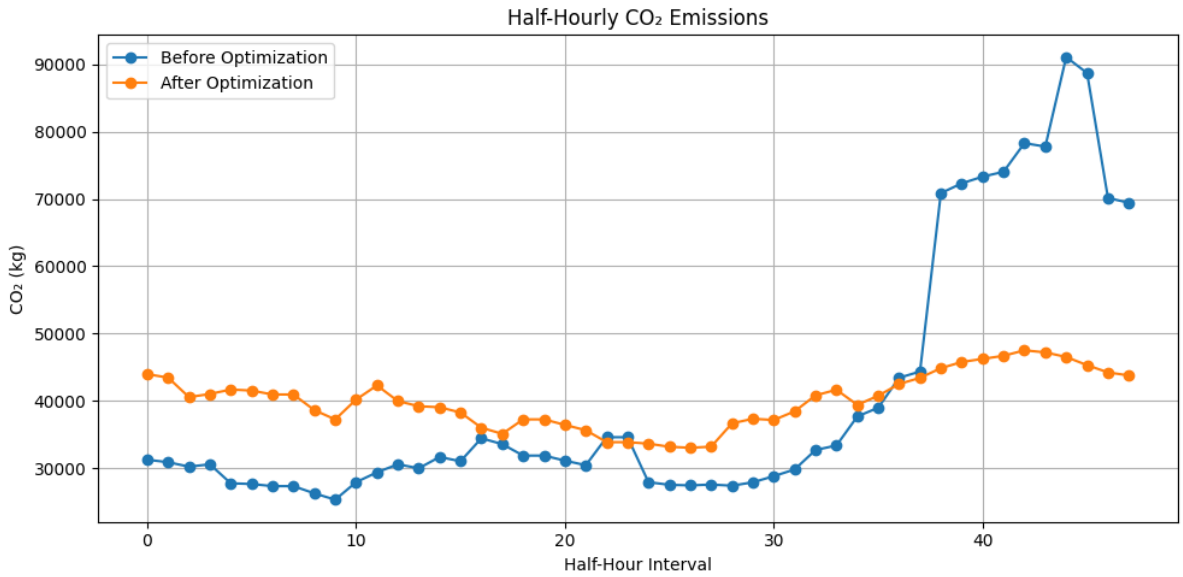


Figure 6-21. Half-hourly distribution of carbon emissions on 21st June under Scenario I with no PV installation capacity (0 kWp). All other parameters remain consistent with the baseline configuration (battery capacity = 24 kWh; charging power = 3 kW; discharging power = 3 kW; EV ownership = 100%; idle rate = 55%; average hourly charging demand = 0.20455 kWh). The total daily carbon emissions of the community grid amounted to 1948173.32 kg before optimization, and were reduced to 1923363.92 kg after optimized V2G scheduling.

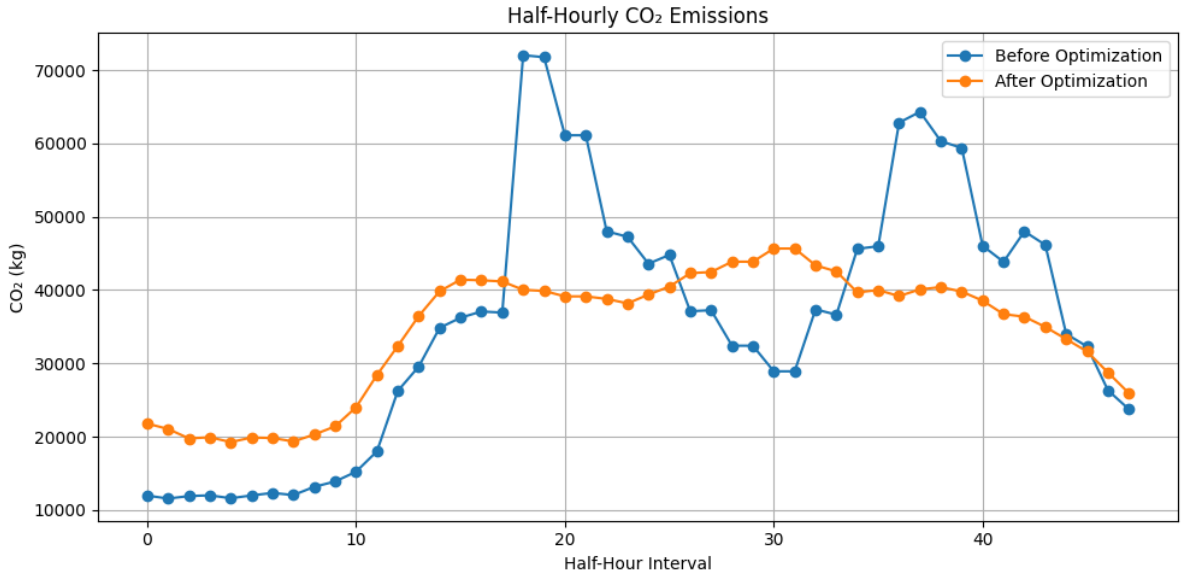


Figure 6-22. Half-hourly distribution of carbon emissions on 11th December under Scenario I with no PV installation capacity (0 kWp). The total daily carbon emissions of the community grid were 1716244.18 kg before optimization and decreased to 1657784.68 kg after optimized V2G scheduling.

6.3.2.2. Low Bidirectional Charging Power and Limited Battery Capacity: Optimized Carbon Intensity Profiles under Boundary Parameter Configurations

Within Scenario I and Scenario II, the analysis of boundary EV scheduling parameters required to maintain the load balance limit provides a useful benchmark for assessing the environmental implications of V2G optimization. Under these boundary configurations, the optimized community grid effectively establishes an upper bound on the achievable reduction in carbon emissions. As illustrated in Figures 6-23 and 6-24, the estimated annual carbon emissions of the community grid prior to optimization amounted to 425561520.90 kg. Following optimization, this value was reduced to -144858765.50 kg, indicating not only the elimination of direct carbon emissions but also the realization of net negative emissions. It should be noted that, for consistency with the previous economic analysis, the calculation of pre-optimization carbon emissions treats any electricity exported from the community grid to the upstream network as contributing zero carbon offset. This approach artificially inflates the total pre-optimization carbon emissions in the assessment. The negative post-optimization emissions arise from the community grid supplying electricity back to the upstream network, thereby offsetting a portion of the generation that would otherwise be required at the system level and functioning as an effective “carbon sink.”

It must be emphasized, however, that the magnitude of this negative carbon balance is highly dependent on the real-time carbon intensity of the upstream grid. Since the database used to characterize carbon intensity reveals strong temporal volatility and uncertainty—ranging from linear increases or decreases to more complex double-peak patterns—the quantitative results cannot be interpreted as an absolute or universally replicable outcome. Instead, they should be regarded as qualitative evidence demonstrating the technical feasibility of the proposed V2G management strategy to drive the community grid toward net-zero or even carbon-negative operation under favourable system conditions.

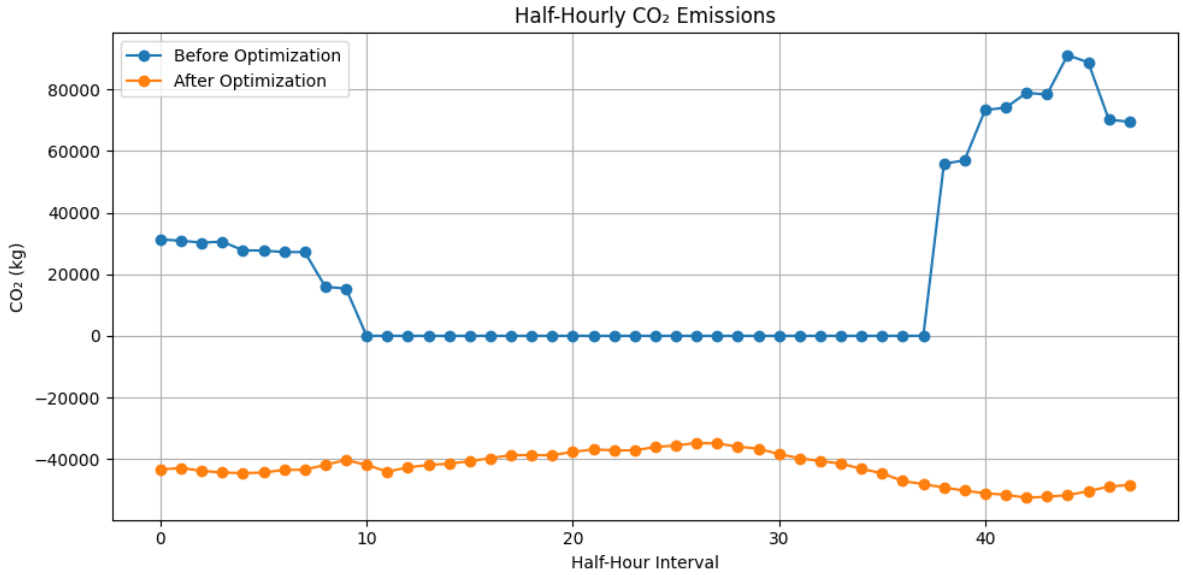


Figure 6-23. Half-hourly distribution of carbon emissions on 21st June under Scenario I & Scenario II with full PV installation capacity (4 kWp). All other parameters remain consistent with the baseline configuration (battery capacity = 24 kWh; charging power = 3 kW; discharging power = 3 kW; EV ownership = 100%; idle rate = 55%; average hourly charging demand = 0.20455 kWh). The total daily carbon emissions of the community grid were 1000715.55 kg before optimization and decreased to –2053303.18 kg after optimized V2G scheduling.

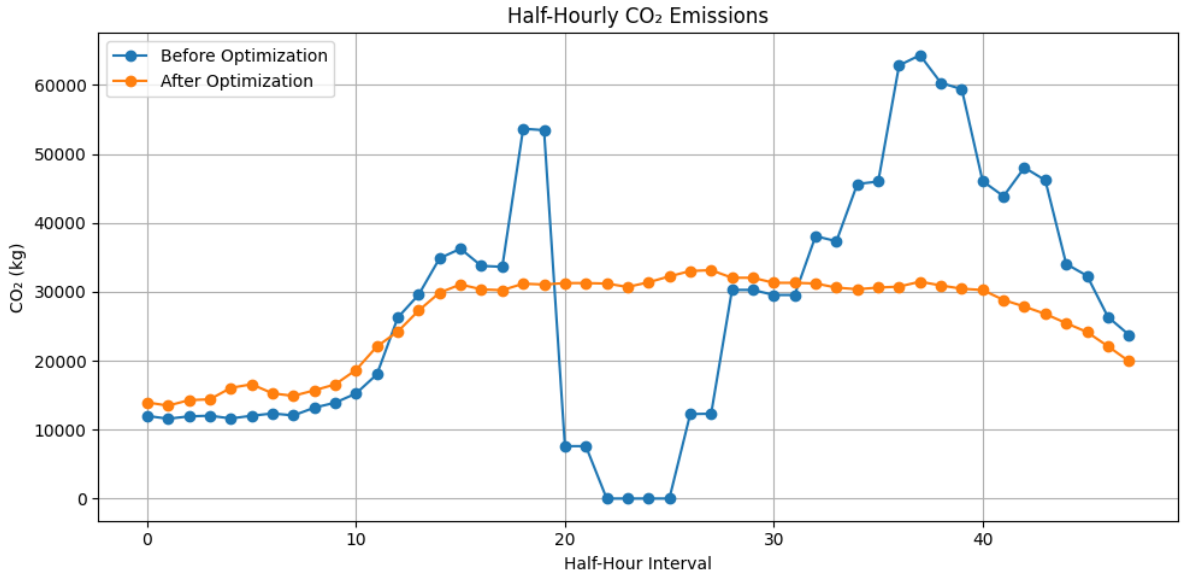


Figure 6-24. Half-hourly distribution of carbon emissions on 11th December under Scenario I & Scenario II with full PV installation capacity (4 kWp). The total daily carbon emissions of the community grid were 1331128.40 kg before optimization and decreased to 1259556.52 kg after optimized V2G scheduling.

For Scenario III, under the boundary parameter configuration with low bidirectional transfer power and limited EV battery capacity, the simulation results reveal a substantial shift in annual carbon emissions. Specifically, the estimated emissions decreased from 301469191.40 kg prior to optimization to -335241648.60 kg after optimization, representing an almost twofold increase in net "carbon absorption" compared to Scenarios I and II. This outcome highlights that, in the absence of additional charging loads from EVs, implementing V2G scheduling solely through idle EVs to achieve load-balance control yields superior results in both economic efficiency and carbon performance.

Taken together, these findings provide strong evidence that V2G scheduling based on the principle of maintaining power load balance constitutes an effective strategy for improving both the economic and environmental performance of community grids. In contrast, optimization approaches that prioritize either cost minimization or carbon reduction in isolation are less effective. This is largely due to the inherent volatility and irregularity of both tariff structures and carbon intensity profiles, which create trade-offs between objectives. A more comprehensive analysis could explore these trade-offs on a Pareto-optimal front, providing insight into the simultaneous optimization of economic and environmental outcomes—a potential avenue for future research. The boundary-parameter-based V2G framework therefore demonstrates its robustness by simultaneously safeguarding load stability while delivering tangible improvements in cost efficiency and carbon emissions reduction.

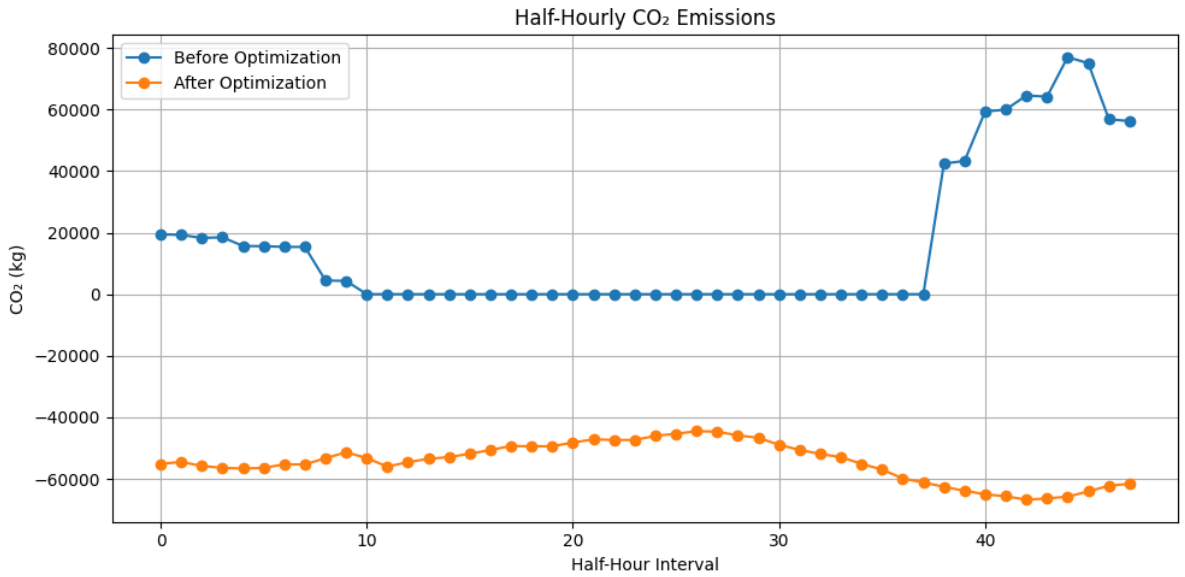


Figure 6-25. Half-hourly distribution of carbon emissions on 21st June under Scenario III with full PV installation capacity (4 kWp; EV ownership = 35%). The total daily carbon emissions of the community grid were 745226.07 kg before optimization and decreased to -2615966.51 kg after optimized V2G scheduling.

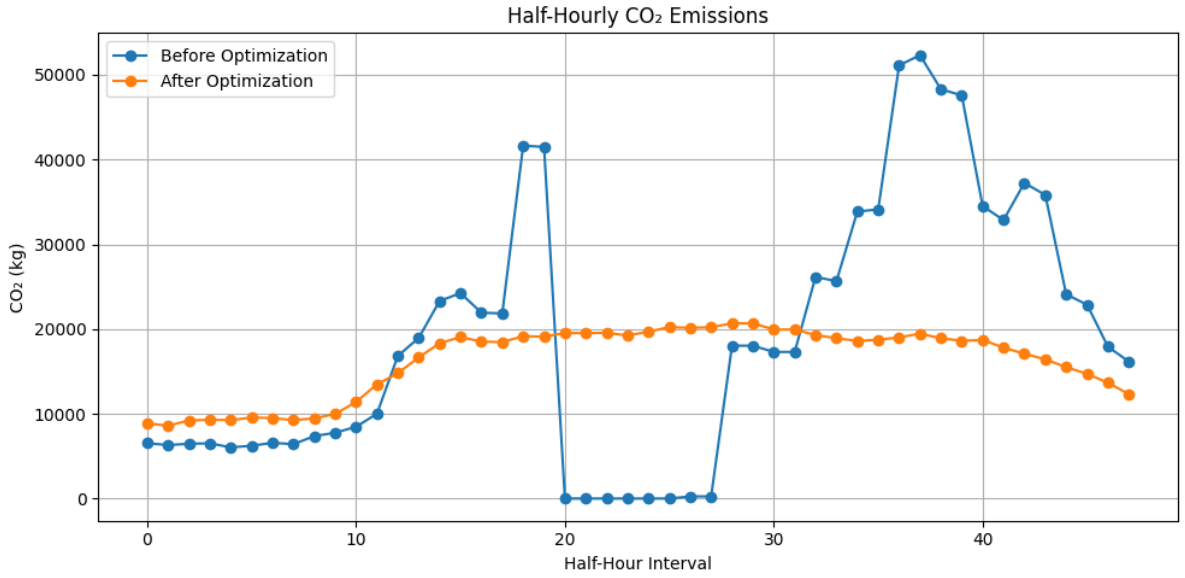


Figure 6-26. Half-hourly distribution of carbon emissions on 11th December under Scenario III with full PV installation capacity (4 kWp). The total daily carbon emissions of the community grid were 906659.91 kg before optimization and decreased to 779025.97 kg after optimized V2G scheduling.

6.3.2.3. Carbon Intensity under Optimal EV Parameter Configurations within the Current Market and Grid Environment

Under Scenarios I and II, when adopting the optimal EV parameter configurations that align with the current EV market and grid environment, the resulting patterns of carbon intensity exhibit a similar trend to that observed in the economic analysis of Section 6.2. Owing to the equivalent scaling method applied in the simulations, the overall charging demand of EVs was significantly amplified, which directly led to an increase in the total carbon emissions compared to the baseline scenario characterized by low bidirectional charging power and limited battery capacity.

More specifically, on the representative summer day, the total daily carbon emissions prior to optimization increased by 25.54% relative to the low-parameter baseline, while the post-optimization value increased by 26.45%. Similarly, on the representative winter day, pre-optimization daily emissions rose by 30.67%, and post-optimization emissions rose by 36.14% under the amplified EV parameters. On an annual scale, the estimated carbon emissions shifted from the previously observed net negative value of -144858765.5 kg to a positive 37328217.85 kg after optimization. This finding reinforces the conclusion drawn from the economic evaluation that, within a comprehensive S-G-L-S grid configuration that fully incorporates EV energy consumption, increasing both the bidirectional transfer power and battery capacity to maximize EV scheduling efficiency may inadvertently compromise both economic performance and carbon reduction effectiveness. This is primarily because larger battery capacities and higher bidirectional power influence EV charging behaviour—reducing external charging and shifting more energy consumption into the community grid—thereby increasing the total electricity demand within the local network.

In contrast, for Scenario III, the situation is fundamentally different. Since the community grid in this scenario only involves power demand from residential users and generation from PV installations, EVs do not contribute directly to the overall load balance. Consequently, adjustments to EV scheduling parameters do not influence the actual power distribution within the grid. As a result, the total and time-varying carbon emissions remain fully consistent with the outcomes previously illustrated in Figures 6-25 and 6-26, confirming that in the absence of EV charging loads, parameter variations have no substantive impact on the carbon intensity of the community grid.

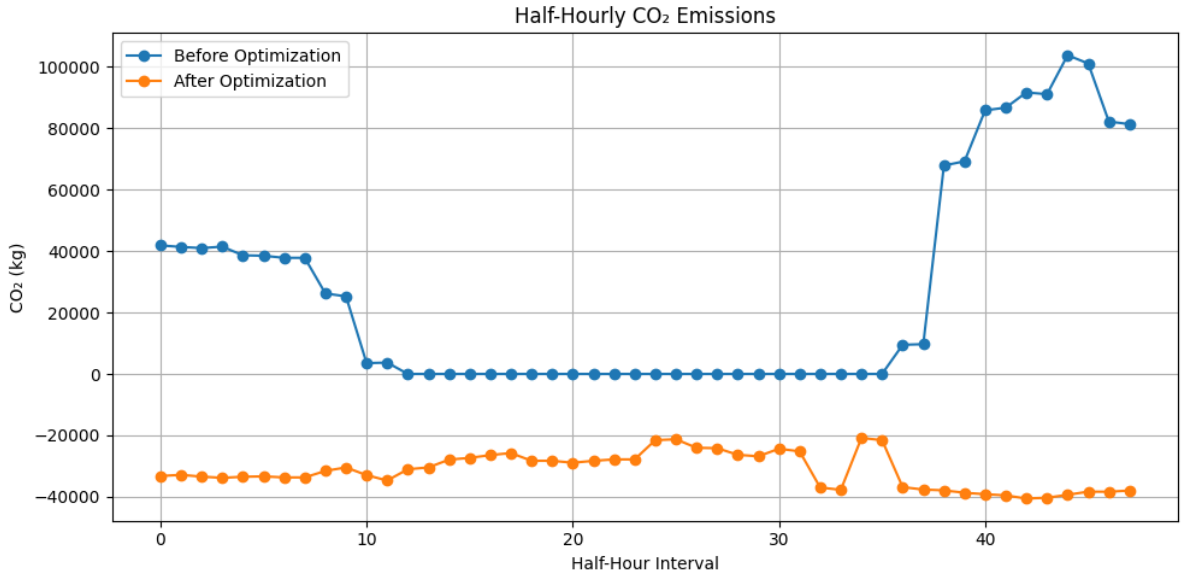


Figure 6-27. Half-hourly distribution of carbon emissions on 21st June under Scenario I & Scenario II with full PV installation capacity (4 kWp). All other parameters remain consistent with the baseline configuration (battery capacity = 82.5 kWh; charging power = 10 kW; discharging power = 7 kW; EV ownership = 100%; idle rate = 15%; average hourly charging demand = 0.20455 kWh). The total daily carbon emissions of the community grid were 1256354.29 kg before optimization and decreased to -1510252.62 kg after optimized V2G scheduling.

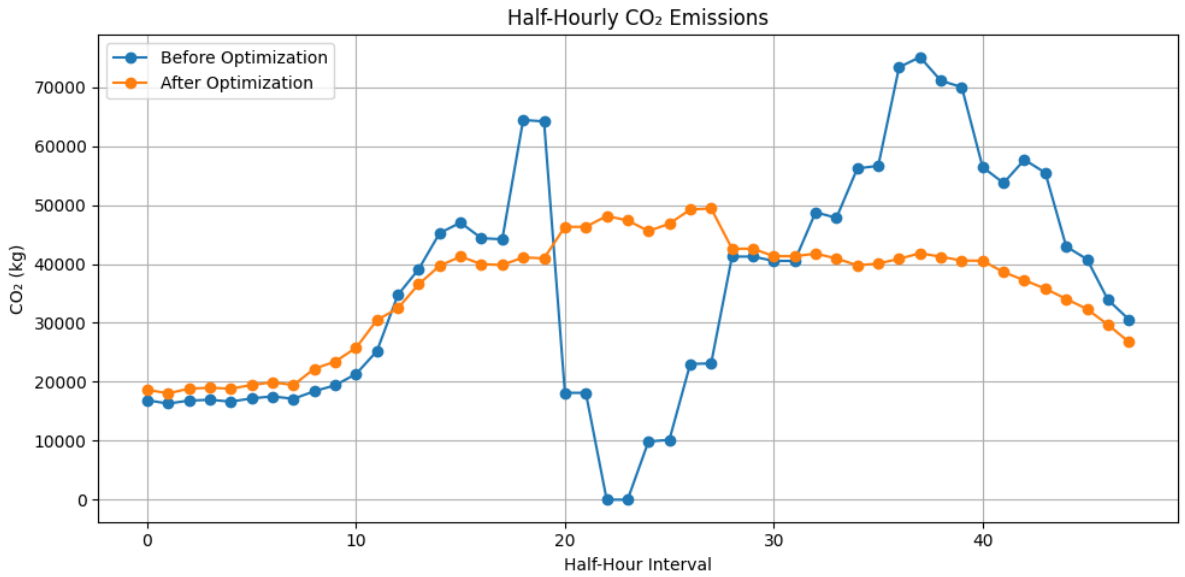


Figure 6-28. Half-hourly distribution of carbon emissions on 11th December under Scenario I & Scenario II with full PV installation capacity (4 kWp). The total daily carbon emissions of the community grid were 1739441.73 kg before optimization and decreased to 1714790.80 kg after optimized V2G scheduling.

6.4. Conclusion

In conclusion, the findings of this chapter demonstrate that the proposed V2G management framework not only achieves its fundamental objective of maintaining power load equilibrium, but also delivers substantial improvements in both economic performance and carbon reduction. This confirms the comprehensive optimization potential of the strategy. Building upon the parameter configurations of community grids and EVs established in Chapter 5, this chapter employed representative summer and winter days as case studies to evaluate the performance of the V2G optimization logic in terms of cost efficiency and carbon intensity. These daily assessments were further extended to annual estimates, enabling a holistic evaluation of the long-term implications of the proposed approach.

The results show that, within a grid environment equipped with full PV installation capacity, adopting the boundary parameter configurations defined in Chapter 5 for achieving load

equilibrium can reduce annual community electricity costs by more than 50% compared with the unoptimized baseline. Furthermore, under a V2G scheduling mode that excludes EV charging loads, the potential savings increase to as much as 76.8%. With respect to environmental outcomes, the analysis suggests that the community grid can in some cases achieve net-zero or even net-negative annual carbon emissions, thereby not only offsetting its own emissions but also contributing to broader system-level decarbonization through reverse power delivery to the upstream grid.

To reach these conclusions, the chapter first examined the temporal patterns of electricity tariffs and carbon intensity, highlighting the inherent volatility of both parameters and their influence on the effectiveness of V2G optimization. The analysis of half-hourly distributions on representative days provided insights into how tariff fluctuations and carbon intensity variability shape the realized benefits of the scheduling logic. The chapter then identified and tested the key factors affecting economic and environmental performance, quantifying their impacts under different boundary conditions. Special attention was given to two boundary cases: one based on low bidirectional transmission power and small EV battery capacity, and another reflecting optimal parameter values aligned with current market-acceptable EV configurations. Both cases were evaluated across daily and annual horizons, consistently confirming the ability of the proposed V2G strategy to deliver significant reductions in cost and carbon emissions when aligned with load-balancing principles.

In addition, from an economic perspective, the chapter examined the two dominant tariff structures in current electricity markets—time-of-use (ToU) pricing and real-time pricing (RTP). By analysing their respective characteristics, the study proposed methods for anticipating cost trends from real-time data to guide V2G scheduling decisions. This enables the formulation of dispatching strategies explicitly oriented toward economic optimization, thereby providing practical support for the development of V2G management models that

prioritize cost-effectiveness while maintaining alignment with broader grid decarbonization objectives.

Overall, this chapter underscores the dual value of the proposed V2G management framework in simultaneously addressing grid stability, economic efficiency, and carbon reduction. By demonstrating both the feasibility and scalability of the optimization strategy under realistic community grid configurations, the results provide a robust foundation for advancing V2G as a critical component of future low-carbon energy systems.

CHAPTER 7. DISCUSSION AND CONCLUSIONS

7.1. Introduction

This chapter summarises the main findings of the research and reflects on their implications. The study developed and evaluated a centralized V2G management strategy for community-scale, net-zero-oriented distribution networks in the UK, with particular emphasis on utilizing the storage capacity of idle EVs. The proposed approach addresses a key limitation in conventional S-G-L-S microgrid configurations, which typically assume uniform EV usage patterns and therefore fail to capture the behavioural diversity of EV users. Such simplifications limit the scalability of traditional V2G strategies when applied to larger community-level systems.

To address this issue, a centralized scheduling model was developed to coordinate EV charging and discharging within a community grid. By integrating EVs with low-rate bidirectional power exchange into a coordinated control framework, the model aims to support load balancing and mitigate peak grid stress. Simulation results presented in earlier chapters indicate that the scheduling strategy can maintain grid power balance under varying operational scenarios while reducing the required level of EV participation under favourable operating conditions.

Beyond technical feasibility, the research also examined the potential economic and environmental benefits of coordinated V2G scheduling. The results suggest that improved utilisation of locally generated PV energy can contribute to both electricity cost reduction and lower carbon emissions at the community level. By enabling local absorption and temporally coordinated release of surplus PV generation, the proposed strategy may also reduce reliance on upstream grid infrastructure and support broader decarbonisation objectives.

Despite these promising outcomes, several methodological limitations remain. The modelling framework relies on hourly resolution input data, which restricts the ability to capture short-term fluctuations in demand and PV generation. In addition, dynamic electricity pricing, demand response mechanisms, and battery degradation effects are not explicitly considered. Addressing these aspects will be important for improving the robustness and practical applicability of future V2G scheduling models.

The remainder of this chapter is structured as follows. Section 7.2 discusses the operational behaviour and performance of the proposed V2G scheduling strategy. Section 7.3 summarises the main contributions of the research. Section 7.4 outlines key limitations of the study, and Section 7.5 identifies directions for future work.

7.2. Summary of Findings

This research, grounded in real-world data from a UK zero-carbon-oriented community grid and an empirically based EV usage model, developed a centralized V2G management algorithm designed to harness the storage potential of idle EVs and achieve extreme balance in community power load distribution.

In the preliminary stage of this research, a detailed analysis was conducted on the temporal distribution of power demand within UK community grids alongside the behavioural patterns of EV usage, in order to establish the foundational scheduling logic for the proposed V2G optimization framework. Using as a baseline a representative community of 500 households, each equipped with rooftop PV systems of 4 kWp installed capacity, the residential demand profile generally increased over the day, with a modest morning peak and a pronounced evening peak between 18:00 and 21:00. Daily electricity consumption within this community typically ranged from 50 kW to 200 kW. Seasonal variations further amplified these fluctuations: during winter, the peak-to-valley difference in daily demand reached as high as 155 kW, with evening

peaks nearly four times greater than the lowest off-peak load. When overlaid with PV generation curves, however, the community grid frequently exhibited negative net loads during daylight hours between 06:00 and 18:00, particularly in high-yielding seasons. On the summer solstice, for example, the maximum net power export reached approximately 491.67 kW, highlighting the community's significant potential to feed surplus energy back into the upstream grid. In parallel, EV usage behaviour was characterized using an empirical EV database, from which an average per-vehicle charging load curve was derived. This analysis confirmed a clear temporal correlation between EV charging demand and household consumption patterns, while also identifying an average daily energy consumption of 0.20455 kWh per vehicle. These insights provided the essential parameters for the design of the V2G optimization logic, ensuring that the proposed scheduling framework was not only technically grounded in real load and generation dynamics, but also aligned with practical EV user behaviour.

By defining grid balancing parameters according to the temporal characteristics of household demand, PV generation, and EV charging requirements, the algorithm enables the realization of load equilibrium within a 24-hour cycle through three tailored scheduling strategies. Based on a community grid model with strong zero-carbon development potential (assuming full PV installation capacity of 4 kWp), this study further identified the boundary conditions of EV parameter configurations required to achieve extreme load balancing under different scheduling scenarios. For Scenario I, which prioritizes active EVs with idle EVs as auxiliary resources, and Scenario II, which avoids interference with active EV charging by relying solely on idle EVs, the results show that with modest EV parameters—bi-directional charging/discharging power of 3.3 kW and battery capacity of 24 kWh—grid equilibrium can be attained when the EV ownership rate reaches 100% and the idle rate exceeds 55%. On the summer solstice, for instance, the system achieved stability by fixing the balancing reference

at –161.64 kW, thereby continuously discharging to the upstream grid, flattening demand peaks, and distributing power more evenly over time. Economically, this reduced annual community electricity costs from £788507.67 to £396061.51, while environmentally, it resulted in an overall net negative annual carbon footprint of –144858765.50 kg, positioning the community grid as a carbon sink for the wider network. These findings demonstrate the robustness of the optimization framework in simultaneously addressing cost efficiency and carbon performance.

When EV configurations were instead based on parameters of commercially available public charging stations—namely, charging power of 10 kW, discharging power of 7 kW, and a battery capacity of 82.5 kWh—the optimal balance was achieved with 100% ownership and only 15% idle EVs. While higher power and capacity reduced the number of EVs required to achieve equilibrium, they also introduced greater energy demand from active EVs due to the amplified driving-related consumption included in the simulation. This led to increased balancing reference values and a heavier economic burden, reflected in a 36.55% reduction in annual electricity costs compared with the baseline, but with pre- and post-optimization costs 27.17% and 60.63% higher, respectively, than those observed under the lower-capacity boundary case. Carbon emissions were also adversely affected: the community grid shifted from a net negative balance of –144858765.50 kg to a positive 37328217.85 kg annually, thereby reducing its carbon absorption potential. These results highlight an important trade-off: while increasing transmission power and battery capacity enhances the scheduling efficiency of EVs, it can simultaneously undermine both economic feasibility and carbon performance.

In contrast, Scenario III—an extreme case where EVs are fully flexible for scheduling—proved to be the most efficient. Under the low-capacity EV configuration (3.3 kW bi-directional power, 24 kWh battery), extreme load balance was already attainable with an ownership rate of just 35%, requiring far fewer EVs compared with Scenarios I and II. Economically, annual electricity costs fell from £563,401.23 to £130,903.61, approximately one-quarter of the

baseline. Environmentally, annual emissions decreased dramatically from 301,469,191.40 kg before optimization to –335,241,648.60 kg after optimization, nearly doubling the community's net carbon absorption relative to Scenarios I and II. Using market-based EV parameters (10 kW charging, 10 kW discharging, 82.5 kWh capacity), extreme balance was achieved with an ownership rate as low as 11%. Notably, because this scheduling strategy does not incorporate any EV charging demand, the economic and carbon outcomes under these conditions remained consistent with those observed in the low-capacity boundary configuration, underscoring the efficiency of idle-EV-centric optimization when unencumbered by active EV charging loads.

7.3. Contributions of Research

The literature review undertaken in this dissertation highlighted a significant gap in existing V2G management strategies. Most prior studies (e.g., Alam et al., 2016; Quammi, 2021) have designed scheduling frameworks within microgrid contexts and have tended to focus on the charging and discharging behaviour of individual EVs. Such approaches, while valuable in localized settings, are fundamentally constrained by the availability of the specific EVs involved. Their capacity to deliver reliable power-load balancing is therefore heavily dependent on user behaviour, which introduces uncertainty and undermines the robustness of the results. Moreover, these microgrid-oriented strategies are inherently limited in scalability. This lack of scalability constitutes a major barrier to the broader deployment of V2G solutions in more advanced grid environments—particularly in zero-carbon community and regional energy systems, as well as in grid models involving large-scale EV clusters—where coordinated and extensible scheduling is essential.

As noted in the introduction, another pressing challenge in the improvement of the UK energy system is the low daily utilisation rate of electric vehicles, particularly household EVs, in their

routine operation (UK Department for Transport, 2022). This underuse translates into a substantial proportion of the fleet remaining idle for extended periods, thereby representing an untapped storage resource. Analysis of the My Electric Avenue database substantiates this observation, indicating that idle EVs consistently account for a significant share of the fleet, with an average daily idle rate of 54.87%. Addressing this underutilisation provided a critical research opportunity: by harnessing the storage potential of idle EVs, it becomes possible to design V2G strategies that are both technically viable and socially scalable.

Against this backdrop, the central contribution of this research lies in the development of a scalable, data-driven centralized V2G scheduling framework specifically designed for UK zero-carbon community grids. The framework is grounded in real residential demand data and empirically observed EV usage patterns, and it is distinguished by its ability to mobilize the short-term storage capacity of large fleets of idle EVs. By integrating this latent capacity into a coordinated optimization process, the proposed strategy achieves extreme load balancing at the community-grid level—something that microgrid-focused, user-dependent models have not been able to deliver. Beyond the theoretical contribution, the staged outputs of the research, from the modelling methodology through to the behavioural simulations and system-level performance analysis, provide valuable insights for both academic research and the practical deployment of smart-grid technologies. Collectively, these contributions not only address the gaps identified in the literature but also advance knowledge on how V2G can be operationalized as a viable component of future community and regional energy systems.

7.3.1. Development of a Representative Community-Scale Grid Model

Another significant contribution of the research is the development of a standardized, community-scale low-carbon energy model, reflective of typical UK apartment communities under net-zero targets. The model integrates realistic household load profiles, rooftop PV

generation (4 kWp per dwelling), and the presence of EVs as mobile storage units. This holistic and modular modelling approach allows for detailed simulation of power flow, load fluctuations, and storage dynamics in a localized energy ecosystem.

The model's structure follows a S-G-L-S architecture, which captures the interconnectedness of supply and demand within decentralized urban energy environments. Its adaptability makes it suitable for replicating or extending to other UK-based low-carbon communities, particularly in the context of pilot microgrids, energy-positive neighbourhoods, or city-scale net-zero initiatives.

Beyond static modelling, the study introduces a behavioural simulation layer that reconstructs individual EV usage profiles using time-stamped driving and charging data, trip distances, and SOC values. This data-driven reconstruction method, which does not rely on high-frequency telemetry, offers a cost-effective yet accurate way to emulate real-world EV behaviour—providing a robust foundation for both academic simulation and commercial application.

7.3.2. Identification and Quantification of Collective EV Behavioural Variables

The study makes a novel methodological contribution by introducing and quantifying several collective behavioural variables that influence grid performance in the presence of V2G assets. These include EV ownership rate, idle rate, average charging intensity, and average bidirectional charging power. By defining mathematical relationships between these variables and the community's net load profile, the research provides a framework to simulate a wide range of future V2G deployment scenarios without the need for extensive real-world experimentation.

This framework allows stakeholders to model different penetration levels, behavioural patterns, and technical constraints, offering a way to stress-test grid performance under various adoption

rates of electric vehicles or renewable generation. Such flexibility is especially valuable in regions where future EV penetration rates are uncertain, or where policy-driven incentives might lead to non-linear adoption curves.

7.3.3. Design and Evaluation of a Centralized V2G Management Strategy

The central innovation of this dissertation lies in the design of a centralized V2G management strategy that dynamically exploits the latent short-term charging and discharging storage potential of idle EVs within the V2G system to perform peak load balancing in a community-scale energy system. By modelling idle EVs as controllable energy storage resources, the proposed strategy overcomes two limitations common in prior V2G schemes (Alam, et.al., 2016; Ma, et.al., 2019): (1) insufficient regulatory capacity to stabilize localized power fluctuations, and (2) lack of reproducibility or scalability due to user behaviour heterogeneity in distributed control models (Kaur, et.al., 2015). Unlike previous approaches, this framework integrates extensive empirical EV usage data—including idle rates and other operational characteristics—into a centralized optimization, enabling coordinated scheduling of EV fleets, particularly idle EVs, without being constrained by fixed individual vehicle operation patterns. This approach is scalable and practically applicable at the community grid level. Moreover, extreme power-load balance reference values are defined at the community level, ensuring optimal peak-load management, rather than relying heavily on the availability of individual vehicles as in prior schemes, whose peak-shaving capability was highly limited.

To demonstrate the efficacy and flexibility of the strategy, three representative simulation scenarios are constructed:

- Scenario I represents a typical high-EV-usage environment, where most vehicles are frequently in motion but exhibit consistent daily patterns.

- Scenario II simulates a low-EV-utilization environment—effectively mimicking the behaviour of a battery swapping station integrated into the V2G system.
- Scenario III explores an extreme idle state, which mirrors the behaviour of a fixed community energy storage unit.

Each scenario is evaluated in terms of its ability to achieve power load flattening, reduce carbon emissions, and offer economic efficiency under real-world constraints. Importantly, Scenario II and III demonstrate that stationary V2G resources—whether idle EVs or swappable batteries—can offer performance on par with dedicated battery energy storage systems, thus supporting cost-effective alternatives to infrastructure-heavy storage investments.

Furthermore, the framework is designed to accommodate asymmetric bidirectional power parameters, allowing for differentiated charging and discharging rates tailored to each EV's battery capacity. This opens the door for personalized V2G configurations in future real-world deployments, especially in car parks containing mixed EV models with varying technical capabilities.

7.3.4. Policy Implications and Practical Significance

Finally, the study delivers a clear and quantifiable message to grid planners and policymakers: even modest V2G participation (up to 11% of idle EVs) using only medium-power configurations (10 kW charging, 7 kW discharging, 82.5 kWh battery capacity) can fully satisfy community-level peak shaving requirements in the simulated environment. This insight is critical for strategic infrastructure planning. It suggests that widespread, high-capacity grid upgrades may not be necessary if intelligent, coordinated V2G strategies are adopted. Moreover, it strengthens the case for policy-driven incentives to encourage idle EV participation, potentially through flexible tariffs, carbon credits, or priority parking schemes.

7.4. Research Limitation

This study proposes a centralized V2G management strategy specifically designed for a UK zero-carbon-oriented community grid environment, focusing on leveraging the flexibility potential of idle EVs to enhance grid power balancing. The approach successfully addresses several critical challenges inherent in existing V2G management frameworks, particularly those related to insufficient regulation capacity—where prior methods fail to adequately meet grid power balancing demands—and issues arising from the heterogeneity in EV usage patterns. Traditional microgrid-based V2G models often lack repeatability and scalability because they assume relatively uniform EV behaviour or rely on fixed usage profiles, limiting their applicability in complex community-scale systems. While this research makes significant progress in overcoming these obstacles, several limitations remain due to data constraints and scope boundaries, which should be carefully considered when interpreting the results.

Firstly, the applicability of the conclusions drawn from this study is inherently linked to the specific community grid context modelled. The simulation environment represents a standard-scale UK apartment community designed with zero-carbon targets in mind. Within this model, electricity consumption patterns exclusively reflect typical apartment household usage, and the PV generation capacity is uniformly set at 4 kWp per household, representing a common specification in UK residential installations. Consequently, the quantitative findings, including the key conclusion that a relatively small number of idle EVs can sufficiently regulate grid power load to maintain operational limits, are directly dependent on this environmental configuration. This context-specific nature implies that the results cannot be indiscriminately generalized to other V2G applications featuring different grid topologies, user behaviours, EV penetration levels, or renewable generation mixes. However, it is important to emphasize that the methodological framework—the core V2G management principles and data processing

approaches developed here—is designed with adaptability in mind. The logic underpinning the exploitation of idle EV flexibility and the corresponding EV usage pattern reconstruction can be extended and tailored to similar regional or community-level grids with centralized V2G architectures. Such flexibility provides a foundation for future research to apply and validate these methods across more diverse and complex settings.

Secondly, the temporal resolution of the input datasets imposes significant constraints on the real-time responsiveness and accuracy of the simulation outcomes. The simulation logic was constructed on Python using historical datasets characterized by relatively coarse sampling frequencies. EV usage data were limited to discrete event reports—charging session start and end times, as well as trip departure and arrival timestamps—recorded with minute-level precision. Community PV generation and household electricity consumption data were aggregated at hourly intervals, while external data streams such as electricity market prices and carbon emission factors were available every 30 minutes. To synchronize these disparate data sources, the simulation was run at an hourly time step, inherently limiting the granularity at which power fluctuations and EV behaviours could be captured. This constraint restricts the ability of the model to fully reflect dynamic, sub-hourly variations that are critical for responsive V2G operation and real-time grid support. Nevertheless, the architecture of the Python-based simulation code is designed to be extensible. Should higher-frequency data become available—for example, with 5 to 10-minute granularity and consistent time alignment across datasets—the current framework can readily incorporate these inputs. This improvement would enable more precise V2G dispatch decisions and enhance the capability to address rapid changes in demand, generation, and EV availability, advancing the model from a retrospective analytical tool to a near-real-time control system suitable for operational deployment in community grids following a S-G-L-S structure.

A further limitation relates to the background datasets used in the case study. The demand and PV generation data representing the community grid were derived by linearly scaling real electricity consumption and centralized PV generation profiles from a standard UK residential community. As a result, the simulated system size—expanded from a smaller empirical dataset to represent a larger community—introduces a degree of uncertainty. In particular, the numerical conclusions presented in this thesis, including specific quantitative estimates of EV participation required for V2G scheduling, may be affected by the assumption of linear scaling when extrapolating from approximately 29 households to a larger community of around 500 homes. In real systems, behavioural diversity, load variability, and PV generation patterns may not scale proportionally, which could influence the precise numerical outcomes reported in this study. Nevertheless, the case study primarily serves to validate the effectiveness of the Python-based V2G scheduling platform and its underlying coordination logic. While the specific numerical values obtained in the simulation should therefore be interpreted with appropriate caution, the functionality and applicability of the proposed platform are not dependent on this particular dataset. In practical applications, users can replace the background data with historical demand and generation data from their own community grids, allowing the platform to perform context-specific simulations and operational assessments.

Lastly, a notable simplification in this study lies in the uniformity of the EV fleet characteristics used for simulation. The EV dataset is sourced exclusively from a single vehicle model—the 2011 Nissan Leaf, equipped with a 24 kWh battery and a rated charging power of 3.3 kW. This uniformity led to assumptions of consistent battery capacities and fixed charging/discharging power ratings across all simulated EVs, which simplifies the complexity inherent in real-world V2G implementations involving diverse vehicle types. In practical centralized car park V2G systems, vehicle fleets typically include a wide range of battery sizes, charging capabilities, and usage patterns. Applying a uniform charging and discharging strategy in such

heterogeneous environments risks accelerating degradation in smaller capacity batteries, which experience faster SoC fluctuations and thus may cycle more frequently. This could lead to disproportionate wear on these vehicles and reduce overall system reliability. However, the V2G scheduling framework developed here maintains flexibility by allowing charging and discharging power to be scaled proportionally to individual vehicle battery capacities, provided that the hardware supports such modulation. This scalability ensures that the core SoC-based coordination logic remains valid and effective even in heterogeneous fleets, thereby extending the applicability of the proposed management strategy to real-world community V2G deployments with complex, mixed EV populations.

In summary, while this study offers a robust foundation for idle EV-based V2G management within a UK zero-carbon community grid context, further work is needed to address these limitations. Future research should explore validation in a broader range of community types and grid configurations, integrate higher-frequency and more granular data sources to improve temporal responsiveness, and incorporate heterogeneous vehicle datasets to better capture fleet diversity and its implications on V2G control and battery health. Addressing these challenges will be critical to advancing the practical deployment and scalability of centralized V2G systems as part of low-carbon community energy solutions.

7.5. Potential Work Directions

Building on the identified limitations of this study, future research will aim to further enhance the V2G management framework developed in Python, particularly by increasing the temporal resolution of the embedded simulation models. The current model operates on an hourly basis due to the constraints of the available dataset. However, the V2G control environment in real-world applications typically requires finer responsiveness to effectively adapt to fluctuations in grid load and user behaviour. By upgrading the time resolution to 5–10-minute intervals, the

model can more accurately reflect the dynamic nature of EV behaviour, grid demand, and PV generation. This enhancement will improve the fidelity of the simulation results and allow for more realistic evaluations of V2G system performance under various operational scenarios.

Once this time-resolution upgrade is implemented, it will be possible to incorporate a broader range of power distribution scenarios and regional grid states into the simulation. Doing so will enable comprehensive testing of the existing centralized V2G management logic across more diverse environmental conditions and usage configurations. Specifically, it would be valuable to evaluate whether the strategy of leveraging idle EVs for grid balancing can be effectively applied in a wider array of regional community grids, especially those with different levels of renewable integration, EV penetration, or consumption behaviours. This would significantly contribute to understanding the adaptability of the current methodology and validate the feasibility of achieving grid-level power balancing via idle EV coordination in broader, real-world contexts.

Another key direction for future work lies in diversifying the EV dataset used in simulation. This study employed a single-model EV dataset (Nissan Leaf 2011), with fixed battery capacity and symmetrical bi-directional power flow parameters. While this approach provides a simplified foundation for model validation, it does not capture the heterogeneity of electrical parameters of actual EV fleets, particularly in centralized V2G-enabled carparks where vehicles vary widely in terms of battery capacity, charging/discharging rates, and usage profiles. Future models should integrate multiple EV types with individually specified charging and discharging parameters, as well as apply the proportional adjustment method proposed in the limitations section—where bidirectional power limits are scaled according to battery capacity. Such a setup would allow the simulation to optimize V2G contributions on a per-vehicle basis and avoid issues such as battery over-cycling or unequal participation, which are especially important for long-term battery health and user acceptance.

In addition to technical improvements, future research should also address the economic dimension of the proposed V2G framework in greater depth. The current study primarily evaluates performance from a grid-level perspective, using electricity prices to assess macro-level optimization benefits. However, for practical deployment and user adoption, a more granular financial assessment is essential. This includes modelling the economic implications of battery degradation due to frequent V2G cycling, as well as conducting Net Present Value (NPV) analyses to determine the payback period and potential profitability of V2G participation from the EV owner's perspective. Quantifying when and how EV users would break even—or profit—from participating in such a system could play a crucial role in encouraging wider participation and supporting the implementation of centralized V2G strategies in residential communities. These evaluations would also help regulators and grid operators design incentive structures that are economically sustainable and equitable.

Moreover, Scenario II proposed in this study—the integration of battery-swap stations into V2G systems—represents another promising research trajectory. While this approach has yet to gain traction in the UK due to the lack of standardized battery specifications and compatible charging infrastructure, it offers significant potential for centralized energy storage and rapid grid response. Future work could investigate the economic feasibility of developing a standardized battery-swap V2G model and assess its potential to serve as a scalable, infrastructure-efficient alternative in high-density EV environments. Demonstrating the financial and technical viability of this model could support its inclusion in broader community energy management strategies, especially in contexts where traditional EV charging infrastructure faces space or throughput limitations.

Lastly, as hardware-level control systems and secure data communication protocols continue to advance, future iterations of this V2G framework could incorporate higher levels of user autonomy. While the current strategy is based on centralized control for system-wide

optimization, enabling user participation through customizable parameters would increase the flexibility and appeal of the V2G scheme. For instance, EV users could be allowed to define their own upper and lower SoC thresholds for participation, based on personal mobility needs and risk preferences. Additionally, users might choose to participate in V2G operations only when electricity prices or carbon intensity cross specific thresholds, effectively allowing them to engage in micro-level electricity or carbon trading. The development of such a user-centric, market-aware V2G environment could represent a new layer of energy market functionality, bridging centralized control with decentralized user agency.

In summary, the next stage of research should explore both technical and economic refinements to ensure that the centralized V2G strategy is scalable, adaptable, and user-inclusive. By increasing simulation granularity, diversifying EV data inputs, assessing real-world economic feasibility, and incorporating user-level decision-making mechanisms, the proposed V2G framework can evolve into a practical, intelligent, and equitable solution for supporting zero-carbon community grids.

7.6. Conclusion

This doctoral thesis has been devoted to addressing the fundamental challenge that conventional microgrid-oriented V2G systems cannot be directly applied to community- or regional-level grids, where the complexity of EV usage behaviour demands more sophisticated centralized coordination. To overcome this limitation, the research has been grounded in the characteristics of UK-standard zero-carbon community grids and the empirically observed usage patterns of EV fleets, with the aim of developing an optimization and management framework capable of achieving load balance at the regional grid scale. The primary objective was to establish, for a standard UK zero-carbon-oriented community, a V2G control logic that leverages the latent storage potential of idle EVs as its foundational design principle, thereby

enabling the community grid to interact with the upstream network in a stable, largely unidirectional manner—buying or selling electricity at approximately constant hourly power levels throughout the day, rather than fluctuating back and forth in response to internal demand variations.

To achieve this goal, the study employed Python-based modelling to design and implement a centralized V2G optimization algorithm that manages EVs according to specified control conditions. Three distinct scheduling scenarios were formulated to explore different operational logics: Scenario I prioritizes active EVs while supplementing with idle EVs, representing the most common V2G deployment model; Scenario II preserves active EV charging behaviours and relies solely on idle EVs, simulating the feasibility of battery-swapping or idle-fleet models within a community grid; Scenario III represents an extreme condition in which all EVs are treated as idle and fully dispatchable, thereby testing the substitutability of large-scale stationary battery storage within community-level grids. For each of these scenarios, the study systematically explored the boundary parameter configurations required to realize extreme load balancing.

The findings demonstrate that under the current operational conditions of community grids and EV usage patterns—specifically, bi-directional charging/discharging power of 3.3 kW, battery capacity of 24 kWh, 100% EV ownership, and an idle rate of 54.87%—the proposed V2G scheduling framework successfully achieves extreme load balance within the community grid. In terms of economic performance and environmental impact, Scenarios I and II yielded a 49.78% reduction in annual electricity costs after optimization, while the community achieved a net negative annual carbon footprint, underscoring the robustness of the framework with respect to both cost-efficiency and carbon emissions reduction. Moreover, by examining EV configurations that align with prevailing market standards, such as charging power of 10 kW, discharging power of 7 kW, and a battery capacity of 82.5 kWh, the study identified boundary

conditions under which scheduling efficiency is maximized—for instance, with 100% EV ownership and a reduced idle rate of 15%. However, while these enhanced configurations improved the efficiency of V2G scheduling, they also diminished overall community-level benefits in terms of economic performance and carbon mitigation, thereby highlighting the inherent trade-offs between maximizing EV utilization and optimizing grid-level outcomes.

Beyond its immediate empirical findings, this research makes a broader contribution to the field by addressing a critical limitation in existing V2G control strategies: the absence of scalable, data-driven frameworks tailored to the operational dynamics of UK community-level grids. The proposed approach not only resolves this gap but also establishes a flexible and extensible model that can inform both future academic inquiries and the practical deployment of intelligent grid systems. Ultimately, the results provide compelling evidence for the feasibility of leveraging idle EVs to achieve power-load balance in centralized V2G systems, while also laying a robust foundation for subsequent research into regional-scale grids and advanced V2G control logics.

REFERENCE

April 2022. Electric Vehicle Charging Research Survey with Electric Vehicle Drivers - Research report. UK Department for Transport

January 2023. Electric Vehicle Smart Charging Action Plan - Affordable, Sustainable Power for Electric Vehicles. UK Department for Business, Energy & Industrial Strategy.

Abdallah, A. & Shen, X. S. 2017. Lightweight Authentication and Privacy-Preserving Scheme for V2G Connections. *IEEE transactions on vehicular technology,* 66**,** 2615-2629.

Abdulaal, A., Cintuglu, M. H., Asfour, S. & Mohammed, O. A. 2016. Solving the multivariant EV routing problem incorporating V2G and G2V options. *IEEE Transactions on Transportation Electrification,* 3**,** 238-248.

Abubakr, H., Lashab, A., Vasquez, J. C., Mohamed, T. H. & Guerrero, J. M. 2023. Novel V2G regulation scheme using Dual-PSS for PV islanded microgrid. *Applied energy,* 340**,** 121012.

Adnan, M., Ali, M., Basalamah, A. & Tariq, M. 2019. Preventing cascading failure through fuzzy co-operative control mechanism using V2G. *IEEE Access,* 7**,** 142607-142622.

Aggarwal, S., Kumar, N. & Gope, P. 2021. An Efficient Blockchain-Based Authentication Scheme for Energy-Trading in V2G Networks. *IEEE transactions on industrial informatics,* 17**,** 6971-6980.

Ahmadi, S. E., Kazemi-Razi, S. M., Marzband, M., Ikpehai, A. & Abusorrah, A. 2023. Multi-objective stochastic techno-economic-environmental optimization of distribution networks with G2V and V2G systems. *Electric Power Systems Research,* 218**,** 109195.

Ahmadian, A., Sedghi, M., Mohammadi-ivatloo, B., Elkamel, A., Aliakbar Golkar, M. & Fowler, M. 2018. Cost-Benefit Analysis of V2G Implementation in Distribution Networks Considering PEVs Battery Degradation. *IEEE transactions on sustainable energy,* 9**,** 961-970.

Ahmed, S., Shamshad, S., Ghaffar, Z., Mahmood, K., Kumar, N., Parizi, R. M. & Choo, K.-K. R. 2021. Signcryption Based Authenticated and Key Exchange Protocol for EI-Based V2G Environment. *IEEE transactions on smart grid,* 12**,** 5290-5298.

Alahyari, A., Fotuhi-Firuzabad, M. & Rastegar, M. 2014. Incorporating customer reliability cost in PEV charge scheduling schemes considering vehicle-to-home capability. *IEEE Transactions on Vehicular Technology,* 64**,** 2783-2791.

Alam, M. J. E., Muttaqi, K. M. & Sutanto, D. 2015. Effective utilization of available PEV battery capacity for mitigation of solar PV impact and grid support with integrated V2G functionality. *IEEE Transactions on Smart Grid,* 7**,** 1562-1571.

Alharbi, A. M., Ali, Z. M., & Diab, A. A. Z. (2025). Comparative techno-economic optimization of microgrid configurations using hybrid battery-hydrogen storage: NEOM case study, Saudi Arabia. *PLOS ONE, 20*(9), e0326050.

Almyaly, A. H. 2019. An Investigation of the DC Charging System and Electric Vehicle in Relation To Autonomous Distributed V2G Implementation. *Journal of physics. Conference series,* 1362**,** 12131.

Al-obaidi, A. & Farag, H. E. Z. 2024. Optimal Design of V2G Incentives and V2G-Capable Electric Vehicles Parking Lots Considering Cost-Benefit Financial Analysis and User Participation. *IEEE transactions on sustainable energy,* 15**,** 1-12.

Alsafran, A. S. 2023. A Feasibility Study of Implementing IEEE 1547 and IEEE 2030 Standards for Microgrid in the Kingdom of Saudi Arabia. *Energies,* 16**,** 1777.

Aluisio, B., Conserva, A., Dicorato, M., Forte, G. & Trovato, M. 2017. Optimal operation planning of V2G-equipped Microgrid in the presence of EV aggregator. *Electric power systems research,* 152**,** 295-305.

Amertet, S. & Gebresenbet, G. 2024. Hybridized Renewable Energy for Smart Vehicle-to-Grid (V2G) Systems. *Energy exploration & exploitation,* 42**,** 292-308.

Amin, A. & Mourshed, M. 2024. Community stochastic domestic electricity forecasting. *Applied Energy,* 355**,** 122342.

Andersen, P. B., Toghroljerdi, S. H., Sousa, T., Soerensen, T. M., Noel, L. & Christensen, B. 2019. The Parker Project: Cross-Brand Service Testing Using V2G. *World electric vehicle journal,* 10**,** 66.

Augello, A., Gallo, P., Sanseverino, E. R., Sciabica, G. & Sciumè, G. 2023. Certifying battery usage for V2G and second life with a blockchain-based framework. *Computer Networks,* 222**,** 109558.

Bai, X. & Qiao, W. 2015. Robust Optimization for Bidirectional Dispatch Coordination of Large-Scale V2G. *IEEE transactions on smart grid,* 6**,** 1944-1954.

Bai, X., Qiao, W., Wei, H., Huang, F. & Chen, Y. 2015. Bidirectional coordinating dispatch of large-scale V2G in a future smart grid using complementarity optimization. *International Journal of Electrical Power & Energy Systems,* 68**,** 269-277.

Banda, M. K., Madichetty, S. & Nandavaram Banda, S. K. 2023. Implementation of Deep Learning-Based Bi-Directional DC-DC Converter for V2V and V2G Applications—An Experimental Investigation. *Energies (Basel),* 16**,** 7614.

Bansal, G., Naren, N., Chamola, V., Sikdar, B., Kumar, N. & Guizani, M. 2020. Lightweight Mutual Authentication Protocol for V2G Using Physical Unclonable Function. *IEEE transactions on vehicular technology,* 69**,** 7234-7246.

Battistelli, C., Baringo, L. & Conejo, A. J. 2012. Optimal energy management of small electric energy systems including V2G facilities and renewable energy sources. *Electric Power Systems Research,* 92**,** 50-59.

Bhoir, S., Caliandro, P. & Brivio, C. 2021. Impact of V2G service provision on battery life. *Journal of energy storage,* 44**,** 103178.

Bi, Y., Wu, C., Xu, J., Li, H., Wang, Y., Shu, G. & Soeiro, T. B. 2023. An Integrated Power Decoupling Method for Single-Phase EV Onboard Charger in V2G Application. *IEEE transactions on power electronics,* 38**,** 1-11.

Bibak, B. & Tekiner-Moğulkoç, H. 2021. A comprehensive analysis of Vehicle to Grid (V2G) systems and scholarly literature on the application of such systems. *Renewable Energy Focus,* 36**,** 1-20.

Bishop, J. D., Axon, C. J., Bonilla, D., Tran, M., Banister, D. & McCulloch, M. D. 2013. Evaluating the impact of V2G services on the degradation of batteries in PHEV and EV. *Applied energy,* 111**,** 206-218.

Blei, D. M. & Lafferty, J. D. Dynamic topic models. Proceedings of the 23rd international conference on Machine learning, 2006. 113-120.

BloombergNEF. 2023. Lithium-ion battery pack prices fall to record low. https://about.bnef.com/blog/lithium-ion-battery-pack-prices-fall-to-record-low/

Board, A., Sun, Y., Huang, P. & Xu, T. 2024. Community-to-vehicle-to-community (C2V2C) for inter-community electricity delivery and sharing via electric vehicle: Performance evaluation and robustness analysis. *Applied Energy,* 363**,** 123054.

Bodo, N., Levi, E., Subotic, I., Espina, J., Empringham, L. & Johnson, C. M. 2016. Efficiency evaluation of fully integrated on-board EV battery chargers With nine-phase machines.

Braeken, A. & Touhafi, A. 2018. AAA-autonomous anonymous user authentication and its application in V2G. *Concurrency and Computation: Practice and Experience,* 30**,** e4303.

Buja, G., Bertoluzzo, M. & Fontana, C. 2017. Reactive power compensation capabilities of V2G-enabled electric vehicles. *IEEE transactions on power electronics,* 32**,** 9447-9459.

Carbon Intensity, A. P. I., Environmental Défense Fund, E., University of Oxford, D. o. C. S. & Wwf 2019. 2019 Real-Time Carbon Intensity of the Electricity System in Great Britain.

Çelik, D. & Meral, M. E. 2022. A coordinated virtual impedance control scheme for three phase four leg inverters of electric vehicle to grid (V2G). *Energy (Oxford),* 246**,** 123354.

CHAdeMO Association 2018. CHAdeMO Protocol: DC Quick Charging for EVs. Tokyo: CHAdeMO Association.

Chamola, V., Sancheti, A., Chakravarty, S., Kumar, N. & Guizani, M. 2020. An IoT and Edge Computing Based Framework for Charge Scheduling and EV Selection in V2G Systems. *IEEE transactions on vehicular technology,* 69**,** 10569-10580.

Chandra Mouli, G. R., Kefayati, M., Baldick, R. & Bauer, P. 2019. Integrated PV Charging of EV Fleet Based on Energy Prices, V2G, and Offer of Reserves. *IEEE transactions on smart grid,* 10**,** 1313-1325.

Chen, H.-C. & Huang, B.-W. 2021. Integrated G2V/V2G Switched Reluctance Motor Drive With Sensing Only Switch-Bus Current. *IEEE transactions on power electronics,* 36**,** 9372-9381.

Chen, P., Han, L., Xin, G., Zhang, A., Ren, H. & Wang, F. 2023. Game Theory Based Optimal Pricing Strategy for V2G Participating in Demand Response. *IEEE transactions on industry applications,* 59**,** 1-13.

Chen, Y., Zhao, Y. & Yiu, S. 2024. Cyber-Physical Authentication Scheme for Secure V2G Transactions. *arXiv preprint arXiv:2409.14008*.

Child, M., Nordling, A. & Breyer, C. 2018. The Impacts of High V2G Participation in a 100% Renewable angstrom land Energy System. *Energies (Basel),* 11.

Chukwu, U. C. & Mahajan, S. M. V2G electric power capacity estimation and ancillary service market evaluation. 2011 IEEE Power and Energy Society General Meeting, 2011. IEEE, 1-8.

Chukwu, U. C. & Mahajan, S. M. 2013. Real-time management of power systems with V2G facility for smart-grid applications. *IEEE Transactions on Sustainable Energy,* 5**,** 558-566.

Chukwu, U. C. & Mahajan, S. M. 2013. V2G parking lot with PV rooftop for capacity enhancement of a distribution system. *IEEE Transactions on Sustainable Energy,* 5**,** 119-127.

Commission, I. E. 2014. IEC 61851-24: Electric vehicle conductive charging system – Part 24: Digital communication between a d.c. EV charging station and an electric vehicle for control of d.c. charging. Geneva, Switzerland: IEC.

Cornélusse, B., Savelli, I., Paoletti, S., Giannitrapani, A., & Vicino, A. 2019. A community microgrid architecture with an internal local market. *Applied Energy, 242*, 547–560.

Dagdougui, H., Ouammi, A. & Dessaint, L. A. 2018. Peak load reduction in a smart building integrating microgrid and V2B-based demand response scheme. *IEEE Systems Journal,* 13**,** 3274-3282.

Dai, S., Gao, F., Guan, X., Yan, C.-B., Liu, K., Dong, J. & Yang, L. 2020. Robust energy management for a corporate energy system with shift-working V2G. *IEEE Transactions on Automation Science and Engineering,* 18**,** 650-667.

Das, D., Weise, N., Basu, K., Baranwal, R. & Mohan, N. 2019. A Bidirectional Soft-Switched DAB-Based Single-Stage Three-Phase AC-DC Converter for V2G Application. *IEEE transactions on transportation electrification,* 5**,** 186-199.

Datta, U., Saiprasad, N., Kalam, A., Shi, J. & Zayegh, A. 2019. A price-regulated electric vehicle charge-discharge strategy for G2V, V2H, and V2G. *International journal of energy research,* 43**,** 1032-1042.

De Los Ríos, A., Goentzel, J., Nordstrom, K. E. & Siegert, C. W. Economic analysis of vehicle-to-grid (V2G)-enabled fleets participating in the regulation service market. 2012 IEEE PES Innovative Smart Grid Technologies (ISGT), 2012. IEEE, 1-8.

Debbarma, S. & Shrivastwa, R. 2019. Grid Frequency Support From V2G Aggregators and HVdc Links in Presence of Nonsynchronous Units. *IEEE systems journal,* 13**,** 1757-1766.

Department for Transport. 2021. Transport decarbonisation plan. UK Government. https://www.gov.uk/government/publications/transport-decarbonisation-plan

Department for Transport. 2023. Transport and environment statistics 2023. UK Government. https://www.gov.uk/government/statistics/transport-and-environment-statistics-2023

Department for Transport. 2023. Vehicle licensing statistics 2023. UK Government. https://www.gov.uk/government/statistics/vehicle-licensing-statistics-2023

Dik, A., Omer, S. & Boukhanouf, R. 2022. Electric Vehicles: V2G for Rapid, Safe, and Green EV Penetration. *Energies (Basel),* 15**,** 803.

Dinh Thai, H., Ping, W., Niyato, D. & Hossain, E. 2017. Charging and Discharging of Plug-In Electric Vehicles (PEVs) in Vehicle-to-Grid (V2G) Systems: A Cyber Insurance-Based Model. *IEEE access,* 5**,** 732-754.

Dong, J., Yassine, A., Armitage, A. & Hossain, M. S. 2023. Multi-Agent Reinforcement Learning for Intelligent V2G Integration in Future Transportation Systems. *IEEE transactions on intelligent transportation systems,* 24**,** 1-10.

Doudou, Y., Cherkaoui, A. & Ezziyyani, M. 2023. The Study of an Energy Management Strategy within a Microgrid with Photovoltaic Production of the <> Project in the City of Tangier and Integrating V2G Technology. *Processes,* 11**,** 2090.

Drude, L., Junior, L. C. P. & Rüther, R. 2014. Photovoltaics (PV) and electric vehicle-to-grid (V2G) strategies for peak demand reduction in urban regions in Brazil in a smart grid environment. *Renewable Energy,* 68**,** 443-451.

Ebrahimi, M. & Rastegar, M. 2023. Data-Driven Charging Load Estimation of Behind-the-Meter V2G-Capable EVs. *IEEE transactions on industry applications,* 59**,** 7949-7956.

Eiza, M. H., Shi, Q., Marnerides, A. K., Owens, T. & Ni, Q. 2019. Efficient, Secure, and Privacy-Preserving PMIPv6 Protocol for V2G Networks. *IEEE transactions on vehicular technology,* 68**,** 19-33.

Eltamaly, A. M. 2023. Optimal Dispatch Strategy for Electric Vehicles in V2G Applications. *Smart cities (Basel),* 6**,** 3161-3191.

Erden, F., Kisacikoglu, M. C. & Erdogan, N. 2018. Adaptive V2G Peak Shaving and Smart Charging Control for Grid Integration of PEVs. *Electric power components and systems,* 46**,** 1494-1508.

Escudero-Garzás, J. J., García-Armada, A. & Seco-Granados, G. 2012. Fair design of plug-in electric vehicles aggregator for V2G regulation. *IEEE Transactions on Vehicular Technology,* 61**,** 3406-3419.

European Committee for Electrotechnical Standardization [CENELEC] 2017. Electric vehicle conductive charging system (European implementation of IEC 61851). *EU 61851*.

Faddel, S., Aldeek, A., Al-Awami, A. T., Sortomme, E. & Al-Hamouz, Z. 2018. Ancillary Services Bidding for Uncertain Bidirectional V2G Using Fuzzy Linear Programming. *Energy (Oxford),* 160**,** 986-995.

Fan, P., Ke, S., Yang, J., Li, R., Li, Y., Yang, S., Liang, J., Fan, H. & Li, T. 2023. A load frequency coordinated control strategy for multimicrogrids with V2G based on improved MA-DDPG. *International journal of electrical power & energy systems,* 146**,** 108765.

Fan, P., Yang, J., Ke, S., Wen, Y., Li, Y. & Xie, L. 2023. Load frequency control strategy for islanded multimicrogrids with V2G dependent on learning-based model predictive control. *IET generation, transmission & distribution,* 17**,** 4763-4780.

Fathabadi, H. 2017. Novel wind powered electric vehicle charging station with vehicle-to-grid (V2G) connection capability. *Energy conversion and management,* 136**,** 229-239.

Gamit, M., Shukla, A., Kumar, R. & Verma, K. 2019. Supplementary frequency control in power systems via decentralised V2G/G2V support. *Journal of engineering (Stevenage, England),* 2019**,** 5287-5291.

Gaolei, L., Jun, W., Jianhua, L., Tianpeng, Y. & Morello, R. 2017. Battery Status Sensing Software-Defined Multicast for V2G Regulation in Smart Grid. *IEEE sensors journal,* 17**,** 7838-7848.

Garcés Quílez, M., Abdel-Monem, M., El Baghdadi, M., Yang, Y., Van Mierlo, J. & Hegazy, O. 2018. Modelling, Analysis and Performance Evaluation of Power Conversion Unit in G2V/V2G Application—A Review. *Energies (Basel),* 11**,** 1082.

Garruto, R., Longo, M., Yaïci, W. & Foiadelli, F. 2020. Connecting parking facilities to the electric grid: A vehicle-to-grid feasibility study in a railway station's car park. *Energies,* 13**,** 3083.

Gerding, E. H., Ceppi, S., Stein, S. & Robu, V. Online mechanism design for vehicle-to-grid car parks. Twenty-Fifth International Joint Conference on Artificial Intelligence, 2016. 286-293.

German Institute for Standardization [DIN] 2014. Electromobility – Digital communication between a DC EV charging station and an electric vehicle for control of DC charging in the Combined Charging System. *DIN SPEC 70121*. Berlin: DIN.

Geske, J. & Schumann, D. 2018. Willing to participate in vehicle-to-grid (V2G)? Why not! *Energy Policy,* 120**,** 392-401.

Gholami, Z., Ildarabadi, R., Heydari-Doostabad, H., Monfared, M. & O'Donnell, T. 2024. Bidirectional wide range and high voltage gain buck-boost DC-DC converter for EV chargers empowering V2G-G2V applications. *IET power electronics,* 17**,** 230-250.

Gough, R., Dickerson, C., Rowley, P. & Walsh, C. 2017. Vehicle-to-grid feasibility: A techno-economic analysis of EV-based energy storage. *Applied energy,* 192**,** 12-23.

Guille, C. & Gross, G. Design of a conceptual framework for the V2G implementation. 2008 IEEE Energy 2030 conference, 2008. IEEE, 1-3.

Guille, C. & Gross, G. 2009. A conceptual framework for the vehicle-to-grid (V2G) implementation. *Energy policy,* 37**,** 4379-4390.

Guo, D. & Zhou, C. 2016. Potential performance analysis and future trend prediction of electric vehicle with V2G/V2H/V2B capability. *AIMS Energy,* 4.

Habib, H. U. R., Subramaniam, U., Waqar, A., Farhan, B. S., Kotb, K. M. & Wang, S. 2020. Energy cost optimization of hybrid renewables based V2G microgrid considering multi objective function by using artificial bee colony optimization. *IEEE Access,* 8**,** 62076-62093.

Habib, S. & Kamran, M. A novel vehicle-to-grid technology with constraint analysis-a review. 2014 international conference on emerging technologies (ICET), 2014. IEEE, 69-74.

Haddadian, G., Khalili, N., Khodayar, M. & Shahiedehpour, M. 2015. Security-constrained power generation scheduling with thermal generating units, variable energy resources, and electric vehicle storage for V2G deployment. *International journal of electrical power & energy systems,* 73**,** 498-507.

Han, H.-S., Oh, E. & Son, S.-Y. 2018. Study on EV Charging Peak Reduction with V2G Utilizing Idle Charging Stations: The Jeju Island Case. *Energies (Basel),* 11**,** 1651.

Han, S. & Han, S. 2013. Economic feasibility of V2G frequency regulation in consideration of battery wear. *Energies,* 6**,** 748-765.

Han, S., Han, S. & Sezaki, K. 2011. Estimation of achievable power capacity from plug-in electric vehicles for V2G frequency regulation: Case studies for market participation. *IEEE Transactions on Smart Grid,* 2**,** 632-641.

Han, W. & Xiao, Y. 2016. Privacy preservation for V2G networks in smart grid: A survey. *Computer communications,* 91-92**,** 17-28.

Hao, X., Chen, Y., Wang, H., Wang, H., Meng, Y. & Gu, Q. 2023. A V2G-oriented reinforcement learning framework and empirical study for heterogeneous electric vehicle charging management. *Sustainable cities and society,* 89**,** 104345.

Haque, M. M., Wolfs, P., Alahakoon, S., Sturmberg, B. C. P., Nadarajah, M. & Zare, F. 2022. DAB Converter With Q Capability for BESS/EV Applications to Allow V2H/V2G Services. *IEEE transactions on industry applications,* 58**,** 468-480.

Hassija, V., Chamola, V., Garg, S., Krishna, D. N. G., Kaddoum, G. & Jayakody, D. N. K. 2020. A Blockchain-Based Framework for Lightweight Data Sharing and Energy Trading in V2G Network. *IEEE transactions on vehicular technology,* 69**,** 5799-5812.

He, D., Chan, S. & Guizani, M. 2018. Privacy-friendly and efficient secure communication framework for V2G networks. *IET communications,* 12**,** 304-309.

He, T., Lu, D. D.-C., Wu, M., Yang, Q., Li, T. & Liu, Q. 2020. Four-quadrant operations of bidirectional chargers for electric vehicles in smart car parks: G2V, V2G, and V4G. *Energies,* 14**,** 181.

Heydari-doostabad, H. & O'Donnell, T. 2021. A wide-range high-voltage-gain bidirectional DC–DC converter for V2G and G2V hybrid EV charger. *IEEE Transactions on Industrial Electronics,* 69**,** 4718-4729.

Hoang, D. T., Wang, P., Niyato, D. & Hossain, E. 2017. Charging and discharging of plug-in electric vehicles (PEVs) in vehicle-to-grid (V2G) systems: A cyber insurance-based model. *IEEE Access,* 5**,** 732-754.

Høj, J., Juhl, L. & Lindegaard, S. 2018. V2G—An Economic Gamechanger in E-Mobility? *World electric vehicle journal,* 9**,** 35.

Hosseini, S. S., Badri, A. & Parvania, M. The plug-in electric vehicles for power system applications: The vehicle to grid (V2G) concept. 2012 IEEE International Energy Conference and Exhibition (ENERGYCON), 2012. IEEE, 1101-1106.

Hou, W., Sun, Y., Li, D., Guan, Z. & Liu, J. 2023. Lightweight and Privacy-Preserving Charging Reservation Authentication Protocol for 5G-V2G. *IEEE transactions on vehicular technology,* 72**,** 1-13.

Hsu, Y.-C., Kao, S.-C., Ho, C.-Y., Jhou, P.-H., Lu, M.-Z. & Liaw, C.-M. 2018. On an Electric Scooter With G2V/V2H/V2G and Energy Harvesting Functions. *IEEE transactions on power electronics,* 33**,** 6910-6925.

Hu, J., Ye, C., Ding, Y., Tang, J. & Liu, S. 2022. A Distributed MPC to Exploit Reactive Power V2G for Real-Time Voltage Regulation in Distribution Networks. *IEEE transactions on smart grid,* 13**,** 576-588.

Hu, K.-W., Yi, P.-H. & Liaw, C.-M. 2015. An EV SRM Drive Powered by Battery/Supercapacitor With G2V and V2H/V2G Capabilities. *IEEE transactions on industrial electronics (1982),* 62**,** 4714-4727.

Huang, S. & Wu, Q. 2019. Dynamic Tariff-Subsidy Method for PV and V2G Congestion Management in Distribution Networks. *IEEE transactions on smart grid,* 10**,** 5851-5860.

Huang, Z., Fang, B. & Deng, J. 2020. Multi-objective optimization strategy for distribution network considering V2G-enabled electric vehicles in building integrated energy system. *Protection and control of modern power systems,* 5**,** 1-8.

Huda, M., Koji, T. & Aziz, M. 2020. Techno Economic Analysis of Vehicle to Grid (V2G) Integration as Distributed Energy Resources in Indonesia Power System. *Energies (Basel),* 13**,** 1162.

Huppmann, D., Rogelj, J., Kriegler, E., Krey, V., & Riahi, K. 2018. A new scenario resource for integrated 1.5 °C research. *Nature Climate Change, 8*(12), 1027–1030.

Hussain, M. A., Brandauer, W. & Lee, M. J. 2019. Mobility-aware vehicle-to-grid (V2G) optimization for uniform utilization in smart grid based power distribution network. *Mobile Networks and Applications,* 24**,** 1701-1712.

Hussein, M. M., Mohamed, T. H., Mahmoud, M. M., Aljohania, M., Mosaad, M. I. & Hassan, A. M. 2023. Regulation of multi-area power system load frequency in presence of V2G scheme. *PloS one,* 18**,** e0291463-e0291463.

Inala, K. P., Kumar, P., & Bose, S. K. 2019. Impact of communication systems on grid node voltage and operation of a vehicle-to-grid controller in a smart-grid scenario. *IET Power Electronics, 12*(13), 3499–3509.

International Electrotechnical Commission 2017. Electric vehicle conductive charging system. *IEC 61851*.

International Electrotechnical Commission 2022. Plugs, socket-outlets, vehicle connectors and vehicle inlets – Conductive charging of electric vehicles. *IEC 62196*.

International Electrotechnical Commission [IEC] 2014. Electric vehicle conductive charging system – Part 23: DC electric vehicle charging station. *IEC 61851-23*.

International Organization for Standardization 2019. Road vehicles — Vehicle to grid communication interface. *ISO 15118*.

International Organization for Standardization [ISO] 2022. Road vehicles — Vehicle to grid communication interface — Part 20: 2nd generation network layer and application layer requirements. *ISO 15118-20*.

International, S. 2018. J3068: Electric Vehicle Power Transfer System Using a Three-Phase Capable Coupler. Warrendale, PA: SAE International.

Iqbal, A., Rajasekaran, A. S., Nikhil, G. S. & Azees, M. 2021. A Secure and Decentralized Blockchain Based EV Energy Trading Model Using Smart Contract in V2G Network. *IEEE access,* 9**,** 75761-75777.

Iqbal, S., Xin, A., Jan, M. U., Salman, S., Zaki, A. u. M., Rehman, H. U., Shinwari, M. F., & Abdelbaky, M. A. (2020). V2G Strategy for Primary Frequency Control of an Industrial Microgrid Considering the Charging Station Operator. *Electronics, 9*(4), 549.

Jafari, M., Kavousi-Fard, A., Niknam, T. & Avatefipour, O. 2021. Stochastic synergies of urban transportation system and smart grid in smart cities considering V2G and V2S concepts. *Energy (Oxford),* 215**,** 119054.

Jahnes, M., Zhou, L., Eull, M., Wang, W. & Preindl, M. 2023. Design of a 22-kW Transformerless EV Charger With V2G Capabilities and Peak 99.5% Efficiency. *IEEE transactions on industrial electronics (1982),* 70**,** 5862-5871.

Jiao, R., Zhu, J., Ma, L., Zhao, Y., Zhang, B., Ding, Y., Gong, C. & Yang, S. 2017. Dead-beat instantaneous power control for off-board charger of electric vehicle for V2G application. *International Journal of Hydrogen Energy,* 42**,** 18174-18180.

Jie, B., Baba, J. & Kumada, A. 2024. Contribution to V2G System Frequency Regulation by Charging/Discharging Control of Aggregated EV Group. *IEEE transactions on industry applications,* 60**,** 1-13.

Jung, S., Yoon, M. & Suh, J. 2019. Optimal Frequency Regulation V2G Control with DOD of EV Battery. *International journal of recent technology and engineering,* 8**,** 75-78.

Karfopoulos, E. L. & Hatziargyriou, N. D. 2015. Distributed coordination of electric vehicles providing V2G services. *IEEE Transactions on Power Systems,* 31**,** 329-338.

Karfopoulos, E. L., Panourgias, K. A. & Hatziargyriou, N. D. 2016. Distributed Coordination of Electric Vehicles providing V2G Regulation Services. *IEEE transactions on power systems,* 31**,** 2834-2846.

Kasturi, K., Nayak, C. K. & Nayak, M. R. 2019. Electric vehicles management enabling G2V and V2G in smart distribution system for maximizing profits using MOMVO. *International transactions on electrical energy systems,* 29**,** n/a.

Kaur, K., Dua, A., Jindal, A., Kumar, N., Singh, M. & Vinel, A. 2015. A Novel Resource Reservation Scheme for Mobile PHEVs in V2G Environment Using Game Theoretical Approach. *IEEE transactions on vehicular technology,* 64**,** 5653-5666.

Kaveh, M., Martín, D. & Mosavi, M. R. 2020. A Lightweight Authentication Scheme for V2G Communications: A PUF-Based Approach Ensuring Cyber/Physical Security and Identity/Location Privacy. *Electronics,* 9**,** 1479.

Kavousi-Fard, A., Niknam, T. & Fotuhi-Firuzabad, M. 2015. Stochastic Reconfiguration and Optimal Coordination of V2G Plug-in Electric Vehicles Considering Correlated Wind Power Generation. *IEEE transactions on sustainable energy,* 6**,** 822-830.

Kempton, W., & Tomic, J. (2005). Vehicle-to-grid power fundamentals: Calculating capacity and net revenue. *Journal of Power Sources, 144*(1), 268–279.

Kempton, W., Udo, V., Huber, K., Komara, K., Letendre, S., Baker, S., Brunner, D. & Pearre, N. 2008. A test of vehicle-to-grid (V2G) for energy storage and frequency regulation in the PJM system. *Results from an Industry-University Research Partnership,* 32**,** 1-32.

Kester, J., de Rubens, G. Z., Sovacool, B. K. & Noel, L. 2019. Public perceptions of electric vehicles and vehicle-to-grid (V2G): Insights from a Nordic focus group study. *Transportation Research Part D: Transport and Environment,* 74**,** 277-293.

Kester, J., Noel, L., de Rubens, G. Z. & Sovacool, B. K. 2018. Promoting Vehicle to Grid (V2G) in the Nordic region: Expert advice on policy mechanisms for accelerated diffusion. *Energy Policy,* 116**,** 422-432.

Kester, J., Noel, L., Lin, X., Zarazua de Rubens, G. & Sovacool, B. K. 2019. The coproduction of electric mobility: Selectivity, conformity and fragmentation in the sociotechnical acceptance of vehicle-to-grid (V2G) standards. *Journal of cleaner production,* 207**,** 400-410.

Kester, J., Noel, L., Zarazua de Rubens, G. & Sovacool, B. K. 2018. Promoting Vehicle to Grid (V2G) in the Nordic region: Expert advice on policy mechanisms for accelerated diffusion. *Energy policy,* 116**,** 422-432.

Khalid, H. M., Flitti, F., Muyeen, S. M., Elmoursi, M., Sweidan, T. & Yu, X. 2022. Parameter Estimation of Vehicle Batteries in V2G Systems: An Exogenous Function-Based Approach. *IEEE transactions on industrial electronics (1982),* 69**,** 9535-9546.

Khalid, H. M. & Peng, J. C. H. 2020. Bidirectional Charging in V2G Systems: An In-Cell Variation Analysis of Vehicle Batteries. *IEEE systems journal,* 14**,** 3665-3675.

Khan, S., Mehmood, K., Haider, Z., Bukhari, S., Lee, S.-J., Rafique, M. & Kim, C.-H. 2018. Energy Management Scheme for an EV Smart Charger V2G/G2V Application with an EV Power Allocation Technique and Voltage Regulation. *Applied sciences,* 8**,** 648.

Khooban, M. H. 2021. An Optimal Non-Integer Model Predictive Virtual Inertia Control in Inverter-Based Modern AC Power Grids-Based V2G Technology. *IEEE transactions on energy conversion,* 36**,** 1336-1346.

Kiaee, M., Cruden, A. & Sharkh, S. 2015. Estimation of cost savings from participation of electric vehicles in vehicle to grid (V2G) schemes. *Journal of modern power systems and clean energy,* 3**,** 249-258.

Kim, J., Kim, J. & Jeong, H. 2022. Key Parameters for Economic Valuation of V2G Applied to Ancillary Service: Data-Driven Approach. *Energies (Basel),* 15**,** 8815.

Kisacikoglu, M. C., Kesler, M. & Tolbert, L. M. 2015. Single-Phase On-Board Bidirectional PEV Charger for V2G Reactive Power Operation. *IEEE transactions on smart grid,* 6**,** 767-775.

Kisacikoglu, M. C., Ozpineci, B. & Tolbert, L. M. Examination of a PHEV bidirectional charger system for V2G reactive power compensation. 2010 Twenty-Fifth Annual IEEE Applied Power Electronics Conference and Exposition (APEC), 2010. IEEE, 458-465.

Kisacikoglu, M. C., Ozpineci, B. & Tolbert, L. M. 2013. EV/PHEV bidirectional charger assessment for V2G reactive power operation. *IEEE Transactions on Power Electronics,* 28**,** 5717-5727.

Kolawole, O., & Al-Anbagi, I. 2019. EV battery wear cost optimization for frequency regulation support in a V2G environment. *IEEE Access, 7,* 114641–114652.

Koubaa, R., Yoldas, Y., Goren, S., Krichen, L. & Onen, A. 2021. Implementation of cost benefit analysis of vehicle to grid coupled real Micro-Grid by considering battery energy wear: Practical study case. *Energy & Environment,* 32**,** 1292-1314.

Koufakis, A. M., Rigas, E. S., Bassiliades, N. & Ramchurn, S. D. Towards an optimal EV charging scheduling scheme with V2G and V2V energy transfer. 2016 IEEE International Conference on Smart Grid Communications (SmartGridComm), 6-9 Nov. 2016 2016. 302-307.

Krueger, H. & Cruden, A. 2020. Multi-layer event-based vehicle-to-grid (V2G) scheduling with short term predictive capability within a modular aggregator control structure. *IEEE Transactions on Vehicular Technology,* 69**,** 4727-4739.

Kumar, D. & Saxena, A. R. 2021. A battery integrated three-port bidirectional charger/discharger for light electric vehicles with G2V and V2G power flow capability. *International journal of circuit theory and applications,* 49**,** 2909-2934.

Kumar, K. N., Sivaneasan, B., Cheah, P., So, P. L. & Wang, D. Z. 2013. V2G capacity estimation using dynamic EV scheduling. *IEEE Transactions on Smart Grid,* 5**,** 1051-1060.

Kwon, M. & Choi, S. 2016. An electrolytic capacitorless bidirectional EV charger for V2G and V2H applications. *IEEE Transactions on Power Electronics,* 32**,** 6792-6799.

Lasseter, R., Akhil, A., Marnay, C., Stephens, J., Dagle, J., Guttromson, R., Meliopoulous, A., Yinger, R. & Eto, J. 2002. The CERTS microgrid concept. *White paper for Transmission Reliability Program, Office of Power Technologies, US Department of Energy,* 2**,** 30.

Lee, B.-K., Kim, J.-P., Kim, S.-G. & Lee, J.-Y. 2017. An isolated/bidirectional PWM resonant converter for V2G (H) EV on-board charger. *IEEE Transactions on Vehicular Technology,* 66**,** 7741-7750.

Li, S., Gu, C., Li, J., Wang, H. & Yang, Q. 2021. Boosting Grid Efficiency and Resiliency by Releasing V2G Potentiality Through a Novel Rolling Prediction-Decision Framework and Deep-LSTM Algorithm. *IEEE systems journal,* 15**,** 2562-2570.

Li, S., Li, J., Su, C. & Yang, Q. 2020. Optimization of bi-directional V2G behavior with active battery anti-aging scheduling. *IEEE Access,* 8**,** 11186-11196.

Li, X., Tan, Y., Liu, X., Liao, Q., Sun, B., Cao, G., Li, C., Yang, X. & Wang, Z. 2020. A cost-benefit analysis of V2G electric vehicles supporting peak shaving in Shanghai. *Electric power systems research,* 179**,** 106058.

Li, Y., Zhang, P. & Wang, Y. 2018. The Location Privacy Protection of Electric Vehicles with Differential Privacy in V2G Networks. *Energies (Basel),* 11**,** 2625.

Liao, J.-T., Huang, H.-W., Yang, H.-T. & Li, D. 2021. Decentralized V2G/G2V Scheduling of EV Charging Stations by Considering the Conversion Efficiency of Bidirectional Chargers. *Energies (Basel),* 14**,** 962.

Liu, D., Zeng, X. & Liu, G. 2019. Control method for EV charging and discharging in V2G/V2H scenario based on the synchronvter technology and H∞ repetitive control. *Journal of engineering (Stevenage, England),* 2019**,** 1350-1355.

Liu, D., Zhong, Q., Wang, Y. & Liu, G. 2018. Modeling and control of a V2G charging station based on synchronverter technology. *CSEE Journal of Power and Energy Systems,* 4**,** 326-338.

Liu, H., Ning, H., Zhang, Y., Xiong, Q. & Yang, L. T. 2013. Role-dependent privacy preservation for secure V2G networks in the smart grid. *IEEE Transactions on Information Forensics and Security,* 9**,** 208-220.

Liu, H., Ning, H., Zhang, Y. & Yang, L. T. 2012. Aggregated-proofs based privacy-preserving authentication for V2G networks in the smart grid. *IEEE Transactions on Smart Grid,* 3**,** 1722-1733.

Liu, H., Zhang, Y., Zheng, S. & Li, Y. 2019. Electric Vehicle Power Trading Mechanism Based on Blockchain and Smart Contract in V2G Network. *IEEE access,* 7**,** 160546-160558.

Liu, P., Wang, C., Hu, J., Fu, T., Cheng, N., Zhang, N. & Shen, X. 2020. Joint Route Selection and Charging Discharging Scheduling of EVs in V2G Energy Network. *IEEE transactions on vehicular technology,* 69**,** 10630-10641.

Liu, X. & Liu, H. 2021. Data publication based on differential privacy in V2G network. *Int. J. of Electronics Engineering and Applications,* 9**,** 34-44.

Logan, K. G., Nelson, J. D., Lu, X. & Hastings, A. 2020. UK and China: Will electric vehicle integration meet Paris Agreement Targets? *Transportation Research Interdisciplinary Perspectives,* 8**,** 100245.

Lotfi, S., Sedighizadeh, M., Abbasi, R., & Hosseinian, S. H. (2024). Vehicle-to-grid bidding for regulation and spinning reserve markets: A robust optimal coordinated charging approach. *Energy Reports, 11*, 925–936.

Lund, H. & Kempton, W. 2008. Integration of renewable energy into the transport and electricity sectors through V2G. *Energy policy,* 36**,** 3578-3587.

Luo, Q., Zhou, Y., Hou, W. & Peng, L. 2022. A hierarchical blockchain architecture based V2G market trading system. *Applied Energy,* 307**,** 118167.

Ma, Y., Chen, Y., Chen, X., Deng, F. & Song, X. 2019. Optimal dispatch of hybrid energy islanded microgrid considering V2G under TOU tariffs. 2019 2019 CEDEX A. CEDEX A: E D P Sciences, 2007.

Madawala, U. 2010. A Bidirectional Inductive Power Interface for Electric Vehicles in V2G System. *IEEE TRANSACTIONS ON INDUSTRIAL ELECTRONIC,* 58**,** 2789-2796.

Manzolli, J. A., Trovao, J. P. F. & Antunes, C. H. 2022. Electric bus coordinated charging strategy considering V2G and battery degradation. *Energy,* 254**,** 124252.

Mattos, M. M., Archetti, J. A. G., Bitencourt, L. d. A., Wallberg, A., Castellucci, V., Dias, B. H. & de Oliveira, J. G. 2024. Analysis of voltage control using V2G technology to support low voltage distribution networks. *IET generation, transmission & distribution,* 18**,** 1133-1157.

Mazumder, M. & Debbarma, S. 2021. EV Charging Stations With a Provision of V2G and Voltage Support in a Distribution Network. *IEEE systems journal,* 15**,** 662-671.

McDonald, S. S. 2013. Personal rapid transit and its development. *Transportation technologies for Sustainability***,** 831-850.

Melo, F. C., da Graça, G. C. & Panão, M. J. O. 2023. A review of annual, monthly, and hourly electricity use in buildings. *Energy and Buildings,* 293**,** 113201.

Mendes, P. R. C., Isorna, L. V., Bordons, C. & Normey-Rico, J. E. 2016. Energy management of an experimental microgrid coupled to a V2G system. *Journal of power sources,* 327**,** 702-713.

Mets, K., Verschueren, T., De Turck, F. & Develder, C. Exploiting V2G to optimize residential energy consumption with electrical vehicle (dis) charging. 2011 IEEE first international workshop on smart grid modeling and simulation (SGMS), 2011. IEEE, 7-12.

Metz, M. & Doetsch, C. 2012. Electric vehicles as flexible loads–A simulation approach using empirical mobility data. *Energy,* 48**,** 369-374.

Miglani, A. & Kumar, N. 2023. Blockchain-Based Co-Operative Caching for Secure Content Delivery in CCN-Enabled V2G Networks. *IEEE transactions on vehicular technology,* 72**,** 1-16.

Ming, T., Ota, K. & Mianxiong, D. 2017. Foud: Integrating Fog and Cloud for 5G-Enabled V2G Networks. *IEEE network,* 31**,** 8-13.

Ming, Z., Supeng, L., Maharjan, S., Gjessing, S. & Jianhua, H. 2015. An Incentivized Auction-Based Group-Selling Approach for Demand Response Management in V2G Systems. *IEEE transactions on industrial informatics,* 11**,** 1554-1563.

Modarresi Ghazvini, A. & Olamaei, J. 2019. Optimal sizing of autonomous hybrid PV system with considerations for V2G parking lot as controllable load based on a heuristic optimization algorithm. *Solar energy,* 184**,** 30-39.

Mokhtar, M., Shaaban, M. F., Ismail, M. H., Sindi, H. F. & Rawa, M. 2022. Reliability Assessment under High Penetration of EVs including V2G Strategy. *Energies (Basel),* 15**,** 1585.

Mortaz, E. & Valenzuela, J. 2018. Optimizing the size of a V2G parking deck in a microgrid. *International Journal of Electrical Power & Energy Systems,* 97**,** 28-39.

Mouli, G. R. C., Kefayati, M., Baldick, R. & Bauer, P. 2017. Integrated PV charging of EV fleet based on energy prices, V2G, and offer of reserves. *IEEE Transactions on Smart Grid,* 10**,** 1313-1325.

Mozafar, M. R., Amini, M. H. & Moradi, M. H. 2018. Innovative appraisement of smart grid operation considering large-scale integration of electric vehicles enabling V2G and G2V systems. *Electric power systems research,* 154**,** 245-256.

Mroczek, B. & Kolodynska, A. 2020. The V2G Process With the Predictive Model. *IEEE access,* 8**,** 86947-86956.

Nguyen, H. N., Zhang, C. & Mahmud, M. A. 2015. Optimal coordination of G2V and V2G to support power grids with high penetration of renewable energy. *IEEE Transactions on Transportation Electrification,* 1**,** 188-195.

Nguyen, H. T. & Choi, D.-H. 2023. Distributionally robust model predictive control for smart electric vehicle charging station with V2G/V2V capability. *IEEE Transactions on Smart Grid*.

Noel, L. & McCormack, R. 2014. A cost benefit analysis of a V2G-capable electric school bus compared to a traditional diesel school bus. *Applied Energy,* 126**,** 246-255.

Noel, L., Zarazua de Rubens, G., Kester, J. & Sovacool, B. K. 2018. Beyond emissions and economics: Rethinking the co-benefits of electric vehicles (EVs) and vehicle-to-grid (V2G). *Transport policy,* 71**,** 130-137.

Noel, L., Zarazua de Rubens, G., Kester, J. & Sovacool, B. K. 2019. Navigating expert skepticism and consumer distrust: Rethinking the barriers to vehicle-to-grid (V2G) in the Nordic region. *Transport policy,* 76**,** 67-77.

Nottingham, U. o. 2025. NUsearch. *University of Nottingham.*

Odetoye, O. A., Olulope, P. K., Olanrewaju, O. M., Alimi, A. O., & Igbinosa, O. G. (2023). Multi-year techno-economic assessment of proposed zero-emission hybrid community microgrid in Nigeria using HOMER. *Heliyon, 9*(9), e19189.

Ofgem 2025. Your tariff might be: Economy 7, Economy 10 or Total Heat Total Control.

O'Malley, C., Badesa, L., Teng, F. & Strbac, G. 2023. Frequency Response From Aggregated V2G Chargers With Uncertain EV Connections. *IEEE transactions on power systems,* 38**,** 3543-3556.

Ota, Y., Taniguchi, H., Baba, J. & Yokoyama, A. 2015. Implementation of autonomous distributed V2G to electric vehicle and DC charging system. *Electric power systems research,* 120**,** 177-183.

Ota, Y., Taniguchi, H., Nakajima, T., Liyanage, K. M., Baba, J. & Yokoyama, A. 2011. Autonomous distributed V2G (vehicle-to-grid) satisfying scheduled charging. *IEEE Transactions on Smart Grid,* 3**,** 559-564.

Ouammi, A. 2021. Peak load reduction with a solar PV-based smart microgrid and vehicle-to-building (V2B) concept. *Sustainable Energy Technologies and Assessments,* 44**,** 101027.

Parameswarath, R. P., Gope, P. & Sikdar, B. 2023. A privacy-preserving authenticated key exchange protocol for V2G communications using SSI. *IEEE Transactions on Vehicular Technology*.

Park, J., Kim, H. & Choi, J.-Y. 2019. Improving TCP Performance in Vehicle-To-Grid (V2G) Communication. *Electronics (Basel),* 8**,** 1206.

Park, K., Park, Y., Das, A. K., Yu, S., Lee, J. & Park, Y. 2019. A Dynamic Privacy-Preserving Key Management Protocol for V2G in Social Internet of Things. *IEEE access,* 7**,** 76812-76832.

Parsons, G. R., Hidrue, M. K., Kempton, W. & Gardner, M. P. 2014. Willingness to pay for vehicle-to-grid (V2G) electric vehicles and their contract terms. *Energy Economics,* 42**,** 313-324.

Peng, C., Zou, J., Lian, L. & Li, L. 2017. An optimal dispatching strategy for V2G aggregator participating in supplementary frequency regulation considering EV driving demand and aggregator's benefits. *Applied energy,* 190**,** 591-599.

Peng, T., Yang, P., Dan, H., Wang, H., Han, H., Yang, J., Wang, H., Dong, H. & Wheeler, P. 2017. A single-phase bidirectional AC/DC converter for V2G applications.

Pokhrel, S. R. & Hossain, M. B. 2022. Data Privacy of Wireless Charging Vehicle to Grid (V2G) Networks With Federated Learning. *IEEE transactions on vehicular technology,* 71**,** 9032-9037.

Popolizio, F., Wik, T., Lee, C. F. & Zou, C. 2025. Nonlinear Online Optimization for Vehicle-Home-Grid Integration including Household Load Prediction and Battery Degradation. *arXiv preprint arXiv:2504.09657*.

Prateek, K., Maity, S. & Saxena, N. 2024. Qska: A quantum secured privacy-preserving mutual authentication scheme for energy internet-based vehicle-to-grid communication. *IEEE Transactions on Network and Service Management*.

Qu, Z., Hou, S., Wang, Y. & Wang, Y. 2019. Synergistic optimization scheduling of a wind–thermal power system considering V2G technology based on probability model. *IEEJ transactions on electrical and electronic engineering,* 14**,** 1008-1015.

Quirós-Tortós, J., Ochoa, L. F. & Lees, B. A statistical analysis of EV charging behavior in the UK. 2015 IEEE PES Innovative Smart Grid Technologies Latin America (ISGT LATAM), 2015. IEEE, 445-449.

Rachid, A., El Fadil, H., Giri, F. & Lassioui, A. 2020. Nonlinear output feedback control of V2G single-phase on-board BEV charger. *Asian journal of control,* 22**,** 1848-1859.

Rachid, K., El Fadil, H., Giri, F., Rachid, A. & Chaoui, F.-Z. 2023. PDE-based modelling and observer design for PEV fleets in V2G charging stations. *International journal of control,* 96**,** 1039-1052.

Rahbari-Asr, N., Chow, M.-Y., Chen, J. & Deng, R. 2016. Distributed Real-Time Pricing Control for Large-Scale Unidirectional V2G With Multiple Energy Suppliers. *IEEE transactions on industrial informatics,* 12**,** 1953-1962.

Raherimihaja, H. J., Zhang, Q., Xu, G. & Zhang, X. 2021. Integration of Battery Charging Process for EVs Into Segmented Three-Phase Motor Drive With V2G-Mode Capability. *IEEE transactions on industrial electronics (1982),* 68**,** 2834-2844.

Rao, Y., Yang, J., Xiao, J., Xu, B., Liu, W. & Li, Y. 2021. A frequency control strategy for multimicrogrids with V2G based on the improved robust model predictive control. *Energy (Oxford),* 222**,** 119963.

Rodrigues, L., Gillott, M., Waldron, J., Cameron, L., Tubelo, R., Shipman, R., Ebbs, N., & Bradshaw-Smith, C. (2020). User engagement in community energy schemes: A case study at the Trent Basin in Nottingham, UK. *Sustainable Cities and Society, 61*, 102187. https://doi.org/10.1016/j.scs.2020.102187

Roman, L. F. A., Gondim, P. R. L. & Lloret, J. 2019. Pairing-based authentication protocol for V2G networks in smart grid. *Ad hoc networks,* 90**,** 101745.

Ru, J., Gillott, M., & Shipman, R. 2025. Vehicle-to-grid (V2G) research: A decade of progress, achievements, and future directions. *Energies, 18*(23), 6148.

Saber, H., Ranjbar, H., Fattaheian-Dehkordi, S., Moeini-Aghtaie, M., Ehsan, M. & Shahidehpour, M. 2022. Transactive Energy Management of V2G-Capable Electric Vehicles in Residential Buildings: An MILP Approach. *IEEE transactions on sustainable energy,* 13**,** 1734-1743.

Saeed, J., Wang, L., & Fernando, N. (2022). Repetitive control of EV battery charger in single-phase vehicle-to-grid (V2G) mode. In *Proceedings of the 13th Asian Control Conference (ASCC)* (pp. 322–327).

Saha, D., Bazmohammadi, N., Vasquez, J. C., & Guerrero, J. M. (2023). Multiple Microgrids: A Review of Architectures and Operation and Control Strategies. *Energies*, *16*(2), 600.

Sahoo, S., Prakash, S. & Mishra, S. 2017. Handshaking V2G strategy for grid connected PV assisted charging station. *IET renewable power generation,* 11**,** 1410-1417.

Sains, N. S. & Al-Anbagi, I. 2018. Optimal charging and discharging for EVs in a V2G participation under critical peak conditions. *IET electrical systems in transportation,* 8**,** 136-143.

Salam, S.S.A., Raj, V., Petra, M.I., Azad, A.K., Mathew, S. and Sulthan, S.M., 2024. Charge scheduling optimization of electric vehicles: A comprehensive review of essentiality, perspectives, techniques and security. *IEEE Access*, 12, pp.121010–121034.

Salvatti, G. A., Emerson Giovani, C., Cardoso, R., da Costa, J. P. & Carlos Marcelo de Oliveira, S. 2020. Electric VehiclesEnergy Management with V2G/G2V Multifactor Optimization of Smart Grids. *Energies (Basel),* 13**,** 1191.

Samadi, M. & Fattahi, J. 2023. Effective self-committed V2G for residential complexes. *Sustainable Energy, Grids and Networks*, 35**,** 101114.

Santos, G. & Smith, O. 2023. Electric vehicles and the energy generation mix in the UK: 2020–2050. *Energy Reports*, 9**,** 5612-5627.

Saxena, N. & Bong Jun, C. 2016. Authentication Scheme for Flexible Charging and Discharging of Mobile Vehicles in the V2G Networks. *IEEE transactions on information forensics and security,* 11**,** 1438-1452.

Schuller, A., Dietz, B., Flath, C. M. & Weinhardt, C. 2014. Charging strategies for battery electric vehicles: Economic benchmark and V2G potential. *IEEE Transactions on Power Systems,* 29.

Semsar, S., Soong, T. & Lehn, P. W. 2020. On-board single-phase integrated electric vehicle charger with V2G functionality. *IEEE Transactions on Power Electronics,* 35**,** 12072-12084.

Seth, A. K. & Singh, M. 2020. Resonant controller of single-stage off-board EV charger in G2V and V2G modes. *IET power electronics,* 13**,** 1086-1092.
Shah, V. & Payami, S. 2023. Integrated Converter With G2V, V2G, and DC/V2V Charging Capabilities for Switched Reluctance Motor Drive-Train Based EV Application. *IEEE transactions on industry applications,* 59**,** 3837-3850.
Shakeel, F. M. & Malik, O. P. 2022. ANFIS Based Energy Management System for V2G Integrated Micro-Grids. *Electric power components and systems,* 50**,** 584-599.
Shams, H., Sadeghfam, A., Rostami, N. & Tohidi, S. 2019. Exact approach for charging of PEVs with V2G capability to improve micro-grid reliability. *IET generation, transmission & distribution,* 13**,** 3690-3695.
Shamshirband, M., Salehi, J. & Samadi Gazijahani, F. 2019. Look-ahead risk-averse power scheduling of heterogeneous electric vehicles aggregations enabling V2G and G2V systems based on information gap decision theory. *Electric power systems research,* 173**,** 56-70.
Shang, B., Dai, N., Cai, L., Yang, C., Li, J. & Xu, Q. 2023. V2G Scheduling of Electric Vehicles Considering Wind Power Consumption. *World electric vehicle journal,* 14**,** 236.
Shang, Y. & Li, S. 2024. FedPT-V2G: Security enhanced federated transformer learning for real-time V2G dispatch with non-IID data. *Applied Energy,* 358**,** 122626.
Sharma, S. & Jain, P. 2023. Risk-averse integrated DR and dynamic V2G scheduling of parking lot operator for enhanced market efficiency. *Energy (Oxford),* 275**,** 127428.
Shen, G., Su, Y. & Zhang, M. 2018. Secure and Membership-Based Data Sharing Scheme in V2G Networks. *IEEE access,* 6**,** 58450-58460.
Shen, J., Zhou, T., Wei, F., Sun, X. & Xiang, Y. 2017. Privacy-preserving and lightweight key agreement protocol for V2G in the social Internet of Things. *IEEE Internet of things Journal,* 5**,** 2526-2536.
Shen, J., Zhou, T., Wei, F., Sun, X. & Xiang, Y. 2018. Privacy-Preserving and Lightweight Key Agreement Protocol for V2G in the Social Internet of Things. *IEEE internet of things journal,* 5**,** 2526-2536.
Shen, K. & Dunn, R. The prediction of flexible load demand in the UK in 2050. 2013 IEEE Power & Energy Society General Meeting, 21-25 July 2013 2013. 1-5.
Shi, R., Li, S., Zhang, P. & Lee, K. Y. 2020. Integration of renewable energy sources and electric vehicles in V2G network with adjustable robust optimization. *Renewable energy,* 153**,** 1067-1080.
Shipman, R. & Gillott, M. 2019. SCENe Things: IoT-based Monitoring of a Community Energy Scheme. *Future Cities & Environment,* 5.
Shirazi, Y., Carr, E. & Knapp, L. 2015. A cost-benefit analysis of alternatively fueled buses with special considerations for V2G technology. *Energy Policy,* 87**,** 591-603.
Shirazi, Y. A. & Sachs, D. L. 2018. Comments on "Measurement of power loss during electric vehicle charging and discharging" – Notable findings for V2G economics. *Energy (Oxford),* 142**,** 1139-1141.
Shobana, S., Praghash, K., Ramya, G., Rajakumar, B. R. & Binu, D. 2022. Integrating renewable energy in electric V2G: Improved optimization assisting dispatch model. *International journal of energy research,* 46**,** 7917-7934.
Shumei, C., Xiaofei, L., Dewen, T., Qianfan, Z. & Liwei, S. The construction and simulation of V2G system in micro-grid. 2011 International Conference on Electrical Machines and Systems, 2011. IEEE, 1-4.
Singh, J. & Tiwari, R. 2020. Cost Benefit Analysis for V2G Implementation of Electric Vehicles in Distribution System. *IEEE transactions on industry applications,* 56**,** 5963-5973.

Singh, K. & Singh, A. 2022. Behavioural modelling for personal and societal benefits of V2G/V2H integration on EV adoption. *Applied energy,* 319**,** 119265.
Society of Automotive Engineers 2017. Electric Vehicle and Plug in Hybrid Electric Vehicle Conductive Charge Coupler. *SAE J1772*.
Society of Automotive Engineers [SAE] 2018. Measurement of the Battery Electric Vehicle Energy Consumption and Range. *SAE J2758*.
Society of Automotive Engineers [SAE] 2019. Communication between Plug-in Vehicles and the Utility Grid. *SAE J2847/1*.
Society of Motor Manufacturers and Traders. 2024. UK new car registrations by fuel type. https://www.smmt.co.uk/vehicle-data/car-registrations/
Song, X., Sun, J., Tan, S., Ling, R., Chai, Y. & Guerrero, J. M. 2024. Cooperative grid frequency control under asymmetric V2G capacity via switched integral reinforcement learning. *International journal of electrical power & energy systems,* 155**,** 109679.
Sortomme, E. & El-Sharkawi, M. A. 2010. Optimal charging strategies for unidirectional vehicle-to-grid. *IEEE Transactions on Smart Grid,* 2**,** 131-138.
Sovacool, B. K., Axsen, J. & Kempton, W. 2017. The Future Promise of Vehicle-to-Grid (V2G) Integration: A Sociotechnical Review and Research Agenda. *Annual review of environment and resources,* 42**,** 377-406.
Sovacool, B. K. & Hirsh, R. F. 2009. Beyond batteries: An examination of the benefits and barriers to plug-in hybrid electric vehicles (PHEVs) and a vehicle-to-grid (V2G) transition. *Energy Policy,* 37**,** 1095-1103.
Sovacool, B. K., Kester, J., Noel, L. & de Rubens, G. Z. 2019. Are electric vehicles masculinized? Gender, identity, and environmental values in Nordic transport practices and vehicle-to-grid (V2G) preferences. *Transportation Research Part D: Transport and Environment,* 72**,** 187-202.
Sovacool, B. K., Kester, J., Noel, L. & de Rubens, G. Z. 2019. Energy Injustice and Nordic Electric Mobility: Inequality, Elitism, and Externalities in the Electrification of Vehicle-to-Grid (V2G) Transport. *Ecological economics,* 157**,** 205-217.
Sovacool, B. K., Kester, J., Noel, L. & de Rubens, G. Z. 2019. Income, political affiliation, urbanism and geography in stated preferences for electric vehicles (EVs) and vehicle-to-grid (V2G) technologies in Northern Europe. *Journal of Transport Geography,* 78**,** 214-229.
Sovacool, B. K., Kester, J., Noel, L. & Zarazua de Rubens, G. 2020. Actors, business models, and innovation activity systems for vehicle-to-grid (V2G) technology: A comprehensive review. *Renewable & sustainable energy reviews,* 131**,** 109963.
Sovacool, B. K., Noel, L., Axsen, J. & Kempton, W. 2018. The neglected social dimensions to a vehicle-to-grid (V2G) transition: a critical and systematic review. *Environmental Research Letters,* 13**,** 013001.
Standardization Administration of China [SAC] 2015. Communication protocol between off-board conductive charger and battery management system for electric vehicle [in Chinese]. *GB/T 27930-2015*.
Standardization Administration of China [SAC] 2015. Connection set for conductive charging of electric vehicles [in Chinese]. *GB/T 20234*.
Standardization Administration of China [SAC] 2015. Electric Vehicle Conductive Charging System—Part 1: General requirements [in Chinese]. *GB/T 18487.1-2015*.
Steffen, T., Fly, A. & Mitchell, W. 2020. Optimal electric vehicle charging considering the effects of a financial incentive on battery ageing. *Energies,* 13**,** 4742.
Steward, D. M. 2017. Critical elements of vehicle-to-grid (v2g) economics. National Renewable Energy Lab.(NREL), Golden, CO (United States).

Strickland, D., Embley, T., Osborne, J., Yang, J., Qiao, Z., Malhotra, A., Corliss, A. & Ashworth, K. 2019. Feasibility study: investigation of car park-based V2G services in the UK central hub. *Journal of engineering (Stevenage, England),* 2019**,** 3967-3971.

Sturmberg, B.C.P., Hapuarachchi, L., Jones, L. *et al.*, 2024. Vehicle-to-grid response to a frequency contingency in a national grid. *npj Sustainable Mobility and Transport*, 1, p.7.

Su, Y., Shen, G. & Zhang, M. 2020. A Novel Privacy-Preserving Authentication Scheme for V2G Networks. *IEEE systems journal,* 14**,** 1963-1971.

Sufyan, M., Rahim, N. A., Muhammad, M. A., Tan, C. K., Raihan, S. R. S. & Bakar, A. H. A. 2020. Charge coordination and battery lifecycle analysis of electric vehicles with V2G implementation. *Electric power systems research,* 184**,** 106307.

Sun, J., Qi, G., Chai, Y., Zhu, Z. & Guerrero, J. M. 2024. An Adaptive V2G Capacity-based Frequency Regulation Scheme with Integral Reinforcement Learning against DoS Attacks. *IEEE transactions on smart grid,* 15**,** 1-1.

Sun, J., Tan, S., Zheng, H., Qi, G., Tan, S., Peng, D. & Guerrero, J. M. 2023. A DoS Attack-Resilient Grid Frequency Regulation Scheme via Adaptive V2G Capacity-Based Integral Sliding Mode Control. *IEEE transactions on smart grid,* 14**,** 3046-3057.

Sun, Q., Lv, H., Gao, S., Wei, K. & Mauersberger, M. 2019. Optimized Control of Reversible VSC with Stability Mechanism Study in SMES Based V2G System. *IEEE transactions on applied superconductivity,* 29**,** 1-6.

Sun, S., Dong, M., & Liang, B. 2014. Real-time welfare-maximizing regulation allocation in dynamic aggregator-EVs system. *IEEE Transactions on Smart Grid, 5*(3), 1397–1409.

Tao, M., Ota, K. & Dong, M. 2017. Foud: Integrating fog and cloud for 5G-enabled V2G networks. *IEEE Network,* 31**,** 8-13.

Tao, M., Ota, K., Dong, M. & Qian, Z. 2018. AccessAuth: Capacity-aware security access authentication in federated-IoT-enabled V2G networks. *Journal of parallel and distributed computing,* 118**,** 107-117.

Tchagang, A. & Yoo, Y. 2020. V2B/V2G on energy cost and battery degradation under different driving scenarios, peak shaving, and frequency regulations. *World Electric Vehicle Journal,* 11**,** 14.

Tepe, B., Figgener, J., Englberger, S., Sauer, D. U., Jossen, A. & Hesse, H. 2022. Optimal pool composition of commercial electric vehicles in V2G fleet operation of various electricity markets. *Applied energy,* 308**,** 118351.

Thingvad, A., Calearo, L., Andersen, P. B. & Marinelli, M. 2021. Empirical Capacity Measurements of Electric Vehicles Subject to Battery Degradation From V2G Services. *IEEE transactions on vehicular technology,* 70**,** 7547-7557.

Triviño-Cabrera, A., Aguado, J. A. & Torre, S. d. l. 2019. Joint routing and scheduling for electric vehicles in smart grids with V2G. *Energy (Oxford),* 175**,** 113-122.

Turker, H. & Bacha, S. 2018. Optimal minimization of plug-in electric vehicle charging cost with vehicle-to-home and vehicle-to-grid concepts. *IEEE Transactions on Vehicular Technology,* 67**,** 10281-10292.

Uddin, K., Jackson, T., Widanage, W. D., Chouchelamane, G., Jennings, P. A. & Marco, J. 2017. On the possibility of extending the lifetime of lithium-ion batteries through optimal V2G facilitated by an integrated vehicle and smart-grid system. *Energy (Oxford),* 133**,** 710-722.

Umoren, I. A., Shakir, M. Z. & Tabassum, H. 2021. Resource Efficient Vehicle-to-Grid (V2G) Communication Systems for Electric Vehicle Enabled Microgrids. *IEEE transactions on intelligent transportation systems,* 22**,** 4171-4180.

Ustun, T. S., Ozansoy, C. R. & Zayegh, A. 2013. Implementing vehicle-to-grid (V2G) technology with IEC 61850-7-420. *IEEE Transactions on Smart Grid,* 4**,** 1180-1187.

Vachirasricirikul, S. & Ngamroo, I. 2017. Robust LFC in a smart grid with wind power penetration by coordinated V2G control and frequency controller. *IEEE Transactions on Smart Grid,* 5**,** 371-380.

Vadi, S., Bayindir, R., Colak, A. M. & Hossain, E. 2019. A review on communication standards and charging topologies of V2G and V2H operation strategies. *Energies (Basel),* 12**,** 3748.

Vaheeda, J. T. & George, B. 2023. In-Vehicle Sensing System to Sense the Ground Pad Configuration in the V2G Mode of EV. *IEEE sensors journal,* 23**,** 1-1.

Van Eck, N. & Waltman, L. 2009. Software survey: VOSviewer, a computer program for bibliometric mapping. *scientometrics,* 84**,** 523-538.

Varajão, D., Araújo, R. E., Miranda, L. M., Lopes, J. P. & Weise, N. D. 2017. Control of an isolated single-phase bidirectional AC-DC matrix converter for V2G applications. *Electric power systems research,* 149**,** 19-29.

Venayagamoorthy, G. K., Mitra, P., Corzine, K. & Huston, C. Real-time modeling of distributed plug-in vehicles for V2G transactions. 2009 IEEE Energy Conversion Congress and Exposition, 2009. IEEE, 3937-3941.

Venkata, J. S. P. A., & Williamson, S. S. 2020. Analysis and design of single-stage, two-mode AC/DC converters for on-board battery charging applications. *IET Power Electronics, 13*(4), 830–843.

Wagner, M. M. & Höyer, B. J. 2024. Investigating the integration of Vehicle-to-Grid (V2G) technology in energy communities with private solar panels and electric vehicles.

Waldron, J., Rodrigues, L., Gillott, M., Naylor, S. & Shipman, R. Towards an electric revolution: a review on vehicle-to-grid, smart charging and user behaviour. Proceedings of the 18th International Conference on Sustainable Energy Technologies (SET 2019), Kuala Lumpur, Malaysia, 2019. 20-22.

Wan, Z., Zhang, T., Liu, W., Wang, M. & Zhu, L. 2022. Decentralized Privacy-Preserving Fair Exchange Scheme for V2G Based on Blockchain. *IEEE transactions on dependable and secure computing,* 19**,** 2442-2456.

Wang, H., Wang, Q., He, D., Li, Q. & Liu, Z. 2019. BBARS: Blockchain-Based Anonymous Rewarding Scheme for V2G Networks. *IEEE internet of things journal,* 6**,** 3676-3687.

Wang, H. & Zhai, Z. J. 2016. Advances in building simulation and computational techniques: A review between 1987 and 2014. *Energy and Buildings,* 128**,** 319-335.

Wang, X., Nie, Y. & Cheng, K.-W. E. 2020. Distribution System Planning Considering Stochastic EV Penetration and V2G Behavior. *IEEE transactions on intelligent transportation systems,* 21**,** 149-158.

Wang, Y., Yang, J.-W., Kim, W.-J., Kwon, T.-H., Lee, T. & Park, S.-J. 2023. Second Harmonic Current Suppression and Dynamic Response Improvement for V2G System. *IEEE transactions on power electronics,* 38**,** 1-16.

Wang, Z., Zhang, Y., You, S., Xiao, H. & Cheng, M. 2020. An Integrated Power Conversion System for Electric Traction and V2G Operation in Electric Vehicles With a Small Film Capacitor. *IEEE transactions on power electronics,* 35**,** 5066-5077.

Wei, H., Zhang, Y., Wang, Y., Hua, W., Jing, R. & Zhou, Y. 2022. Planning integrated energy systems coupling V2G as a flexible storage. *Energy (Oxford),* 239**,** 122215.

Wen, S., Lin, N., Huang, S., Wang, Z. & Zhang, Z. 2023. Lithium battery health state assessment based on vehicle-to-grid (V2G) real-world data and natural gradient boosting model. *Energy (Oxford),* 284**,** 129246.

Xiao, N., Wang, Z. & Sun, X. 2025. A secure and efficient authentication scheme for vehicle to grid in smart grid. *Frontiers in Physics,* Volume 13 - 2025.

Xiong, Z., Shen, X., Wu, Q., Guo, Q. & Sun, H. 2023. Stochastic planning for low-carbon building integrated energy system considering electric-heat-V2G coupling. *International journal of electrical power & energy systems,* 151**,** 109148.
Xu, J. & Huang, Y. 2022. The short-term optimal resource allocation approach for electric vehicles and V2G service stations. *Applied Energy,* 319**,** 119200.
Xu, M., Ren, H., Chen, P. & Xin, G. 2024. On the V2G capacity of shared electric vehicles and its forecasting through MAML-CNN-LSTM-Attention algorithm. *IET generation, transmission & distribution,* 18**,** 1158-1171.
Yammani, C., Prabhat, P. & Dahal, K. 2019. Optimal Dispatch of Vehicle-to-Grid (V2G) Battery Storage Using p-ELECTRE Method and Its Impact on Optimal Scheduling of DGs in Distribution System. *Electric power components and systems,* 47**,** 1362-1374.
Yang, Z., Yu, S., Lou, W. & Liu, C. 2011. $ P^{2} $: Privacy-preserving communication and precise reward architecture for V2G networks in smart grid. *IEEE Transactions on Smart Grid,* 2**,** 697-706.
Yu, Q., Wang, Z., Song, Y., Shen, X. & Zhang, H. 2024. Potential and flexibility analysis of electric taxi fleets V2G system based on trajectory data and agent-based modeling. *Applied energy,* 355**,** 122323.
Zabetian-Hosseini, A., Joos, G. & Boulet, B. 2023. Control Design for Effective Usage of Electric Vehicles in V2G-Enabled DC Charging Stations. *IEEE transactions on power delivery,* 38**,** 4335-4346.
Zahid, Z. U., Dalala, Z. M., Chen, R., Chen, B. & Lai, J.-S. 2015. Design of bidirectional DC–DC resonant converter for vehicle-to-grid (V2G) applications. *IEEE Transactions on Transportation Electrification,* 1**,** 232-244.
Zecchino, A., Prostejovsky, A. M., Ziras, C. & Marinelli, M. 2019. Large-scale provision of frequency control via V2G: The Bornholm power system case. *Electric power systems research,* 170**,** 25-34.
Zecchino, A., Thingvad, A., Andersen, P. B. & Marinelli, M. 2019. Test and Modelling of Commercial V2G CHAdeMO Chargers to Assess the Suitability for Grid Services. *World electric vehicle journal,* 10**,** 21.
Zhang, C., Sheinberg, R., Narayana Gowda, S., Sherman, M., Ahmadian, A., & Gadh, R. 2023. A novel large-scale EV charging scheduling algorithm considering V2G and reactive power management based on ADMM. *Frontiers in Energy Research, 11*, 1078027.
Zhang, L., Cheng, L., Alsokhiry, F. & Mohamed, M. A. 2023. A Novel Stochastic Blockchain-Based Energy Management in Smart Cities Using V2S and V2G. *IEEE transactions on intelligent transportation systems,* 24**,** 915-922.
Zhang, L., Ma, H., Shi, D., Wang, P., Cai, G. & Liu, X. 2017. Reliability Oriented Modeling and Analysis of Vehicular Power Line Communication for Vehicle to Grid (V2G) Information Exchange System. *IEEE access,* 5**,** 12449-12457.
Zhang, Y., Chen, X., Gu, Y., Li, Z., & Wu, K. (2023, July 1). Deep reinforcement learning-based battery conditioning hierarchical V2G coordination for multi-stakeholder benefits. *arXiv*. https://doi.org/10.48550/arXiv.2308.00218
Zhang, Y., Chen, X., & Zhang, Y. 2022. Transfer deep reinforcement learning-based large-scale V2G continuous charging coordination with renewable energy sources. *arXiv*. https://doi.org/10.48550/arXiv.2210.07013
Zhang, Y., Zou, J. & Guo, R. 2021. Efficient privacy-preserving authentication for V2G networks. *Peer-to-Peer Networking and Applications,* 14**,** 1366-1378.
Zhao, G. & Baker, J. 2022. Effects on environmental impacts of introducing electric vehicle batteries as storage-A case study of the United Kingdom. *Energy Strategy Reviews,* 40**,** 100819.

Zhong, W., Yu, R., Xie, S., Zhang, Y. & Yau, D. K. Y. 2018. On Stability and Robustness of Demand Response in V2G Mobile Energy Networks. *IEEE transactions on smart grid,* 9**,** 3203-3212.

Zhou, C., Qian, K., Allan, M. & Zhou, W. 2011. Modeling of the cost of EV battery wear due to V2G application in power systems. *IEEE Transactions on Energy Conversion,* 26**,** 1041-1050.

Zhou, T. & Sun, W. 2020. Research on multi-objective optimisation coordination for large-scale V2G. *IET renewable power generation,* 14**,** 445-453.

Zhu, H., Hu, S., Tahir, M., Bai, Y. & Wu, X. 2023. CLLC Modeling and Control in V2G Mode to Mitigate Double Line Frequency Current for High Power Density On-board Charger. *IEEE Journal of Emerging and Selected Topics in Power Electronics*.

APPENDIX I: DATA PROCESSING

Processing of Residential Electricity Consumption Data

```
import pandas as pd
file_path = "HourlyTotalsData2019.xlsx"
df = pd.read_excel(file_path, sheet_name="in")
device_counts = df.groupby(["day",
"hour"])["deviceId"].nunique().reset_index(name="device_count")
df_grouped = df.groupby(["day", "hour"], as_index=False)["kWh"].sum()
df_grouped["kWh"] = df_grouped["kWh"] / 1000
df_grouped = df_grouped.merge(device_counts, on=["day", "hour"])
df_grouped["adjusted_kWh"] = (df_grouped["kWh"] / df_grouped["device_count"]) * 500
df_grouped.to_excel("HouseConsumption_Processed.xlsx", index=False)
print("Saved as HouseConsumption_Processed.xlsx")
```

Processing of PV Generation Data

```
import pandas as pd
import glob
file_pattern = "PV2019*Process.xlsx"
file_list = glob.glob(file_pattern)
all_data = pd.DataFrame()
for file in file_list:
    df = pd.read_excel(file)
    df.columns = ['usage', 'date', 'hour']
    df['date'] = pd.to_datetime(df['date'], format="%d/%m/%Y")
    all_data = pd.concat([all_data, df], ignore_index=True)
all_data = all_data.sort_values(by=["date", "hour"])
all_data.to_excel("Total_PV2019.xlsx", index=False)
print("Saved as Total_PV2019.xlsx")
```

```
import pandas as pd
file_path = "Total_PV2019.xlsx"
df = pd.read_excel(file_path)
df.columns = ['usage', 'date', 'hour']
df['date'] = pd.to_datetime(df['date'], format="%d/%m/%Y")
df_grouped = df.groupby(["date", "hour"], as_index=False)["usage"].mean()
df_grouped["usage"] = df_grouped["usage"] * 10
df_grouped = df_grouped.sort_values(by=["date", "hour"])
df_grouped.to_excel("Total_PV2019_Processed.xlsx", index=False)
print("Saved as Total_PV2019_Processed.xlsx")
```

Processing of EV Charging Data

```
import pandas as pd
file_path = "EVCharging.xlsx"
df = pd.read_excel(file_path)
df.columns = df.columns[:1].tolist() + ['date'] + df.columns[2:3].tolist() + ['date_col4'] +
df.columns[4:].tolist()
df['date'] = pd.to_datetime(df['date'], format="%d/%m/%Y")
df['date_col4'] = pd.to_datetime(df['date_col4'], format="%d/%m/%Y", errors='coerce')
df_2014 = df[df['date'].dt.year == 2014].copy()
df_2014['date'] = df_2014['date'].apply(lambda x: x.replace(year=2019))
df_2014['date_col4'] = df_2014['date_col4'].apply(lambda x: x.replace(year=2019) if pd.notna(x) else
x)
df_2014 = df_2014.sort_values(by="date")
df_2014.to_excel("EVCharging_2019.xlsx", index=False)
print("Saved as EVCharging_2019.xlsx.")
```

Processing of EV Driving Data

```
import pandas as pd
file_path = "EVTrip.xlsx"
df = pd.read_excel(file_path)
df.columns = ['vehicle_id', 'date', 'start_time'] + df.columns[3:].tolist()
df['date'] = pd.to_datetime(df['date'], format="%d/%m/%Y")
df['start_time'] = pd.to_datetime(df['start_time'], format="%H:%M:%S")
df_2014 = df[df['date'].dt.year == 2014].copy()
df_2014['date'] = df_2014['date'].apply(lambda x: x.replace(year=2019))
df_2014['hour'] = df_2014['start_time'].dt.hour
df_filtered = df_2014.groupby(['vehicle_id', 'date'])[['hour']].min().reset_index()
df_filtered = df_filtered.sort_values(by=["date", "vehicle_id"])
df_filtered.to_excel("EVTrip_2019.xlsx", index=False)
print("Saved as EVTrip_2019.xlsx")
```

```
import pandas as pd
file_path = 'EVTrip.xlsx'
df = pd.read_excel(file_path)
print("Original Column:", df.columns)
df = df.iloc[:, :5]
df.columns = ['Vehicle_ID', 'Start_Date', 'Start_Time', 'End_Date', 'End_Time']
df['Start_Date'] = pd.to_datetime(df['Start_Date'])
df['End_Date'] = pd.to_datetime(df['End_Date'])
df_2014 = df[df['Start_Date'].dt.year == 2014].copy()
df_2014['Start_Date'] = df_2014['Start_Date'].apply(lambda x: x.replace(year=2019))
df_2014['End_Date'] = df_2014['End_Date'].apply(lambda x: x.replace(year=2019))
df_2014['Start_Hour'] = pd.to_datetime(df_2014['Start_Time'], format='%H:%M:%S').dt.hour
df_2014['End_Hour'] = pd.to_datetime(df_2014['End_Time'], format='%H:%M:%S').dt.hour
df_final = df_2014[['Vehicle_ID', 'Start_Date', 'Start_Hour', 'End_Date', 'End_Hour']]
df_final = df_final.sort_values(by=['Start_Date', 'Start_Hour']).reset_index(drop=True)
```

```
output_path = 'EVTrip_2019ALL.xlsx'
df_final.to_excel(output_path, index=False)
print(f"Saved as {output_path}")
```

Calculation of Daily Average Initial and Final SOC of Electric Vehicles

```
import pandas as pd
file_path = "EVCharging_2019.xlsx"
df = pd.read_excel(file_path)
df.columns = ['vehicle_id', 'start_date', 'start_time', 'end_date', 'end_time', 'start_soc', 'end_soc',
'charging_duration']
df['start_date'] = pd.to_datetime(df['start_date'], format="%d/%m/%Y")
df['end_date'] = pd.to_datetime(df['end_date'], format="%d/%m/%Y")
df['start_datetime'] = pd.to_datetime(df['start_date'].astype(str) + ' ' + df['start_time'].astype(str))
df['end_datetime'] = pd.to_datetime(df['end_date'].astype(str) + ' ' + df['end_time'].astype(str))
earliest_start_soc = df.loc[df.groupby(['vehicle_id', 'start_date'])['start_datetime'].idxmin(),
['start_date', 'vehicle_id', 'start_soc']]
latest_end_soc = df.loc[df.groupby(['vehicle_id', 'end_date'])['end_datetime'].idxmax(), ['end_date',
'vehicle_id', 'end_soc']]
avg_earliest_start_soc = earliest_start_soc.groupby('start_date')['start_soc'].mean().reset_index()
avg_latest_end_soc = latest_end_soc.groupby('end_date')['end_soc'].mean().reset_index()
avg_earliest_start_soc.rename(columns={'start_date': 'date', 'start_soc': 'avg_earliest_start_soc'},
inplace=True)
avg_latest_end_soc.rename(columns={'end_date': 'date', 'end_soc': 'avg_latest_end_soc'},
inplace=True)
final_df = pd.merge(avg_earliest_start_soc, avg_latest_end_soc, on='date',
how='outer').sort_values(by="date")
output_file = "EVCharging_SOC_Averages.xlsx"
final_df.to_excel(output_file, index=False)
print(f"Saved as {output_file}")
```

Interpolation of SOC Values During Charging Periods

```
import pandas as pd
import numpy as np
charging_file = "EVCharging_2019.xlsx"
trip_file = "EVTrip_2019.xlsx"
output_file = "EVSOC_2019.xlsx"
df_charging = pd.read_excel(charging_file)
df_trip = pd.read_excel(trip_file)
SOC_STEP = 0.1375
sheets_data = {}
def fill_soc_values(start_hour, end_hour, initial_soc, final_soc):
    soc_values = {}
    current_soc = initial_soc
    for hour in range(start_hour, end_hour + 1):
```

```
        soc_values[hour] = min(current_soc, final_soc)
        current_soc += SOC_STEP
    return soc_values
for _, row in df_charging.iterrows():
    vehicle_id, start_date, start_time, end_date, end_time, start_soc, end_soc, _ = row
    same_day = start_date == end_date
    if same_day:
        sheets_data.setdefault(start_date, {}).setdefault(vehicle_id, {}).update(
            fill_soc_values(start_time, end_time, start_soc, end_soc)
        )
    else:
        sheets_data.setdefault(start_date, {}).setdefault(vehicle_id, {}).update(
            fill_soc_values(start_time, 23, start_soc, end_soc)
        )
        last_soc_prev_day = sheets_data[start_date][vehicle_id][23] + SOC_STEP
        sheets_data.setdefault(end_date, {}).setdefault(vehicle_id, {}).update(
            fill_soc_values(0, end_time, last_soc_prev_day, end_soc)
        )
for _, row in df_trip.iterrows():
    vehicle_id, trip_date, departure_time = row
    if trip_date in sheets_data:
        sheets_data[trip_date].setdefault(vehicle_id, {})[departure_time] = 0.929496004
with pd.ExcelWriter(output_file, engine='xlsxwriter') as writer:
    for date, vehicles in sorted(sheets_data.items()):
        df_result = pd.DataFrame.from_dict(vehicles, orient="index")
        df_result.index.name = "vehicle_id"
        df_result.reset_index(inplace=True)
        all_columns = ["vehicle_id"] + list(range(0, 24))
        df_result = df_result.reindex(columns=all_columns, fill_value=np.nan)
        sheet_name = date.strftime("%Y-%m-%d")
        df_result.to_excel(writer, sheet_name=sheet_name, index=False)
print("Saved as EVSOC_2019.xlsx")
```

Allocation of Non-Charging Periods

```
import pandas as pd
import numpy as np
charging_file = "EVCharging_2019.xlsx"
trip_file = "EVTrip_2019.xlsx"
soc_file = "EVSOC_2019.xlsx"
output_file = "EVSOC_2019_UPDATED.xlsx"
df_charging = pd.read_excel(charging_file)
df_trip = pd.read_excel(trip_file)
with pd.ExcelFile(soc_file) as xls:
    sheet_names = xls.sheet_names
    dataframes = {sheet: xls.parse(sheet) for sheet in sheet_names}
```

```
for _, trip in df_trip.iterrows():
    vehicle_id, trip_date, departure_time = trip
    charge_rows = df_charging[(df_charging.iloc[:, 0] == vehicle_id) & (df_charging.iloc[:, 1] ==
trip_date)]
    if charge_rows.empty:
        continue
    sheet_name = trip_date.strftime("%Y-%m-%d")
    if sheet_name not in dataframes:
        continue
    df_soc = dataframes[sheet_name]
    if vehicle_id not in df_soc["vehicle_id"].values:
        continue
    start_time = charge_rows.iloc[:, 2].min()
    row_index = df_soc[df_soc["vehicle_id"] == vehicle_id].index[0]
    for hour in range(departure_time, start_time):
        if hour in df_soc.columns and pd.isna(df_soc.at[row_index, hour]):
            df_soc.at[row_index, hour] = -1
with pd.ExcelWriter(output_file, engine='xlsxwriter') as writer:
    for sheet_name, df in dataframes.items():
        df.to_excel(writer, sheet_name=sheet_name, index=False)
print("Saved as EVSOC_2019_UPDATED.xlsx")
```

Assignment of All Other Data

```
import pandas as pd
charging_df = pd.read_excel("EVCharging_2019.xlsx")
charging_df.columns = ["Vehicle_ID", "Start_Date", "Start_Time", "End_Date", "End_Time",
"Start_SOC", "End_SOC", "Charging_Duration"]
trip_df = pd.read_excel("EVTrip_2019.xlsx")
trip_df.columns = ["Vehicle_ID", "Start_Date", "Departure_Time"]
soc_file = "EVSOC_2019_V3_OPERATE.xlsx"
xls = pd.ExcelFile(soc_file)
DEFAULT_SOC = 0.929496004
with pd.ExcelWriter("EVSOC_2019_V4_EXTRA.xlsx") as writer:
    for sheet_name in xls.sheet_names:
        soc_df = pd.read_excel(xls, sheet_name=sheet_name)
        date = sheet_name
        for vehicle_id in soc_df["vehicle_id"].unique():
            soc_vehicle_df = soc_df[soc_df["vehicle_id"] == vehicle_id].copy()
            soc_vehicle_df.iloc[:, 1:25] = soc_vehicle_df.iloc[:, 1:25].astype(float)
            trip_row = trip_df[(trip_df["Vehicle_ID"] == vehicle_id) & (trip_df["Start_Date"] == date)]
            departure_hour = int(trip_row["Departure_Time"].values[0]) if not trip_row.empty else None
            charge_rows = charging_df[(charging_df["Vehicle_ID"] == vehicle_id) &
(charging_df["End_Date"] == date)]
            last_charge_soc = None
            last_charge_hour = None
            first_charge_soc = None
```

```
            first_charge_hour = None
            if not charge_rows.empty:
                last_charge = charge_rows.iloc[-1]
                last_charge_hour = int(last_charge["End_Time"])
                last_charge_soc = last_charge["End_SOC"]
                first_charge = charge_rows.iloc[0]
                first_charge_hour = int(first_charge["Start_Time"])
                first_charge_soc = first_charge["Start_SOC"]
            if departure_hour is not None:
                if last_charge_hour is not None and last_charge_hour <= departure_hour:
                    soc_vehicle_df.iloc[:, last_charge_hour+1:departure_hour+1] = last_charge_soc
                else:
                    soc_vehicle_df.iloc[:, 1:departure_hour+1] = DEFAULT_SOC
            if last_charge_hour is not None:
                if soc_vehicle_df.iloc[:, last_charge_hour+1:25].isna().all().all():
                    soc_vehicle_df.iloc[:, last_charge_hour+1:25] = last_charge_soc
            if departure_hour is not None:
                soc_vehicle_df.iloc[:, departure_hour+1:25] = (
                    soc_vehicle_df.iloc[:, departure_hour+1:25].fillna(-1)
                )
            if first_charge_hour is not None:
                soc_vehicle_df.iloc[:, 1:first_charge_hour+1] = (
                    soc_vehicle_df.iloc[:, 1:first_charge_hour+1].fillna(first_charge_soc)
                )
            soc_vehicle_df.iloc[:, 1:25] = soc_vehicle_df.iloc[:, 1:25].fillna(-1)
            soc_df.update(soc_vehicle_df)
        soc_df.to_excel(writer, sheet_name=sheet_name, index=False)
print("Saved as EVSOC_2019_V4_EXTRA.xlsx")
```

Determination of Return Times

```
import pandas as pd
trip_file = 'EVTrip_2019ALL.xlsx'
df_trip = pd.read_excel(trip_file)
df_trip = df_trip[['Vehicle_ID', 'End_Date', 'End_Hour']]
df_trip['End_Date'] = pd.to_datetime(df_trip['End_Date']).dt.strftime('%Y-%m-%d')
soc_file = 'EVSOC_2019_V4_EXTRA.xlsx'
xls = pd.ExcelFile(soc_file)
output_file = 'EVSOC_2019_V5_FINAL.xlsx'
with pd.ExcelWriter(output_file, engine='openpyxl') as writer:
    for end_date, group in df_trip.groupby('End_Date'):
        if end_date in xls.sheet_names:
            df_soc = pd.read_excel(soc_file, sheet_name=end_date)
            df_soc.columns = df_soc.columns.map(str)
            df_soc.rename(columns={'vehicle_id': 'Vehicle_ID'}, inplace=True)
            hour_columns = [str(i) for i in range(24)]
            df_soc[hour_columns] = df_soc[hour_columns].astype(float)
```

```
        for _, row in group.iterrows():
            vehicle_id = row['Vehicle_ID']
            end_hour = str(row['End_Hour'])
            if vehicle_id in df_soc['Vehicle_ID'].values and end_hour in df_soc.columns:
                idx = df_soc[df_soc['Vehicle_ID'] == vehicle_id].index[0]
                if all(df_soc.loc[idx, str(hour)] == -1 for hour in range(int(end_hour), 24)):
                    for hour in range(int(end_hour), 24):
                        df_soc.loc[idx, str(hour)] = 0.519998013
        df_soc.to_excel(writer, sheet_name=end_date, index=False)
print(f"Saved as: {output_file}")
```

LimeJump Bills

```
import pandas as pd
import os
time_labels = [f"{int((t-1)//2):02}:{'30' if (t-1) % 2 else '00'}" for t in range(1, 49)]
columns = ["Date"] + time_labels
full_year_df = pd.DataFrame(columns=columns)
for month in range(1, 13):
    file_name = f"Bills2020{month:02}.csv"
    if not os.path.exists(file_name):
        print(f"Document {file_name} is not exist")
        continue
    df = pd.read_csv(file_name)
    df.iloc[:, 0] = df.iloc[:, 0].astype(str).str.strip()
    df.iloc[:, 0] = df.iloc[:, 0].replace(["NULL", "N/A", "", "nan"], pd.NA)
    date_formats = ["%d/%m/%Y", "%Y-%m-%d", "%m/%d/%Y"]
    df["Bill_Date"] = pd.NA
    for fmt in date_formats:
        temp = pd.to_datetime(df.iloc[:, 0], format=fmt, errors="coerce")
        df.loc[temp.notna(), "Bill_Date"] = temp[temp.notna()]
    invalid_dates = df[df["Bill_Date"].isna()].iloc[:, 0].unique()
    if len(invalid_dates) > 0:
        print(f"Warning: {file_name} has unresolved dates: ", invalid_dates)
        continue
    df["Time"] = df.iloc[:, 1]
    df["Bill_Date"] = df.iloc[:, 4]
    df = df[df["Time"].between(1, 48)]
    pivot_df = df.pivot(index="Bill_Date", columns="Time", values="Bill_Price")
    pivot_df = pivot_df.reindex(columns=range(1, 49))
    print(f"Processing {file_name} - Number of columns in pivot table: ", len(pivot_df.columns))
    pivot_df.columns = time_labels
    pivot_df.reset_index(inplace=True)
    pivot_df.rename(columns={"Bill_Date": "Date"}, inplace=True)
    full_year_df = pd.concat([full_year_df, pivot_df], ignore_index=True)
full_year_df.sort_values(by="Date", inplace=True)
output_path = "LimeJump Bills 2020.xlsx"
```

```
full_year_df.to_excel(output_path, index=False)
print("Saved as 'LimeJump Bills 2020.xlsx'")
```

NESO Bills

```
import pandas as pd
file_path = 'NESO Bills.xlsx'
sheet_name = 'analytics_db_model price_data 2'
df = pd.read_excel(file_path, sheet_name=sheet_name, usecols=[0, 4, 5], names=['date', 'price',
'time'])
df.loc[(df['date'] == '2019-12-31') & (df['time'] == 24), 'date'] = '2020-01-01'
df.loc[df['time'] == 24, 'time'] = 0
df['date'] = pd.to_datetime(df['date'])
df = df[(df['date'] >= '2020-01-01') & (df['date'] < '2020-12-31') | ((df['date'] == '2020-12-31') &
(df['time'] < 24))]
df = df.groupby(['date', 'time'], as_index=False).first()
pivot_df = df.pivot(index='date', columns='time', values='price')
pivot_df.columns = [f'{int(c)}:{int((c % 1) * 60):02d}' for c in pivot_df.columns]
pivot_df.reset_index(inplace=True)
output_file = 'NESO Bills 2020.xlsx'
pivot_df.to_excel(output_file, index=False)
print("Saved as:", output_file)
```

Generation of 7 kW Charging Simulation Data

```
import pandas as pd
import numpy as np
charging_file = 'EVCharging_2019.xlsx'
soc_file = 'EVSOC_2019_V5_FINAL.xlsx'
output_file = 'EVSOC_2019_7kW.xlsx'
df_charging = pd.read_excel(charging_file)
sheets_soc = pd.read_excel(soc_file, sheet_name=None)
for sheet_name, df_soc in sheets_soc.items():
    df_soc.set_index(df_soc.columns[0], inplace=True)
    df_soc.columns = df_soc.columns.astype(str)
    df_new_soc = df_soc.copy()
    date_filtered_charging = df_charging[df_charging.iloc[:, 1] == sheet_name]
    for vehicle_id in date_filtered_charging.iloc[:, 0].unique():
        vehicle_charging_data = date_filtered_charging[date_filtered_charging.iloc[:, 0] == vehicle_id]
        vehicle_charging_data =
vehicle_charging_data.sort_values(by=[vehicle_charging_data.columns[2]])
        if vehicle_id not in df_soc.index:
            print(f" Warning: Vehicle ID {vehicle_id} is not in SOC data, skip...")
            continue
        prev_new_soc_end = None
        prev_original_soc_end = None
```

```
    for _, row in vehicle_charging_data.iterrows():
        start_time_str = str(row.iloc[2])
        end_time_str = str(row.iloc[4])
        start_hour = int(start_time_str.split(':')[0])
        end_hour = int(end_time_str.split(':')[0])
        start_soc = row.iloc[5]
        end_soc = row.iloc[6]
        if end_hour < start_hour:
            valid_hours_1 = [str(h) for h in range(start_hour, 24) if str(h) in df_soc.columns]
            if valid_hours_1:
                new_soc_values_1 = np.arange(start_soc, start_soc + len(valid_hours_1) * 0.2917,
0.2917)
                new_soc_values_1[new_soc_values_1 > 1] = 1
                df_new_soc.loc[vehicle_id, valid_hours_1] = new_soc_values_1[:len(valid_hours_1)]
                prev_new_soc_end = new_soc_values_1[-1]
                prev_original_soc_end = end_soc
            next_day = str(pd.to_datetime(sheet_name) + pd.Timedelta(days=1))[:10]
            if next_day in sheets_soc:
                df_next_day = sheets_soc[next_day]
                df_next_day.set_index(df_next_day.columns[0], inplace=True)
                df_next_day.columns = df_next_day.columns.astype(str)
                if vehicle_id in df_next_day.index:
                    valid_hours_2 = [str(h) for h in range(0, end_hour + 1) if str(h) in df_next_day.columns]
                    if valid_hours_2:
                        new_soc_values_2 = np.arange(prev_new_soc_end, prev_new_soc_end +
len(valid_hours_2) * 0.2917, 0.2917)
                        new_soc_values_2[new_soc_values_2 > 1] = 1
                        df_next_day.loc[vehicle_id, valid_hours_2] = new_soc_values_2[:len(valid_hours_2)]
                        sheets_soc[next_day] = df_next_day.reset_index()
            continue
        valid_hours = [str(h) for h in range(start_hour, end_hour + 1) if str(h) in df_soc.columns]
        if not valid_hours:
            print(f" Warning: Vehicle {vehicle_id} charging time on {sheet_name} {start_hour}-
{end_rour} No valid SOC data, skip...")
            continue
        if prev_new_soc_end is not None:
            start_soc = row.iloc[5] + prev_new_soc_end - prev_original_soc_end
        new_soc_values = np.arange(start_soc, start_soc + len(valid_hours) * 0.2917, 0.2917)
        new_soc_values[new_soc_values > 1] = 1
        df_new_soc.loc[vehicle_id, valid_hours] = new_soc_values[:len(valid_hours)]
        if len(new_soc_values) > 0:
            prev_new_soc_end = new_soc_values[-1]
            prev_original_soc_end = end_soc
    sheets_soc[sheet_name] = df_new_soc.reset_index()
with pd.ExcelWriter(output_file) as writer:
    for sheet_name, df_soc in sheets_soc.items():
```

```
        df_soc.to_excel(writer, sheet_name=sheet_name, index=False)
print(f'Saved as {output_file}')
```

Generation of Annual Time-of-Use Simulation Data for 7 kW Charging

```
import pandas as pd
from collections import defaultdict
from datetime import timedelta
charging_file = "EVCharging_2019.xlsx"
soc_file = "EVSOC_2019_7kW.xlsx"
df_charging = pd.read_excel(charging_file)
sheets_soc = pd.read_excel(soc_file, sheet_name=None)
cleaned_soc = {}
for sheet_name, df_soc in sheets_soc.items():
    df_soc = df_soc.copy()
    df_soc.columns = df_soc.columns.astype(str)
    df_soc.set_index(df_soc.columns[0], inplace=True)
    df_soc.replace(-1.0, pd.NA, inplace=True)
    cleaned_soc[pd.to_datetime(sheet_name).strftime("%Y-%m-%d")] = df_soc
hourly_charging_stats = defaultdict(float)
df_charging['date'] = pd.to_datetime(df_charging['date']).dt.strftime('%Y-%m-%d')
df_charging['date_col4'] = pd.to_datetime(df_charging['date_col4']).dt.strftime('%Y-%m-%d')
for _, row in df_charging.iterrows():
    vehicle_id = row['ParticipantID']
    start_day = row['date']
    end_day = row['date_col4']
    start_hour = int(row['Hour'])
    end_hour = int(row['Hour.1'])
    if start_day == end_day:
        hours = list(range(start_hour, end_hour + 1))
        dates = [start_day] * len(hours)
    else:
        hours = list(range(start_hour, 24)) + list(range(0, end_hour + 1))
        dates = [start_day] * (24 - start_hour) + [end_day] * (end_hour + 1)
    for hour, date in zip(hours, dates):
        hour_str = str(hour)
        if date not in cleaned_soc:
            continue
        df_soc_day = cleaned_soc[date]
        if vehicle_id not in df_soc_day.index:
            continue
        soc_value = df_soc_day.at[vehicle_id, hour_str] if hour_str in df_soc_day.columns else None
        if pd.notna(soc_value) and float(soc_value) < 1:
            hourly_charging_stats[hour] += 1
df_hourly_stats = pd.DataFrame({
    "Hour": list(range(24)),
    "EffectiveChargingHours": [round(hourly_charging_stats[h], 2) for h in range(24)]
```

```
})
output_file = "HourlyCharging_EffectiveOnly.xlsx"
df_hourly_stats.to_excel(output_file, index=False)
output_file
```

APPENDIX II: MAIN LOGIC

```
import numpy as np
import pandas as pd
import matplotlib.pyplot as plt
import random
import string
import math
import os

# User Input
ownership_rate = 0.8
idle_rate = 0.5
charge_power = 3.3
discharge_power = 3.3
battery_capacity = 24
target_date = '2019-03-15'
ev_hourly_charge_power = 0.20455129
strategy = 'I'

# Utility Function
def generate_virtual_ids(prefix, count):
    return [f"{prefix}_{''.join(random.choices(string.ascii_uppercase + string.digits, k=4))}" for _ in
range(count)]
# Data Loading
def read_all_data():
    house = pd.read_excel('HouseConsumption_Processed.xlsx')
    pv = pd.read_excel('Total_PV2019_Processed.xlsx')
    ev_soc_all = pd.read_excel('EVSOC_2019_V5_FINAL.xlsx', sheet_name=None)
    ev_charge_log = pd.read_excel('EVCharging_2019.xlsx')
    price = pd.read_excel('LimeJump Bills 2020.xlsx')
    carbon = pd.read_excel('Carbon_Intensity_Data_2019.xlsx')
    return house, pv, ev_soc_all, ev_charge_log, price, carbon

# Data Preprocessing
def preprocess_data(house, pv, price, carbon):
    house['timestamp'] = pd.to_datetime(house['day'].astype(str) + ' ' + house['hour'].astype(str) +
':00')
    pv['timestamp'] = pd.to_datetime(pv['date'].astype(str) + ' ' + pv['hour'].astype(str) + ':00')
    house.set_index('timestamp', inplace=True)
    pv.set_index('timestamp', inplace=True)

    price = pd.melt(price, id_vars='Date', var_name='hour', value_name='price')
    price['timestamp'] = pd.to_datetime(price['Date'].astype(str) + ' ' + price['hour'])
    price = price.groupby('timestamp').mean(numeric_only=True)

    carbon = pd.melt(carbon, id_vars='date', var_name='hour', value_name='carbon')
```

```
    carbon['timestamp'] = pd.to_datetime(carbon['date'].astype(str) + ' ' + carbon['hour'])
    carbon = carbon.groupby('timestamp').mean(numeric_only=True)

    return house, pv, price, carbon

# Active EV Data Augmentation
def expand_active_evs(ev_soc_all, target_date, required_count):
    day_data = ev_soc_all.get(target_date)
    if day_data is None:
        raise ValueError(f"No data for date {target_date}")
    current = len(day_data)
    if required_count <= current:
        sampled = day_data.sample(n=required_count).copy()
    else:
        sampled = day_data.copy()
        remaining = required_count - current
        all_days = list(ev_soc_all.values())
        while remaining > 0:
            new_rows = random.choice(all_days).sample(n=min(remaining, 5)).copy()
            new_ids = generate_virtual_ids('virtual_A', len(new_rows))
            new_rows.iloc[:, 0] = new_ids
            sampled = pd.concat([sampled, new_rows], ignore_index=True)
            remaining -= len(new_rows)
    sampled.to_excel('Expanded_Active_EV_SOC.xlsx', index=False)
    return sampled

# Initial SOC Distribution & Idle EV Data Generation
def get_soc_distribution(ev_charge_log):
    soc_series = ev_charge_log['Starting SoC Percentage'].dropna()
    levels = (soc_series * 12).round().astype(int)
    dist = levels.value_counts(normalize=True).sort_index()
    return dist

def generate_idle_evs(count, ev_charge_log):
    soc_series = ev_charge_log.iloc[:, 5].dropna()
    levels = (soc_series * 12).round().astype(int)
    level_dist = levels.value_counts(normalize=True).sort_index()

    print("Start SOC level Distribution： ")
    print(level_dist)

    ids = generate_virtual_ids('virtual_I', count)
    soc_levels = np.random.choice(level_dist.index, size=count, p=level_dist.values)
    soc_vals = soc_levels / 12

    df = pd.DataFrame({'Vehicle_ID': ids})
    for h in range(24):
        df[str(h)] = soc_vals
```

```
    filename = 'Updated_Idle_EV_SOC_Output.xlsx'
    df.to_excel(filename, index=False)
    print(f" Idle EV dataset generated: {filename}")

    return df

# Reference Curve Calculation
def generate_reference_curve(house, pv, ev_avg_power, active_ev_count, target_date):
    target = pd.to_datetime(target_date)
    month = target.month
    house_month = house[house.index.month == month]
    pv_month = pv[pv.index.month == month]

    hourly_avg_house = house_month.groupby(house_month.index.hour)['adjusted_kWh'].mean()
    hourly_avg_pv = pv_month.groupby(pv_month.index.hour)['usage'].mean()

    reference = hourly_avg_house.values - hourly_avg_pv.values + (ev_avg_power * active_ev_count)
    return reference


# Power Curve Calculation
def calculate_loads(house, pv, active_ev_count, charge_power, target_date):
    day_mask = house.index.date == pd.to_datetime(target_date).date()
    house_power = house.loc[day_mask, 'adjusted_kWh'].values
    pv_power = pv.loc[day_mask, 'usage'].values
    ev_load = active_ev_count * charge_power
    original_net = house_power + ev_load - pv_power
    baseline = house_power - pv_power
    baseline = house_power - pv_power
    print(f"Baseline on {target_date}:")
    for h in range(len(baseline)):
        print(f"{h}h: house={house_power[h]}, pv={pv_power[h]}, baseline={baseline[h]}")
    return original_net, baseline

# EV Scheduling Update Tool
def update_ev_soc(df, hour, new_soc, ev_idx):
    for h in range(hour, 24):
        df.at[ev_idx, str(h)] = new_soc
    return df

def get_ev_soc(df, hour, idx):
    val = df.at[idx, str(hour)]
    return -1 if val == -1 else float(val)

# Participating EV Scheduling Logger
def init_participation_tracker():
    return {'hour': list(range(24)), 'active_EV': [], 'idle_EV': []}
```

```
def record_participation(tracker, hour, active_num, idle_num):
    tracker['active_EV'].append(active_num)
    tracker['idle_EV'].append(idle_num)

# SOC Threshold
def determine_soc_threshold(level_dist):
    soc_start_mode = level_dist.idxmax()
    threshold = 1 - soc_start_mode / 12
    return threshold

#  Strategy I
def dispatch_strategy_I(active_df, idle_df, ref_curve, baseline,
                        charge_power, discharge_power, threshold, battery_capacity,
                        P_potential, critical_charge_level):
    updated = active_df.copy()
    idle = idle_df.copy()
    participation = {
        'active_charge': [], 'active_discharge': [],
        'idle_charge': [], 'idle_discharge': []
    }

    if isinstance(P_potential, (int, float)):
        potential_ev_load = np.full(24, P_potential, dtype=float)
    else:
        potential_ev_load = np.array(P_potential, dtype=float)

    for h in range(24):
        P_ref = ref_curve[h]
        P_base = baseline[h]
        P_pot = potential_ev_load[h]

        active_charge = active_discharge = 0
        idle_charge = idle_discharge = 0

        # Forced Charging Principle
        low_soc_active = updated[(updated[str(h)].astype(float) < critical_charge_level) &
(updated[str(h)] != -1)]
        low_soc_active = low_soc_active.sort_values(by=str(h))
        for idx, row in low_soc_active.iterrows():
            soc = get_ev_soc(updated, h, idx)
            new_soc = np.minimum(critical_charge_level, soc + charge_power / battery_capacity)
            updated = update_ev_soc(updated, h, new_soc, idx)
            active_charge += 1

        # Adjustment of ΔP: Subtracting the Power Generated by Forced Charging First
        deltaP = P_ref - (P_base + P_pot)
        deltaP -= active_charge * charge_power
```

```
# Existing Scheduling Logic
if deltaP > 0:
    needed = math.ceil(deltaP / charge_power)
    eligible_active = updated[(updated[str(h)].astype(float) < threshold) & (updated[str(h)] != -1)]
    eligible_active = eligible_active.sort_values(by=str(h))
    for idx, row in eligible_active.iterrows():
        if active_charge >= needed + active_charge:
            break
        soc = get_ev_soc(updated, h, idx)
        new_soc = np.minimum(1, soc + charge_power / battery_capacity)
        updated = update_ev_soc(updated, h, new_soc, idx)
        active_charge += 1

    if active_charge < needed + active_charge:
        needed_idle = needed + active_charge - active_charge
        eligible_idle = idle[(idle[str(h)].astype(float) < 1)]
        eligible_idle = eligible_idle.sort_values(by=str(h))
        for idx, row in eligible_idle.iterrows():
            if idle_charge >= needed_idle:
                break
            soc = get_ev_soc(idle, h, idx)
            new_soc = np.minimum(1, soc + charge_power / battery_capacity)
            idle = update_ev_soc(idle, h, new_soc, idx)
            idle_charge += 1

elif deltaP < 0:
    needed = math.ceil(abs(deltaP) / discharge_power)
    eligible_active = updated[(updated[str(h)].astype(float) > threshold) & (updated[str(h)] != -1)]
    eligible_active = eligible_active.sort_values(by=str(h), ascending=False)
    for idx, row in eligible_active.iterrows():
        if active_discharge >= needed:
            break
        soc = get_ev_soc(updated, h, idx)
        new_soc = np.maximum(threshold, soc - discharge_power / battery_capacity)
        updated = update_ev_soc(updated, h, new_soc, idx)
        active_discharge += 1

    if active_discharge < needed:
        needed_idle = needed - active_discharge
        eligible_idle = idle[(idle[str(h)].astype(float) > 0)]
        eligible_idle = eligible_idle.sort_values(by=str(h), ascending=False)
        for idx, row in eligible_idle.iterrows():
            if idle_discharge >= needed_idle:
                break
            soc = get_ev_soc(idle, h, idx)
            new_soc = np.maximum(0, soc - discharge_power / battery_capacity)
            idle = update_ev_soc(idle, h, new_soc, idx)
```

```
                idle_discharge += 1

        participation['active_charge'].append(active_charge)
        participation['active_discharge'].append(active_discharge)
        participation['idle_charge'].append(idle_charge)
        participation['idle_discharge'].append(idle_discharge)

    # Calculation of Net Adjustment
    net_adjustment = [
        charge_power * (ac + ic) - discharge_power * (ad + idc)
        for ac, ad, ic, idc in zip(
            participation['active_charge'], participation['active_discharge'],
            participation['idle_charge'], participation['idle_discharge']
        )
    ]

    optimized_net = baseline + potential_ev_load + np.array(net_adjustment)

    return updated, idle, optimized_net, pd.DataFrame(participation)

# Strategy II
def dispatch_strategy_II(idle_df, ref_curve, original_net, charge_power, discharge_power,
battery_capacity):
    updated = idle_df.copy()
    participation = {
        'idle_charge': [],
        'idle_discharge': []
    }

    for h in range(24):
        deltaP = ref_curve[h] - original_net[h]
        idle_charge = idle_discharge = 0

        if deltaP > 0:
            needed = math.ceil(deltaP / charge_power)
            eligible = updated[(updated[str(h)].astype(float) < 1)]
            eligible = eligible.sort_values(by=str(h))
            for idx, row in eligible.iterrows():
                if idle_charge >= needed:
                    break
                soc = get_ev_soc(updated, h, idx)
                new_soc = min(1, soc + charge_power / battery_capacity)
                updated = update_ev_soc(updated, h, new_soc, idx)
                idle_charge += 1

        elif deltaP < 0:
            needed = math.ceil(abs(deltaP) / discharge_power)
            eligible = updated[(updated[str(h)].astype(float) > 0)]
```

```
            eligible = eligible.sort_values(by=str(h), ascending=False)
            for idx, row in eligible.iterrows():
                if idle_discharge >= needed:
                    break
                soc = get_ev_soc(updated, h, idx)
                new_soc = max(0, soc - discharge_power / battery_capacity)
                updated = update_ev_soc(updated, h, new_soc, idx)
                idle_discharge += 1

        participation['idle_charge'].append(idle_charge)
        participation['idle_discharge'].append(idle_discharge)

    net_adjustment = np.array([
        charge_power * ic - discharge_power * idc
        for ic, idc in zip(participation['idle_charge'], participation['idle_discharge'])
    ])
    optimized_net = original_net + net_adjustment

    return updated, optimized_net, pd.DataFrame(participation)


# Strategy III
def dispatch_strategy_III(idle_df, ref_curve, baseline, charge_power, discharge_power,
battery_capacity):
    updated = idle_df.copy()
    participation = {
        'idle_charge': [],
        'idle_discharge': []
    }

    for h in range(24):
        deltaP = ref_curve[h] - baseline[h]
        idle_charge = idle_discharge = 0

        if deltaP > 0:
            needed = math.ceil(deltaP / charge_power)
            eligible = updated[(updated[str(h)].astype(float) < 1)]
            eligible = eligible.sort_values(by=str(h))
            for idx, row in eligible.iterrows():
                if idle_charge >= needed:
                    break
                soc = get_ev_soc(updated, h, idx)
                new_soc = min(1, soc + charge_power / battery_capacity)
                updated = update_ev_soc(updated, h, new_soc, idx)
                idle_charge += 1

        elif deltaP < 0:
            needed = math.ceil(abs(deltaP) / discharge_power)
```

```
            eligible = updated[(updated[str(h)].astype(float) > 0)]
            eligible = eligible.sort_values(by=str(h), ascending=False)
            for idx, row in eligible.iterrows():
                if idle_discharge >= needed:
                    break
                soc = get_ev_soc(updated, h, idx)
                new_soc = max(0, soc - discharge_power / battery_capacity)
                updated = update_ev_soc(updated, h, new_soc, idx)
                idle_discharge += 1

        participation['idle_charge'].append(idle_charge)
        participation['idle_discharge'].append(idle_discharge)

    net_adjustment = np.array([
        charge_power * ic - discharge_power * idc
        for ic, idc in zip(participation['idle_charge'], participation['idle_discharge'])
    ])
    optimized_net = baseline + net_adjustment

    return updated, optimized_net, pd.DataFrame(participation)

# Calculation of Carbon Emissions and Electricity Costs
def calculate_cost_emission(original_net, optimized_net, carbon, price, target_date):
    day_mask_carbon = carbon.index.date == pd.to_datetime(target_date).date()
    day_mask_price = price.index.date == pd.to_datetime(target_date).date()

    carbon_factor = carbon.loc[day_mask_carbon, 'carbon'].values
    price_factor = price.loc[day_mask_price, 'price'].values

    if len(carbon_factor) != 48 or len(price_factor) != 48:
        raise ValueError(f"Carbon/price data for {target_date} does not have 48 half-hourly values.")

    original_net_30min = np.repeat(original_net, 2)
    optimized_net_30min = np.repeat(optimized_net, 2)

    original_clipped = np.clip(original_net_30min, 0, None)
    hourly_co2_before = original_clipped * carbon_factor
    hourly_cost_before = original_clipped * price_factor

    hourly_co2_after = optimized_net_30min * carbon_factor
    hourly_cost_after = optimized_net_30min * price_factor

    total_co2_before = np.sum(hourly_co2_before)
    total_co2_after = np.sum(hourly_co2_after)
    total_cost_before = np.sum(hourly_cost_before)
    total_cost_after = np.sum(hourly_cost_after)

    return (total_co2_before, total_co2_after, total_cost_before, total_cost_after,
```

```
        hourly_co2_before, hourly_co2_after, hourly_cost_before, hourly_cost_after)

# Plotting Function
def plot_results(original_net, optimized_net, baseline, reference,
                 soc_matrix, updated_soc, participation,
                 hourly_co2_before, hourly_co2_after, hourly_cost_before, hourly_cost_after,
                 active_soc=None, updated_active_soc=None):
    import matplotlib.pyplot as plt
    import numpy as np
    import pandas as pd

    hours = np.arange(24)

    # Printing Plot-Related Parameters
    print("original_net:", original_net)
    print("optimized_net:", optimized_net)
    print("baseline:", baseline)
    print("reference:", reference)
    if not soc_matrix.empty:
        print("soc_matrix:\n", soc_matrix)
    if not updated_soc.empty:
        print("updated_soc:\n", updated_soc)
    if isinstance(participation, pd.DataFrame):
        print("participation:\n", participation)
    print("hourly_co2_before:", hourly_co2_before)
    print("hourly_co2_after:", hourly_co2_after)
    print("hourly_cost_before:", hourly_cost_before)
    print("hourly_cost_after:", hourly_cost_after)

    # 1. Comparison of Load Curves
    plt.figure(figsize=(10,6))
    plt.plot(hours, original_net, label='Original Net', marker='o')
    plt.plot(hours, optimized_net, label='Optimized Net', marker='o')
    plt.plot(hours, baseline, label='Baseline', linestyle='--')
    plt.plot(hours, reference, label='Reference', linestyle='--')
    plt.title('Load Profiles')
    plt.xlabel('Hour')
    plt.ylabel('Power (kW)')
    plt.grid(True)
    plt.legend()
    plt.tight_layout()
    plt.show()

    # 2. SOC Distribution Histogram
    frames_before = []
    frames_after = []
    if active_soc is not None and not active_soc.empty:
        frames_before.append(active_soc)
```

```
if not soc_matrix.empty:
    frames_before.append(soc_matrix)
if updated_active_soc is not None and not updated_active_soc.empty:
    frames_after.append(updated_active_soc)
if not updated_soc.empty:
    frames_after.append(updated_soc)

if frames_before and frames_after:
    all_before = pd.concat(frames_before, ignore_index=True)
    all_after = pd.concat(frames_after, ignore_index=True)

    init_soc = (all_before.iloc[:, 1:] * 12).round().astype(int)
    final_soc = (all_after.iloc[:, 1:] * 12).round().astype(int)

    init_levels = init_soc.iloc[:, 0].value_counts().sort_index()
    final_levels = final_soc.iloc[:, -1].value_counts().sort_index()

    x = np.arange(13)
    plt.figure(figsize=(10, 5))
    plt.bar(x - 0.2, init_levels.reindex(x, fill_value=0), width=0.4, label='Start SOC')
    plt.bar(x + 0.2, final_levels.reindex(x, fill_value=0), width=0.4, label='End SOC')
    plt.xticks(x)
    plt.xlabel('SOC Level (0-12)')
    plt.ylabel('Number of EVs')
    plt.title('SOC Distribution Before and After')
    plt.legend()
    plt.grid(True)
    plt.tight_layout()
    plt.show()

# 3. Histogram of Participating EV Counts
if isinstance(participation, pd.DataFrame):
    hours = participation.index

    if 'active_charge' in participation.columns:
        active_charge = participation['active_charge']
    else:
        active_charge = pd.Series(0, index=hours)

    if 'idle_charge' in participation.columns:
        idle_charge = participation['idle_charge']
    else:
        idle_charge = pd.Series(0, index=hours)

    if 'active_discharge' in participation.columns:
        active_discharge = participation['active_discharge']
    else:
        active_discharge = pd.Series(0, index=hours)
```

```
    if 'idle_discharge' in participation.columns:
        idle_discharge = participation['idle_discharge']
    else:
        idle_discharge = pd.Series(0, index=hours)

    charge_total = active_charge + idle_charge
    discharge_total = active_discharge + idle_discharge

    width = 0.35
    x = np.arange(len(hours))  # [0, 1, ..., 23]

    plt.figure(figsize=(12, 6))

    plt.bar(x - width / 2, active_charge, width, label='Active Charge', color='tab:blue')
    plt.bar(x - width / 2, idle_charge, width, bottom=active_charge, label='Idle Charge',
color='tab:cyan')

    plt.bar(x + width / 2, active_discharge, width, label='Active Discharge', color='tab:orange')
    plt.bar(x + width / 2, idle_discharge, width, bottom=active_discharge, label='Idle Discharge',
            color='navajowhite')

    plt.xlabel('Hour')
    plt.ylabel('Number of EVs')
    plt.title('EV Participation per Hour (Charge & Discharge)')
    plt.xticks(x)
    plt.grid(True, axis='y')
    plt.legend()
    plt.tight_layout()
    plt.show()
```

 # 4. Carbon Emissions Line Chart

```
plt.figure(figsize=(10, 5))
half_hours = np.arange(48)
plt.plot(half_hours, hourly_co2_before, label='Before Optimization', marker='o')
plt.plot(half_hours, hourly_co2_after, label='After Optimization', marker='o')
plt.title('Half-Hourly CO₂ Emissions')
plt.xlabel('Half-Hour Interval')
plt.ylabel('CO₂ (kg)')
plt.legend()
plt.grid(True)
plt.tight_layout()
plt.show()
```

 # 5. Electricity Cost Line Chart

```
plt.figure(figsize=(10, 5))
plt.plot(half_hours, hourly_cost_before, label='Before Optimization', marker='o')
plt.plot(half_hours, hourly_cost_after, label='After Optimization', marker='o')
```

```
    plt.title('Half-Hourly Electricity Cost')
    plt.xlabel('Half-Hour Interval')
    plt.ylabel('Cost (pence)')
    plt.legend()
    plt.grid(True)
    plt.tight_layout()
    plt.show()

# Main Function
def main():
    # User Input Parameters
    strategy = input("Select strategy (I / II / III): ").strip().upper()
    ownership_rate = float(input("Enter EV ownership rate (0~1, default=0.8): ") or 0.8)
    idle_rate = float(input("Enter idle EV rate (0~1, default=0.5): ") or 0.5)
    avg_ev_power = float(input("Enter average EV hourly charging power (kW, default=0.20455129):
") or 0.20455129)
    target_date = input("Enter target date (YYYY-MM-DD, default=2019-03-15): ") or '2019-03-15'

    charge_power = 3.3
    discharge_power = 3.3
    battery_capacity = 24

    # Data Reading and Processing
    house, pv, ev_soc_all, ev_charge_log, price, carbon = read_all_data()
    print("Data loaded.")
    house, pv, price, carbon = preprocess_data(house, pv, price, carbon)
    print("Data preprocessed.")

    # Calculation of EV Count
    if strategy != "III":
        total_ev = int(500 * ownership_rate)
        active_ev = int(total_ev * (1 - idle_rate))
        idle_ev = total_ev - active_ev
    else:
        idle_ev = int(500 * ownership_rate)
        active_ev = 0

    # EV Data Generation
    level_dist = get_soc_distribution(ev_charge_log)
    print("SOC distribution:\n", level_dist)
    if strategy == "III":
        idle_soc = generate_idle_evs(idle_ev, ev_charge_log)
        active_soc = pd.DataFrame()
    else:
        active_soc = expand_active_evs(ev_soc_all, target_date, active_ev)
        idle_soc = generate_idle_evs(idle_ev, ev_charge_log)

    # Curve Calculation
```

```
day_mask_house = house.index.date == pd.to_datetime(target_date).date()
day_mask_pv = pv.index.date == pd.to_datetime(target_date).date()

house_power = house.loc[day_mask_house, 'adjusted_kWh'].values
pv_power = pv.loc[day_mask_pv, 'usage'].values

if len(house_power) != 24 or len(pv_power) != 24:
    raise ValueError(f"Data for {target_date} does not have 24 hourly values.")

# Unified EV Potential Array
ev_potential = active_ev * avg_ev_power if strategy != "III" else 0
P_potential = np.full(24, ev_potential, dtype=float)

original_net = house_power + ev_potential - pv_power
baseline = house_power - pv_power
reference = np.mean(original_net) * np.ones(24)
print(f"Baseline on {target_date}:")
for h in range(len(baseline)):
    print(f"{h}h: house={house_power[h]}, pv={pv_power[h]}, baseline={baseline[h]}")

soc_start_mode = level_dist.idxmax()
soc_threshold = (12 - soc_start_mode) / 12

# Critical Charging SOC Input
try:
    critical_input = input(f"Enter critical charging SOC (0~1, default={soc_threshold:.2f}): ").strip()
    if critical_input:
        critical_charge_level = float(critical_input)
        if not (0 <= critical_charge_level <= 1):
            print("Value out of range [0,1], using default.")
            critical_charge_level = soc_threshold
    else:
        critical_charge_level = soc_threshold
except ValueError:
    print("Invalid input, using default critical charging SOC.")
    critical_charge_level = soc_threshold

# Strategy-Based Scheduling
if strategy == "I":
    updated_active, updated_idle, optimized_net, participation = dispatch_strategy_I(
        active_soc,
        idle_soc,
        reference,
        baseline,
        charge_power,
        discharge_power,
        soc_threshold,
        battery_capacity,
```

```
        P_potential,
        critical_charge_level
    )
elif strategy == "II":
    updated_idle, optimized_net, participation = dispatch_strategy_II(
        idle_soc, reference, original_net, charge_power, discharge_power, battery_capacity
    )
    updated_active = active_soc.copy() if not active_soc.empty else pd.DataFrame()
elif strategy == "III":
    updated_idle, optimized_net, participation = dispatch_strategy_III(
        idle_soc, reference, baseline, charge_power, discharge_power, battery_capacity
    )
    updated_active = pd.DataFrame()
else:
    print("Invalid strategy selected.")
    return

# Output Saving
updated_idle.to_excel('Updated_Idle_EV_SOC_Output.xlsx', index=False)
if not updated_active.empty:
    updated_active.to_excel('Updated_Active_EV_SOC_Output.xlsx', index=False)
participation.to_excel('EV_Participation_Log.xlsx', index=False)

# Calculation of Carbon Emissions and Electricity Costs
co2_b, co2_a, cost_b, cost_a, h_co2_b, h_co2_a, h_cost_b, h_cost_a = calculate_cost_emission(
    original_net, optimized_net, carbon, price, target_date
)

print(f"Total CO2 before optimization: {co2_b:.2f} kg")
print(f"Total CO2 after optimization: {co2_a:.2f} kg")
print(f"Total cost before optimization: {cost_b:.2f} pence")
print(f"Total cost after optimization: {cost_a:.2f} pence")

# Result Plotting
plot_results(
    original_net=original_net,
    optimized_net=optimized_net,
    baseline=baseline,
    reference=reference,
    soc_matrix=idle_soc,
    updated_soc=updated_idle,
    participation=participation,
    hourly_co2_before=h_co2_b,
    hourly_co2_after=h_co2_a,
    hourly_cost_before=h_cost_b,
    hourly_cost_after=h_cost_a,
    active_soc=active_soc,
    updated_active_soc=updated_active
```

```
    )

if __name__ == "__main__":
    main()
```

APPENDIX III: DATA APPENDIX—2020 TIME-OF-USE ELECTRICITY TARIFF DATA PROVIDED BY LIMEJUMP

Table III-1 TIME-OF-USE Electricity Tariff Data (00:00–05:30), 2020, Provided by LimeJump — Part 1

Date	00:00	00:30	01:00	01:30	02:00	02:30	03:00	03:30	04:00	04:30	05:00	05:30
01/01/2020	50.9	51	29.37006	28.52	25.78	24.77018	50.5	50	23.93006	23.93006	6	6
02/01/2020	2.5	2.5	49	2.5	2.5	8	25.85	25.85	49	27.74	31.85	2.5
03/01/2020	2.5	17.15	51	51	50	50	2.5	2.5	7.13	8	20.99	50
04/01/2020	2.5	49.49	2.5	0	2.5	2.5	2.5	2.5	5	2.5	0	2.5
05/01/2020	21.88	22.66	24.71	21.96	48.99	48.98	48.98	2.5	2.5	5	5	19.83
06/01/2020	4.5	19.39962	44.62	31.4	24.81	22.23	21.36	14.6	17.6	17.1	0	0
07/01/2020	5.1	23.72	24.08	22.8	22	5.1	2.5	0	5.1	0	0	0
08/01/2020	2.5	2.5	2.5	2.5	14.56	14.28	2.5	2.5	28.26	29	21.65	31.7
09/01/2020	25.99	23.61011	9.14053	2.5	2.5	2.5	6	6	16.88	16.88	48	49.5
10/01/2020	49	49.24	49.24	49	16.95013	10	7	8	49	21.99	6	6
11/01/2020	49.95	49.95	49.99	28.99	28.51	27.17	27.85	26.66	27.98	26.57	27.18	27.17625
12/01/2020	49.95	49.95	54.45	49.95	54.45	49.95	49.95	49.95	54	54	49.95	49.95
13/01/2020	0.5	0.5	0.5	0.5	46	0.5	46	46	4.5	0.5	35.84	35.9699
14/01/2020	50	52	52	52	50	12.42	11.99	11.35	18.04	50	2.5	50
15/01/2020	12	26.44	50	49.49	26.44	12	2.5	-11.21	2.5	2.5	2.5	31.91
16/01/2020	50	50	50	49.99	50	12	0	1	19.42	21.13	35.9699	38.49
17/01/2020	21.26	49.49	35	36.66222	20.3	19.84	40	28.45	21.01	21.6	24.2	24.2
18/01/2020	0	0.86628	45	2.1	2.1	19.23	45	49.5	49.5	49.5	33.88	32.64
19/01/2020	49.5	49.5	49.5	23.74	22.85	22.85	49	49.5	49.5	49.5	49.5	49

20/01/2020	19	28.25	48.5	27.07	26.73	48.5	12.5	12.5	2	2	48.5	48.99
21/01/2020	27.65	46	32.46	32.19	31.13	32.33	33.23	45.85	30	45.9	49.5	49.5
22/01/2020	5.2	44.5	22.9	22.9	43.5	42.75	42.75	31.8	42.75	46	50	50
23/01/2020	38.60995	38.4	46	25.45	25.3	25.3	25.45	35.46	39.77	25.45	25.5	25.5
24/01/2020	27.06	27.15	27.15	27.15	27.15	27.15	27.06	10	27.15	27.15	27.15	27.2
25/01/2020	10.98699	3	3	3	2.2	22.41	18.7	17.9	18.33	18.41	17.95	18.26
26/01/2020	48	48	47.5	45.5	45.5	45.5	45.5	29.35	29.71	30.96	30.99	30.3
27/01/2020	2.5	13.38	46	28	10.76	2.5	0	0	2.5	2.5	2.5	3
28/01/2020	21.07	16.55	19.55	30.85	31.2	45	45	18.31	2.5	0	2	2
29/01/2020	27.59	45.44	45.99	45.44	45.44	45.44	45.44	26.47	45	45	24.29	45
30/01/2020	2.1	13.85	13.14	14.54	14.1	14.9	44.75	45.75	45.75	44.75	31.72	23.56
31/01/2020	16	43.68	42.99	42.89	17.63	16.82	25.93029	25.93029	20	2.5	2.75	36.39185
01/02/2020	46	47.9	46	46	45.9	45.9	17.65	4.15	7.43	20.89	45.9	45.9
02/02/2020	46	47.7	46	45.85	9.95	9.95	45.8	45.85	45.75	42.5	45.75	45.75
03/02/2020	15.72	13.76	10.07	3.16	0.3	-1.34	15	-8.87	-11	-6.74	9.47	16.55
04/02/2020	46.9	45	15.6	12.43	11.23	8.91	7.13	4.31	7.19	8.38	2.5	27.49
05/02/2020	10	41	18.18	0	40	40	29.13	2.35	0	2.1	0	0
06/02/2020	42	12.13	12.13	3	2	2.2	7.34711	12.15	12.15	3.5	41.5	54.39129
07/02/2020	40	40	39	23.53	39	38.89	38.89	3	38.75	18.45	40.96	40.96
08/02/2020	16.88029	2.5	2.5	11.34	17.2	13.03	-20	-65.14	-11.21	8.22	10.92	12.49
09/02/2020	43.5	43.5	47	43.5	43.5	43.5	43	47	43	2.5	1.55	2
10/02/2020	42	42	43.95	3.6	41.9	41.9	41.9	2.5	43.9	43.9	8.5	44
11/02/2020	2.5	8.53	2.5	1.71	4.63	4.79	7.64	2.5	7.92	43.67	45	45
12/02/2020	13.72	10.86	42	10.03	2.5	2.5	2.5	2	13.7	10.22	2.5	26.3901
13/02/2020	40	24.63	15.49	2.5	2.5	2.5	40	16.98	17.77	17.27	31.48	31.48
14/02/2020	44.5	44.5	43.5	41.5	41	41	40.9	20	40	40	36.18	17.7
15/02/2020	20.51	39.5	39	39	39	39	41	39	39	0	0	-60
16/02/2020	43.75	43.75	40	14.97	43.75	43.75	43.75	40	40	39.95	16.47	14.04
17/02/2020	41	42.9	42.9	42.89	2.5	11.24	42.89	42.75	42.89	42.75	42.5	42.74
18/02/2020	40	41	40	12.57	2.5	2.5	40.9	2.5	2.5	2.5	2.5	25.45

19/02/2020	2.5	2.5	15.02	15.66	14.34	13.57	15.48	14.24	24.4	15.34	16.13	41.99
20/02/2020	2.5	2.5	41	2.5	0	0	0	0	2.5	2.5	2.5	31.77
21/02/2020	15	41.85	42.3	14.61	21.21	18.52	21.32	9.81	22.87	22.87	21.14	43
22/02/2020	44.98	46	45	45	39.5	45	45.9	45.9	44.9	17.14	20.65	44.9
23/02/2020	12.29	42	45	42	42	43.9	43.9	43.9	46.4	46.4	46.4	47
24/02/2020	49	49	49	47	46.99	45	45	13.38	4.39814	2.2	10	2.1
25/02/2020	42	42	42	42	42	31.11	26.27	26.81	41.95	41.95	42	42
26/02/2020	19.49	19.41013	14.14	13.94012	18.26649	21.38501	21.31	21.54	41.95	41.95	24.55	39.98
27/02/2020	6	42.35	42.3	31.87	21.12	42	41.95	7	41.75	23.48419	42.5	42
28/02/2020	6	6	8.25	24.41	24.16	17.32	6	6	27.94	28.52	40.5	2.2
29/02/2020	9.05	44	9.81004	4	4	4	4	4	2.34	2.34	5.14	7.44
01/03/2020	7.74	9.46	9.76	4.05022	20	4	2.44	1.04	0.25	0.75	4	4
02/03/2020	43.8	43.8	43.8	43.8	43.8	43.8	43.8	43.8	43.8	43.8	43.9	45
03/03/2020	23.52	25.17	29.76	30.31	27.35	26.92	26.66	27.67	28.91	39.85	39.85	39.85
04/03/2020	42	8.1	42	42	41	41	41	41	34.86	41	39.85	20.25
05/03/2020	23.5	42.5	42.5	0	0	0	40	23.5	0	0	0	0
06/03/2020	40	40	41.5	40	41.5	40	40	30.74	32.11	40	32	50
07/03/2020	43.5	43.5	43.5	43.5	24.12	24.1	19.66	15.52	15.04	2.2	2.2	2.1
08/03/2020	-9.24	1.72	3.84	4.81	4.69	3.83	2.5	2.5	4.09	4.97	2.5	2.5
09/03/2020	19.29	43.9	43.9	25	19.59	18.09	17.83	2.5	2.5	2.5	43.94	43.95
10/03/2020	2.5	2.5	11.46	2.5	2.5	2.5	2.5	2.5	2.5	7.22	43.25	2.5
11/03/2020	43	44	44	44	44	40	6.54	5.47	17.12	18.14	22.34	0
12/03/2020	44	44	3.11	2.5	-4.43	-8	-0.68	-8	2.5	2.5	6.46	16.07
13/03/2020	28.48	43.85	43.85	15.4	9.36	9.36	2.5	2.5	2.5	13.26	21.54	21.57
14/03/2020	42.4	43.85	24.93	3	10.66	3	7.53	3	10.53	8.8	14.48	2.5
15/03/2020	2.5	45	45	2.5	45	45	2.5	2.5	2.5	2.5	2.5	45
16/03/2020	41.75	41.75	41	40.75	41	41	41.75	41.75	41.75	13.8104	7.75	3
17/03/2020	14.49	42.5	42.5	19.66	30	2.5	21.28	2.1	19.22	19.93	2.5	32.61
18/03/2020	15.73	17.27	16.47	22.24	22.17	17.24	42.5	17.2	25.35	40.5	42.95	42.95
19/03/2020	40.5	40.5	40	16	16	16	16	16	22.86	24.64	1.95	1.95

20/03/2020	16.55	17.9	17.9	17.9	17.9	17.85	17.9	17.9	18	17	18	18
21/03/2020	6.44	9.94	40	40	6.13	40	40.75	40	39.95	39.95	5.03008	5.03008
22/03/2020	40	41	41	41	40	41.9	41.9	41.9	41.9	42.5	43	42.5
23/03/2020	6.24	7.03006	7.3	5.33013	2.5	5.58	4.72	4.72	15.92	15.88	16.21	16.05
24/03/2020	40.5	40	40	13.52	13.63	13.49	14.39	13.62	14.71067	2.5	2.5	2.5
25/03/2020	2.5	2.5	15.61012	15.87	14.75	39.5	39.5	39.5	25.97	19.99	21.26	22.34
26/03/2020	11.5	12.75	41.4	41.4	29.58	41.4	41.4	49	49	41.4	40	15.42108
27/03/2020	38.8	38.8	14.29	12.35	12.62125	12	11.97	13.7	10.63863	10.7	36.55	36.55
28/03/2020	4	17.68	17.84	17.84	15.26	14.74	14.74	14.22	15.13002	14.41008	15.41	14.88
29/03/2020	4.27	4.27	2.77	4	1.38	1.08	2.5	2.5	2.5	2.5	0.81	2.5
30/03/2020	39	19.2	19.19	38.25	41	41	41	41	43.71478	39	39	35
31/03/2020	14.94	14.94	15.64	36.85	36.85	37	36.85	36.85	36.85	18.03006	22.16	35.5
01/04/2020	38.75	38.75	38.75	38.8	38.8	38.8	38	38	37.95	37.8	37.95	37.95
02/04/2020	17.99	25.33	37	37	36.85	36.85	36.85	16.16	36.75	2.5	26.13	25.12
03/04/2020	35.95	14.63	13.03	36.8	36.8	36.8	36.8	36.75	14.52	29.15	28.88	29.29
04/04/2020	18.64	18.2	10	17.5	36	36	36	36	35.85	35.85	35.85	35.64385
05/04/2020	9.22	2.02	-0.37	7.87	39.95	4.02	38	38	42	38	41.25	41.25
06/04/2020	-29.24	-12.09	12.15	12.15	8.97	-0.34	-8	-8	-49	-8	-49.67	18.96
07/04/2020	14.38	14.9	14.6	14.64	14.68	14.42	15.63	37	36.9	37	37	37.4
08/04/2020	13.86	14.93008	35.85	35.85	35.85	35.49	14.27	14.69	35.25	35.25	10.37	10.1
09/04/2020	35.9	35.75	35.75	35.86257	35.5	16.36	13.3	35	20.94	13.5	35.5	35.5
10/04/2020	35	34.85	34.75	34.75	34.75	34.75	34.75	35	35.9	35.9	36.5	36.4
11/04/2020	9.71	9.09	9.54	21.44	19.11	20.33	13.36	5.13863	6.6	2.5	10.06	13.87
12/04/2020	36.25	36	35.95	35.95	37.5	37	36	32.95	35.99969	35.95	36	36.2
13/04/2020	5.78	-50	-50	-55	-50	-8	-60	-60	-60	-60	-60	-50
14/04/2020	8.24	5.19	4.92	6.1812	4.62	4	12.7	12.7	10.88	5.82	9.77	10.24
15/04/2020	34.5	13.03	12.29	13.21	12.52	11.29	13.25	9.05	11.99	13.48	9.6	18.54
16/04/2020	34.5	34.5	34.45	34.45	34.45	14.72711	34.4	34.4	34.45	34.45	34.45	34.45
17/04/2020	36	10.13	9.21	9.21	24.35	35.7	36	36	26.05	24.05	30.37	30.37
18/04/2020	13.45	13.01	4	9.58	11.3	11.45	6.09	5.45	2	2	9.01	9.58

19/04/2020	36.1	36.1	36.1	36.5	36.4	35.99	36	36	36	36	36.5	36.4
20/04/2020	0.5	0.5	36	36	8.8	0.5	0.5	0.5	0.5	15.73013	22.73	35.8
21/04/2020	37.48	12.48788	6.83	6.83	8.15	0.5	6.3	6.3	37.45	37.45	37.07	37.45
22/04/2020	40.93689	39.45	9.8	30	1.79	0.5	0.5	0.5	2.74	35.75	39.45	35.75
23/04/2020	34.5	34.5	34.5	35.6	38	35.75	35.75	35.75	35.75	35.75	40	35.6
24/04/2020	37	37	37	37	37	25.5	13.39	13.18	12.67	12.11	14.89	14.89
25/04/2020	35.5	35	35	35	34.5	35	35	34.5	35	38.5	38.5	30
26/04/2020	33	13.88	33	33	14.54	21.94	9.16	12.13991	9.16	10.6104	9.24	8.64
27/04/2020	15.69	15.69	32	33.5	32	12.74	10.2	10.54	12.39015	12.15	15.23	15.23
28/04/2020	34	34	32.5	32.5	32.5	32.5	32.5	20.07	32.5	32.45	32.5	10.56
29/04/2020	32	13.01	11.98	11.98	12.54	13.04	32	32	32	32	9.45008	9.1
30/04/2020	27	11.09	27	27	9.46	3.26	2.93	2.23	2.59	3.67	3.14	2.43
01/05/2020	33.5	33.5	33.5	33.5	33.5	33.5	33.5	33.5	33.5	33.5	1.04	25
02/05/2020	35.5	33.1	33.05	33.05	33.05	15.77	33	33	33	33	5.3101	4.12
03/05/2020	33	10.93	8.63	33	33.5	33.5	33.5	32	32	33	33.5	33
04/05/2020	35.5	34.25	34	34	33.95	33.95	33.9	33.9	33.9	33.33	33.81	33.81
05/05/2020	5	2.5	0.5	0.5	0.5	0.5	10.07729	10.07729	11.56	11.46	8.97	6.00921
06/05/2020	15.2702	16.03	15.96	32.95	32.95	14.75	13.69	13.62	33.95	33.95	33.95	18.64
07/05/2020	34.25	33.95	33.75	33.5	33.45	33.3	33.2	33	32.95	32.95	14.61	32.95
08/05/2020	33.05	33	32.95	32.5	32.5	32.5	32.45	32.45	32.4	32.4	32.4	30
09/05/2020	37	37	40	37	36	34.95	34.95	34.95	34.95	34.95	35	35.35129
10/05/2020	44	43.8	33.99	32.82	34.05	33.17	44	43.8	46.8	17.8	15.8	5.83
11/05/2020	1	0.5	-7	-5	-5	-10	-10	-10	-10	-10	-12.29	-10
12/05/2020	39.95	39.95	40.5	42	42	42	40.5	40.5	38.5	38.5	13.69	16.44
13/05/2020	17.77	4.25	4.25	5	5	9	16.3	16.36	16.06	15.64	4.25	5
14/05/2020	36.5	35.15	35.15	35.15	35.15	35.15	34	24.22	34	23.37	35.15	35.15
15/05/2020	14.23	14.28	20.44	34.9	34.95	34.9	34.9	23.31	22.79	22.41	22.48	22.29
16/05/2020	14.64	13.66	13.07	13.46	13.21	13.21	34	11.89	10.89	11.1	11.22	11.22
17/05/2020	36	36.2	36.2	36	36.2	36	36	36	36	36	6.8	6.8
18/05/2020	12.42	8.99	7.13	6.89	36.5	9.26	36.5	36.45	36.25	36.45	36.45	36.45

19/05/2020	20	16.15	30	11.6	12.03	12.03	11.5	10.55	11.21	12.46	11.99	11.99
20/05/2020	35	35	35	34.98	34.92	30	34.85	13.62	13.32	13.31	10.53	10.54998
21/05/2020	16.46	16.2	34.95	30	12.59	12.44	11.34	11.34	12.39	12.09	9.5	9.36
22/05/2020	40	12.82	34	-13	-13	-60	-59.95	-60	-60	-68.67	-69.39	-70.492
23/05/2020	14.7528	49	59	59	59	51.89	12.75	11.6	11.86	11.16	11.91	11.91
24/05/2020	54.5	51	-50	-43.7704	-50	-50	-19.05	-17.05	-15.86	-21.98	7	51
25/05/2020	52.25	51	51.89	51.89	51.89	43	51.89	51.89	50	50	49.72	48.5
26/05/2020	42.95	12.44	42.95	43	43	43	42.95	43	43	43	43	43
27/05/2020	14.66	16.62	37	37	17.5	13.58	13.39	10.98	9	8.11	21.83	36.4
28/05/2020	11.34	22.97	11.34	12.5	36.75	36.75	36.75	36.6	11	10.45013	13.21013	1.5
29/05/2020	16	17.19	31	20	30	7.71	8.69	15.79	11.89	10.21	10.11	10.44
30/05/2020	12.51	33	33	33	33	33	9.94	9.76	8.13	8.13	8.57	8.57
31/05/2020	6.83	7.06	7	7.2	7.41	7.25	4.77	5.54	3.82	3.29	0.58	0.89
01/06/2020	6.88	6.65	6.76	6.76	3.77	4.07	6	6	39.8	39.8	39.8	25
02/06/2020	39.8	39.65	39.65	38.5	38.5	38.5	38.5	38.5	38.5	38.5	38.9	38.9
03/06/2020	36	19.69	6.51	2.5	2.5	5	11.25	13.52	22.47	22.45	28.79	0.8
04/06/2020	16.13006	15.53	14.2	14.49	35	13.94	30	13.18	12.65	12.43	20.45	16.67
05/06/2020	37.5	25.92	14.52	14.52	19.11	15.28	11.9	11.18	15.73	9.4	8	6.3701
06/06/2020	0.5	-38.82	-3.62	-2.79	0.5	-3.9	-44.95	0.5	3.58	-55	-55	-55
07/06/2020	44.5	15.24	11.71	11.71	9.38	8.68	7.22	7.35468	8.07	8.07	8.04	44.5
08/06/2020	37	20	18.51	18.51	17.8	17.13	15.98	17.11	37	37	37	18.58
09/06/2020	37	36.95	37	37	36.95	36.95	37	36.95	36.95	19.17	36.95	34
10/06/2020	19.57	23.90055	17.5	17.5	17.22	20.25	30	20.96	21.32	20.32	10.1	8.3
11/06/2020	35.6	18.84	36	16.57	36	0.55	0.55	13.31	13.55	0.55	0.5	0.55
12/06/2020	14.76	14.31006	13.98	13.98	39	11.53	39	11.39	39	11.55	12.46	12.07
13/06/2020	39	38.5	15.39003	38.5	38.5	30	39	38.9	39	15.69	15.96	38.9
14/06/2020	38	30	40	39.5	38	30	30	15	15.8	23.68	37.8	30
15/06/2020	37.95	37.75	37	37	37	20	37	37	37	37	37.5	37.9
16/06/2020	28.45	24.32	25.89	22.05	21.79006	21.15013	4	21.75	24.97	36.45	36.75	11.1
17/06/2020	36	36	25.87	35.85	24.59	35.85	35.9	35.72	24.21	14	28.03	23.83

18/06/2020	22.87	19.92	30	21.84	30	10	22.1	18.84	34.8	10	13.5	13.5
19/06/2020	21.21	24.83	26.01	34.69	1.2	1.1	1.1	34.65	34.65	34.65	37	39.5
20/06/2020	42	38.5	38.5	36	36	18.16	17.12	17.12	16.73003	16.48	18.07	18.07
21/06/2020	20.1	17.12	45.94	39	21.87	0.5	18.19	0.5	0.5	0.5	0.5	0.5
22/06/2020	25.98	16.97015	15.84	15.21067	16.72	16.88	39.85	39.85	39.85	17.41	39.85	43
23/06/2020	29.39	0.5	0.5	29.75	28.45	29	42	45.5	46.75	48	49	46.04741
24/06/2020	40	40	40	38.94	24.92	0.5	0	17.16	24.14	0	0.55	0.55
25/06/2020	39	8	37.95	8	37.85	37.85	37.85	1.5	37.95	37.95	38	37.95
26/06/2020	40	40	40	39.9	5.92	39.9	39.9	39.9	5	5	40	33.5
27/06/2020	39	39	39	38.95	23.27	23.07	22.76	22.87	22.47	22.22	20.79	1.5
28/06/2020	21.72	0.5	0.5	0.5	0.5	-50	-50	-50	-60	-60	-60	-60
29/06/2020	0.5	0.5	0.5	0.5	0.5	0.5	0.5	18.18	20.3	0.5	0.5	-50
30/06/2020	1.83	0.5	0.5	0.5	6.21	10	10	21.68	25.93	24.42	30.91	33.45
01/07/2020	39.6	38	39.6	39.6	8	30	7.65	8	39.4	39.4	35.22988	34.29
02/07/2020	40	40	41	40	38.5	28.14	38.5	40	40	30.45	37.75	37.75
03/07/2020	40	40	40	39.9	11	11	11	39.9	39.83	0.6	36.75	11
04/07/2020	5.11	0.5	0.5	0.5	0.5	0.5	0.5	10.92	10.25	0.5	0.5	0
05/07/2020	-59.76	-59.76	4.87	50	60.5	46	46	46	46	46	2.29	-0.9
06/07/2020	0.5	-55	-59.9982	-60	0.5	0.5	-58.95	0.5	0.5	0.5	0.5	21.65013
07/07/2020	2	8.28	23.59	23.59	24.54	23.18	22.73	22.73	22.81	22	45	41.9
08/07/2020	11.62	39	38	38	38	37.75	30	12.49	27.27	27.27	1.6	33.28
09/07/2020	36.5	11.2642	32.16	1.15	29.82	1.15	27.52	1.15	0.6	1.15	0.6	0.55
10/07/2020	33.18	33.08	31	5.25	25.3	29.46	29.41	29.41	30.33	35	35	35.4
11/07/2020	10.05	26	25	25	24	24	23	23	36.95	23	8.2	23.36
12/07/2020	24.73	24.73	36.75	25	21.05	21.05	20.75	21.02	20.26	20.26	18.13	18.13
13/07/2020	38.25	21.05	25	1.15	6.5	6.5	38	38	38	38	37.5	36.02
14/07/2020	38	37	36.5	36.5	36.5	27.48	36.5	36.49	36.49	36.49	36.49	36.5
15/07/2020	30.28	30.1104	29.02	29.01	1.15	28.06	7	1.15	30.93	16.31	22.62	25.16
16/07/2020	31.41	31.26	29.2	29.2	28.99013	28.1	17	25.8	27.1	32.07013	28.65003	6
17/07/2020	30.66	30.72	28.53	28.59	28.29	27.44	12	1.05	7	1.05	21	21

18/07/2020	38	29.37	37.9	25.31	37.9	27.49	27.45	9	9	9	1.49	22.93
19/07/2020	24.22	37.5	37.5	37.5	37.5	19.85	21.19	21.06	9	1.05	1.05	0.55
20/07/2020	22.49	21	21.4	21.76	21.05	21	21	42	9	5.8	37.8	9
21/07/2020	14.5	14.5	37.8	37.95089	37.5	37.3	37.3	37.1	37.5	37.5	31.9301	14.5
22/07/2020	18.23	9.85957	17.56	36.95	36.8	23.38	36.69	7	36.42	7	31.96	10
23/07/2020	33.1904	31.72	29.67	29.79007	27.96	27.9	25.85	25.85	29.81	29.81	35.99	35.66
24/07/2020	37.25	37	37	37	37	37	37	37	16.94	37	37.5	37.5
25/07/2020	24.81	24.79	23.09	7	21.29	37	37.5	37	37.5	37.5	37.5	7
26/07/2020	39	17.13	16.01	16.1104	12.94	13.6	39.8	39.8	39.8	40	39.75	39.75
27/07/2020	18.11	18.11	42.5	42.5	42.5	30	6	6	22	19.75	44	2
28/07/2020	0.5	15	18.07	18.07	17.91	17.77	17.82	17.42	21.61	15	15	15
29/07/2020	28.09	10	7	10	11.51	25.36	10	24.33	25.37	11.0904	30.03	15.03022
30/07/2020	16.64591	1.05	40	40	39.9	39.9	38	38	17.5	38	35.38	17.5
31/07/2020	43	1.05	31.22	30.39	1.05	1.05	1.05	15.58	28.92	28.92	37.15	36.16
01/08/2020	10	10.89	1.05	1.05	20.73	18.93	17.34	1.05	1.05	1.05	17.63	21
02/08/2020	38.99	38.5	43	38.3	20.53	38.3	42.9	42	20.69013	20.56	18.65032	17.83
03/08/2020	40.95	25.71	5	39.8	41	39.8	2.65561	3.5	27.07	26.29	34.55	3.8
04/08/2020	40	39.8	39.75	38	39.75	8	1.1	1.05	35.82117	1.05	30.98713	30.65
05/08/2020	0.5	0.5	0.5	0.5	0.5	0.5	0.5	6.24	8.43	10.97	1.2	1.2
06/08/2020	44.5	43	42.5	43	42.5	42.5	43	42.99	43	42.5	35.9504	15
07/08/2020	12.75	7	24.8	7	35	40	40	40	40.95	40.95	36.49	36.68
08/08/2020	43	42.75	40	27.24	25.92	24.48	25.39	24.39	39.95	24.45	30.76	25.92
09/08/2020	40	28.86	28.53	27.92	40	36	40	40	40	40	40	24.22
10/08/2020	41.9	23.23018	43.5	41.45	25	29.39	41.45	41.45	43	43	44.45	43.5
11/08/2020	42.5	42.5	42.5	24.11	10	29.09	26.84	41	40.95	40	40.95	40.95
12/08/2020	17	39.5	39.5	34.57	15	5	26.34	38.97	38.75	24.57537	30.53	1.7
13/08/2020	39.69	39.5	38	37.74	37.74	19.09	37.74	37.9	37.7	37.55	37	37
14/08/2020	37.99	37.99	37	37	36.5	32	20.1	20.1	20.1	20.05	20.05	32.71
15/08/2020	29.89	29.89	38	38	38	38	38	25.85	24.84	24.21008	38	39.5
16/08/2020	42	25.15	24.48	30	39.75	35.52	32.51	32.17	31.3	31.26	39.7	39.7

17/08/2020	24.62	25.12	39.45	39.45	39.45	39.25	23.89	30	29.42	22	22.1	35.06
18/08/2020	38.99	38.99	38.99	38.45	38.45	0	0.6	24.81	37.9	37.79	36.61	36.58
19/08/2020	43	42	37	37	36.9	36.88	36.84	36.84	36.8	36.69	36.88	36.88
20/08/2020	43	1.5	2	2	42.9	2	2	1.6492	2	2	31.74	42.9
21/08/2020	52.5	52.5	52.5	52.5	51.48985	50.59	35.59	34.1	31.38	2	2	28.49
22/08/2020	18.91008	14.72	2	16.61	22.49	22.49	47.5	28.98	28.39	26.1	50.41	28.62
23/08/2020	18.15	18.02	16.37022	16.7904	14.82	13.98	10.6	10.84	8.07	8.20196	10.43	11.42
24/08/2020	7.5	7.5	22.94	22.88	21.88	21.53	23.53	23.53	24.52	23.43	46	46
25/08/2020	48	45	46	1.7	50	0.6	49	43	35.06	27.22	10	1
26/08/2020	50	26.79	2	20.57011	15.08	14.59	2	2	50	52.5	52.5	49.75
27/08/2020	48.69	48.69	56.99	48	48	47.5	47.5	47.5	47	47	47	50
28/08/2020	30	20	20	10	10	10	12.97067	18.73013	47.45	47	47.45	47.45
29/08/2020	48.5	48.5	49.5	49.5	50.5	49.95	49.5	49.5	49.5	49.5	49.5	49.5
30/08/2020	49.75	49.95	26.89	49.45	25.96	48	51.5	25.66	48	48	24.94	25.35
31/08/2020	36.96	46.95	47	46.4	46.4	46.35	46.3	46.45	47	46.3	47	46.3
01/09/2020	0.5	2	46.4	46.3	46.3	46	46	46	46	46	46	27.8
02/09/2020	46	45	15	31.45	44.75	45	45	45	45	2	15	3
03/09/2020	55	47.4	51.5	35.96	2.05	2	2.05	2.05	27.96	55.75	55.75	45.95013
04/09/2020	37.14	2	2	2	23.4	32.4504	49.98	49.98	49.95	50	40.71	40.71
05/09/2020	1.5	0	2	51	28.48	27.38	29.42	29.42	2	28.3	2	49
06/09/2020	49	49	34.5	49	49	49	49	49	52.5	52.5	49	49
07/09/2020	25.07	28.75	24.43	24.05	25.89013	25.89013	47.5	24.1904	15	0.6	48.1	48.1
08/09/2020	49	30	49	47.75	47.75	47.75	20.2	15	15	22.81	21.15709	11.22
09/09/2020	25.02	23.27	19.328	15	15	15	18.84	18.84	30	23.19	44.9104	48
10/09/2020	27.82	30.76	47.5	47.3	47.3	30	20.8	23.55311	34.17	2	45.63	48
11/09/2020	48.5	23.18	30	48	10	23.3	36.42	36.39	40.4	22.42	0.6	1.19
12/09/2020	42.22	2	0.55	0.55	0.5	0.55	0	0	0	0	0	-5
13/09/2020	53.4	52	58	52	52	30	29.79	29.11018	28.65011	28.21	29.73	29.41
14/09/2020	50.5	50	49.95	50	49.95	27.58	35.1	27.15	2	0	46.22	23
15/09/2020	26.71	30	26.8	30	30	30	30	45.37339	44.9	42.62	52.97	57.83013

16/09/2020	51.25	50.68	48	48	36.66	37.48	30.75	44.95	46.22	31	28	28
17/09/2020	29.41	30.06	28.63	28.07	27.39	26.91	26.96	28.06	47	29.78	45.62394	28.9
18/09/2020	15	20.38	15	24.57692	15	0.6	15	26	31.3304	31.15	26	0
19/09/2020	15.2	2	1.5	2	15	2	21.05	24.24	24.24	21.05	25.16	47.5
20/09/2020	2.5	2	2.5	15	47.95	29.13	28.95	29.09013	30.9	34.4	29	28.9
21/09/2020	16	24.87	47.3	29.27	29.66	28.52	46.5	28.85	43.29006	43.29006	54.22	20.5
22/09/2020	20.69884	30	49.5	49	47.25	30	20.5	0.6	0.6	0	0	2
23/09/2020	44.5	44.35	49.45	49.45	49.4	45	30	48.9	48.9	48.9	53.89933	54.45
24/09/2020	48	32.2	26	26	22	22	10.39	10.39	30	48.65	48.59	49.5
25/09/2020	52	26.66	2	2	2	2	23.49	23.49	2	0.5	0	1.5
26/09/2020	50.5	50.5	52	52	52	50.5	27.05	17.32	27.82	10.5	1.5	2
27/09/2020	14.76	14.29	12.6704	12.26	6.65	5.89	5.66	5.66	8.47	8.91	11.77	11.89
28/09/2020	50.5	50.25	50.5	50.25	32.39	24.49	12.3	12.3	12.3	50	50.88	49.32
29/09/2020	55	55	52	54.75	52	52	52	30.98	52	28.2	61.4	64.84
30/09/2020	56	37.5	55	12.3	12.3	12.3	55	55	55	52.75	47.76	12.5
01/10/2020	28.22552	25	22.48	23.93	22.7	22.34	23.02	22.05	26.5	26.41	35.02	34.29
02/10/2020	55	53	35	35	51.5	19.56	16.1	14.42	9.23	9.05	20.61	20.79
03/10/2020	33	23.56	50	50	15.06	15.06	49.8	49.8	58	58	51.5	49.8
04/10/2020	12.7	12.71	9.07006	9.07006	3.69	3.73	0.5	-0.25	0.19	0.72	2.52	4.83
05/10/2020	58	57	57	57.1	57.1	57	56.5	5.91	56.5	56.9	58.5	57
06/10/2020	22.46	27.59	20.03	23.1	25.2	27.88	55.5	30	21.82	11	29.08	28.74
07/10/2020	53.25	1.5	2	2	53.25	2	53.25	2	2	53.25	36.5	53.25
08/10/2020	32.52	29.54	57.8	57.8	57.5	19.99	17.95018	7	0.55	0	0.5	4.5
09/10/2020	29.92	29.71	33.7492	28.22	31.1	26.55	27.55	26.04	26.83	27.21	37.65	53.95
10/10/2020	26.18	0	27.66	58.5	60.5	58.5	58	58.5	60.5	58	0	0
11/10/2020	24.7025	24.66	24.03	57	57.25	57	21.38	21.25	21.77	20.3904	22.59	22.76
12/10/2020	56.5	56.19	56.19	57	56.19	56	19	26.18	55	25.4704	56.19	13
13/10/2020	58.35	57	24.91	24.91	24.91	56.9	57	27.38	29.22	29.9	63	60
14/10/2020	54	54	28.69013	53	53	25.52	31.99	31.34	28.34	28.34	33.93	32.23
15/10/2020	22.22	14	13.14	14	53.9	53.5	53	52.5	52.9	53	54	27.32

16/10/2020	3.85	22.11	53	53.5	53.9	53	52	20.1	20.2	20.2	51.95	55
17/10/2020	34.8	34.8	32.58	53.5	30.9	31.1504	33	29.6904	31.39	52.5	31.87	30.89
18/10/2020	32.56	32.36	53.75	53.75	53.75	53.75	53.75	53.75	53.75	30.27	33.32	53.75
19/10/2020	56.5	29.79	55.9	55.9	55.9	55.9	55.9	55.9	55.94	55.9	15	15
20/10/2020	24.39	24.54	22.62	22.66	52.45	52.45	52.45	52.90332	56.45	52.45	28.78	28.92
21/10/2020	20.38	23.72	19.61013	23.93	21.25	16.3	17.96	18.62	26.65	5	3.9	4.5
22/10/2020	25	23.5	57.5	57.4	18.68	15.24	14.1	12.7	20.97	21.1	31.87	57.4
23/10/2020	54.25	57	58	58	58	56	56	54.25	54.25	31.7	54.25	58.4
24/10/2020	33.37	5	5	4.5	5	4.5	-4	-4.58	11.61	1.41	9.57	12.22
25/10/2020	0.83	-18.81	-18.78	-18.78	-29.8	-39.32	-24.5	-24.5	-25.46	-32.4862	-32	-27.44
26/10/2020	13.12	15.09	14.17	13.9304	8.66	9.4104	12.72	12.67018	19.19	21.1904	62	33.6
27/10/2020	33.05	58.9	30.86	30.35	27.34	25.46	26.76	26.69	58.75	58.9	35.09013	62
28/10/2020	63	63	63	60	34.98	24	24	5	5	4.5	23	36.92
29/10/2020	22.85	60	34.6	22.26	6.58	6.58	7.8504	7.8504	19.96	19.96	29.45	62
30/10/2020	-2.47	0.73	-4.52	-9.23	-9.56	-9.82	-7.03	-7.77	-6.34	-5.81	12.6	60
31/10/2020	26.98	60	69	25.48	65	30	60	4.5	5	24.62	19.36	18.53
01/11/2020	0	5	58.75	5	59	-59.99	-59	-17.35	-8.57	-28.39	-20.22	-18.71
02/11/2020	-9.55	-7.15	-2.51	-2.51	-14.3	-14.3	-10.1	-27.25	-15.6	-24.19	5	5.99
03/11/2020	23.12	21.76	17.83	17.77	15.22	15.05	19.86	59	63.5	70	70	65
04/11/2020	33.46	38.52	38.55	30	33.7	30	32.57	32.04	29.75	37.07	58.5	5
05/11/2020	4	3.9	3.95	3.9	3.9	18.21	24.51	24.2	24.02	23.58	5	43.71043
06/11/2020	60	58.5	25.22	59	60	59.96704	56.7	56.7	56.7	56.7	62	58.5
07/11/2020	27.72	57	29.03	26.67	22.5	15	15	8	25.52	21.85	56	56
08/11/2020	58.05	59	57	56	56	55.9	55.9	56	55.9	25	55.9	56
09/11/2020	59	59.55	59.55	59.55	59	59	59	59	28.49	28.49	55	59
10/11/2020	54.7	54.7	55	28.62	23.1	39.9	36.56	34.8	37.24	34.8	53	53
11/11/2020	58.28	58.28	58.28	29.15	35	35	30.37	28.52	29.93	29.45	43.2102	43.2102
12/11/2020	0	5	5	16.11	4.5	5	4.5	0	4.5	4.5	22.52	27.85
13/11/2020	59.7	58	34.95	28.01	27.17	26.72	30.04	30.6	30.9	30.9	36.01	62
14/11/2020	32.76	57.9	35.3	30.05	63.9	63.9	63.85	26.92	37.16	6.1	5	5

15/11/2020	0.17	0.36	-0.42	-0.62	-2.91017	-2.91017	-5.9	-5.9	-4.64	59	-1.02	-1.02
16/11/2020	-15.95	14.77	2.63	-59.99	-59.99	0	-8.27	-8.27	-11.52	-63.93	35.53	39.9
17/11/2020	58.95	58.9	58.9	27.57	26.18	15.4	18.27	3.02	10.46	28.81	3.9	3.9
18/11/2020	59.9	59.9	62	59.85	27.21	26.25	26.76	26.48	30.97	30.48	37.64	38.35
19/11/2020	4.5	5	59.9	59	58.9	58.9	8.7	8.05	6.1	16.84	4.5	59
20/11/2020	15	28.9	58	55	28.28	25.08	30	4	28.32	31	52.07018	15.1
21/11/2020	4.5	6.01814	4.5	11.2	15.94	6	6	2.2	6	6	6	6.05893
22/11/2020	30	30	35.95	35	30.63	30.03	6.1	6.1	21.72	30	21.48	25.37
23/11/2020	21.52	29.94	29.6	27.82	28.06	27.7	30.68	20.55	22.47	30.1	57	55.8
24/11/2020	20.11	38.15	36.98	36.25	35.44	34.71	35.56	36.4	40.22	56.13	56.13	56.13
25/11/2020	15.55	24.96	27.9	30.06	56	56	40.42	38.65	38.65	30.46	56	56
26/11/2020	20	35	55	53	20.75	7	20.75	7	7	20.75	56.5	9
27/11/2020	55	57.95	54	33.5	33.5	33.5	54	0	4	33.5	53.45	52.45
28/11/2020	36.1	36.2	53	36.1	53	55	52.95	52.95	52.95	52.95	52.9	52.9
29/11/2020	57	59.9	59.9	54	36.1	36.1	36.1	57	36.32	32.02	32.7	43.81
30/11/2020	35.91	25.2	25.2	25.2	52	9	52	9	52.5	6	6	5.95
01/12/2020	54.75	57.7	53	42.61	41.64	40.19	40.07	37.48	52.9	52.9	50.19	46.88
02/12/2020	32	57.89	57.77	30.5	37.19	5.9	57.77	32.15	57.88	58	59	57.14
03/12/2020	18.7	20	37.77	32.72	55.9	56	59.7	56	56	35	11.12274	12
04/12/2020	58	37.17	58	57	11.34	8.55013	6	0	0	0	0	0
05/12/2020	18.49	25.55	13.68	12.32	7.5	12	12	7.5	5.74015	5	30.55	57.9
06/12/2020	59.95	21.25	60	21.25	17.37	21.25	21.25	21.25	21.25	21.25	21.5	21.5
07/12/2020	29.8	54	54	29.8	23	23	52.9	52.9	52.9	52.9	72	30.05
08/12/2020	6	53.7	27	34.18	30	30	33.7	22.25	33.65	5	5	49.25
09/12/2020	53.5	53.5	53.5	30	6	5.9	20	11	11	25.10441	33.5	30.05
10/12/2020	5.95	11	9.79	11.48	11.28	7.02	23.9	19.61	20.08	20.58	50.77	12.31357
11/12/2020	17.5	25.24	25.96	26.89	55	57.45	6.5	57.4	6	17	9.5	45.6501
12/12/2020	60	62	63	62	59.9	59.85	59.7	59.7	59.7	59.7	59.7	59.7
13/12/2020	59.7	59.7	61.95	32.25	32.2	32.29	60.6	60.6	60.6	32	6	32.08
14/12/2020	38	64.4	64.4	38	64	17.45	24.74	8.2	-1.13	0.42	42.9	42.9

15/12/2020	55.87	32.15	29.78	7.5	7.5	38.81	29.27	28.06	7.5	7.5	7.5	5.9
16/12/2020	62	62	59.5	34.76	35.06	7.5	29.42	5.9	7	2.5	2.5	7
17/12/2020	38.72	62.5	62.75	45.08	62.5	62.75	63	63	62.75	63	63	63
18/12/2020	14.2	21.55	24.17	21.47	24.97	7.5	3.5	0	0	0	29.78	64
19/12/2020	7	7.5	27.1	7.5	22.93	7.5	18.96	13.49	69	65	65	68.5
20/12/2020	7.5	65	65	65	63.95	7.5	7.5	63.9	63.9	65	65	65
21/12/2020	63	65.5	65.5	65.5	66	66	66	66	66	66	66	36.14
22/12/2020	6	5.76	6	6	6	6	10.84	58	14.59	12.87	5.95	5.95
23/12/2020	32	65	65	65	65	65	64.9	28.25	62	25.91	21	28.96
24/12/2020	65.5	66.5	65	7.5	7	7	7	7	7	7	7	7
25/12/2020	65	65	65	64.5	63.45	64	63.45	63.45	63.45	63.45	63.45	63.95
26/12/2020	25.78	66	66	20.65	66	64	7.5	7	-59.95	-60	-60	-60
27/12/2020	7	74.5	77	74.5	74.5	74	74	74	72.5	68	70	7.5
28/12/2020	22.63	59.9	59.9	22.6	20.1	10.01	10.52	58.5	58.5	65	58.5	65.5
29/12/2020	75.6	75	75	75	75	75	70.08742	69	69	69	69	69
30/12/2020	72	72	71.9	70.5	70	69	69	65.0271	69	69	69	70.5
31/12/2020	66.75	67.75	66.75	66.75	67.75	67.75	66.35	38.25	38.4	38.4	66.25	66.23

Table III-2 TIME-OF-USE Electricity Tariff Data (06:00–11:30), 2020, Provided by LimeJump — Part 2

Date	06:00	06:30	07:00	07:30	08:00	08:30	09:00	09:30	10:00	10:30	11:00	11:30
01/01/2020	23.82	31.69	23.98	52	52	52	52	51	51.9	51	25.59	7.5
02/01/2020	7.5	0.5	42.12	7.5	6	7.55	6	6	6	7.8	7.8	7.8
03/01/2020	24.65	2.5	-3	0.2	6	6	49.2	9	53.5	49.2	49.2	9
04/01/2020	0	2.5	0	5	6	9.6	6	7	7.75	49.45	6	6
05/01/2020	48.5	48.98	2.5	0	2.5	2.5	2.5	48.94	29.4	48.94	48.94	5.1
06/01/2020	2.5	48.5	5	5.1	50	10	50	52.3	49	49	32.85	48.94
07/01/2020	2.5	2.5	52.5	54	54	51.75	51.75	51.75	56	56	51.5	50

08/01/2020	48.95	7	50	50	54.5	50	50	51.5	50	14	4.5	4.5
09/01/2020	48.99	14.56	6	16.5	16.5	16.5	16.5	15.3	15.3	18	18.06	18.25
10/01/2020	11	49.24	49.24	69	100	115	100	60.5	60.5	60.5	58	52
11/01/2020	29.98	49	32.85	49	5	49.95	50	50	50	50	50	54.5
12/01/2020	49.95	49.95	20.61	18.35	19.57	49.95	54	50	54	49.95	16.03	10.01
13/01/2020	52.75	50	50	51.12	56.5	55	55	10.05	54.5	10.15	10.5	10.55
14/01/2020	52	53.5	52	53.5	54	54	54	54	55	55	54	58
15/01/2020	10	51	10	53	53.5	53.5	57.5	53.6	53	52.75	51	50
16/01/2020	42.9	50	50	57	50	12.8	37.32	50	50	50	12.5	50
17/01/2020	49	4.5	10	52	60.75	60.75	60.75	15.5	15.5	18	56	56
18/01/2020	49.5	49.5	49.99	49.75	49.5	49.99	50	49.75	49.75	49.5	49.5	49.5
19/01/2020	30.1	30.1	41	49.7	49.5	49.7	49.45	49.45	49.45	19.25	49.45	19.25
20/01/2020	49.45	10	53.32	55.51	19.5	59.5	59.5	59.5	59.5	20	20	20
21/01/2020	60	58.4	57.32	84.5	84.5	86.5	86.5	84.5	21.25	21.35	21.8	21.8
22/01/2020	50	60	54.42	74.95	74.95	23.15	40	90	90	90	105	105
23/01/2020	25.5	55.55	25.5	52	29.96882	25.5	62.25	68	57.35338	67.85	51	58
24/01/2020	54.88	56.25	27.2	59.95	27.3	59.95	55	27.3	27.5	59.95	57	57
25/01/2020	19.2	20.59	32.85	39.59	43.17013	50	29.97	53	53	53	53	53
26/01/2020	31.12	30.4699	27	2.5	10	31.36	32.57	33.82	3	3	3	49
27/01/2020	46	47	47.49	49	55	47.49	14.11	14.15	3	51	3.5	3.5
28/01/2020	40.12	39.58	14	50	49.25	49.25	49.25	50	49	48.5	48.5	16.25
29/01/2020	46.5	46.5	47.2	47.2	47.25	47.25	48.5	47.25	48.5	20	18.2	18.2
30/01/2020	2.75	33.53	2.75	47.9	28.4	33.4	47.8	22.95	5	2.75	2.75	7.5
31/01/2020	46	51.45	50.04624	51.7	48	13.1	13.1	47	13.03801	47	47	47
01/02/2020	46.8	46.8	28	2.35	14.52	46.8	2.5	45	-65.14	-66.25	45	-11.34
02/02/2020	46	45.75	5.05	14.51	46	46.85	48	49	48	48	48	46.85
03/02/2020	35	48	38.05	39.86	2.5	2.35	13.1	26.36	13.1	13.1	10.05	10.05
04/02/2020	46.5	48	46.9	48	48	48	47.9	47.9	47	48.5	48.95	48.95
05/02/2020	15.15	15.15	15.2	47.73	15.25	0	0	7.5	15.55	15.6	2.35	0
06/02/2020	80	115	80	84.5	15.45	85	76.9463	15.5	15.41	15.55	50	15.62

07/02/2020	39.9	45.54	50	53.34	50	50	46	17.6	17.6	17.49	17.49	43.75
08/02/2020	2.5	44.5	44.33	43.95	44.5	46	46	47	44.5	43.95	43.8	43.95
09/02/2020	2.5	2.5	2.5	2.5	2.5	44.95	45.45	48	48	48.5	48	48.45
10/02/2020	47	49.9	48.48	49.9	49.9	49.9	49.9	45.75	40	13	46	45.75
11/02/2020	47.5	49.5	47.5	47.5	47.5	47	47	46.5	45.5	45	45	45
12/02/2020	43.89	43.9	43.25	43.25	44.29	13.45	2	2	40	13.6	13.65	13.65
13/02/2020	41.99	40	15	37.46	35.02	38	41.98	43	43	44	44.5	44.5
14/02/2020	40	45.5	46.5	48.86	46.5	45.5	46.2	30	46.2	43.75	45.5	43.25
15/02/2020	-60	0	2.1	2.5	2.5	41	41	41	41	38	42	41.5
16/02/2020	39.95	16.13	3.47013	1	-60	1.85	1.85	6.63	16.19	43	43.4	43.4
17/02/2020	44.99	45	45	44.9	18.25	44.5	42.5	6.5	6.5	6.51711	6.63093	28.36
18/02/2020	26.07	2.5	2.5	7	11	42.9	42.9	42.8	42.8	11.2	11.2	42.3
19/02/2020	41.99	2.5	8	12.1	13.1	13.5	46.28	45	45	46.28	47.61	46.28
20/02/2020	15.15	7	7	10	44	48.78	48	47.5	45	45	45	44.8
21/02/2020	44	45.68	44	40	2	44	44	43.95	44.25	46.9	44	44
22/02/2020	44.9	46.5	46	46	45.5	46	45.5	46.4	46.4	34	17.86	27.93
23/02/2020	47	45.8	46.4	14.48	43.9	16.66	22.6	16.03	7	2.25	2.5	2.1
24/02/2020	45	47.95	47.95	52	45	48	55	58	55	55	57.95	54.5
25/02/2020	44.5	46	54.5	54.5	66	46	46	13.5	13.5	13.5	13.68	46
26/02/2020	46	52	52	45.25	45.25	16.15	45.25	45.25	45.25	45.25	44.85	44.85
27/02/2020	42.5	45.26	7.25	46	50	18.1	46	46	17.6	17.6	17.15	17.1
28/02/2020	2.35	10	20.86	13.5	13.25	13.5	13.7	14.19	14.5	45	45	44.75
29/02/2020	37.55	43.8	10.15013	11.25005	44	44.5	44.5	44.5	44	44	44	15.05
01/03/2020	4.69	5.38	5.75	5.75	4	4	2.35	2	4	4	4	4
02/03/2020	47	47	56	56	55	52	49	47	18.4	17.3	45	45
03/03/2020	54.5	64.4	45	46.5	45	45	45	44.99	19.5	19.75	19.75	19.86
04/03/2020	20.25	47.08	21	66	22.5	22.25	22.3	22.55	39.35322	22.61	0	0
05/03/2020	0	22.7	22.7	23	0	0	66	87	80	41.5	23.98	24
06/03/2020	50	23.9	105	125	105	49	32.5	23.8	23.8	23.75	23.75	23.8
07/03/2020	21.13013	24.23	2.35	27.7	11.95	11.95	32.51	13.06	0	0	0	2.1

08/03/2020	2.5	2.5	2.5	2.5	2.5	10.55	8	8.93	11.05	9.52	10.63	12.47
09/03/2020	43.95	43.94	56.14	59.16437	45	45	50	50	24.6	15	43.75	43.75
10/03/2020	21.58	43.75	0.5	0.5	1.85	19.93	42.4	42.4	42.25	42.25	42.4	42.25
11/03/2020	0	44	45	45.9	14.5	30.1	47	45.9	45	35	13.1	13.1
12/03/2020	44	46	46	46	46	46	15.75	45	46	46	44	44
13/03/2020	45	45	10.31773	15.15	13.6	15.05	47	47	47	47	16	42.5
14/03/2020	2.5	12.05	2.5	2.5	25.61	31.18	44	44	44	45	43.85	43.85
15/03/2020	2.5	45	47.5	47.5	17.83	45	9.35	45	47.5	46.5	44.25	46.5
16/03/2020	15	47.5	15.62	10.06	2.5	2.5	2.5	-61.21	-11.21	2.5	41.75	41.5
17/03/2020	2	22	1.95	42	41.9	42	41.9	5.05	15	42	41.9	4.50618
18/03/2020	24.31	1.95	2	5	43	43	65.6	44.95	44.95	15.7	44.95	44.95
19/03/2020	0	0	0	0	17	66	65	66	65	65	65	65
20/03/2020	17.99488	17.9	17.85	17.9	18	18	18	18	18	18	18	18
21/03/2020	39.95	7.76	40	10.17	3.42	3	3	2.5	0.5	0.09	0.09	0.09
22/03/2020	42.5	42.5	42.5	42.25	26.85	6.52	6.16	3.3	0.89	2.5	2.5	2.5
23/03/2020	30	18.83	1.95	1.95	2.1	3.85	4.1	4.1	8.03	4.1	4.1	20.65
24/03/2020	0	2.5	1.95	1.95	1.95	4.5	9.62985	9	2.1	1.95	0	0
25/03/2020	24.66	9	2	1.85	1.85	4	5.3	5.90813	7	7.3	7.9	7.9
26/03/2020	11.5	11.8	14.2	45	11.8	14.2	45	11.3	11.5	11.5	12.206	14.4
27/03/2020	12.3	21.42	12.35	38.85	38.9	38.9	14	13	13	13	13.05	13
28/03/2020	4	4	4	2.5	4.48	4.48	1.11	1.33	-0.42	0.22	4.5	38
29/03/2020	4	4	35	2.6	-4.9	0.01	1.21	0.5	4	4.68	39	41.8
30/03/2020	17.78	11.3	4	38.75	39	4	17.36	38.75	16.19	5.01	38.75	38.75
31/03/2020	36.85	6.5	2	5	39	41	41	41	41	41	39	41
01/04/2020	7.36	7.25	7.35	40	42.48	42.48	42.48	42	42	8.16	7.8	1.25
02/04/2020	21.83	23.19	1	19.06	36.85	36.85	26	16.61	14.75006	2.5	2.5	15.27006
03/04/2020	37.7	37.7	36	36.8	5	40	36	39	42	38	37.9	37.4
04/04/2020	35.85	36	38.5	38.5	38.75	38.75	38.75	38.6	36.2	36	11.26	10.64
05/04/2020	43	40	41.25	41.25	38	-8	-11.53	-25	-8	-8	-25	-28
06/04/2020	4.95	7.52	30	35	35	2.5	2.5	16.15	15.19	14.55	18.48	18.76

07/04/2020	37.4	37.4	40	42.5	42.5	40.74	40.74	39	38.9	38.5	13.57013	8.5
08/04/2020	9.11	7.5	7.49538	9.25	6	2.2	9.75	37	23.93	10.55	2.2	2.2
09/04/2020	16.30992	14.1	23.85013	37.85	42.95	42.95	40	40	36.65	35.95	35.95	35.95
10/04/2020	36.35	36.21347	37	38.45	36	37.95	41	39	39	38.9	36	36
11/04/2020	10.17	12.93	14.7	18.41	22.07	15.73	24.94	23.86	7.98	6.32	2.5	4.27
12/04/2020	36.2	36.2	37.25	37.75	35.95	37.25	37.2	37.2	37.25	37.25	37.25	38
13/04/2020	-8.4	-7.4	-8	2.5	-14.34	-8	-10.61	-7.11	2.5	2.5	36	37
14/04/2020	14.4	5.58	3.1	16.47013	38.5	38.5	4.16	4.16	22.39	8.66335	4.27	12.41156
15/04/2020	34.5	34.5	18.67	13.56	11.6	18.6	13.96	2.2	1.25	9.17	35	35
16/04/2020	8.6302	34.45	30	36	40	39	15.51	8.23	1.25	9.45	36.5	20.23
17/04/2020	8.41	8.41	1.25	8.94	23.74	36	36	36	36	28.62	27.27	36
18/04/2020	10.44	10.15	11.35	12.14	9.75	10.84	35.7	35.75	39.5	41	42	42
19/04/2020	36.5	36.5	36.4	36.4	8.69	8.69	6.49	5.87	0.5	0.5	0.5	0
20/04/2020	24.33	36.5	9.77013	10.22	8.90745	10.29	6.04	1.83	-3.48	-8.79	-8	-8
21/04/2020	5.7	36.2	10.53	37.25	37.25	40	42	36.2	42	11.91	15.19	35
22/04/2020	40	42	44.5	44.5	44	44	44	44	43	42	41.88	39.99
23/04/2020	40	18.46	15.23537	41.85	45	41.97	41.97	33.95	40	33.95	41	33.95
24/04/2020	15.36	16.06	0	2.2	17.61	17.87	16.28	16.28	2.5	2.5	35	35
25/04/2020	30	11.78	11.1	24	36.9	37	37	36.9	36.9	36.5	36	35.95
26/04/2020	8.63	8.63	8.74	8.35	6.25	6.35	3.55	8.02	10.69	9.9	10.12	11.25
27/04/2020	14.6	2.25	0	2.51	2.51	33.8	20	10.88	2.5	33.85	3.1	3
28/04/2020	15.25	4	1.1	37.5	43	50	38.75	38.75	38.75	36	35	36
29/04/2020	31.9	33	31.9	11.69	4	7.6	34.97	34.97	37.9	37.8	34.97	4.05
30/04/2020	5.48	6.48	5.86	33.9	33.8	33.9	33.9	33.9	33.95	33.95	33.95	33.94472
01/05/2020	23.25	2	4.05	35	36.95	35.95	36.95	37	37	37	37	37
02/05/2020	5.17	5.27	6.83013	5.96	5.69	6.57	6.78	6.78	8.15	33.5	7.72	35.45
03/05/2020	23.68	30	33	7.52	6.71	6.71	24.07	36	39	39	39	39.5
04/05/2020	34	34.25	34.25	34.25	34.9	36.94	37	36.94	16.3	34.9	36.94	36.94
05/05/2020	11.57	12.02	14.39	16.38	34.44	34.44	34.44	34.44	15.95	15.82	15.27	15.27
06/05/2020	22.08	21.49	21.43	21.11	25.77	34.5	34.5	16.95	16.42	25	25	18.9

07/05/2020	33	33	34	34	34.9	35	35	35	34.8	34.9	34.9	34.9
08/05/2020	15.87	23.27	33.35	16.19	18.05	34.07	34.07	34.07	34.07	35.32	34.07	33.75
09/05/2020	40.95	35	16.36	35.5	30	16.85	39	39	39	39	39.5	39
10/05/2020	44	15.96	47	12.12	-13	0.5	0.5	0.5	15.1	15.1	43	45.8
11/05/2020	-4.86	0.5	0	0.5	0.5	0.5	0.5	0.5	11.63	11.88	13.41	13.41
12/05/2020	38	24.58	2.5	2.25	2.25	4.5	4.5	5	4.5	4.5	16.05	17.1
13/05/2020	20.61	21.01	36.25	40	5.1	19.0304	6.5	15.71	35.55	22.27	35.5	36
14/05/2020	35.24	35.24	35	35.24	35.24	35	35	35	35	19.07	27.09	27.97
15/05/2020	34.9	34.95	34.75	34.75	19.26	34.75	6.5	17.93	30	34.1	15.55	4.9
16/05/2020	12.48	12.83	23.47	26.16	34.5	10.6	9.31	9.31	8.56	8.83	10.13	9.83
17/05/2020	8.99	8.99	37	38.5	30	38.25	38.5	38.45	38.45	38.45	4.44	3.94
18/05/2020	36.45	36.45	36.5	39	38.5	38.5	38.5	38.5	38.5	38	9.89	9.89
19/05/2020	16.45	16.6467	17.71	20.72	36.42	36.42	36.42	36.42	36.42	37	36.42	36.42
20/05/2020	15.27	34.29	36	36	37.05	37	37	37	30	15.82	20	30
21/05/2020	14.6	15.43008	1.1	13.6	35	37	37	35	35	12.29	9.64	9.64
22/05/2020	-70.17	-60	-65.94	-13	-11	2.14	17.4	-37.44	10	-68.67	15.24	-13
23/05/2020	18.75	17.85	19.19	16.71	16.84	17.78	20.12	51.75	51.75	16.3	14.18	4.05
24/05/2020	7	7	5.18	5	-50	9	-36.59	46	8.49	5	-60	-65.94
25/05/2020	48.5	46	49	48.5	48.75	48.5	42	42	42	15.30997	13.1	12.3
26/05/2020	43	38	1.3	3	13.49	5.41426	4.8	14.29	15.6	13.66	15.57	15.82
27/05/2020	20.52	20.34	36.4	40	40	40	40	40	16.66	17.29685	18.37	36
28/05/2020	12.9	13.15	17.3	36.6	36.6	15.03013	15.17013	6.3	15.19	37	36	35.75
29/05/2020	31	17.82	34.95	27.78	18.08	36.9	17.65649	17.43015	35.9	34.95	14.65	14.56
30/05/2020	6.83	6.83	9.4	9.4	8.9	8.9	6.5	6.5	3.94	3	4.37	4.17
31/05/2020	2.9	39	39	39	0.27	0.27	0.5	38.25	38.25	38.25	38.25	38.25
01/06/2020	39.8	39.8	39.8	40	41.7	42	42.23	42	41.65	40	40	40
02/06/2020	39.7	39.7	20.78	38	19.81	38	37.75	37.5	37.5	37.5	17.68	0.8
03/06/2020	0.8	0.8	0.95	38	3	3.1	3.1	3.25	23.26	38	25	22.57
04/06/2020	22.45	21.79	0.8	26.02	36.95	36.95	40.5	40	41	39.98	39.5	39.38
05/06/2020	12.44	12.44	24.19	24.26	24.27	24.27	18.76	18.56	14.64	0.5	0.5	0.5

06/06/2020	-46.8	0.5	-4	-1.41	-6.55	-0.85	-4.1	-2.75	-3.91	-1.4	-0.5	0.5
07/06/2020	10.61	10.61	11.74	11.74	10.35012	11.42	23.39	23.78	26.72	25.11	26.74	20
08/06/2020	41.5	44	41	37.64	44	44	44	45	44	44	27.7301	44
09/06/2020	36.95	36.95	28.09	6.1	46.50337	48	42.06	6.1	6.1	6.1	6.1	7.15
10/06/2020	7.05	34.38	8.3	36.5	8.2	30.65	36.5	36.5	40.75	41	36.5	40.75
11/06/2020	0.55	42	25.45	39.5	41	35	40.95	40.75	41.25	40.5	40.25	39.45
12/06/2020	16.62	19.14	23.28	39	39	39	39.5	17.66	19.32	17.18	16.91	39
13/06/2020	39	39	16.54	16.06	15.74	38.5	38.5	38.5	39.8	38.5	38.5	38.5
14/06/2020	26.38	30	23.5	37.8	37.8	37.8	38	41.25	41.9	41.5	41	37.5
15/06/2020	37.9	37.95	37.95	44	44	44	45.9	45.9	44	44	44	44
16/06/2020	11.1	1.1	35.99	40.33	36.61	41	50	45	51.5	49.6	47	37.61
17/06/2020	36	36.25	15.25	37.69	39.6	41.6	10.99	10.72	47.99	11.5	11.5	9.35
18/06/2020	32.42	12.70445	35.46	35.21	13.6	45.75	45.75	46.5	45.75	45.75	45.6	46.9
19/06/2020	39.5	40.9	39.5	39.5	40.9	48.49	48	46	43.27	40.9	39.5	38
20/06/2020	21.22	37.5	38.5	38.5	20.57003	42.9	43	44.94	44.94	44.94	44	43
21/06/2020	0.5	13.98	16.2	17.02	-16	0.5	10.09	10.09	0.5	0.5	0.5	12.82
22/06/2020	43	43	42	31.9	28.5	27.33	27.04	28.77	25.93008	1.65	5.27355	0.55
23/06/2020	43.36	43.28	41.45	41.45	41	41.5	36.36	3.5	3.5	3.5	40.5	40.5
24/06/2020	38.9	38.9	1.1	41.28	42.5	42.5	42.5	44.94	44.94	43.25	4.7	43.25
25/06/2020	45	45	45	45	43.25	45	45	44.5	44.5	43.25	8.15	8.15
26/06/2020	33.3	40	8.5	49.25	45.5	45.5	45.5	43	40.5	10	39.94	10
27/06/2020	0.5	0.5	0.55	23.51	23.73	38.9	28.25	28.49	20.76	20.47	8	16.19
28/06/2020	-60	-60	-60	-60	-65.94	-60	-48.0978	-16	-16	0.05	-13.39	-9.9
29/06/2020	34.89	35.84	39.32	40.9	34.9901	44	49.99	32.5	48	48	8.32	48
30/06/2020	39	39	39	11	47	45	45	39	45	45	45	45
01/07/2020	37.48	7.87	5	8.03	8.11	46.5	46.99	46.5	0	5	43	43
02/07/2020	40	40.77	8.6	43.77	41.9	41.98	42.4	42.4	42.3104	42.4	42.4	46
03/07/2020	11	11	47	47	41.85	42.85	11	11	11	11	11	11
04/07/2020	0.5	8.05013	0.5	10.25013	0.5	19.93	18.2	40.5	44.25	44.25	44.25	43.25
05/07/2020	3.57	6.8	-1.52	46	-3.35	46	47	47.25	15.22	4.37	8.83	46

06/07/2020	0.5	45.56331	31.4	45	22.25	43.75	24.49	42.75	41	41	46	45
07/07/2020	46	2	5	38	39.5	5.15	5.15	5.5	6	6.17	44	44
08/07/2020	1.6	4	15	15	42.58	42.58	12.5	49	47	15.1	35	50
09/07/2020	0.55	0.6	5	10.1	10.1	12.1	47.02	26.22	48.25	48.25	14	45.94
10/07/2020	39.7	39.5	5.25	41.49	42.39	42.8304	16	16	16	40.12	44.25	44.25
11/07/2020	36.75	37.49	25	25	36.75	25	23.33	27.65	21.5	21.5	22.91	37.7
12/07/2020	19.02	35.95	35.5	15.25	13.44	19.22	20	13.78	13.38	38	38	39
13/07/2020	39.89	4.05	7	39.23	4	4.45	4.7	46.25	46.25	46.25	37.5	4.48437
14/07/2020	36.5	38.57	40.5	39.95	39.75	40.5	40.25	40.25	41.95	41.95	41.95	40.25
15/07/2020	26.52	36.15	39.5	25	35.8	36.39	44.99	44.99	35.66	18.06	18.22	18.22
16/07/2020	35.3	36.1	47	52.55	58.35	48	48	42.86	43.67	42.78	42.87	42.74
17/07/2020	21	21	11	20	21.21	21.25	21.25	20	20	20	38.53	38.07
18/07/2020	37.8	38.75	45	38.75	22.2	22.58	23.16	23.46	23.52	23.31	27.39004	27.39004
19/07/2020	0.5	0.5	22.64	41.75	20.18	20.89	20.64	20.57	37.45	14.7104	6.6704	12.54
20/07/2020	38.5	38.99013	38	37.43014	9	12	12	12	12	12	44	44
21/07/2020	37.97	37.98	36.9996	39.26	41	15.75	41	2	15.75	15.81	38.97	41
22/07/2020	35.98	36.18	18.25	37.51	13	15	30	40	18.5	18.5	18.5	18.5
23/07/2020	38.54	20.15	37.44614	40.97013	36.36	37.01	30	15.25	15.2	15.2	17	17.05
24/07/2020	41.49	41.49	38.21	52.5	53	52.5	52.5	49.99	52.5	52.5	52.5	52.5
25/07/2020	4.91	30	1.01	39.9	13	22	30	43.55	43.55	43.55	43.55	43.55
26/07/2020	39.75	39.75	39.75	39.7	16.11	16.22	40	40	13.89	12.66	15	16.53
27/07/2020	16	4	10	68.85	16	75	10.5	73.88	10.5	10	10	10
28/07/2020	15	35.55	33.27	32.47	11.91	38.68	38.28	38.28	15	9.77	2.56	2.56
29/07/2020	37.46	37.23	16.44	16.44	1.05	6	38.41	2.65	11.84	38.77	38.87	11
30/07/2020	37.89	38.21	42.38	43.34	46.5	46.5	46.5	43.38	55	45	15.3	15.3
31/07/2020	39	39.25	40.95	42.48	40.3	43.95	43.95	29.7	42.91	19.57	15	15
01/08/2020	39.5	38.95	40.5	20	15.58	43	2	24.15	43	27.57	5.25	10
02/08/2020	1.05	1.05	15.52	38.55	29.75	29.48	22.01	28.12	21.22	23.06	38	38
03/08/2020	41	8	6	40.34	19	19	19.5	19	49.73	19.5	47.29006	47.29006
04/08/2020	35	36	15.1	39	45	45	45	38.35011	37.57	37.76	45	38.33

05/08/2020	1	33.52	45	46	45	44.9	44.9	44.9	44.9	43.95	1.2	30.88
06/08/2020	42.03	38.48	7	46.99	47.4	47.5	48	47.5	47.4	46.99328	47	47.4
07/08/2020	39.61	39.55	15	40.56	45.65	45.65	45.6	45.6	45.6	17.2	43.5	17.25
08/08/2020	32.97	33.05952	5	34	42	42	41.95	25.02	24.98	1.2	0.6	1.2
09/08/2020	28.04	23.43005	29.72	40	40	43	43	44.2	44.95	44.5	43.95	30
10/08/2020	45	40.74	38.4	46	45.9	46.99	46.98999	46	46.99	54	47	43.25
11/08/2020	40.95	40.95	40.9	47.95	47	50	49.5	47.79811	49.5	11.33	45.133	48.47031
12/08/2020	15	15.2	15.3	41.83	1.7	15	15	16	75	16.31	15.36	15.36
13/08/2020	37	18.6	39.95	40.87	40.98	52	52	52	52	49.9	49.6	52
14/08/2020	34.98	35.89	37.83	40.9	54.95	60	59.94	54.95	52.7	53	53	49.5
15/08/2020	41	41	21.5	21.5	21.5	42.5	45.67	45.67	45.67	49	45.67	49
16/08/2020	39.86742	39.75	24.47	24.17	24.59	23.77	21.55	42.4	43.8	43.8	43.8	43.8
17/08/2020	41	22.1	22.1	44.3	42.98	52	75	96.16	79.02	82.11	92.16	77.16
18/08/2020	40.8	40.8	43.76	47	24.6	49.95	24.6	38.33	34.99	49.95	24.7	24.7
19/08/2020	45.14	43.8	25.52	47	51.45	56	65	63.75	74	74	65	65
20/08/2020	43	49.99	48.5	49.99	49.99	49	49	49	48	48	29.14933	30.66
21/08/2020	37.03013	52.4	31.81	51	31.56	51	47.5	28.03	27.02	27.26339	48	48
22/08/2020	28.76	51.9	22.01	48	24.66	26.86	22.5	23.24	22.06	19.62	46	17.03
23/08/2020	45	44.8	17.42	45	17.82	44.7	44.8	44.75	45	44.75	44	44.75
24/08/2020	44	7	10	10	7.6	10	0.6	10.20059	1.7	10	10	10
25/08/2020	12	45.8	2	48.27	44.43013	45.07	43.57022	42.82	39.47	20.25073	39.87	40.03
26/08/2020	52.5	52.5	52.5	52.5	31.42	49.95	49.95	49.95	49.95	49.75	45.95	35.1
27/08/2020	50	68	17.4	50	50	17.4	22.05	75	75	75	75	75
28/08/2020	47.45	47.45	15.25	45.5	50	51.25	50	15.45	15.25	15.25	15.25	15.6
29/08/2020	24.03	24.63	26.97	31.53007	29.2	31.7	29.78	29.75	28.17	28.17	27.89	30.87
30/08/2020	49.25	50	49	50	49	49	48.95	48.95	48.95	26.11	17.4	30
31/08/2020	64.27	7.6	52.9	63.25	45	55.11	26.5	12.3	12.25	12.26795	26.75	27
01/09/2020	54.45	54.45	55.45	68	64.02	62.3698	55.8	28.05	53.0504	28.25	28.5	49.7904
02/09/2020	27.85	28.81	53	56	56	56	53.5	36.44	24.8	50.74	46.91	46.53
03/09/2020	54.8	52.09808	49.88	52.8	53	53	52.95	52.95	55	52.85	52.95	52.95

04/09/2020	45.6	43.08	47.84	55	56	58.5	58.5	55	55	44	39.9	53
05/09/2020	1.5	50.85	30.68	50.85	53	52.25	53	52.25	53.9	53	53	52.25
06/09/2020	49	49	26.04	26.67	49	40	49	49	29.31	18.6	40	53
07/09/2020	55.29	57	57	57.75	57	57	51.88	45.87735	51.88	30	51.88	54
08/09/2020	52	52	59	59.85	59	57.7	53.35	52.94	52.94	52.94	56.97	52.94
09/09/2020	52.5	35	15	19.7	55.25	55	55	55	30	15	19.7	30
10/09/2020	48	52.25	59.5502	61.79	73.84998	73.85003	73.85	73.85	73	44.85	73.85	29.25
11/09/2020	50.5	49.95	52.52	56.4	52.52	54	55	55	52.52	52	51.75	51.75
12/09/2020	-5	0	15	35.59	2	28.18	23.34	23.74	15	0	6.13369	15
13/09/2020	30	30.21	17.22345	53	53	53	13.8	15	2	2	15	2
14/09/2020	23.3	59.89	23.35	70	62	52.15005	47.97	50.86	65	65	58	59
15/09/2020	87.04	88.94	96.32	100.07	91.74	96.74	99.99	99.99	101	30	99.98993	85
16/09/2020	28.5	31.1	79.5	86.57	79.5	80	85	80	79	31.15	31.15	31.15
17/09/2020	26.55	53.73	30.65514	79.89	31.4	0	58.95	15	52.23	31.5	31.5	31.55
18/09/2020	26.01	50.5	26.1	60	60	27.02	27.02	26.1	26	15	27.25	27.5
19/09/2020	53.75	53.75	53.5	53.5	53	52.7	52.65	50	50	18.89013	15	2
20/09/2020	28.62	29	53	53	30.46	31.09	29.5	29.04	31.67	49.5	49.5	49.5
21/09/2020	2	15	15	25	69	46.4	22.5	20.5	20.5	15	20.5	30
22/09/2020	30	60	58.75	58.75	61.5	26.12	58.75	26.18	40	26.2	46.5	30
23/09/2020	54.45	49	21.5	26.57	26.57	30	62	62	62	62	60	60
24/09/2020	49.5	53	60	58.5	58.5	65	64.5	25	20.5	20.5	58.95	64.5
25/09/2020	5	20.5	20.5	60	62	25	65	26.6789	57.88	57.88	57.88	57.88
26/09/2020	14.26	20.97	29.89	52.5	35.37	53.95	54.25	53.95	53.95	32.06	37.82	53.25
27/09/2020	16.32	16.37	50.3	50.3	52	53	28.02	39.93	29.83	28.89	31.24	30.3
28/09/2020	57.75	58.44	60.5	62.65	64	64	60.5	60.5	63.8	63.8	60.5	60.5
29/09/2020	68.44	71.22	86.48	110.81	101.68	101.37	139.7	108.4	108.4	40	139.7	40
30/09/2020	56	25	63.5	68.5	63.5	64.33	63.5	63.5	68.2096	70	70	70
01/10/2020	22.5	20.3	12.3	25	65	28	22	22	65	28.25	64	64
02/10/2020	53.5	50	5	53.5	56.2	53.5	53.5	57.5	65.5	57.5	56.2	15.5
03/10/2020	58	58.25	60	58.25	62	62.99	62.99	66	69	62.99	62.99	67.5

04/10/2020	8.8	6.26	7.22	7.22	2	61	15.69959	14.71029	58.75	58.75	62	62
05/10/2020	58.13996	57	16.25	20.15	68	68	68	68	64.9	21.16	21.28	55
06/10/2020	21.3	15.75	62.25	62.25	62.25	62.25	62.25	24.12	15.7	57	56.5	56.5
07/10/2020	53.2	53.25	16.34736	30	59.5	59.5	59.49342	59.25	57	9	15.5	15.7
08/10/2020	4.5	10	50.91	58.9	61.48598	62	62	58.9	62	58.9	26.16	26.01
09/10/2020	49.9	37	59.6	60.4	60	60	64.5	62	28.55	28.55	28.55	28.55
10/10/2020	0	57.95	31.56	59.5	33.45	33.45	59.5	63.4	60	59.5	59.4	53.5
11/10/2020	25.57	26.49	57	57	36.92	36.48	40.27	41.36	35.13	36.73	31.66	56.95
12/10/2020	56.19	27	27	67.8	72	67.92173	72	72	27	72	72	72
13/10/2020	63.95	57.8	74.17	76.32	74	74	74	65.5	70	74	65.5	35.08372
14/10/2020	54	54	27.96	66.5	69	66.5	28.11	28.12	64.49	57.5	64.49	64.49
15/10/2020	28	54	29.25	53	73.8	67.71844	73.8	58	60	13	13	60
16/10/2020	68	30.36	30.36	32.15	30.45	13	72	67.5	67	32	13	32
17/10/2020	24.1	29.63022	25	53.5	61.5	64.85	59.5	64.85	53.25	30.5	59.5	13
18/10/2020	58.75	57	15.25	27	60	57.5	27	57.5	60	65	66.85	67
19/10/2020	28.25	17.2	68.36	69.86	62.5	62.5	62.45	27.05	62.45	62.4	27	27
20/10/2020	41.4	40.15013	15	58	58.8	58	58	58	58	58	58	58.7
21/10/2020	0	0	22.55	28.13	62.05	67	62.05	67	67	67	67.89	62.05
22/10/2020	58.75	5	18	58.5	18.1	18	31.25	15	58.5	27.1	30	57
23/10/2020	58.5	53.84	55.51	56.17	32.21	32.22	32.22	32.25	32.27	32.35	74.5	74.5
24/10/2020	12.48	20	20	24.82	3.17628	5	27.4	63.3	64.25	64.25	63.4	63.3
25/10/2020	62.9	63.95	63.95	63.95	64.45	63.4	5	62.9	62.95	62.95	62.95	12.77
26/10/2020	37	39.15008	20	20	20	68.4224	20	20	18	11	9	11
27/10/2020	72	22.5	22.5	22.6	68.25	68.25	69	68.25	68.25	68.25	27	23.51
28/10/2020	5	23	23.56	40.51	60	64	64	63.94	24	23.75	23.75	63.94
29/10/2020	67.5	62	51.12	12	12.05	12.11	63.55	63.55	69.5	67	63.5	63.5
30/10/2020	61.5	65	3.85	3.85929	3.85	3.9	12.65	33.45	36.73	56	34.27	55.95
31/10/2020	34.01	34.69	30	4.5	5	4.5	19.42	20.37	22.89	29.13	27.54	26.27
01/11/2020	-18.85	1.89	7.2	15.74	-61	-61	-60	-0.71	62	62	25	18.5
02/11/2020	18.13	27.57	63	64	63	28.86	18.01	18.01	18.00771	18	18	18

03/11/2020	69.69	61.5	61.5	61.5	63	63	67	63	61.5	16.5	16.5	17
04/11/2020	16	4.5	61.85	64.8	64.8	64.75	62	17.87	27.1	27.1	18.2	18.04
05/11/2020	50.3	56.7	3.85	62.05	64.5	64.5	64.5	62.05	59.8	3.85	57	57
06/11/2020	22	22.3	64.5	64.5	64.5	65	65	64.5	64	23	23	23.1
07/11/2020	59	59	59	59	59	59	59	59	59	59	59	59
08/11/2020	56.5	56	5	5	5	5	5	56	59.25	59.5	59.5	59.95
09/11/2020	59	19.2	29.5	65	64	65	65	66.99	66.99	65	66	65
10/11/2020	23.1	23.15	23.15	53.21	23.1	23.1	24.1	23.25	24	24	65	58.95
11/11/2020	58	58	39.51	59.9	61	25	42.03	59.9	59.9	25	59.8	59.9
12/11/2020	26.71	63.95	5	37.47	66.9	63.85	64.81989	63.81994	11	11.0004	11	6
13/11/2020	68	68	65	66.9	61.98	61.95	61.95	61.9	60	55	4	6
14/11/2020	29.83	6.1	33.13	63.35	62	35.18	34.33	34.48	35.23	59.8	59.89297	61.9
15/11/2020	-2.9	-2.9	-30	5.02	4.5	11.91	9.78	20.1	26	19.01	26	5
16/11/2020	43.22	55.91	-60	47.15	59	59.8	59.8	59.8	59	59.8	59	59
17/11/2020	7.03	40.89	41.38	45.55	37.9	59	59.95	59.95	62	59.95	6.1	6.80327
18/11/2020	45.81	47.09	44.94	46.08	35.59368	32.61658	6	30	33.64	63	63	63
19/11/2020	19.22	63	63	59.9	59.7	66.9	69	75	68	59.95	58.75	16.5
20/11/2020	58.8	60.36	63	66.88	18.17	74	74	58.8	18.2	61.5	18.26	15
21/11/2020	31.96	6	6	0	0	27.12	23.16	26.55	27.85	29.57	36.44	5
22/11/2020	25.48	30.38	32.02	38.07	26.73	5	59	33.39	28.05	59	58	6.6
23/11/2020	5.1	2.5	7.2	57.25	57.25	-15	61	60	57.25	60	57	57
24/11/2020	58.45	58.45	54.71011	55.18	58.5	25	9.22	10	58.7	58.75	9	58
25/11/2020	58	52.1	50.43	51.8	59.25	60	16	60	60	60	65.98	60
26/11/2020	67.9	66.8	3.85	68.9999	82	86	75	69	144	84.99	84.88378	75.0003
27/11/2020	54	66.66	33.52	78.23	34	69.00011	66.66	66.66	33.6	66.66	66.66	72.25
28/11/2020	53	36.37	53.88915	53.88061	36.3	59.75	62	62	62	70	60	67.98
29/11/2020	54	56	44.1	42.6704	56	54	35	65.00048	68.98	66.85	63	72.7
30/11/2020	6	3.85	6	3.85	3.85	52	3.85	53	54.75	53	52.69	52.65
01/12/2020	76.34256	52.9	70	70	72	74	69.25	69.25	72	68.96	69.25	58.17006
02/12/2020	56	29.6	85	85	88.17122	106.74	103.28	100	98.9	90	79.36	79

03/12/2020	56	57.92	35.1	67.05	85	92.75882	135	135	135	80	34.5	90
04/12/2020	6	20	29	55	67	69.95	69.4	69.4	86	90	80	75
05/12/2020	57.9	5.9	5.95	10	30	56.47	64.9	65	64.9	63	15.4	30
06/12/2020	21.75	10	21	21.5	0	53	22	73.5	25.75	70.79	25.75	25.25
07/12/2020	72	61	30.15	125	188	188	188	188	199	192.3374	351.2	349
08/12/2020	53.5	25	5	71.05	85	56	32.80928	86.38	123	120	36.15	36.3
09/12/2020	33.45569	33.55	33.55	89.99	37.12	98.73	99.47	144	98.97	97.48	99.29	98.95
10/12/2020	67	5	6	67	55	55	80	89.34	89.82	66.85	36	36
11/12/2020	59.5	56.77	5	60.5	60.5	60.5	5	5	5	5	85	88.99
12/12/2020	59.7	59.7	36.61	32.15	33.5	62	62	32.2	32.25	34.15	62	62
13/12/2020	32.2	6	60.6	6	25	63.5	61.9	49.65	49.77	63.5	63.5	68.9
14/12/2020	7.5	7.5	55.75	53.4	0	6	64.46	64	62.75	62.75	65	62.75
15/12/2020	69	65	57.5	73	72.98	72.98	69.90804	60.46	57.22	57.76	23.35	23.4
16/12/2020	59.5	7	59.45	61.95	59.45	60.72996	62	61	62	62.6	60	62.6
17/12/2020	63	62.5	58.59067	62.51	73.5	73.5	69.95	20.2	70	23.5	20.5	23.5
18/12/2020	65	65	55	56.24	23.75	56.98	64	68	23.75	23.86595	65	65
19/12/2020	65	66	67	65	65	65	66	65	64.95	30.18	36.1	18.6
20/12/2020	64.75	66	64.75	65	39.29	65	65	65	64.75	64.5	64.5	64.5
21/12/2020	66.75	66	49.9	20.2	20.1	35	70	70	66	70	70	67
22/12/2020	6	4.5	4.5	4.5	4.5	4.5	74.98	74.8	75.9	40	5.15	70
23/12/2020	21	25	23.81	23.81	27.1	69.45	72	72	77.7	77.75	78	77.7
24/12/2020	24.6	64	65	64.95	38.44	7.5	64.95	64.95	64.95	64.95	64.95	64.25
25/12/2020	63.95	64.5	64.5	62	35	68	73.5	74.98	75.75	75.75	75.5	78.85
26/12/2020	-63.93	-19.07	-30.26	-20.67	-25	14.58	0	0	18.1	20.58	36.55	41.31
27/12/2020	7.5	70	71	72.5	7.5	20.2	35	23.76	20	64.5	18.6	18.6
28/12/2020	65.5	20.3	54.27	25	25	68.9	71.87497	85	94	85	85	84.99
29/12/2020	75	75	32.11	32.11	32.11	32.11	32.11	67	74	74	74	74
30/12/2020	70.5	69	65	63	31.55	31.65	31.65	31.65	45	72	72	72
31/12/2020	68	66.15	66.15	66.1	33.41	33.41	72	73.5	73.5	73.5	73.5	35.5

Table III-3 TIME-OF-USE Electricity Tariff Data (12:00–17:30), 2020, Provided by LimeJump — Part 3

Date	12:00	12:30	13:00	13:30	14:00	14:30	15:00	15:30	16:00	16:30	17:00	17:30
01/01/2020	51.9	51.9	51	51	50.75	7.5	7.5	50.8	52	50.8	52	52
02/01/2020	50	50	52	50.5	50	8.8	50.5	50	8.8	8.8	8.9	8.9
03/01/2020	9	9	9	9	9	9	9	9	9	52.5	55.5	55.5
04/01/2020	6	7.75	7.75	7.5	6.75	49.9	49.9	52	80	150	150	150
05/01/2020	8	48.94	48.94	48.95	49	49	48.94	50.45	51	50.5	52.7	51
06/01/2020	11	48.94	48.94	48.94	53	53	53	57.5	53	56.5	56.5	56.5
07/01/2020	43.26	43.09	42.24	41.41	11.85	11.85	11.9	40	49.5	51.75	49.5	49
08/01/2020	51.95	51.95	51.95	14	4.5	51.95	50.95	60.84	22.5	60.84	4.5	18
09/01/2020	18.55	50	18.5	50	69	69	69	70	19	19.1	18.05	19
10/01/2020	55	52	19	19	19.11	19.16	43.11	43.11	57	57.75	57	55
11/01/2020	54.5	60	60	50	54.5	54.5	19.4	19.4	10.25	49.95	10.25	19.25
12/01/2020	10.01	15.29	10.2	10.11	10.26	10.26	10.26	10.35	58	58.85	58.95	58.95
13/01/2020	54	54	53.45	54	11.3	53.45	53.45	55	54	54	54	53.25
14/01/2020	58	58	55	55	55	55	55	55	59.75	59.75	59.75	58
15/01/2020	13	12.5	50	12.5	5	10	10	11.55	50	54.25	54.75	54.75
16/01/2020	50	49.85	12.5	32.79	47.97	20	46.98	47.97	49.45	49.45	49.45	50
17/01/2020	15.7	15.7	15.85	16	15.95	16.05	16	16.2	16.25	54.5	54.5	54
18/01/2020	16	16	16	11.75	16	16	49.5	52.5	19	50.07992	52.5	52.5
19/01/2020	19.25	49.45	49.45	19.25	19.25	19.25	51.9	54.83213	55.5	54.65	55.5	60.9
20/01/2020	40	20	3.5	3.5	3.5	20.5	20.51	20.51	5	20.6	20.35	21
21/01/2020	21.8	21.8	22.25	22.5	22.5	22.5	22.65	83.75	84.5	99.5	99.8	98
22/01/2020	150	150	23.85	23.85	24	28	28	100	24.3	99	99	99
23/01/2020	58	26	25.85	25.8	25.5	25.9	26.05	72	26.1	26.1	26.1	26.1
24/01/2020	57	27.31	27.3	27.3	27.3	27.3	74.85	47.24	27.3	27.3	27.3	27.3
25/01/2020	53	53	50	46.15	50	46.15	27.25	46.15	50	50	50	50

26/01/2020	50.5	50.49	49	11.1	11.1	11.1	49	47.5	53.5	57	57	57
27/01/2020	17.39969	54.75	55	55	49.9	54.5	62.75	62.75	62.75	62.75	62.75	62.75
28/01/2020	49	50	50	50	48.5	16.25	17	50	17	17.15	51.7	55.7
29/01/2020	18.51	18.61	18.77	18.77	19	47.2	18.1	47.5	49	49.75	51	51
30/01/2020	45.5	45.5	45.5	2.75	2.75	5	44.9	32.7	18.25	44	44.85	44.83
31/01/2020	47	47	47	40	48.7	13	13	2.2	3	3	48.7	48.7
01/02/2020	3.13	40	11.3	12.24	13.13	46.5	46.5	40	48	51.5	57.2	57.2
02/02/2020	46.85	8.25	8.36	8.55	47.7	47.7	47.7	47.7	47.7	48	53.9	53.9
03/02/2020	47.75	47.75	47.75	47.75	47.75	47.75	47.75	47.75	47.75	49.5	50	50.5
04/02/2020	56	56	56	56	48.95	47	13.4	13.25	13.35	14	47.9	15
05/02/2020	0	2.35	2.35	15.9	16	16.1	16.12	16.21	16.38	16.4	16.53	16.45
06/02/2020	15.5	16	16.22	16.3	16.5	17.12	17.25	34.6	38.37769	17.45	17.95	115.71
07/02/2020	17.45	12.5	17.8	12.5	43.95	44.8	44.8	44.95	44.8	46.51279	47.5	48.6
08/02/2020	43.8	37.19	29.9	12.13	12.13	28.64	34.65	43.8	43.8	43.8	44.3	47
09/02/2020	51.5	51.5	51.5	48.5	48	47.8	8.2	8.6	10.25	48.5	48	48.5
10/02/2020	45.75	45.75	45.45	45.5	45.5	45.45	45.5	44.95	46.65	46.65	46.65	48.84
11/02/2020	45	45	45	44.9	44.8	44.8	13.35	45	45	45	47.5	51.15
12/02/2020	3.57	23.08	13.6	13.6	13.6	2	42.9	45	45	51.03	36.75523	50.28271
13/02/2020	44.5	44.5	41.98	44.5	44.7	41.98	16.5	16.5	16.55	58.29	58.29	69.29
14/02/2020	43.15	41	40	40	42.23	42	38	38	38	38	41.85	41.85
15/02/2020	42	42	42	40	40	40	41.5	41.5	41.5	42	42.5	43
16/02/2020	43.45	43.4	43.84	43.4	43.4	43	21.78	2.5	42.5	43.4	43	45
17/02/2020	42	23	27.41	26.57	39	7.1	7	7	7.5	9.1	13.1	50
18/02/2020	42	41.75	41.7	41.7	41.7	42.4	42.4	42.3	49.75	49.8	49.8	51
19/02/2020	46.28	45.9	45.9	43.45	43.45	43	15	42.79	14.75	2.2	2.2	48.5
20/02/2020	44	43.5	43	40	12	12	2.2	2.1	2.1	13	50.8	50.9
21/02/2020	44	44	44	44	44	43.7	21.47	44	44	10	7.6	49
22/02/2020	46.3	46.3	46	46.3	46.2	46.2	46.2	46.2	44.61459	47.7	47.7	51
23/02/2020	2	2	0	1.4	2.15	8.13	2.1	45.1	45.4	45.4	45.4	51.15
24/02/2020	52	49	49	55.95	49	49	10	13.1	48	47.8	47.8	13.2

25/02/2020	46	49	70	47.9	70	69.9	48	69.99	48	67.1	67.79	77.29
26/02/2020	43.25	16.2	2.35	14.1	14.1	14.1	16.55	2.35	2.5	16.55	55.5	83
27/02/2020	17.65	17.85	17.92	17.92	17.92	17.92	18.11	18.1	18.15	43.5	52.55	55.9
28/02/2020	45	45	45	45	45.75	45	15.5	15.6	39.45	45	15.95	45.75
29/02/2020	4	4	4	2.35	2.75	4	0	2.35	2.35	44	45.95	46.8
01/03/2020	42	42	5.31	5.15	4.53	4.44	4	4	5.1	42	46	46.7
02/03/2020	46.5	30	18.5	17.53	18.5	17.53	15	13.9	17.53	43	48	49
03/03/2020	46.5	47.5	57.5	47.5	52.99	44.75	45.5	44.75	44.25	51.4	59.5	71.9
04/03/2020	22.8	37.35	72	38.5978	38.35	23.35	23.35	23.47	125	125	119.14	144.14
05/03/2020	24	24	25.05	25	25.35	47	42.8	25.25	47	47	25.35	25.35
06/03/2020	23.8	23.8	23.9	23.9	23.9	0	0	0	24	42.9	23.99	24
07/03/2020	2.35	2.2	5	20.17	21.14	21.06	25.38	22.4	2.35	2.35	2.1	2.35
08/03/2020	7.8	7.8	42.75	42.75	42.75	14.4701	43	43.5	43.84	48	50	52
09/03/2020	43.75	15.05	13.6	14.53	1.85	13.1	13.75	2.2	42.7	42.45	47.95	54
10/03/2020	42.25	42.25	42	15.36	14.98659	26	13	13	13.1	42.25	42.25	45
11/03/2020	13.1	13.1	18.28	43.95	43	13.1	13.18049	14.5	41.99	41.99	47.5	52
12/03/2020	44	43.85	43.85	21.12	43.85	43.85	44	46	44	46	48	48
13/03/2020	42.5	16	16	16	16.5	16.5	16.5	47.25	47.25	17.26	16.5	20
14/03/2020	43.85	44	43.85	15.96	17.97013	16.52	12.10288	2.89	2.5	2.5	2.5	46.5
15/03/2020	46.5	46	46.5	46.5	46	44.25	2.5	3	44.5	44.5	45	47.45
16/03/2020	41.5	40.95	40.95	2.5	41.5	2.5	2.5	2.5	20.48294	34	40.95	2.5
17/03/2020	1.95	1.95	5	42	42	42	42	43.85	44.5	49.5	40.45	2.1
18/03/2020	44.95	44.95	44.95	43.43	35.69	8.01	43.35	46	49.49	49.49	58	58
19/03/2020	105	17.02	65	17.02	17.1	17.24	17.24	17.24	17.4	17.76	17.76	17.9
20/03/2020	18.5	39.69	39.5	39.5	39.5	18	39.49	18.55	18	18	18	18.55
21/03/2020	0.68	1.93	0	0	2.21	2.38	4.58	3.58	42	43	43.75	46
22/03/2020	41.9	41.9	41.9	2.5	1.95	1.95	2	1.95	3.55	3.7	3.75	3.75
23/03/2020	22.31	41	40	16	16	23.15	40	14.52	40	41	41.9	49
24/03/2020	2	2.5	11.03	2.1	0	2.1	23.74	2.5	2.5	2.5	39	44
25/03/2020	7.9	7.9	7.9	7.9	7.9	3.1	9	9	9.5	9.65	9.65	11.2

26/03/2020	15.25	15.2	37.5	16	12	12.25	14.4	15.3	15.3	34	15.2	15.35
27/03/2020	13	13	13.06	3.5	11.31	3.5	3.5	3.5	36.75	37	44	44
28/03/2020	39	41.8	41.8	38	4	-6.07	-1.06	0	7.99	41.5	41.25	41.25
29/03/2020	40	41.8	41.8	40	40	39.5	42	44	42	44	45	45
30/03/2020	42	40.5	39	38.25	5.9	5.9	5.91	6.13	6.14	39	40.5	41.95
31/03/2020	54.69131	41	41	6.55	6.55	6.55	6.6	6.61	41	7	7	42.65
01/04/2020	40	40	40	40	40	40	40.6	40.6	40.6	40.6	40.6	43.45
02/04/2020	38	38	38	9.83	8	2.5	22	22	22	36.75	38	40
03/04/2020	9.25	37.4	9.35	9.4	9.35	9.35	9.7	9.75	9.7	9.95	10	39
04/04/2020	8.21	6.66	6.96	6.96	7.49	3	2.25	2.75	2.5	37	40.5	44
05/04/2020	-25	-8	-8	40.65	-58.4	-50	47.99	-37	-8	50	48	50.5
06/04/2020	37	37	6.77	3.69	3.45	2.5	6.97	8.88	7.5	2.09494	3.1	18.2
07/04/2020	8.6	7.7	36.5	36.5	7.82	8.6	7.3	36	19.43	8.6	8.6	42
08/04/2020	10.6	10.69	11.15	11.15	11.15	11	2.2	10	11.4	11.55	11.55	11.7
09/04/2020	35.5	35.5	35.5	35.25	12.76	13.75013	9.2	34.5	34.5	35.75	35.75	38.2
10/04/2020	36	36	36	36	36	36	35.9	30	36	39.9	39.9	45.6
11/04/2020	4.98	5.78	2.5	1.99	3	3.35	10.35	33	33	33.75	33	37.8
12/04/2020	39.5	39.5	39.5	38	37.5	38	38	40	40	45	45	43.95
13/04/2020	37	38.75	39	38.75	36.5	36.5	36.5	3	38.75	3	38.75	49.5
14/04/2020	4.34	4.3	4.30083	4.3	4.3	2.2	4.75	4.75	5.1	2.2	2.1	30
15/04/2020	35.8	35.8	34.9	20.99	30	4.95	7.27013	7.27013	2.2	35.8	6.1	36.5
16/04/2020	36.5	36.5	25	0.6	7.99013	36	36	7.69013	9.27059	36.4	40	42.5
17/04/2020	36	20	10.71	2	1.25	1.25	8.54	36	36	36	38	40
18/04/2020	42	42	41.5	41	40.95	40.95	40.95	12.06	37	41.5	47.75	47.75
19/04/2020	0	0	0	-8	-8	-8	35.75	36.4	40	45	39.25	43.25
20/04/2020	-8.42	-45	-53.68	-55	-55	-55	-61	-65	-65	-50	-8	10.68
21/04/2020	-50	-56.61	0	-48.8	-50	-55	-55	-53.76	-42.7979	0.85	0.5	41
22/04/2020	39.99	29.78	42	42	39.99	40	41.88	41.88	41.9	41.5	41.5	43
23/04/2020	33.95	41.95	41.95	41.95	40	33.95	11.72	2.5	2.5	41.95	51	43
24/04/2020	11.22	2.5	0	2.5	2.5	5	2.5	2.5	2.5	2.5	5	5

25/04/2020	34.5	34.5	7.39	7.04	7.32	7.24	8.57	8.57	5.4	6.13	35.9	36
26/04/2020	8.74	34	34	34.25	33.85	33.5	33.5	33.85	33.85	34.25	36.1	39.75
27/04/2020	13.45	33.85	10.87	5	5	33.25	33.1	5.05	5.05	33.85	36	5.5
28/04/2020	42	51.95	55	47	40	38.75	38.75	38.75	38.75	48.25	48.25	51.95
29/04/2020	37	34.95	34.5	10.86974	4	4	4.05	3.5	4	7.36	33.74	33.74
30/04/2020	33.95	33.95	33.95	4.56	3.8	4.05	10.02	6.61	34.95	38	34.95	35.95
01/05/2020	37	37	38.5	37	35.95	35.95	35.95	4.15	4.05	4	4.15	4.15
02/05/2020	35.45	35.45	35.45	35.45	35.45	6.4	6.81	6.62	8	8	37	38.85
03/05/2020	50.5	50.5	48	41	39.5	39.5	39.5	39.5	49	51	51	49.25
04/05/2020	37	37	36.92	34.9	34.9	10.47013	33.25	7.63	7.93	5.6	36.94	39.45
05/05/2020	14.45	14.45	32.98	13.11	12.65	12.65	12.77	19.71	33	13	15.83	43.33
06/05/2020	33.5	25	12	9.02	3.5	2.3	3.1	2.1	0	4.56	2.1	5
07/05/2020	34.9	34.9	34.9	34.9	34.9	34.9	35	34.9	40	4.11	4.2	30
08/05/2020	33.75	33.75	12.17	4.75	5	13.09	5	5	5	5	4	14.26
09/05/2020	39.5	39	39	12.89	12.18	12.11	39	39.5	42	39.75	39.75	44.5
10/05/2020	45.8	46	46	45.95	45.8	44	44	43.9	43.9	44	43.9	43.9
11/05/2020	9.11	8.61	6.54	41.5	5.87	3.36	1.91011	-13	4.82	6	4.5	10.94
12/05/2020	37.9	37.85	13.55	6.75	6.75	6.75	20	6.6	4.6	4.3	4.55	7.5
13/05/2020	36.25	39.75	36.25	36.25	36	35.5	36	30	30	13.1	12.8	13.3
14/05/2020	34.5	34.5	15.02	10.84	0.6	1.1	1.1	0.6	1.1	1.1	5.15	12.5
15/05/2020	15.21	15.21	34.1	4.6	4.6	1.65	4.5	4.5	4.8	4.8	13.72	13.72
16/05/2020	9.48	9.48	6.65	6.34	6.89	6.93	7.45	7.24	10.69	10.69	16.45	41.5
17/05/2020	30	0.6	0.6	0.09	0.5	-8	-5	-4.08	0.6	38.45	39.8	41.95
18/05/2020	38	11.08	10.05	10	10.01	9.77	38	38	13.22	39.95	40	40.7
19/05/2020	36.42	36.42	14.58	14.0984	14.4	14.42	15.2	1	1	1	22.31	40.21
20/05/2020	36	36	36	13.08	11.18	1.21	12.45	13.07	16.5	14.88136	1.21	1.5
21/05/2020	35	34.5	35	9.65	34.5	35	35	35	34.5	34.5	34.5	39.53
22/05/2020	-13	-64.5	-60	-65	-60	-60	-65	15.34	15.64	16.98	-50	16.58
23/05/2020	54.5	54.5	54.5	13.26	51.75	51.75	18.86	17.6	7.25004	51.25	40	51
24/05/2020	-60	-60	-22.54	-21.21	-48.4	-55	-55	-60	-17.12	54	54	54.5

25/05/2020	8.8	0	10.9	5.36	7.25	5.17	6.17	6.46	9.86	9.86	0.55	17.5
26/05/2020	14.73024	14.73024	41	15.99013	41.2	4.8	3.61	14.77	4.8	41	41	46
27/05/2020	36	41.99	41.99	36	35.75	16.25	14.11	13	6	34.5	34.5	34.5
28/05/2020	26.23	25.48	22.98	22.19	34.4	34.5	21.73	34.3	34.2	34.2	37.5	34.5
29/05/2020	13.19	8.35	10.34	10.25008	8.12	8.12	6.33	7	14	14	18.05	19.22
30/05/2020	0.5	0.5	-2.72	-2.54	-3.07	-3.43	-1.89013	-1.85	1	1.5	9.54	11.28
31/05/2020	43.25	38.25	38.25	36	36	0.6	0.6	0.55	0.55	36	38.25	43
01/06/2020	41.7	41.7	35.99	35.7	4.37463	4	4	0.8	9.52	9.84	4.15	43.5
02/06/2020	16.46	16.7	35	34.9	35	34.9	20.17	30	24	35	38	39.8
03/06/2020	21.58	21.9	22.76	30	30	38	38	38	24.67	23.0101	20.06	38
04/06/2020	37	37	39.5	38.9	37	41.5	41.85	42	32.95	41.8	39.5	42
05/06/2020	8.83	16.47	3.58	2.83	3.08	0.5	-13	-0.9	-1.01	5.54	15.54	19.94
06/06/2020	-0.92	-0.61	0.5	-3.5	0.5	0.5	0.5	-1.4	3.13	5.36	47	48
07/06/2020	42	41.9	42	41.9	42	43.95	43.95	44	44	42.1	42	42.1
08/06/2020	43	43	44	43	24.55	43	43	43	26.11	26.11	37.11	36.76
09/06/2020	43.75	40.8	43.5	6.1	6.1	43.5	43.5	43.5	1.5	45	7.5	7.5
10/06/2020	36.5	36.5	40.75	36.5	40.75	8.56	39.94	36.5	39.75	43.34	30.69008	30.76
11/06/2020	39.45	39.45	39.4	20	39	39	39	39	39.35	39	39.4	39.4
12/06/2020	39	39	39	39	38	39	39	39	43.65	43.65	43.85	44.5
13/06/2020	38.5	38.5	38.5	38.5	38	38	38.5	30	16.42	38.45	45	45.5
14/06/2020	37.5	37.5	37	12.49	11.42	11.42	12.18	30	2.5	2.8	27.78	37
15/06/2020	45.9	9.01	9.15	9.21	49.75	46.7	50	48.5	10.15	5.6	46.5	40
16/06/2020	45	48	45	13.77	11.2	13.6	13.6	14.1	14.5	48	14.61	14.61
17/06/2020	11.5	12	40	40	1.40525	1.1	40	12.7	12.7	48	48	64.5
18/06/2020	45.75	46.9	45.6	14.5	45.75	45.75	45	45	43.5	45	43.5	43.5
19/06/2020	6.5	6.15	6.5	6.2	6.6	6.6	7.73	37	30.02	29.7	6.8	34.42
20/06/2020	42.85	15.38	12.96	13.12	12.4	11.68	13.85	13.58	2	19.46988	23.35	23.8
21/06/2020	8.55	8.37	5.44	4.81	0.5	-16	-16	-16	0.5	14.84	0	0
22/06/2020	5	0.6	0.55	20.13	30	19.56	22.35	20.30017	20	42	32.22	34.52
23/06/2020	40.5	39	39	40.5	40.5	40.5	3.7	3.7	3.65	35	1.1	42

24/06/2020	43.25	43.25	43.25	8	43.25	9	43.25	43.25	43.25	43.25	44.85	44.85
25/06/2020	43	38	38	8.57	8.5	8.5	8.57	8.5	9.6	36.21	8.57	40
26/06/2020	10	10.5	10.55	39.94	39.94	43	43	31.88	39.9	43	44	39.94
27/06/2020	16.68	16.68	12.72	0.5	0	-15	0	-15	0.5	18.55	41.95	41.95
28/06/2020	-16	-16.76	-16	-61	-16	-16	-16	0.5	-14.57	46	21.5	22.01
29/06/2020	45	45	47.9	5.27	45	46	44.5	45	45	46.5	46.5	46.5
30/06/2020	45	5.15	46.85	46.85	47.8	46.85	47	46.8	46.95	49	49	46.95
01/07/2020	42	1.1	1.1	0	1.1	1.1	8.5	9	7	9	1.1	9
02/07/2020	46	42.4	42.4	10	10	10	39	42.4	49.99	49	10.4	10.35
03/07/2020	10.25	8.3	11	5.12	0.55	8.18	10.25	22.7	39.07848	39.45	39.45	39.45
04/07/2020	43.25	43.25	40.5	40	37	37	37	37	40	40.5	49	50
05/07/2020	46	46	-3.83	-3.83	50	50	46.99	46.99	51	51.75	51.75	50
06/07/2020	44	44	42	44	44	44	39.9	39.8	14.51013	15.36	2	5
07/07/2020	42.00913	39.75	44.16	8.01	8.5	9	9.15	44	44	44	10.5	43.5
08/07/2020	47	46.95563	46.5	16.55	42.34	17.58	17.58	17.6	60.36	62.36	23	64.07
09/07/2020	39.98	36.7	36.7	36.7	31.48	15.58	36.7	36.7	39.31	39.36	17.6	18
10/07/2020	44	36.99	16	16.05	16.05	22.42	1.5	36.6	26.14	16.5	15.99381	15.9
11/07/2020	37.7	21.06	18.5	10.05	10.69408	18	21.02	20.5	8.4	1.15	1.15	9
12/07/2020	35	12.94	11.79	9.69	0.6	10.25	0.85	0.6	0.55	17.67048	0.6	0.6
13/07/2020	4.81	6.16	47.25	6.17	22.7704	22.32	44.93	30.88	7	7.05	8	46
14/07/2020	12.5	12.5	40.25	16.45	40.25	40.25	40.25	40.25	14.1	44.5	48.75	14.5
15/07/2020	18.22	18.25	31.94	30.73	43.3	29.43	21.01	27.72	27.5	46.94	46.94	33.85
16/07/2020	24	42.43	30	20	20	20	20.5	20	20.6	57.42	50	21.1
17/07/2020	20.2	20.27	20.69	20.56	20.6	20.56	20.56	20.56	20.69	20.73	20.69	20.73
18/07/2020	23.71	23.71	37.5	1.05	37.75	37.5	37.5	37.5	37.5	38	32.44	37.5
19/07/2020	20.63	20.28	37.45	16.22	9.66	1.05	3.5	1.05	1.05	22.56	37.9	38.5
20/07/2020	13.5	14.5	44	44	14.75	14.75	14.75	14.6	14.87	15.01	15.05	15.11
21/07/2020	43.5	44.85	44.85	16.45	44.85	41	16.72	37	16.72	44.85	17.18151	45.99
22/07/2020	18.5	18.7	19	19	19	19	19	39.36	40	40	20.39183	20.5
23/07/2020	42.5	41	17.5	17.75	42.75	18	17.8	17.8	34.2	34.2	38.45	38.64

24/07/2020	46.5	20.05	45.5	40	52.5	52.5	49	20.25	20.25	20.41	22	49
25/07/2020	44.9	45	45.45	45.45	43.55	43.55	43.55	43.55	45.45	45.5	45.5	45.5
26/07/2020	15	30	7.92	0.5	15	15	15	15	30	39	40	42
27/07/2020	10	10	30	30	38.01	15.18	16.4	10.52	10.52	18.6	42.35	42.35
28/07/2020	1.2	1.2	0.5	-17.13	0.1	0.5	0.5	0.55	8.56	35.54	0.5	45.9
29/07/2020	11	4.65	11	3.4	12	12	12	12	12	11.5	13.85	46.6
30/07/2020	55	55	55	16	15.35	15.35	15.35	15.35	17	63.9804	70.42	17.55
31/07/2020	15.5	15.4	15.4	15.4	18	21.59096	81.74	81.19	85.26	84.35	92.14	18.5
01/08/2020	13	19	44	15.3	45	45	44	20	10	45	32.69	45.5
02/08/2020	23.73	22.99	14.84	30	9.49	1.05	19.87	11.7	24	38	37.9	47.85
03/08/2020	47.29006	47.71	12.7	13.5	36.13	35.99	13.8	14.1	15	36.56	15	36.90995
04/08/2020	38.38	38.38	44.75	42	32.48	1.05	30.98	1.05	27.68	32.26	34.2	34.93
05/08/2020	43.95	44	44.75	44.75	44.75	44.7	43.95	6.5	6.5	1.2	44.7	47.95
06/08/2020	45.9	15.11	14.5	13.15	15.11	15.11	15.11	48.40695	45.9	16.25	16.25	46.8
07/08/2020	45.65	43.5	45	45.65	43.5	45	45	45	49	45	18.05	25.3
08/08/2020	41.75	27.86	17.57	6	6.07	22.99	40	40	40	41.95	44.95	46.99
09/08/2020	43.95	43.95	43	43.95	34.14	33.22	32.7	32.4	43.41002	44.5	43	46.98999
10/08/2020	19.5	43.25	43.25	43.25	43.25	43.25	54	52.5	54	60	55	52.5
11/08/2020	49.5	47	49.5	48.952	45	49.5	13.16745	49.5	13.4	61.95	87	87
12/08/2020	64	60	52	58	1.7	16.55	16.6	16.9	16.91	17.2	17.26	17.3
13/08/2020	54.95	54.95	52	51.85	51.5	51.5	51.85	51.85	51.5	51.9	51.5	59.85
14/08/2020	20.76	53	1.7	20.64455	49.5	49	21.21	21.21	58	51.8	51.8	51.8
15/08/2020	49	47	49	49	45.67	42.5	42.5	42.5	45.67	45.67	47	66.75
16/08/2020	50.5	43.8	43.9	43.9	43.8	43.8	43.8	43.9	43.9	54.5	43.9	54.5
17/08/2020	77.16	22.75	22.2	16.6	22.2	1.7	23	23	59.56	77.56	23.76	30
18/08/2020	24.75	24.8	30.66	25	25	28.9104	24.9	25	24.9	25.11	24.9	25.11
19/08/2020	63.75	26.15	51	50.75	50	26.3	26.3	26.5	48.5	48.7	48.5	52
20/08/2020	26.92	25.81	26.26	24.1	26.16	5	48	2	5	54.9	44.14	60
21/08/2020	48	48	48	48	48	48	48	48	48	48	50	33.62
22/08/2020	8.54	3.51	5.2	3.04	2	3.21	12.15	12.55	25.25	46	46	46.95

23/08/2020	33.76052	43	44.75	44	43	42.9	30	5.1	7.2	7.2	45	43.8
24/08/2020	11.66609	10	12.7	10	12.7	13.36	13.69	14.11	14.36	79.44547	21	29.55
25/08/2020	48.75	45	49.5	49	2	47	47	52	50	51.9	52	53.95
26/08/2020	30	49.95	53.5	51.76503	53.9	49.95	35	35	1	13.92522	16.1	21
27/08/2020	75	71.62068	17.65	22.65	34	75	59.4	34.4	24	34.55	34	34.55
28/08/2020	15.55	48	51.25	15.6	51.25	51.25	39.86	41.37	15.55	47.5	2	26.66006
29/08/2020	47	49	49	48.25	48.25	47	48.25	38.41	38.72	47.25	36.72	50
30/08/2020	48.8	48.95	49.75	48.95	48.7	23.48	23.04	33.43838	3.1	3.1	3	3
31/08/2020	27	2	7.6	0	0	27.1	27.1	27.1	26.5	26.5	27.1	27.2
01/09/2020	48.8104	48.46	29.49825	28.35	28.35	28.4	28.35	28.4	27.85	28.35	28.6	81.24
02/09/2020	46.37	45.4	30	42.72	43.96	43.96	58.65	58.35	61.24003	63.75	67.16	67.16
03/09/2020	52.85	51.8	52.75	17.4	17.4	17.4	17.4	49	37.18994	17.4	17.4	17.5
04/09/2020	17	15	17	47.5	15	15	30	49	51.95	53	57.35	57.35
05/09/2020	53	52.25	27.54	27.54	50.5	25.32	30	40	47.5	40	17.6	40
06/09/2020	54.3	54.3	54.3	40	18.65	18.65	20	52	54.3	58	58.85	75
07/09/2020	54	51.88	55.75	51.88	20	19.05	19	19	44.72	45.4	51.88	53.42
08/09/2020	52.94	53.35	52.94	52.94	56.97	53.35	56.97	53.35	59.5	52.94	57.31	56
09/09/2020	20	19.7	19.5	19.5	19.75	15	2	2	50	52.5	59	59
10/09/2020	29.25	22.1	22.15	22.2	30	40	68.84	68.96	75.6	76.9	89.34	89.34
11/09/2020	49.8	49.8	49.8	24	41.93	41.93	23.18	2	30	44.14	23.35	53.27
12/09/2020	15	11	2	1.51	0	0	2	15.3	11	23.56	51.75	51.89
13/09/2020	1.5	0.5	0.5	0.5	1.5	15	15	15	27.1	29.05	54	59
14/09/2020	15	30	80	23.8	15	15	52.9	76.46	24.25	108.72	26	116.43
15/09/2020	85	31.6	127.59	32	120	110.07	82.98	108.23	175.0901	182.54	377.07	369.8
16/09/2020	31.15	31.15	31.15	31.15	73.2	31.3	31.3	31.3	31.3	31.3	31.35	31.35
17/09/2020	31.6	31.6	31.75	50.71	38.5	31.8	31.6	31.75	31.75	32	32	34.6
18/09/2020	27.5	27.5	27.25	20.21148	1	27.55328	27.25	52	46.25	28.5	27.5	28.5
19/09/2020	2	19.35	15.99789	15	21.91013	26.67	26.6704	30.43	34.39021	34.5702	52	59.95
20/09/2020	49.5	32.92	26.23	18.18	23.88	2.75	19.7	27.5904	30	59.95	59.95	68.95
21/09/2020	15	15	20.5	15	15	15	15	50	26	44.32	20.5	60

22/09/2020	40	30	30	40	26.63	44.6	50.65013	54	58.69	63	65	62.25
23/09/2020	69.95	68.89	68.89	27.27	27.2	21.33	20.5	83.5	40.5	50.5	40.5	40.5
24/09/2020	58.95	53	68	54	58.5	58.5	56.71	67.71	76.71	72.56	70.65072	75.56
25/09/2020	51.9	51.5	63.9	50.96	17.08	0.55	0.55	18.01	50.25	61.5	9.15	63
26/09/2020	53.9	52.85	52.85	53.95	53.95	53.95	53.95	54.2	29.04	54.2	53.95	60
27/09/2020	35.34	35.1	55	50.25	55	27.78	39	27.88	26.7	56	55	61.25
28/09/2020	60.5	60.5	67.5	60.5	60.5	63.7439	74.74	78.0901	86.14	91.05	118.2666	118.34
29/09/2020	40.15	40	30	30	30	30	30	91.26	31.5	31.5	31.65	35.05
30/09/2020	63	62.5	47.15004	61.5	62	62	56.5	73.5	73.5	69	70	110
01/10/2020	80	60	29.95	22	28.25	28.25	28.25	29	29	29	32.26	34.15
02/10/2020	53.5	53.5	53.5	53.5	53.5	53.5	15.7	15.7	15.7	16.1	64.5	65
03/10/2020	68	70	75.5	68.5	66	66	66	66	66	66	65	62
04/10/2020	62	62	62	62	62	62	62	66	67.95	66	67.95	66
05/10/2020	35	21.51	64.9	68	64.5	22.26	64.5	75	74	22.5	23.31	23.31
06/10/2020	59	56.5	24.27	53.5	53.5	53.5	53.45	24.5	63.75	63.75	64.7	64.7
07/10/2020	25	57	57	25	57	57	24.5	57	62.45	62.5	64.75	64.75
08/10/2020	26.25	58.9	58.9	58.9	58.9	58.9	58.9	63.95	27.51	27.56	63.95	65.5
09/10/2020	28.55	28.55	28.55	59.5	35	53.75	27.5	28.55	62	64	28.55	28.55
10/10/2020	58.5	42.51	58.5	24.27012	27.11	26.2504	33.14	29.31	31.11	59.4	28.55	65.75
11/10/2020	56.95	56.95	57	56.95	8.05	10	27	56.95	56.95	27	65	66
12/10/2020	27.25	25.31	25.37	25.45	25.5	25.5	47.9	46.5	26	52.63	57.34	25.71
13/10/2020	34.03468	33.4546	43.78	44.78	43.62	41.58	44.81	44.7	53.54	56.93	73.5	73.5
14/10/2020	64.49	64.49	57.5	57.5	57.2	64.4	29.17	71.63	71.63	95.73	95.73	95.73
15/10/2020	59.5	13	57.5	57.5	57	69	30.36	30.36	30.36	30.36	30.45	103.81
16/10/2020	13	32.5	55	52.45	52.45	52.45	52.45	52.5	65	65	75	67
17/10/2020	59.5	59.5	30.35	59.5	59.5	59.5	57.94319	3.85	6.46817	67	69	67
18/10/2020	66.9	66.9	66.5	58.4	57.5	57.5	58.4	57.5	69	73	74.25	74.45
19/10/2020	17.2	17.2	19	27	27	27	27.3	28	28.25	64	67.5	67.5
20/10/2020	58.7	58.7	58.7	35	57.95	40	20.1	58.8	61	22.5	22.55	64.2
21/10/2020	65	72.5	72.5	62.05	67	31	31	72.25	78.4	66	31.01	31.05

22/10/2020	56.5	31.3	30.1	30.1	30.1	30.1	30	62.02	31.32	30.1	30.25	32.01
23/10/2020	69.79	65	62	32.53	32.56	33.8	33.75	33.81	34	44.54	33.81	74.85
24/10/2020	63.2	63	62.95	52	62.95	61	61	62.95	63.3	64.45	63	70
25/10/2020	62.9	12.52	12.7	12.7	14.92	24.17	26.18	25.68	28.53013	29.16	68.2	73.45
26/10/2020	58	57.75	4	15	20	20	46.55	52.25	64.25	70	74.5	84
27/10/2020	27.5	57.5	59.95	27	23.59	23.59	41.61	23.59	23.65	23.66	69	71.85
28/10/2020	63.95	63.95	63.94	63.94	63.94	63.94	63.94	63.94	24.52	69.5	78	78
29/10/2020	63.55	63.55	67	67	67	63.2	63	15.27	15.27	66.5	66.5	60
30/10/2020	65.5	66	65.5	55.95	27	9.17305	3.85	55.95	18	91.95	117.55	117.55
31/10/2020	22.63	21.2	19.6	3.95	23.09	22.64	25.26	25	3.85	35.88	52.47	63.5
01/11/2020	11.83	23.14	26.01	62	63.25	62	9.51	0	0	64.25	63.5	5
02/11/2020	18.01	18.01	59.95	59.25	59	59	62	18.5	13.1	67.75	68	68
03/11/2020	17	61.5	61.5	61	59.9	61.5	59.9	61	80.92	86.79028	95.02	95.92
04/11/2020	18.2	62	62.69	62	18.82	62	18.82	19	3.85	3.85	3.85	0
05/11/2020	57	57.5	57.5	55	55	30	3.85	57	55	140	160	145
06/11/2020	64	64	65	65	64.5	58.8	36.79	23.55	23.4	81.64	82.39	82.14
07/11/2020	62	59	59	23.6	23.65	23.6	23.65	23.65	69	72.95	73.9	72.95
08/11/2020	68	59.95	69	67.4	69	72	70	69.49	88.28	94.28	104.28	104.28
09/11/2020	68	68	68	64	74	64	50.6	29.5	128.31	153.41	240.7728	168.41
10/11/2020	65	65	49.3	24.6	24.45	24.45	24.6	30	27.25	40.9	25	30
11/11/2020	59.9	59.8	59.5	52.82	59	25	21.5	59	21.5	59	64.65	59.5
12/11/2020	6	6	11.1	63.25	6.1	63.8	68	68	66	68	68	67.8
13/11/2020	6	6	58.9	60	60	6	6.01	27	27	64.95	27	64
14/11/2020	61.9	61.9	61.9	29.91	41.22	39.48	59.7	59.7	63.25	63.25	63.25	63
15/11/2020	5	12.49	62.8	63.9	63.9	62.95	63.9	62.95	67.9	69.75	69.75	68
16/11/2020	59.8	59.8	59.8	59.8	60	65.98	67.4	69.5	66.5	67	67	65.5
17/11/2020	59.95	59.95	62	59.95	59.95	6.1	63	64	64	66.25	69	69
18/11/2020	62.5	62.5	62.5	62.4	6.1	6	6	6	6	6.1	61	61
19/11/2020	16.5	16.5	15.1	15	15.1	14.5	0	16	16	70	15.1	16
20/11/2020	18.2	3.55255	61.4	59	58	54.02	52.7	52.7	18.4	59	0	4

21/11/2020	5	5	26.11	55	58	58	55	31.52	25	59	60	60
22/11/2020	6	6	5.25	5.25	5.25	7	7	9	60	68.5	69	68.5
23/11/2020	58.9	57	58	58	60	58	8.1	47.26	58	62	62	62
24/11/2020	58	58.75	60	60	46.97007	46.58	48.48	48.6	13.5	65	68.95	68.97
25/11/2020	58.29	18.6	19	19.07	19.5	19.57	20.2	21.5	20.57	22.02	25.11	25.61
26/11/2020	97	97	97	97	37	134.95	32	35	32.5	145	36.5	35.5
27/11/2020	72.25	72.39961	34	34	60.89007	61.4304	66.76	64.98	35.5	129.8896	35.56	125
28/11/2020	78.00017	68.5	60	60	36.6	36.7	36.7	36.7	80.71	38.5	86.43	86.43
29/11/2020	69	70	69	69	63	63	63	85.51	97.46	105.33	105.33	91.51
30/11/2020	52.55	52.55	52	51.98	51.5	6	25.5	52.29	63.1371	63	3.85	6
01/12/2020	62.82	68.96	63.23	62.42	62.9	69.25	79	88	88	130	195	31.13
02/12/2020	79	63	70	85	133	72.67	85	85	38	224.5	38.25	215
03/12/2020	90	130	36.01	36	36	159.99	36.22	145	145	38	38	37.25
04/12/2020	78	70.79	67	25.25	0	0	6	6	0	0.05	6	0
05/12/2020	15.75	16.55	17.11	17.11	64.9	63	17.75	17.75	18	123.26	20	70.56
06/12/2020	62	65	27	27	27	72.98	27.1	28	399.41	720.41	720.41	575.41
07/12/2020	495	495	495	495	37.21	36.7	37.2	412.4604	37.2	37.2	11	10
08/12/2020	120	37.1	66.62	66.62	72.71	72.71	71.99	74.57	37.5	38.25	145	38.45
09/12/2020	40.1	40.1	225	38	40	225	38.5	107.37	395	39.1	38.62	5
10/12/2020	95	95	94.84995	92	94.85	36.7	36.4	36.4	36.7	36.71	6	6
11/12/2020	88	88.98	92.99	36	5	38.55	37.3	88	37.3	102	125	92.5
12/12/2020	62	62	62	62	62	35.38	35.4	35.4	37.01	37.06	37.22	70
13/12/2020	68.9	68.5	68.9	68	64	63.5	58.67	50.46	71.5	71	67.75	67.75
14/12/2020	62.75	65	62.75	65	65	72	72	12	72	72.9	74.5	74.5
15/12/2020	23.4	23.4	79	75.5	75.5	74	63.25059	72.55	23.5	23.6	25	37.7
16/12/2020	63	63	63	63	63	63	63	64	73.98	75.55	76	75.55
17/12/2020	69.95	69.95	69.95	69.95	73.5	69.95	23.6	23.6	77	78	78	36.5
18/12/2020	65	64.95	64	23.81	64	23.9	63.9	24	24.05	24.05	68	71
19/12/2020	31.52	38	55	30.26635	63.95	18.65	65	20.1	20.2	42.69	68.95	68.95
20/12/2020	65	65	65	65	65	20.11	65	67	75.85	75.95	75.95	75.95

21/12/2020	70.99991	75	76.5	75	75	76.5	87.88	87.88	80	80	75	79.4927
22/12/2020	70	72.95	70	70	73	73	73	75.00058	74	72.9	27.85	72
23/12/2020	78	73	30.1	30.1	73.5	73	31.05	31.05	31.12	31.15	31.15	31.15
24/12/2020	64.95	64.95	64.25	64.25	64.25	64.25	66	74.5	74.5	75.95	75.95	76.67
25/12/2020	78.85	78.85	79.89986	79.5	78.85	75.75	72	72	66	66	66	65
26/12/2020	64	64	64	64	64	43.92	39.02	44.64	68.5	68.5	69	69
27/12/2020	30	66	20.1	18.6	18.6	18.6	18.6	79	79.95	145	169.95	157.9987
28/12/2020	87.25	95	94	90	105	130	119.5	130.83	170.83	849.8154	791.6856	268.2942
29/12/2020	85	79	85	74.60068	74	77.5	33.26	85.66	124.66	142.66	142.66	142.66
30/12/2020	33.25	70	72	35	35	34.66	35	35	35	238.35	238.35	238.35
31/12/2020	73.5	73.5	73.5	73.5	73.5	35.5	85	88	80	93.5	93.5	93.5

Table III-4 TIME-OF-USE Electricity Tariff Data (18:00–23:30), 2020, Provided by Limejump — Part 4

Date	18:00	18:30	19:00	19:30	20:00	20:30	21:00	21:30	22:00	22:30	23:00	23:30
01/01/2020	51.9	51.5	49.95	8	7.5	51.5	49.45	51.5	51.5	49.45	50.05	49.95
02/01/2020	9.2	8.9	8.9	9	9	8.9	9	20.99	6	2.5	15.83	2.5
03/01/2020	52	10	9.6	9.8	9.6	9.6	49.5	9.6	40	5.1	5	2.5
04/01/2020	55.5	55.5	55.5	49.9	49.9	49.9	9.65	8	8	9	24.17	23.48
05/01/2020	51	48.95	9.6	8	8	8	9.6	5.1	5	2.5	48.88	0
06/01/2020	56.5	56.5	52.5	45	11.35	49.75	51	51	49.99	18.1472	4.5	2.5
07/01/2020	12.15	49	49.5	49.5	49	12.25	20.1	10.9	2.5	2.5	28.16	4.5
08/01/2020	19.15	56	56	52	51.5	19.15	21.25	50	18	18	25.44	46
09/01/2020	19	68.5	65	57.5	53	50	19	49.95	51	19	49	49.25
10/01/2020	56.2	52.97	19.25	19.16	48.17	50.32	52	49.95	52.98	49.95	49.95	49.95
11/01/2020	19.25	10.5	10.25	10.25	10.25	12	12	13.10991	13.1101	10	17.25	49.8
12/01/2020	58.85	58	10.55	10.59	53.95	10.61	52	23	5	0.5	22.33008	22.33008
13/01/2020	52.8	52.8	52.8	53.25	52	52	50	5.1	10	2.5	50	50

14/01/2020	54.5	53.6	54.5	53.6	54	53	52.8	52	51.99	50	51.5	50
15/01/2020	54.25	53	52.85	13.1	10	9	49.99	49.99	50	2.1	2.08294	2.5
16/01/2020	5	50	50	50	50	50	50	32.65	27.71	25.1	49.89	45
17/01/2020	61.95	46.4	16.55	55.5	54	50	49.5	16.3	16.21	3	14.95	0
18/01/2020	52.5	50	52.5	50	19.5	49.85	49.85	19.25	49.75	49.75	49.5	49.5
19/01/2020	54.65	19.5	54.65	50	49.45	49.45	49.45	49.4	49.1	19.35	19.35	12.5
20/01/2020	21	49.4	49.4	49.45	21	21	20.5	3.5	46.7	20	20	28.51
21/01/2020	165.96	183.6762	160	105	105	99.93	99	99	99	99	99	99
22/01/2020	99	99	25.1	60.75	66.5	25.15	50	47	45	25.25	38.41	38.41
23/01/2020	26.15	27	60	59	27.06	27.06	50	50	45	27.06	27.06	27.06
24/01/2020	27.25	27.25	57	27.6	50.5	48	47.23	45.9	27.45	43.48	16.61	3
25/01/2020	50	50	50	17.75	17.5	17.5	48	48	48	48	47.5	48
26/01/2020	57	51	57	51.5	47.5	12.05	46	46	12.15	46	19.21	3
27/01/2020	62.75	24	53	62.75	53	49.5	51	48.45	48.4	48.35	46	46
28/01/2020	55.7	55	55	55	48.5	48.5	48.05	48.5	48	47.5	47.49	45.99
29/01/2020	49.75	49	49.75	47.25	19.25	18.1	18.1	2.2	2.1	0	2.5	2.1
30/01/2020	44.83	44.75	44.75	44.75	2.75	32.6	22.78	10	2.2	2	5	16
31/01/2020	48.7	47	48.5	48	47	3	45.25	21.86	45.25	13.4	47.9	45.25
01/02/2020	53.38779	53	51.45	51.4	51.4	51.4	51.4	51.4	48	48	48	47.7
02/02/2020	51	9.66	48	10.49	48	48	48	22.62	47	2.5	14.23	14.92
03/02/2020	50	48	48	5	13.3	13.25	26.97	26.97	22.28	2.5	45.5	45.5
04/02/2020	14	14.1	46.5	49	80	46.5	46	45.9	45	44.25	10	10
05/02/2020	16.75	16.75	17.5	47	45	17.9	44.85	17.9	17.95	17.9	42.5	42
06/02/2020	105.71	90.71	17.99	45	45	44	44	44	43	43	42	25.72
07/02/2020	44.8	17.8	17.8	17.8	20	44.5	12.5	12.15	42.5	2.5	2.5	2.5
08/02/2020	47	44.3	44.3	44.3	44.3	43.8	43.8	43.8	43.8	43.5	43.5	43.5
09/02/2020	47.5	12.5	47.5	47.5	46	43.5	44	44	44	42	6	3.15
10/02/2020	48.84	48.5	48.5	46.5	44.5	46.7	46	44.5	44	2.5	10.84	10.52
11/02/2020	51.15	50	51	49.1	45	45	45	44.44	44.44	2.5	2.5	-60
12/02/2020	51.03	51.03	51.03	45	44.99	14.1	15	15	15	13.6	15.1	20

13/02/2020	64.24	64.24	58.29	58.29	51.95	46	50	48	41.25	17.55	17.35	44.5
14/02/2020	45.5	44.9	41.85	19.2	19.05	19.2	41	41.5	40	40	21.37	21.29
15/02/2020	45	45	43	42	41.5	42	42	41.5	42	34.17	45	43.75
16/02/2020	45	45	43	18.87	43	42	43	43.74	43	2.5	43	42.95
17/02/2020	50	46.5	46.3	46.3	44.85	44.25	44	43.9	40	40	41	15.15
18/02/2020	51	49.8	49.75	13.5	14	14	13.5	41	39.99	10.2	13	13
19/02/2020	43.25	48.5	48.35	45	45	15.18381	15.15	43	43	26.88	41.99	2.5
20/02/2020	53	50.75	43.5	13	43.2	43.5	42.9	41	41	11.72	40.5	2.5
21/02/2020	44	20	44	44	46	21.4	7.65	7.65	39.5	7.7	43.8	43.8
22/02/2020	51	50	47.5	47	15	47	47	46.5	20.39	19.16	42	2.5
23/02/2020	49.00708	47.95	47.95	46.75	47	47	47.95	47	47	5.4779	44.01	47
24/02/2020	55	48.6	55	48.6	48.6	47.8	47.75	47	40	40	13.5	25.5
25/02/2020	79.74	79.79	79.79	79.74	57.5	49.8	48	48	43.5	43.5	20.75	20.75
26/02/2020	55.95	120	98	55.5	55.95	17.5	17.1	19.2	17.5	17.05	25.91485	7.2
27/02/2020	55.9	81	55.9	52	18.25	18.25	44	43.7	42	18.35	42	13.5
28/02/2020	45.75	45.75	44	16.25	43	15.81	2.35	15.8	18.91	43	44	10.63407
29/02/2020	49	49	43.98	39.45	48	13.15012	46.01	48	45	43	12.66	7.79303
01/03/2020	49	49	49	46.95	46.7	45.5	44.5	44.72	44.5	43.9	43.8	43.8
02/03/2020	49	49	49	48	47	17.8	17.8	17.4	8	2.5	20.25	20.25
03/03/2020	54	125	59.5	20.4	20.28468	44.13406	53	50	47.5	20.5	0	2.1
04/03/2020	2242.307	1708.052	23.35	0	25.05	66.5	104	45	50	55	23.5	23.5
05/03/2020	2.2	23.75	26	48	26	25.5	23.75	25.45	25.5	25.5	25.7	40
06/03/2020	24.25	66	48	24.3	49.5	47	45.75	100	44.75	44	43.25	43.5
07/03/2020	29.06	40	13.57567	13.06	43.75	27	42.75	19.95	19.33	-9	-8	-8.92
08/03/2020	54.9	54.9	52	50	48.84	46	22.24125	23.81	23.36	42.9	43	19.57
09/03/2020	47.95	16.15	13.1	2.21755	43.75	1.85	2.2	15.15	43	43.75	43	2.5
10/03/2020	52.8	55	52.8	50.9	50.9	20	43	44.4	43	42.9	44	44
11/03/2020	53	53.46	53.46	53.46	52.2	48	45	46	44	44	46	44
12/03/2020	48.7	49	49	48	16.52	16.52	20.25	44	43.5	43.5	25.41	18.46
13/03/2020	20	80	65.7	44	44	15	16.6	16	16	16	44	44

14/03/2020	46.4	46.45	46.4	4	2.2	2.5	45	45	45	45	45	2.5
15/03/2020	50.5	50.5	60	50.5	50.5	47.5	60	47.5	43.75	15.65	7.5	15.65
16/03/2020	48.5	49	2.5	2.5	2	2.1	15.8	7.5	42.5	42.5	7.27134	5
17/03/2020	15.7	49.25	49.25	49.25	49.25	45	42.95	21.53	18.75	18.75	18.36	16.88
18/03/2020	58	58	58	15.99	58	8.01	35	41.98825	43.35	41	40.5	40.5
19/03/2020	128.39	127.99	127.99	18	18	17.9	0	18	41.75	41.75	40.75	18
20/03/2020	18.55	43.75	47.5	18.55	18.55	18	18	16.1	16.1	40.75	12.33	12.67
21/03/2020	52	53	53	46.5	46	46	12.24	10.78	43.5	43.5	30	42.5
22/03/2020	29.0375	55	53	4.1	3.65	3.2	4.05	11.85	8.02	9.39	9.75006	10.1
23/03/2020	50	50	9.5	4.5	4.5	2.1	4.5	40.75	40.75	40.75	40.75	40
24/03/2020	44	44	44	13	3	2.2	4	3	2.5	2.5	17.24	2.5
25/03/2020	11.2	50.95	11.5	11.5	11.4	11.55	14.2	11.55	40	40	13.92	12.5
26/03/2020	16.5	16.5	25	16.6	16.6	15.3	14.4	10	15.35	42	38.75	38.72
27/03/2020	44	44	44	40	41.5	38	38	35	11.5	3.55	3.7	16.18
28/03/2020	43	43	43	41.18	41	6.3	6.15	5.15	13.57	13.35	42	42
29/03/2020	45	43.25	42.5	42.5	40.25	39.5	38.5	39.25	40.25	39		
30/03/2020	41.95	40.5	40	40	41.95	40	36.98	36.85	18.35013	36.85	36.85	18.67006
31/03/2020	43	41	7.06	41	41	41	52	39	38	40	39	39.95
01/04/2020	47.5	43.6	43.45	43.6	47.5	40.6	38.6	38.45	38.45	37.85	37.85	37.8
02/04/2020	40	40	40	40	44.85	44.35	40	40	39.98	38	38	35.95
03/04/2020	39	38.85	38.85	38.85	40.5	10.05	10.05	10	10	10	36.5	36.5
04/04/2020	47	47	44	44	43.95	39.2	40.5	40	39.2	39.2	39	13.62
05/04/2020	52	48	48	15.99	40.89852	42	45	6.05	38.5	-20	38.5	-8
06/04/2020	38	49.15	37.67	41	49.15	49.15	49.15	39.5	37.67	37.67	16.59	14.47
07/04/2020	42	46	9.1	46	14.02	30	18.35	7.00464	13.44	35.9	13.03	9.1
08/04/2020	11.8	12.1	48	48	48	43.5	37	12.4	37	12.7	36	36.9
09/04/2020	38.2	38.2	39	38	39	38	38	38	35.7	35.5	35.25	35.25
10/04/2020	45.6	49	45.6	45.6	45.6	39.9	39.9	39.9	19.27	18.46	36	36
11/04/2020	18.44	11	11	11	38	45.5	45	45.5	45.5	38	38	38
12/04/2020	40	32.14383	13.54	2	2.5	2.5	6.24	2.5	40	39	41.9	13.47

13/04/2020	44.95	44.95	4.37	4.37	3.01	4.15	39	38	38	7.2	36	36
14/04/2020	42.5	42.5	42.42	6.01	6.1	6.26	6.26	4.75	2.2	1.25	15.46	35.5
15/04/2020	37	37	38.85	7.05	7.1	36.5	36.5	7.5	20	35	34.75	34.5
16/04/2020	40	36	42	42	42	42	13.98	16.19	40	36	36	35.95
17/04/2020	40.9	39	39	39	37.5	37.5	36	36	37.5	37	34.5	16.33
18/04/2020	47.75	47.75	47.75	41.8	41.8	44	44	41.8	37.5	36.95	37.5	37
19/04/2020	43.25	43.5	40.95	40.5	40.95	40.95	100	43.5	43.5	39.95	36.6	-20
20/04/2020	16.44	10.03	25.44	26.68	42.35	39.9	37.25	37.25	37.45	3.2501	42	37.45
21/04/2020	41	25.59	28.75	40	41.7	41.9	41.95	41	40.97	31.23	37.5	2.23
22/04/2020	42	42.98	42	40	40	40	38	38	36.8	16.1	42.95	42.95
23/04/2020	43	42.78	43	5.15	43	43	41.9	41.9	38	5.5	38	40
24/04/2020	0	39.5	39.5	19.04	22.92	39.5	36.5	7.2	6.61	2.5	13.31	35.5
25/04/2020	35.9	36	36	36	41.25	41.25	45.99	36	35	34	41	35.5
26/04/2020	36.1	35.5	35.5	35.8	39.75	39.75	39.75	35.25	19.62	34.25	33.85	16.2
27/04/2020	5.25	5.5	5.5	5.5	5.69	5.8	46	5.8	6	34	34.25	34
28/04/2020	48.25	47.95	48.25	47.95	40	10.3	7.6	0	6.5	31.9	33.5	33
29/04/2020	4.25	16.51	36.45	34	38.5	38.5	38.5	33.74	13.16	13.46	34	13.01
30/04/2020	34.95	4.18511	4.07	34.95	35.95	33.9	33.9	4.5	3.5	33.9	33.9	33.9
01/05/2020	16.25	44	45.35	44	40.4	40.4	40.4	37.5	35.95	36	36	35.5
02/05/2020	38.85	38.85	37.7	37.7	21.3	38.85	38.85	38.85	37.24	32	32.94	33
03/05/2020	49.25	45	45	45	41.75	41.75	39.8	39.8	33.5	33.5	37	37
04/05/2020	39.45	16.37	12.96	5.92	5.92	5.6	36.92	36.92	35	11.64	12.22	0.55
05/05/2020	43.33	41	41	41	37.45	37.45	41	37.45	35	33	16.09	15.89
06/05/2020	5	39	39	39	39	39	39	39	36	33.4	34.75	34.75
07/05/2020	49.8	49.8	49.8	49.8	49.8	45	45	44.95	39.75	37.5	34	36
08/05/2020	15.42	37	37	37	37	37	49.5	39.75	39.75	35	44	41
09/05/2020	45	39.5	44.5	44.5	42.5	40	45	42.5	20	17.65	39.1	42
10/05/2020	10.54	9.82	-13	-10	0.5	10.93	11.64	11.41	7.86	0.5	1.5	0.5
11/05/2020	14.47	14.47	13.9	13.61	16.02	16.5	19	19.29	42.5	35	17.1	39.95
12/05/2020	7.5	42.8	42.8	42.8	42.8	42.8	7.6	4.8	1	4.7	19.17	19.42

13/05/2020	15.69	15.66282	13.4	6.5	12.21	12.75	14.58	14.55	12.0101	12.23	37	36.75
14/05/2020	15.88	34.1	15.54	14.96	37.75	37	37	37	36.45	36.25	36.25	36.08601
15/05/2020	39.8	39.8	18.31	18.91	39.8	39.78	39.95	42.5	39.8	34.25	35.8	34
16/05/2020	37.4	37.4	41.5	41.5	42	42	42	42	36.75	36.75	36.75	36.2
17/05/2020	41.95	39.8	39	39	41.95	39	39.8	37.5	30.35	27.78	37	14.17
18/05/2020	40.7	40	40.7	40.7	37.89	37.89	39.01998	38.5	38.5	37.45	35.5	36
19/05/2020	40.5	40.21	40.5	40.5	40.5	40.5	40.21	40.21	35	2.21	36	35.95
20/05/2020	14.99	14.99	38.11	40.25	37.5	37.5	35.5	36.9	25.73	36.25	35.95	17.02
21/05/2020	39.53	39	16.16	15.2	15.19	1.51	17.88	15.92	15.19	14.98	16.07	16.78
22/05/2020	-15	-15	40	-15	20.11	40	49.72	51.5	51.75	18.78	15.6	14.38
23/05/2020	7	49.24	-59.95	18.61	9.88	-61.2	12.84	22.4	40	28.4	51	9
24/05/2020	54	46	54	54	54	46	49.72	54	54.5	54	54.5	54.5
25/05/2020	19.69	43.5	43.5	43.5	43.5	43.5	43.5	43.5	43.5	43	43	17.76
26/05/2020	46.97	46.97	45	45	17	5	17	45	45	45.5	43.25	37
27/05/2020	6.26	14	36	41.75	41.75	6.41	41.75	6.43	41.75	37.5	37	14.74
28/05/2020	37.5	37.5	19.16	14.45	15	15	37	37.5	37	34.34	31	16
29/05/2020	21.25	36.9	38	38.75	38.75	38	38	38	36.9	34	15.02	14.6
30/05/2020	43.5	43.5	43.4	41.5	43.4	11.8	36.73	36.73	38.5	38.5	39.99	8.15197
31/05/2020	43	43	43.25	43.25	43	43	43	42.9	41.99	41.99	39.8	8.7
01/06/2020	43.5	43.5	43.5	43.5	41.7	4.75	40	13.1	39.7	40	40	39.8
02/06/2020	42.5	42.5	42.5	39.8	40	40	39.8	40	39.1	33.5	21.07	36.5
03/06/2020	26.83	23.62	22.8101	22.8101	18.4	23.48	22.75512	19.23	30	19.94	37.5	18.57
04/06/2020	43	42	41.85	33.21	25.11	24.5	25.78	29.52	30	30	38	37.95
05/06/2020	40.2	40.2	40.2	10	17.76	14.9902	40.2	40.2	40.2	10	7.25	0.5
06/06/2020	48	47.8	45	45	18.74	36.7	20.19	45	41.25	41.25	45	44.5
07/06/2020	42	42	39.31	38.94	29.6498	37.67	1.33	0.5	0.5	1.3	39.5	41.5
08/06/2020	36.88	37.78	45.13	44	44	25.3302	38.75	38.75	21.87	21.4	22.37	22.6
09/06/2020	28.46	27.51	30	8.05	45.5	8.15	45.5	45.5	37.75	8.2	19.65	21.21
10/06/2020	39.75	36.5	29.8	9.15	9	9.05	9	8.55	8.55	27.5	20.02	35.55
11/06/2020	42.95	42.95	42.75	42.75	42.75	42	41.75	39.45	20.03	19.41007	37.2	17.16

12/06/2020	43.85	43.85	43.65	43.65	39	39	39.8	43.65	41	39.9	39.5	39.9
13/06/2020	45	44	44	43	43	23.8	6.1	2.11	2.15	2.1	19.99	39.35
14/06/2020	34	41.9	36.95	30	28.02	41	41.9	27.17	21.89	3.6	39	39
15/06/2020	10.25	47	56	55	45	47	47	10.45	47.99	5.6	10.76	37.95
16/06/2020	16.5	14.1	14.75	14.75	50	48.66	49.99	15	1.1	1.1	1.1	36.5
17/06/2020	52	48	50	51.5	52	13.3	13.2	1.1	13.35	37	37	36
18/06/2020	43.5	43.5	44.88	42	41.99	16	41	16.12	1.1	37	36	34.9
19/06/2020	42	40	7.02	38.95	39	39	39	39	38.75	39	38.5	42.9
20/06/2020	25.02	25.77	42.75	42.75	42.75	42.75	42.85	42.75	42.75	42.75	25.73	24.73
21/06/2020	1	19.96	21.09	21.09	23.42	23.7102	35.55	26.63	36	33.18	44.5	42
22/06/2020	44.25	44.25	44.25	34.22	35.02	31.03	29.57471	25	30	17.15	22.79	8.89505
23/06/2020	50	47.35	52.9	50	50	46.5	47.4	46	47.35	46	4.22	40
24/06/2020	9	44.85	44.85	44.85	44.85	43.25	44.85	43	42.75	9	9	42
25/06/2020	40.56	40.56	10.6	40.5	40.65	40.65	40.5	39.08	36.49	38	38	40
26/06/2020	11.11	12	44	44	44	43.5	38.95	35.39	11.86	10.25	10.55	42
27/06/2020	26.15	25.8	21.26	21.37	41.95	30	30	30	21.69	0	0.5	0.5
28/06/2020	18.58	21.47	0.5	35	23.54	0.5	0.5	22.24	18.46	-60	24.86	0.5
29/06/2020	35.51	35.46	0.5	0.5	34.46	30.01	46.99	46.5	8.37	5.84	30.77	7
30/06/2020	47	46.95	49	49	49	46.95	46.99	46.99	47.2	39.6	15.9	39.6
01/07/2020	47	49	49	47.8	47	46	47.8	46	9.6	8.3	41	41
02/07/2020	50	10.8	10.8	11	11	11	47	15	35	11	11	40
03/07/2020	39.45	39.45	10.25	0.55	39.45	39.45	39.45	39.45	40.5	39.45	21.5	2.89
04/07/2020	50.9	47.94	40	18.2	16.98	13.53	6.88	1.88	2.93	-7.93007	0	-55
05/07/2020	49	12	46	12.35	49	18.7	21.09	19.59013	2.75	-5	26.33	0.5
06/07/2020	5	30.01	42	30.51	42	30.75	30.77	29.65	46.5	0.6	42	25.80959
07/07/2020	20	43.5	45.5	45.5	45.5	47	43	11.6	1.1	11.6	11.6	39
08/07/2020	53.62	50.46	47.2	42.94	37.97	20.21	20.22	20.27	20.5	20.51	38	38
09/07/2020	58.5	20	20	50.51	41.93	37.18	50.85	34.56	43.48	42	35	35
10/07/2020	1.15	1.15	43	43	33.94	17	36.43	36.25	37.24	36.64	0.6	17.41
11/07/2020	31	31	11.25	44.25	44.25	44.25	34.6	38.75	38.75	14.12	28.57	27.93006

12/07/2020	0.6	11.55	30.5	30.5	30.1	29.6	30.1	39	39	30.1	30	30
13/07/2020	46	8	39.99048	39.98	46	46	46	46.8	46	34.03	41	37.9
14/07/2020	14.65	14.85	41	41	47	41	40	40	38	38	16.28	1.15
15/07/2020	50	47.78	50	50	40	21.75	46.94	22.05	22.1	38	34.19	34.93632
16/07/2020	48	49.74629	48	21.21	38	21.25	34.43	21.55	21.55	21.61	5	1.05
17/07/2020	20.7	20.71	30	21	38.52	21	25.67	26.07	27.52	35.63	20.5	38
18/07/2020	34.08	38	38.5	38.5	38.5	38.5	38.5	38.5	38.45	33.46	31.03	29.34
19/07/2020	38.5	38.5	38.5	38.5	38.5	38.5	42.47938	42.5	44	42.25	42	27.54
20/07/2020	15.11	15.31	50.04	50.04	45.8	45.8	45.99	45.8	43.5	14.7	15.69	14.5
21/07/2020	45.75	44.85	17.51	44.85	44.85	18	44.85	44.85	18.13	41	40.4	38.75
22/07/2020	45.99	21	21	21	21	20.05	39.88	41.41	41.31	39.88	38.4	36.16
23/07/2020	39.55	39.45	47.9	38.18	36.5	46	45.45	45.45	45.45	32.62	25.1645	37.5
24/07/2020	49	45	45	45	44.5	20.65	45	45	43.95	1.05	38.5	38.5
25/07/2020	45.5	45.45	45.45	45.5	45.5	47	48	45.5	44.5	40.88455	44.5	41.5
26/07/2020	44.75	42	30.03	30.5	28.05013	32.75	44.75	37.3	27	8	28	23.69
27/07/2020	4	1.05	39.9	44	39.9	39.9	39.9	39.9	15	10	15	0.5
28/07/2020	46	47	46.5	46.5	46.5	46.5	46.5	46.5	46.5	46.5	44	44
29/07/2020	47.5	50	44	45.7	44.73	44.73	45.7	49.5	42.85	16.75	43.9	1.05
30/07/2020	20	84.73	80.1	62.99	50.95	50.95	49	49	42.61	42.61	44	44
31/07/2020	59.5	59.76	52.4698	30	45	46	40.75	42.4	41.58	41.58	0	0
01/08/2020	32.78	32.96	29.59	32.63	32.1	4.55	21.03	45.5	27.23008	1.05	25.71	39
02/08/2020	46.5	45	45	30.83	32.52	32.52	43.25	40	28.92	3.5	18	1.05
03/08/2020	15.25	45.9	45.9	45.9	47	47	45.9	32.72	15	15.25	26.77	26.77
04/08/2020	30.41	31.22	31.82	1.2	20	36.46	35.04	36.75	1.2	5	37.79	33.15
05/08/2020	7	7	3.5	3.5	7	7	45.9	46.2	46.95	46.75	42	44.75
06/08/2020	51.28	49.95	49	60	50	45.45	47	45.45	44.95	20	40	39.95
07/08/2020	45	26.5	19.05	26.5	45	19.05	44.45	20.5	44.45	44.45	43.5	44
08/08/2020	41.25	47.8	35.7	36.42	41.25	43	34.32	35.45	35.45	44.5	41.5	44
09/08/2020	47.5	49.9	49.9	49.9	49.9	47.8	49.9	45	45	45	44.45	43.5
10/08/2020	48.9	52.5	48.9	48.9	43.25	52.5	65	55	55	47	9.75	9.25

11/08/2020	87	80	85	85	85	87	93.55	94.90354	85	49.95	0	15
12/08/2020	17.32	17.5	17.5	17.55	97.75	17.95	59	18.25	18.21	18.35	18.25	18.38
13/08/2020	51.5	1.7	51.5	20.05	53.6	20.15	49.75	20.05	20.05	20.05	1.7	0.55
14/08/2020	58	53	38.77	40	54.95	55	54	37.04	21.43	42.5	42.45	42.45
15/08/2020	66.75	62	66.75	62	60	56.5	53.5	45	21.91	41	39.5	43
16/08/2020	54.5	54.5	54.5	61.5	56	58.05	54.9	43.9	43	39.75	39.8	40
17/08/2020	89.56	88.06	89.56	80	60	80	51.88	24.2	51	24.11	41	38.99
18/08/2020	25.18	25.11	25.18	36	65	65	65	52	52	52	43.8	42
19/08/2020	49.75	48.02	39.8	43.08	52.5	52.5	1.7	26.55	26.1	43	47	29.64
20/08/2020	59	59	51.68	59	59	61.99	61.99	53	53	47	51	52.5
21/08/2020	48	48	48	48	48	52	51.2	33.5	31.5	1.7	25.31	22.55008
22/08/2020	50.89	50.89	50.89	52	52	50.89	51.95	47.35	47.35	27.55	47.1	21.13448
23/08/2020	0.6	7.3	7.3	8.2	59	54	8.2	7.5	0	3	8.2	1.7
24/08/2020	30	21	30	21	30	77	58.5	16.5	7.6	10.2	17.01	17.01
25/08/2020	53.95	50	20.4	2	2	2	11.31	2	28.94	15.29	12.54	7.58
26/08/2020	16	56.99	59.1709	80	33.00038	89	21	17.25	88	54	59.95	48.69
27/08/2020	70.4	29	24	20	20	24	48.5	25.1	24	2	25.11	48.25
28/08/2020	15.56	47	55	55	55	47	44.13	44.5	54	55	48.9	30.45
29/08/2020	51.15	52.95	50	51.15	51.15	50	36.88	36.75704	32.51	39.33	50.35	49.75
30/08/2020	3	10	48	28	59.88	59.66	47	46.9	4.2	4.2	48.5	46.85
31/08/2020	27.3	27.35	27.2	40	60	59.89	62	27.7	50	30	46.45	46.45
01/09/2020	28.6	28.7	81.24	64.99	64.99	28.65	28.7	28.7	2	2	47.5	45.5
02/09/2020	76.58003	68.75	62.06	64.02	53	16.6	16.7	52.55005	43.46	44.15	50.9	53.5
03/09/2020	56	56.5	54.75	54.75	52.95	17.61	50	17.5	54	55	54	50
04/09/2020	57.35	57.35	57.35	57.35	54.75	52.45	52.25	25.1	51.5	17.62	1.5	0
05/09/2020	59.5	60	59.5	59.5	55.5	20	35.1	23.72567	27.03008	18.25	28.93	52.85
06/09/2020	58.85	30	58.85	18.8	58.85	30	18.85	53.9	18.85	18.7	50	49.5
07/09/2020	56.1	56.1	51.88	54.19	55.25	19.25	2	18.95	51	51	22.2904	21.77
08/09/2020	59.98	61.7711	54.75	54.45	61.9	53	19.72	19.72	2.5	2	22.60554	25.4
09/09/2020	59	64.97	59	64.97	60	52.75	52.75	52.75	52.75	0.6	2	20.3

10/09/2020	88.09	29.25	68.75	70	55.88	23.61	51	20	42.85	43.9	24	49.5
11/09/2020	54.1	59.5	15	30	2	2	53.9	54	44.23	52.5	52.5	51
12/09/2020	15	37.75	51.89	51.89	41.6	12.15	12.15	2	30	2	58	2
13/09/2020	57.45	58.9	57.45	59.5	60	58.9	58.9	34.46	31.77	36.86	51.85	50.5
14/09/2020	181.91	181.91	121.1	145	155	30	85	65	61.5	49.32	66.28	44.96
15/09/2020	540.22	530.07	315.49	355.49	40.5	34	73.58	41.1	21.35	20	55.96	53.53
16/09/2020	31.35	31.35	68.8	69.8	68.8	68.8	65	31.4	31.4	15	0.6	15
17/09/2020	53.67	32	32	32	42.9904	32	52	15	47.85	15	47.5	15
18/09/2020	30	28.5	28.25	54.95	28.25	26	30	30	28.25	28.25	30	22.2
19/09/2020	56.25	59.95	60	60	60	59.95	57	38.42	22	29.95	32.97	28.08
20/09/2020	59.95	59.95	59.95	59.95	59.95	48	48	48	48	15	2	21
21/09/2020	20.5	59.9	27	69	24.36649	20.5	15	33.2	54	53.5	33.2	53.9
22/09/2020	60	28	58.69	26.83	26.81	26.87	30	27	54.9	54.9	41.75	44.5
23/09/2020	83.5	78.5	40	27.55	27.57	20	57	27.57	26.7	50	49.95	49.65
24/09/2020	82.71	87.71	88	85	75	30.11	56	56	55	51	50.95	53
25/09/2020	63	63	63	63	63	63	63	63	58.75	54.75	54.75	54
26/09/2020	60	61.5	61.5	60	58.5	28.04	23.4	25.02	54	29.04	52.5	21.57
27/09/2020	61.25	61.25	61.25	61.25	61	12.3	55	26.75	35.81	35.81	29.29	27.69
28/09/2020	88.33	50	79.5	35	35	72.52401	64	50.5	68.99	65	63	59.95
29/09/2020	35.68	35.68	99.5	37.5	32.39	32.4	32.4	32.4	32.47	32.4	32	55
30/09/2020	34	37.35551	70	56.5	80	70	60	56.5	20.3	20.45	22.58	23.48987
01/10/2020	32.27	35.15	84.9	40	72.73067	79.8	33.03	33.03	33.03	33.03	55	55
02/10/2020	63.24	60.25	16.17	16	16.1	16.1	53.5	53.5	55.5	53.5	55.5	53.5
03/10/2020	65	67.99	65	61	36.3	17.1	31.2	33.35	26.06	2	21.72	0.5
04/10/2020	66	67.95	74.47	70	67.95	66	67.95	67.95	65	62	61.5	58.4
05/10/2020	23.32	23.32	23.47	60	35	60	62	58	57.35	57.35	57	24.94
06/10/2020	64.7	64.7	64.7	62.9	62.9	24.56	58	24.56	57.5	24.27	53.3	26.1
07/10/2020	64.75	66.5	64.75	62.5	62.5	25.86	59	25.76	25.76	58.95	25.9	37.02
08/10/2020	69.5	195.175	200	170	105	64.75	65.5	63.95	46.59013	52.5	54	52.5
09/10/2020	64	65	65.5	59.75	28.61	28.61	59.75	62	62	62	32.15	30.56

10/10/2020	28.55	68	68	68	65.75	65.75	58.5	58.5	58.25	57.95	57.7	28.37
11/10/2020	66	66	66	65	65.5	66	58	57.95	56.25	27	56.19	56.19
12/10/2020	25.71	25	25.71	26	26.1	26	26.1	26	58.4	59.5	26.25	23.76
13/10/2020	82	82	73.5	28	73.5	28	46.71977	27.09	2.5	2.2	1	8.77
14/10/2020	29.51	81.03	84.73	73.23	29.51	29.51	29.5	29.63	29.61	13	29.61	26.38
15/10/2020	103.81	108.81	102.31	88.81	30.61	31.15	68	30.85	60	20	2	20
16/10/2020	80	85	75	33.25	32.8	13	62	60	33	33	55	55
17/10/2020	66.5	67	66.5	66.49	32	64	66.5	57	53.75	53.75	32.15	53.75
18/10/2020	75	74.25	29	28.2	28.13	27	28.13	59	56.9	29.05	56.9	56.9
19/10/2020	69.8	67.5	29.1	17.2	29.1	28	19	15	24.99	52.5	27.24	26.24
20/10/2020	67.5	66.5	66	60	22.55	22.5	58.5	58	57.85	57	57.45	25.95
21/10/2020	78.4	74.45	69.8	31.05	68	60	31.1	57.9	32.51	32.5	57.9	20.4
22/10/2020	94.92	97.17	32.15	32.06	32.06	32.2	32.2	54.25	54.25	54.25	54.25	58.4
23/10/2020	75	75	77.8	56.5	35	34.1	64.5	35	33.81115	33	59.75	34.6
24/10/2020	78	83	78	63	61	22.92	61	63	59.5	13.2	59.3	4.5
25/10/2020	83.2	83.2	73.2	10.2	31	20.1	2.2	18	20.2	3.95	20.86	5
26/10/2020	74.5	70	69.7	69.5	27.05	21	4	15	15.55	59	62	32.75
27/10/2020	69	24.06	24.35	24.35	24.37	65	65	24	29.81	24	60	28.54
28/10/2020	78	69.5	24.95	24.95	24.95	64	65	65	65	59.9	22.74	5
29/10/2020	50.28	15.27	12.61	12.66	30.57022	12.66	3.9	-63.93	3.9	3.9	3.9	-8.15
30/10/2020	116.95	35.11	116.95	79.5	80.5	80.5	63	59	56.9	63	63	62
31/10/2020	54.91	49.32	31.66	63.5	63	34	23	5	62.5	20	30	0
01/11/2020	5	35.15	63.5	1	3.9	4	5	3.95	3.9	-31.38	-2.63	-1.61
02/11/2020	67.75	63.9	63.9	35	14	62.5	63	62.95	20.36	13	24.47	24.47
03/11/2020	85.02	17.65	17.5	3.9	3.85	17.62	56.9	56.9	36.19	3.85	24.3099	41.2
04/11/2020	0	0	3.85	3.85	64.5	3.85	3.85	3.85	3.85	3.85	3.85	3.9
05/11/2020	22	22	75	25	25	25	67	64	22.25	60	63	62
06/11/2020	24	23.5	23.5	23.5	23.5	23.5	23.5	23.55	59	23.5	30.18	58
07/11/2020	72.95	71.5	72.95	71.5	69	64	23.75	23.7	23.7	31.56	59.5	59
08/11/2020	92.78	88.28	73	72	73	72.45	61.5	59.95	59	56	59.55	59

09/11/2020	168.41	40	56	56	56	56	56	56	56	21.5	55	29.43
10/11/2020	97.85	25.1	25	3.85	19	3.85	3.85	15	19.1876	3.85	33.7	29.58
11/11/2020	12	12	60	12	10	10	29.28	28.89	26.0163	23.12	5	4.5
12/11/2020	66.1	6	64	64	6	5	34.05	34.6	36.57	27.84	59	34.51
13/11/2020	63.9	63.9	11.2	11.3	11.3	58.5	11.3	34.17	37.45	36.81	46.47	32.76
14/11/2020	62.9	62.5	59	29.14	27.25	22.78	21.5	5	5	-5	59	59
15/11/2020	35.26	6.51	6.76	6.22	6.22	6.25	16.47	10.68	9.42	0	67.9	-59.99
16/11/2020	24	14.11	50	14.11	25	6	34.07	34.15	5	-5.75003	59	5
17/11/2020	69	66.25	66.25	63.95	30	30.69	60	36.26	7.1704	6	42.89	4.5
18/11/2020	63	63	6.1	6	20.1	39.79	26.26	0	23.25	4.5	5	-17.13
19/11/2020	3.85	60	30	17.95	17.95	17.95	58.5	18.12	18.12	15.1	15	15
20/11/2020	60	60	39.15	60	41.07	3.95	5.22	3.95	58.9	32.98	6	0
21/11/2020	59	59	59	15.80497	42.47	23.66	59	37.45	59	59	20.63	3.95
22/11/2020	65	25	25	9	12	12	60	59	20.2	20.2	21.43	21.43
23/11/2020	50.26	45.93	6.24804	42.07	57	3.95	57	9	45.58	34.89	9.1	7.11
24/11/2020	68.95	68.95	68.95	15.57	25	59.75	58.95	58.95	58	58	30.49	15.55
25/11/2020	26.5	25.77	26	26.2	26.71	28	58.25	57.5	3.85	28.5	56.6	26
26/11/2020	32.6	32.6	36.5	35	33.12	33.15	52.5	33.15	58.25	59	54	54
27/11/2020	109	83.40251	66.85	59.9	59.9	34.6	36.16	36.16	36.2	45.58	56.25	54
28/11/2020	86.43	86.43	72.72	72.72	72.72	72.72	67	67	59	67	59	57
29/11/2020	97.51	25.11	67	25.15	63	63	62.5	25.2	3.85	27	52.5	52.5
30/11/2020	64	54	61	61	59	6	59	23	30	38.25	54.75	54.75
01/12/2020	31.19984	80	85	70	68.9	65	52.75	58	58	52.75	57.9	32
02/12/2020	155	100	69.98	67.77	38.5	59.48	30	54.88	56	6	2.5	5.95
03/12/2020	38.25	38.42	60	60	80	80	68	65	58	37	38.6	33
04/12/2020	65	62	61	61	61	61	59	39.43	30	3	3	22.9197
05/12/2020	304.76	68.93885	300	64.95	87.21978	68	65	61.5	61.5	31.25	31.25	31.25
06/12/2020	38.5	38.5	525	39	39	27.56	38.5	38.85	67	29	32.49	33.21
07/12/2020	34.26713	37	70	5	61	36.5	60.75	60.75	60.75	60	60	53.8
08/12/2020	133	39	139.8704	39.05	39.05	39	0	0	6	6	38.55	53.5

09/12/2020	38.62	5	38.62	38.62	39.12	39.21	39.14	38.6	20	5	5	2
10/12/2020	6	36.75	6	5	5	56.9	5	36.87	41.22	5	17.5	5.95
11/12/2020	92.5	85	92.5	92.5	90	74.5	68	37.9	63	63.75	63	62
12/12/2020	95	95	78	70	69	62.5	63	62	0	0	60.45	59.7
13/12/2020	68.9	69.88	7.5	10	45.64	63	43.75	37.72	37	-42.79	-61	-61
14/12/2020	72.9	72.9	72.9	22	67	69	65	65	65	63	63	63
15/12/2020	23.6	23.6	23.6	23.5	65	65	65	63	37.31	63	63	63
16/12/2020	75.55	72	71.5	63	65	63	63	64.5	63	63	30.03	7.5
17/12/2020	30	73	73	63	34.46817	20.1	62	18.6	61.5	38.61	0	0
18/12/2020	72	71.7	71	66	31.01	66	66	30.83	29.07	63.69	31.35	7.5
19/12/2020	68.45	20.24	42.28	44.85	66	67	66.95	66	66	65	65	7
20/12/2020	75.85	71.75	71.5	67	25.15	25.15	39.96	66	65.5	63.45	65.5	65.5
21/12/2020	80	67	75	75	66	25.5	66	65.95	62.75	22.7	6.9	6
22/12/2020	72.9	72.98483	79	65	72.9	33	65	33	33	65	65	64
23/12/2020	32	32	32	67.5	67.5	65	65	65	29.1	29.1	65	65.5
24/12/2020	79.9	76.67	75.95	75.95	75.95	75.95	67	65	65	65	65	65
25/12/2020	27.29	27.3	65	65	65	37.86	7.5	20.5	34.32	20.5	66	65.75
26/12/2020	68.5	68.5	46.43	64	20.59	15.56	64	3.84	7	7	18.7	14.9
27/12/2020	24	81.4	78.99	23.8	24.5	24.25	24.25	69	65	58.5	59.9	59.9
28/12/2020	190.83	35	145	35	84.99	77	69	35.1	35.16	69	76	75.6
29/12/2020	142.66	131.66	113	113	113	95	95	74	72.5	70.5	70.5	70.5
30/12/2020	238.35	220.9594	222	94	222	74.95	76.5	38.1	75.45	38.2	38.2	38.21
31/12/2020	93.5	89.95	90	88	74	74.9	74.9	74.9	73.15	67	72	73.15